DESIGN INTEGRATION AND NOISE STUDY FOR A LARGE STOL AUGMENTOR WING TRANSPORT

TASK I REPORT

D6-60139

Distribution of this Report is provided in the interest of information exchange. Responsibility for the contents resides in the author or organization that prepared it

Prepared Under Contract NAS2-6344 by
THE BOEING COMPANY
Commercial Airplane Group
P.O. Box 3707
Seattle, Washington 98124

JAN 1976
RECEIVED
NASA STI FACILITY
INPUT BRANCH

For
Ames Research Center
NATIONAL AERONAUTICS AND SPACE ADMINISTRATION

DESIGN INTEGRATION AND NOISE STUDY FOR A LARGE STOL AUGMENTOR WING TRANSPORT

TASK I REPORT

D6-60139

Distribution of this Report is provided in the interest of information exchange. Responsibility for the contents resides in the author or organization that prepared it

(NASA-CR-146111) DESIGN INTEGRATION AND NOISE STUDY FOR A LARGE STOL AUGMENTOR WING TRANSPORT, TASK 1 REPORT (Boeing Co., Seattle, Wash.) 449 p

N76-71551

Unclas

00/98 17864

Prepared Under Contract NAS2-6344 by
THE BOEING COMPANY
Commercial Airplane Group
P.O. Box 3707
Seattle, Washington 98124

For
Ames Research Center
NATIONAL AERONAUTICS AND SPACE ADMINISTRATION

CONTENTS

Page

1.0 SUMMARY 1

2.0 INTRODUCTION 3

3.0 SYMBOLS AND ABBREVIATIONS 5

4.0 TASK I INTRODUCTION 11
- 4.1 General Program Objectives 11
- 4.2 General Program Approach 11
  - 4.2.1 Task I–Noise Suppression–Nozzles 12
  - 4.2.2 Task II–Noise Suppression–Entire Augmentor Wing Flap System 13
  - 4.2.3 Task III–Aerodynamic Investigations 13

5.0 SYSTEM DESIGN STUDIES 15
- 5.1 Introduction and Background 15
- 5.2 Augmentor System Duct/Nozzle/Flap Integration 17
  - 5.2.1 Baseline Definition 17
  - 5.2.2 Test Hardware Requirements 18
  - 5.2.3 Nozzle Studies 19
  - 5.2.4 Flap Studies 20
- 5.3 Wing Geometry Studies 21
  - 5.3.1 Wing Planform Parametric Studies 21
  - 5.3.2 Duct Geometry 22
- 5.4 Duct System Studies 24
  - 5.4.1 Duct System Concept Evolution 24
  - 5.4.2 Alternate Duct Systems 25
  - 5.4.3 Engine Spacing 27
  - 5.4.4 Engine - Out Rolling Moment 27
  - 5.4.5 System Pressure and Pressure Loss Studies 27
- 5.5 Engine Cycle Studies 30
  - 5.5.1 Introduction and Scope 30
  - 5.5.2 System Design Study Engines 32
  - 5.5.3 Splitter Through Fan Concept 36
  - 5.5.4 Parametric Engine Cycle Study 37
- 5.6 Three-Stream System 44
  - 5.6.1 Introduction 44
  - 5.6.2 Three-Stream Duct, Nozzle, and Flap Integration 45
  - 5.6.3 Airplane Sizing 45
  - 5.6.4 Noise 46
  - 5.6.5 Conclusions 46

CONTENTS–Concluded

Page

6.0 STATIC RIG TEST PROGRAM 163
6.1 Introduction 163
6.1.1 Background 163
6.1.2 Design Principles 165
6.1.3 Test Objective 167
6.2 Technical Approach 167
6.3 Apparatus and Test Procedures 169
6.3.1 Performance Data Acquisition 170
6.3.2 Performance Data Reduction 171
6.3.3 Acoustic Data Acquisition 172
6.3.4 Acoustic Data Reduction 174
6.3.5 Acoustic Data Reduction Processing 175
6.3.6 Model Descriptions 177
6.3.7 Test Variables 179
6.4 Data Accuracy and Repeatability 179
6.4.1 Performance Measurements 179
6.4.2 Acoustic Data Measurements 180
6.5 Results 181
6.5.1 Performance Results 181
6.5.2 Primary Nozzle Jet Profile 184
6.5.3 Acoustic Results 189
6.6 Applications 200

7.0 AERODYNAMIC DESIGN OF AUGMENTOR WING SECTION 381
7.1 Introduction 381
7.2 Design and Analysis Method 381
7.2.1 Description of Existing Potential Flow Analysis Computer Program 381
7.2.2 Application of the Program to Augmentor Wing 382
7.3 Flap "A" Design 382
7.4 Results of Potential Flow Calculations 383

8.0 CONCLUSIONS TASK I 391

9.0 TASK II AND III RECOMMENDATIONS 393
9.1 Static Rig Tests 393
9.2 Wind Tunnel Tests 395
9.3 System Design Studies 396

REFERENCES 403

1.0 SUMMARY

The task I effort of contract NAS2-6344, described in this report, consisted primarily of initial system studies and static rig testing to establish the design characteristics and performance and noise levels of a large STOL transport airplane. In general, work to date indicates that completion of tasks II and III will confirm that noise suppression will equal or exceed original estimates.

The baseline configuration airplane studied incorporated a two-stream engine with the fan air ducted to the augmentor nozzles through a plenum system. This was accomplished with a takeoff nozzle pressure ratio of 2.0, which was the original target.

Wing optimization studies showed that the augmentor wing airplane design is particularly responsive to wing thickness and its effect on ducting capacity. Therefore, the optimizations showed substantial improvement by using a wing aspect ratio of approximately 5.5 for the STOL mission. System studies also showed that minimum takeoff gross weight is achieved by utilizing high duct velocities with total pressure duct losses up to 25%.

Static rig testing included slot nozzles with aspect ratios between 50 and 400, convergent-divergent nozzles, and various multi-element nozzles with lobes and tubes. All testing, both performance and noise, showed good accuracy and repeatability. Performance testing of nozzles showed high velocity coefficients.

Noise testing of nozzles without flaps has confirmed original noise estimates quite closely, including the effects of aspect ratio, nozzle breakup, and shock-induced noises of underexpanded nozzles. The high-breakup lobe-type nozzle has the best noise characteristics to date. A firm base has been established for task II static testing with the complete flap system.

A preliminary study of the three-stream augmentor wing design shows that the takeoff gross weight is equivalent to that of the two-stream design at higher levels of wing thrust (50% and above), but the noise will be substantially higher.

Using test data generated to date, and applying reasonable noise technology improvements, it is evident that the two-stream augmentor wing airplane has a noise potential of 90 PNdB at a 500-ft sideline.

2.0 INTRODUCTION

The aerodynamic development of the augmentor wing concept has been pursued by NASA and de Havilland Aircraft of Canada for a number of years. More recent emphasis on very low noise levels for commercial STOL aircraft has focused attention on the fact that the augmentor of the augmentor wing airplane has the inherent characteristics of a very effective ejector-suppressor.

Studies by The Boeing Company showed that the augmentor wing airplane has a lower noise potential than other systems being studied, particularly if all the fan air could be directed to the wing and silenced by the augmentor. This work resulted in a contract (NAS2-6344) for the augmentor wing noise program, which has the objective of developing through analysis, design, experimental ground rig testing, wind tunnel testing, and design integration studies, an augmentor wing jet flap for a jet STOL transport aircraft having maximum propulsion and aerodynamic performance with minimum noise generation. This program has three basic elements: (1) static rig testing of a scale wing section to demonstrate augmentor performance and noise characteristics, (2) two-dimensional wind tunnel testing to determine flight speed effects on performance, and (3) system design and evaluation which optimizes the complete system and ensures compatibility of the design with the requirements for a large (150 passenger) STOL transport.

The results of task I, accomplished between January 1 and June 30, 1971, are described in this report. Included are initial static rig testing with a variety of augmentor nozzles and completion of work preparatory to testing with the complete augmentor flap system, design and fabrication of the two-dimensional wind tunnel model, and establishment of a baseline airplane with a parametric optimization of wing design and propulsion system.

3.0 SYMBOLS AND ABBREVIATIONS

A	area
A*	blowing nozzle area at Mach number = 1.0
a	local velocity of sound
ail	aileron
AR	airplane aspect ratio or nozzle aspect ratio, b/h
AR	augmentor primary nozzle array area ratio, area enclosed by array/nozzle flow area
b	span
BPR	bypass ratio, engine secondary airflow/engine primary airflow
C_D	drag coefficient or nozzle discharge coefficient (mean airflow/ideal airflow)
C_G	nozzle thrust coefficient
C_L	lift coefficient
C_{LP}	design lift coefficient
C_P	pressure coefficient
C_R	roll moment coefficient
C_V	nozzle velocity coefficient
C_μ	blowing momentum coefficient, augmentor primary nozzle isentropic thrust/qS
c	chord
C-D	convergent-divergent nozzle
CTOL	conventional takeoff and landing
D	diameter
dB	decibel
F	engine thrust or augmentor primary nozzle thrust
F_I	ideal nozzle thrust
f	frequency (Hertz)
FPR	fan pressure ratio
g	gravitational constant

GND	ground plane
GW	airplane gross weight
GW'	airplane corrected gross weight
H	nozzle array height
h	height (Y direction)
Hz	Hertz, unit of frequency
K_F	duct loss velocity head factor
L	length (X direction, usually)
LE	leading edge
M	Mach number
m	airflow
NPR	nozzle pressure ratio
OASPL	overall sound pressure level
$OASPL_{max}$	maximum OASPL along a noise radiation line with respect to the jet axis
OPR	overall pressure ratio of engine
P	static pressure or lobe or tube centerline pitch
PNdB	unit of perceived noise level
PNL	perceived noise level
PNL_{max}	maximum PNL along a noise radiation line (arc) with respect to the jet axis
q	dynamic pressure
R	radius from nozzle exit centerline to microphone or observer
R_N	Reynolds number
R_c	coanda radius
S	wing area
S_N	Strouhal number
sfc	specific fuel consumption
SLS	sea level static

SPL	sound pressure level
STOL	short takeoff and landing
T	temperature or airplane net thrust
t	wing thickness
T/O	takeoff power setting
Thumbprint	plot of $(T/W)_{unin}$, GW, and W/S
TOFL	takeoff field length
TOGW	takeoff gross weight
T/W	airplane thrust/weight ratio
T/S	airplane thrust/wing area ratio
V	velocity
W	weight or airplane weight
w	lobe width
WCP	wing chord plane
W/S	wing loading
X	axial distance downstream from augmentor primary nozzle
Y	vertical coordinate from nozzle centerline or WCP
Z	spanwise coordinate
α	angle of attack
β	plenum rotation or slot nozzle orientation with respect to flyover position
$\Delta F/F_{sec}$	fan air gross thrust loss ratio
ΔGW	airplane gross weight correction based on engine installed thrust/weight ratio relative to thumbprint thrust installation factor
$\Delta P/P_F$	fan air total pressure loss fraction relative to fan exit total pressure
δ_F	flap rotation angle with respect to WCP
δ_N	augmentor primary nozzle deflection angle with respect to WCP
δ_{tur}	augmentor flap air turning angle, $\delta_F - \delta_N$

$\delta_{1/2}$	at a given jet axial station, the "Y" distance from the jet centerline to the point where the jet velocity is half the maximum jet velocity in the same plane
θ	noise radiation angle with respect to inlet centerline
θ_{DIFF}	augmentor diffuser angle
θ_I	augmentor intake angle
θ_{LIP}	lip angle with respect to WCP
Λ	airplane wing sweep of quarter chord
λ	wavelength
ρ	jet density, lb/cu ft
ϕ	thrust installation factor, $(T_{in}/T_{unin}) = (T/S)_{in}/(T/S)_{unin}$

Subscripts

A	airplane
AP	augmentor primary nozzle
APC	section from augmentor primary nozzle to coanda
APIG	isentropic gross thrust of the augmentor primary nozzle associated with installed engine and ducting, excluding nozzle losses
APTH	section from augmentor primary nozzle to flap throat
aug	total augmentor per wing
diff	diffuser section, flap throat to flap exit
duct	duct system
E	equivalent nozzle, i.e., same nozzle area per unit span
EX	augmentor flap exit
eng	bare engine
exp	fully expanded jet
F	fan exit total conditions
G	gross

I or IJ	ideal, fully expanded jet (as applied to velocity)
in	installed
J	jet at augmentor primary nozzle exit ($V_J = C_V V_I$)
L	lobe of augmentor primary breakup nozzle
lip	lip on lower side of augmentor primary nozzle
lipc	end of lip to nearest point of coanda parallel to lip surface
M	maximum for any axial (or "X") station downstream of nozzle
MD	main wing duct
MDR	baseline system main wing duct
mix	total mixing section, augmentor primary nozzle to flap exit
N	net
NS	nacelle and strut
P	augmentor primary nozzle exit
pod	bare engine plus nacelle and strut
pri	primary
R	relative jet
S	slot nozzle
SD	subduct
SLS	sea level static
sec	secondary, engine stream, or induced flow regions of the augmentor
secin	secondary air inlet to augmentor
sect	particular augmentor section
T	total (for total pressure, total temperature)
TH	augmentor flap throat
tot	engine pads plus duct system
unin	uninstalled
4	turbine inlet
∞	ambient

4.0 TASK I INTRODUCTION

4.1 GENERAL PROGRAM OBJECTIVES

The objective of the augmentor wing noise program is to develop through analysis, design, experimental ground rig testing, wind tunnel testing, and design integration studies an augmentor wing jet flap configuration for a jet STOL transport aircraft having maximum propulsive and aerodynamic performance with minimum noise generation. The program is primarily a technology development effort, with a parallel system integration design study to assess the feasibility of all augmentor wing concepts considered for low noise for meeting various propulsion and aircraft design requirements of commercial STOL transport aircraft. The technology development effort consists of three major tasks: (1) studies of various nozzle design parameters for noise suppression of slot-type nozzles, (2) studies of the entire augmentor wing jet flap, with acoustic treatment of various segments of the flap for noise suppression, and (3) aerodynamic studies at forward speed to assess the effects of noise suppression modifications on the performance of the flaps.

To achieve the primary goals of the program, emphasis is placed on the following factors:

1) Augmentor wing jet flap concepts for noise reduction are selected with consideration for STOL aircraft performance, stability, control, and field length to minimize degradation of airplane operating capabilities and economics for the entire flight envelope.

2) Investigations include noise measurements of nozzle and augmentor wing jet flap configurations, thrust measurements, and wind tunnel tests on augmentation efficiency, aerodynamic drag, and propulsive thrust.

3) Consideration is given to selection of test hardware, test conditions, and the potential for presenting tradeoff data and design curves over a wide range of application.

4.2 GENERAL PROGRAM APPROACH

The development of the augmentor wing jet flap for best thrust performance and noise reduction requires a thorough understanding of the basic mechanisms of noise generation and suppression, as well as the basic mechanisms of thrust augmentation in ejector/flap combinations. In the proposed program, particular emphasis is placed on understanding those elements of the augmentor wing jet flap that generate noise or affect the resultant noise field. The configurations will be designed to combine nozzle and ejector thrust performance with noise reduction to permit application of the results to other similar configurations.

The objective of task I is the determination of component noise sources and propulsion characteristics. The work will evaluate the effects of basic slot nozzles, suppressor nozzles with breakup, nozzle lip and nozzle placement variation, and the identification of required

[illegible] characteristics. Candidate configurations will be selected for task II tests. [illegible] system analysis will be performed to ensure that the candidate configurations are [illegible] to meet the airplane installation and performance requirements. The parameters of [illegible] to be conducted are described in sections 4.2.1 through 4.2.4.

4.2.1 Task I–Noise Suppression–Nozzle

Develop a program to optimize an augmentor wing jet flap concept over a broad [illegible] of operating conditions for low noise. The goal is to meet a 95 PNdB noise level at a [illegible] sideline distance for a 100/150-passenger STOL transport aircraft having a 2000-ft [illegible] field length.

Static Rig Tests

Conduct studies and static rig tests of large-scale models of various nozzle configurations to determine noise attenuation and propulsion efficiency for various nozzle types and conditions, including nozzle aspect ratio, nozzle pressure ratio, shock structure with convergent-divergent nozzle, and multi-element nozzles. The most promising nozzle configurations will be investigated in conjunction with the coanda surface having various lengths of lip and deflection angles with respect to the jet axis to determine the effects on noise suppression and performance.

System Design and Evaluation

Conduct preliminary studies of system design and analysis wherein integration of the propulsion system and augmentor wing jet flaps with the airplane will be started during this task. These studies shall include preliminary design of practical aircraft wings to assess the optimum combination of wing thickness, area, aspect ratio, and span location to accept ducting and augmentor wing jet flap requirements. The studies shall also include preliminary design of practical basic ducting layouts for independent and plenum chamber systems to assess engine-out duct and valve requirements for various engine number and spacing. The studies shall also include a preliminary assessment of a range of engine cycle pressure ratios, fan pressure ratios, turbine temperatures and bypass ratios for providing low primary nozzle noise. The results of the initial system integration studies carried out in this task will be continued during task II and III.

General

Conduct preliminary studies and program definition for the task II and task III parts of the program. In task II, consideration is given to tests of the noise levels of the entire augmentor wing jet flap with acoustic lining and to continuation of the systems integration effort started in task I. In task III, aerodynamic performance of the low noise level augmentor wing jet flap is investigated.

4.2.2 Task II--Noise Suppression--Entire Augmentor Wing Flap System

Task II will be composed of static rig tests of the noise levels of acoustically treated augmentor wing jet flap systems utilizing the various nozzles developed in task I which indicated the greatest potential for accomplishing the objectives of the program.

Static Rig Tests

The investigations shall include measuring the acoustic noise levels and static performance of augmentor wing jet flaps with a number of parameters such as coanda lip length, slot heights, and diffuser height to nozzle height ratio varied to define near-optimum ejector performance with low noise levels for the basic augmentor flap.

Investigations shall also include measuring the noise and static performance levels of augmentor wing jet flaps with systematic installation of various acoustic lining on several positions on the lower flaps, upper flaps, intake door, and coanda surface. The types of lining should include, first, a broadband acoustic treatment, followed later by tuned lining which will be selected during the task I preliminary studies for definition of task II.

System Design and Evaluation

Continue preliminary studies of system design and analysis, of which the integration of the propulsion system and augmentor wing jet flap portion was started in task I. In addition to the task I items, the studies shall include ducting component design layouts for minimum pressure loss and weight, diverter valves, variable nozzle area, and other components related to ducting air from the engine fans to the flaps. The results of these and the task I systems integration studies will be continued in task III.

4.2.3 Task III--Aerodynamic Investigations

The studies are to include analyses and experimental investigations of the effects of various modifications to the augmentor wing jet flap for reduction of noise levels on the sectional aerodynamic characteristics at forward speed conditions by conducting wind tunnel tests of two-dimensional models. The task I and II investigations will determine the static performance of the configurations, and a certain limited number of configurations will be investigated during task III. Specific objectives are to:

1) Determine the baseline performance with a two-dimensional model of the basic NASA-Ames Phase VI augmentor wing jet flap.

2) Modify the two-dimensional model with the augmentor wing jet flap nozzle configuration changes, acoustic lining treatment, upper and lower flap, and slot and coanda surface changes based on the results of task II and determine the effects on performance at forward speed.

3) Modify the two-dimensional model to determine dependence on augmentor wing ejector efficiency and requirements versus lift coefficient with wing leading edge devices and leading edge blowing in the vicinity of a leading edge slat to provide data for design trades with trailing edge flap momentum coefficients, flap chord ratio, and flap deflection.

4) The design integration studies for the propulsion system and augmentor wing jet flap will be completed in task III and shall include, in addition to task I and task II studies, the investigation of the total system integration to determine interrelationship of duct designs, wing thickness, engine specific fuel consumption, and weight, and their effects on STOL transport aircraft performance and noise.

   The studies shall also include, with assistance from engine manufacturers, evaluation of existing fan-jet engines and components to determine modifications that may be possible for a demonstrator augmentor wing fan jet engine. The purpose of these studies will be to define a program with a full-scale fan jet engine combined with an augmentor wing jet flap of partial span to demonstrate with static tests the noise suppression capable with an integrated system.

5.0 SYSTEM DESIGN STUDIES

5.1 INTRODUCTION AND BACKGROUND

The purpose of the system design effort is to integrate the airplane mission and installation requirements with the static and wind tunnel augmentor flap testing. To perform this function a baseline airplane was sized to the mission constraints of a 2000-ft field length, 500-nmi range, and 150-passenger capacity (see fig. 5-1). The noise target is 95 PNdB at the 500-ft sideline. The baseline thrust and wing area are used to size the test hardware. Installation and feasibility studies are performed on nozzle, flap, and duct systems. The augmentor flap concept of major interest is the "two stream" configuration, with all the fan airflow ducted to the wing and with the augmentor flap used as the primary propulsion source during takeoff and landing. The engine cycle for this system has a high pressure ratio (2.5 to 3.5), multistage fan, and low-velocity, low-noise primary jet. This system is shown on figure 5-2. It is felt that the suppression potential of the flap system, combined with the low primary jet velocity and choked inlet, provides the two-stream concept with the best potential to meet the noise target. However, three-stream systems, with a low-pressure fan providing jet thrust and a high-pressure fan of 30% to 50% blowing thrust ducted to the wing, are also evaluated and compared to the two-stream system.

The wing planform and duct system on the baseline airplane is systematically varied to determine the amounts of thrust that can be ducted to the wing as a function of wing and duct system parameters. Engine cycle studies are conducted to evaluate engine weight and performance.

A sketch of the augmentor flaps for a two-stream system is shown in figure 5-3. The major change from previous augmentor flaps is the amount of air ducted to the wing. Previous augmentor flaps, like the modified DHC Buffalo (NASA contract NAS2-6025), are similar to three-stream systems investigated, with about one-third of the thrust ducted to the augmentor flaps. The increase in the wing thrust split and the increased wing loading desirable for ride quality require about three times as much thrust into a given sized flap system. The increased flap thrust necessitates geometry changes and reoptimization of the nozzle-flap system. Multi-element augmentor primary nozzles appear likely to be used for noise reduction and to improve augmentor performance by increasing the mixing rate inside the flap system. Several configuration changes from the Buffalo flaps are shown in figure 5-3; it is expected that changes in this direction will be required to optimize the flaps for the increased thrust per unit wing area, and to realize the noise suppression potential of the flap system. Important changes will likely include the long lip, the increased flap spacing, and the larger coanda radius. These and other features are being evaluated in the system design and test programs.

Suppressor nozzle design experience developed at Boeing, as well as available information from NASA and the industry, have revealed the existence of several avenues for large improvement in augmentor wing jet flap noise suppression. These include:

1) Breakup of the nozzle into multi-element segments and spread to an overall cross-sectional area considerably larger than that of a single jet of the same total flow

area. This process in general reduces the level of low-frequency noise but may shift some of the energy to higher frequencies. Configuration constraints often determine the upper limit for flow breakup.

2) Effective use of lining material on the long flap-ejector surfaces. Ejectors promote mixing of ambient air with the jet to reduce velocity (and noise) and provide shielding of the high-frequency energy generated close to the jet exit. Lining with acoustically absorbent material provides additional noise attenuation primarily in the high frequencies.

3) Use of convergent-divergent (C-D) nozzles to minimize the shock-induced noise effects commonly measured on conventional convergent nozzles operated at supersonic pressure ratios.

4) Extension of the nozzle lip to shield high-frequency noise generated close to the jet exit.

5) Improvement in the augmentation ratio to decrease the nozzle pressure ratio. The resulting lower jet velocity will generate less augmentor primary nozzle noise.

6) Direct decrease in nozzle pressure ratio (with corresponding increase in airflow) to reduce nozzle velocity and noise.

7) Use of the favorable directionality characteristics of the high-aspect-ratio slot nozzle to decrease sideline noise.

The effects of given changes in suppressor geometry can only be predicted in a general way. A more detailed discussion of these suppression principles, especially those involving primary nozzles, is presented in section 6.0.

The target noise level for the augmentor wing STOL airplane is 95 PNdB or less at a runway sideline distance of 500 ft. This objective has been expressed in at least two technical reports (refs. 5-1 and 5-2). The American Airlines study of the feasibility of a floating Manhattan STOLport, (ref. 5-3) recommended complying with the New York City requirement of 85 PNdB at about one-half mile from the nearest residential development. Correcting for distance this is close to the 95 PNdB objective at a 500-ft distance. Robinson of the National Physics Laboratories in England has used a criterion of 90 PNdB in the business and industrial areas of cities and about 85 PNdB in residential areas (ref. 5-4). A definite target number is difficult to determine, because subjective response to aircraft noise is a complex phenomenon involving several interrelated factors: intensity peak, duration of peaks, discrete tones, harmonics, and the general quality of the sound.

5.2 AUGMENTOR SYSTEM DUCT/NOZZLE FLAP INTEGRATION

5.2.1 Baseline Definition

An augmentor wing airplane configuration with 80% of the engine thrust ducted to the wing was established to:

1) Determine thrust and wing loading requirements

2) Guide sizing of test hardware

3) Provide a reference point for further wing, duct, flap, and weight studies

The airplane was designed for 150 passengers, a 2000-ft field length, a 500-nmi range, and a cruise requirement of Mach 0.8 at a 30,000-ft altitude. This configuration (see fig. 5-1), was designed around the STF-369C engine, which has a fan pressure ratio of 2.45. Assuming a 15% pressure loss in the ducts, this gives a nozzle pressure ratio of about 2.0. A supercritical airfoil section was used to meet the cruise speed requirement, with a thicker than conventional airfoil. The wing planform had an aspect ratio of 6.5 and a thickness ratio of 12% outboard increasing to 16.3% at the fuselage. A thrust-to-weight ratio (T/W) of 0.39, a wing loading (W/S) of 84 lb/sq ft, and a gross weight of 185,000 lb were initially selected. This gave an engine size of 18,000 lb (uninstalled) and a wing area of 2200 sq ft. The thrust to the wing was split 85% to the augmentor nozzle, 10% for leading edge BLC and 5% for aileron BLC.

A subduct plenum augmentor duct system was installed on the baseline airplane. The subduct plenum has a separate duct that is closed during engine-out operation to reduce the nozzle area to compensate for the lost engine. The subduct was installed on the inboard and outboard augmentor nozzle sections. It was not extended through the center portion because this is a critical area for duct volume during engine-out operation. A schematic of the duct system is shown in figure 5-4, and the resulting nozzle spanwise blowing distribution in figure 5-5. The augmentor blowing nozzle arrangement and dimensions are shown in figure 5-6. The separate nozzles are installed into an adapter plate that has integral turning vanes and also supports the duct. The main duct air flows into lobe nozzles, and the subduct flows into a slot nozzle below the lobe nozzle array. This nozzle arrangement was used to minimize the nozzle vertical space requirements and to allow room for support structure on the inboard flap sections. The nozzle exit plane was placed over the aft duct to allow the flow from the nozzle elements to merge into a jet sheet before encountering the coanda turning section in the flaps and to permit installation of as much acoustic lining material as possible between the nozzle exit plane and the flap exit. The subduct slot nozzle was placed close to the lobe nozzle to obtain a long lip to allow the flow from the lobes to attach to the lip when the subduct is closed during engine-out operation. Additional ducting schemes are described in section 5.4 and other nozzle arrays in section 5.2.3.

A flap system using a simple pivot for both the flap and shroud was designed for the baseline airplane and is shown in figure 5-7. The flap nose and lip were contoured to give a substantial lower ventilation gap at the takeoff flap setting of 35° to improve thrust augmentation. The gap gradually closes with increasing flap angles to enhance the lift and flow

turning capability. A small door seals the lower gap during cruise flight. The upper shroud and door are connected by a roller and slot arrangement which allows the shroud and door length to telescope as the flap angle increases. This action exposes the upper BLC suction slot (which is built into the shroud) at flap angles greater than about 25°. The flaps are broken into three spanwise segments per side and are actuated by a rotary actuator.

A parametric study of thrust loading, wing loading, and estimated airplane gross weight was performed; the results for the baseline airplane are shown in figure 5-8. This figure was developed by determining the T/W and W/S relationship for the takeoff and landing field length. The gross weights were determined by conventional parametric methods. The duct volume is for a duct system similar to the baseline. The design point is the intersection of the duct volume and takeoff lines and shows that a gross weight of 203,000 lb is required to meet the mission. However, the wing and thrust loading remained at 84 and 0.39, and therefore the relationships of engine and duct size to wing area remain the same as in the previous design work. Additional wing geometry studies are described in section 5.3.

The assumptions for the STF-369C engine data used in the noise calculation procedure for the baseline was for an installed configuration, standard day sea level performance, and 100 kn speed. The noise calculation procedures of reference 5-16 were used to predict the inlet, primary jet, and flap (basic cycle) noise.

The curves of figure 5-9 relate peak PNL to altitude for the baseline airplane. The low primary jet noise levels are attributed mainly to the low jet exit velocity. Inlet noise has been suppressed 22 PNdB by the application of inlet guide vanes and sonic choking. The technical basis for this suppression estimate was founded in previous Boeing sonic inlet development work. Augmentor wing/jet flap noise levels are based on technology associated with other Boeing suppressor design programs and available test reports. It is the purpose of the testing portion of this program to provide test data that will permit improvement in these predictions.

5.2.2 Test Hardware Requirements

The baseline airplane was designed around an STF-369C engine because it is expected that lower nozzle pressure ratios will result in lower noise. However, the test program will evaluate this assumption. The major effect of increasing the NPR at constant thrust is to reduce the nozzle and duct area. This relationship is shown in figure 5-10. It shows that increasing the NPR from 2.0 to 2.5 will decrease the nozzle area to about 0.7 of the former area. This reduces the equivalent nozzle slot height. h_E (augmentor nozzle area per side/nozzle span), from 2.1 in. at NPR = 2.0 to 1.47 in. at NPR = 2.5. This reduction in h_E increases the nozzle aspect ratio from 220 at NPR = 2.0 to 320 at NPR = 2.5 (see fig. 5-11). Therefore a realistic evaluation of the effect of NPR on noise will include these configuration variables. Increasing the NPR also decreases the duct diameter, and this reduces the chordwise volume of space occupied by the duct. If the rear spar is kept at 50% of chord, the flap length will vary inversely to the duct volume. This is shown in figure 5-12 for a common duct system and for a typical independent duct system (27% crossover) described in section 5.4. The independent ducts require more chordwise volume and a higher NPR (2.7 vs 2.0 on the plenum) to obtain the same flap chord. The duct volume, nozzle exit plane, and equivalent nozzle height determine the mixing length ratio, which is a nondimensional

measure of the length available to mix the nozzle flow and attenuate the noise inside the flaps. For constant wing planforms, the mixing length ratio increases with increasing nozzle pressure ratio (fig. 5-12).

Figure 5-13 presents schematics of several suppressor nozzle types. Slot nozzles provide an effective means of increasing the mixing perimeter of a jet nozzle to reduce noise and are compatible with the augmentor wing configuration. The slot height reduction is effective in reducing the level of low-frequency noise but may shift some of the energy to higher frequencies. C-D nozzle designs operated at design pressure ratio have demonstrated a capability to attenuate shock-induced noise.

Lobe and tube nozzles have also been shown to be effective suppressors. The major variables are element dimension (size and shape) and array area ratio. Large array area ratios are necessary for good low-frequency noise reduction. A decrease in element dimensions (with adequate spacing) tends to provide better mixing and shift the noise energy to a higher frequency, which is more amenable to shielding and attenuation.

The test nozzles are described in section 6.2 and were designed to give parametric trade curves of these variables.

The expected mixing characteristics of a breakup nozzle are shown in figure 5-14. The flow from the individual nozzle elements mixes with and entrains the surrounding ambient air. As this occurs, the mixing regions expand and merge together to form a thick, continuous, lower velocity jet.

5.2.3 Nozzle Studies

Several nozzle configurations were studied to determine their feasibility for use with the duct and flap systems. Considerations included wing volume, flow losses, noise suppression potential, and nozzle installation and manufacture. The array height is limited by the available vertical space in the wing for structure, nozzles, and ducts. Figure 5-15 shows the nozzle pressure ratio required for nozzle array area ratios of 2.5 and 4.0 using a plenum duct and nozzle location similar to that of the baseline airplane. This figure shows the vertical space allocations for structure, aft duct, and nozzles at the nozzle exit plane.

The interwoven lobe concept is shown in figure 5-16. An independent duct system (each engine has a separate duct) is used here and is described in section 5.4.2. The nozzles are attached to the ducts with an adapter plate with integral turning vanes. The lobe nozzles are alternately attached to two ducts, and this arrangement could also be applied to the subduct plenum system. The advantages of this concept are a uniform breakup of the nozzles and good ventilation between the lobes for access of entrained mixing air. The severe bend to the nozzles from duct 2 may cause high internal losses unless special care is taken in the design of the internal contours. Engine-out conditions would shut off the lobes from one duct, and the effective spacing of the remaining lobes would be increased. This would require a longer distance for the flow from the lobes to mix and would need to be considered when integrating the nozzles and flaps.

The "stacked" lobe concept (fig. 5-17) is similar to the interwoven lobes, except that the nozzles from each duct are arranged vertically. This relieves the severe bend on the nozzles from the aft duct. The effective lobe spacing remains constant during engine-out operation, but the nozzle array height is reduced. However, a gap exists between the upper nozzle row and the coanda flap during engine-out with the lower nozzle row inoperative, and this will require evaluation for adverse effects at higher flap angles.

Tube nozzle arrays are shown in figures 5-18 and 5-19. The tubes could be arranged either in an interwoven or a stacked array. The upper row of tubes is shown with elliptical shapes to increase the ventilation area for entrained air. The nozzle/duct adapter plate would become rather complex for the four-tube row nozzle array. The tube nozzles require more individual pieces for the entire augmentor nozzle than do the lobe nozzles, but each tube can be lighter and simpler than a lobe.

The tandem nozzle (fig. 5-20) combines a breakup nozzle array with a slot nozzle. This nozzle type was used on the baseline airplane but has a wider application and could lend itself to some innovative duct/nozzle schemes. A potential advantage of this nozzle is that the slot nozzle portion can be used as a BLC device to enhance the turning of the breakup nozzle flow at steep flap angles. This would require a duct system having continuous blowing to this nozzle, especially during engine-out operation. One way to achieve this would be to add a trailing edge plenum duct similar to the leading edge BLC system. The slot nozzle might be fabricated as a series of lobe nozzles laid end to end. Evaluation of these described nozzle types is continuing and will require integration of the test data with system design.

5.2.4 Flap Studies

The airplane constraints for wing area, wing chord, nozzle area, and flap chord were used to size the test flap configurations. The test hardware and test plan are discussed in section 6.0, and the results of the testing will be used to evaluate and optimize the flap system during task II. In addition to the baseline flap system, conceptual flap arrangements were synthesized to provide alternate solutions and possible improvements to the flap system.

The lower gap acoustic shield (fig. 5-21) provides a method to suppress the noise leakage through the lower gap while maintaining the performance advantages associated with this gap. The acoustic shield creates an acoustically lined channel to attenuate and redirect the noise leakage away from a direct path to the ground. The modulating flap concept (fig. 5-22) attempts to provide a means to modulate the thrust during approach without incurring large changes in lift. The flaps are deployed conventionally until the go-around flap setting (approximately 45°) is reached. Then the major flap components remain in position and additional flap deflection is obtained by modulating the trailing edge of the flaps. Rapid control rates could be achieved during modulation because only the modulating portion of flaps would be moved. Flap deflections over 90° could be achieved with this scheme with the possibility that flow separation at high flap deflections could be confined to the modulating portion of the flaps rather than the entire flap system. The main flap would have a reduced range of deflection compared to other augmentor flaps, and this would allow the nozzle lip and flap nose to be tailored to a specific flap angle rather than compromised over a large range of flap angles. The effective coanda turning radius could be made larger than that of the baseline flap; this would enhance the performance when breakup nozzles were used.

5.3 WING GEOMETRY STUDIES

5.3.1 Wing Planform Parametric Studies

The effects of wing planform changes were studied using the 751-103 configuration (fig. 5-1) planform as a reference. Takeoff thrust requirements were updated to incorporate the augmentor performance of working paper 271, NASA Ames, and to balance all-engine and engine-out field length requirements. Aspect ratio and sweep effects were included in lift and drag. Weights of the fuselage, wing, and surface controls were adjusted for differences due to wing planform.

The volume required to house augmentor ducting between the rear spar and the augmentor flaps imposes an upper limit on wing loading. Figure 5-24 shows that the 751-103 configuration planform is duct volume limited to an 81 lb/sq ft wing loading by the takeoff thrust requirements. Higher wing loadings are desired for improved airplane economics and better passenger ride quality.

The duct volume constraint on wing loading can be eased somewhat by wing planform changes to increase wing chord and thickness. The relationships between duct volume limits, thrust requirements, wing loading, and takeoff gross weight (TOGW) are shown in figures 5-23 through 5-31 for wing aspect ratios of 5, 5.5, and 6.5 and sweep angles of 20°, 25°, and 30°. All planforms studied had wing loadings limited by duct volume to less than the optimum wing loading for minimum TOGW.

Figure 5-32 summarizes the effect of sweep and aspect ratio on STOL and CTOL takeoff gross weights. The minimum STOL TOGW occurs at 5 aspect ratio and 30° sweep. The minimum CTOL TOGW occurs at 5.5 aspect ratio and 30° sweep.

The effect of wing planform on block fuel is shown in figure 5-33 for the STOL and CTOL missions. Planform changes caused variations of only -2.7% to +4.2% in STOL block fuel and -2.5% to +5.5% in CTOL block fuel.

Wing loading and thrust loading are plotted in figure 5-34 for the duct volume limits of the planforms studied. The highest wing and thrust loading are obtained with the 5 aspect ratio and 30° sweep planform.

Significant improvements in TOGW and wing loading can be made by wing planform changes. The lightest TOGW and the highest wing loading occur at 5 aspect ratio and 30° sweep. However, since a configuration with 5.5 aspect ratio and 30° sweep weighs only 0.75% more and has better growth capabilities and lower CTOL operating costs, it is recommended that 5.5 aspect ratio be considered a lower limit. A three-view and specification are shown in figure 5-35 for an airplane with 5.5 aspect ratio and 30° sweep. The STOL TOGW of this airplane is 11,500 lb lighter than the reference 6.5 aspect ratio, 25° sweep configruation and the CTOL weight is 8000 lb lighter. Wing loading is 94.3 lb/sq ft, whereas that of the reference airplane is 81.4 lb/sq ft.

5.3.2 Duct Geometry

The wing planforms discussed in section 5.3.1 above were examined through a systematic series of preliminary drawing layouts to establish available duct installation space relative to the baseline wing (aspect ratio 6.5, 25° sweep). As discussed in section 5.2.1, a supercritical type airfoil section (fig. 5-36) was adopted to provide maximum internal space without penalizing cruise speed. Wing thickness, t/c, was varied for the several planforms to maintain constant critical Mach numbers, and the inboard engine location was selected as typical for parametric studies. Major dimensions of the space available at the inboard engine bounded by upper and lower surfaces, the 50% chord plane and the 75% chord plane, are given in table 5-1 and shown graphically in figure 5-37 for the 2200-sq-ft reference wing area. The gross areas thus defined are plotted in figure 5-38. The expected trends are evident in these figures, and it is significant that increasing sweep angle for a given aspect ratio causes the space geometry to tend toward a square, which favors the installation of a plenum duct. Conversely, lower sweep angles provide a space with longer fore and aft dimension more appropriate to several small side-by-side ducts of an independent system.

Cross-section views of the independent and plenum systems shown in figure 5-39 indicate the space allowances for structure and clearances. By applying these space allowances at the inboard engine location (27% b/2) of the wing planforms, the duct areas shown in figure 5-40 are obtained. These curves represent the areas available for a plenum-type system similar to the baseline described in section 5.4.2. These and similar data generated for the independent duct system (also described in section 5.4.2) were used as a basis for duct pressure and available thrust studies presented in section 5.4.5.

The effect on available plenum system duct area of locating the rear wing spar at 50% and 55% is shown in figures 5-41, 5-42, and 5-43 for the planform range studied. For the plenum system the available duct area increases with sweep angle and decreases as the spar moves rearward. Area required for wing loadings of 80, 90, and 100 lb/sq ft are shown based on the system described in section 5.4.2 at NPR = 2.0 and $\Delta P/P_F$ of 15%. The revised baseline design point discussed in section 5.3.1 is identified in figure 5-43 (6.5 apsect ratio, 25° sweep), which shows a possible shift of the rear spar to 52% to 53% or, alternatively, an increase in wing loading approaching 90 lb/sq ft with a change to 30° sweep at 6.5 aspect ratio.

At aspect ratio 5.5, figure 5-42, a sweep angle of 30° would provide 95 lb/sq ft wing loading with the rear spar at 50% chord; at 80 lb/sq ft wing loading, the rear spar could be shifted to 54% chord. Similar trends are shown for aspect ratio 5.0. However, as discussed in section 5.3.1, the airplane weight advantage would not be significant for this aspect ratio.

A preliminary assessment indicates that the effect on wing weight of rear spar location in the 50% to 60% chord range is less significant than the effect of higher wing loading possible with the 50% location. An evaluation in greater depth of the effect of rear spar location on wing weight will be necessary to establish the optimum compromise.

Figures 5-44 and 5-45 show available and required areas for an independent duct system with 27% cross-body flow as in the scheme described in section 5.4.2 with 2.6 NPR. Wing sweep angles of 25° and 30° were examined at aspect ratios of 5.5 and 6.5. The inter-

TABLE 5-1.– WING PLANFORM AREA STUDY
(S = 2200 SQ FT SECTIONS AT b/2 = 27%)

Λ	AR	Depth, in. 50% chord	62.5% chord	75% chord	Chordal length, in. 50 - 75% chord	Area, sq in. 50 - 75% chord	Overall chord length, in.*
20°	5.0	36.2	31.5	23.9	75.7	2320	300
		37.4	31.5	23.6	78.2	2430	313
	5.5	34.8	30.3	23.3	72.0	2140	288
		35.6	30.3	22.0	75.0	2210	300
	6.5	31.6	27.8	21.8	65.3	1770	261
		32.7	27.8	23.3	68.8	1870	275
25°	5.0	39.7	34.3	26.5	72.7	2460	291
		40.3	34.3	25.2	78.2	2650	313
	5.5	38.1	33.0	25.5	69.5	2240	277
		38.9	33.0	25.3	75.0	2430	300
Baseline	6.5	34.5	30.1	23.2	63.6	1955	254
		35.6	30.1	22.1	68.8	2045	275
30°	5.0	42.6	37.3	28.6	70.0	2570	280
		44.0	37.3	27.5	78.2	2880	313
	5.5	41.2	36.0	27.6	66.9	2420	267
		42.2	36.0	26.6	75.0	2650	300
	6.5	37.6	33.0	25.0	60.8	1970	243
		38.8	33.0	24.1	68.6	2330	275
35°	5.0	46.0	40.5	31.2	66.1	2620	264
		47.8	40.5	29.8	78.2	3120	313
	5.5	44.1	39.0	30.3	63.5	2420	254
		46.1	39.0	28.6	75.0	2870	350
	6.5	40.7	36.0	27.2	58.1	2030	230
		42.2	36.0	26.4	68.8	2430	275

*Overall chord length perpendicular to 50% chord plane, streamwise

relation of the blowing nozzles from opposite engines dictates a side-by-side arrangement of the ducts similar to that shown in the section views on figures 5-44 and 5-45. Thus, the greater duct area is available at the lower sweep angle where the fore and aft dimension is longer. The effect of increasing the fore and aft dimension was examined by assuming the rear duct limit at 72.5% chord (2.5% shorter flap chord).

This shows a substantial increase in available duct area and indicates (fig. 5-44) that a solution would be possible at about 71% chord in the 6.5 aspect ratio, 25° sweep wing. The more favorable fore and aft dimension of the 5.5 aspect ratio wing would permit a solution with the rear duct at 70% chord for the assumed 80 lb/sq ft wing loading or alternatively would allow a higher wing loading with a more rearward duct limit.

As lift coefficient may be very sensitive to flap chord, further trades are necessary to assess thrust required and establish the net effects on installed system weight. The effects of duct system flow loss, augmentor nozzle pressure ratio, and comparison of installed thrust available for plenum and independent systems are discussed in section 5.4.5.

5.4 DUCT SYSTEM STUDIES

5.4.1 Duct System Concept Evolution

The air distribution system of the initial baseline reference configuration described in section 5.2.1 was derived through a series of exploratory point design layouts, which were directed toward providing full 50% cross-body flow with independent ducts. A nozzle pressure ratio of 2.0 was set as a goal to provide maximum potential for community noise control.

The appendix contains a series of drawings that are representative of the various configurations studied. They include a version with independent cross-body ducts in the wing leading edge, LO-AWNP-001 (which left insufficient space for stowing the leading edge device) and versions of concentric ducts at two pressure levels, LO-AWNP-003 and 004. The concentric ducts are considered undesirable primarily from the safety inspection standpoint.

Versions of interconnected (plenum) systems were examined including variable augmentor nozzle concepts to address the problem of rematching the nozzle to avoid overarea with an engine-out condition, LO-AWNP-005, 006, 007, and 011. If the nozzle area were not adjusted, the resulting thrust loss would be 8% to 15% of the remaining three-engine thrust.

The complexity of the variable augmentor nozzles led to consideration of the plenum concept with subducts that carry blowing nozzles to handle the equivalent airflow of one engine and that are valved off the line upon loss of power from one engine.

Drawings LO-AWNP-008 and 012 are representative of attempts to incorporate this concept. In LO-AWNP-008, the subduct was limited to the inboard flap only and caused excessive reduction in the local blowing coefficient when shut off. In both systems the ducts were integrated with each other and with their supporting structure. An independent bridgework structure shown in LO-AWNP-009 was used to support the flaps from the rear wing spar.

Further refinement of the duct structural concept to provide circular duct sections with independent support structure resulted in additional constraints on duct area. Subduct blowing was limited to the inboard and outboard flaps to retain sufficient cross-flow area between engines with subducts valved off. This concept, LO-AWNP-017, together with the diverter/check valve arrangement of LO-AWNP-019, was adopted for the baseline study reference as described in section 5.2.1. The design nozzle pressure ratio of that system is 2.0

Continuing effort to establish an independent duct system concept by varying the augmentor nozzle pressure ratio as well as the amount of cross-body flow is described in section 5.4.2. Drawing LO-AWNP-026 is representative of the general arrangement of such a system,

having a nozzle pressure ratio of 2.2 and 27% cross-body airflow. However, additional space allowance is needed for duct support structure. The probable results of such space allowance are discussed in sections 5.3.2 and 5.4.5.

5.4.2 Alternate Duct Systems

Preliminary evaluations were made of alternate duct system configurations that would collect the engine fan air and deliver it to the appropriate blowing nozzles. The alternate configurations included completely separate engine and duct systems and plenum systems wherein the fan air from all four engines was supplied in parallel to a single duct system. The baseline airplane selected for the evaluation was the model 751-103 powered by P&WA STF-369C turbofan engines (sec. 5.5.2).

5.4.2.1 Completely Separate Engine and Duct Systems

The completely separate engine and duct system configurations provide separate independent fixed fan air nozzles for each engine. The primary advantage is that the problems associated with engine interactions caused by an inoperative engine and different engine dynamic response characteristics are eliminated. The primary disadvantages are the duct system complexity resulting from limited spacing for duct runs and potential asymmetric rolling moments resulting from an inoperative engine.

Three configurations were studied. These included semispan with no cross-body flow, 27.5% cross-body flow, and 50% cross-body flow. Pertinent features of each configuration are as follows:

Semi-span with no cross-body flow.—Each engine provides its fan air to an independent separate nozzle that spans the associated wing (e.g. left engine(s)--left wing). No airflow is ducted across the fuselage to the other wing. The configuration results in an engine-out rolling moment coefficient equivalent to an externally blown flap airplane (fig. 5-46). This is not considered acceptable for the augmentor wing STOL airplane studied. A typical system configuration is shown in figure 5-47.

Twenty-seven and one-half percent cross-body flow.—The duct and nozzle systems are configured such that 27.5% of the total augmentor nozzle flow on each wing is provided from the engines on the opposite wing. In addition, the duct system is arranged to partially alleviate the rolling moment resulting from an inoperative engine. A typical configuration is shown on figure 5-48. (A plenum system to provide balanced leading edge and aileron blowing with a 20% of the total fan flow is included in the figure. This shows how the leading edge blowing and balanced aileron blowing might be incorporated.) Preliminary study results show that the engine-out roll moment requirement is within the capability of the airplane, and therefore additional lateral control system capability and associated weight would not be required with this duct system configuration.

Fifty percent cross-body flow.—The duct and nozzle systems are configured such that 50% of each engine's augmentor nozzle flow is supplied across the body to the opposite wing. In addition, the ducting is arranged to alleviate the rolling moment resulting from an inoperative engine (fig. 5-46). A typical configuration is shown in figure 5-49.

The 50% cross-body flow system could eliminate all lateral control requirements resulting from lift asymmetry with an inoperative engine. However, the augmentor nozzle pressure ratio required is excessive. The reference airplane would require a nozzle pressure ratio of approximately 3.3 to achieve the required thrust within the available baseline wing ducting envelope. The resulting noise level would exceed the 95-dB objective selected for the study. Therefore, this configuration is considered unacceptable unless means are found to reduce the noise level to acceptable limits.

5.4.2.2 Plenum (Interconnected) Duct Systems

The plenum systems are duct configurations wherein the engine fan air from all of the engines is supplied to a common duct and nozzle system. The plenum systems were evaluated with fixed-area nozzles, variable-area nozzles, and subduct nozzle area control. The fixed-area nozzle was eliminated because of incompatibility with the engines with one or more engines inoperative. The incompatibility is caused by fan nozzle overarea, which results in an excessive thrust loss and potential engine mismatch. The variable-area nozzle configurations were in general not acceptable. They did provide the capability to rematch the engine fan nozzle area, but the weight and mechanical complexity required to provide variable nozzle area were judged to be excessive.

A typical variable nozzle design was discussed in section 5.4.1. The subduct nozzle system provides for engine fan nozzle rematch during engine-out operation by shutting off sections of duct with 25% of the total nozzle area. A typical configuration is shown in figure 5-50. The rolling moment is essentially balanced for both normal and engine-out operation (fig. 5-46). Because of the relatively simple means used to control nozzle area, and the ability to retain a high level of performance with an inoperative engine, this configuration was selected for the baseline airplane.

Blowing system performance, $C\mu$, is shown in figure 5-51. Nozzle area distribution and augmentor duct sizes for the airplane are included in figure 5-50.

5.4.2.3 Potential Augmentor Airflow and Engine Surge Control Problems

Engine-interconnected duct system concepts have significant unresolved control problems which increase the technical risk of the augmentor wing airplane. The following control problems were identified during task I with engine-interconnected systems:

1) Prevention of engine surge during dynamic or steady-state conditions resulting from a drop in engine rpm of one engine relative to the other three.

2) Inadvertent closure of one or more subduct valves (nozzle underarea), which drives all engines toward surge.

3) Detection of an engine failure to signal all subduct valves closed to preclude nozzle overarea and excessive thrust loss.

4) Control logic for diverter valve operation considering flap position, engine power, actuation time, and "flow area" variation during valve movement.

With the exception of diverter valve control, the independent duct system concepts are exempt from these control problems, and consequently provide less technical risk for a STOL airplane.

The identified control problems will be further evaluated during tasks II and III of the augmentor wing contract.

5.4.3 Engine Spacing

The effect of engine spanwise location on the wing was examined to establish the optimum locations from the standpoint of duct area requirements in the critical flow areas adjacent to the main delivery pipe junction. A plenum system with full-span subducts and constant spanwise blowing coefficient was assumed to permit a parametric approach. A comparison of the assumed blowing distribution with the baseline system in terms of the ratio of blowing nozzle height to chord length is given in figure 5-52.

The results of the study are given in figure 5-53, which shows that the inboard engine location may range from 48% to 55% b/2 while the inboard engine could be located as far outboard as 30% b/2 with equivalent duct constraint (equal flow Mach number at the critical duct cross-section). A cursory review of wing flutter constraints indicates that these ranges of engine locations would permit an acceptable solution.

5.4.4 Engine-Out Rolling Moment

The criterion that the airplane must reach a bank angle of 6° within one second of application of full lateral control requires that the lateral control system have a capability of $C_L = 0.13$. A 30-kn crosswind landing will require $C_L = 0.09$. The recommended limit engine-out rolling moment of 0.04 shown in figure 5-54 on engine-out 30-kn crosswind landing would require $C_L = 0.13$.

The roll moments due to engine-out are also plotted in figure 5-54 for various amounts of crossover flow between right and left wing ducts. These roll moments were calculated using a C_L vs C_J relationship on a sectional basis with no lift carryover assumptions. A crossover of at least 25% is needed to avoid the necessity to oversize the lateral control system to handle engine-out rolling moments.

5.4.5 System Pressure and Pressure Loss Studies

The baseline system pressure loss has been established as approximately 15% of total fan discharge pressure. This includes the losses from the fan face to the augmentor nozzles. The equivalent fan thrust loss is 9%, excluding the nozzle velocity loss coefficient. Most of the pressure loss occurs in the fan air collector duct and the wing ducts. The diverter valve, which accounts for 1/4 of the loss is required to shift from the augmentor nozzles to the engine fan nozzles. The loss summary is shown in figure 5-55. The effects of varying different parameters are described in the following paragraphs.

5.4.5.1 Duct Pressure Level

Higher pressure levels in the duct system result in lower thrust losses for the same percentage duct pressure loss. This is shown in figure 5-56, where a comparison of losses is presented for the STF-369C and higher pressure ratio STF-395 engines. The STF-395 is less sensitive to duct system pressure losses.

5.4.5.2 Duct Pressure Losses, $\Delta P/P_F$, at Constant Installed Thrust

If engine-installed thrust and the duct loss velocity head factor, K_F, are held constant, an increase in duct losses would result in smaller ducts and lower duct weight because both the airflow and duct internal flow velocity would increase. However, the engine bare weight and installed pod weight would increase because a larger uninstalled engine would be required. These characteristics are shown in figure 5-57 for the STF-369C. If the sum of the engine pod and augmentor duct weights is compared against the duct pressure losses, the minimum augmentor system weight is obtained when $\Delta P/P_F$ is approximately 6% (fig. 5-58). However, insufficient duct volume exists within the baseline wing planform to take advantage of this characteristic. The significant parameters for the above comparison are presented in table 5-2. In addition, the effects of $\Delta P/P_F$ on bare engine thrust-to-weight ratio are shown in figures 5-59 and 5-60 for the STF-369C and STF-395, respectively. The higher pressure ratio STF-395 engine is less sensitive to duct $\Delta P/P_F$ than the STF-369C but is approximately 30% heavier for the same thrust.

5.4.5.3 Wing Planform Effects

Increasing wing sweep angle and decreasing wing aspect ratio provides more wing volume and consequently more duct flow area for a constant wing area. This characteristic, based on design layout studies, is shown in figures 5-61 for a plenum system and figure 5-62 for an independent duct system. These data indicate that a 5.5 aspect ratio and 30° sweep, provide maximum duct flow area A_D/S, and maximum wing nozzle area, A^*/S, for a plenum duct system. Maximum duct and nozzle area for an independent system results with a 5.5 aspect ratio and 25° sweep.

The effect of wing planform changes on installed thrust per square foot of wing area $(T/S)_{in}$ is shown in figure 5-63 for the subduct plenum system. Installed $(T/S)_{in}$ vs $\Delta P/P_F$ for varying aspect ratio and constant sweep (25°) is shown in figure 5-64 for the STF-369C and 5-65 for the STF-395 engines. It can be concluded from these data that a maximum $(T/S)_{in}$ can be attained for a particular wing planform by increasing augmentor nozzle area, A^*/S. The augmentor duct pressure loss, $\Delta P/P_F$, increases with increasing A^*/S due to higher duct Mach number.

5.4.5.4 Augmentor Wing Blowing System and Airplane Aerodynamic Relationships

To establish the relationships between the augmentor wing airplane aerodynamics and blowing system dynamics, the lines of constant $(T/S)_{unin}$ corresponding to a unique $\Delta P/P_F$ are plotted on the airplane thumbprint for 6.5 aspect ratio and 25° sweep (fig. 5-66).

TABLE 5-2.—AUGMENTOR WING AIRFLOW SYSTEM VARIABLES

SLS, Standard Day, Constant Installed Thrust

	Pressure loss $\Delta P/P_F$, %	F_p, lb	F_{sec}, lb	W_E, lb	W_{NS}, lb	W_{pod}, lb	NPR	W_{sec}, lb/sec	M	(A_D/A_{D_R})	W_A, lb	W_T, lb
Four STF 369C engines	6.5	11,440	51,080	11,600	6,290	17,850	2.2	315	.190	1.43	5,650	23,500
	15.1	11,920	50,600	12,120	6,560	18,700	2.0	329	.30	1.0	5,150	23,850
	18.5	12,200	50,320	12,360	6,700	19,050	1.92	336	.335	.935	5,050	24,100
	25.5	12,920	49,600	13,120	7,100	20,300	1.75	356	.391	.840	4,940	25,240
	31.	13,600	48,920	13,800	7,460	21,300	1.62	375	.441	.826	4,900	26,200
Four STF 395 engines	6.5	17,360	46,720	13,880	6,300	20,180	2.74	251	.190	.91	5,020	25,200
	15.*	18,080	45,600	14,440	6,560	21,000	2.42	262*	.30	.64	4,640	25,640
	18.4	18,160	45,920	14,520	6,561	21,031	2.39	263	.335	.59	4,540	25,621
	31.	18,720	45,360	14,950	6,760	21,710	2.03	271	.441	.48	4,330	26,040

Symbol definition:

$\Delta P/P_F$ — Duct pressure loss relative to fan exit total pressure

F_P — Engine primary thrust

F_{sec} — Engine secondary thrust

W_E — Enigne bare weight

W_{NS} — Nacelle and strut weight

W_{pod} — Engine bare weight plus nacelle and strut

NPR — Nozzle pressure ratio

W_{sec} — Engine secondary airflow

M — Duct Mach number at engine fan exit station

(A_D/A_{D_R}) — Duct area ratio relative to baseline system duct area

W_A — Duct system weight

W_T — Total weight, engine pods and duct system

The gross weights shown on the thumbprint were computed on the basis of constant engine thrust-to-weight ratio where $\Delta P/P_F = 15\%$. Therefore, the airplane gross weight must be adjusted to compensate for increments of engine weight when the duct system losses are not equal to 15%. The method used to adjust airplane gross weight is shown in table 5-3. Adjusted airplane gross weights versus installed thrust-to-weight ratio $(T/W)_{in}$ and installed thrust per square foot of wing area $(T/S)_{in}$ for a constant 2000-ft takeoff field length are given in figure 5-67 for the STF-369C and 5-68 for the STF-395 engine.

The effect of nozzle pressure ratio (NPR) on wing loading capability with a plenum duct system is shown in figure 5-69 for a wing planform of 6.5 aspect ratio, 25° sweep and in figure 5-70 for 5.5 aspect ratio, 30° sweep. It is noted that the lower aspect ratio and higher sweep (30°) result in higher wing loading at constant NPR. (NPR lines and equivalent ride quality line is shown in fig. 5-71 as a function of aspect ratio with constant sweep (25°)). The effect of NPR on wing loading capability with an independent duct system (27% crossover) is shown in figure 5-72 with 5.5 aspect ratio, 25° sweep. Engine NPR data were obtained from engine cycle studies conducted for 1978 technology. Installed thrust $(T/S)_{in}$ vs wing nozzle area, A*/S, is shown in figure 5-73 for NPR = 2.2, 2.4, 2.9.

The following conclusions for a wing aspect ratio of 6.5 and sweep of 25° were drawn from this section.

1) An augmentor wing airplane with characteristics shown in figure 5-66 with STF-369C engines could be designed with a wing loading factor from approximately 62.2 lb/sq ft to approximately 89.3 lb/sq ft. The higher wing loading results in lower gross weight. The minimum weight airplane would result from a total augmentor duct system pressure loss of approximately 25% for the STF-369C engine and 15% for the STF-395.

2) The STF-395 engine cycle provides much higher wing loading capability. However, airplane gross weight may not be lighter since the thumbprint gross weight lines in figure 5-66 are based on the airplane structural weight associated with the higher thrust-to-weight ratio of the lighter weight STF-369C engine. The method used to adjust gross weight shown in table 5-3 provides a general approximation for both duct losses and engine weight. To further refine the engine/airplane match, it would be necessary to recalculate the thumbprint for each duct system loss variation and each engine cycle.

5.5 ENGINE CYCLE STUDIES

5.5.1 Introduction and Scope

Engine studies have been concerned with two main topics. The first has been the study and application of augmentor flap engines designed by Pratt & Whitney and Rolls-Royce. The second has been a parametric engine study in which thermodynamic engine cycles with the same primary jet noise base were established. Approximate weight and size for these cycle engines were also calculated. Additional side studies have included cycle definition of a turbostream engine with 60% blowing thrust and an investigation of thrust loss reduction, under plenum system engine-out conditions, by use of a splitter through the fan concept.

TABLE 5-3.– AIRPLANE GROSS WEIGHT ADJUSTMENT FOR ENGINE WEIGHT INCREMENTS

	$(T/W)_{unin}$	$(T/W)_{in}$	W/S, lb/sq ft	$(T/S)_{in}$, lb/sq ft	T, lb	GW, lb	$\Delta P/P_F$, %	T/W_E	ΔGW, lb	GW', lb
STF 395 engines	.407	.352	82.0	28.9	73,630	209,170	6	4.58	4,470	213,640
	.443	.383	96.5	37.0	76,450	199,600	10	4.52	5,190	204,790
	.471	.407	107.2	43.6	80,110	196,830	15	4.46	5,980	202,810
	.486	.420	113.0	47.5	82,240	195,800	20	4.34	7,500	203,300
	.495	.428	116.0	49.6	83,670	195,500	25	4.22	8,970	204,470
STF 369C engines	.361	.312	62.2	19.4	75,000	240,000	6.2	5.40	-1,750	239,250
	.387	.335	73 5	24.6	74,040	221,000	10.5	5.28	-860	220,140
	.405	.350	81.0	28.4	73,500	210,000	15	5.15	0	210,000
	.418	.362	86.5	31.3	74,280	205,200	21.7	4.94	1,550	206,750
	.422	.365	88.2	32.2	74,510	204,150	25	4.81	2,530	206,680

Symbol definitions:

$(T/W)_{unin}$ – Uninstalled thrust/weight ratio

$(T/W)_{in}$ – Installed thrust/weight ratio

W/S – Wing loading

$(T/S)_{in}$ – Installed thrust/sq ft (2,000-ft takeoff field requirement)

T – Installed thrust required

$\Delta P/P_F$ – Augmentor duct pressure loss ($\Delta P/P_F \Rightarrow (T/S)_{in}$

(T/W_E) – Engine installed thrust/weight ratio ($\Delta P/P_F \Rightarrow (T/W_E)$

ΔGW – Corrected gross weight based on engine installed (T/W_E) relative to thumbprint thrust installation factor

ΔGW = 2.5 (Δ engine weight)

$$\Delta GW = 2.50\ T/(T/W_E)_R \left[\frac{(T/W_E)_R}{(T/W_E)} - 1\right],\ (T/W_E)_R = 5.14N \text{ (STF 369C at } \Delta P/P = 15\%)$$

GW' – Airplane corrected gross weight

5.5.2 System Design Study Engines

5.5.2.1 STF-369 and STF-395 Engines

The STF-369 and STF-395 are the two principal engines designed by Pratt & Whitney for application to an augmentor wing airplane, with all the fan or secondary air going to the wing. Both engines are dual rotor, unaugmented axial flow turbofans incorporating a scalable advanced engine high spool. The engines provide approximately 20,000 lb of takeoff thrust, flat rated to 90° F at sea level, and have a maximum flight Mach number capability of 1.0.

Both engines were designed to achieve low primary jet and forward arc fan inlet noise levels. The noise target was 95 PNdB, for four engines at a 500-ft sideline at 100 kn. Our estimates for the noise of these engines indicate that the target was not achieved.

The basic cycle parameters for these two engines are, for sea level static, standard day conditions:

STF-369: Fan pressure ratio = 2.45
Bypass ratio = 2.5
Overall pressure ratio = 19.6

STF-395: Fan pressure ratio = 3.0
Bypass ratio = 1.82
Overall pressure ratio = 24.0

The noise estimates (1971-72 technology) with four engines, 500-ft sideline, 100 kn, standard day are:

STF-369 Inlet noise = 116.5 PNdB (basic)
= 96.5 PNdB (choked)
Primary jet = 96.5 PNdB
Augmentor jet flap = 109 PNdB (basic slot)
= 94 PNdB (suppressed)

STF-395: Inlet noise = 113 PNdB basic)
= 93 PNdB (choked)
Primary jet = 99.0 PNdB
Augmentor jet flap = 114 PNdB (basic slot)
= 97 PNdB (suppressed)

Their physical characteristics are:

STF-369: Length = 91.6 in.
Diameter = 55.5 in.
Weight = 3065 lb

STF-395: Length = 102.5 in.
Diameter = 54.5 in.
Weight = 4080 lb

The STF-369 employs a two-stage fan and the STF-395 a four-stage fan.

A full airplane configuration has not been done using the STF-395 engines. The STF-369 and its derivatives have been the only two-stream engines matched to an augmentor wing airplane.

The baseline engine, designated the STF-369C, is a derivative of the original P&W STF-369 with adjustments made by Boeing to meet the noise requirements. This amounted to increasing the bypass ratio to 2.6 to lower the primary jet noise to 94-95 PNdB, and adding an inlet guide vane (IGV) in front of the fan with the supposition that this device would reduce the forward arc fan inlet noise to the desired level. Reference should be made to section 5.2.1 and figure 5-9 for baseline airplane noise estimates. The weight allowance for the IGV amounted to 8% of the bare engine weight and the increment on length was estimated to be 12 in.

Some of the principal performance characteristics of the STF-369C and STF-395 are given in table 5-4. Installed performance figures were generated by Boeing using computer-aided cycle simulation techniques. Basic P&W performance estimates may be found in references 5-5 and 5-6.

TABLE 5-4.—PERFORMANCE CHARACTERISTICS

Parameter	STF-369C	STF-395
Uninstalled SLS thrust	20,000 lb	20,000 lb
Maximum cruise SFC, installed (30,000 ft, 0.8 Mach, 100% primary nozzle area)	0.867	0.869
Uninstalled thrust/weight (SLS)	5.93	4.99
Uninstalled thrust/total airflow (SLS)	37.9	42.4
Installed secondary/total thrust (SLS)	0.79	0.716
Installed maximum cruise/SLS takeoff uninstalled thrust	[a]0.228	0.232
% Installed loss, SLS thrust	14%	11.5%

[a]Actual ratio required for baseline airplane (3% higher than P&W's original maximum cruise rating); new airplane/engine requirements will likely decrease this value, see section 5.3.1.

Further performance data are shown in figures 5-74 through 5-77.

5.5.2.2 RB-419 Type Engines

The Rolls-Royce RB-419 family of engines uses what is known as the three-stream concept, this term originating from the fact that, in addition to the conventional primary and secondary exhaust streams, a large quantity of continuous air bleed is taken from the exit of the IP compressor to be used as blowing air for lift augmentation devices.

Rolls-Royce Ltd. has supplied Boeing with performance data for one particular engine, the RB419-01, reference 5-7, and for a parametric family of engines, reference 5-8. Since the RB419-01 delivers a quantity of blowing air that is consistent with the requirements of the augmentor flap airplane, the characteristics of this particular three-stream model will be described. Reference should be made to section 5.6 to see how this engine is matched with an augmentor system and an augmentor flap airplane.

The RB419-01 is a two-spool geared fan that develops a minimum uninstalled takeoff thrust of 19,190 lb at sea level static conditions and is flat rated to 86°F. A blowing air mass flow of 159 lb/sec is extracted from the IP compressor exit at a pressure ratio of 3.0 and, at this exit plane (i.e., not accounting for duct losses), is equivalent to 7470 lb of thrust, which is 39% of the total thrust. The bleed air is diverted to a rearward-facing propelling nozzle during cruise and can be diverted to a forward-facing nozzle to facilitate thrust reversal after touchdown. A reduction gearbox is incorporated between the intermediate compressor and the single-stage LP fan. This permits the operation of the fan at a low tip speed optimized for minimum noise generation. The fan is of a variable pitch design which, in combination with an automatic adjustment to the engine control system, allows thrust modulation on approach over a very wide range while maintaining constant bleed airflow and pressure. The fan may also be used to supply reverse thrust down to 0 kn. The IP compressor is comprised of four stages and, along with the coupled fan, is driven by a two-stage low-pressure turbine. The eight-stage high-pressure compressor is driven by a single-stage high-pressure turbine. The combustion chamber is of annular construction.

The engine thermodynamic cycle is arranged such that the gas generator exhaust velocity is low (900 ft/sec). Boeing calculations estimate this to give 96 PNdB for four engines at 500-ft sideline (see sec. 5.6.4). Further details on the RB419-01, scaled to a sea level static uninstalled thrust size of 20,000 lb for comparison with the STF-369 and STF-395, are listed below. Items marked with an asterisk entail Rolls-Royce estimates for losses due to air bleed from HP compressor, power from HP shaft, IP bleed duct pressure loss, and acoustic treatment in air intake and fan delivery duct.

Bare engine weight = 4290 lb
Uninstalled thrust/weight = 4.66
Uninstalled thrust/total airflow = 26.3
Uninstalled maximum cruise SFC = 0.73 lb/hr/lb (30,000 ft, Mach 0.8)
Uninstalled maximum cruise thrust = 4770 lb
*Installed maximum cruise SFC = 0.778 lb/hr/lb
*Installed maximum cruise thrust = 4290 lb
Installed maximum cruise/SLS takeoff uninstalled thrust = 0.214
*% installation loss, SLS takeoff thrust = 6.7%

Comparing the three-stream concept, represented by the RB419-01, with that of the two-stream concept represented by the STF-369 and STF-365, the following is observed. The thrust/weight and thrust/total airflow ratios are better for the two-stream engines. The three-stream engine has a lower maximum cruise SFC than the two-stream engines—even when the two-stream engine employs a variable primary nozzle area (estimate for the STF-369C is 0.818 lb/hr/lb at 65% area). The two-stream thrust lapse rate is less than that of the three-stream engine, although not significantly so. The sea level static thrust installation loss is considerably less for the three-stream engine, principally due to the smaller quantity of blowing air subjected to duct pressure losses.

The parametric family of three-stream engines produced by Rolls-Royce, with varying quantity of blowing thrust, will not be discussed in detail. Pertinent curves of performance data for the whole family are included, however, in figures 5-78 through 5-81. Due to the parametric nature of the study, the cycle parameters at 39% blowing thrust do not compare exactly with those of the specific RB419-01 engine design.

5.5.2.3 60% Thrust Split with Two-Stream Engine

A study was performed to ascertain whether it is possible to reduce the secondary/total thrust split from the presently typical 80% to about 60% and still obtain an engine that is both practical and quiet.

Use was made of a P&W parametric augmentor wing engine study, reference 5-9, and of their performance, noise, and weight results for a series of engines with the same fan pressure ratio, 2.45, but varying bypass ratio and turbine inlet temperature. The STF-369 engine was one of these engines and, in fact, it was from this particular parametric study that P&W selected the STF-369 cycle as the best suited for augmentor wing application.

A plot of primary jet noise versus bypass ratio for varying design turbine inlet temperatures is shown in figure 5-82. Lines of constant thrust split and relative weight are also shown plotted in the figure. It is seen that the lowest turbine inlet temperature considered by P&W, 1800° F, was too high to give a 60% thrust split and achieve a low enough primary jet noise as well. Additional cycles were therefore examined at lower turbine inlet temperatures. These are shown as cycles 1, 2, and 3 in figure 5-82. The noise and performance estimates for these cycles and the STF 369 are listed in table 5-5.

From P&W's weight trends, engines 1, 2, and 3 would probably be in the relative weight range of 1.5 to 1.7 times the weight of the STF-369.

The large increase in bare engine weight and the large increase in cruise SFC, associated with achieving a thrust split of 60% in conjunction with acceptable primary jet noise, would cause a very large increase to the airplane TOGW. This would certainly outweigh any advantage gained by the reduced wing weight occasioned by the reduced wing airflow.

TABLE 5-5.—COMPARISON OF VARIOUS THRUST SPLIT CYCLES

Engine	Standard day T_4, °F	BPR	Thrust split, %	Primary jet noise, PNdB ±2	Cruise SFC, lb/hr/lb
1	1190	0.82	61.7	91.0	—
2	1300	1.05	65.4	94.0	—
3	1250	0.9	60.5	95.0	0.926
STF-369	2220	2.5	77.0	95.5 P&W)	0.81

5.5.3 Splitter Through Fan Concept

A study was undertaken to see whether by extending the engine splitter forward through the fan stages, a reduction could be made in the thrust loss suffered during an engine-out condition for engines operating on an augmentor wing common plenum system. A summary of the study and further developments since the study will be given here.

With the aid of a thermodynamic computer program, performance data were obtained for the STF-369C cycle for different values of secondary nozzle overarea up to 35%—the one engine-out case would correspond to a nozzle overarea of 33.3%. Parallel sets of data were obtained for a splitter behind the fan and for one running through the fan. The aft splitter gave a thrust loss of 26.2% due to nozzle overarea for the engine-out case, whereas the splitter through the fan reduced this to 4.25%. Thrust and thrust loss variation with nozzle overarea are shown in figure 5-83. Fan speed variation is shown in figure 5-84 and bypass ratio variation in figure 5-85. The splitter through the fan effectively keeps the primary airflow disassociated from changes in the secondary stream, and this is reflected by the almost constant bypass ratio and fan speed increase.

P&W's estimate of the thrust loss due to secondary nozzle area mismatch of 33.3% was 15%. After the study, P&W were requested to consider this concept and either verify the results or prepare some other way of dealing with the thrust loss using innovative engine design methods.

Although no formal report of their results has been received from P&W, they have indicated that the concept is valid. However, they state that the mechanical complexity of the design does not warrant further detailed analysis in the light of new evidence about aft splitter designs. P&W have stated, on the basis of a review of test data obtained from TF30 and JTF20 engines, that the fan root pressure drop due to an increased fan nozzle area is not so large as was originally thought. Consequently, P&W now estimate the thrust loss to be only 7.5% or half of their original estimate and conclude that it is not worthwhile to employ a splitter through the fan to try to eliminate this thrust loss.

P&W have been requested to study the weight penalty and other effects associated with having an emergency rating (increase in T_4) to cope with supplying 7.5% more thrust per engine when one engine goes off the plenum.

5.5.4 Parametric Engine Cycle Study

5.5.4.1 Introduction

The object of the parametric engine study was to produce a family of engines that could be used as a basis for augmentor wing propulsion system and airplane configuration trade studies. The whole family uses the device of passing all the secondary fan air of a dual-spool, turbofan engine to the augmentor wing. The engines are conventionally configured with two-shaft turbomachinery consisting of a fan, high-pressure compressor, and high- and low-pressure turbines.

The variables studied were fan pressure ratio, overall pressure ratio, and turbine inlet temperature. Of principal interest is the fan pressure ratio because it has a direct effect on the augmentor nozzle and wing duct system design.

Performance, noise, weight, and size data were generated for nine engine cycles, all of which satisfy the basic ground rule of a 90 PNdB primary jet noise level with four engines at a 500-ft sideline. Four cycles examine the effect of varying the fan pressure ratio in the range from 2.2 to 3.6; three are used to investigate an overall pressure ratio range from 18 to 30, and the remaining two examine turbine inlet temperatures ±200°F about the expected 1978 technology value.

5.5.4.2 Method of Analysis

Performance data.—To put all the engines on the same primary jet noise base, it was necessary to use one cycle parameter for varying the amount of energy extracted from the primary stream. The bypass ratio was used for this purpose. The bypass ratio that met the primary jet noise requirement was established for each engine by first running three cases with bypass ratios that gave three noise values about the target value. By interpolation, the exact bypass ratio required was found and the performance data for the fully defined cycle was then generated. The nine engine cycles that meet the 90 PNdB primary jet noise criterion are defined in table 5-6.

Initially it was not known whether to make the fan of engine 1 three or four stage and that of engine 3 two or three stage. A side study was therefore performed to examine the alternatives before making a selection. This side study is reported in section 5.5.4.3.

The performance data for the above nine engine cycles were generated using computer program GSA, reference 5-10. In addition to the design point performance, off-design data were generated which included installed sea level performance at takeoff power setting and speeds to 150 kn, sea level installed part power performance at 80 kn, and installed and uninstalled cruise performance at 30,000 ft, Mach 0.8.

The terms "installed" and "uninstalled" are used on the basis of the following assumptions.

Uninstalled:

Ram recovery = 100%
No external bleed or power extraction
Fan duct total pressure loss ratio, $\Delta P/P_F = 0.02$
Primary nozzle $C_V = 0.99$
Secondary nozzle $C_V = 0.987$

Installed:

Ram recovery = 97% sea level, sonic inlet engaged
= 99% cruise, sonic inlet retracted
External bleed = 0.93 lb/sec sea level
= 0.72 lb/sec cruise

(The customer bleed port was established on the high-pressure compressor at a pressure ratio of approximately 3.5 at sea level static takeoff thrust).

Power extraction = 225 HP sea level
= 50 HP cruise

Fan duct pressure loss ratio, $\Delta P/P_F = 0.15$ sea level
= 0.05 cruise

Primary nozzle $C_V = 0.99$

Secondary nozzle C_V = 0.965 sea level, augmentor nozzle
= 0.987 cruise nozzle

TABLE 5-6.—DEFINITION OF BASIC CYCLE CHARACTERISTICS

Engine cycle number	FPR[a]	OPR[b]	Bypass ratio	Design T_4, °F[c]	Maximum T_4, °F[d]
1	3.6	22.0	1.85	2395	2550
2	3.0	↑	2.32	↑	↑
3	2.75	↓	2.60		
4	2.2	22.0	3.4		
5	2.75	18.0	2.71		
6	↑	26.0	2.44	↓	↓
7		30.0	2.25	2395	2550
8	↓	22.0	2.29	2205	2350
9	2.75	22.0	2.82	2585	2750

[a]FPR = fan pressure ratio

[b]OPR = overall pressure ratio

[c]Design T_4 = standard day turbine inlet temperature

[d]Maximum T_4 = hot day, 90° F, turbine inlet temperature

The engine component technology used in the analysis was consistent with that expected for a 1978 engine introduction.

Engine weight data.—The weight of each engine was estimated using computerized, correlated engine data. The estimation uses the technique of predicting the weight of individual engine components as a function of the corrected inlet airflow to the component. The component weight-airflow functions were derived by statistical correlation of engine manufacturers' data for 22 turbofan and turbojet engines.

The weights calculated by this technique are for a 1975 level of technology. To adjust to that for 1978, an expected weight decrease of 5% was assumed for this 3-year period.

Engine size data.—An engine-sizing computer program was used to calculate the major dimensions of the parametric engines. This program has been in use for about 1 year at Boeing and the majority of its assumptions are considered valid for this study. The major assumptions used are as follows:

Fan:

a) Specific corrected weight flow at design point = 41.0 lb/sec/sq ft,

b) Design point hub loading parameter for first rotor stage, $(2g\,J\Delta h)/u^2_{hub}) = 3.2$
where: Δh is the stage enthalpy rise, u_{hub} is the wheel velocity at the wheel hub, and J is the mechanical equivalent of heat

c) Rotor aspect ratio = 2.5, stator aspect ratio = 3.5

d) Mean line stagger angle (angle between chord and axial direction) for rotor = 45°; for stator = 15°

High-pressure compressor:

Performance and geometry scaled from an advanced engine HPC design

Burner:

Length of burner scaled from an advanced engine burner design

High-pressure turbine:

a) HPT loading parameter, $(u^2_{mean})/2gJ\Delta h) = 0.3$
where: u_{mean} is the wheel velocity at the wheel mean radius.

b) Length scaled by square root of corrected weight flow. An advanced engine single-stage HPT length and the JT9D two-stage HPT length were used as reference turbines.

Low-pressure turbine:

a) Inlet and outlet axial Mach number = 0.4

b) Mean radius same as HPT mean radius

c) Length/mean radius same as JT9D for four stages, linear ratio for more stages

d) Nominal loading parameter per stage = 0.25

Rear frame:

Length assumed to be 6 in. for all engines. Engines sized for sea level static, standard day, uninstalled takeoff condition.

Noise data prediction and extrapolation.—Noise for these engines was predicted using method 1 (ideal jet velocity) of SAE AIR 876 (ref. 5-11). The predicted spectrum derived from this method is the peak spectrum at a distance of 200 ft off axis. The values of air absorption used to extrapolate the predicted spectrum were derived from SAE ARP 866 (ref. 5-12), and the calculations of perceived noise levels (PNdB) were based on SAE ARP 865 (refs. 5-13 and 5-14). This procedure was computerized as reported in reference 5-15.

5.5.4.3 Results

Performance.—The performance data are presented mainly in the form of figures that show the variation of certain cycle characteristics with fan pressure ratio, overall pressure ratio, and turbine inlet temperature.

The side study to determine the number of fan stages for engine cycles 1 and 3 indicated that, using minimum airplane TOGW as the criterion, three-stage fans should be used for both engine cycle 1 (FPR = 3.6) and engine cycle 3 (FPR = 2.75). The factors that controlled this decision were bare engine weight and cruise SFC, which in turn were functions of fan efficiency. A more detailed analysis of fan design, taking into account such things as forward-arc fan noise, maintainability, production costs, and dynamics might indicate a different decision. Some performance figures show the results for the alternate fan designs.

Engine 2 (FPR = 3.0) has three fan stages and engine 4 (FPR = 2.2) has two fan stages.

The effects of varying the fan pressure ratio, overall pressure ratio, and turbine inlet temperature on the designated cycle characteristics are shown in the following figures:

Characteristic	Figure
Bypass ratio	5-86, 5-87, and 5-88
$\frac{\text{Uninstalled thrust}}{\text{Total airflow}}$	5-89 and 5-90
Secondary airflow	5-91 and 5-92
Installed cruise performance	5-93 through 5-97
$\frac{\text{Uninstalled cruise thrust}}{\text{Uninstalled SLS takeoff thrust}}$	5-98 and 5-99
Installation effects on SLS takeoff thrust, cruise thrust, cruise SFC	5-100, 5-101, and 5-102

The effects of employing a variable primary nozzle at cruise were investigated. This entailed shutting down the primary nozzle until the minimum SFC was obtained. The results of this study are shown in figure 5-103. The study was done for only one of the parametric engines, engine 3 (FPR = 2.75). As the figure shows, for the baseline engine installed thrust requirement the cruise SFC can be reduced from 0.86 to 0.793 lb/hr/lb by reducing the primary nozzle area from 100% to 50%. This is a saving of 7.8%.

Noise.—As an indication of how the engine bypass ratio was obtained to give a cycle with the desired primary jet noise, reference should be made to figures 5-104 and 5-105. These figures show plots of bypass ratio vs. primary jet noise for engines of varying fan pressure and overall pressure ratios.

Figure 5-106 is an example of the final plots of the primary jet noise as a function of altitude for engine 1 through 4. An altitude of 550 ft is equivalent to a sideline distance of 500 ft. As shown, the engines are within ±1.0 PNdB of the target figure of 90 PNdB, four engines, 500 ft sideline.

Figure 5-107 shows the effects of varying design fan pressure ratio on the augmentor nozzle 500-ft sideline, four-engine noise level. Two noise levels are shown. The higher level is for the augmentor nozzle configured as a basic slot in conjunction with unlined flaps. The lower level is for the augmentor nozzle and flap system fully optimized for noise reduction according to expected 1978 technology.

Sizing and weight.—The major results of the sizing and weight calculations are given in table 5-7. The values of the engine uninstalled thrust/weight ratios are plotted against design fan pressure ratio in figure 5-108 and against design overall pressure ratio and T_4 in figure 5-109. The weight values are for expected 1978 technology.

5.5.4.4 Conclusions and Recommendations

The effects of varying cycle fan pressure ratio, overall pressure ratio, and turbine inlet temperature will be discussed in turn. The effects will be mainly confined to those on engine weight, augmentor noise, and cruise performance.

Wing duct volume has a strong influence on wing weight. This produces an incentive to go to as high a fan pressure ratio as possible. The higher the fan pressure ratio, the lower the bypass ratio necessary to achieve the required primary jet noise. The low bypass ratio and high fan pressure ratio give poor cruise SFC performance as indicated by figure 5-96. The SFC is reflected by the cycle overall efficiency, which in turn is the product of the thermal and propulsive efficiencies. The cruise SFC in figure 5-96 for the design fan pressure ratio of 3.6 is associated with a propulsive efficiency of 0.469, a thermal efficiency of 0.454, and an overall efficiency of 0.213. At the other end of the fan pressure ratio range, the propulsive, thermal, and overall efficiencies for a pressure ratio of 2.2 are 0.69, 0.349, and 0.241, respectively. The predominating factor is the large increase in propulsive efficiency that results from the decreased secondary nozzle jet velocity as fan pressure ratio is decreased. The secondary jet velocity decreases from 1860 to 1477 ft/sec. Even for the lower fan pressure ratio cycle, the overall efficiency is poor. This, however, can be improved upon somewhat by using a variable primary nozzle to increase the thermal efficiency.

TABLE 5-7.—PARAMETRIC CYCLE STUDY—ENGINE SIZE AND WEIGHT

Engine cycle number	Fan stages	HP turbine stages	LP turbine stages	Fan tip diameter, in.	Engine overall length, in.	Bare engine weight	Thrust/ weight
1_4 1_3	4 3	2 2	5 5	49.6 49.7	116.7 107.4	4260 4110	4.69 4.86
2	3	2	5	50.9	111.7	4050	4.94
3_3 3_2	3 2	3 3	5 5	51.6 –	116.3 –	4170 4225	4.79 4.73
4	2	3	5	54.4	111.5	4000	5.0
5	3	2	5	51.4	114.6	4120	4.85
6	3	2	5	51.8	115.1	4050	4.94
7	3	3	5	52.3	117.7	4300	4.65
8	3	2	5	52.1	112.2	4375	4.57
9	3	3	5	51.4	119.7	3980	5.03

Figure 5-107 shows the increase in augmentor system noise with increasing fan pressure ratio. If it is accepted that the augmentor noise should be no greater than the 90 PNdB of the engine primary nozzle jet, then it follows that the fan pressure ratio should be kept below 2.92, which corresponds to 2.48 at the augmentor nozzle, assuming a 15% duct total pressure loss.

Figure 5-108 shows a downward trend in the engine thrust/weight ratio with increasing fan pressure ratio. The discontinuity in the engine weights can be partly attributed to changes in the number of turbine stages. For instance, engine 2 with a fan pressure ratio of 3.0 has only two high-pressure turbine stages compared with engine 3 (FPR = 2.75) which has three. Note also that a three-stage fan engine is lighter than a two-stage fan engine for engine 3. This is attributed to the much higher efficiency of the three-stage fan reducing the weight of all engine components except the fan, by virtue of a decreased airflow (see fig. [illegible]) by an amount greater than the increase in the fan weight. For the fan pressure ratio [illegible] engine, the increase in fan efficiency in going from three to four stages was insufficient to offset the fan weight increase. The downward trend in the thrust/weight curve is slight, and it is suggested that actual hardware engines could possibly show a different type of trend depending on the ground rules to which they were designed.

The advantages in going to a high fan pressure ratio are a decreased secondary air flow, [illegible], a higher cruise thrust, figure 5-98, and lower installation losses, figure 5-100. In [illegible] the engine maximum diameter and length decrease, as can be seen from table 5-7.

Comparing the fan tip diameter (first rotor) of engines 1_3 (three fan stages) and 4 shows a decrease of 8.5% in going to the higher fan pressure ratio. The lower installation losses will tend to offset the weight increase trend, but it is probable that the higher cruise thrust cannot be taken advantage of because of the indication that engines will be sized by takeoff requirements.

Figure 5-93 shows the installed cruise performance for different fan pressure ratio engine cycles in detail. The installed cruise thrust required by each engine is not known accurately, so the corresponding maximum cruise power setting cannot be defined. However, the baseline airplane thrust requirement is shown.

The conclusion in regard to the effects of varying the fan pressure ratio is that augmentor nozzle noise will probably dictate the upper level to be in the 2.9-3.0 region. It is recommended that further trade studies be done with the data made available on engine weight/wing weight/fuel weight/engine installation relationships.

For a given fan pressure ratio, increasing the overall pressure ratio decreases the bypass ratio required to meet the primary jet noise requirements. The cruise SFC shown in figure 5-97 has a minimum at an OPR of about 22.0, which is also shown in the details of figure 5-94.

Augmentor noise is not sensitive to OPR for a given fan pressure ratio because the secondary airflow is relatively constant with OPR, figure 5-92.

The increasing weight of the high-pressure compressor as the OPR increases gives a downward trend in the engine thrust/weight ratio, although not a steep one.

The conclusion in regard to OPR effects is that the magnitude of performance, noise, and weight changes is slight over the range from 18 to 30. Operation in the range from 20 to 24 is preferable, however.

Increasing values of turbine inlet temperature, T_4, increases the BPR and although the total airflow decreases the secondary or wing airflow increases. This increase is relatively small, however, being 3% over a design T_4 range of 380° F. The cruise SFC shows a small bucket, although the maximum-to-minimum variation is only 1% (fig. 5-97). Variation in T_4, for constant fan pressure ratio and OPR, does not appreciably affect the augmentor nozzle noise. The principal T_4 effect is the decrease in engine weight as T_4 increases (fig. 5-109). The engine weight decreases by 9% in going from a design T_4 of 2665° to 3045° R.

It is concluded that increasing T_4 is probably beneficial but that investigation of wing weight changes and SFC effects should be further studied.

It has already been indicated that the results of this parametric study must be considered together with noise and wing duct system requirements. An in-depth appraisal has yet to be made, but in the meantime it is worthwhile to specify the most likely range of engine parameters.

Bypass ratio = 2.0 to 2.7

Fan pressure ratio = 2.7 to 3.3

Overall pressure ratio = 20 to 24

Design T_4 = 2665° to 2855° R

The range extremes of these parameters would result in the following approximate engine characteristics:

Uninstalled thrust/weight = 5.2 to 4.5

Installed cruise SFC lb/hr/lb = 0.78 to 0.84
(with variable primary nozzle)

Uninstalled thrust/total airflow = 38 to 42

Frontal area (to fan tip diameter), sq ft = 13.5 to 15.0

A summary of the parametric study results is shown in figure 5-110. Six important characteristics are plotted against the study independent variables, namely, fan pressure ratio, overall pressure ratio, and turbine inlet temperature. The fan pressure ratio is the variable with the strongest effect on the engine characteristics, except for the effect on engine weight, where turbine inlet temperature predominates. Increasing the fan pressure ratio rapidly reduces the secondary airflow and hence duct volume and wing weight. However, the penalties in doing this are a rapid increase in cruise SFC and an increase in augmentor flap system noise.

5.6 THREE-STREAM SYSTEM

5.6.1 Introduction

Exploratory design and analysis was performed on a three-stream augmentor system to compare the two- and three-stream concepts. The three-stream system was developed around the RB419-01 engine described in section 5.5.2. This engine had 39% of the thrust ducted to the wing at a bleed pressure ratio of 3.0. Typical duct losses of 15% pressure drop would give a blowing nozzle pressure ratio of about 2.5. A schematic of an engine installation is shown in figure 5-111. Of interest is the required engine inlet and fan duct noise treatment. The wing air thrust reverser could be mounted in the strut or spanwise behind the augmentor nozzles. The RB419 low-pressure fan has variable pitch blades, and this feature gives thrust modulation during approach. Although most of the design effort was expended on the 39% thrust split cycle, 30% and 50% wing thrust split systems were also evaluated.

5.6.2 Three-Stream Duct, Nozzle, and Flap Integration

Conceptual duct layouts were made for a subduct plenum and an independent duct system using a wing area of 2200 sq ft, 20,300-lb-thrust engines, and a 39% wing thrust split. A section of the subduct plenum system is shown in figure 5-112. Because this system was not volume critical, the subduct was mounted above the main duct to minimize any flow geometry changes caused by shutting off the subduct during engine-out operation. The main duct is shown with a slot nozzle because the reduced nozzle flow area should probably make multi-element nozzles unnecessary from a noise standpoint. The subduct nozzles are small, widely spaced lobes which were used to allow free ventilation of ambient air to the slot nozzle while reducing the distance from the subduct to its nozzle exit plane. The main duct slot nozzle, nozzle lip, and flap were patterned after the Ames phase VI augmentor configuration. Although the rear spar is shown at 50% chord, it could be moved to 57% chord if the flap chord was reduced from 35% to 27%.

An independent duct system for the three-stream engine is shown in figure 5-113. This duct system, 27% crossover, is described in section 5.4.2. Interwoven lobe nozzles are used, and the dimensions at the exit plane are shown. The system occupies 20% of the wing chord compared to 13% on the plenum at the 39% thrust split.

The equivalent augmentor nozzle height as a function of the wing thrust split is shown in figure 5-114 along with the flap mixing length ratio. The mixing length ratio for 39% wing thrust split is about 110 compared to 40 to 60 for two-stream systems. This higher value of mixing length ratio is very similar to the Buffalo augmentor wing model and phase VI augmentor flaps. This would allow the test data and design information for these flaps to be directly applicable to the three-stream system. A summary curve relating the chordwise duct volume requirements to the wing thrust split is shown in figure 5-115 for plenum and independent duct systems.

5.6.3 Airplane Sizing

Thumbprints for three-stream configurations at 40%, 50%, and 30% blowing thrust are shown in figures 5-116, 5-117, and 5-118. The weights were adjusted from the two-stream configuration for the increased weight of the RB419 engine and for the smaller duct system. The design point is the intersection of the takeoff and landing field length lines because, if a plenum duct system is used, the duct volume is not critical. As the wing thrust split is reduced the landing line shifts to lower wing loadings because the reduced blowing reduces the lift coefficients. This causes an increase in airplane weight with decreasing wing thrust split. These curves are somewhat pessimistic because the lift coefficients were based on a flap length of 29% chord. As figure 5-115 implies, the flap chord could be increased and this would shift the landing line to higher wing loadings and lower gross weights. Further improvements may be possible with additional work on the split flow configurations.

5.6.4 Noise

The three-stream engine reintroduces the aft fan noise problem. The engine as presently envisioned has two lined splitters in the inlet and one splitter in the low-pressure fan duct to attenuate the fan noise. A choked inlet would give much higher thrust and SFC penalties on the three-stream engine than the two-stream engine because the pressure losses associated with choking are a much higher percentage of the fan pressure ratio. The estimated noise levels are given in table 5-8 and the prediction procedures were similar to those described in section 5.5.4.2. The augmentor flap noise is estimated in the same way as the baseline two-stream flap because the noise increase caused by the higher augmentor pressure ratio in the three stream, 2.5 compared to 2.0 on the baseline, is nullified by the reduced airflow and increased nozzle aspect ratio of the three-stream. On the three-stream system, the engine fan noise appears to dominate the augmentor flap noise.

5.6.5 Conclusions

The major comparison between the two- and three-stream augmentor systems is the tradeoff of flap and duct system complexity against engine complexity. Considerable effort is required on the two-stream to fit the ducting into the wing and to obtain the augmentor flap and choked engine inlet suppression. The three-stream system relieves the duct space problems and reduces the development required on the flap system but requires substantial engine development to achieve the noise goal with the low-pressure fan inlet and exhaust and to achieve inflight thrust modulation. The smaller size and reduced weight of the ducts and flaps in the three-stream system does not appear to compensate completely for the increased engine weight of the three-stream engine. The two-stream airplane configuration also appears to offer a much better noise reduction potential than the three-stream configuration.

TABLE 5-8.—THREE-STREAM AUGMENTOR NOISE[a]

Component	Untreated	Treated
Inlet	107 PNdB	99 PNdB
Aft fan	111	99
Primary jet	96	96
Secondary jet	76	76
Augmentor flap	112	92
Total	115 PNdB	99 PNdB

[a]Four RB419-01 engines
20,300 lb thrust
39% thrust to wing
500-ft sideline
Takeoff power

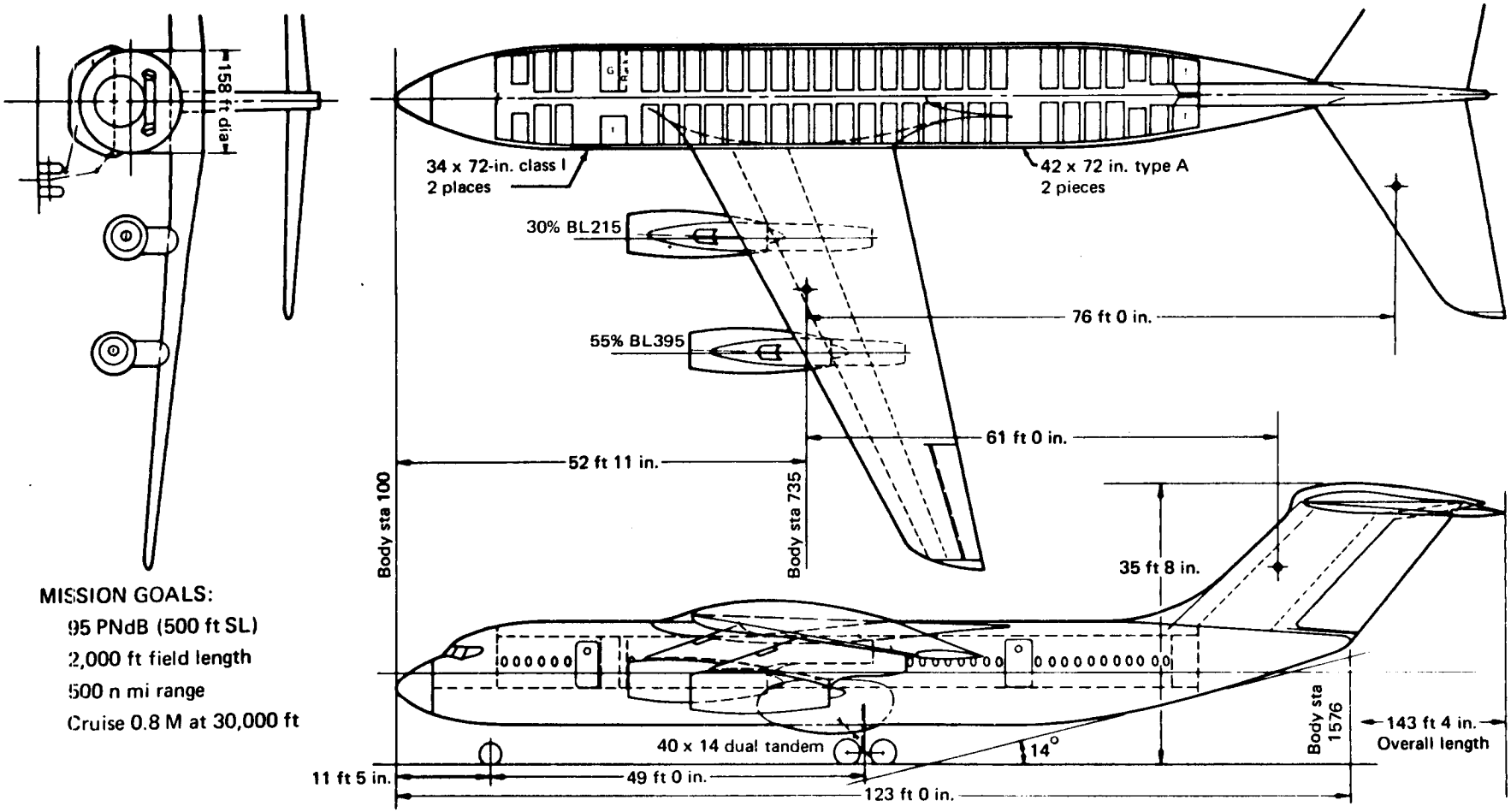

MISSION GOALS:

95 PNdB (500 ft SL)

2,000 ft field length

500 n mi range

Cruise 0.8 M at 30,000 ft

FIGURE 5-1.– MODEL 751-103 AUGMENTOR WING GENERAL ARRANGEMENT

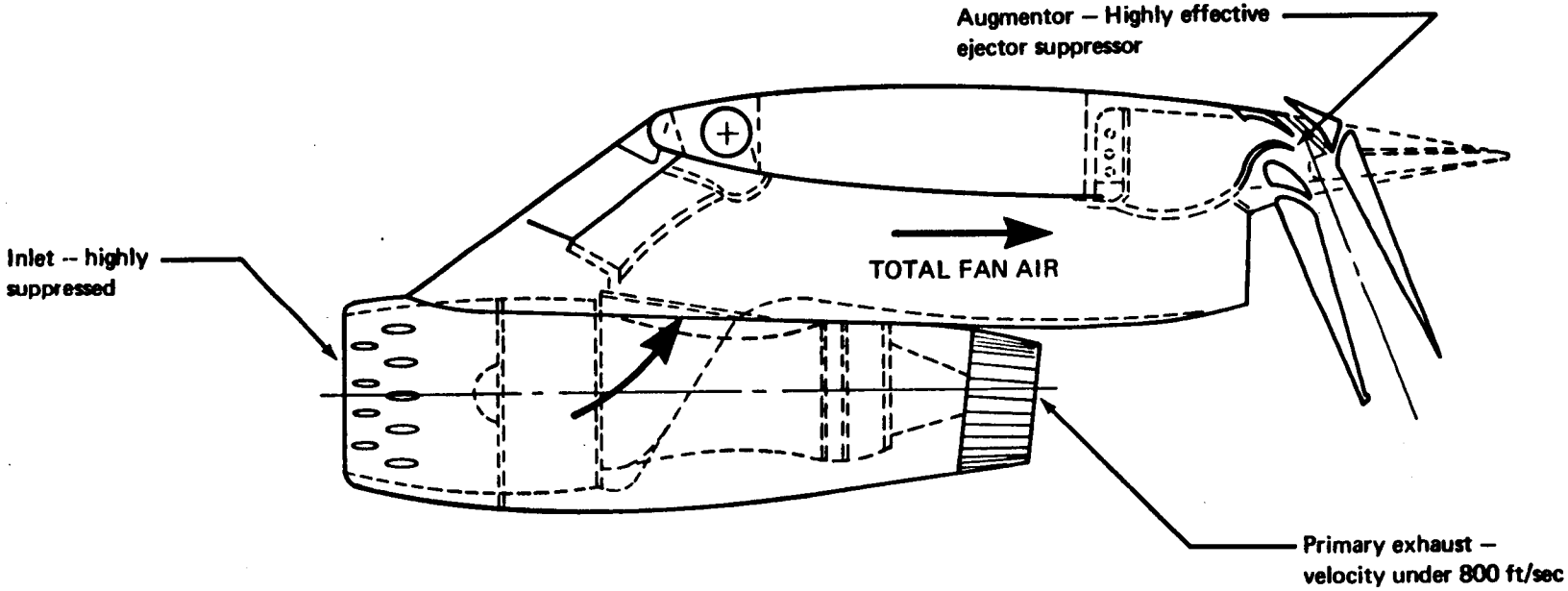

FIGURE 5-2.–TWO-STREAM ENGINE

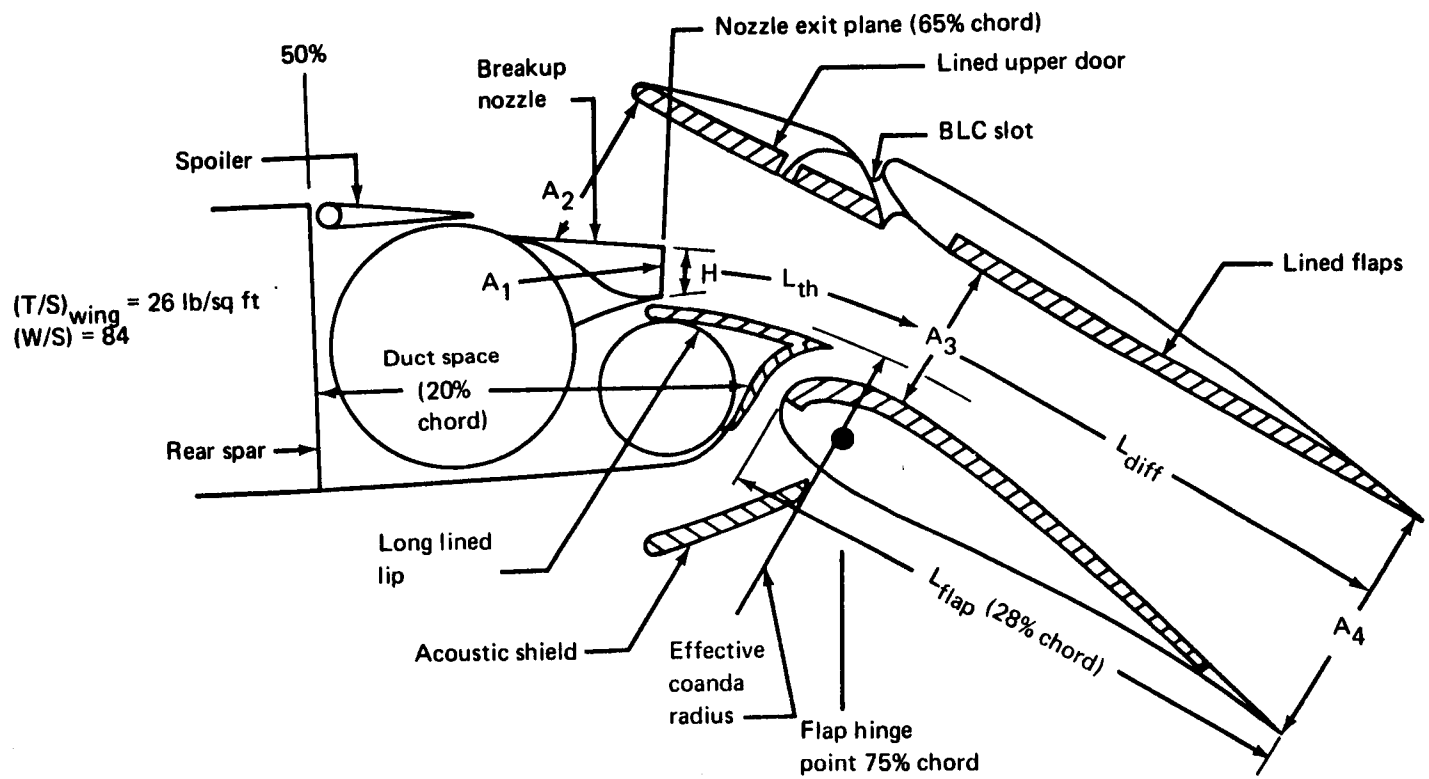

Two-stream engine

FIGURE 5-3.–PRELIMINARY SIZING OF 751 AUGMENTOR FLAP WITH NOISE SUPPRESSION TECHNIQUES

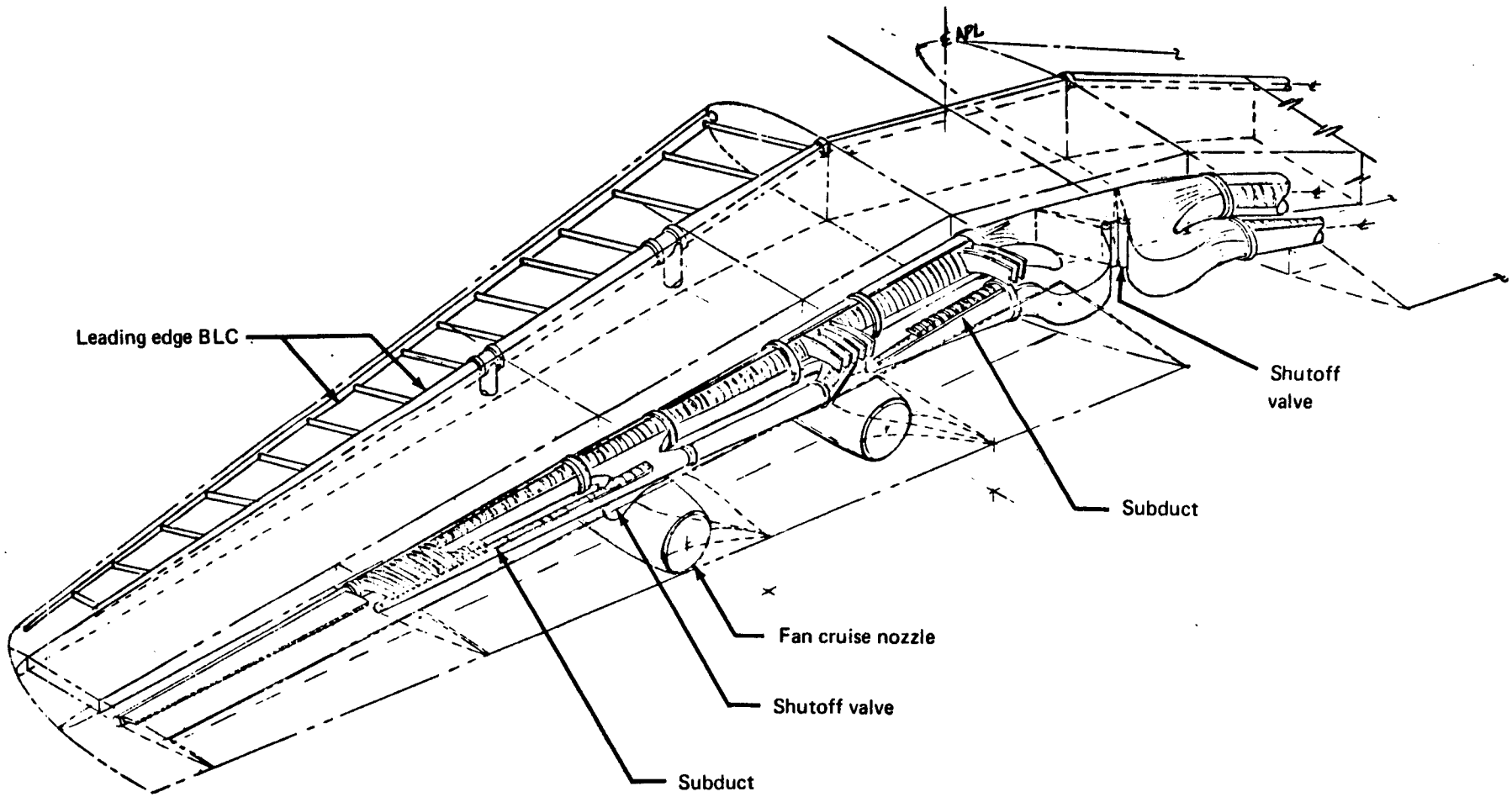

FIGURE 5-4.–BASELINE AIRPLANE SUBDUCT PLENUM SYSTEM

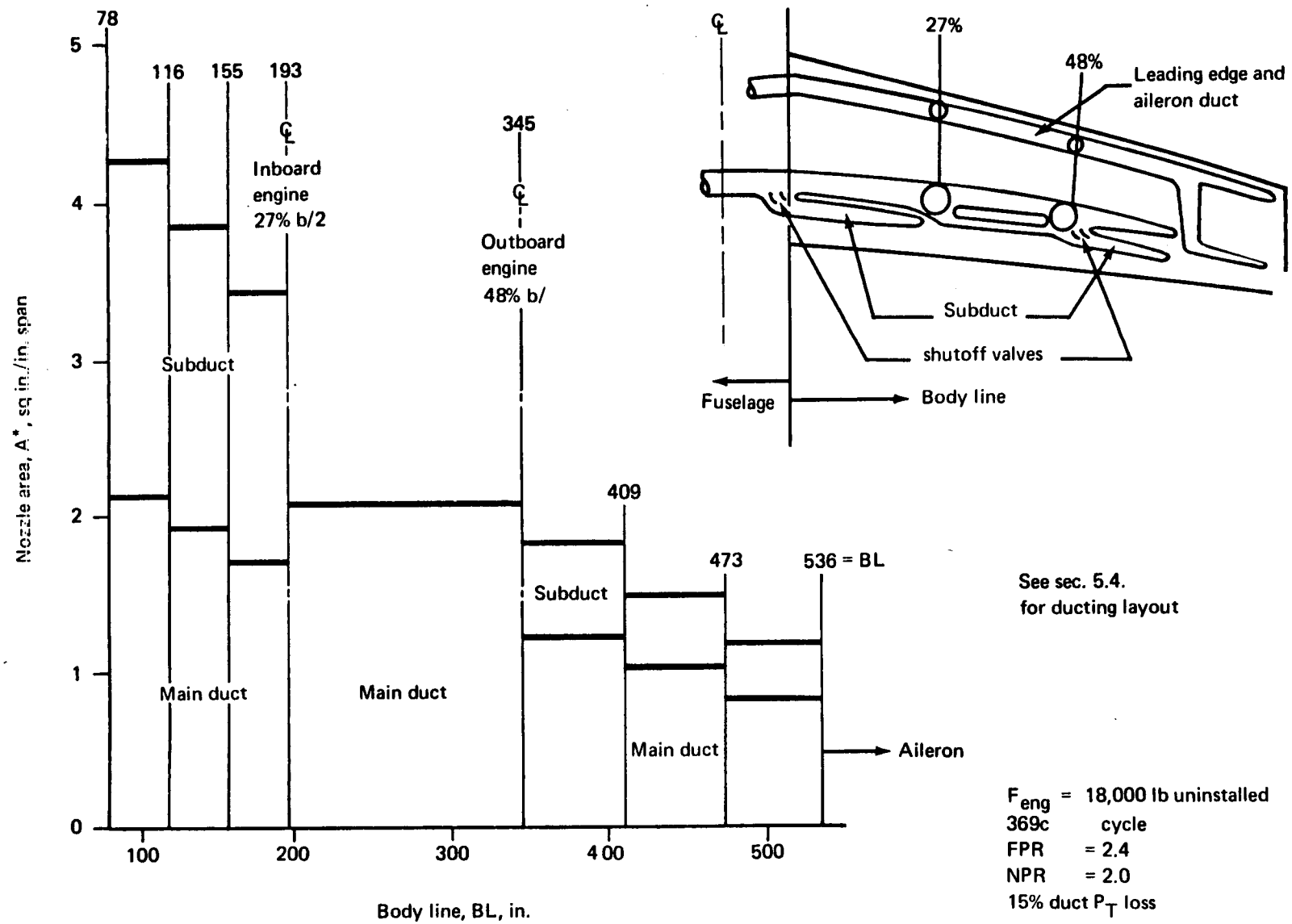

FIGURE 5-5.—BASELINE AUGMENTOR NOZZLE AIRFLOW DISTRIBUTION

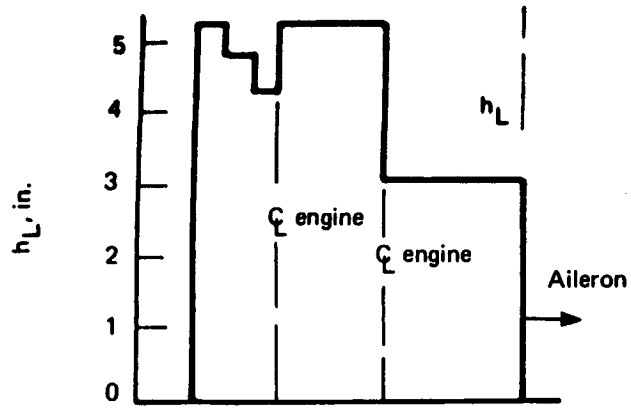

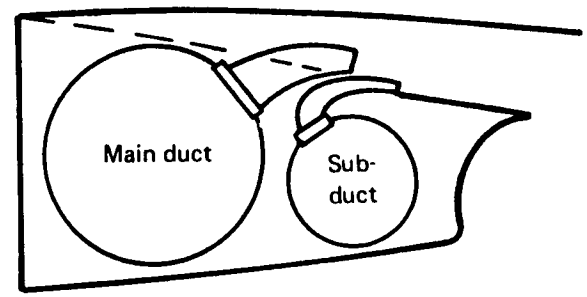

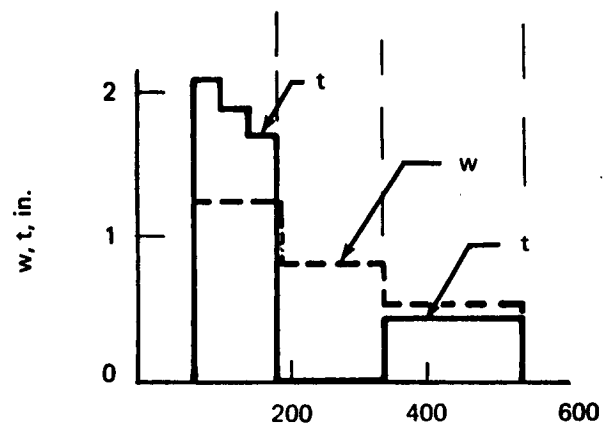

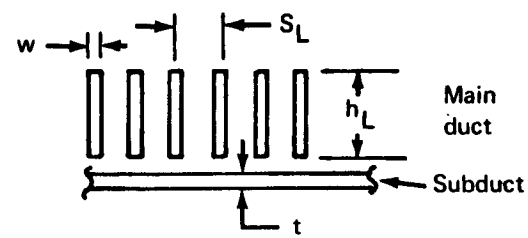

$S_L = 2.5\ w$

No subduct from BL193 to BL345

FIGURE 5-6.–BASELINE AIRPLANE NOZZLE DIMENSIONS

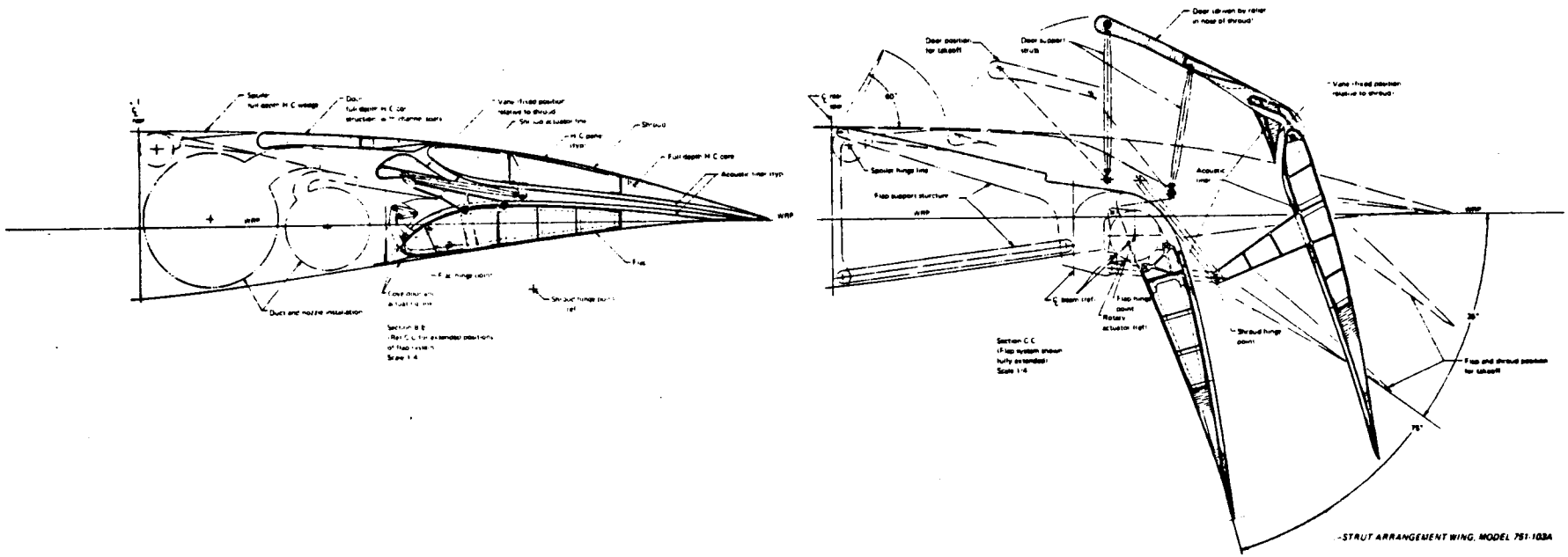

NOT DEVELOPED
UNDER NASA CONTRACT
(REFERENCE DWG. B/A-LO-STR-033, SHT 2)

FIGURE 5-7.—BASELINE AIRPLANE FLAP SYSTEM

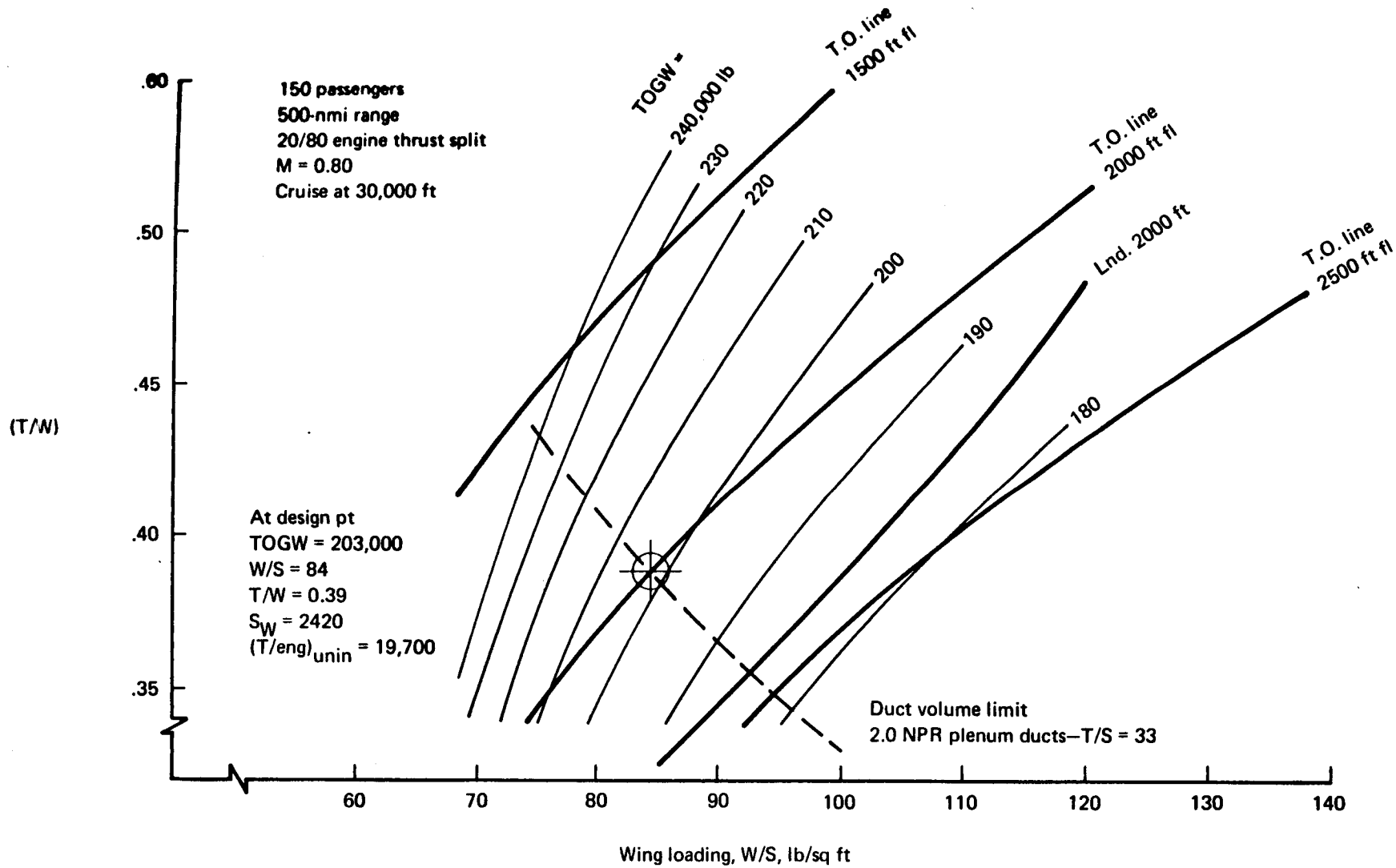

FIGURE 5-8.—AUGMENTOR WING BASELINE DESIGN PARMETERS

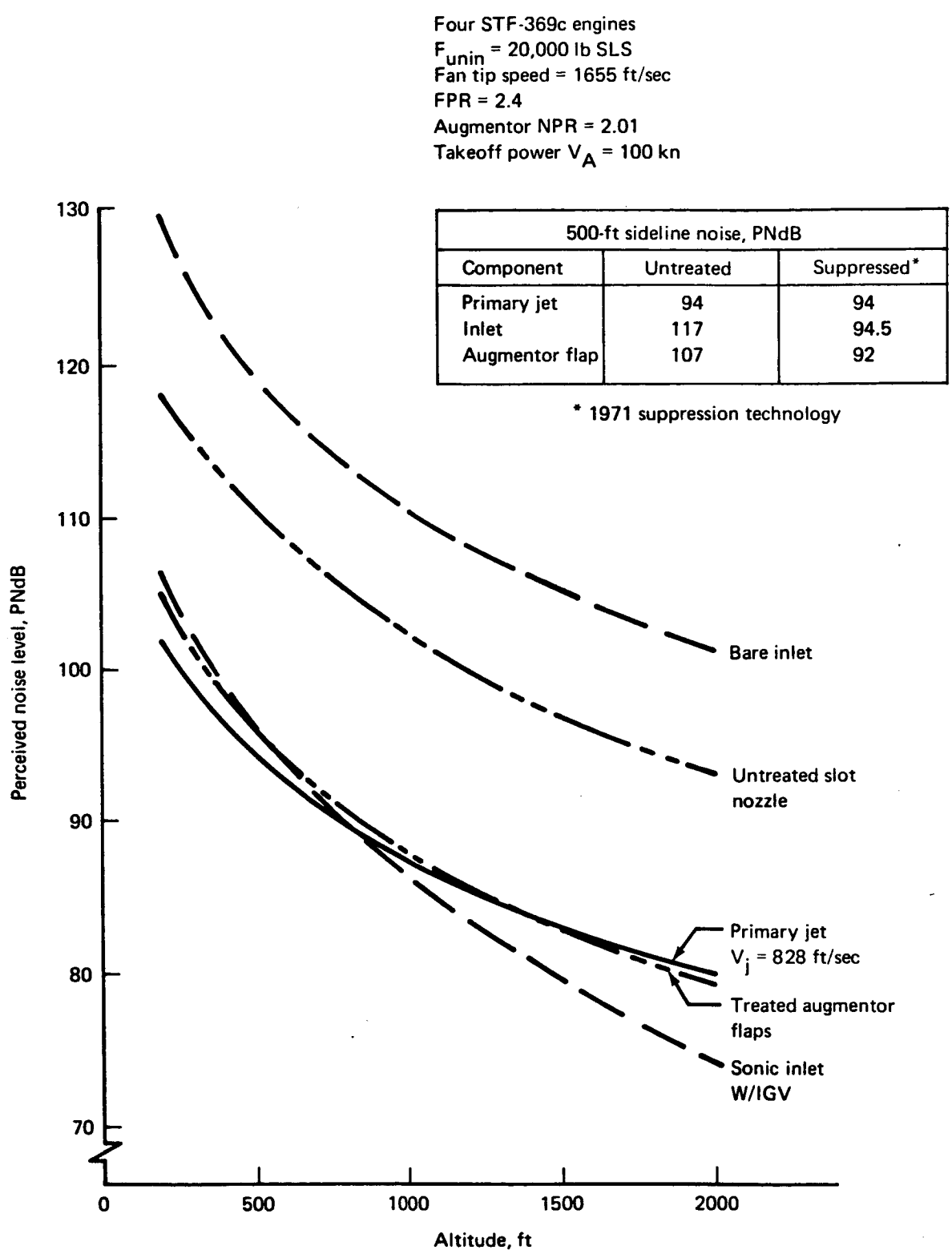

FIGURE 5-9.—BASELINE AIRPLANE NOISE ESTIMATES, PERCEIVED NOISE LEVEL VS ALTITUDE

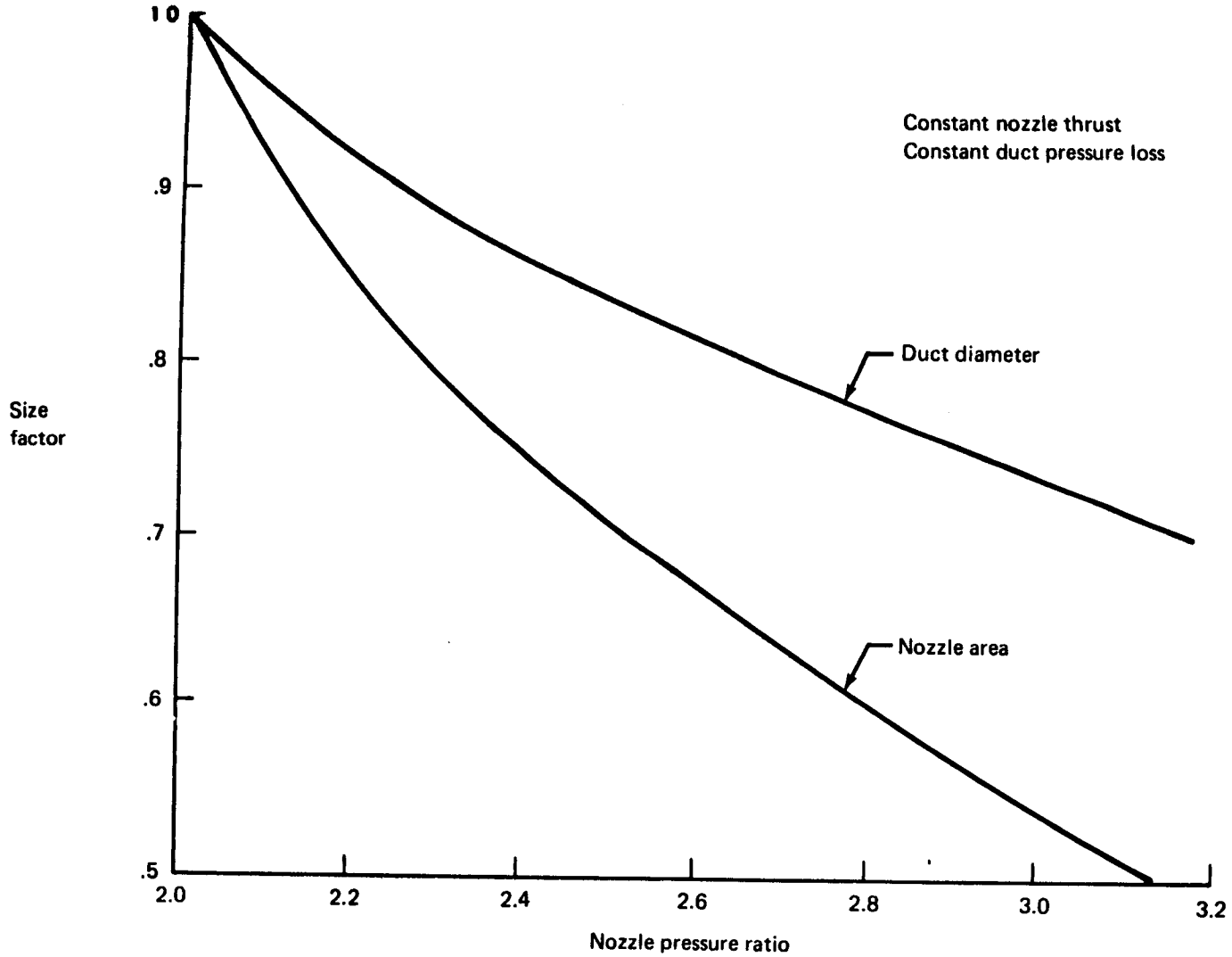

FIGURE 5-10.–NOZZLE AREA AND DUCT DIAMETER AS A FUNCTION OF NPR

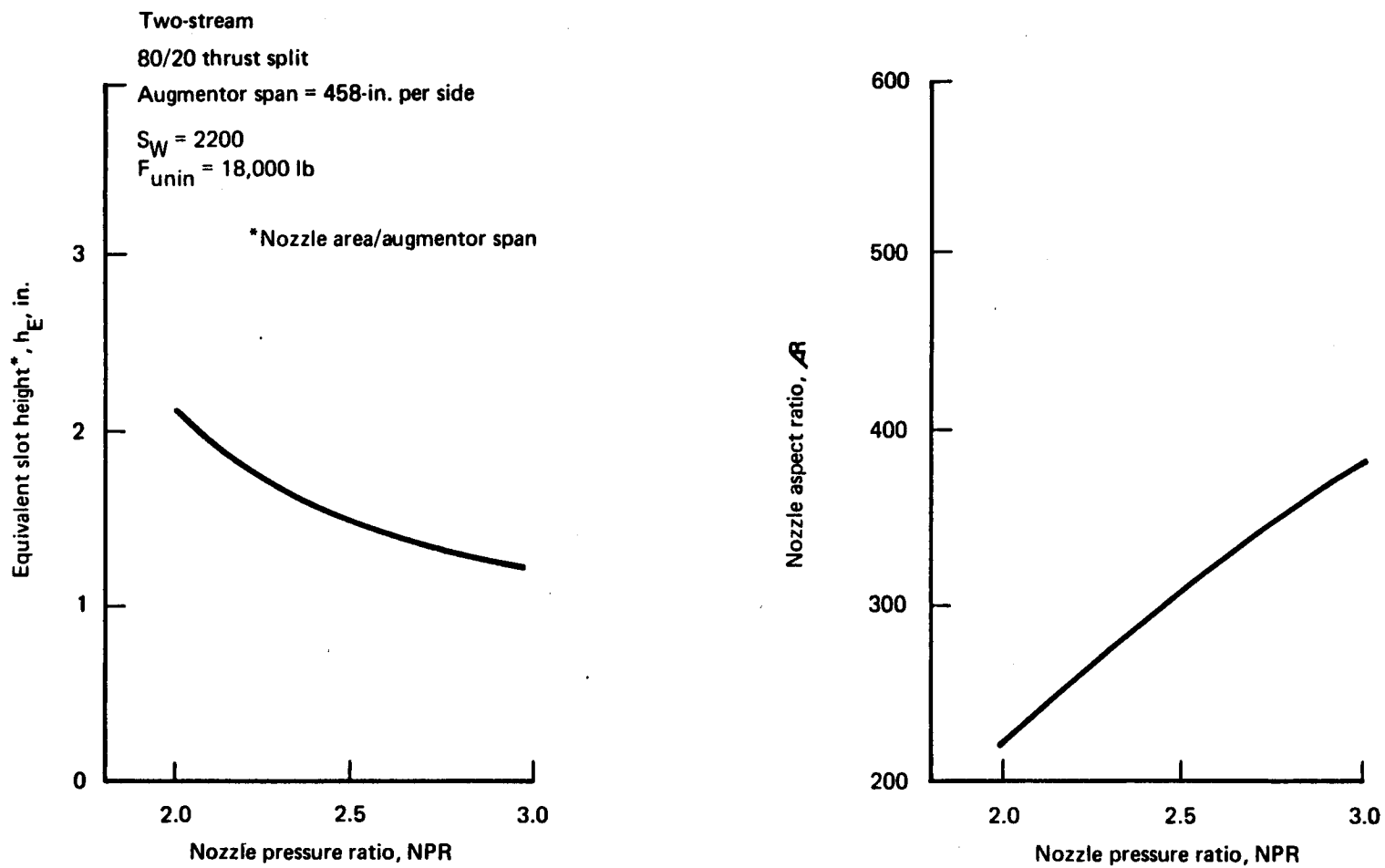

FIGURE 5-11.–AUGMENTOR NOZZLE HEIGHT AND ASPECT RATIO

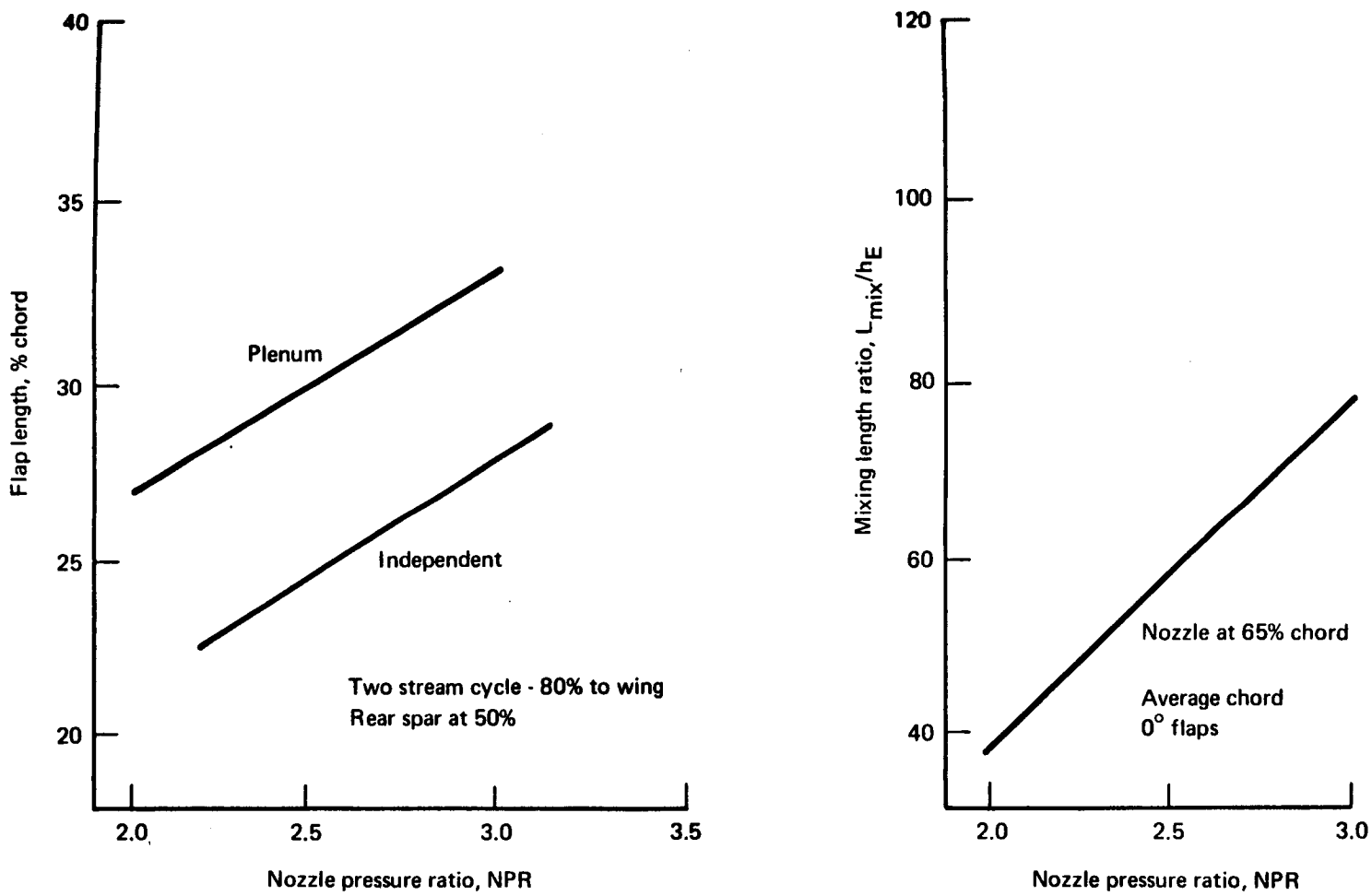

FIGURE 5-12.—FLAP LENGTH AND MIXING LENGTH VS NOZZLE PRESSURE RATIO

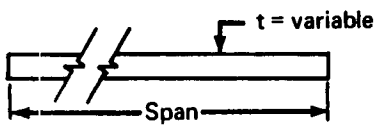

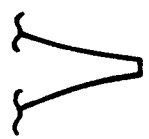

Area = span x t

Aspect ratio = span ÷ t

Slot nozzles

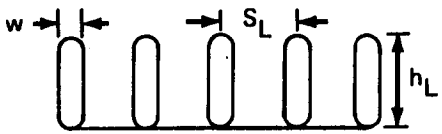

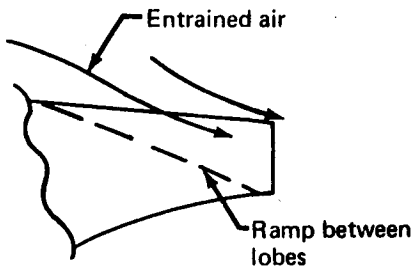

Area = N x h_L x w

N = Number of lobes

= span/S_L

Area ratio = AR_N

= $h_L/t_{eq\ slot}$ = S/w

Lobe nozzles

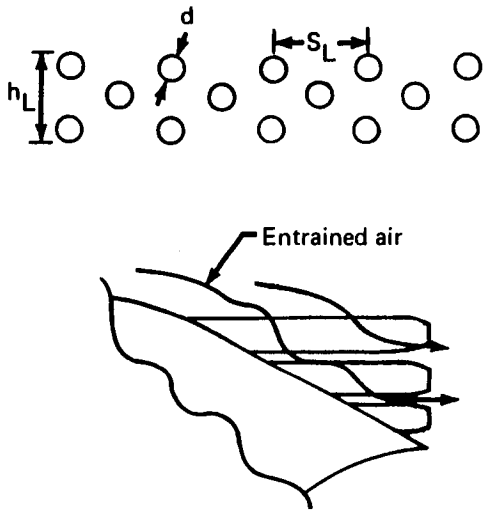

Area = N x $\frac{\pi}{4} d^2$

N = No. of tubes

$\simeq$ No. of rows x $\frac{\text{span}}{S_L}$

Area ratio = h_L/t

$\simeq (S_L/d)^2$

Tube nozzles

FIGURE 5-13.–NOZZLE PARAMETERS

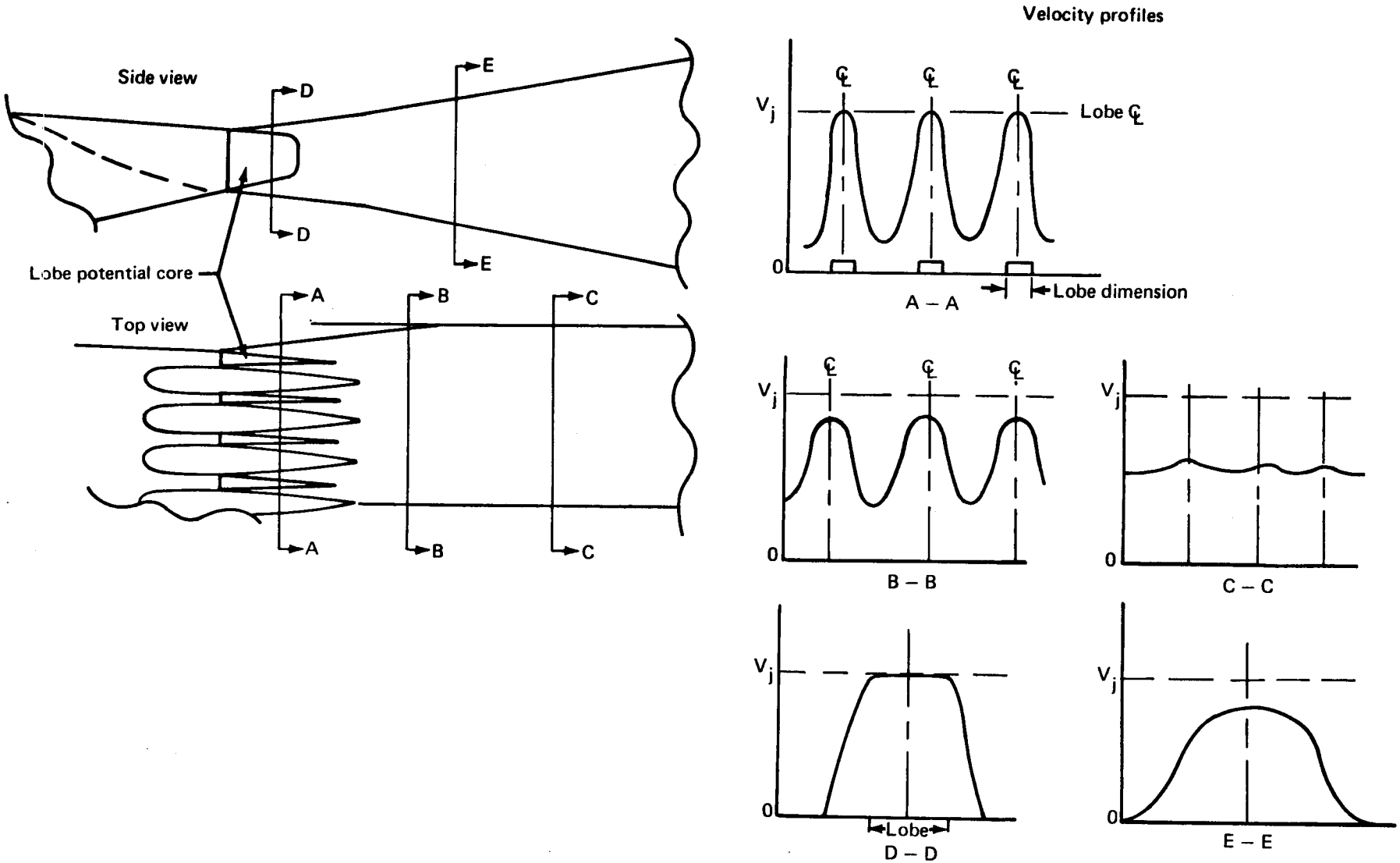

FIGURE 5-14.–BREAKUP NOZZLE MIXING CHARACTERISTICS

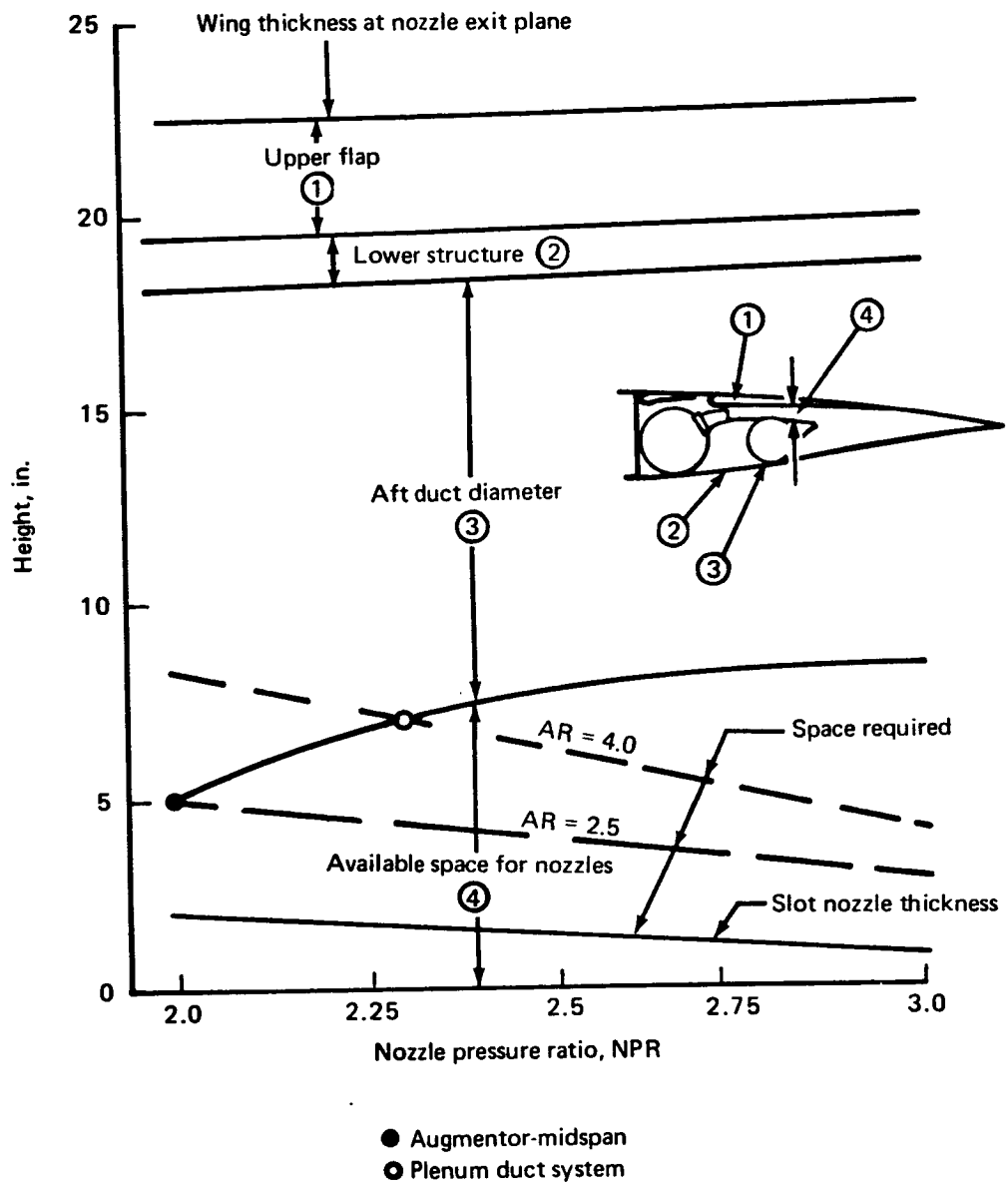

FIGURE 5-15.—WING VERTICAL SPACE UTILIZATION AS A FUNCTION OF NOZZLE PRESSURE RATIO

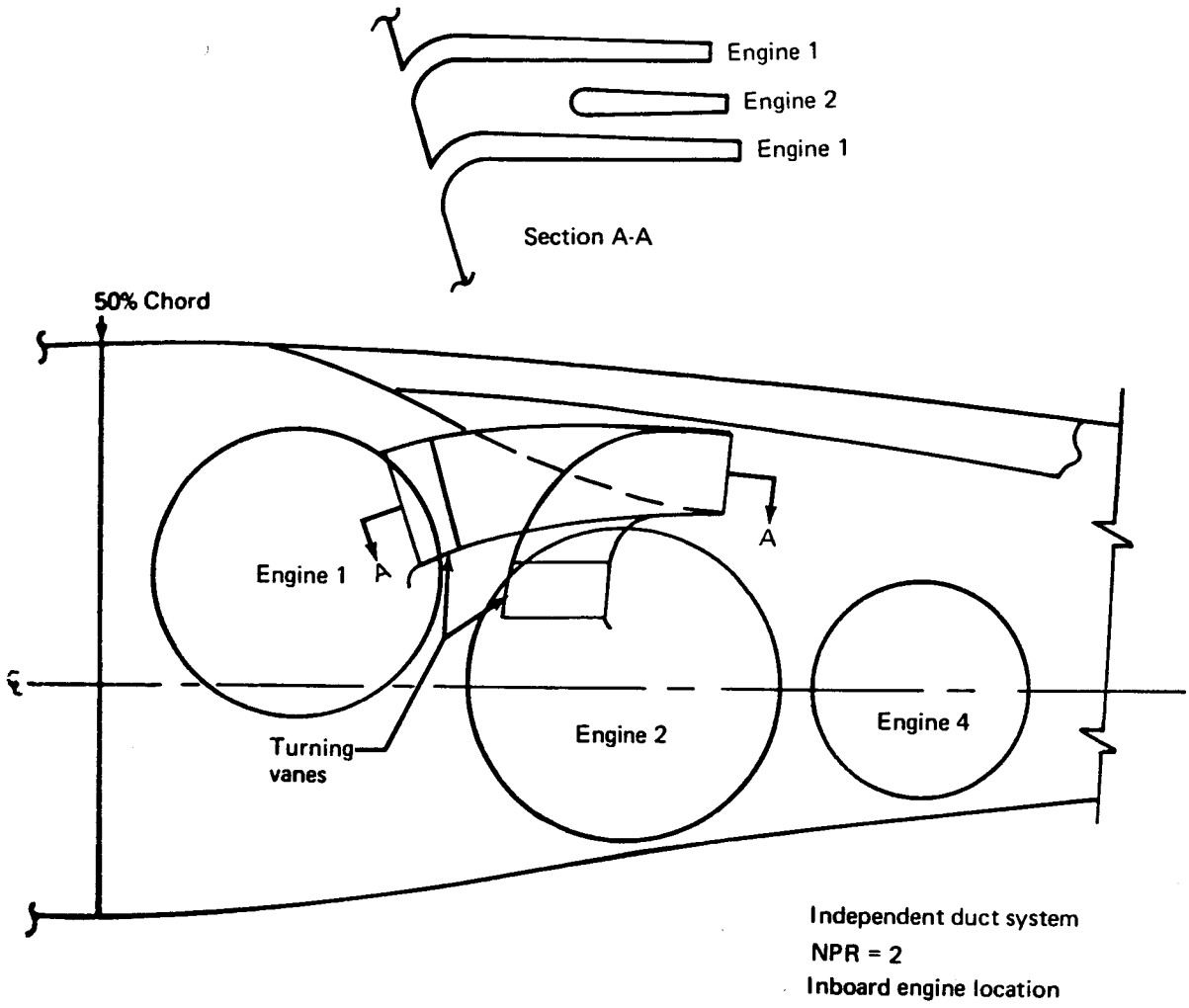

FIGURE 5-16.–INTERWOVEN LOBE CONCEPT

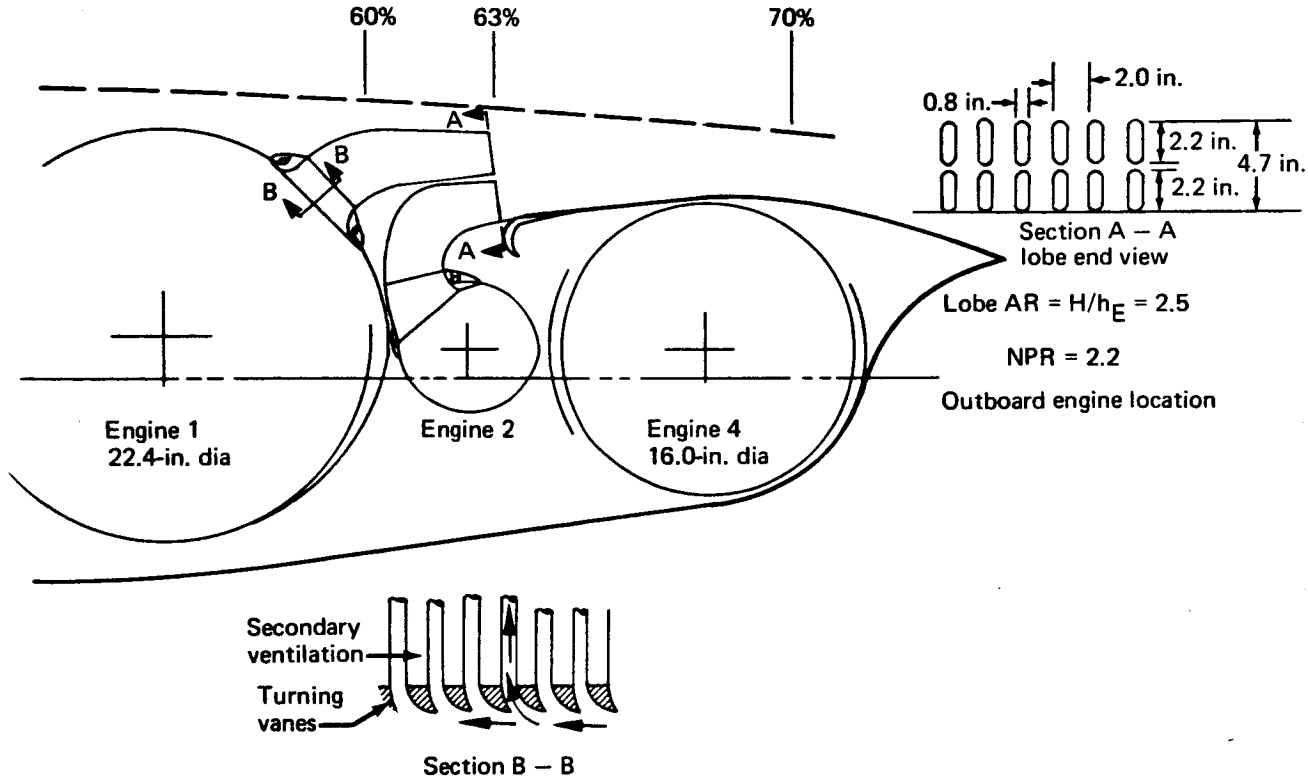

FIGURE 5-17.–STACKED LOBE NOZZLES ON INDEPENDENT DUCT SYSTEM

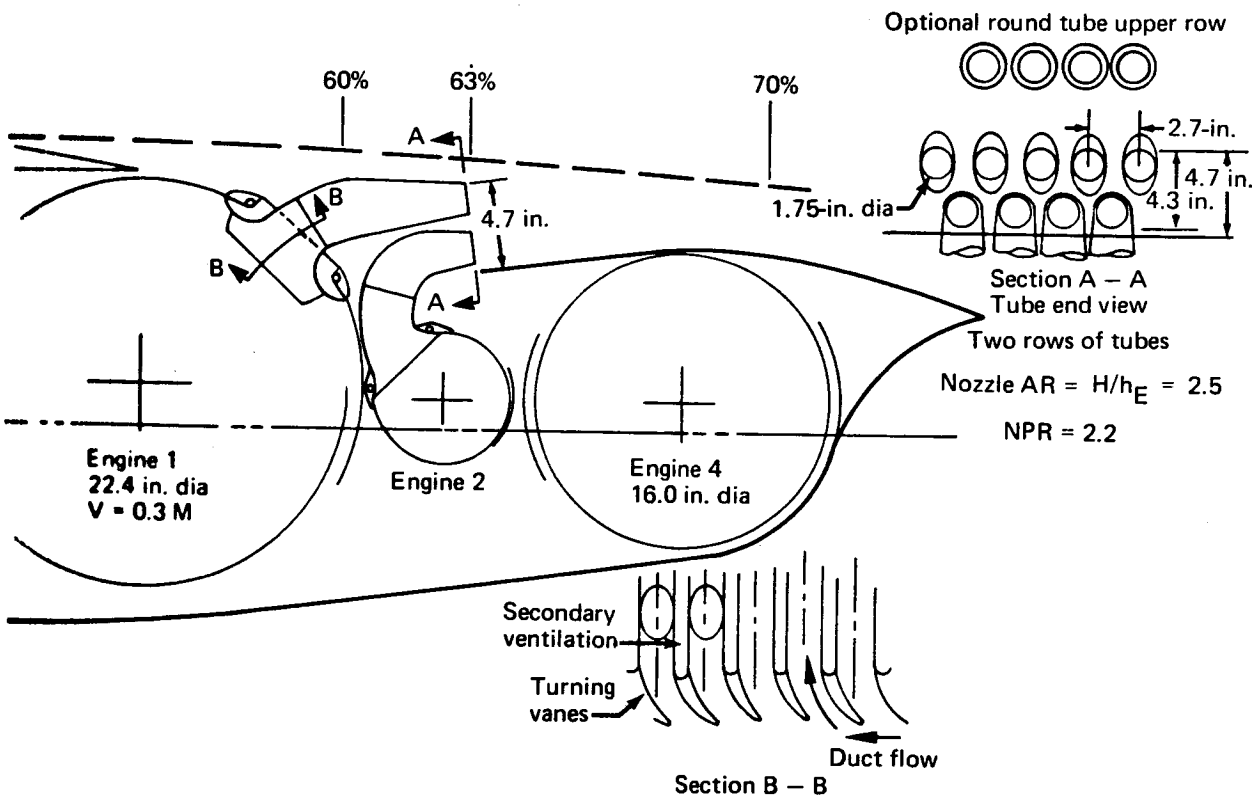

FIGURE 5-18.–TWO-ROW TUBE NOZZLE ARRAY ON INDEPENDENT DUCT SYSTEM

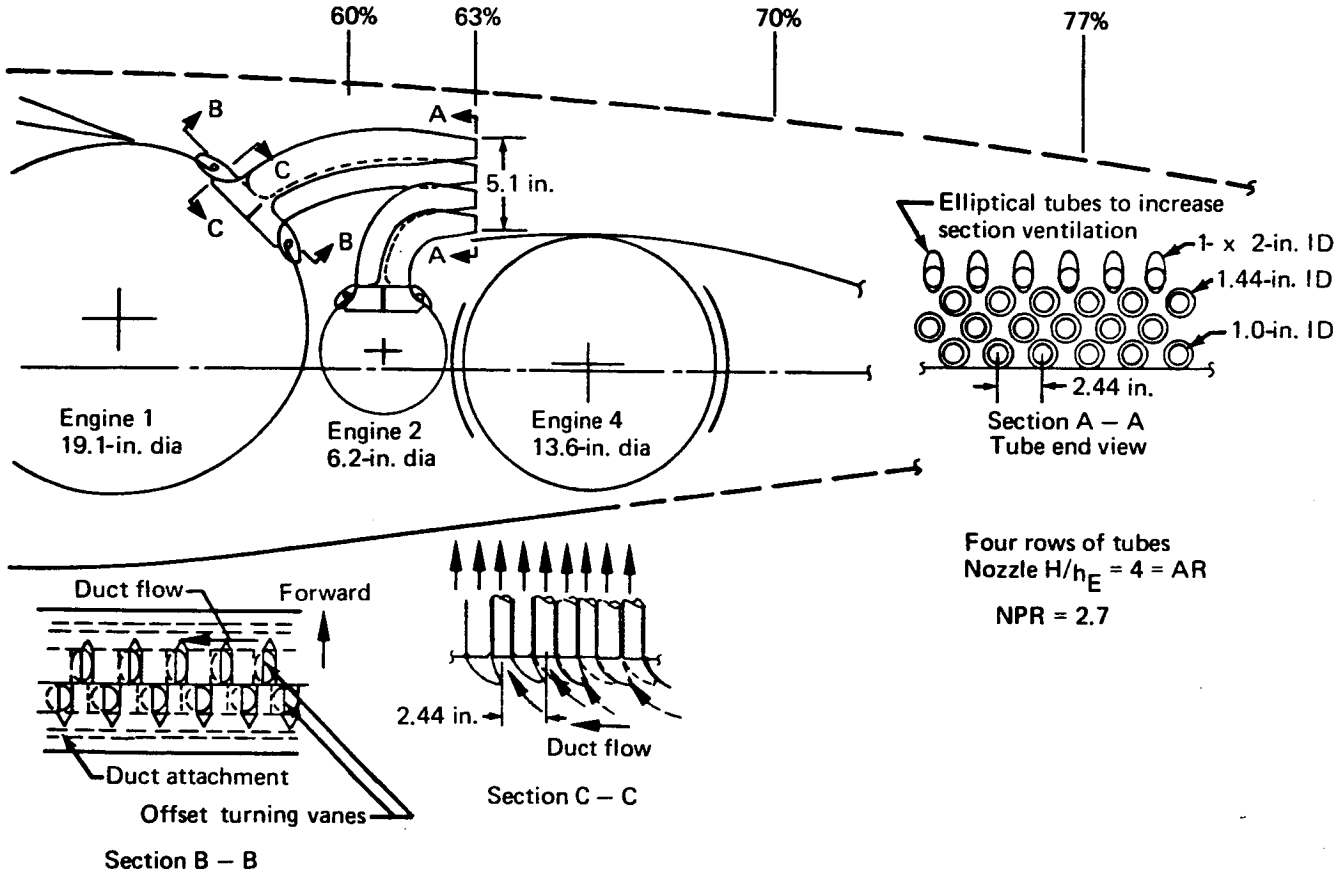

FIGURE 5-19.–FOUR-ROW TUBE NOZZLE ARRAY ON INDEPENDENT DUCT SYSTEM

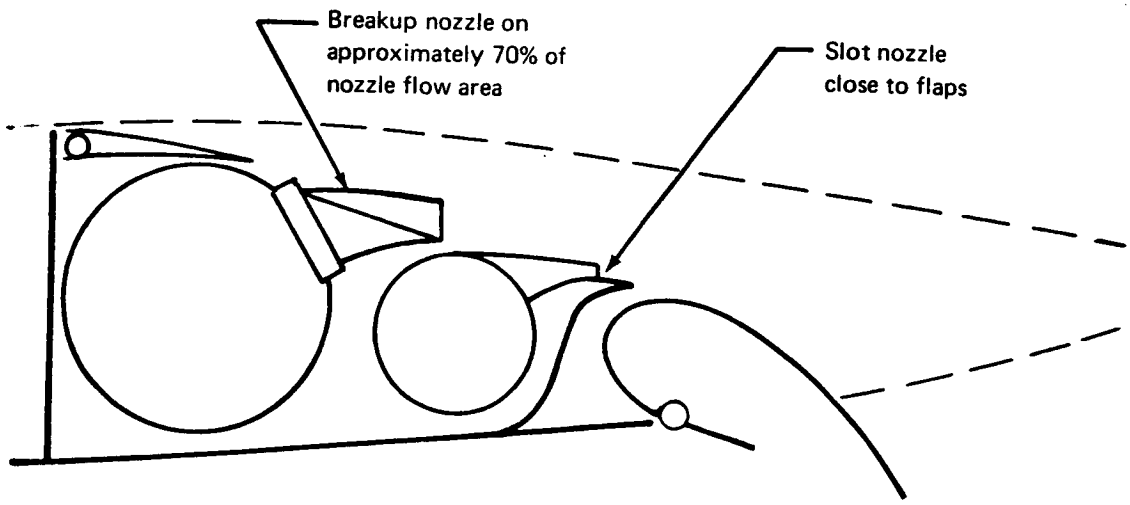

Applications:
- Subduct plenum
- Independent duct system
- Independent duct system with trailing edge BLC plenum

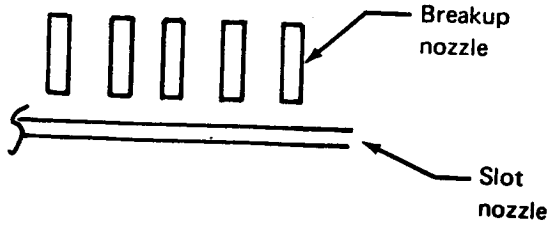

FIGURE 5-20.—TANDEM NOZZLE

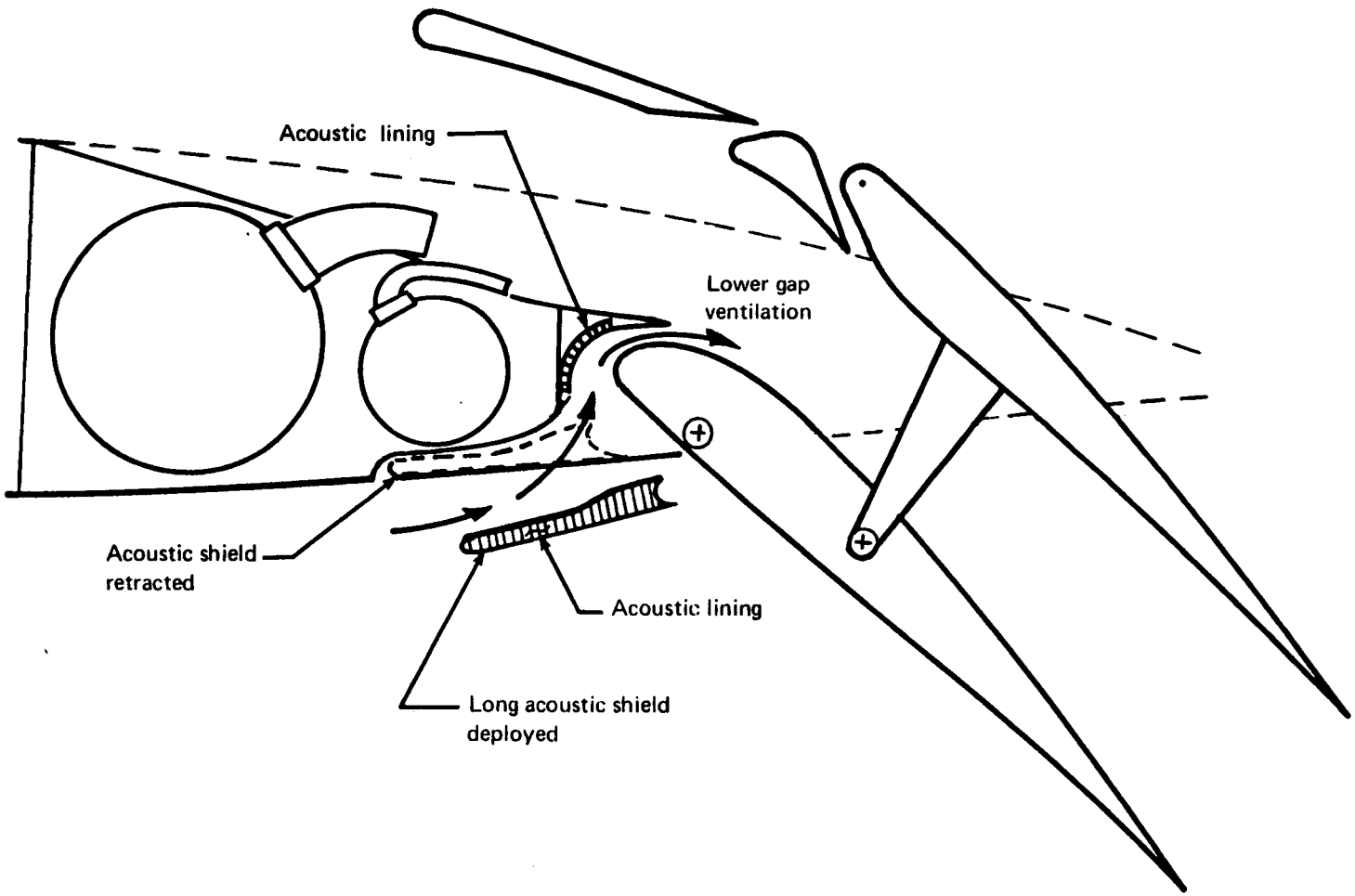

FIGURE 5-21.–LONG LOWER GAP ACOUSTIC SHIELD

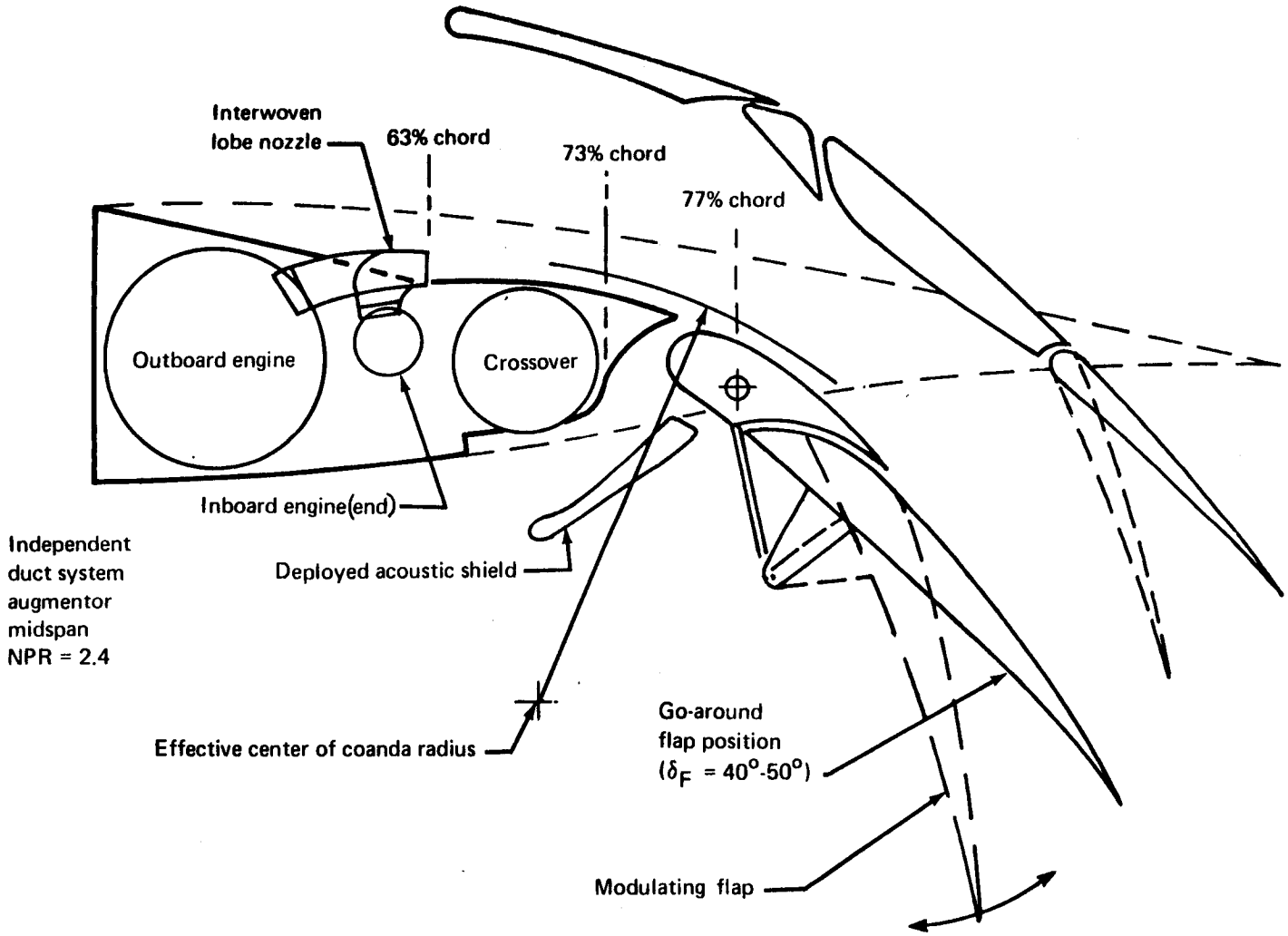

FIGURE 5-22.–MODULATING FLAP CONCEPT

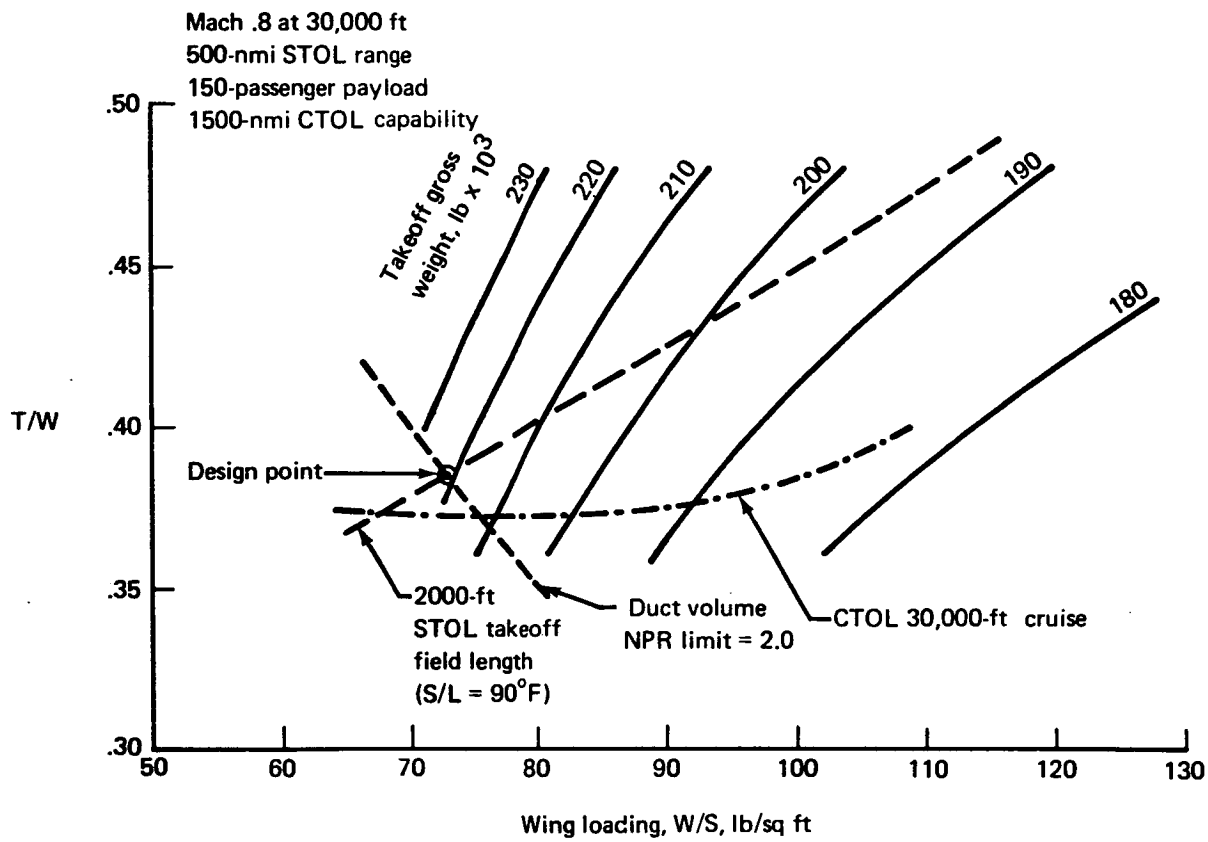

FIGURE 5-23.– AIRPLANE/ENGINE DESIGN RELATIONSHIP, TWO-STREAM AUGMENTOR WING, AR = 6.5, Λ = 20°

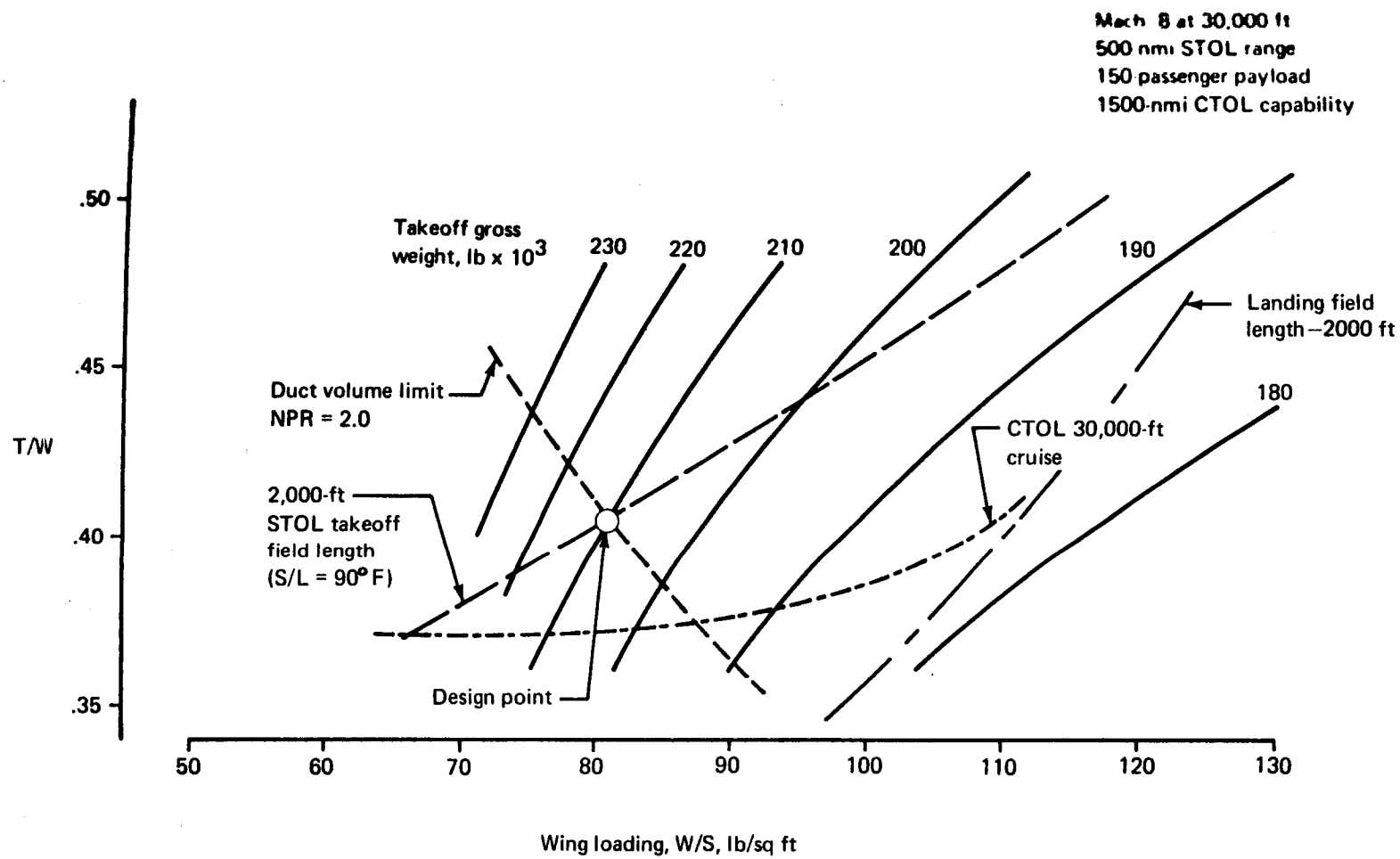

FIGURE 5-24.—AIRPLANE/ENGINE DESIGN RELATIONSHIP, TWO-STREAM AUGMENTOR WING, AR = 6.5, Λ = 25°

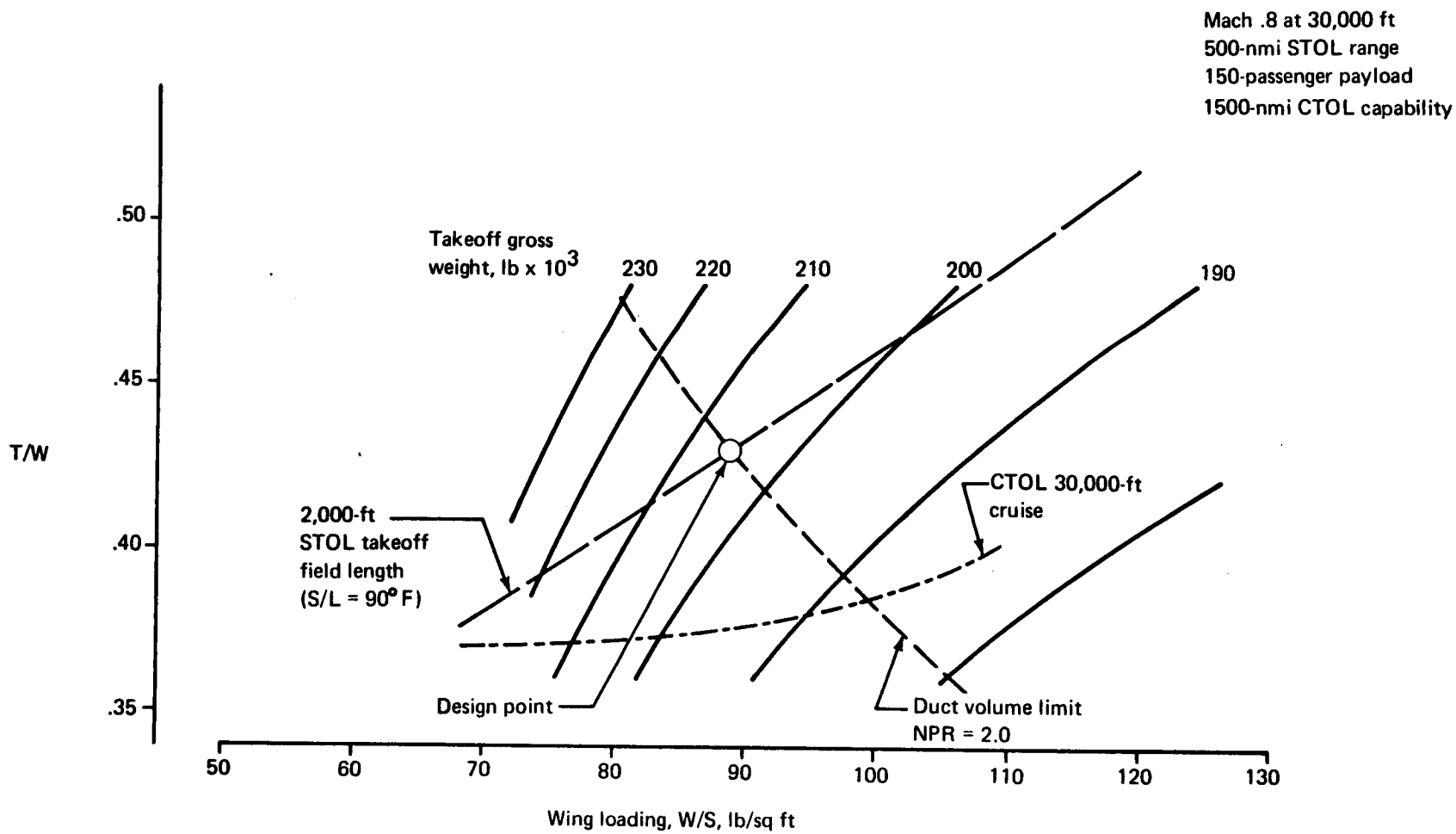

FIGURE 5-25.—AIRPLANE/ENGINE DESIGN RELATIONSHIP, TWO-STREAM AUGMENTOR WING, AR = 6.5, Λ = 30°

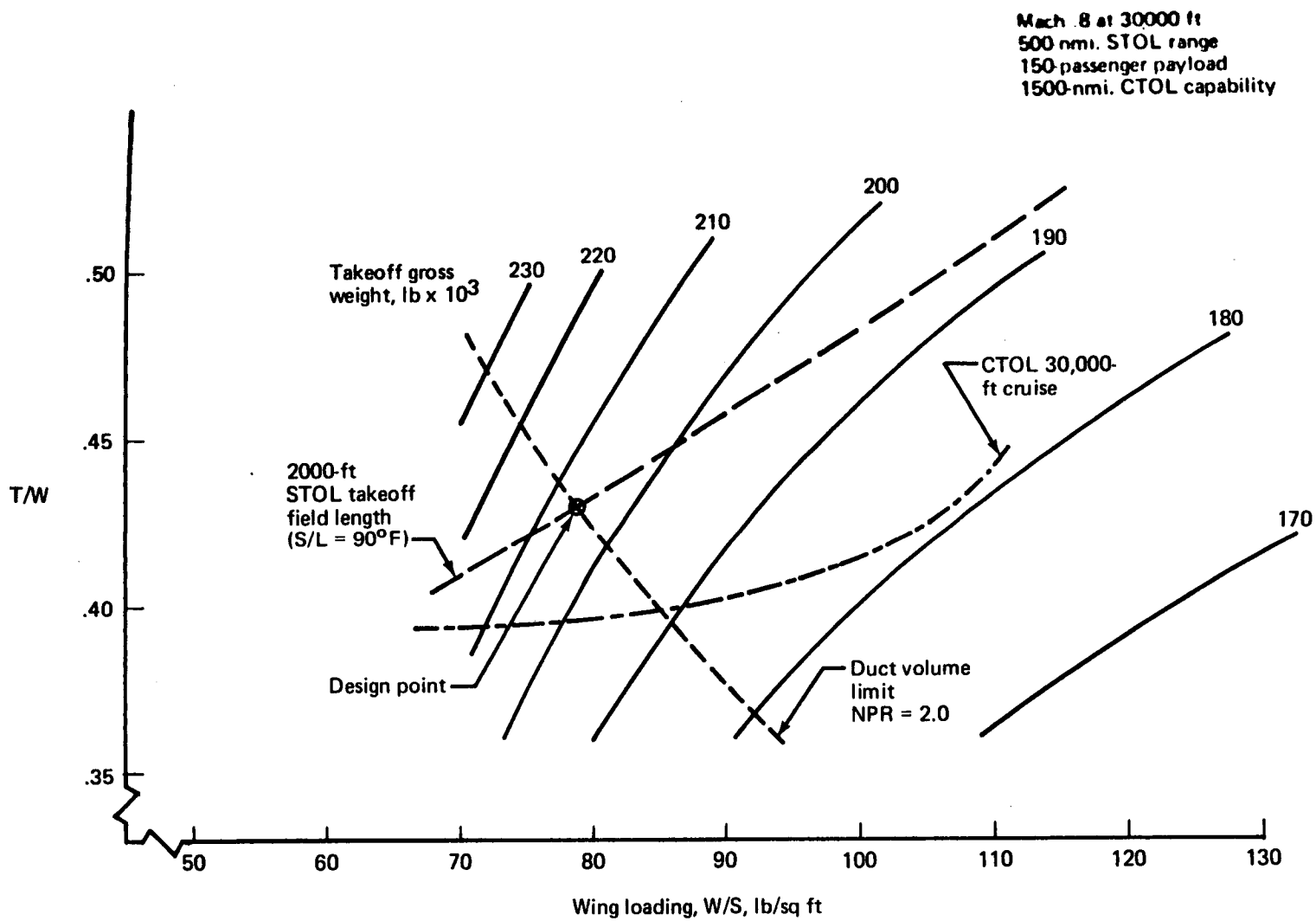

FIGURE 5-26.—AIRPLANE/ENGINE DESIGN RELATIONSHIP, TWO-STREAM AUGMENTOR WING
$AR = 5.5$, $\Lambda = 20°$

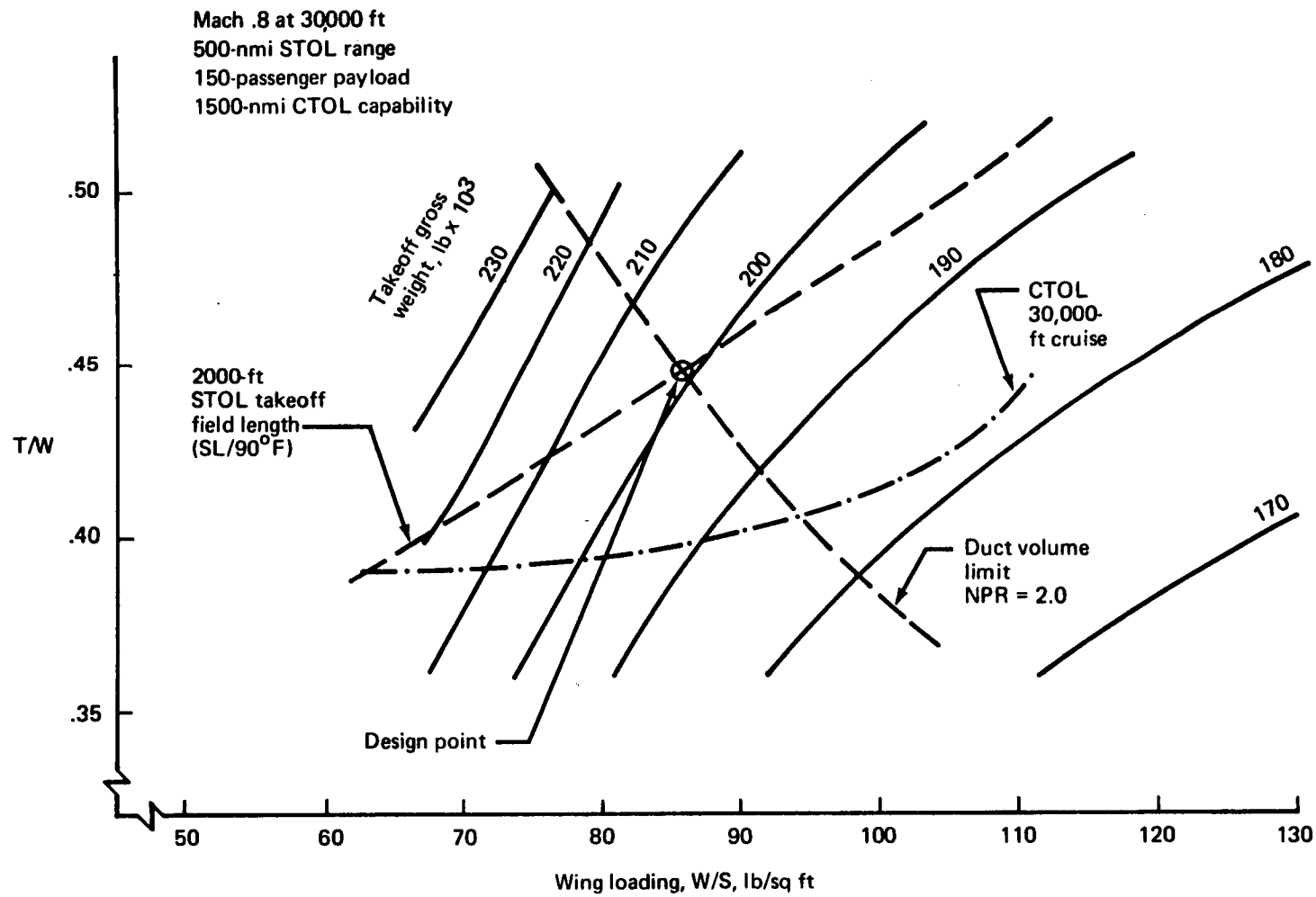

FIGURE 5-27.—AIRPLANE/ENGINE DESIGN RELATIONSHIP, TWO-STREAM AUGMENTOR WING
$AR = 5.5$, $\Lambda = 25^{\circ}$

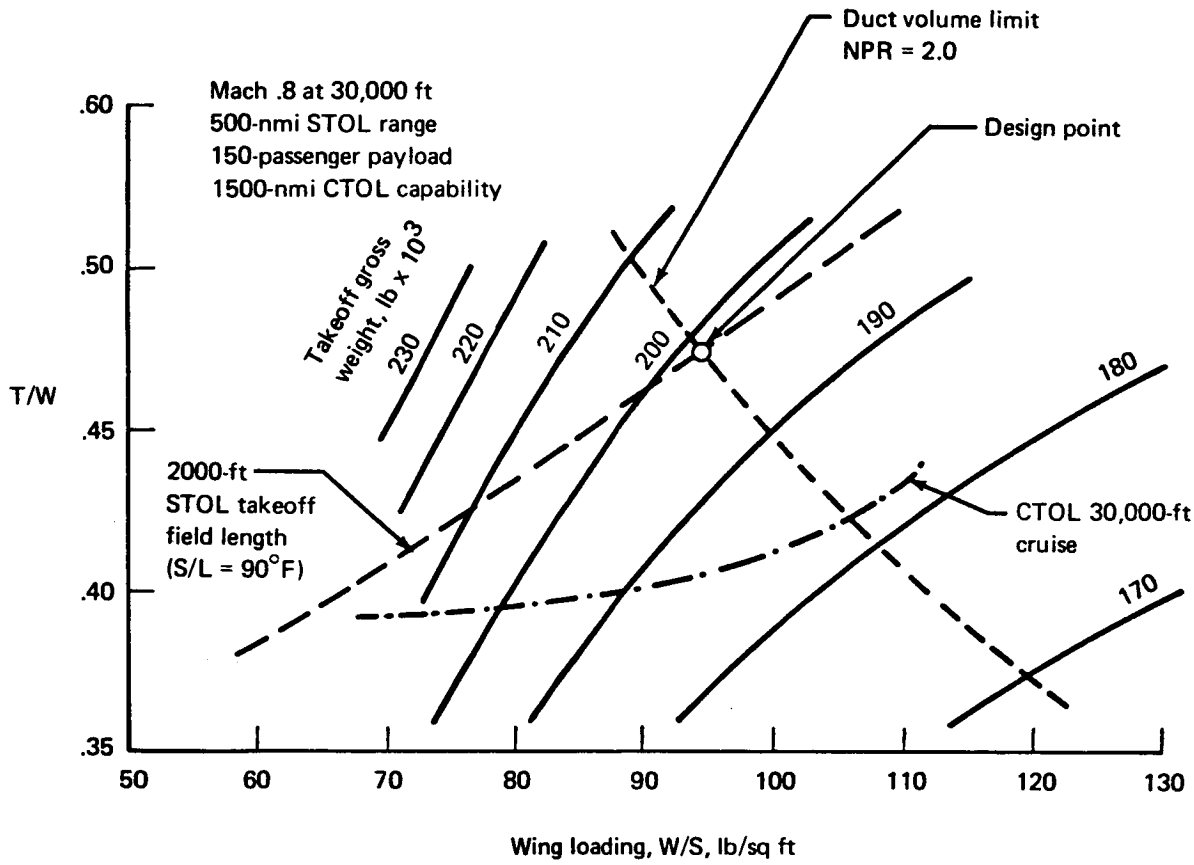

FIGURE 5-28.—AIRPLANE/ENGINE DESIGN RELATIONSHIP, TWO-STREAM AUGMENTOR WING, AR = 5.5, Λ = 30°

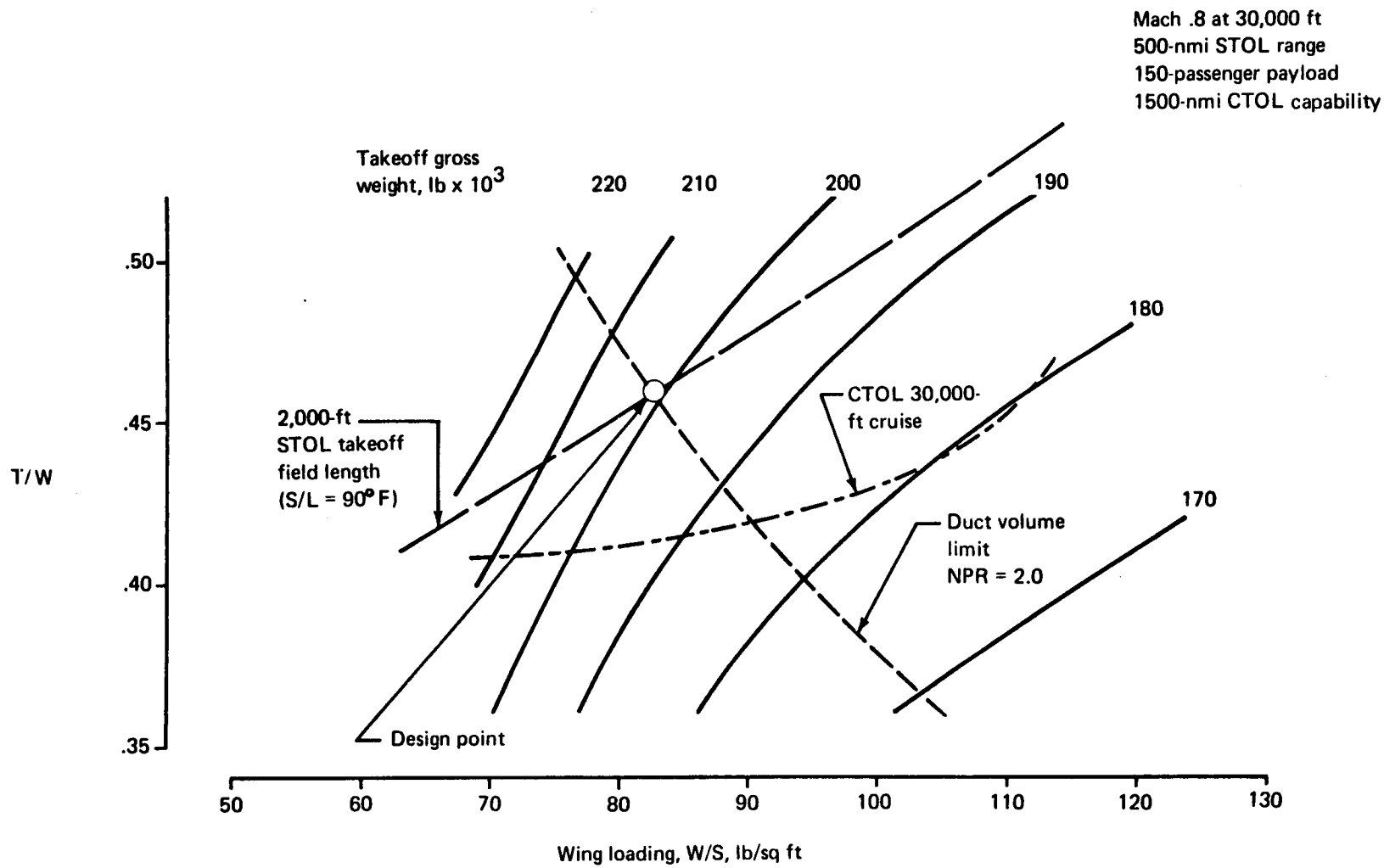

FIGURE 5-29.– AIRPLANE/ENGINE DESIGN RELATIONSHIP, TWO-STREAM AUGMENTOR WING, AR = 5.0, Λ = 20°

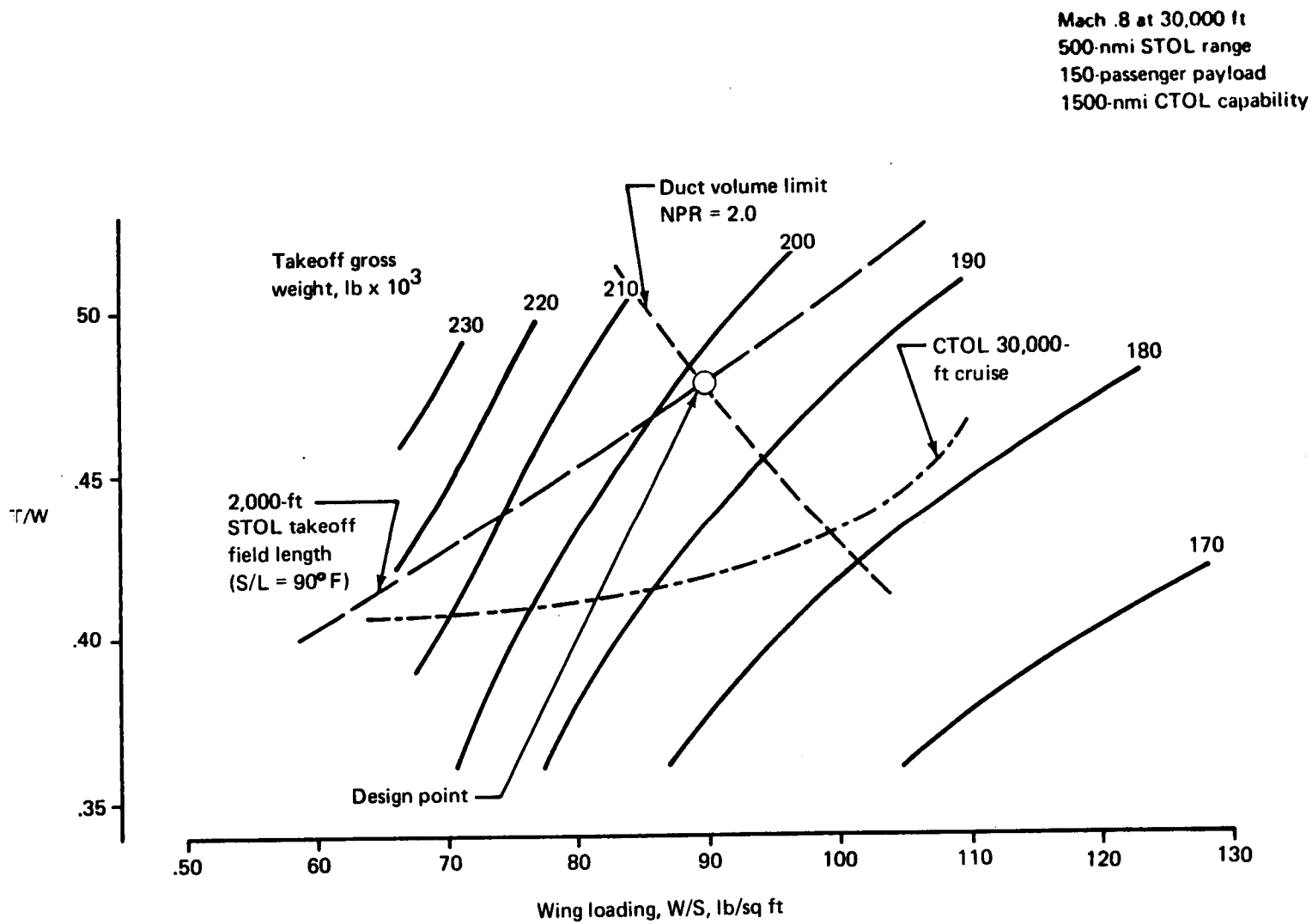

FIGURE 5-30.—AIRPLANE/ENGINE DESIGN RELATIONSHIP, TWO-STREAM AUGMENTOR WING, AR = 5.0, Λ = 25°

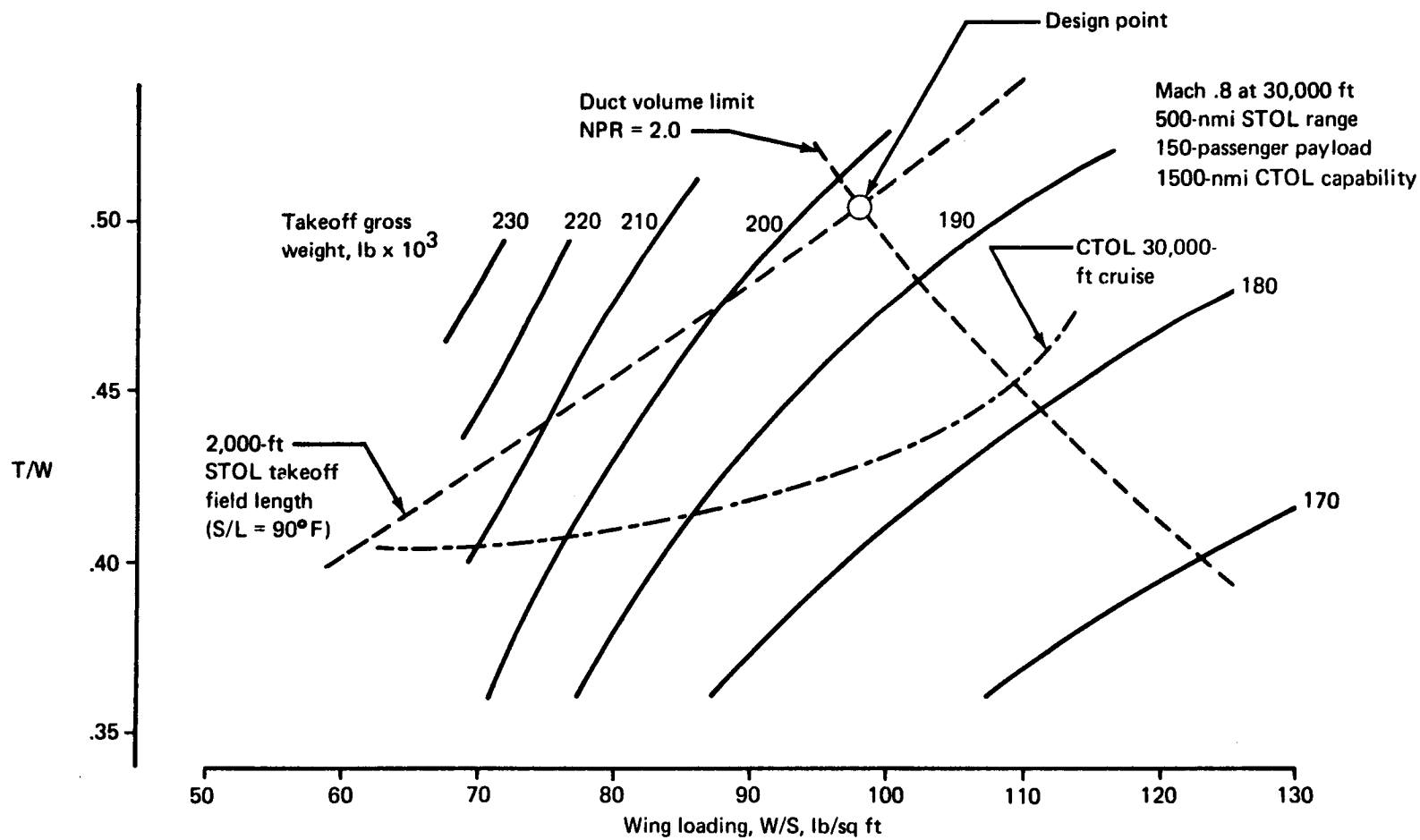

FIGURE 5-31.—AIRPLANE/ENGINE DESIGN RELATIONSHIP, TWO-STREAM AUGMENTOR WING, AR = 5.0, Λ = 30°

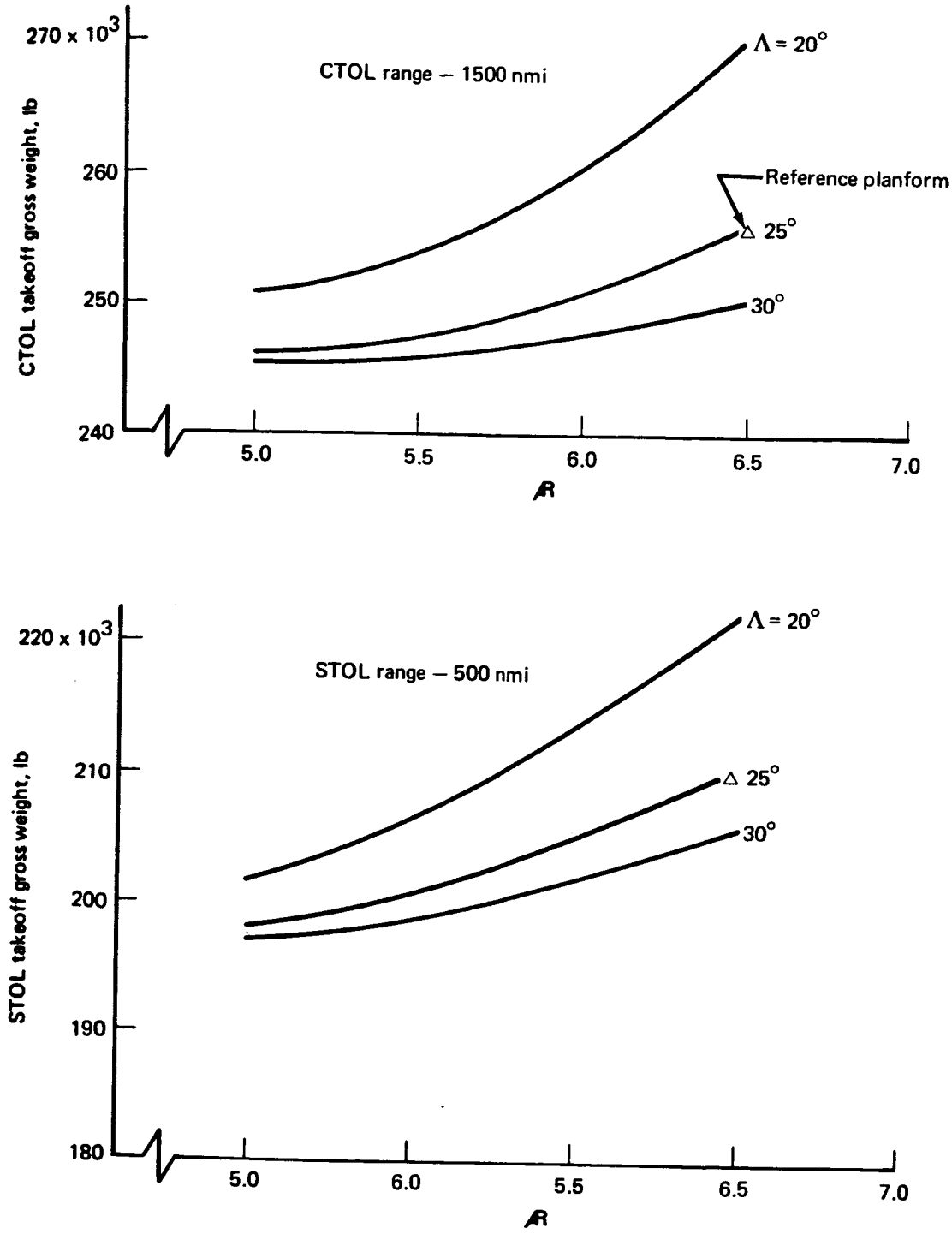

FIGURE 5-32.–PLANFORM EFFECTS ON MISSION TAKEOFF GROSS WEIGHT

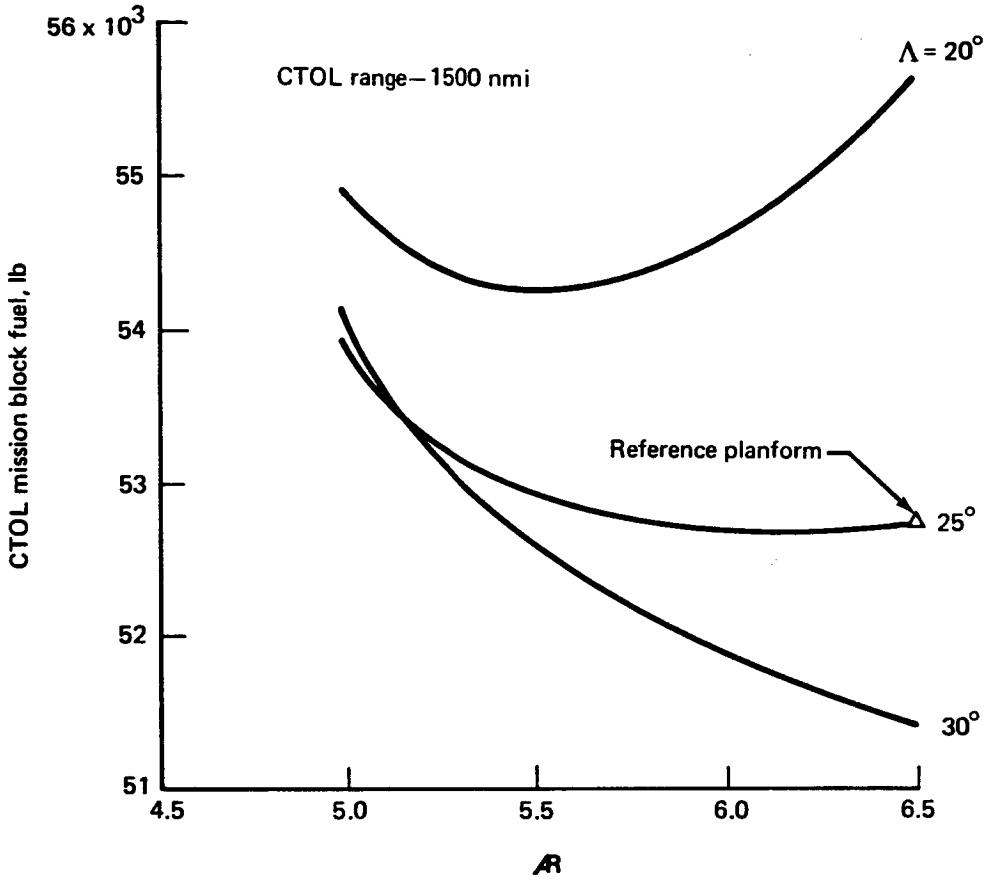

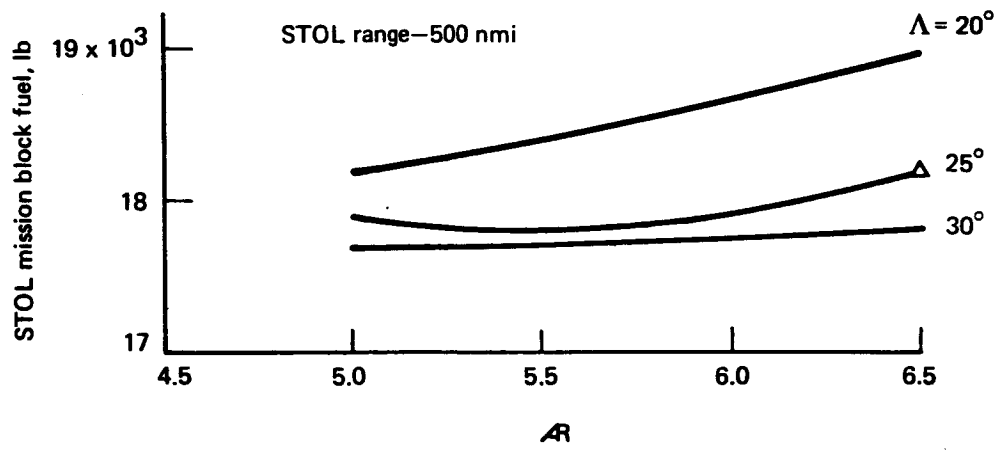

FIGURE 5-33.– PLANFORM EFFECTS ON BLOCK FUEL

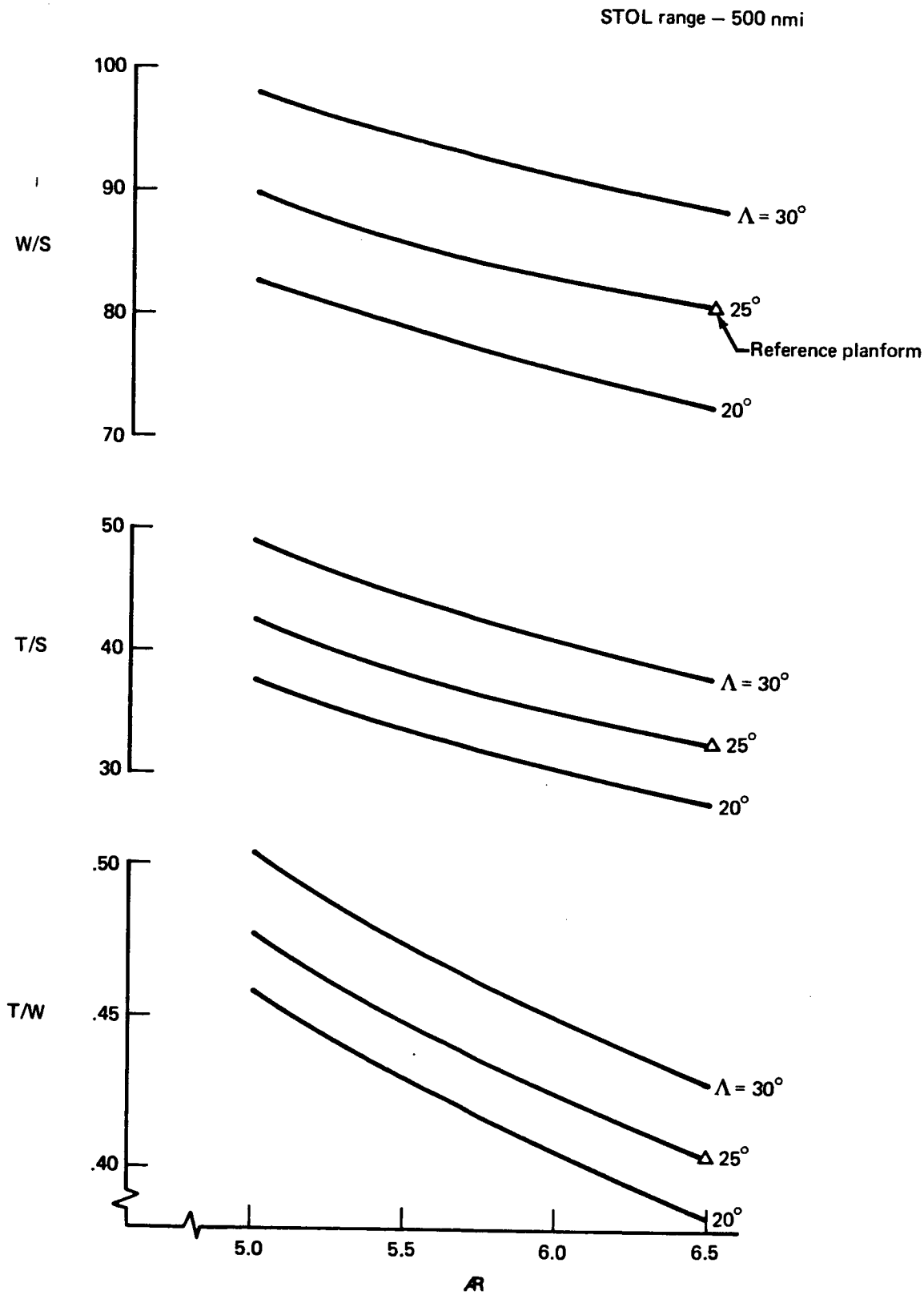

FIGURE 5-34.—PLANFORM EFFECTS ON WING AND THRUST LOADING—STOL MISSION

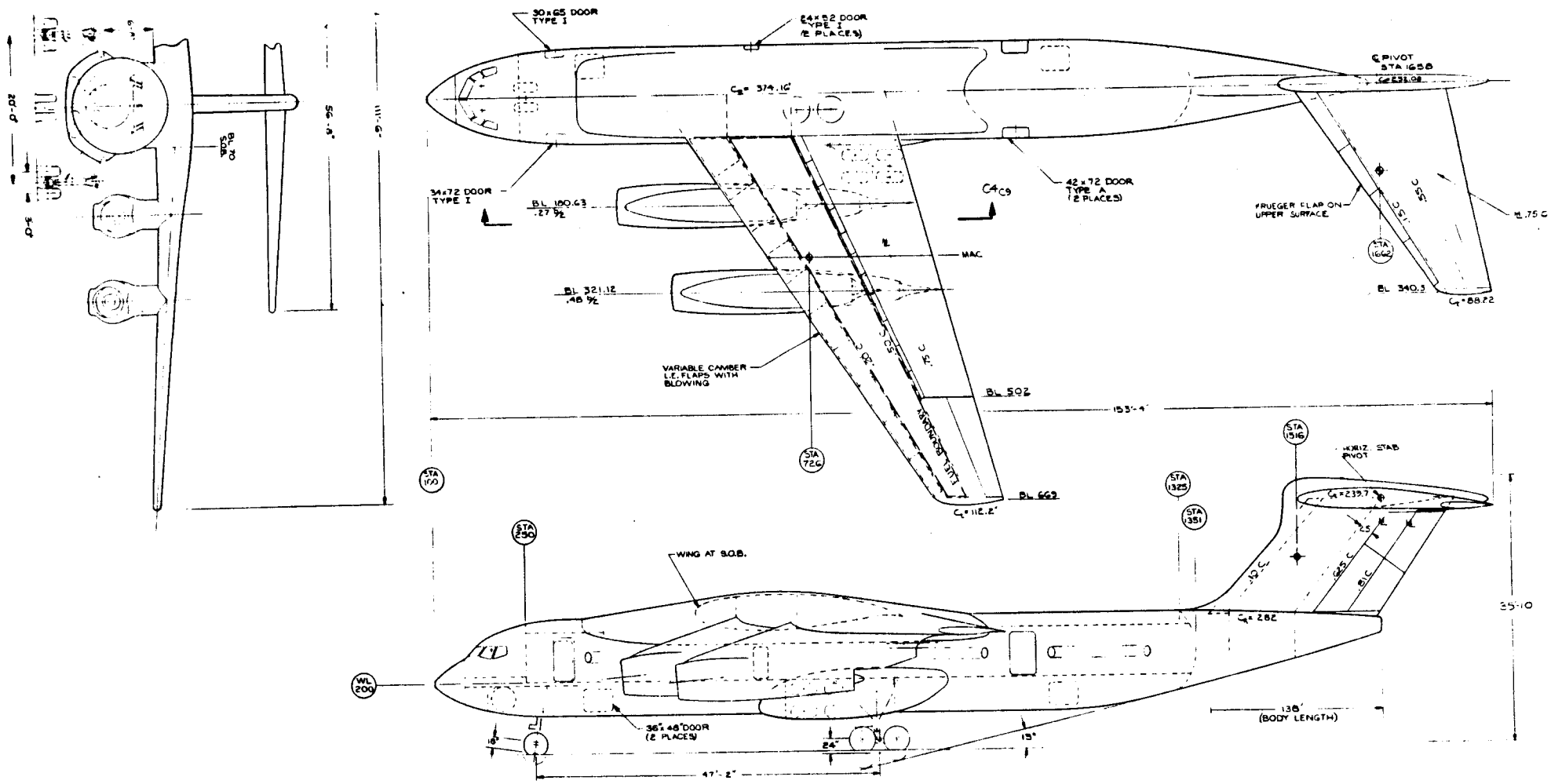

Ref dwg LO-AWNP-041

FIGURE 5-35.– MODEL 751-106 AUGMENTOR WING GENERAL ARRANGEMENT

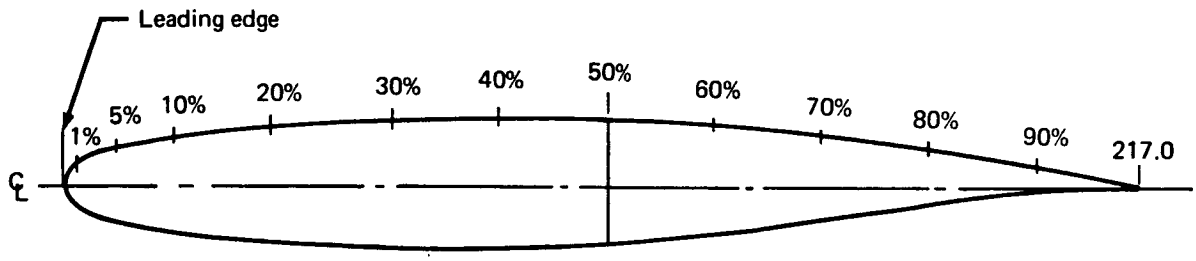

(modified TR-38)
t/c = 12%

FIGURE 5-36.—STREAMWISE WING SECTION AT 52% b/2

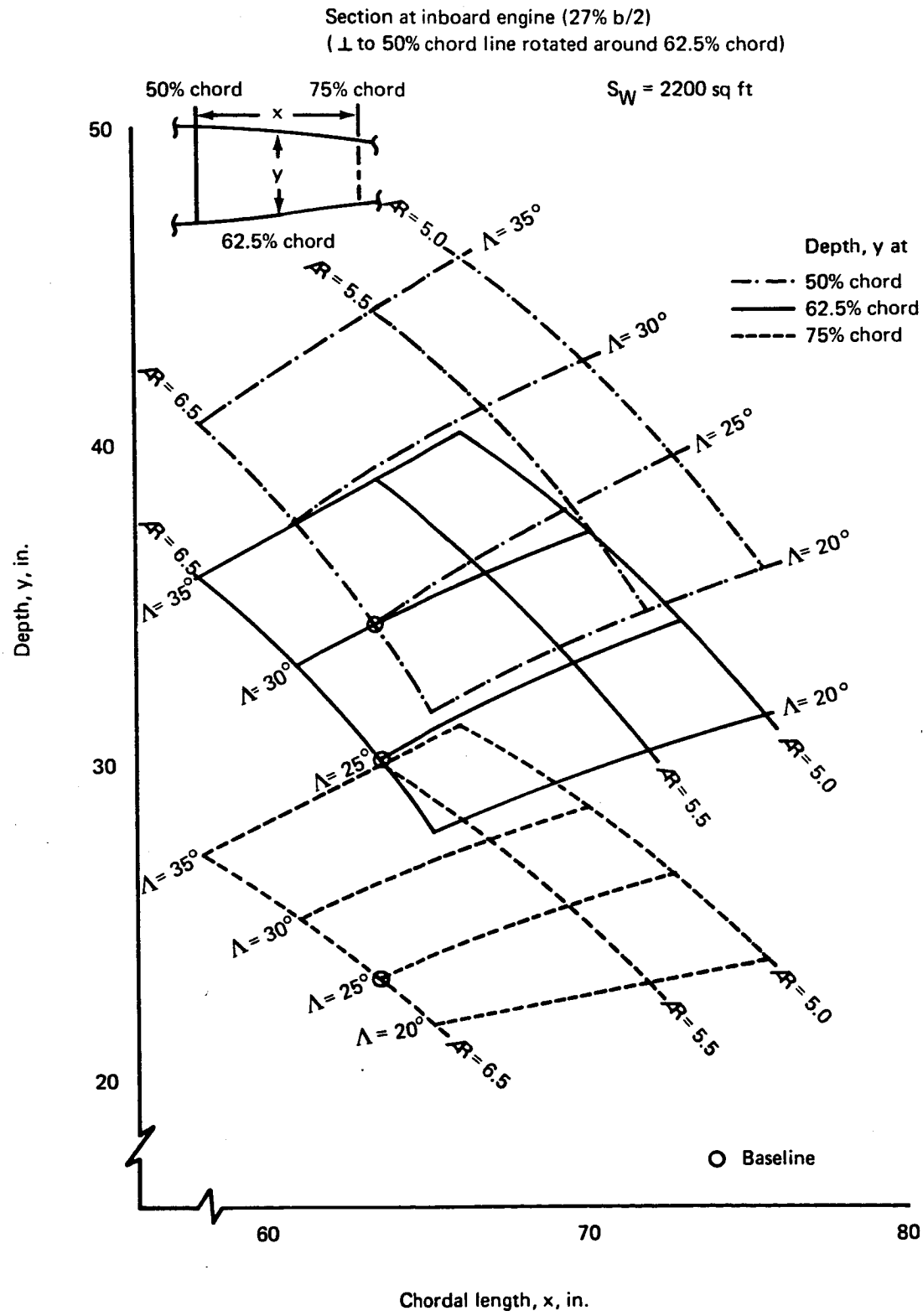

FIGURE 5-37.—AUGMENTOR DUCT INSTALLATION SPACE

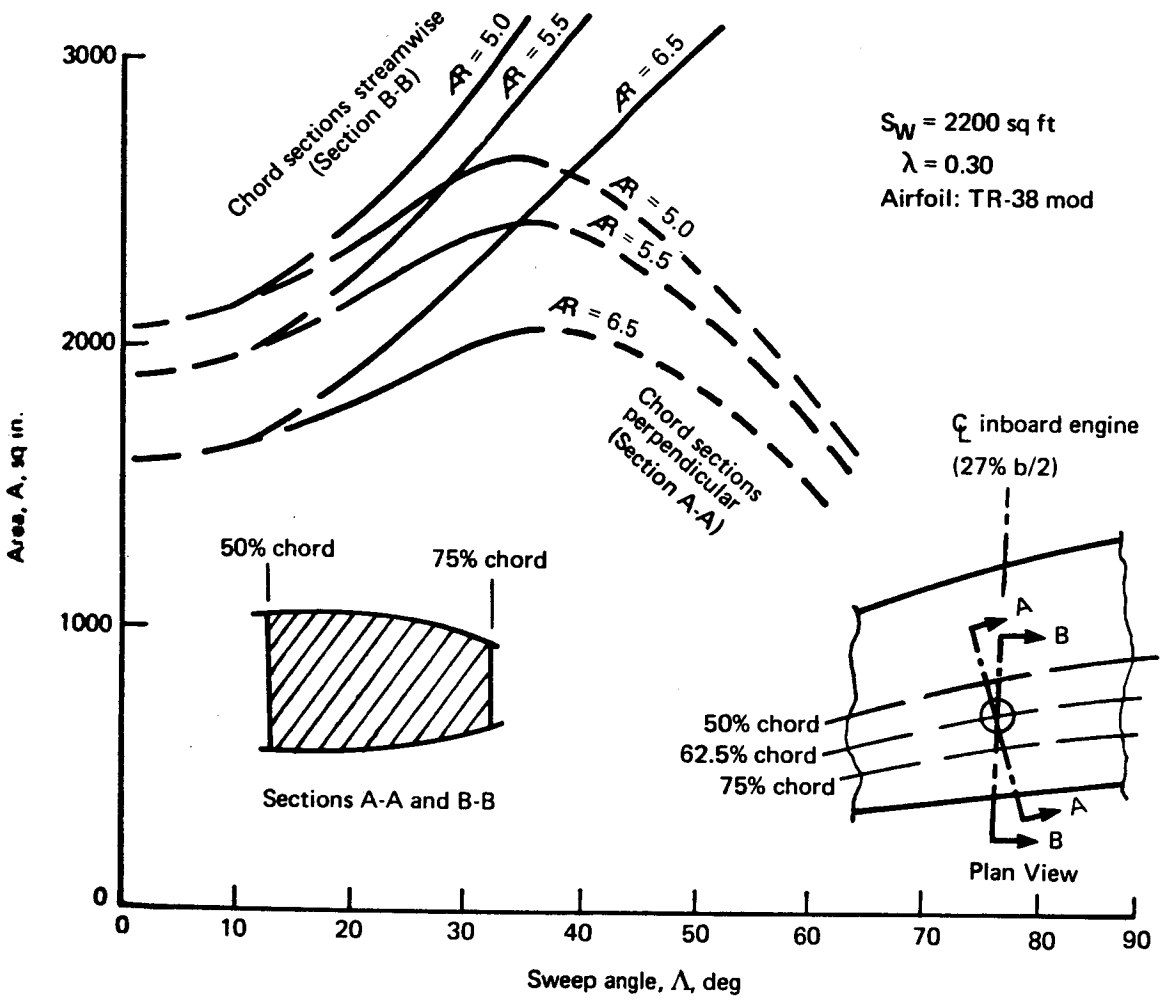

FIGURE 5-38.—AUGMENTOR DUCT INSTALLATION SPACE

Independent Duct System—Section at Inboard Engine

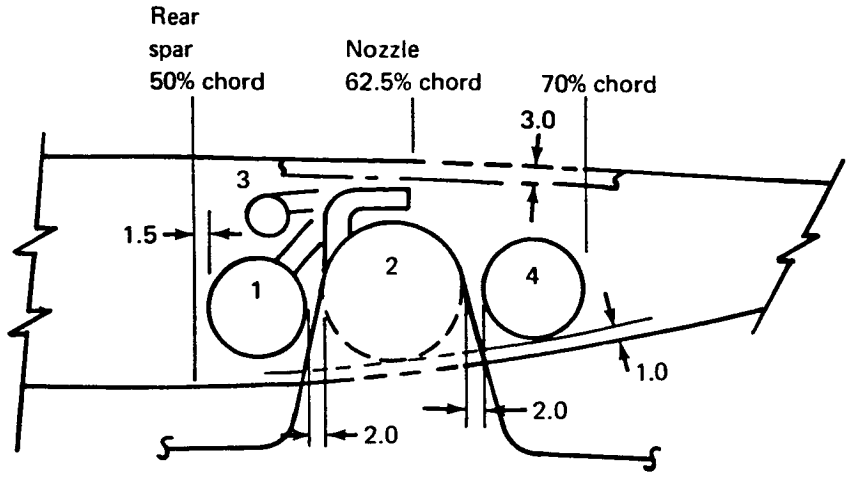

Plenum Duct System—Section at Inboard Engine

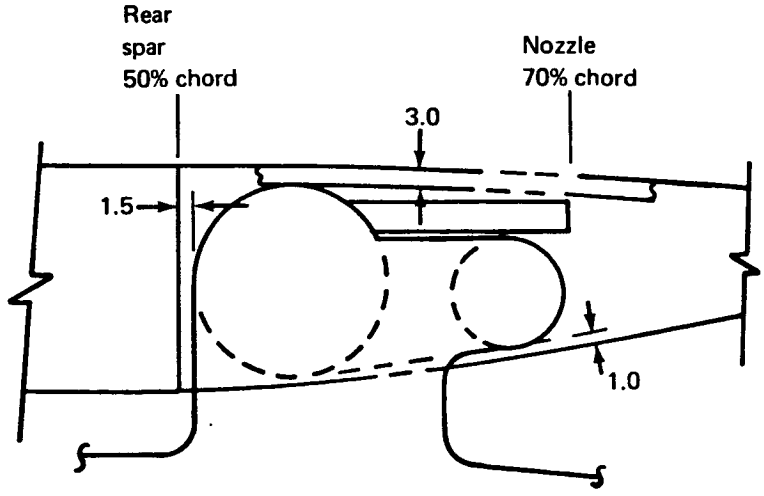

FIGURE 5-39.—DUCT SYSTEMS

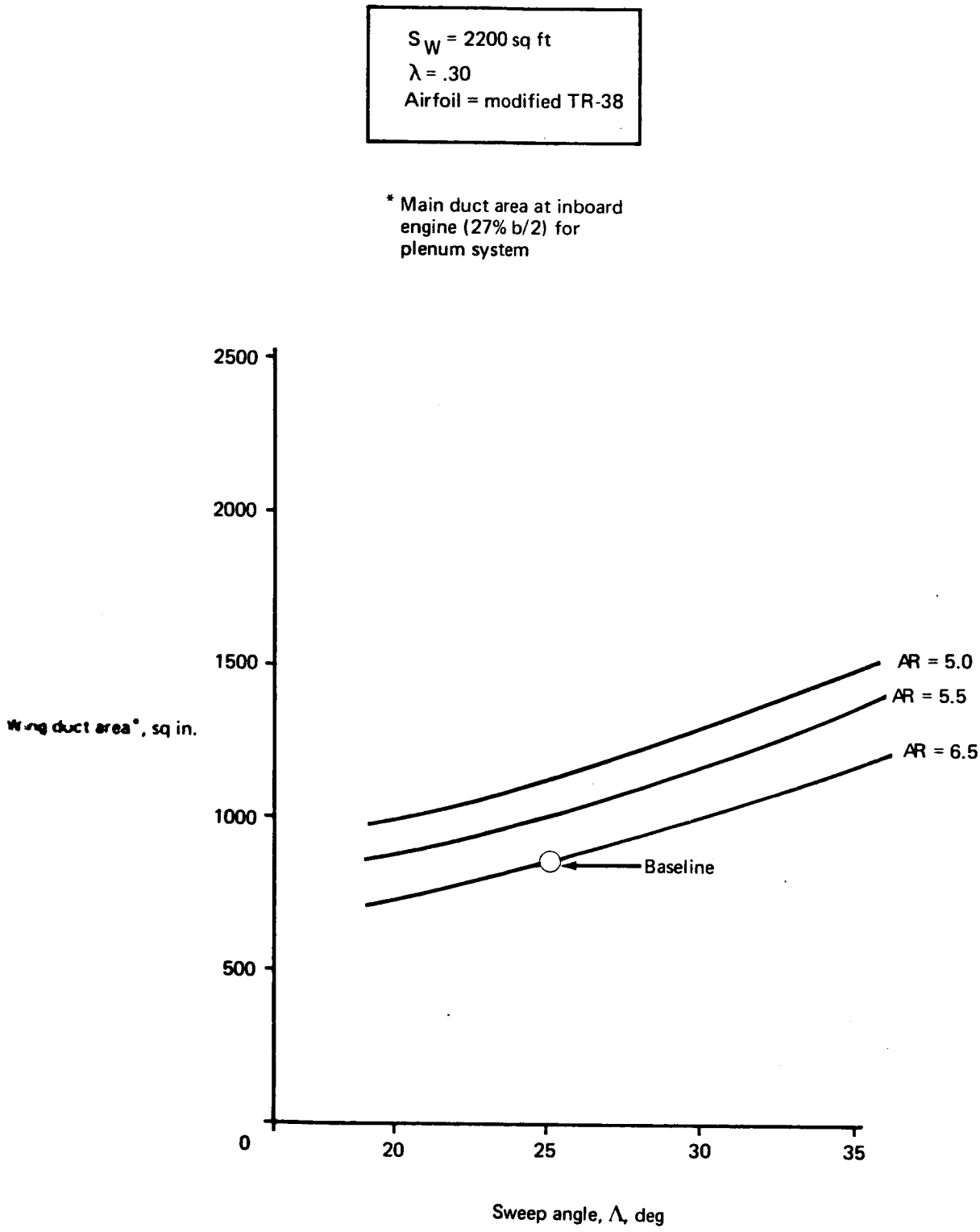

FIGURE 5-40.–VARIATION OF AVAILABLE DUCT AREA WITH WING PLANFORM

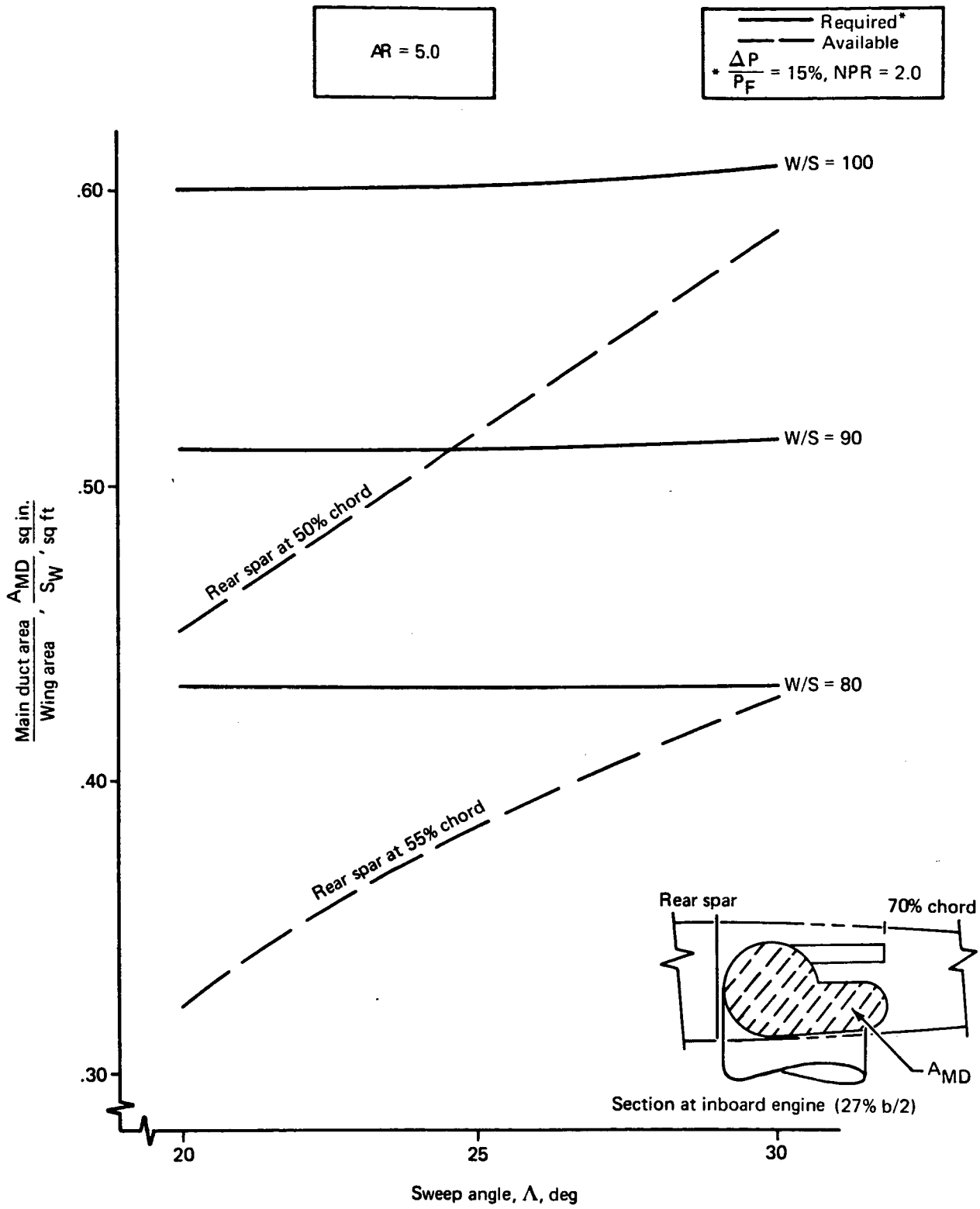

FIGURE 5-41.– REQUIRED AND AVAILABLE DUCT AREA–EFFECT OF REAR SPAR LOCATION, PLENUM SUBDUCT SYSTEM

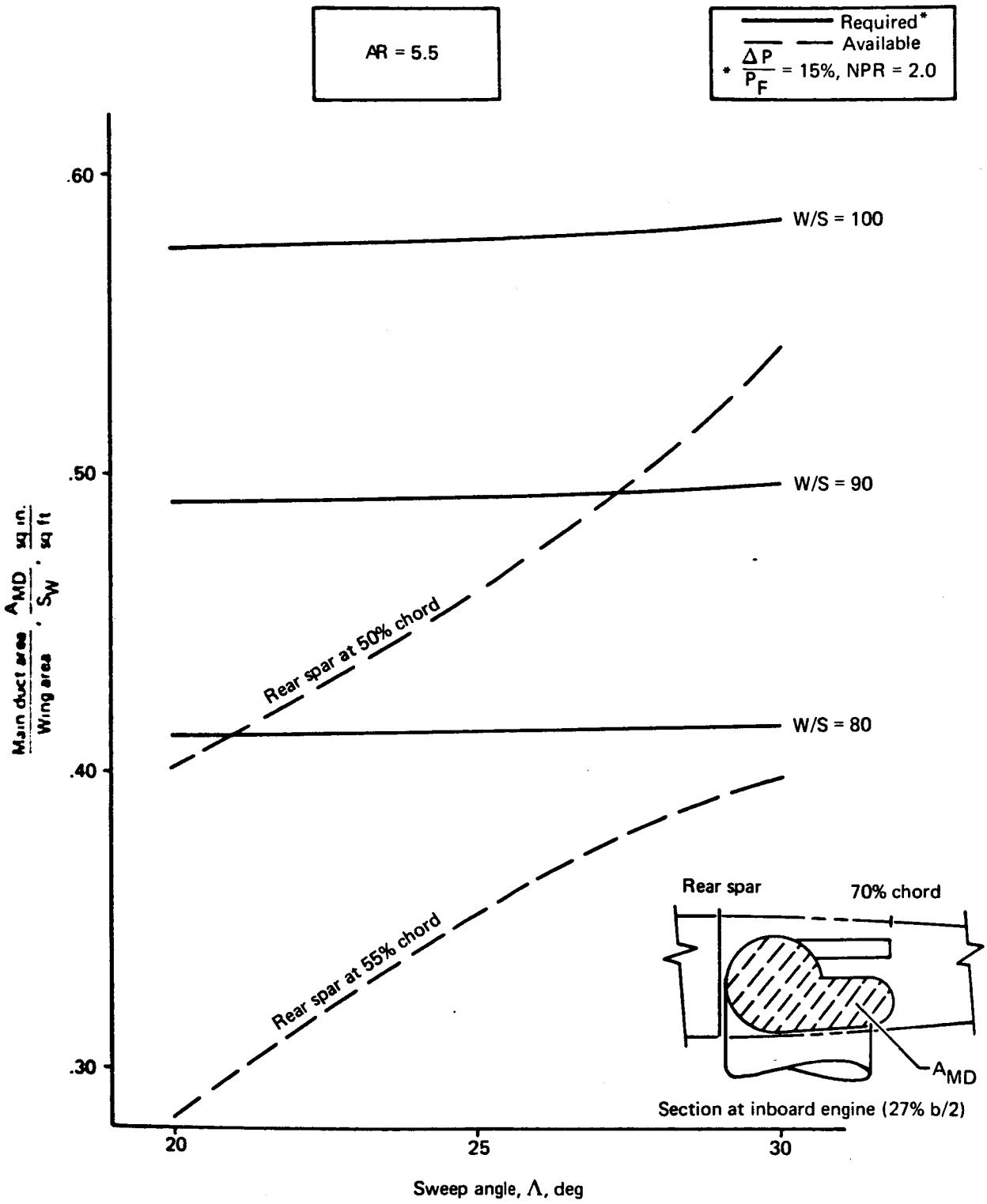

FIGURE 5-42.– REQUIRED AND AVAILABLE DUCT AREA–EFFECT OF REAR SPAR LOCATION, PLENUM SUBDUCT SYSTEM

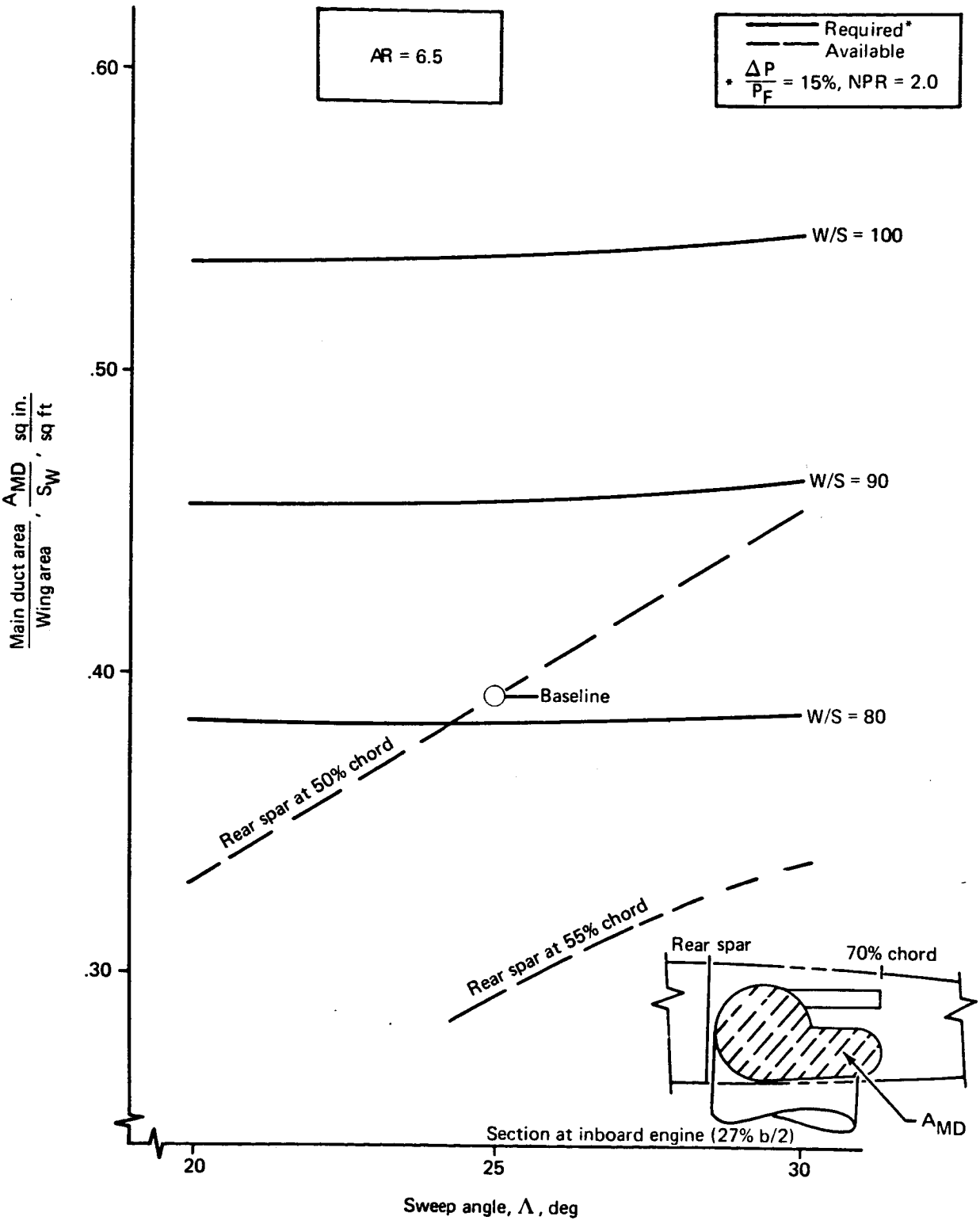

FIGURE 5-43.– REQUIRED AND AVAILABLE DUCT AREA–EFFECT OF REAR SPAR LOCATION, PLENUM SUBDUCT SYSTEM

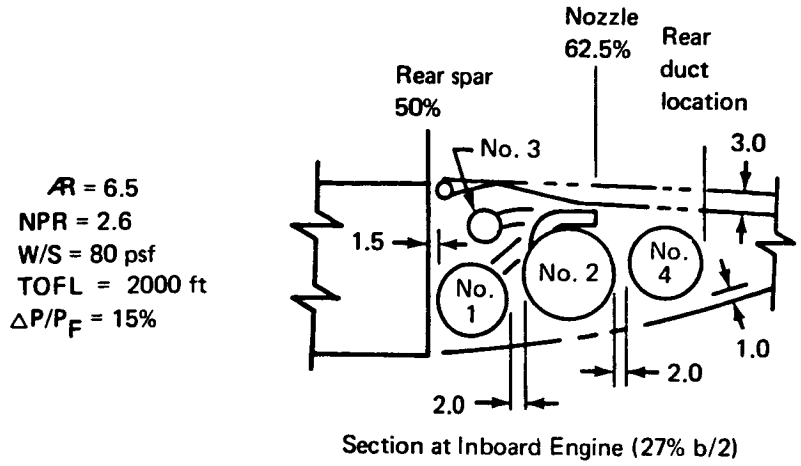

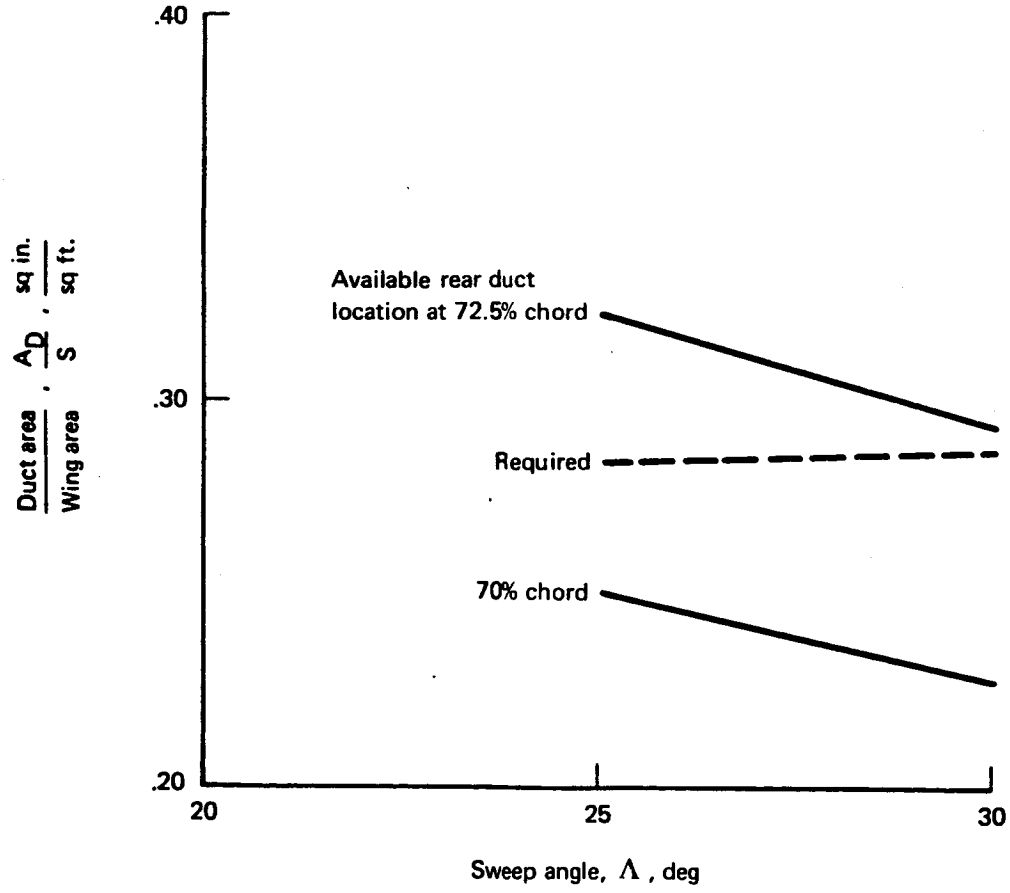

FIGURE 5-44.–REQUIRED AND AVAILABLE DUCT AREA–EFFECT OF REAR DUCT LOCATION, INDEPENDENT DUCT SYSTEM

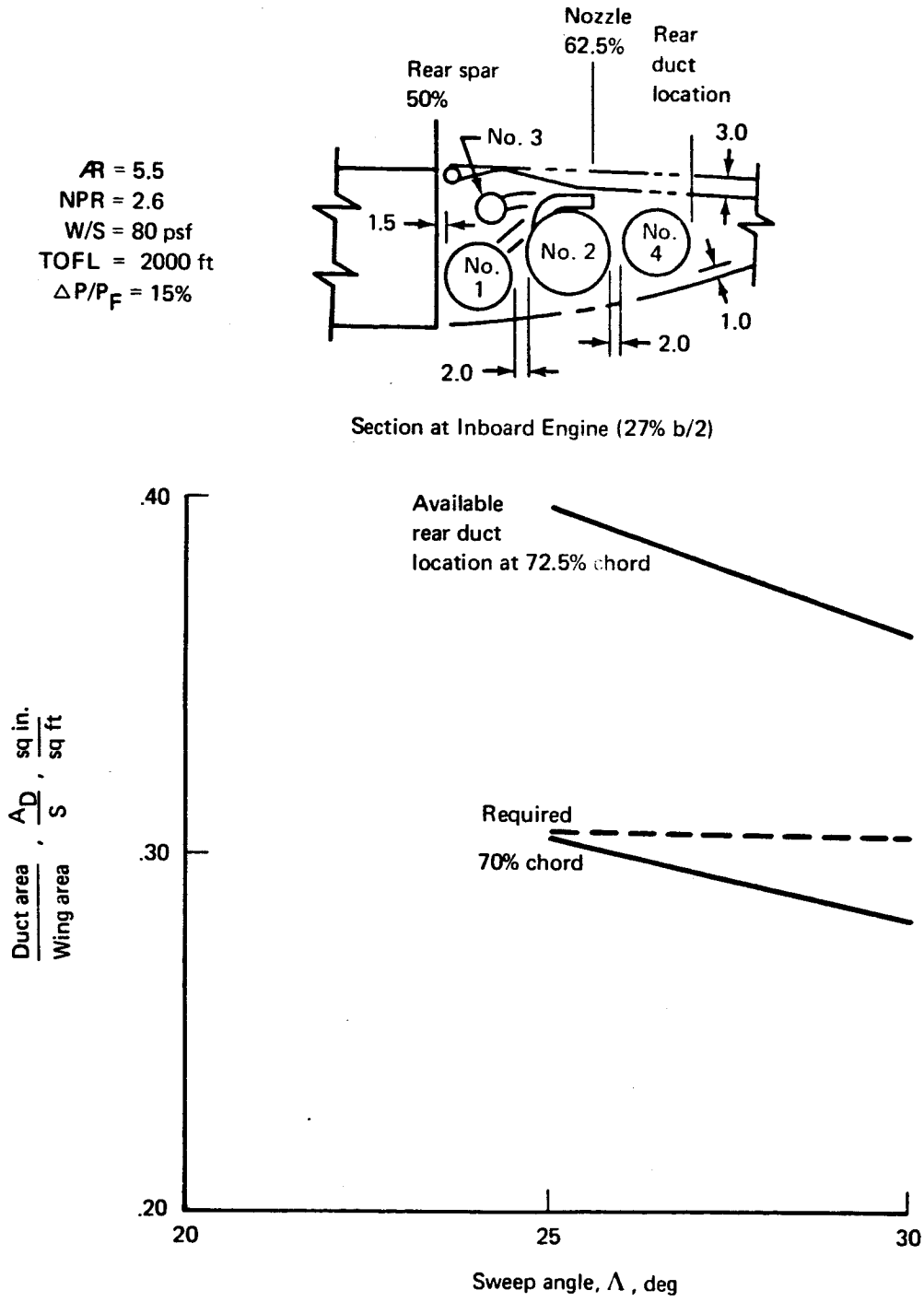

FIGURE 5-45.—REQUIRED AND AVAILABLE DUCT AREA—EFFECT OF REAR DUCT LOCATION, INDEPENDENT DUCT SYSTEM

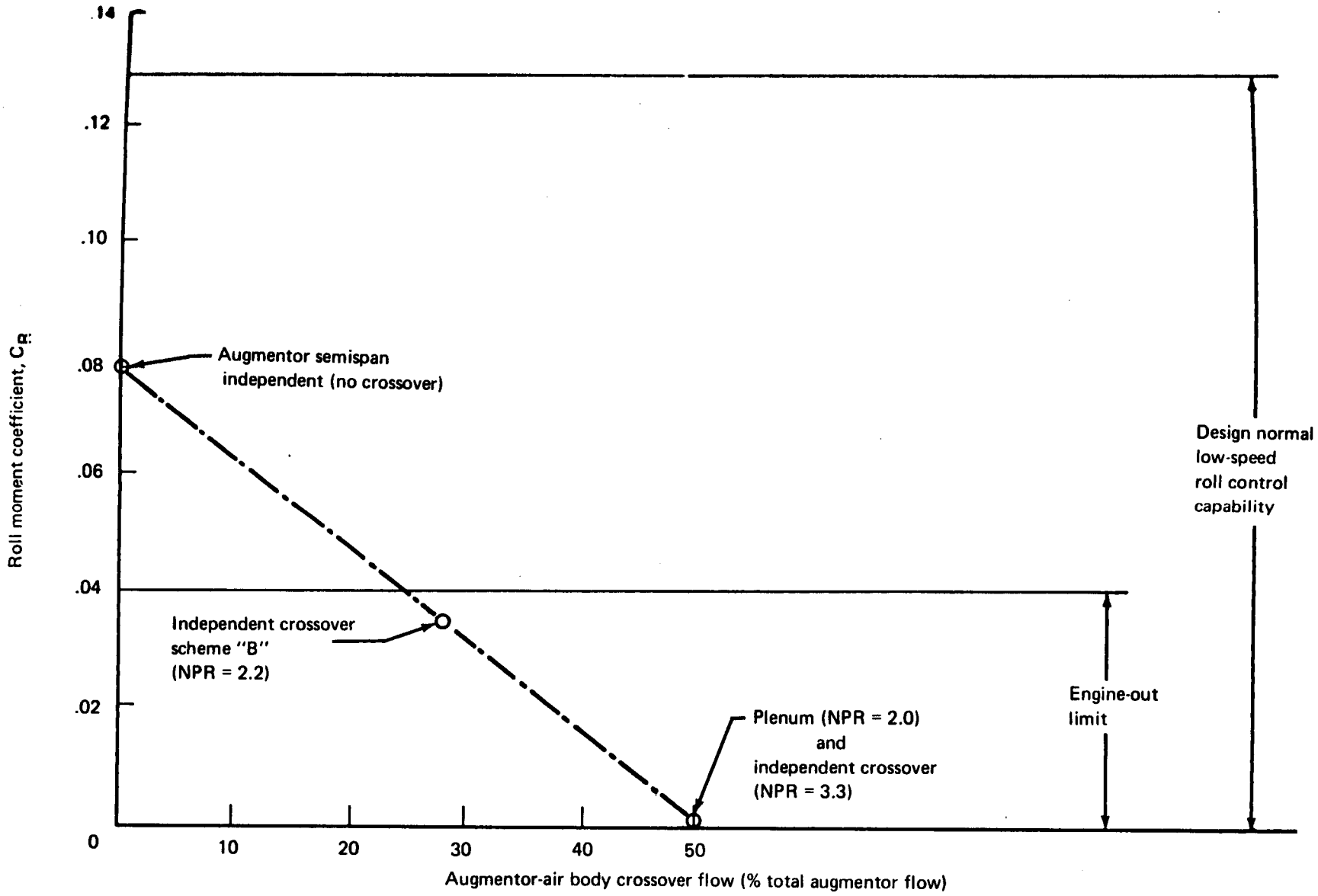

FIGURE 5-46.—ENGINE-OUT ROLL MOMENT COMPARISON

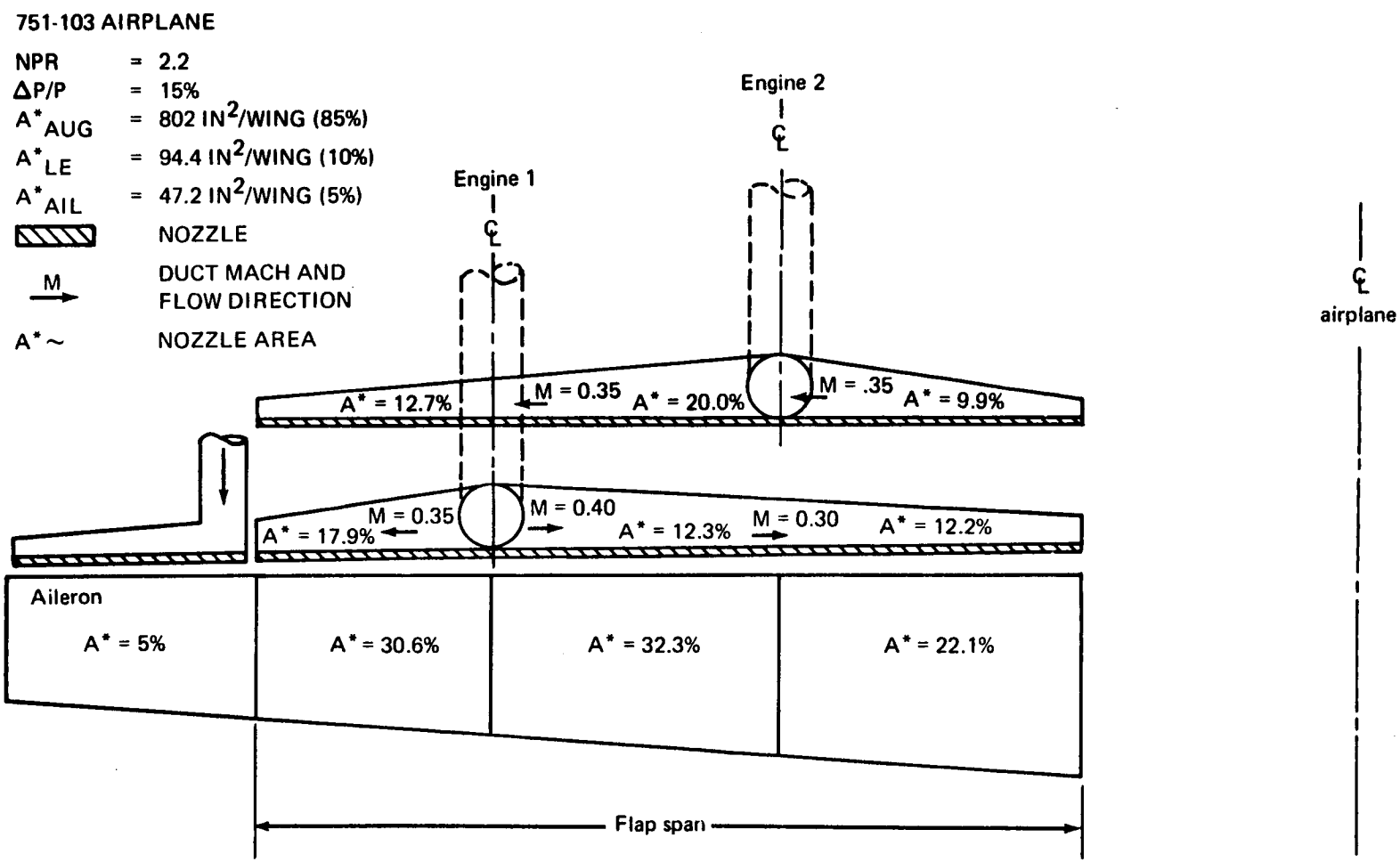

FIGURE 5-47.– INDEPENDENT DUCT SYSTEM SEMISPAN WITH NO CROSS-BODY FLOW

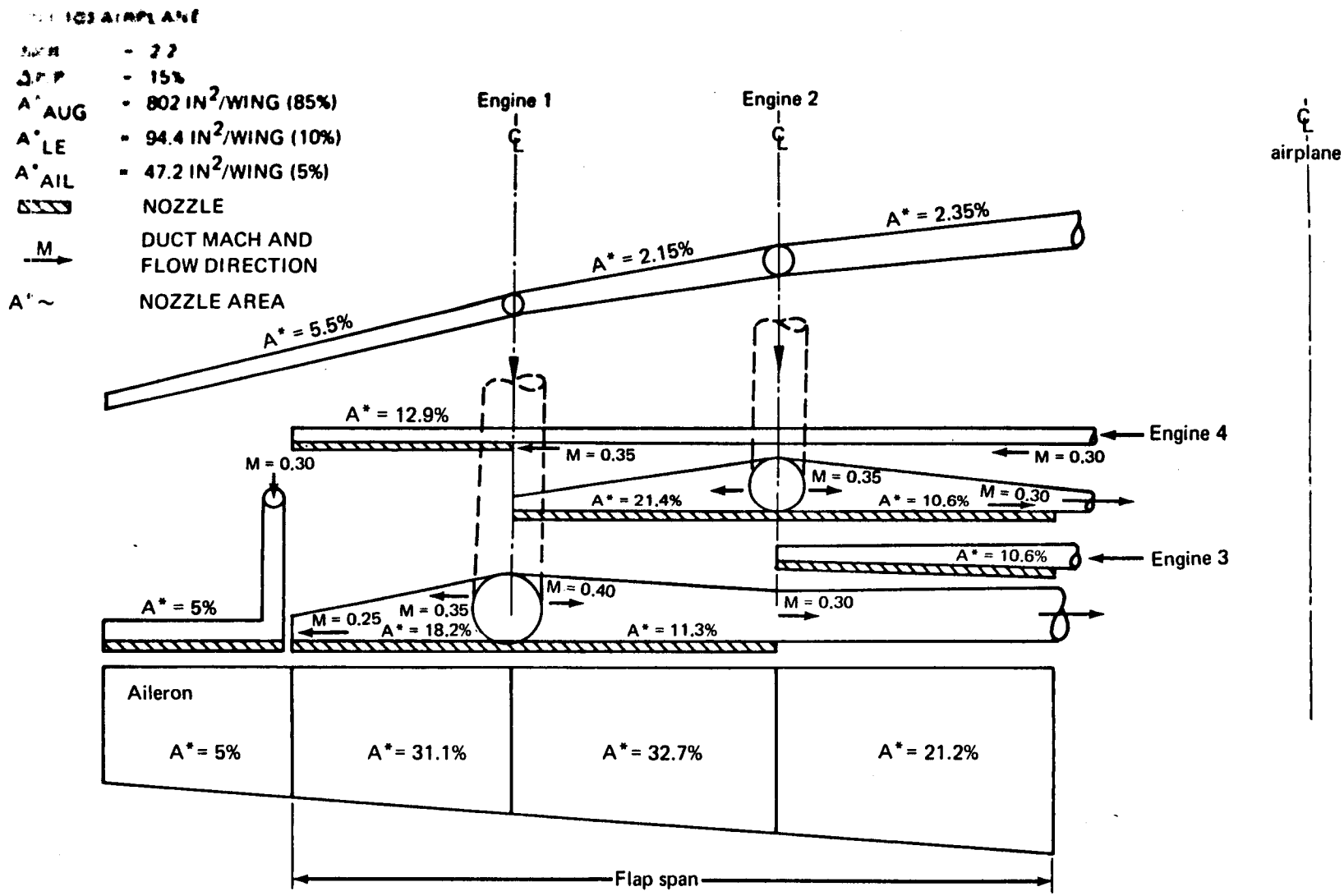

FIGURE 5-48.– INDEPENDENT DUCT SYSTEM, 27.5% BODY CROSSFLOW

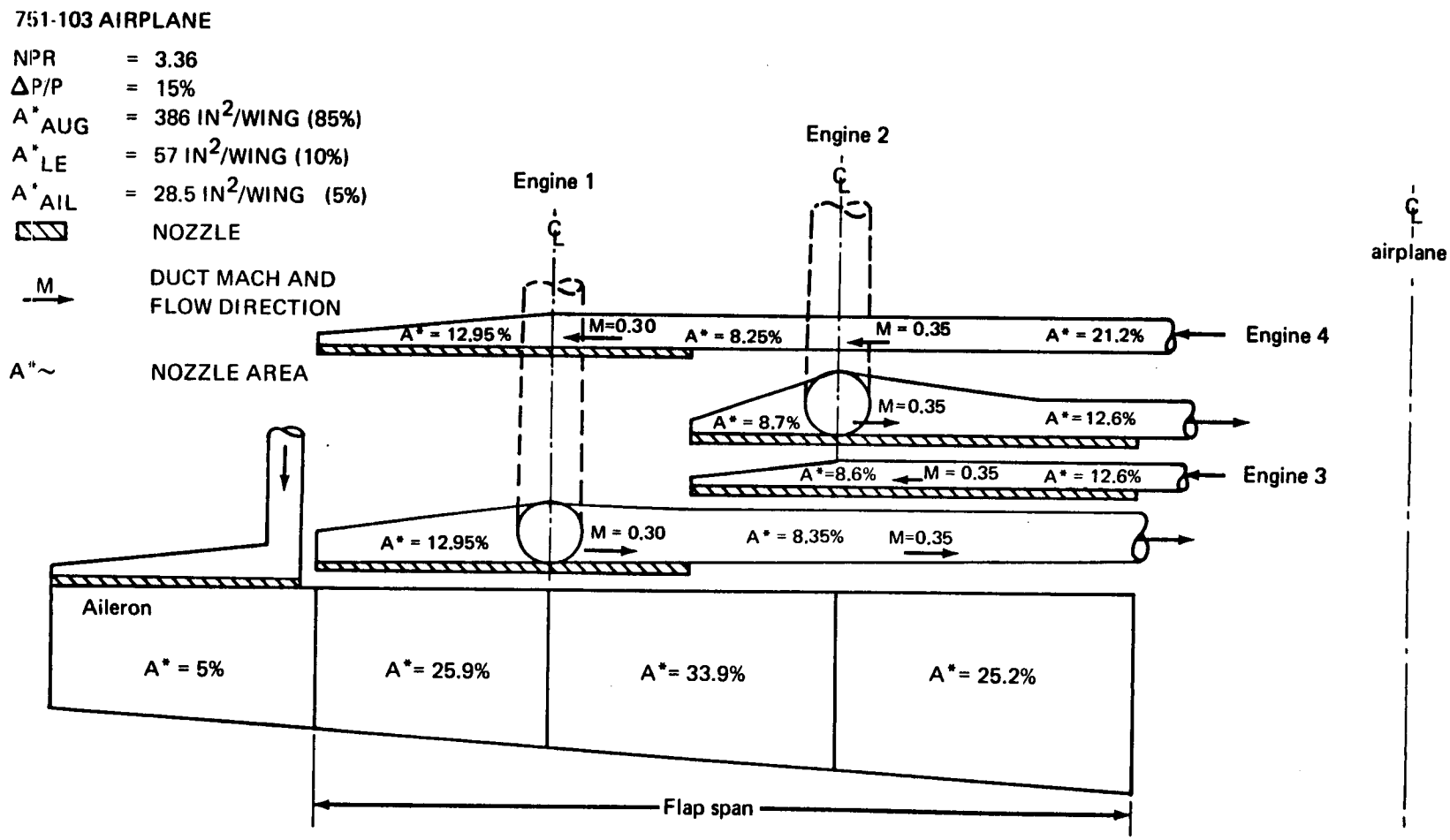

FIGURE 5-49.—INDEPENDENT DUCT SYSTEM, 50% BODY CROSSFLOW

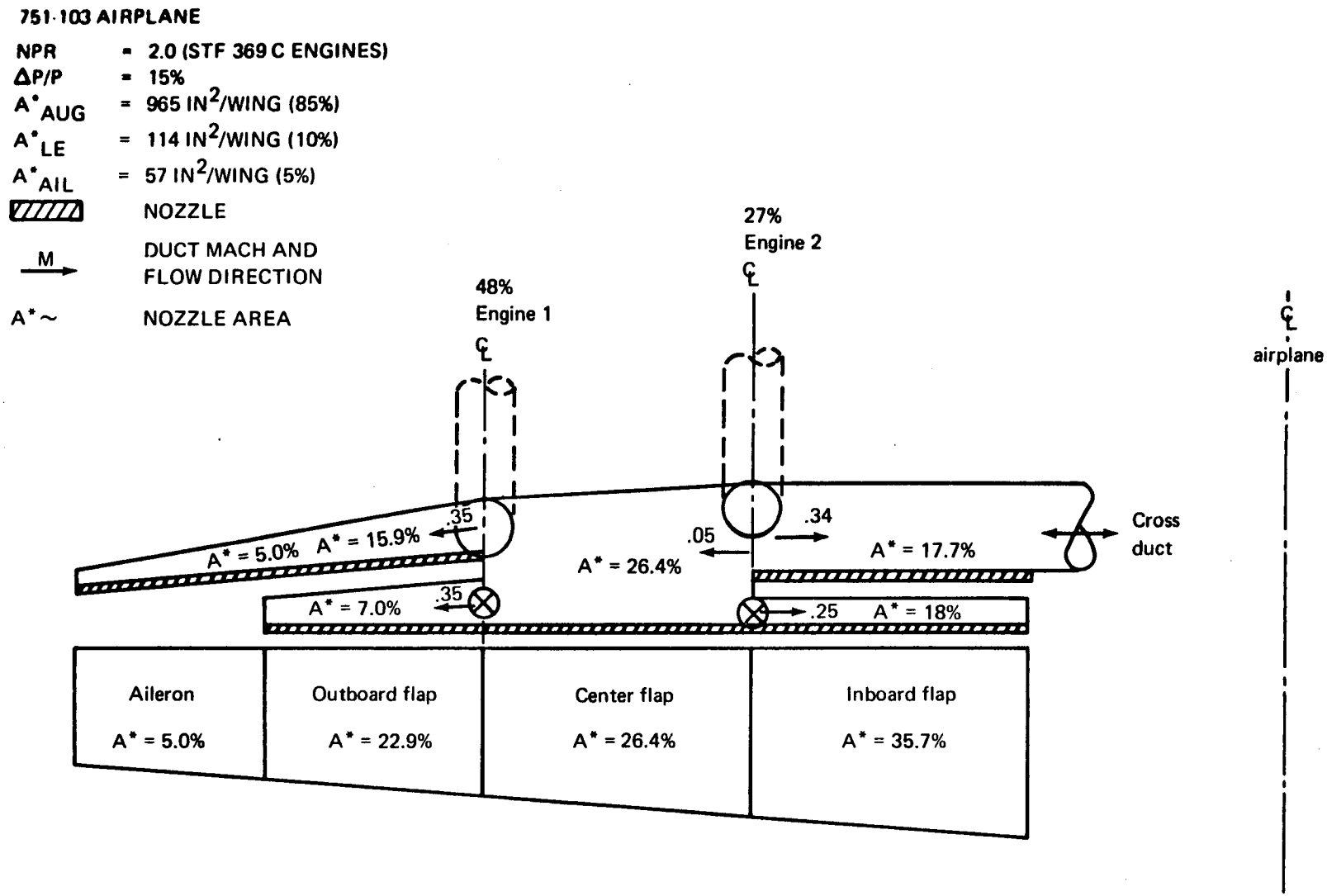

FIGURE 5-50.– INTERCONNECTED DUCT (PLENUM) SYSTEM

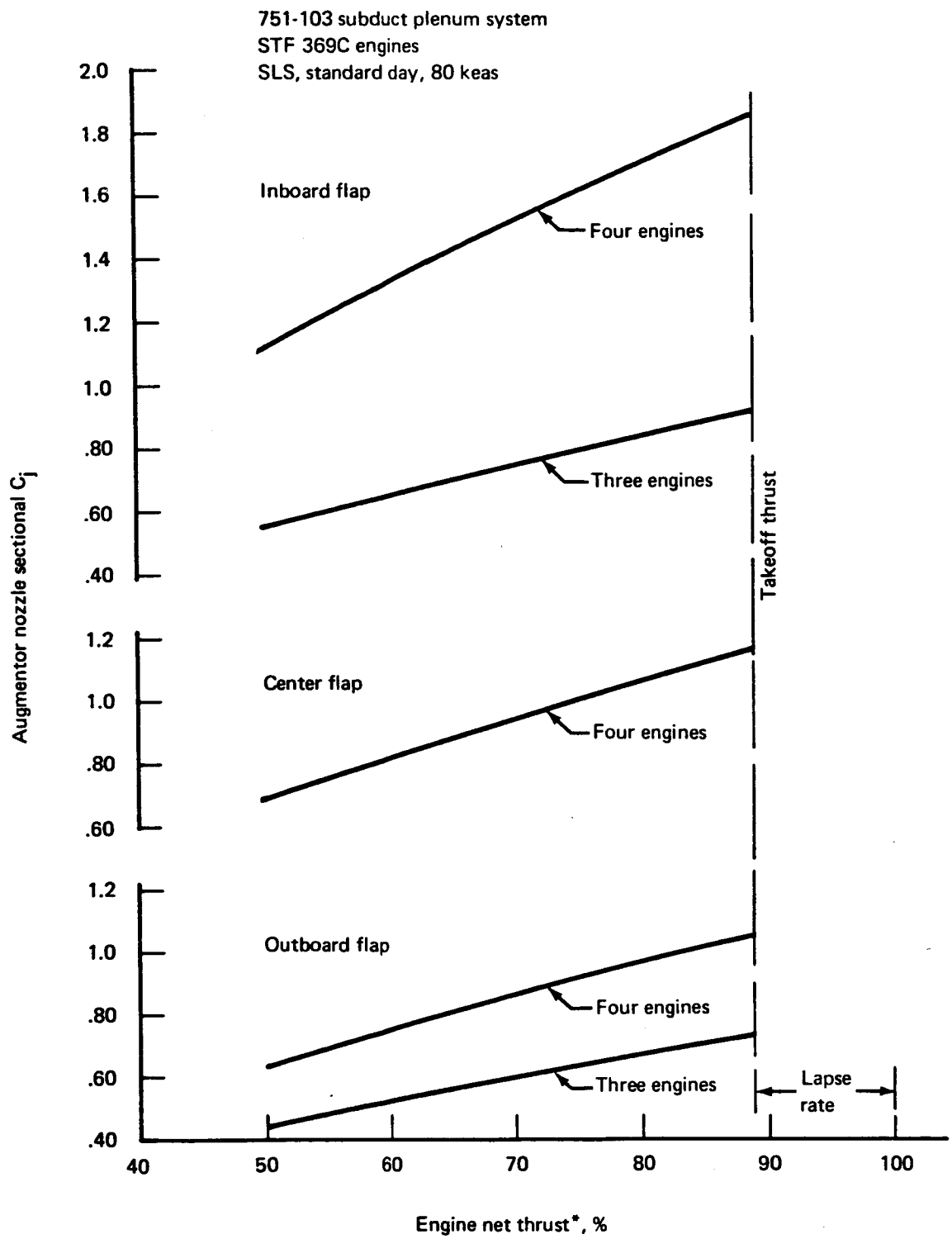

*Net sea level static installed thrust

FIGURE 5-51.—AUGMENTOR NOZZLE MOMENTUM COEFFICIENT

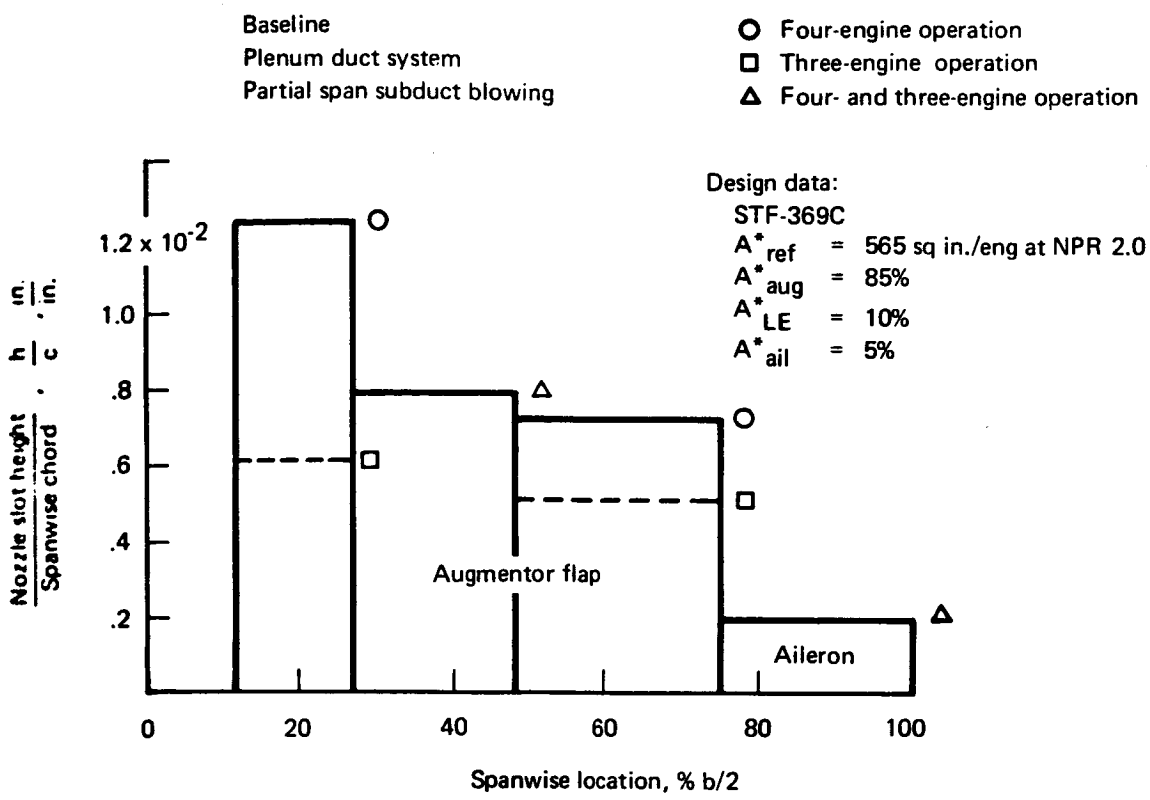

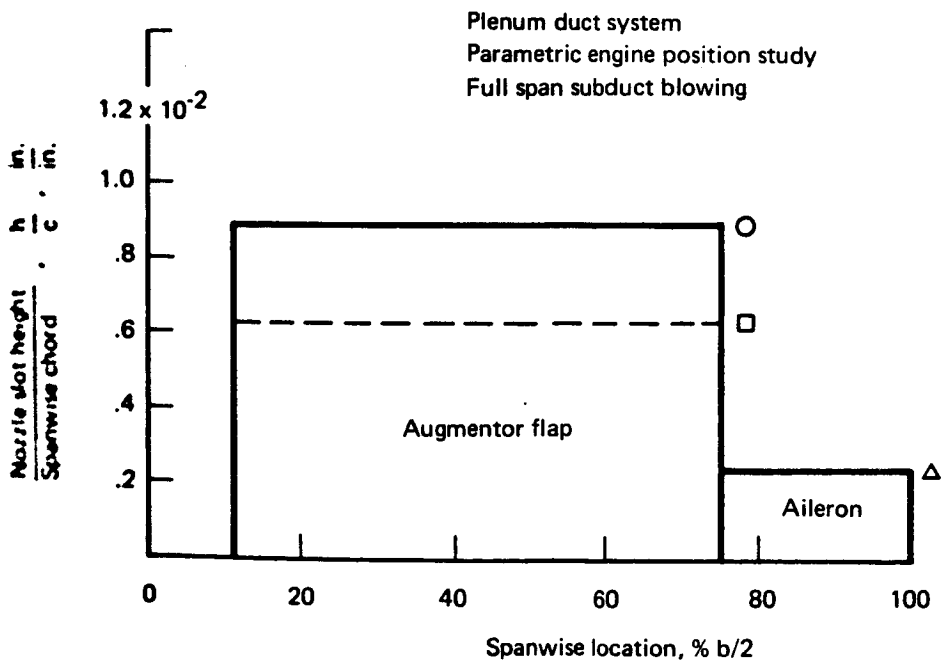

FIGURE 5-52.– AUGMENTOR NOZZLE AIR DISTRIBUTION COMPARISON

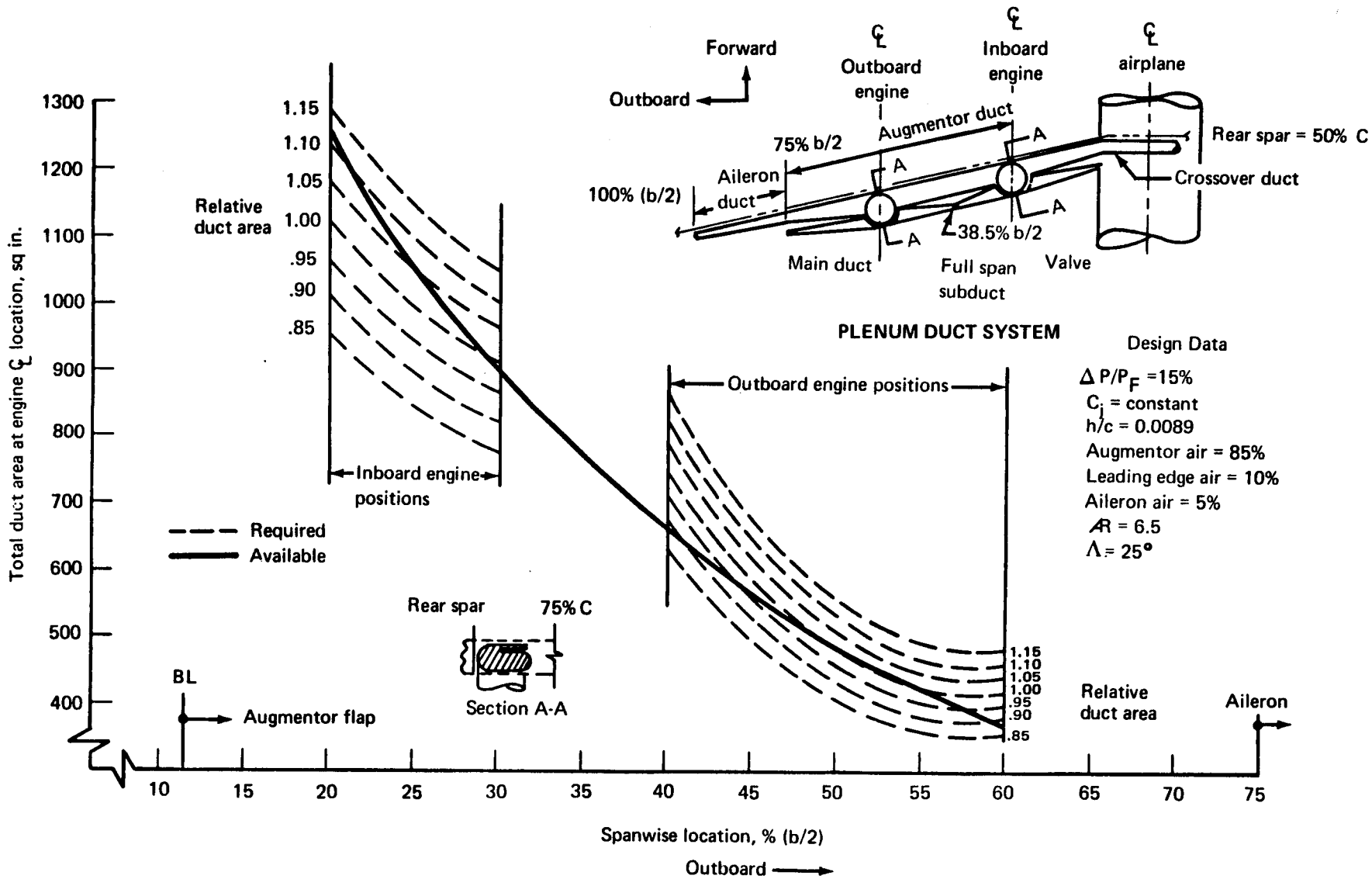

FIGURE 5-53.–PLENUM DUCT SYSTEM ENGINE POSITION STUDY

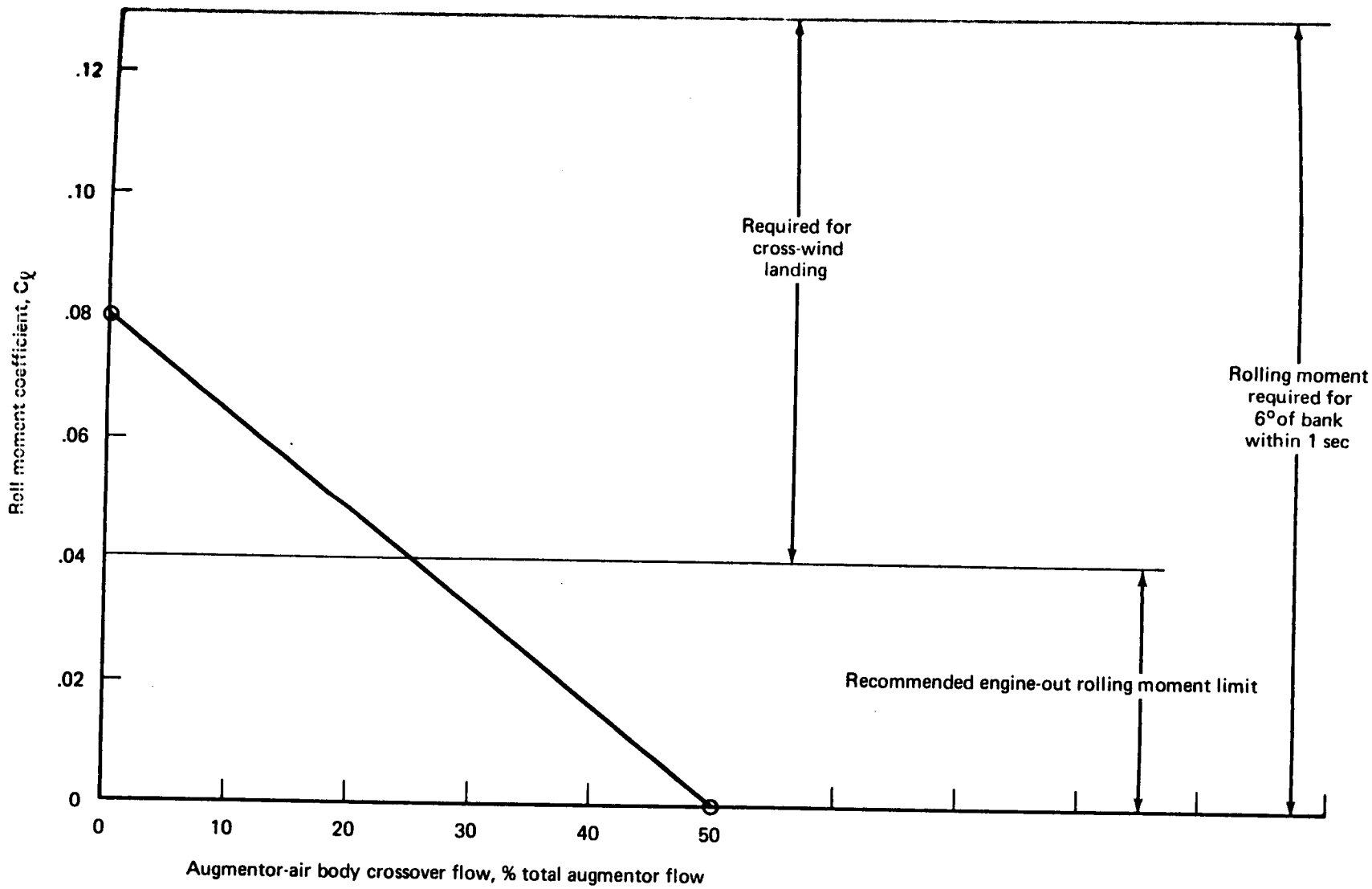

FIGURE 5-54.—ENGINE-OUT ROLL MOMENT

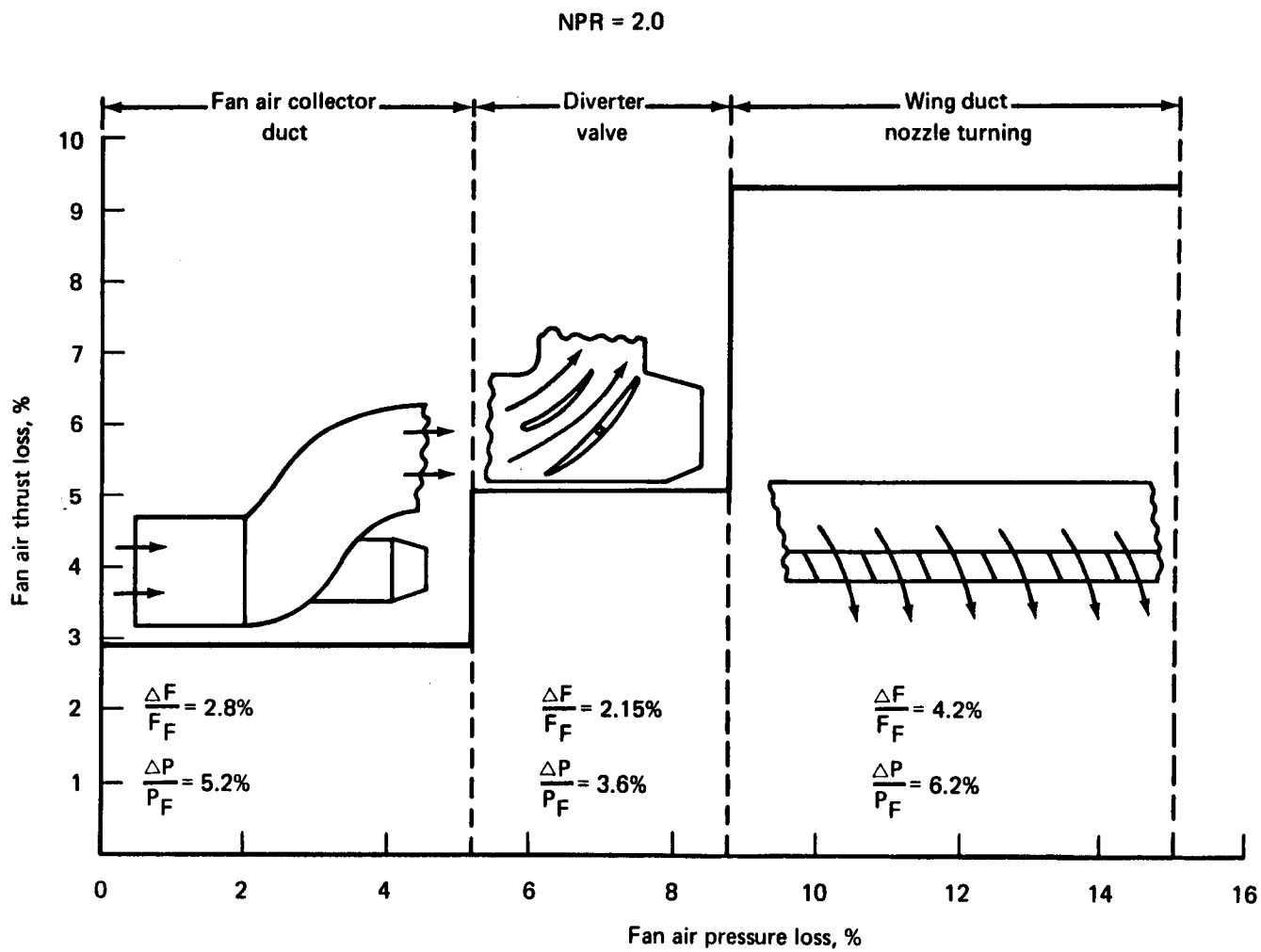

FIGURE 5-55.—AUGMENTOR WING AIRPLANE DUCT PRESSURE LOSS DISTRIBUTION

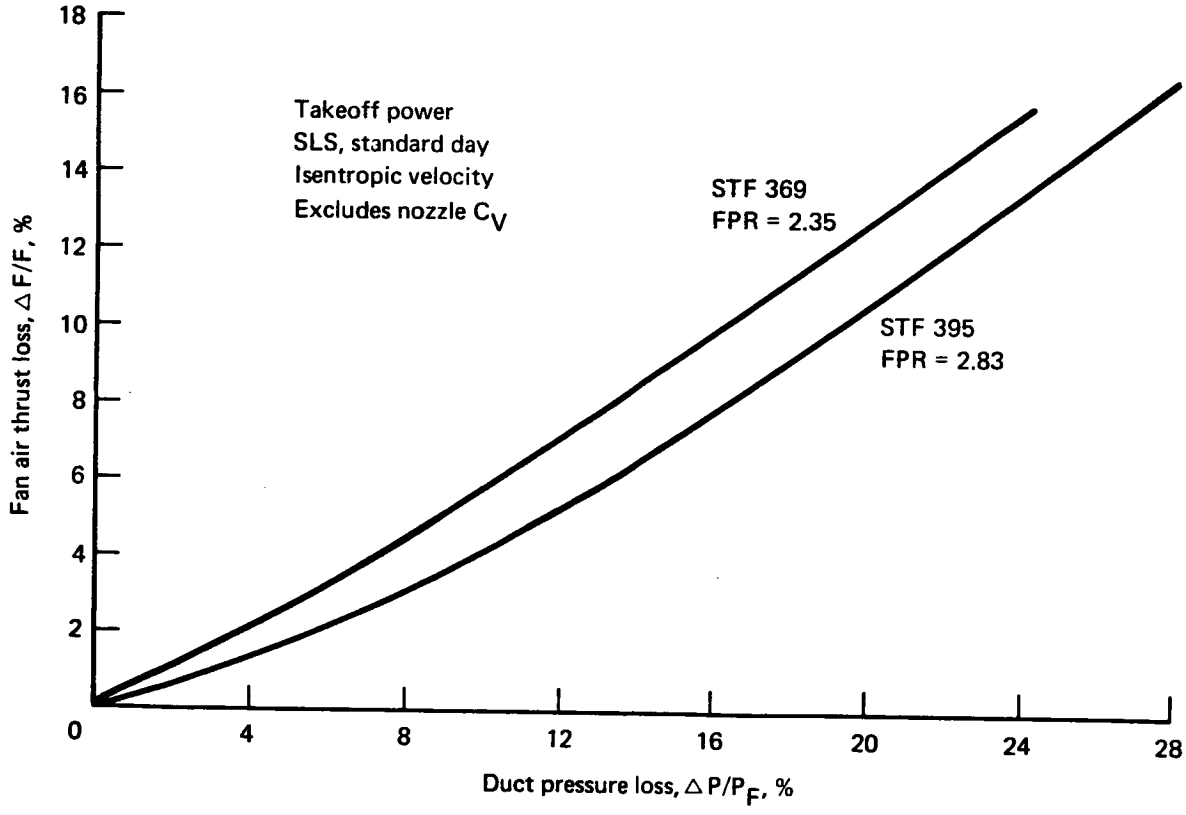

FIGURE 5-56.–DUCT LOSS EFFECT ON ENGINE THRUST

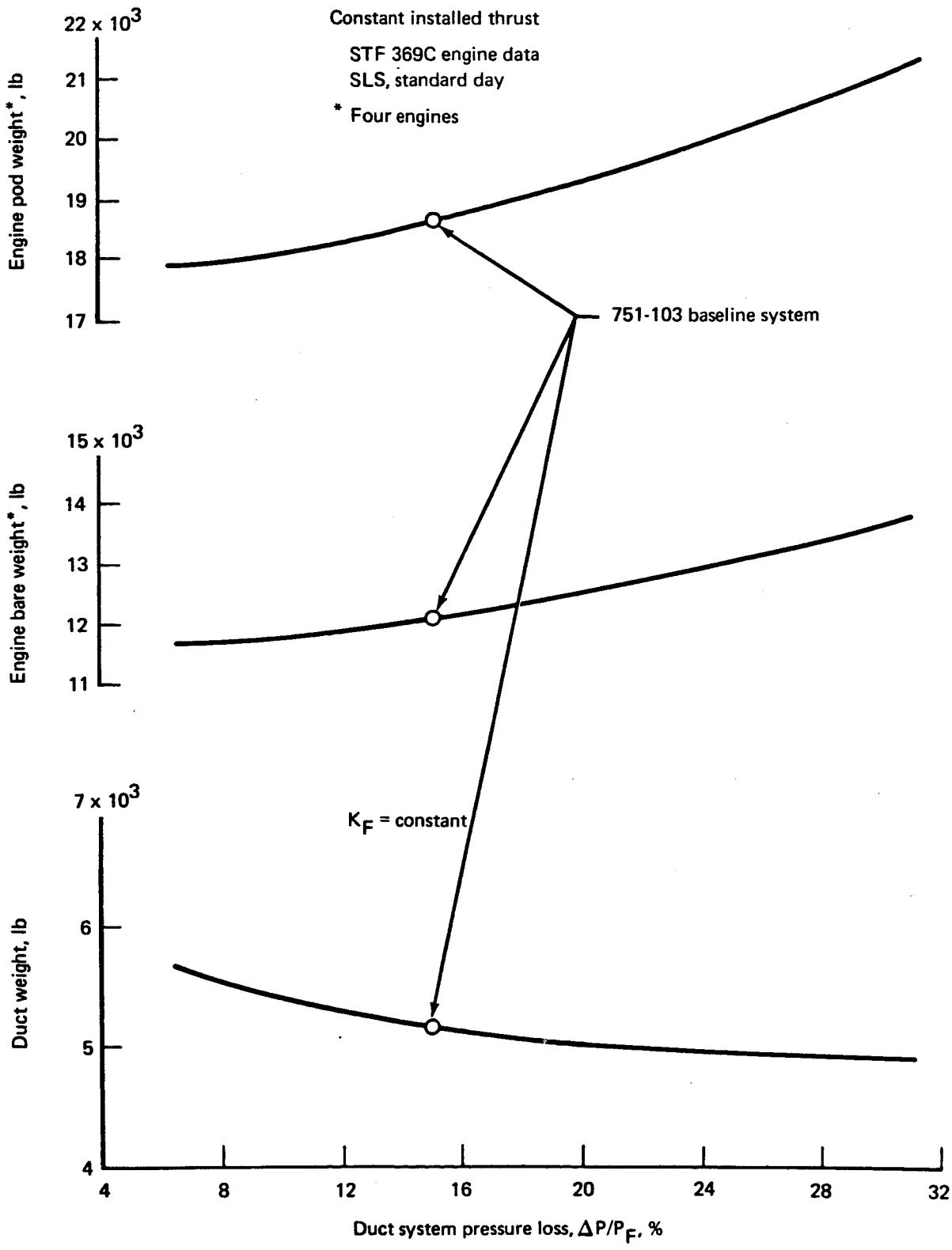

FIGURE 5-57.—AUGMENTOR AIRFLOW SYSTEM WEIGHT SCALING BREAKDOWN

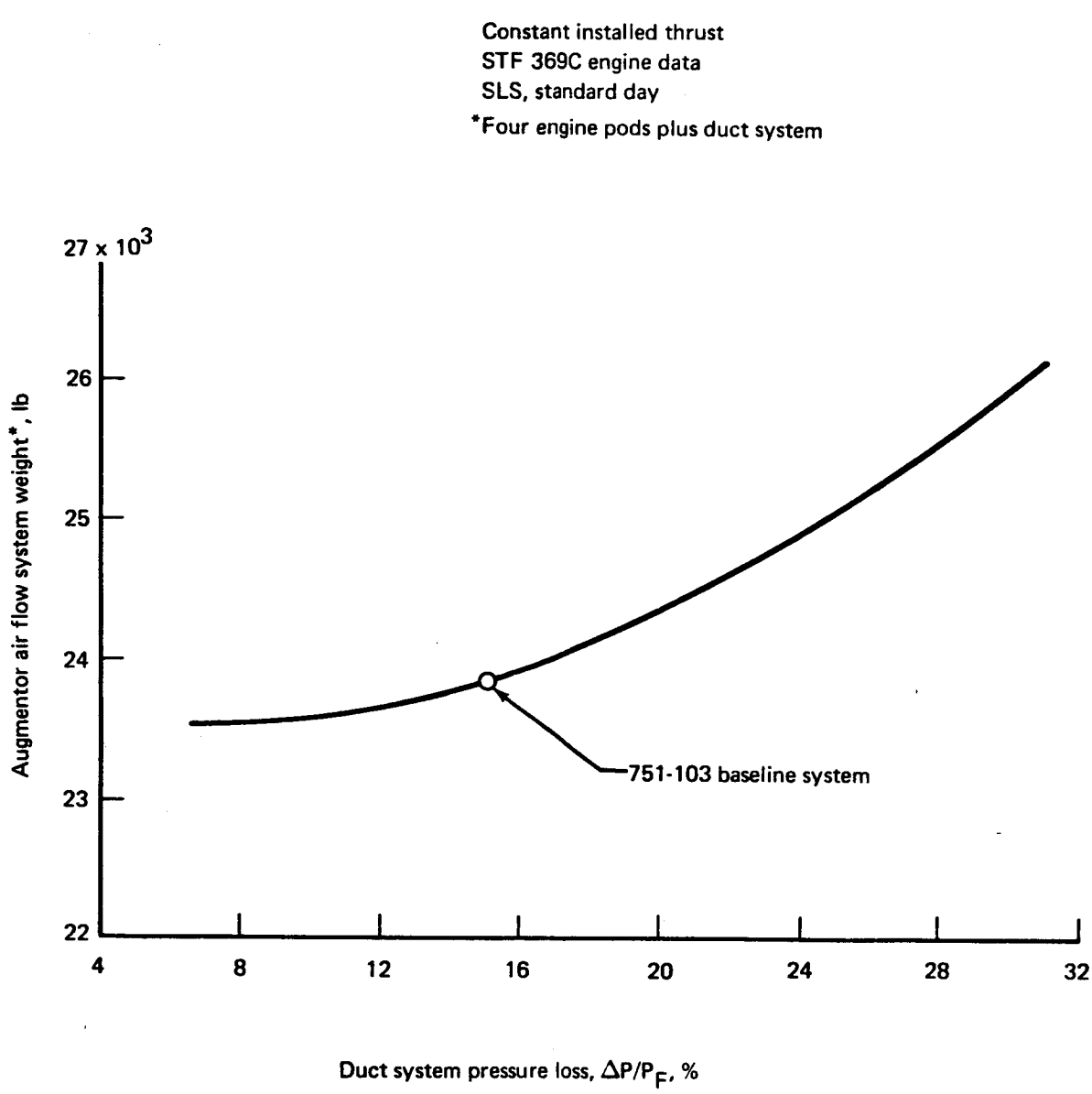

FIGURE 5-58.–AUGMENTOR AIRFLOW SYSTEM WEIGHT SCALING SUMMARY

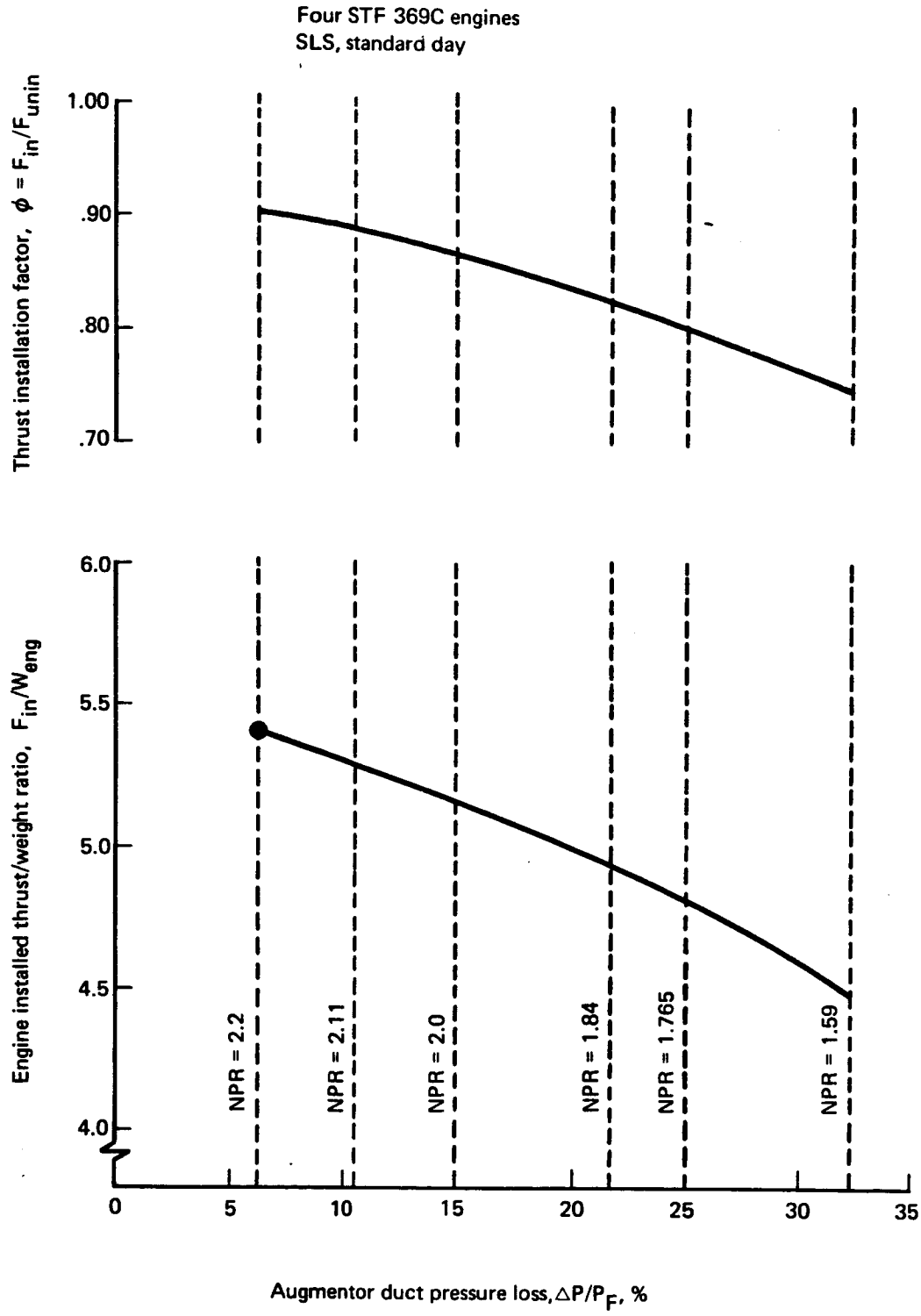

FIGURE 5-59.—THRUST INSTALLATION FACTOR AND ENGINE INSTALLED THRUST/WEIGHT RATIO—STF 369C

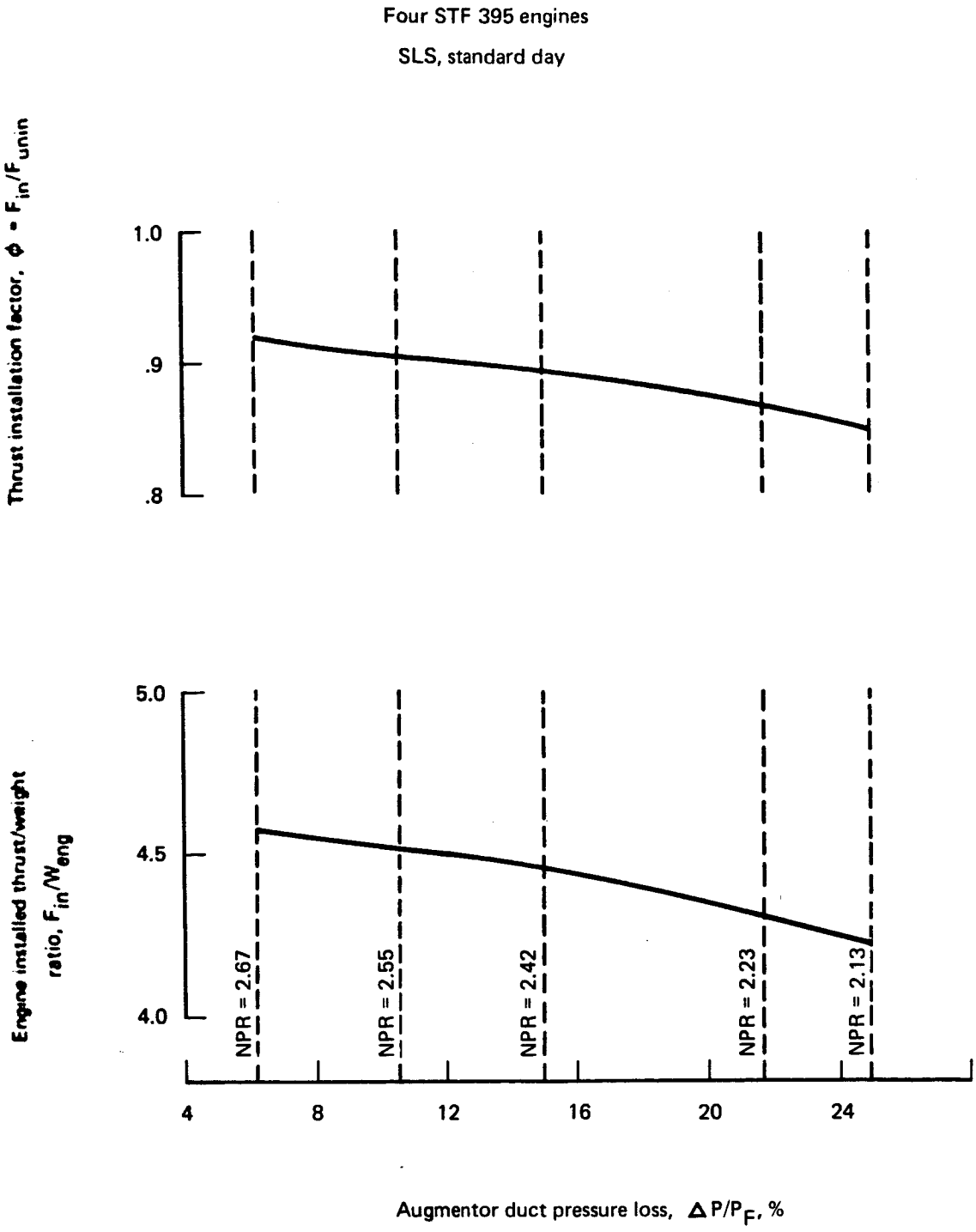

FIGURE 5-60.–THRUST INSTALLATION FACTOR AND ENGINE INSTALLED THRUST/WEIGHT RATIO–STF 395

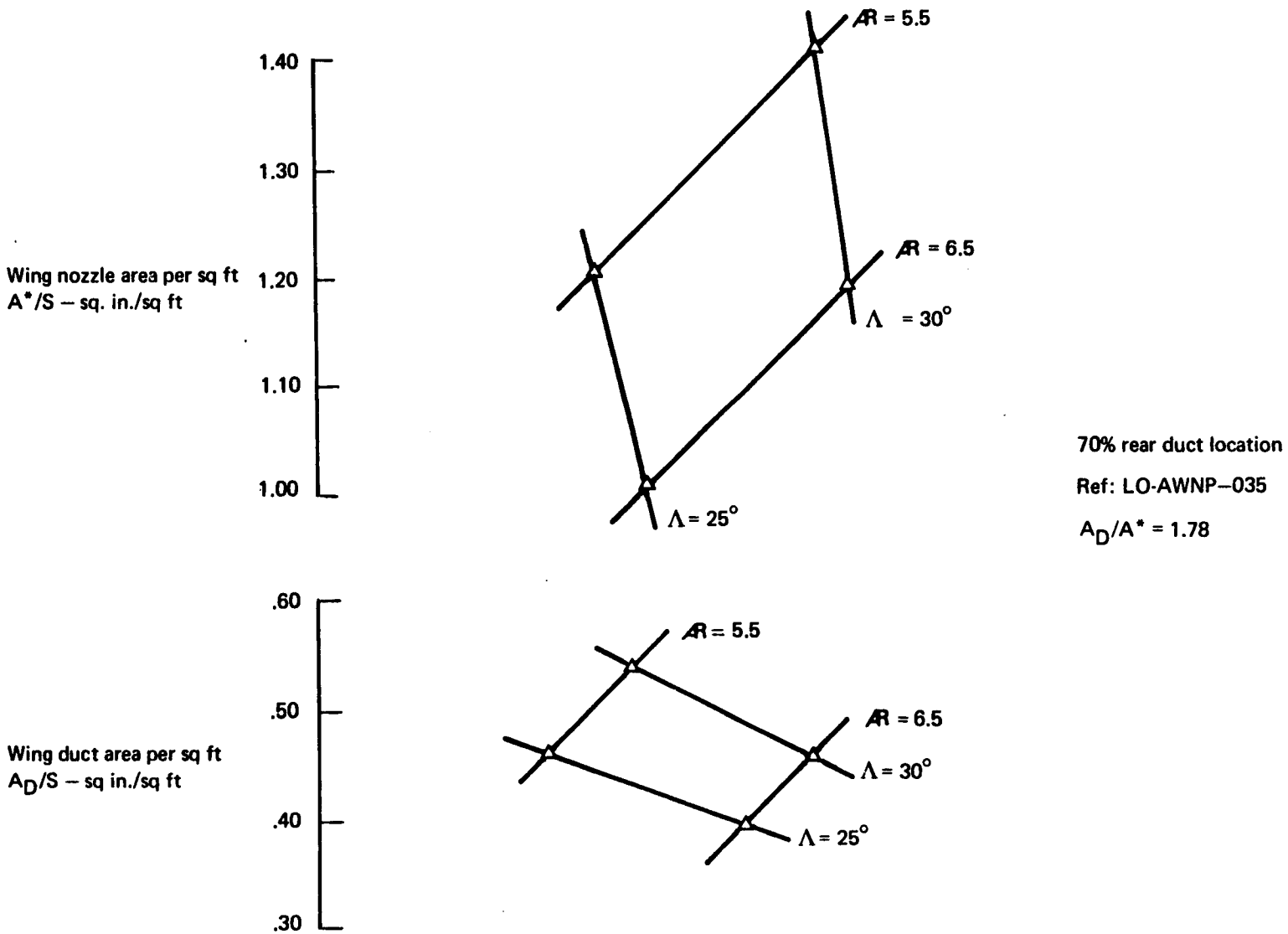

FIGURE 5-61.–WING PLANFORM EFFECT ON AVAILABLE DUCT AND NOZZLE AREA–PLENUM DUCT SYSTEM

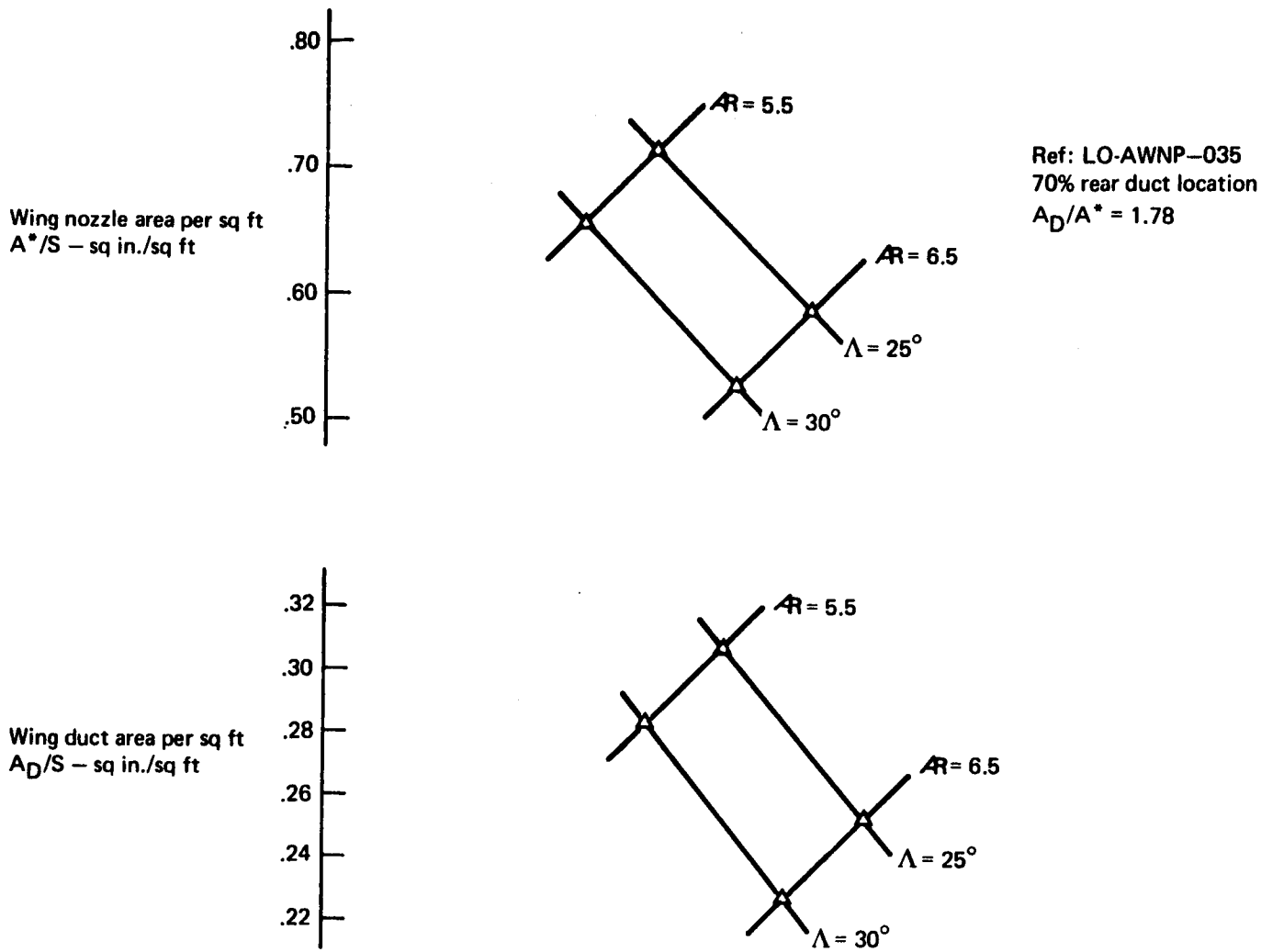

FIGURE 5-62.–WING PLANFORM EFFECT ON AVAILABLE DUCT AND NOZZLE AREA–INDEPENDENT DUCT SYSTEM (27% CROSSOVER)

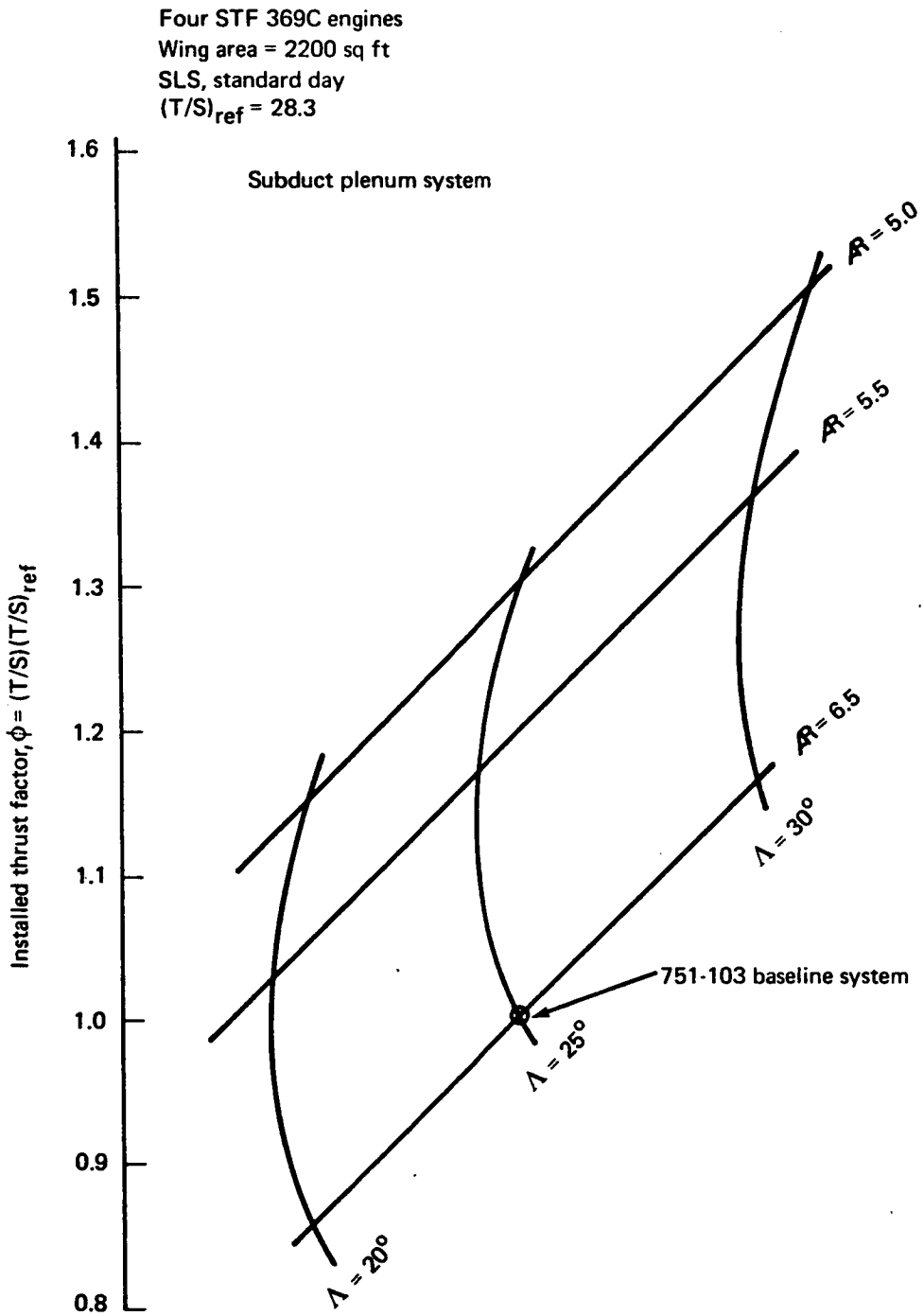

FIGURE 5-63.—WING PLANFORM EFFECT ON INSTALLED THRUST

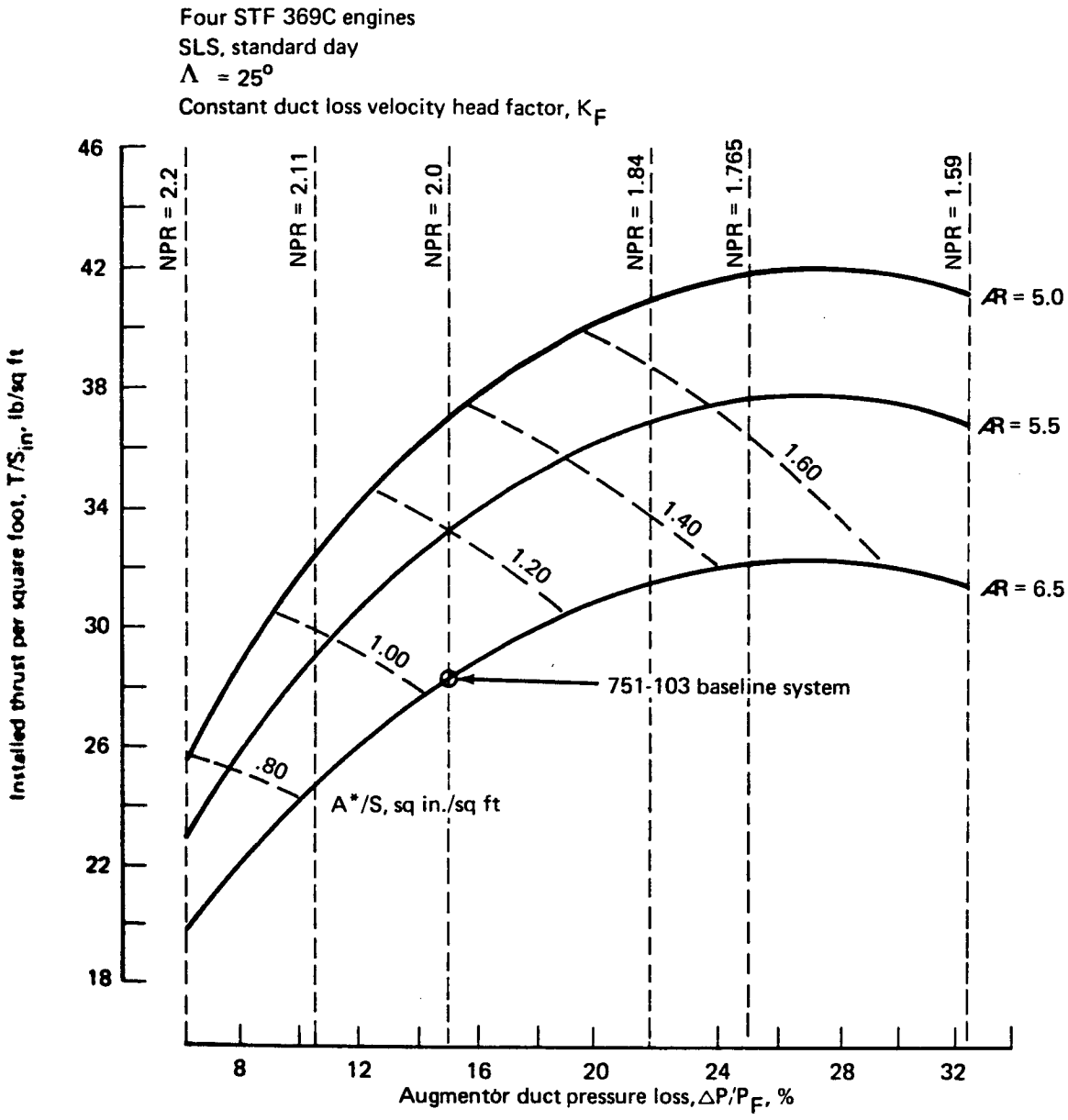

FIGURE 564 –INSTALLED THRUST PER SQUARE FOOT OF WING AREA–STF 369C ENGINES

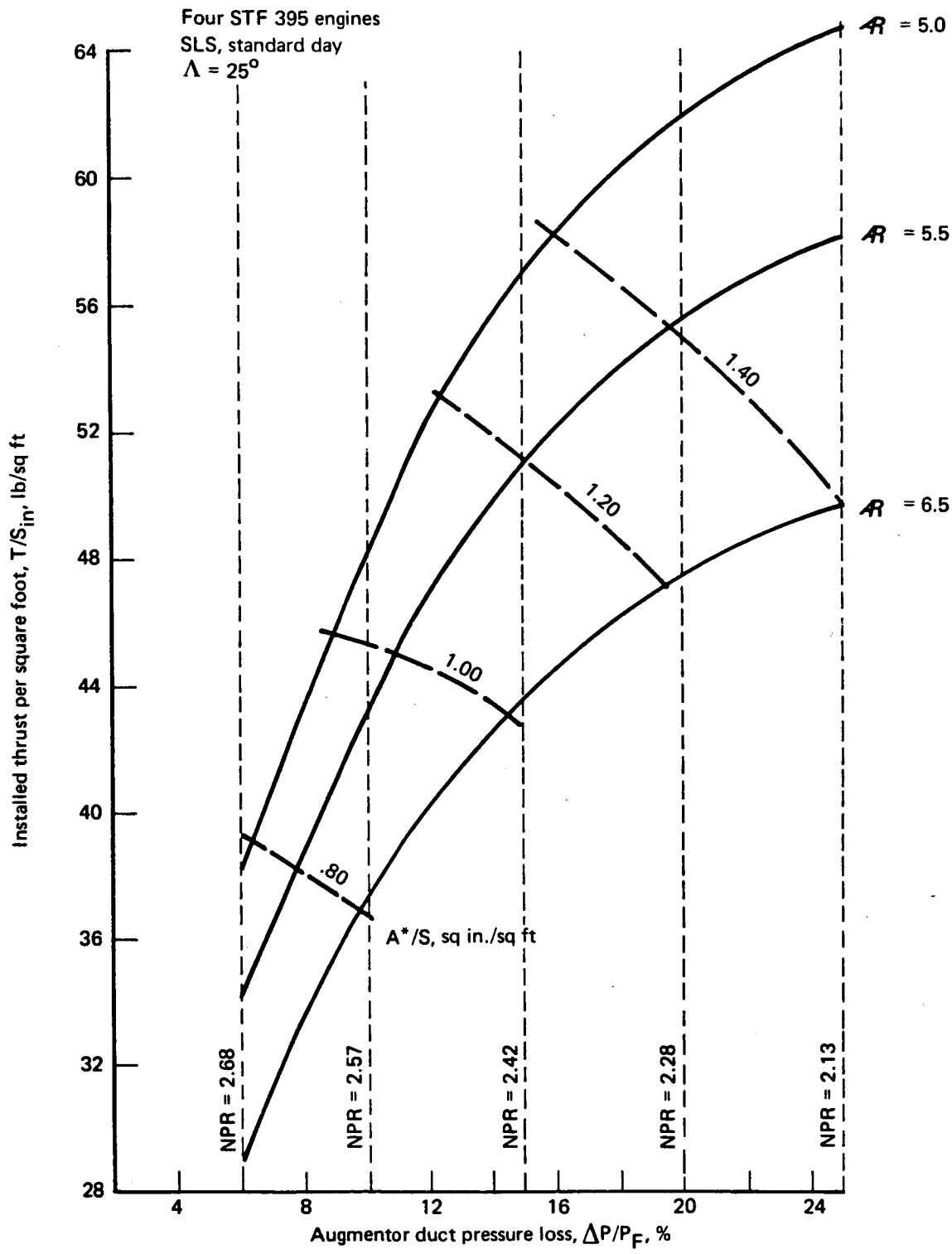

FIGURE 5-65.—INSTALLED THRUST PER SQUARE FOOT OF WING AREA—STF 395 ENGINES

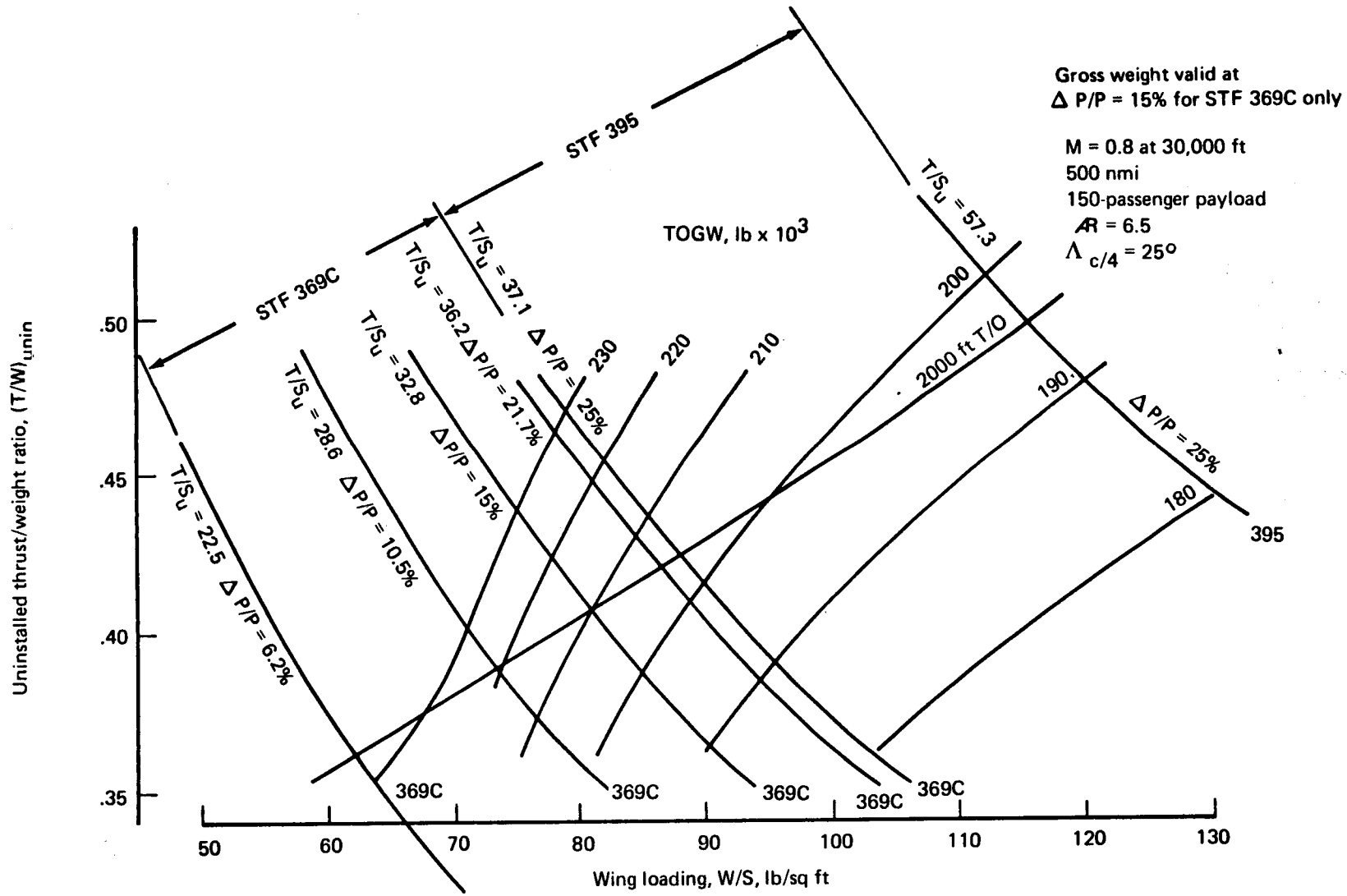

FIGURE 5-66.– AUGMENTOR WING BLOWING SYSTEM AERODYNAMIC RELATIONSHIP

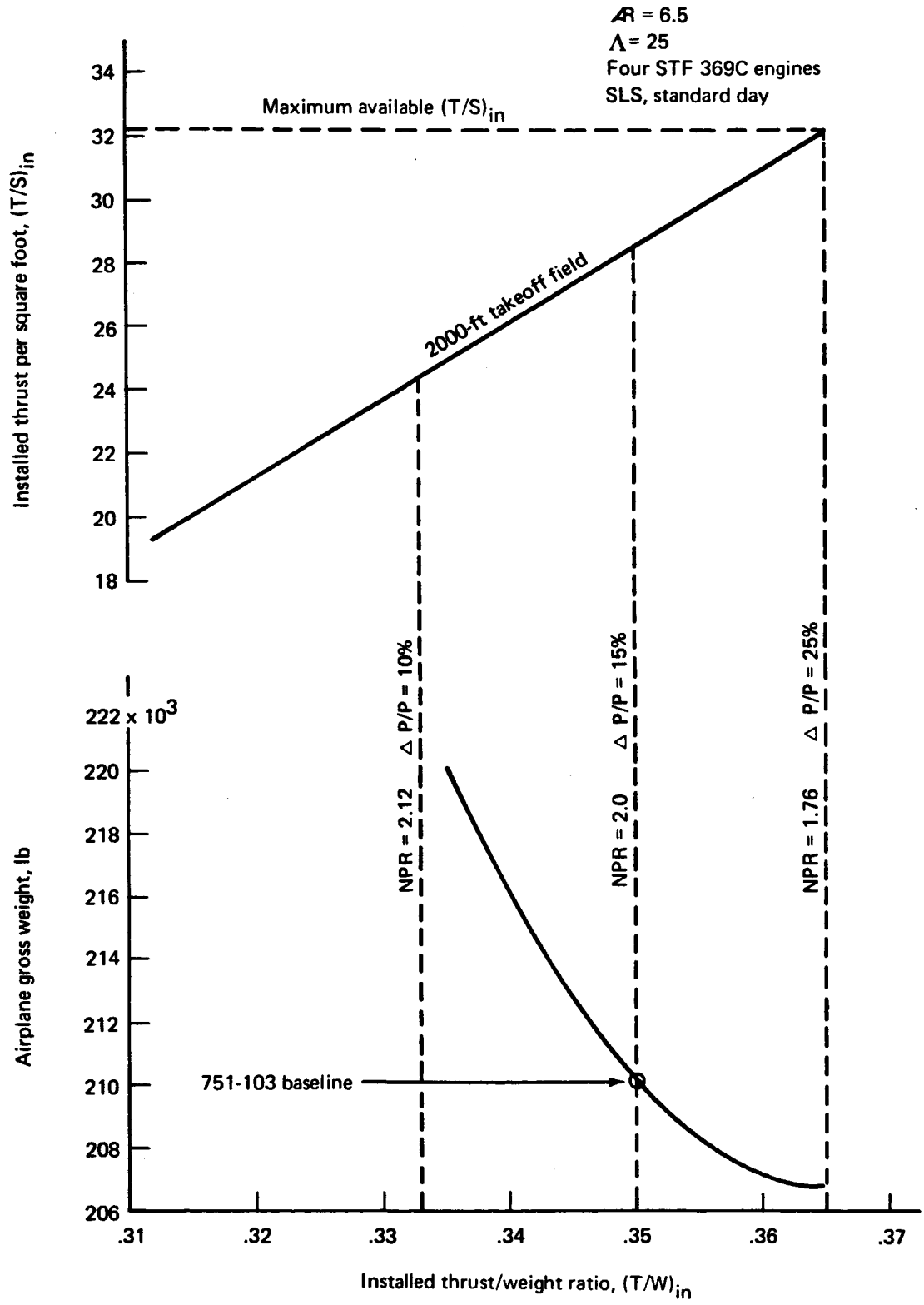

FIGURE 5-67.– EFFECT OF NOZZLE PRESSURE RATIO AND DUCT LOSS ON GROSS WEIGHT

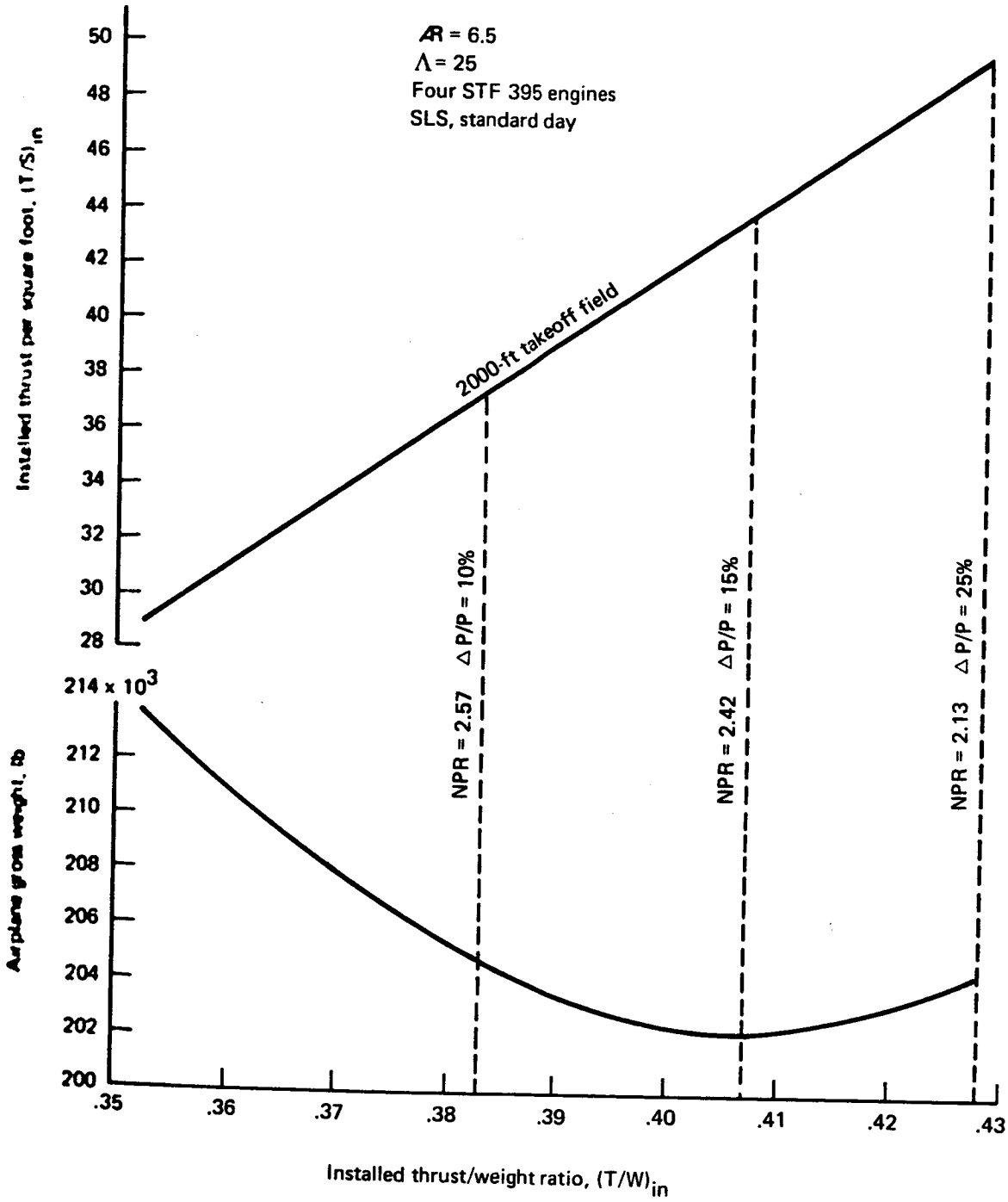

FIGURE 5-68.—EFFECT OF NOZZLE PRESSURE RATIO AND DUCT LOSS ON GROSS WEIGHT

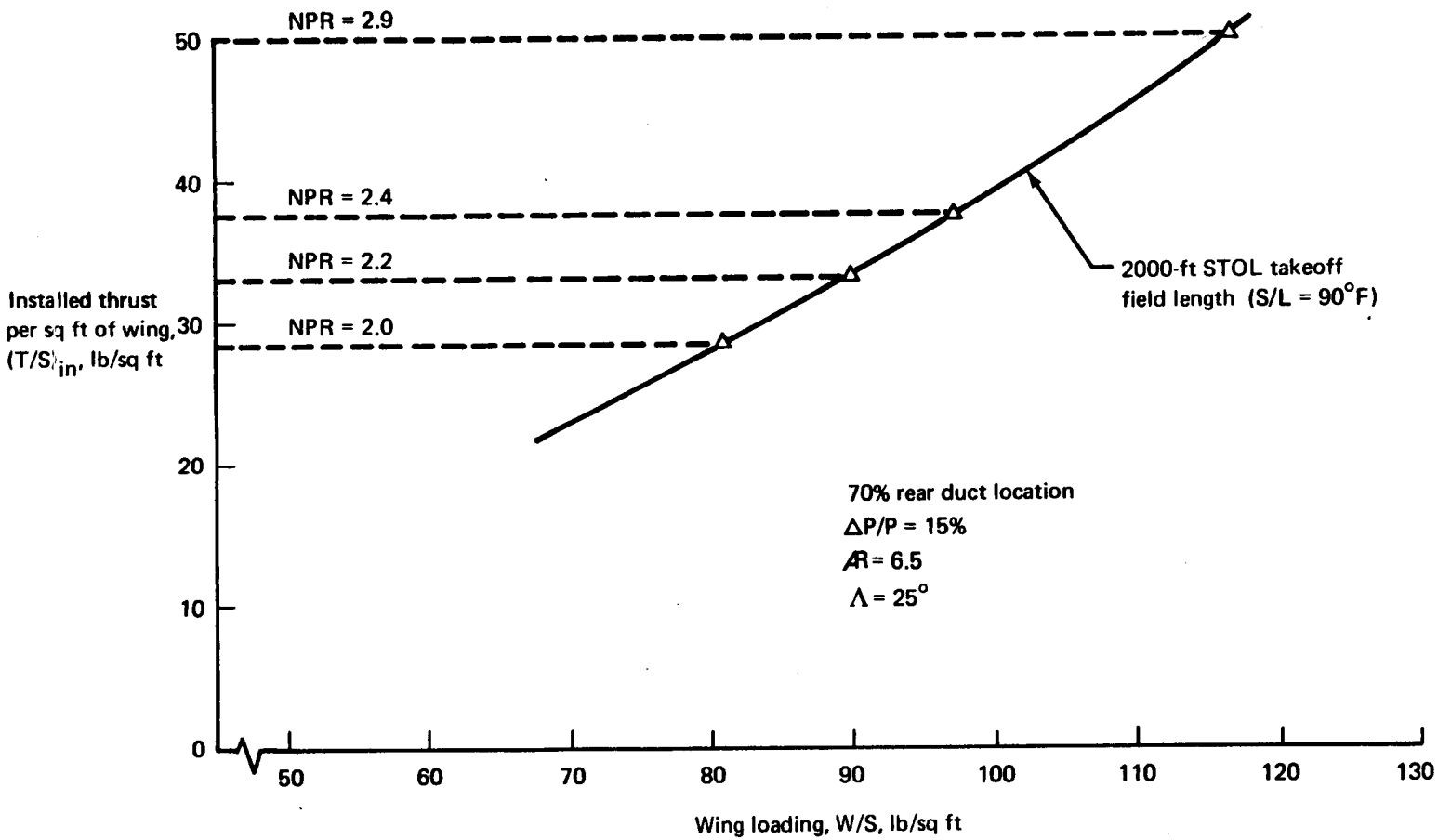

FIGURE 5-69.—INSTALLED THRUST AS A FUNCTION OF WING LOADING AND NOZZLE PRESSURE RATIO—PLENUM DUCT SYSTEM

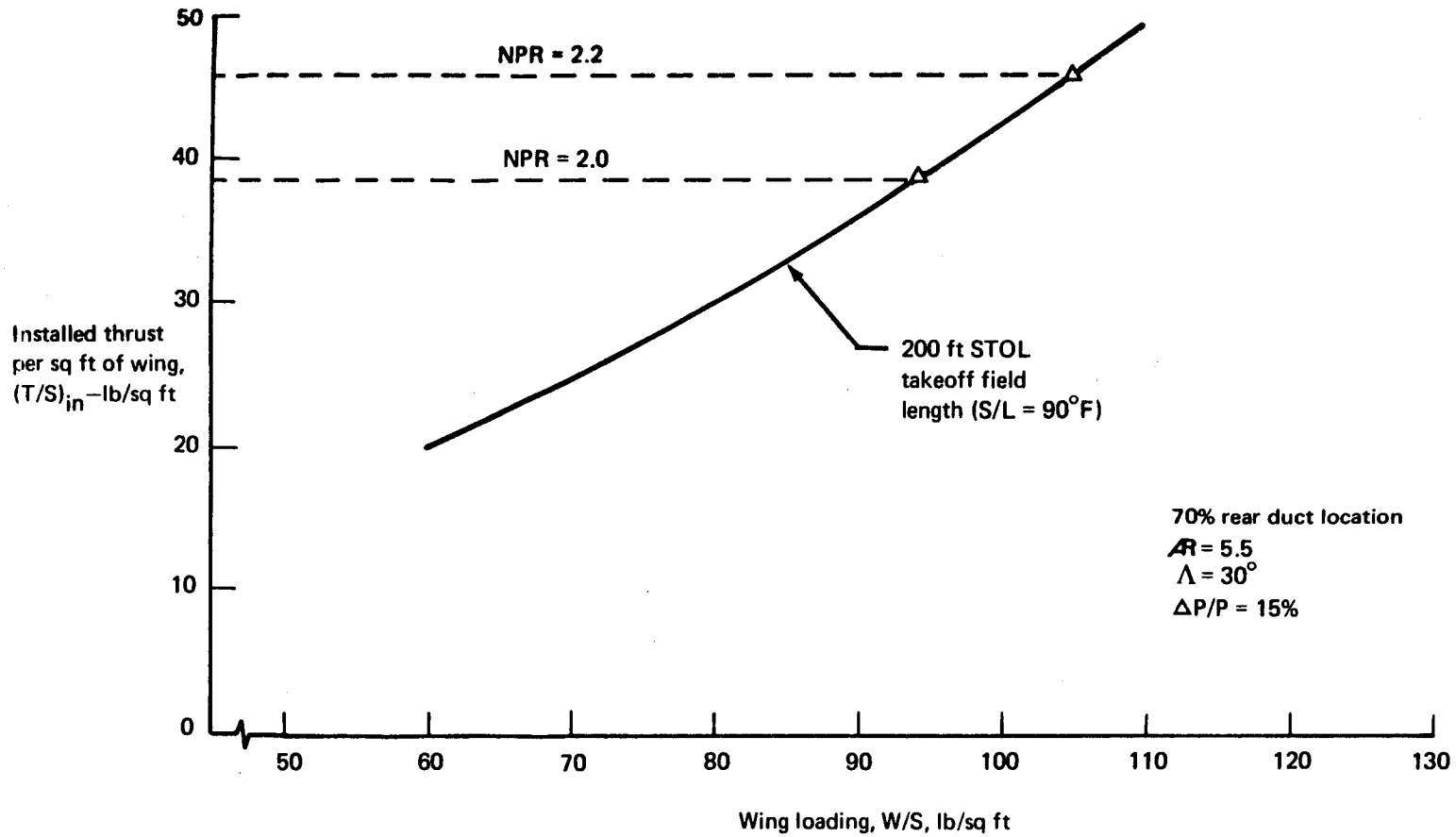

FIGURE 5-70.—INSTALLED THRUST AS A FUNCTION OF WING LOADING AND NOZZLE PRESSURE RATIO—PLENUM DUCT SYSTEM

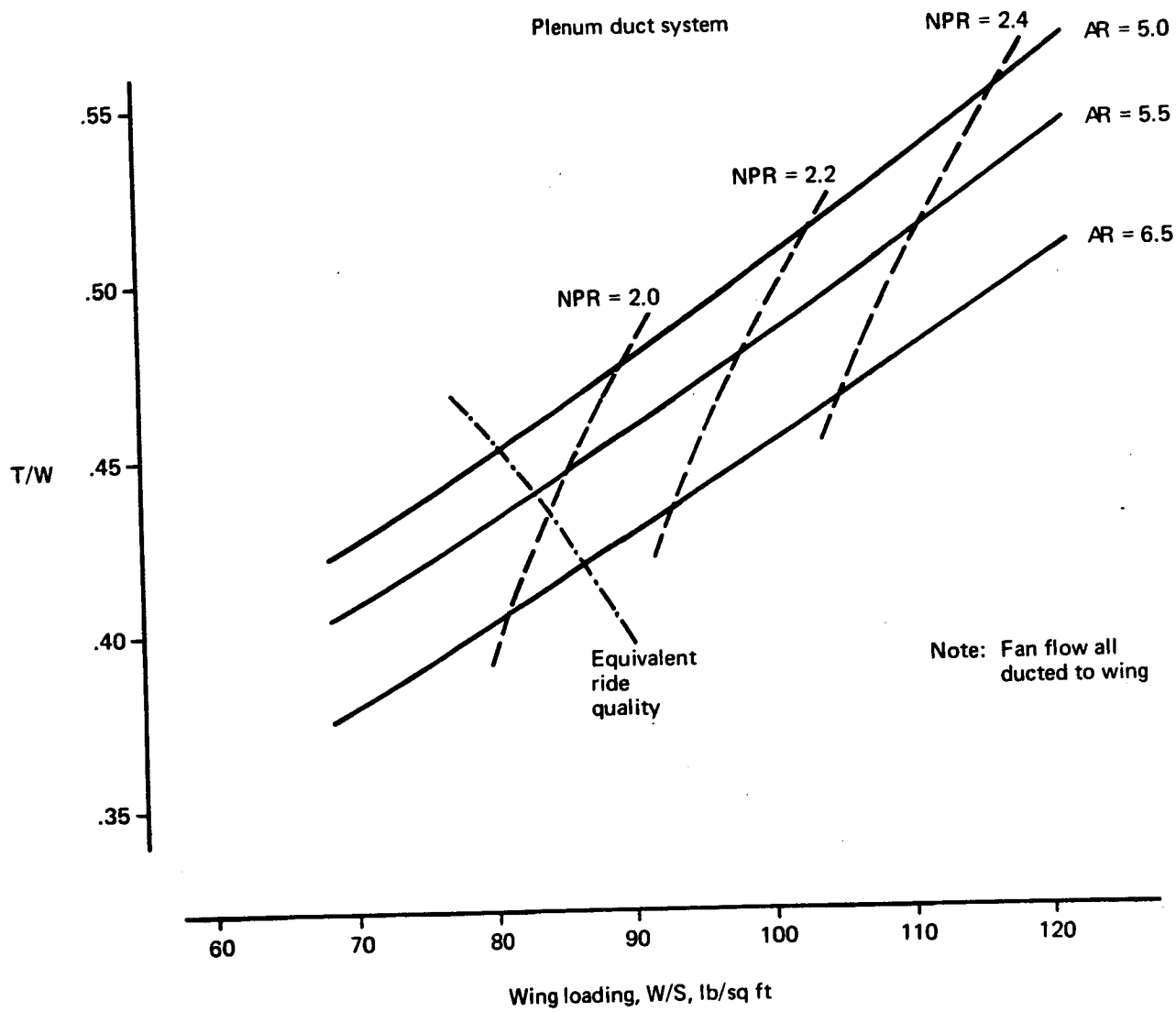

Takeoff field length = 2000 ft

$t/c_{(tip)} = .12$

Duct pressure loss, $\Delta P/P = 15\%$

$\Lambda = 25^\circ$

FIGURE 5-71.– EFFECT OF NOZZLE PRESSURE AND WING ASPECT RATIO ON AIRPLANE T/W AND W/S

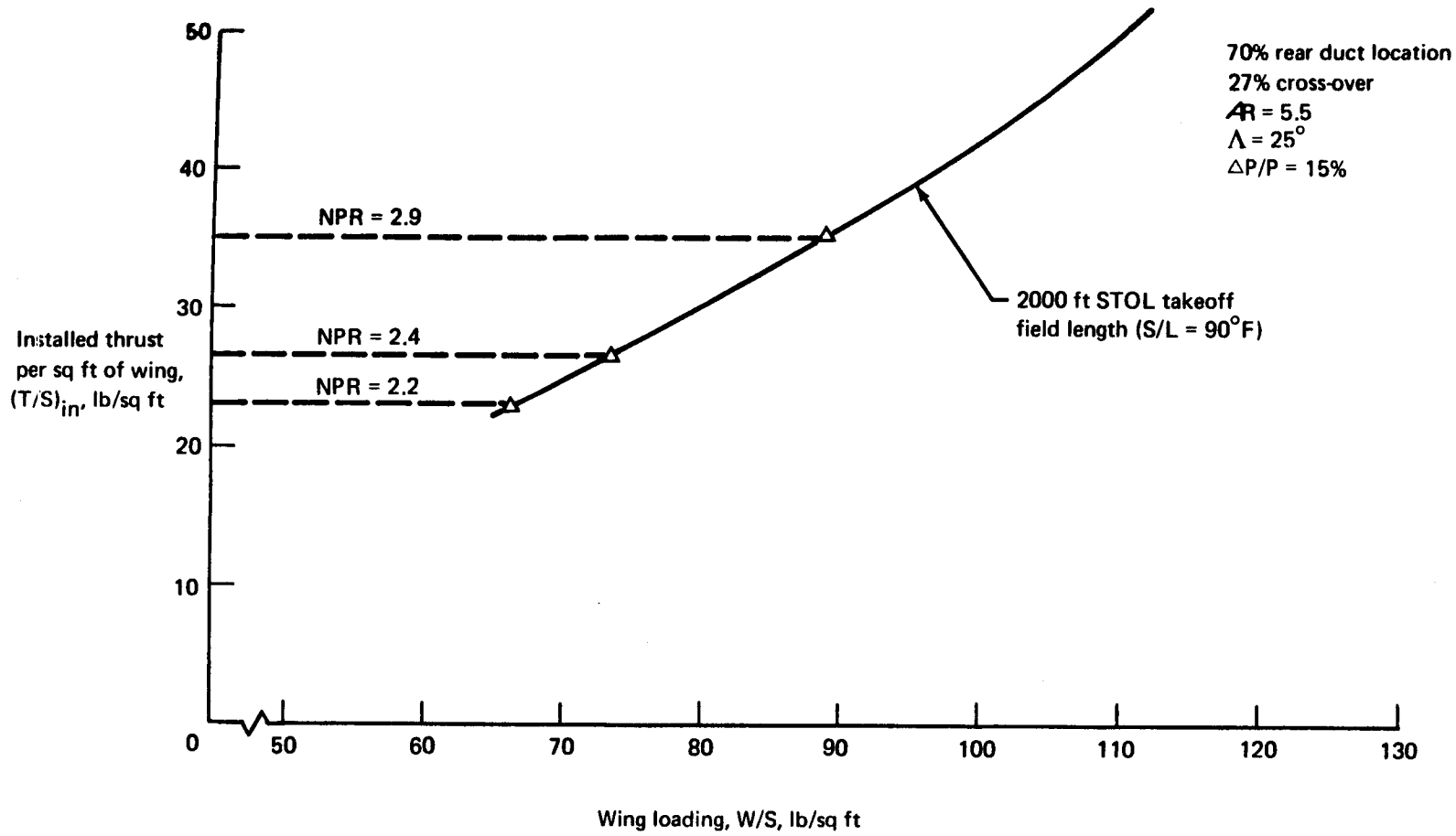

FIGURE 5-72.–INSTALLED THRUST AS A FUNCTION OF WING LOADING AND NOZZLE PRESSURE RATIO–INDEPENDENT DUCT SYSTEM

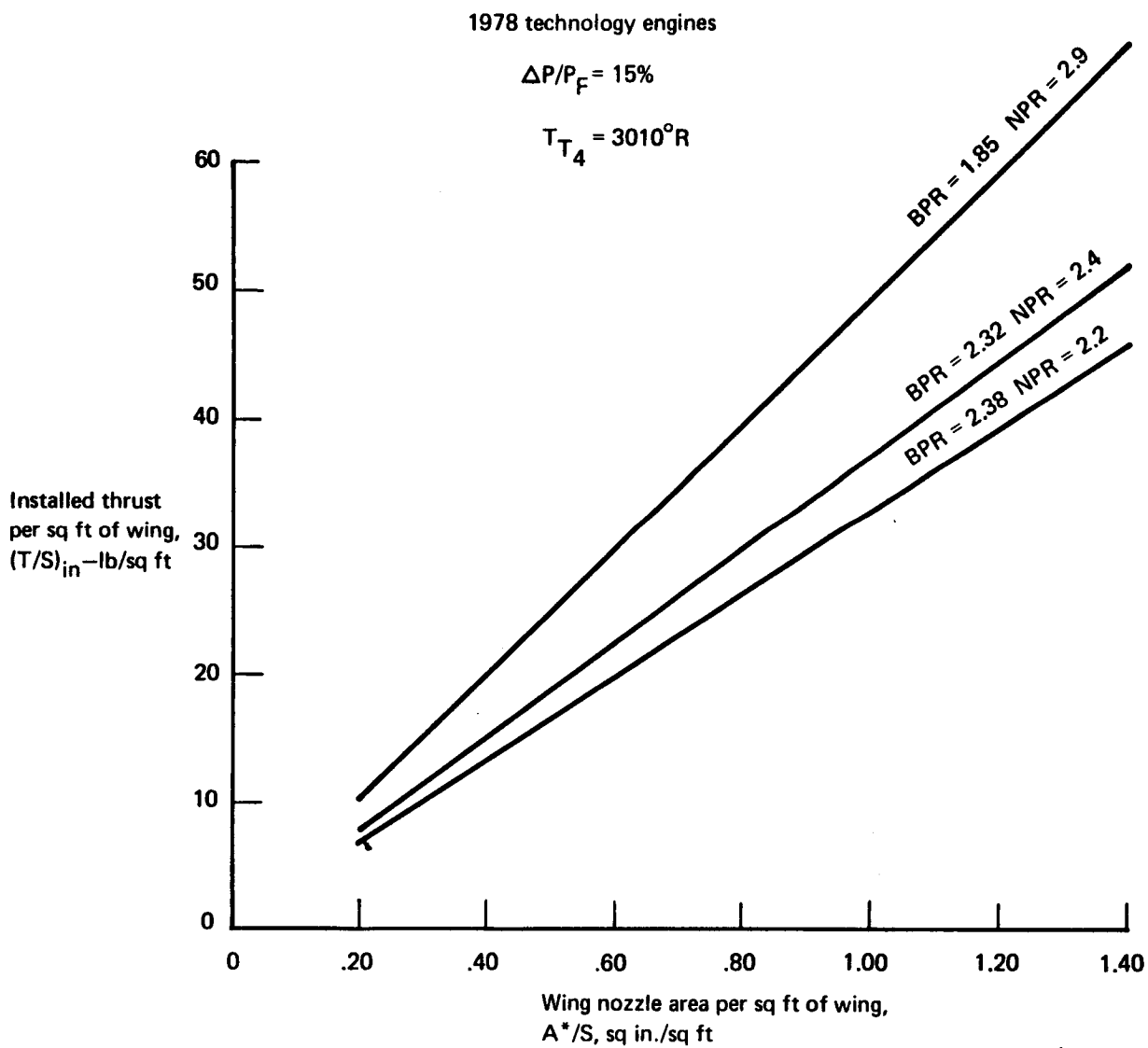

FIGURE 5-73.—INSTALLED THRUST AS FUNCTION OF NOZZLE AREA AND PRESSURE RATIO

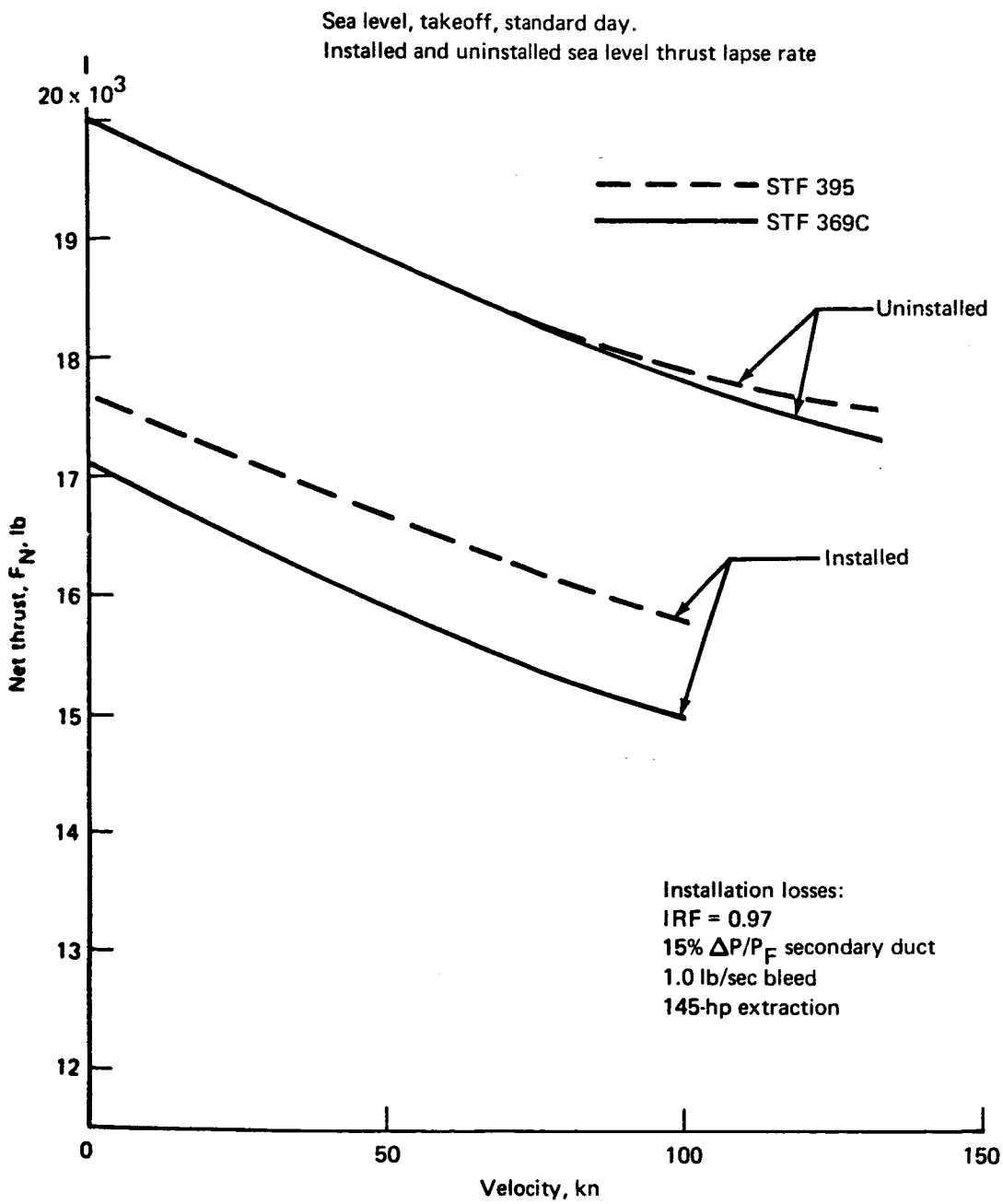

FIGURE 5-74.—STF 369C and STF 395 INSTALLED AND UNINSTALLED SEA LEVEL TAKEOFF DATA

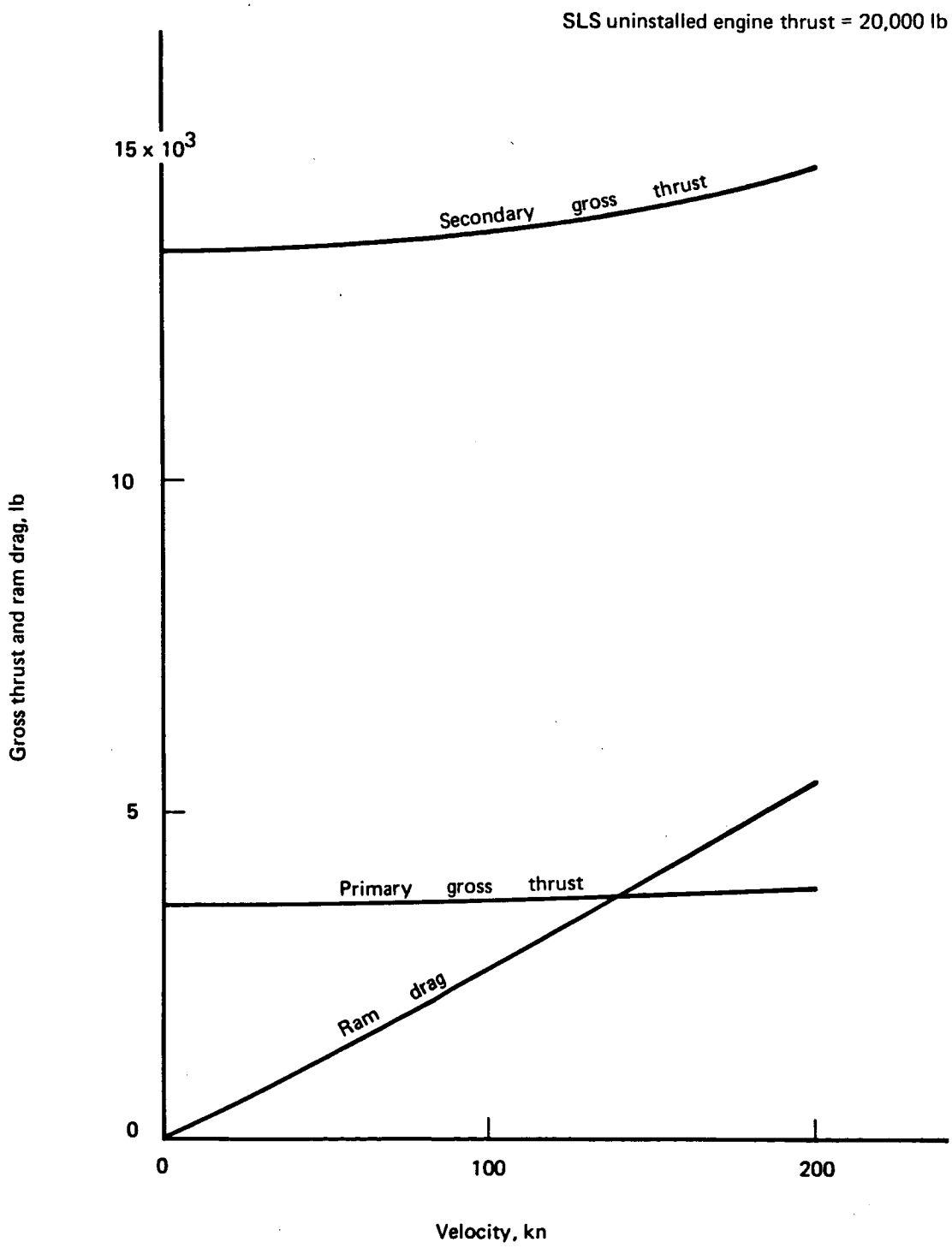

FIGURE 5-75.– INSTALLED, SEA LEVEL, TAKEOFF, 90 °F DAY DATA FOR STF 369C ENGINE CYCLE

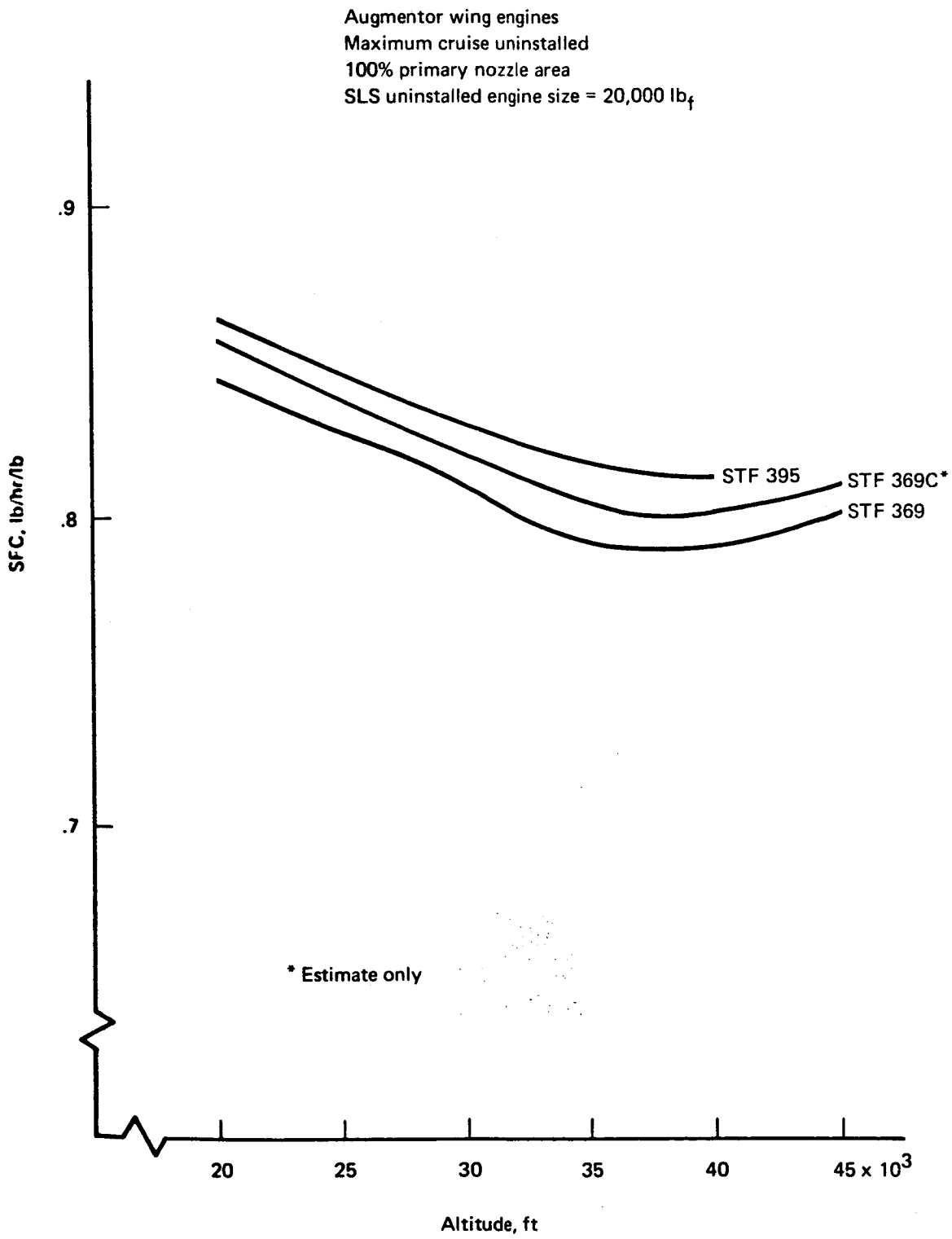

FIGURE 5-76.—SFC VS ALTITUDE AT MACH .8 FLIGHT SPEED FOR STF 369, 369C, AND 395 ENGINES

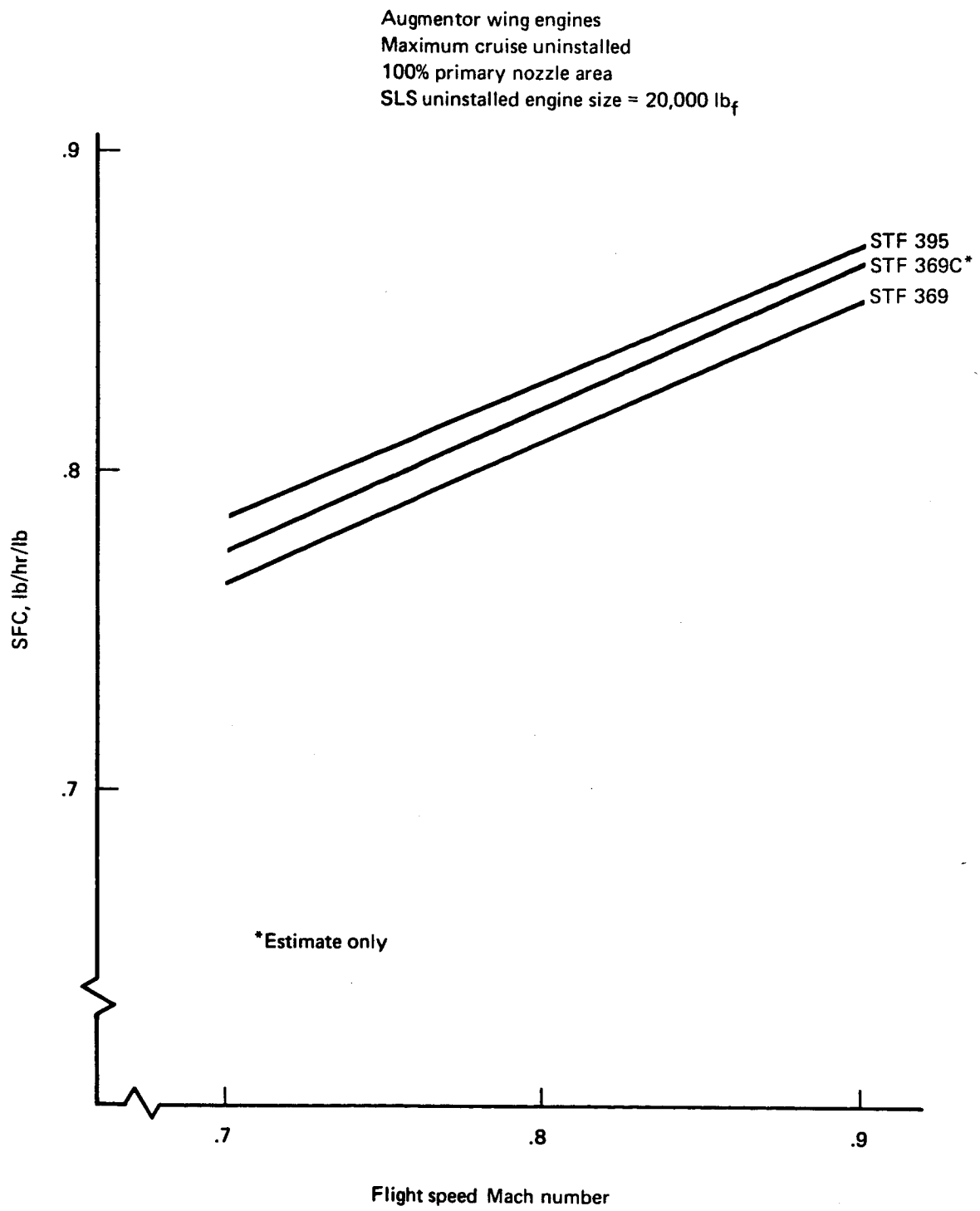

FIGURE 5-77.—SFC VS FLIGHT SPEED AT 30,000 FT FOR STF 369, 369C AND 395 ENGINES

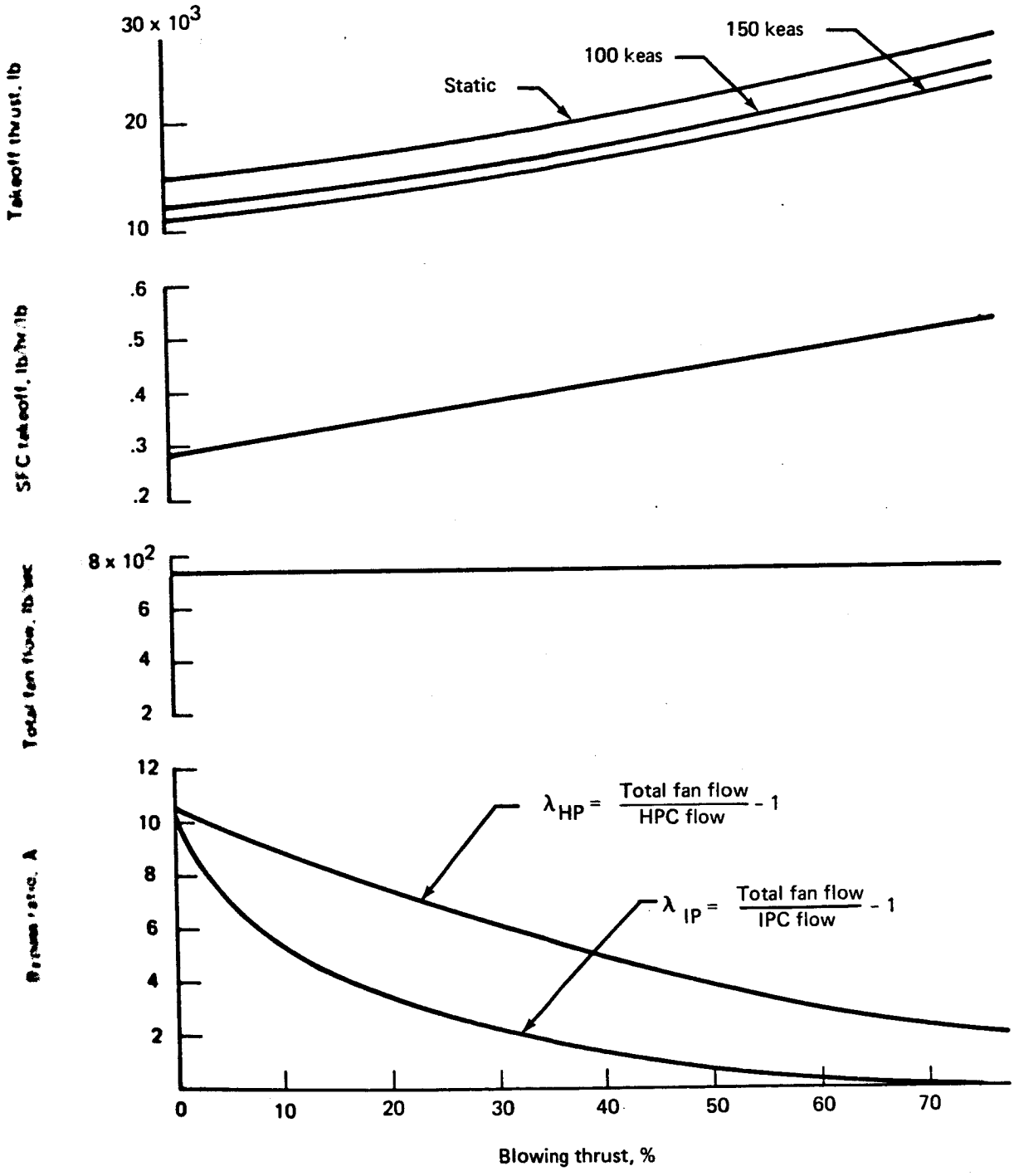

FIGURE 5-78.– RB419-TYPE ENGINES, SLS TAKEOFF PERFORMANCE

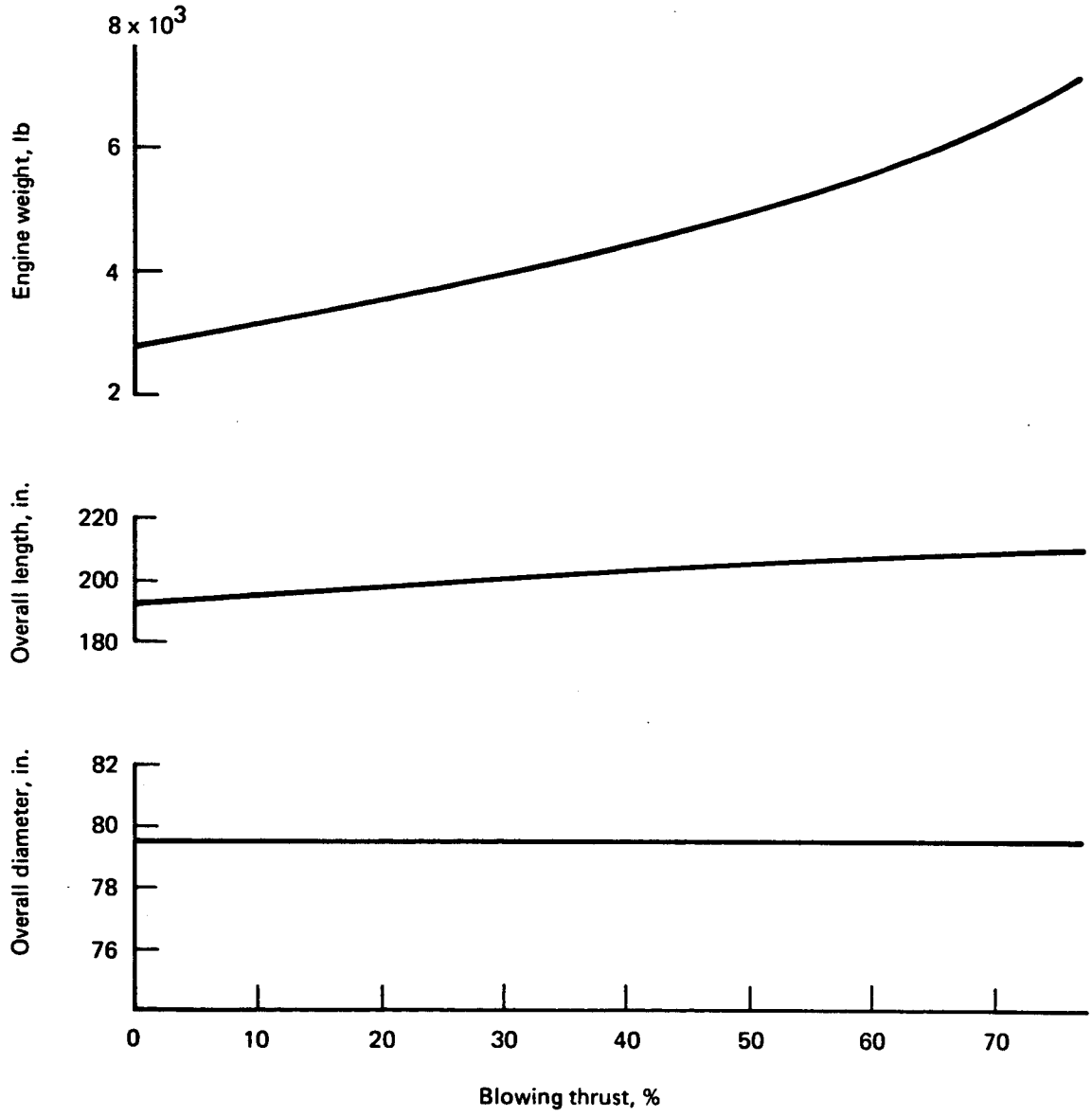

FIGURE 5-79.– RB419-TYPE ENGINES, SIZE AND WEIGHT

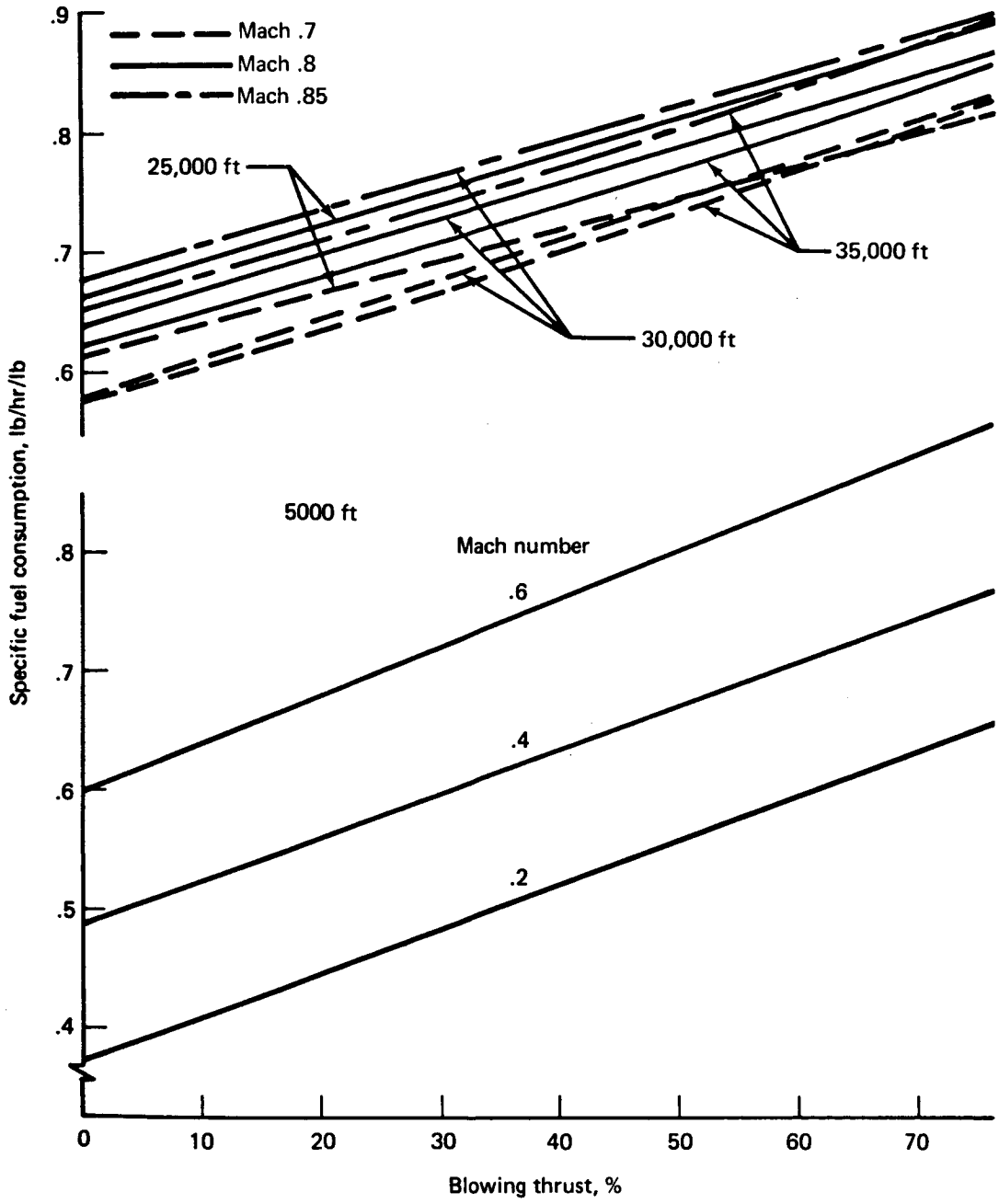

FIGURE 5-80.– RB419-TYPE ENGINES, CRUISE SPECIFIC FUEL CONSUMPTION

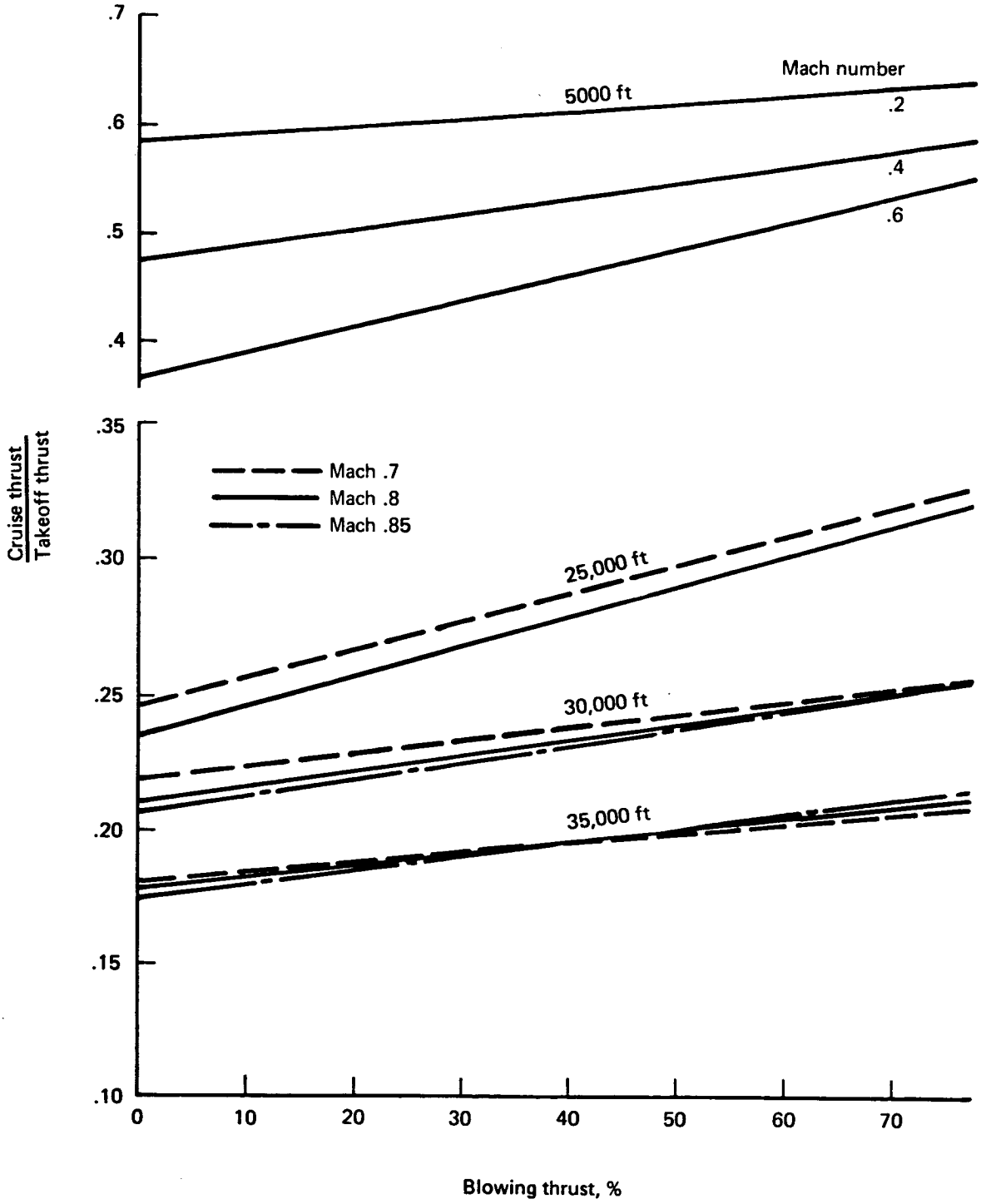

FIGURE 5-81.—RB419-TYPE ENGINES, CRUISE THRUST

FPR = 2.45
Overall pressure ratio = 19.6
Noise for four-engines at 500-ft sideline, 100 kn

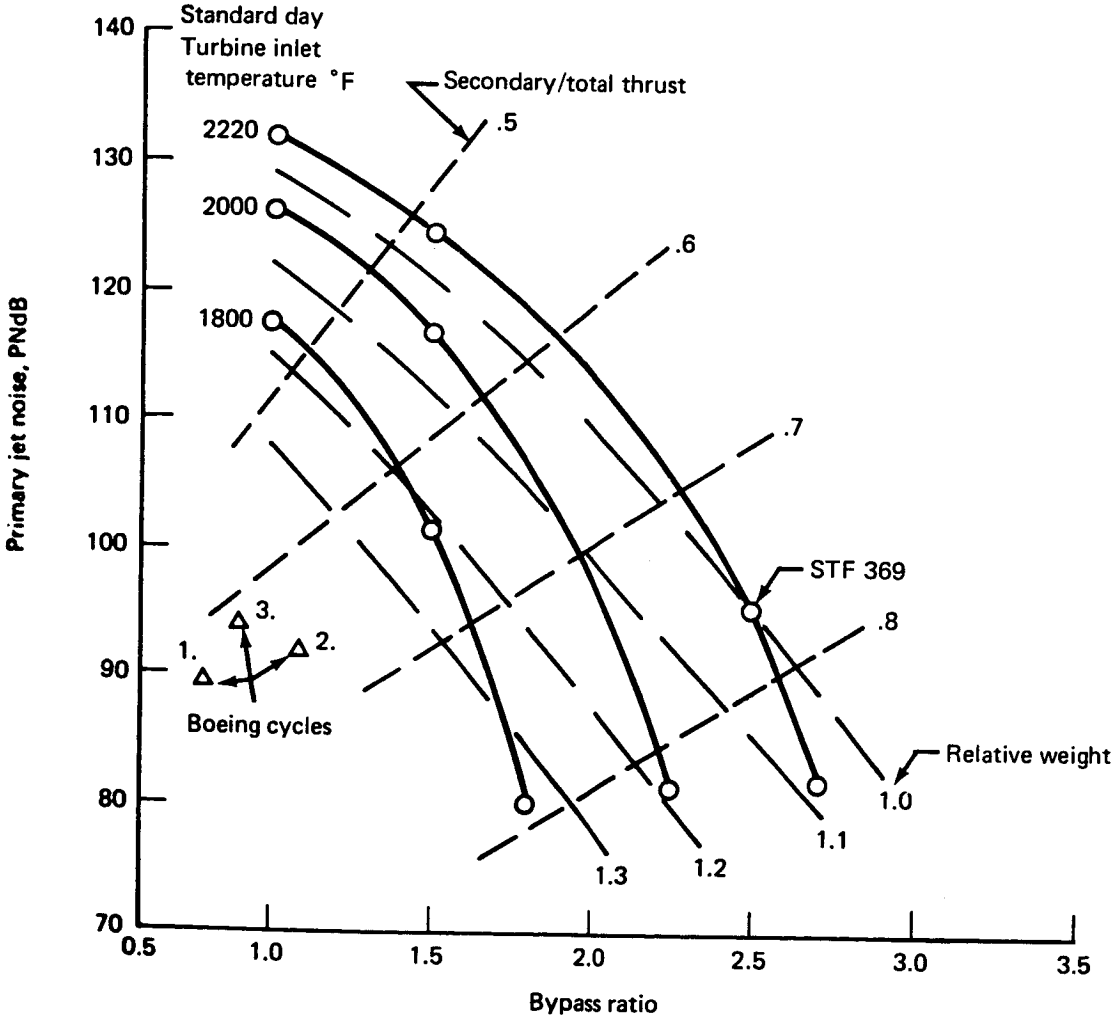

FIGURE 5-82.—P&W AUGMENTOR WING ENGINE STUDY—RELATIVE WEIGHT AND SECONDARY/TOTAL THRUST OVERPLOT

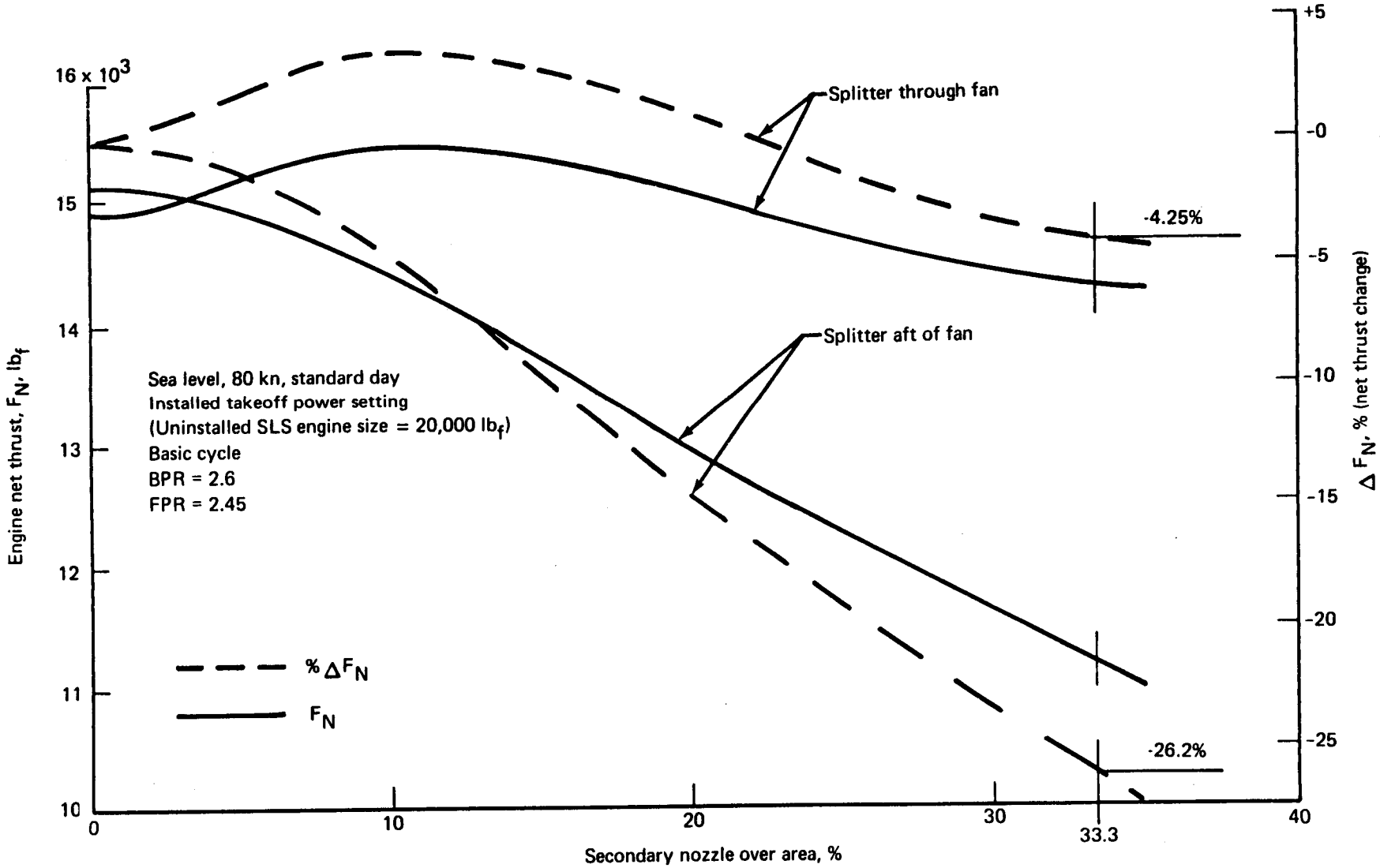

FIGURE 5-83.–THRUST AND THRUST LOSS VS SECONDARY NOZZLE OVERAREA

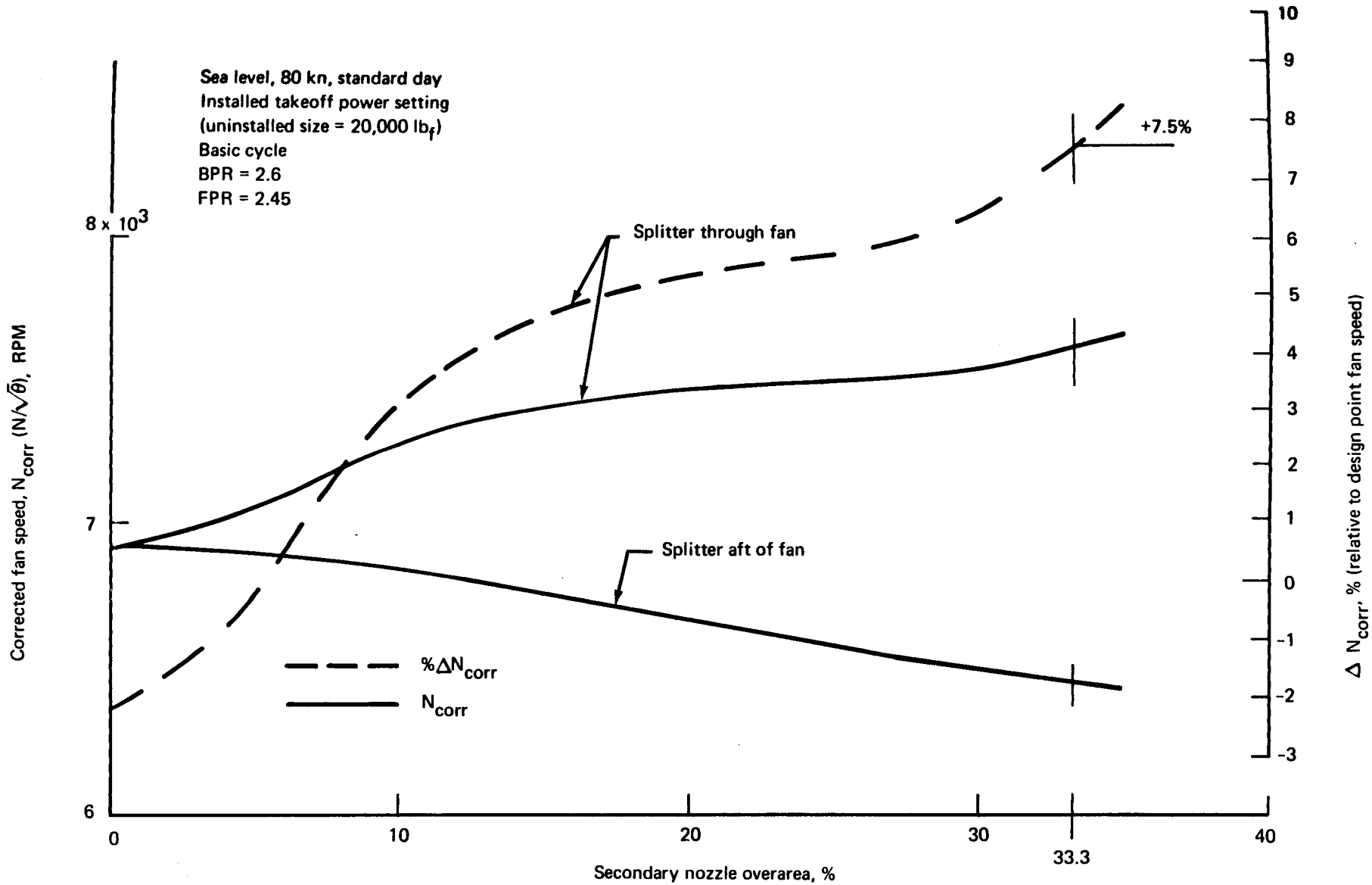

FIGURE 5-84.—CORRECTED FAN SPEED AND SPEED CHANGE VS SECONDARY NOZZLE OVERAREA

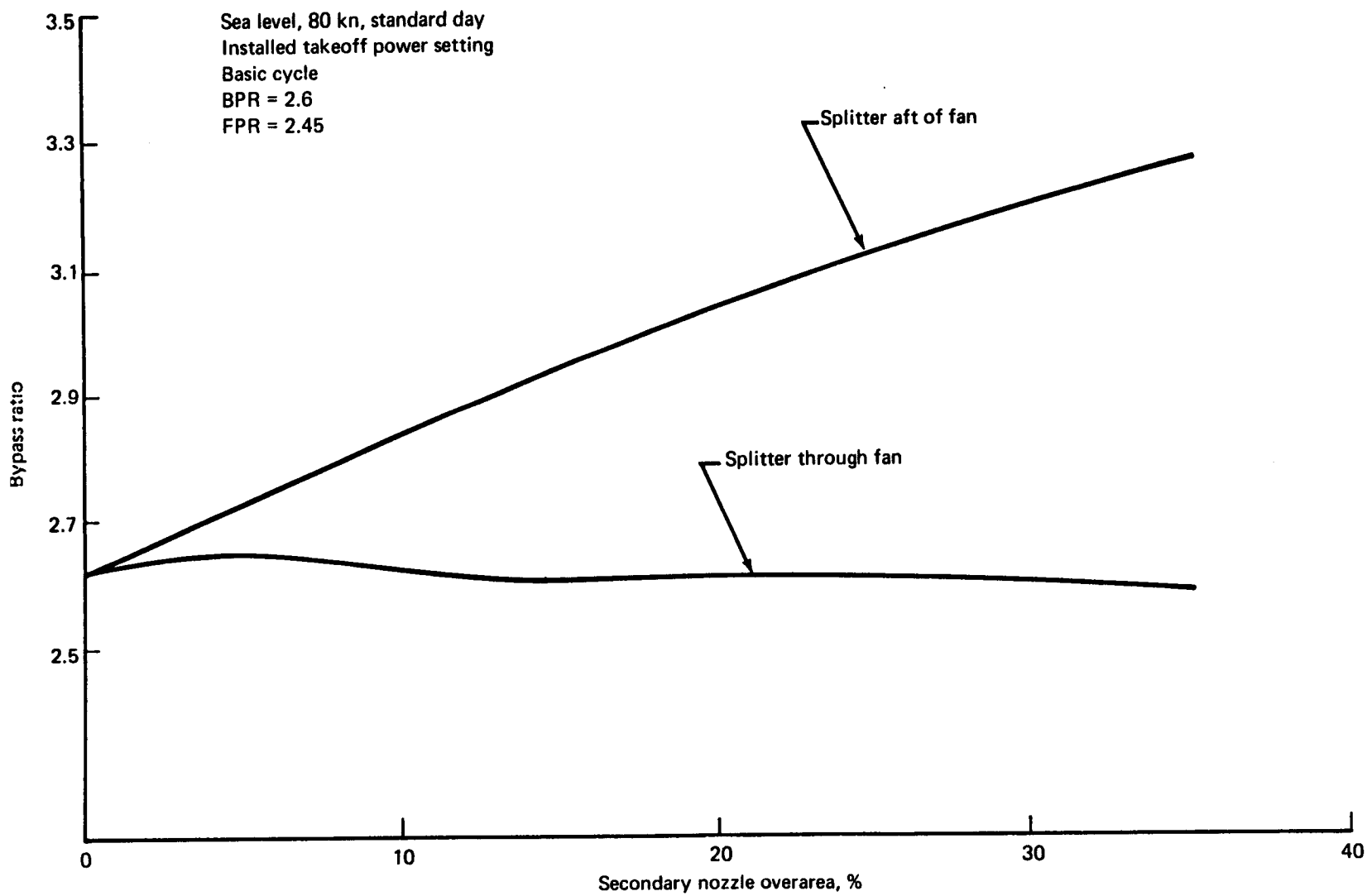

FIGURE 5-85.– BYPASS RATIO VS SECONDARY NOZZLE OVER AREA

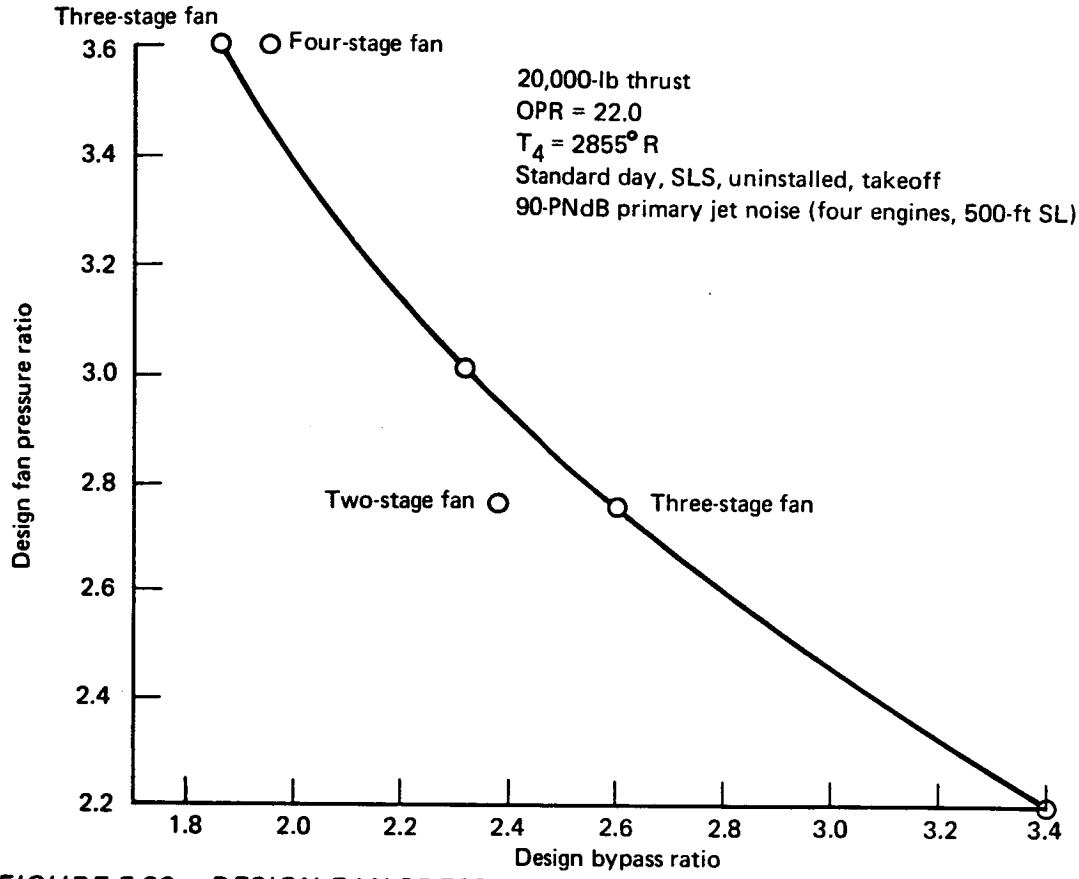

FIGURE 5-86.– DESIGN FAN PRESSURE RATIO VS DESIGN BYPASS RATIO

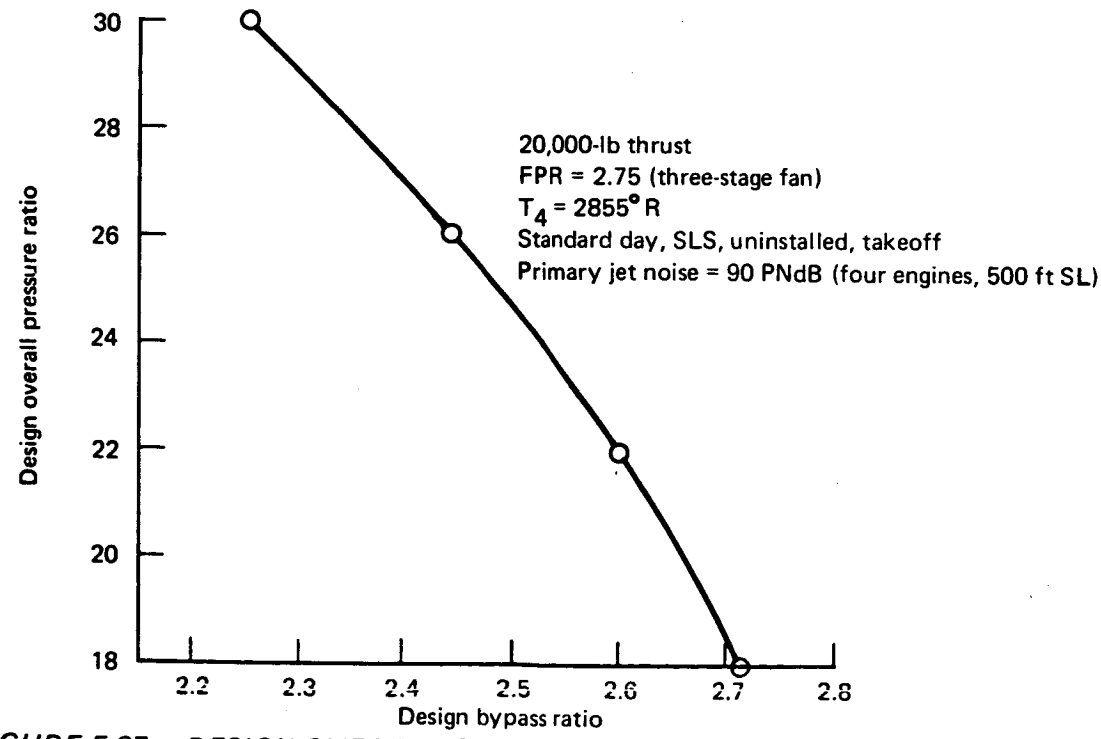

FIGURE 5-87.– DESIGN OVERALL PRESSURE RATIO VS DESIGN BYPASS RATIO

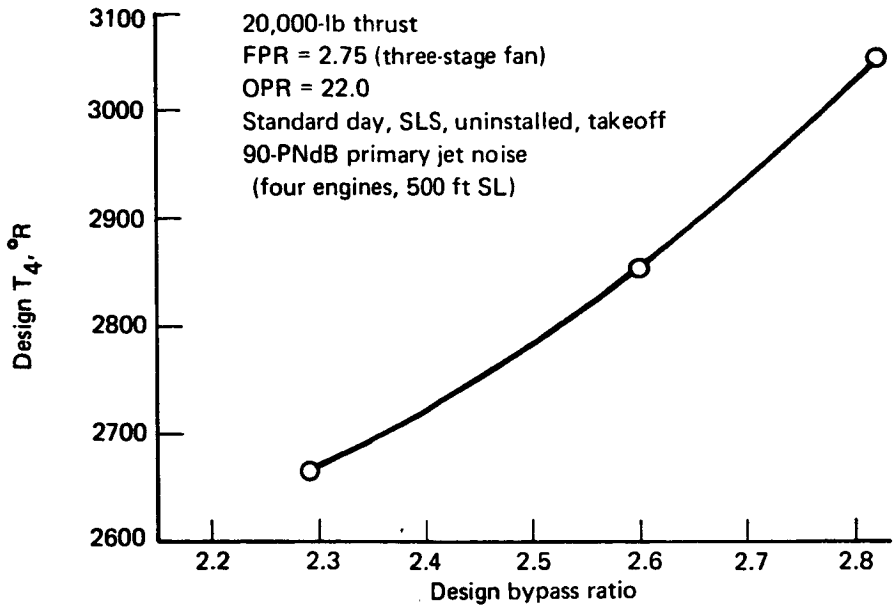

FIGURE 5-88.—DESIGN T_4 VS DESIGN BYPASS RATIO

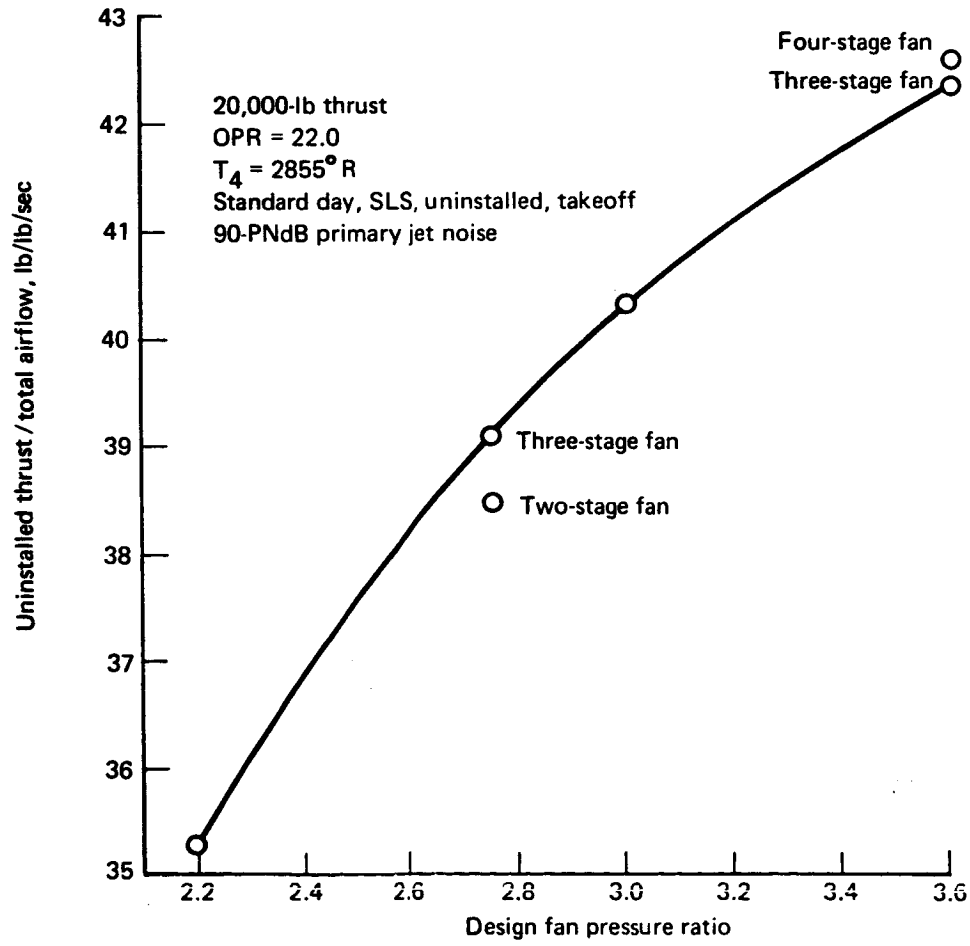

FIGURE 5-89.—UNINSTALLED THRUST/TOTAL AIRFLOW VS DESIGN FAN PRESSURE RATIO

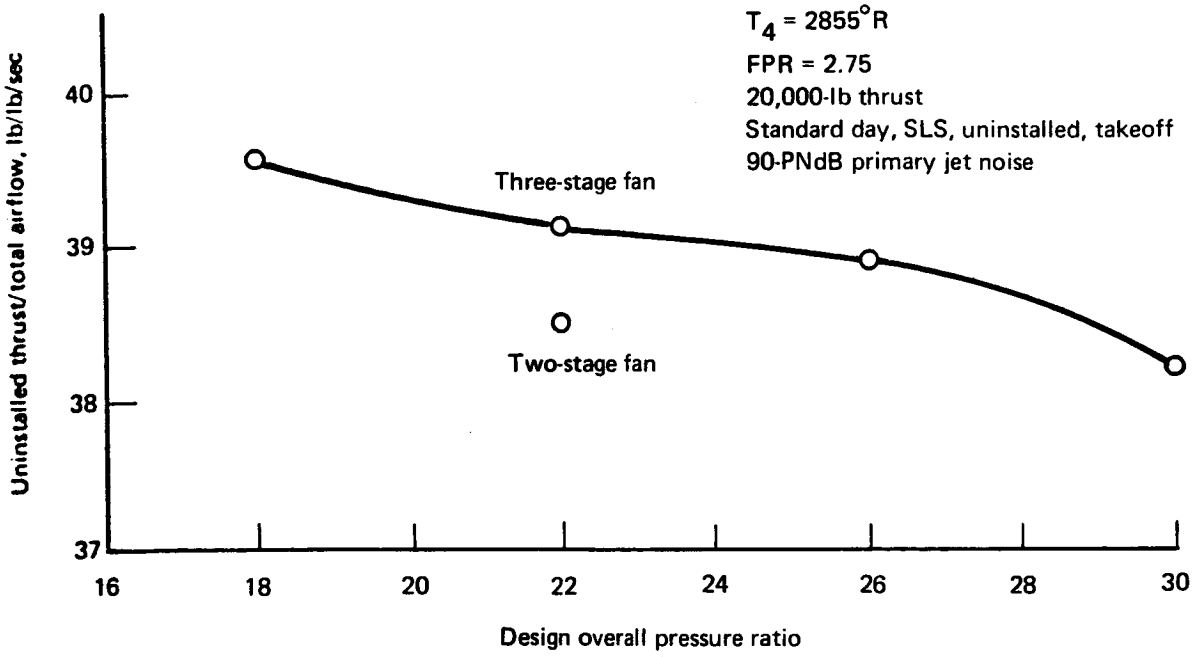

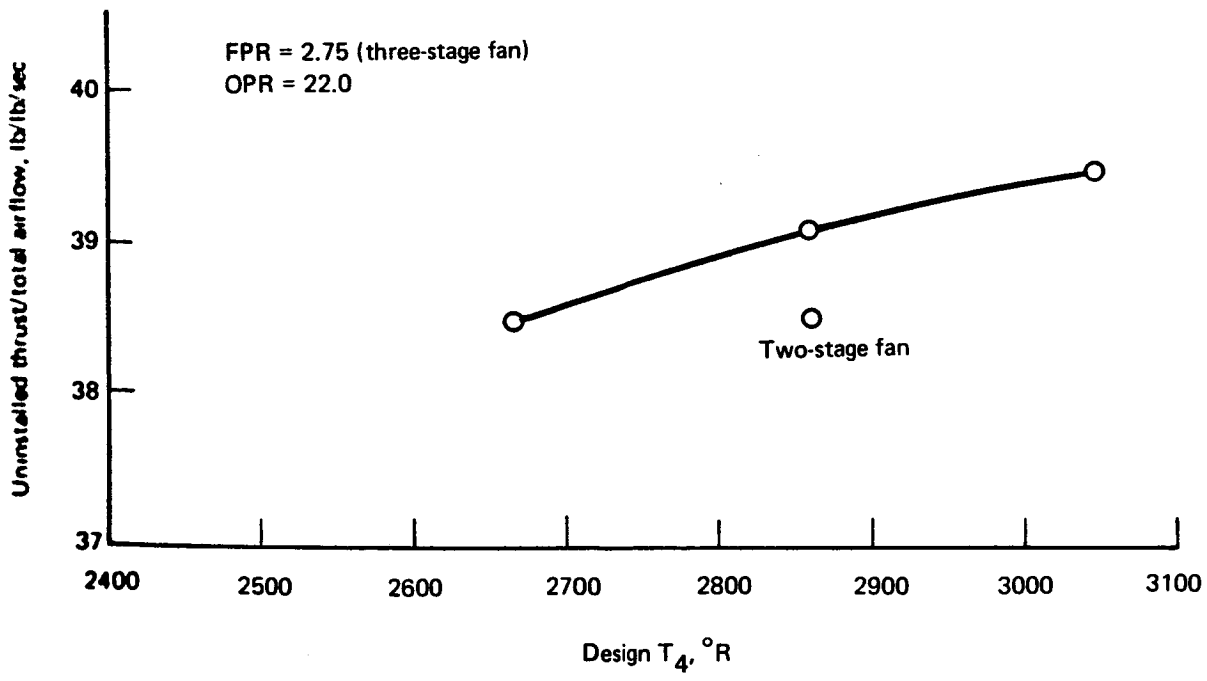

FIGURE 5-90.– UNINSTALLED THRUST/TOTAL AIRFLOW VS DESIGN OVERALL PRESSURE RATIO AND DESIGN T_4

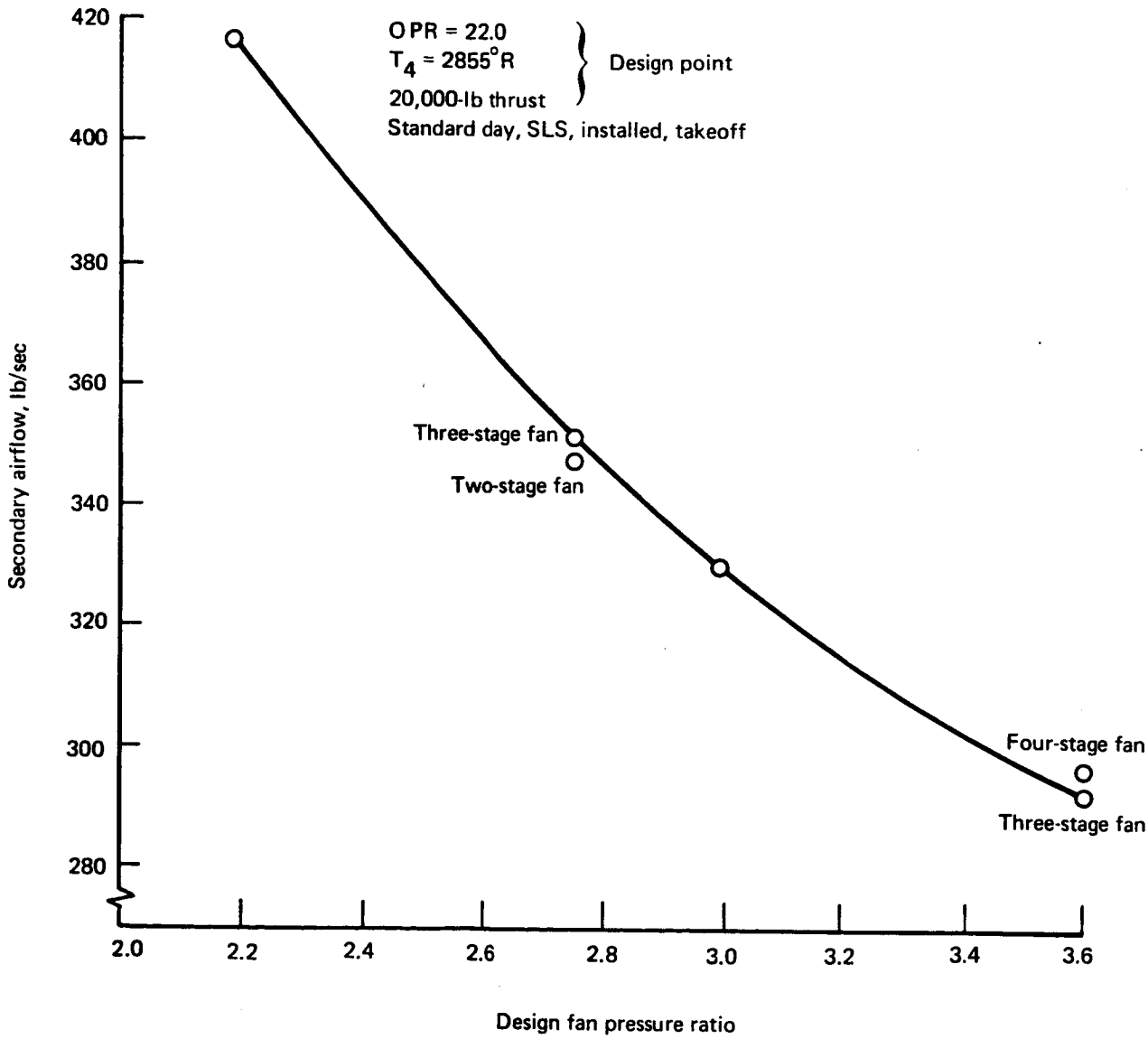

FIGURE 5-91.– SECONDARY AIRFLOW VS DESIGN FAN PRESSURE RATIO

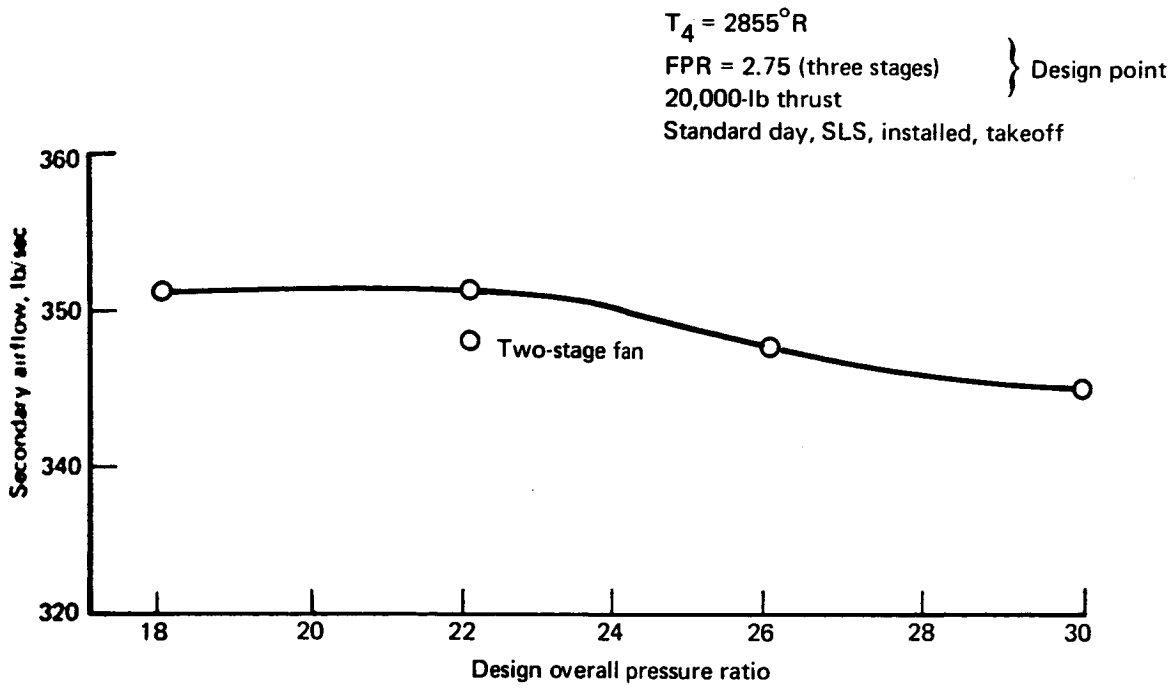

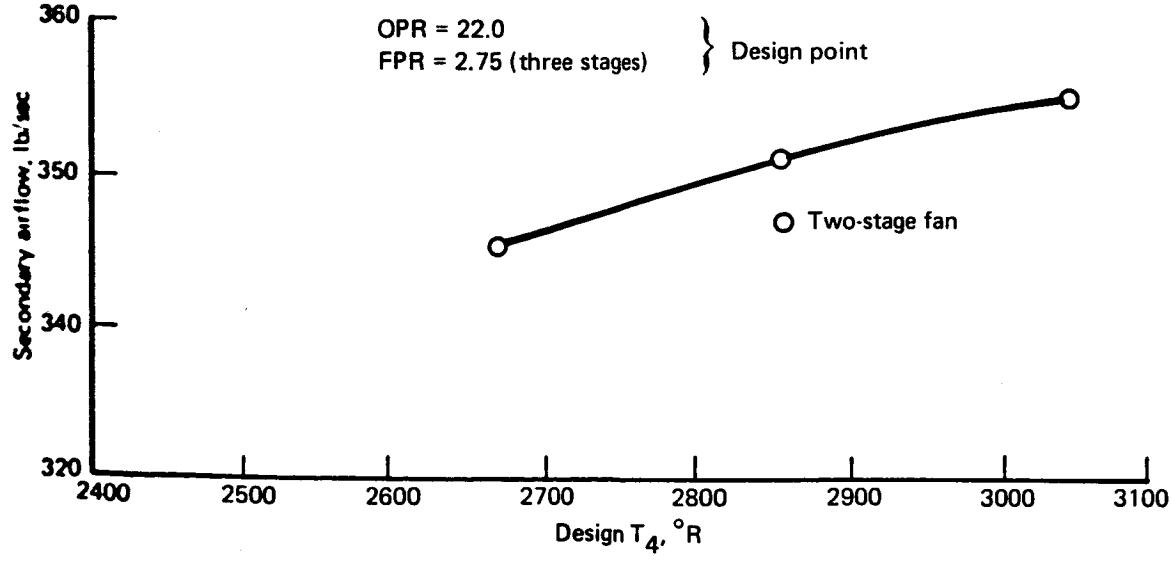

FIGURE 5-92.– SECONDARY AIRFLOW VS DESIGN OVERALL PRESSURE RATIO AND DESIGN T_4

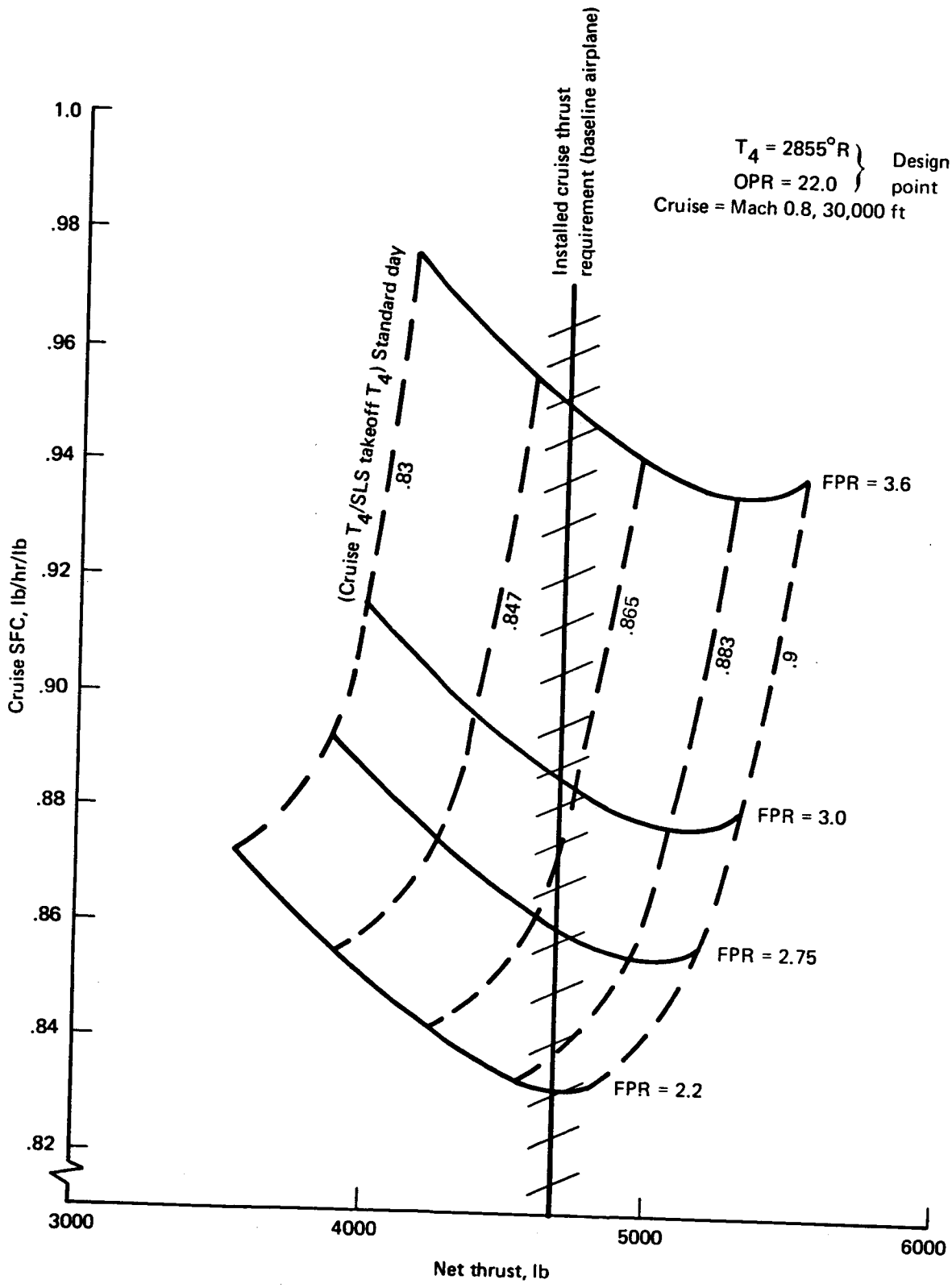

FIGURE 5.93.– INSTALLED CRUISE PERFORMANCE, ENGINES 1, 2, 3, AND 4

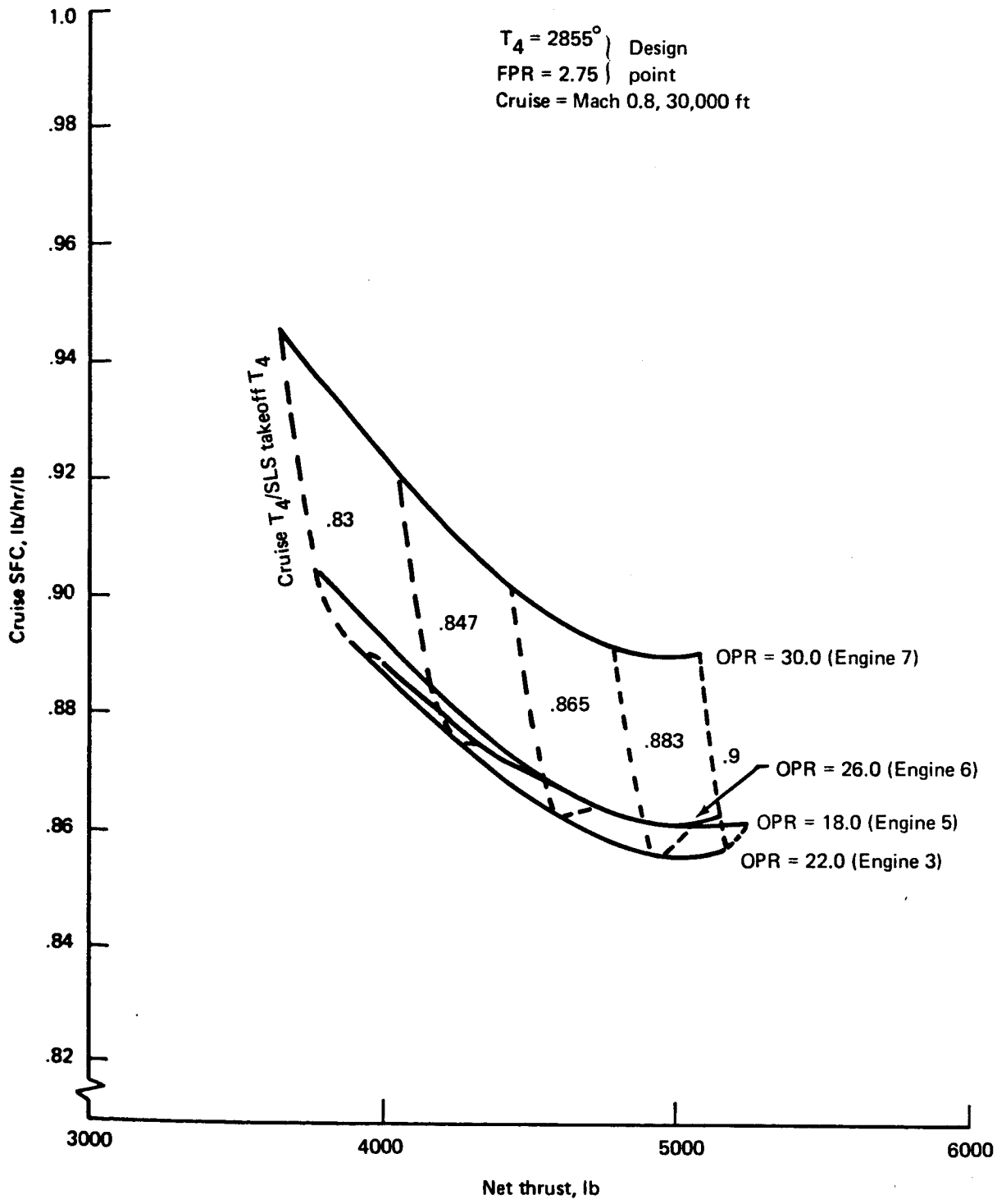

FIGURE 5-94.– INSTALLED CRUISE PERFORMANCE, ENGINES 3, 5, 6, AND 7

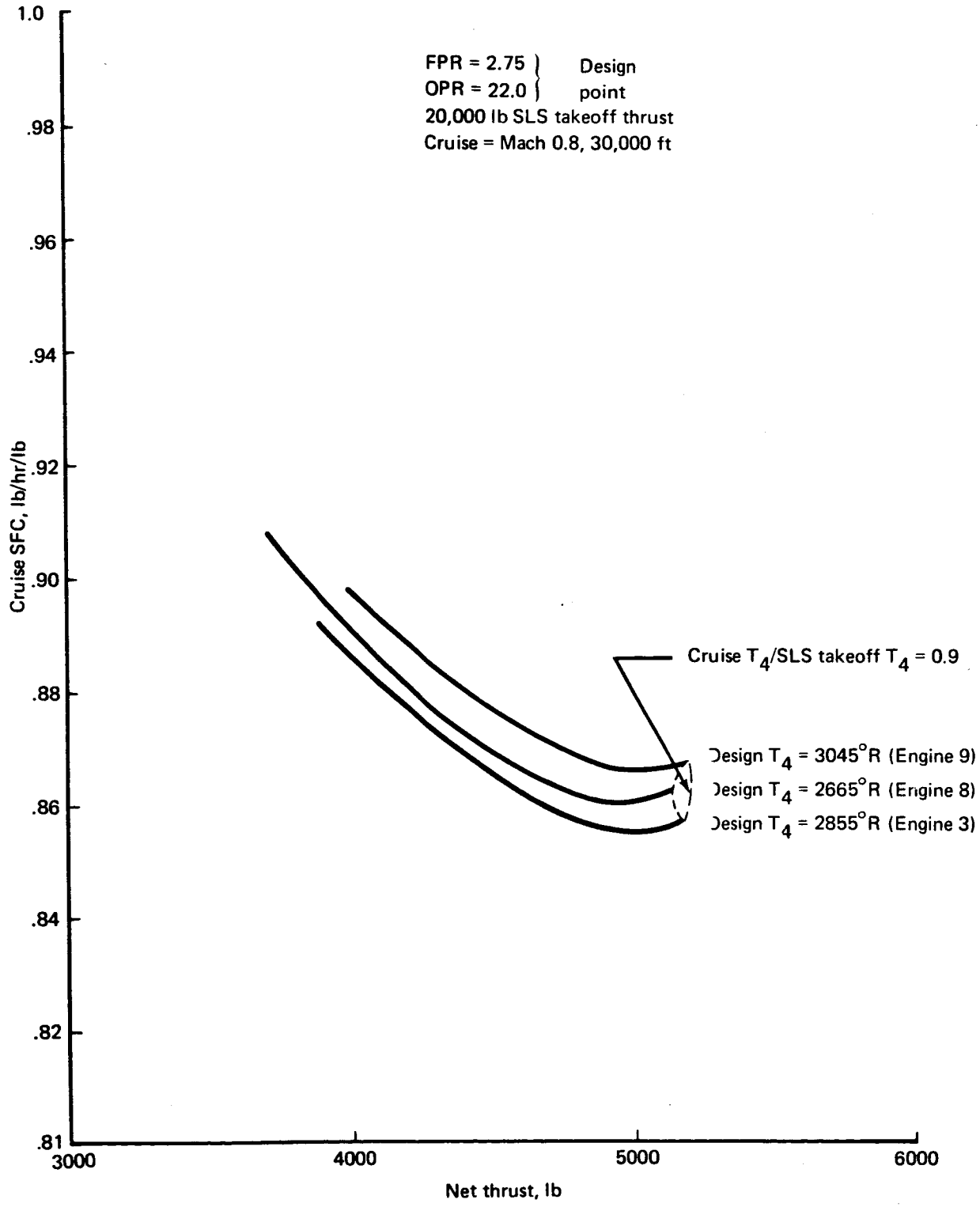

FIGURE 5-95.—INSTALLED CRUISE PERFORMANCE, ENGINES 3, 8, AND 9

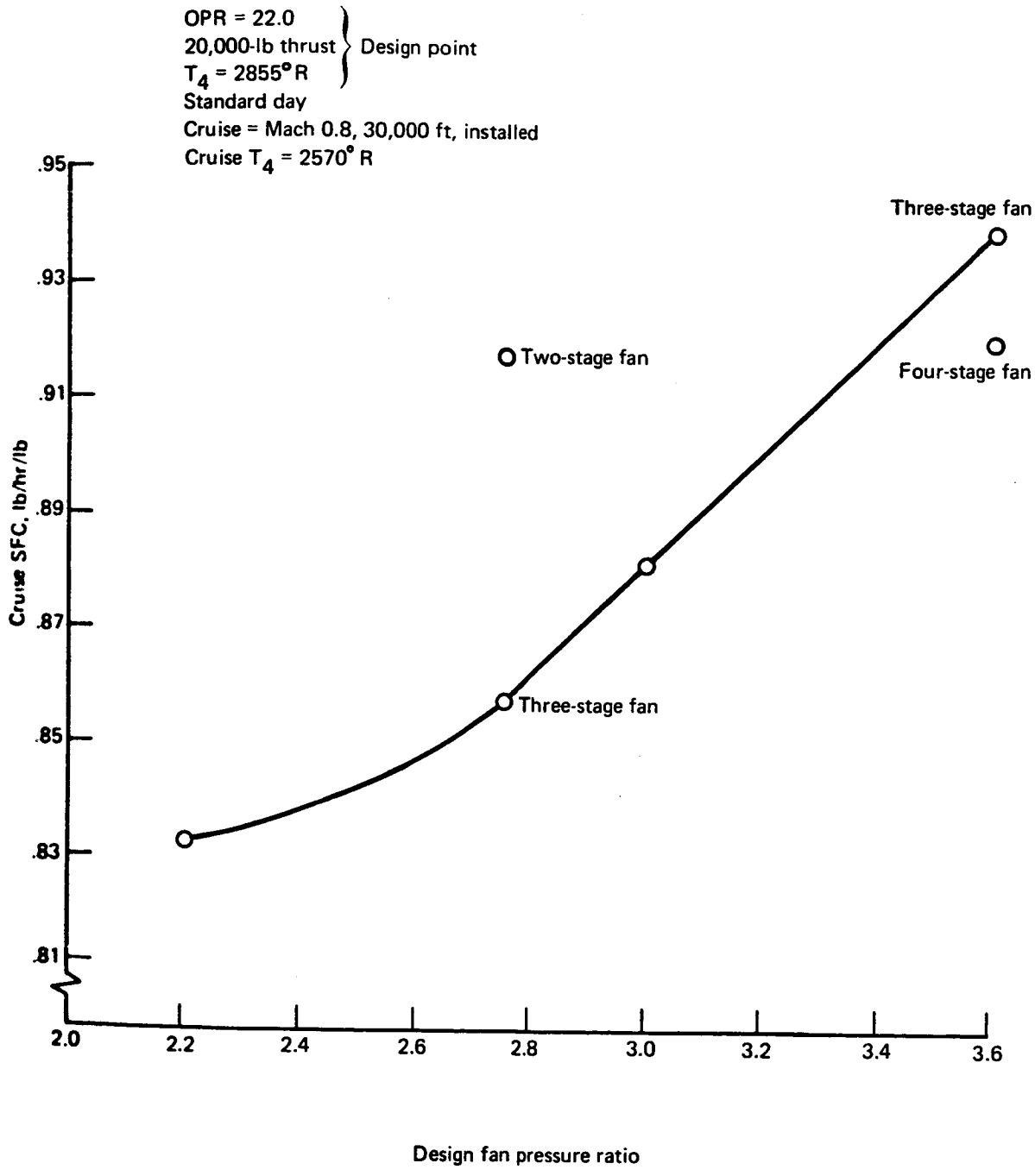

FIGURE 5-96.– INSTALLED CRUISE SFC VS DESIGN FAN PRESSURE RATIO

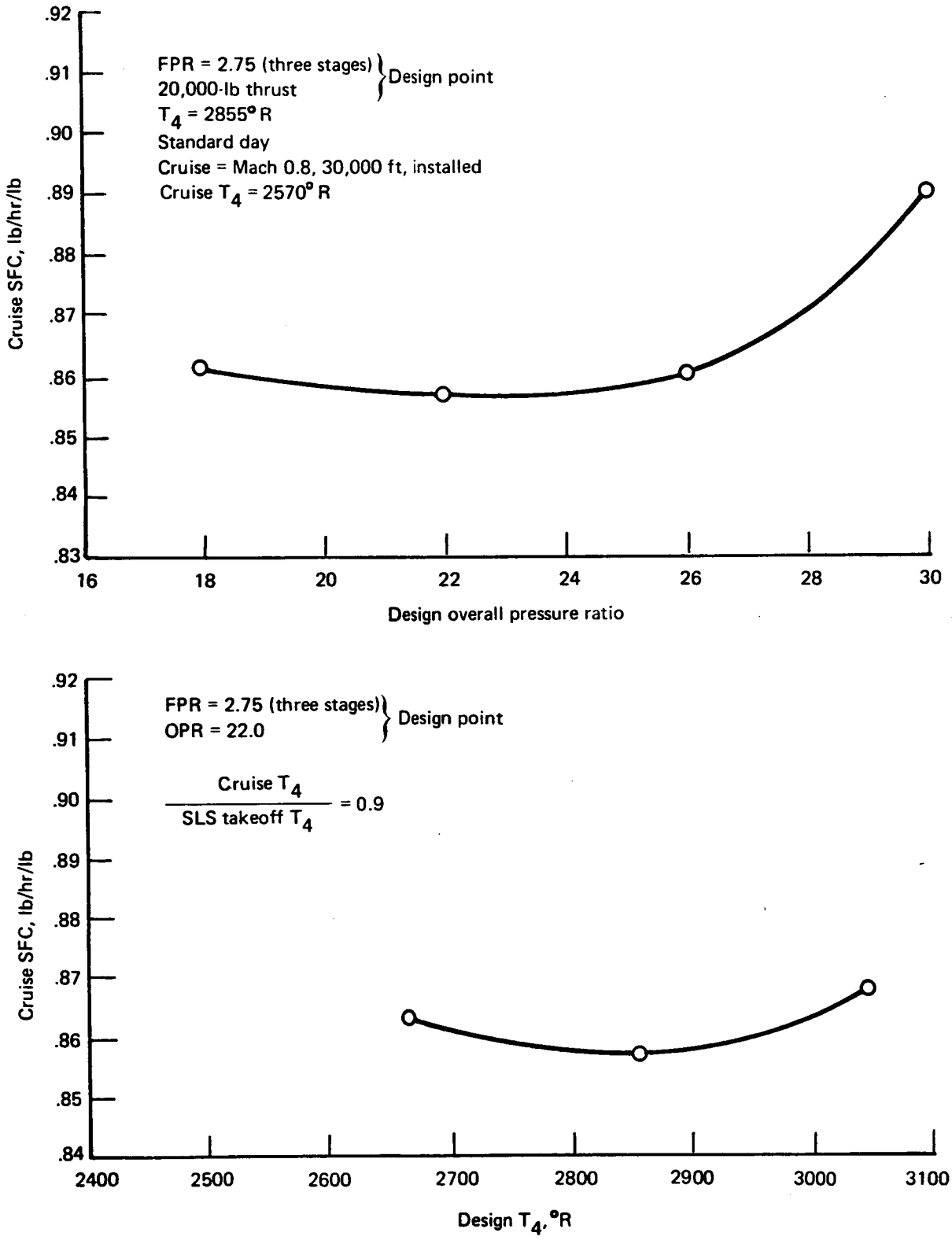

FIGURE 5-97.—INSTALLED CRUISE SFC VS DESIGN OVERALL PRESSURE RATIO AND DESIGN T_4

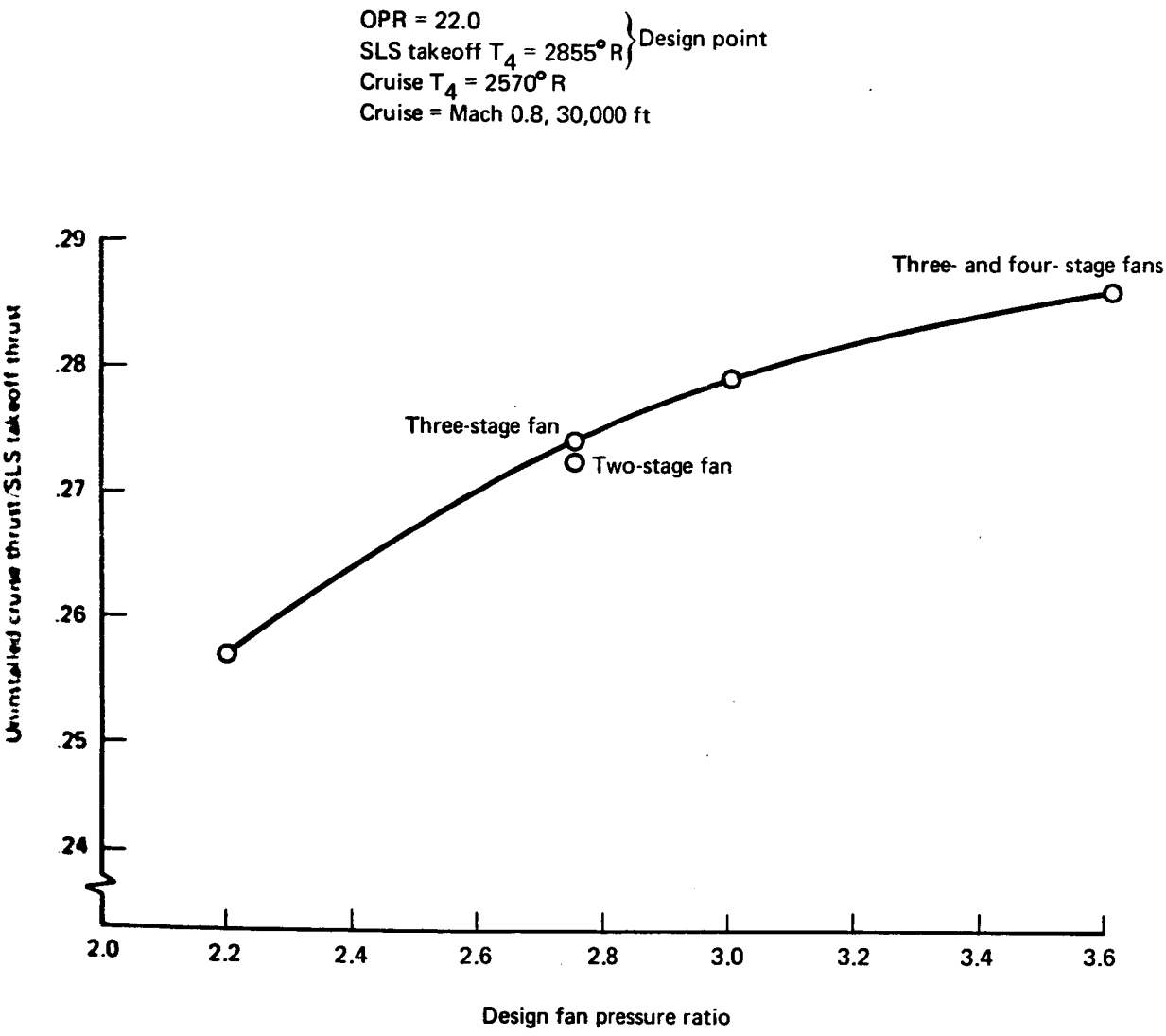

FIGURE 5-98.—UNINSTALLED CRUISE THRUST/SLS TAKEOFF THRUST VS DESIGN FAN PRESSURE RATIO

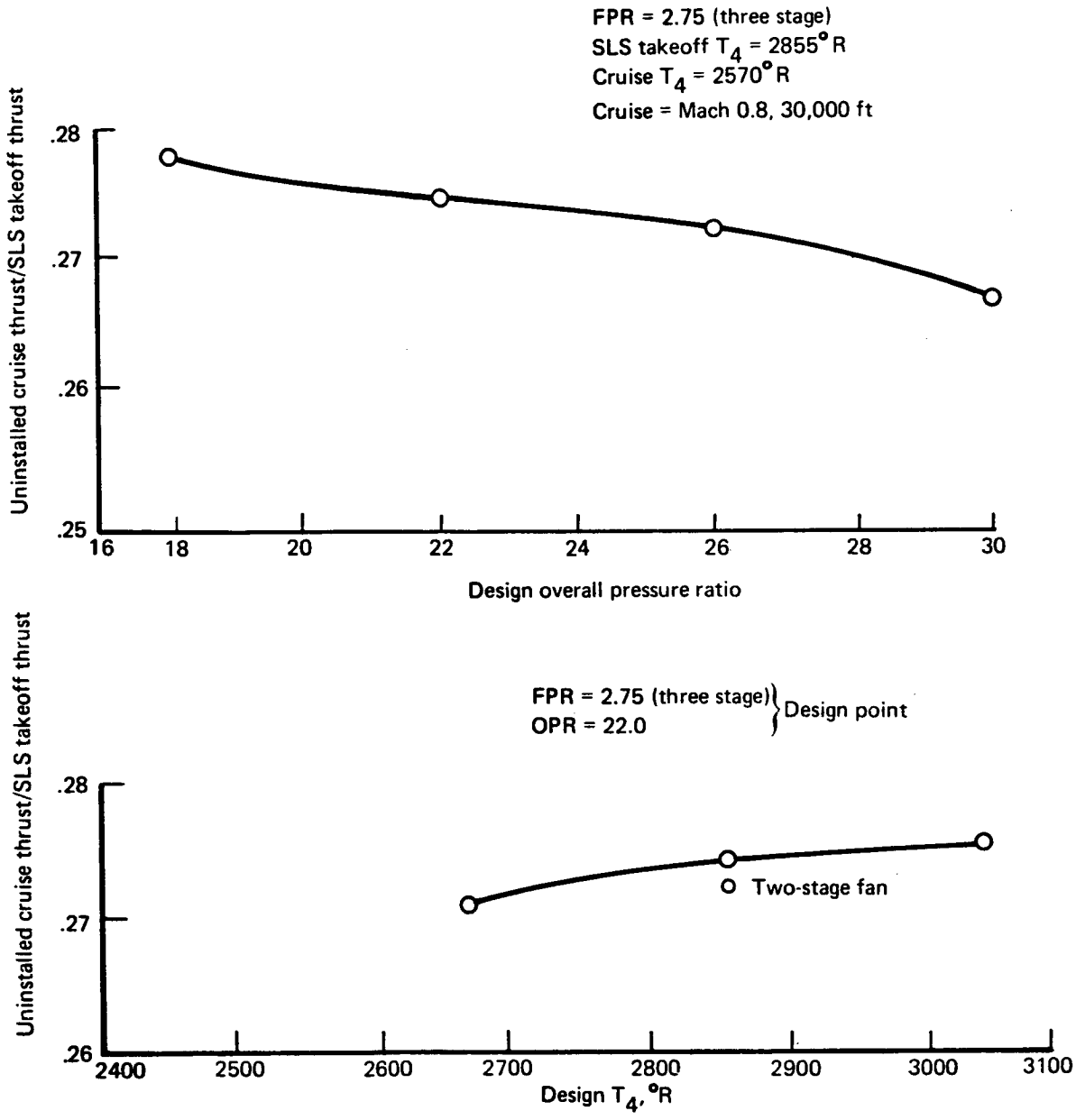

FIGURE 5-99.—UNINSTALLED CRUISE THRUST/SLS TAKEOFF THRUST VS DESIGN OVERALL PRESSURE RATIO AND DESIGN T_4

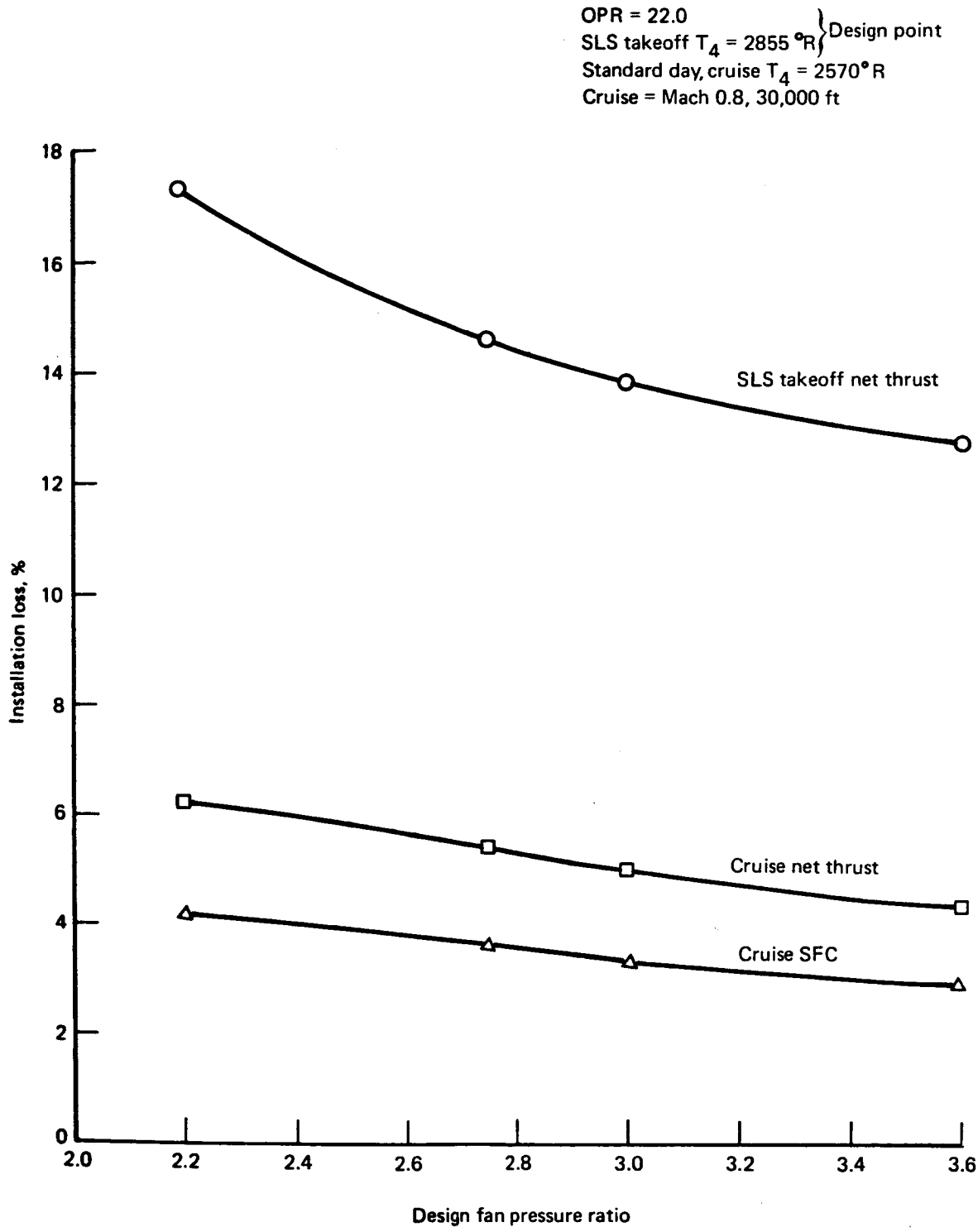

FIGURE 5-100.– INSTALLATION EFFECTS–PERCENT LOSSES IN SEA LEVEL STATIC TAKEOFF THRUST, CRUISE THRUST, AND CRUISE SFC VS DESIGN FAN PRESSURE RATIO

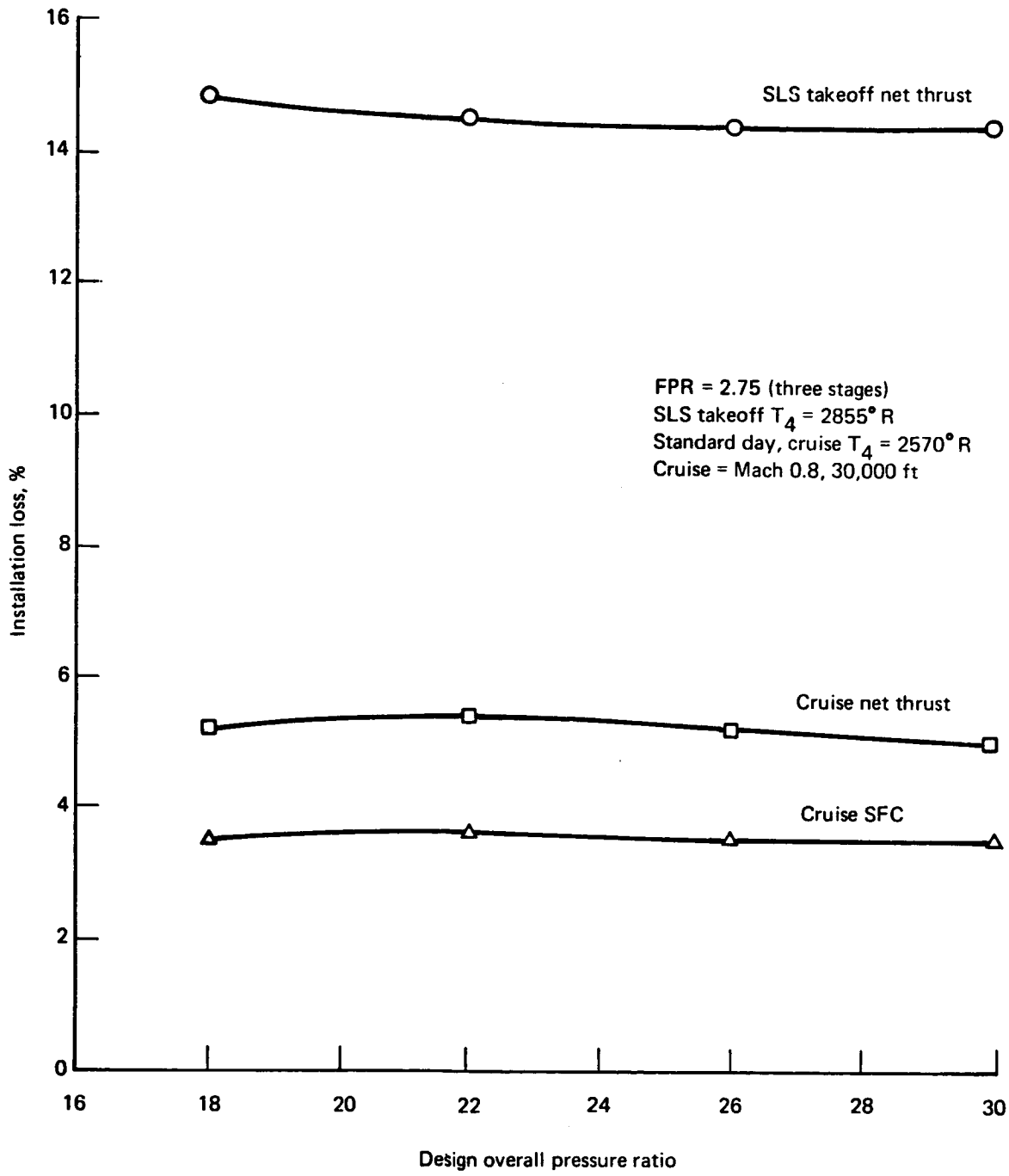

FIGURE 5-101.– INSTALLATION EFFECTS–PERCENT LOSSES IN SEA LEVEL STATIC TAKEOFF THRUST, CRUISE THRUST, AND CRUISE SFC VS DESIGN OVERALL PRESSURE RATIO

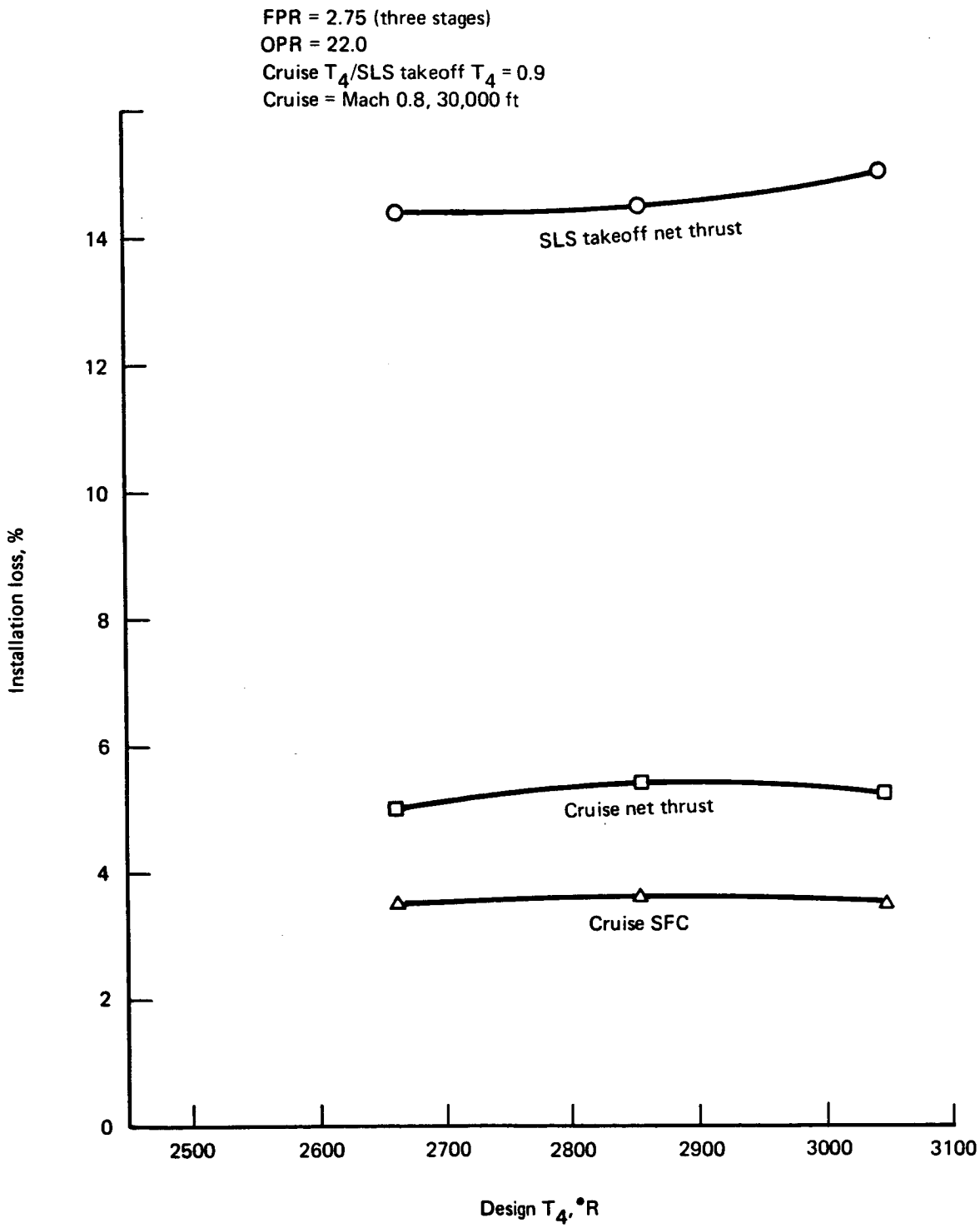

FIGURE 5-102. INSTALLATION EFFECTS—PERCENT LOSSES IN SEA LEVEL STATIC TAKEOFF THRUST, CRUISE THRUST, AND CRUISE SFC VS DESIGN T_4

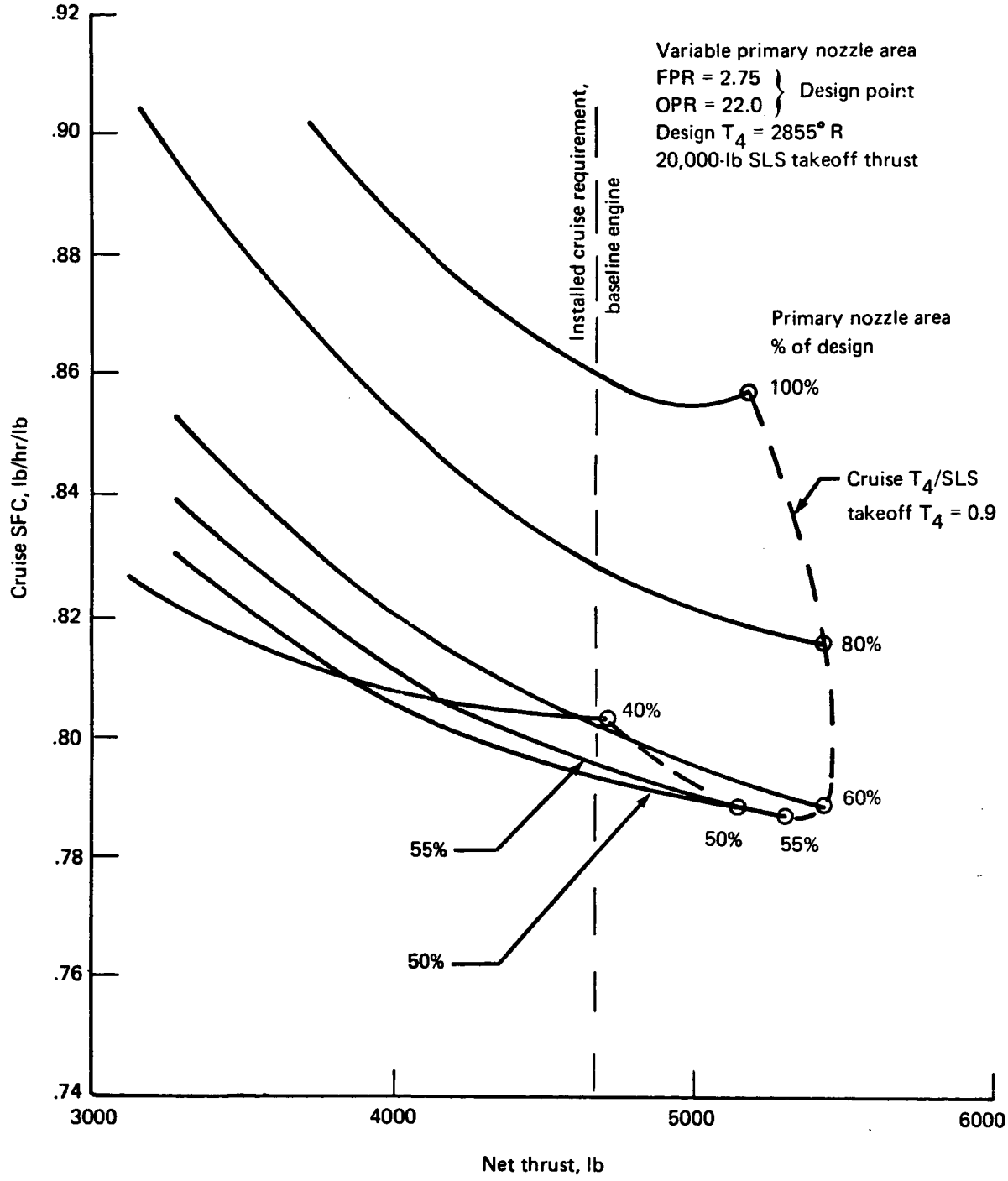

FIGURE 5-103.– INSTALLED CRUISE PERFORMANCE WITH VARIABLE PRIMARY NOZZLE AREA, ENGINE 3

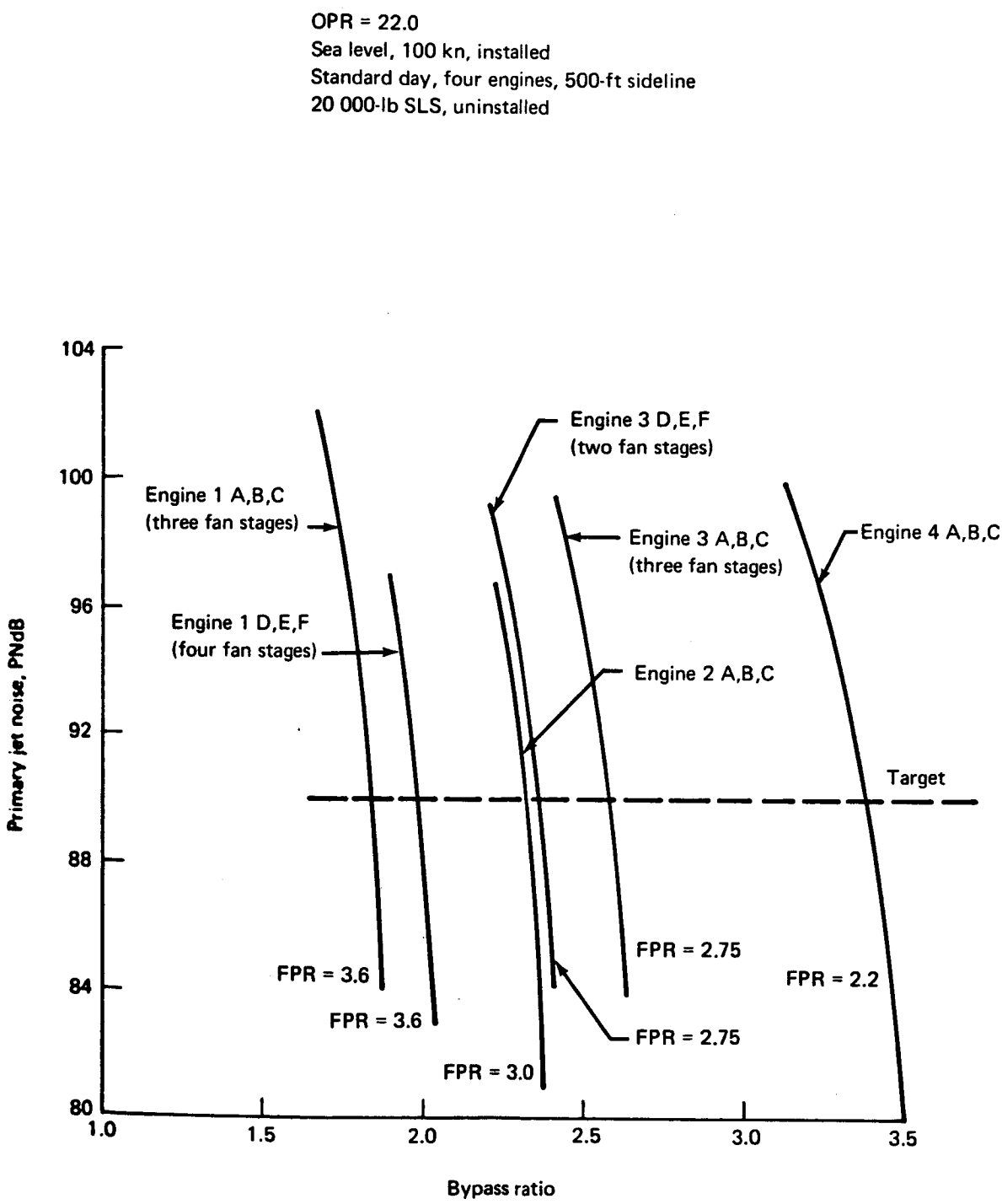

FIGURE 5-104.– PRIMARY JET NOISE VS BYPASS RATIO FOR VARYING FAN PRESSURE RATIO

FPR = 2.75
Sea level, 100 kn, installed
Standard day, four engines, 500-ft sideline
20,000-lb SLS thrust
Design T_4 = 2855° R

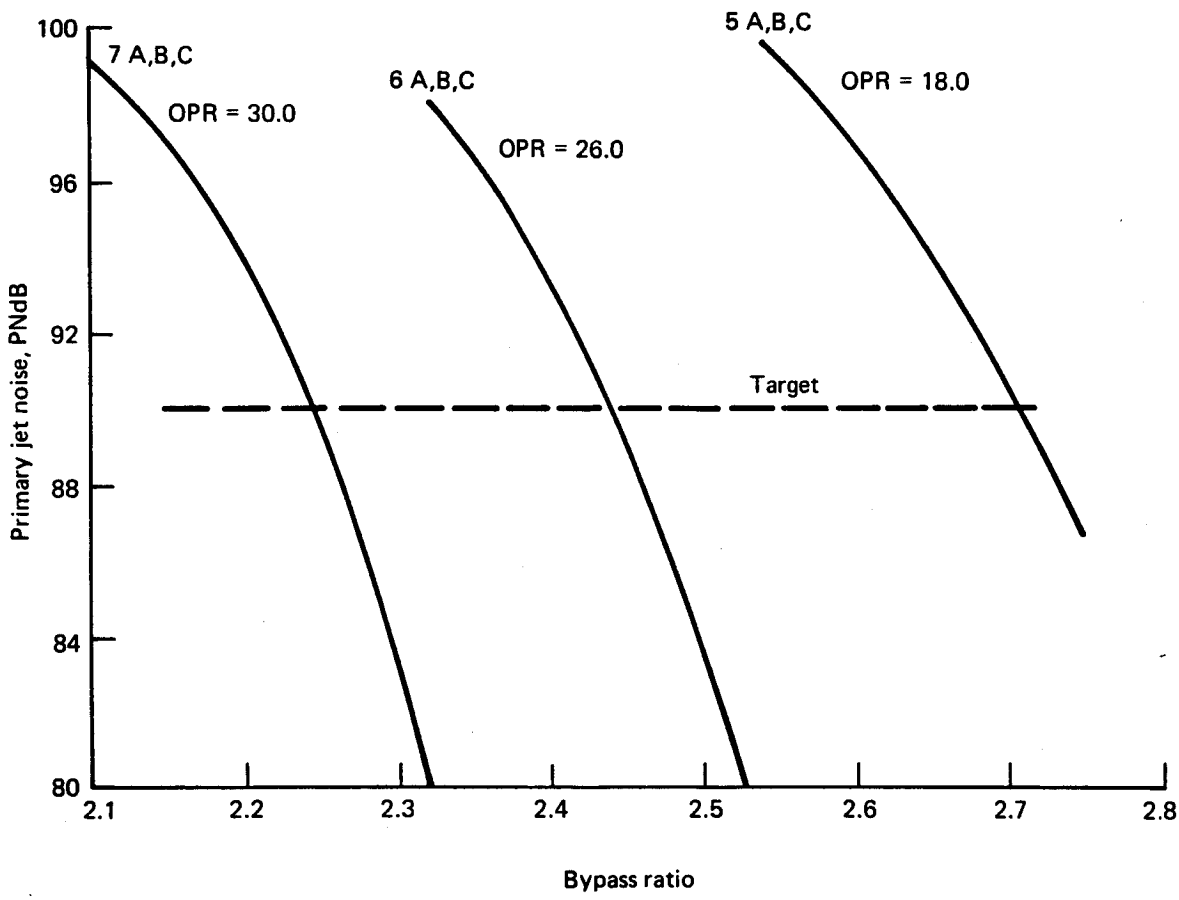

FIGURE 5-105.– PRIMARY JET NOISE VS BYPASS RATIO FOR VARYING OVERALL PRESSURE RATIO

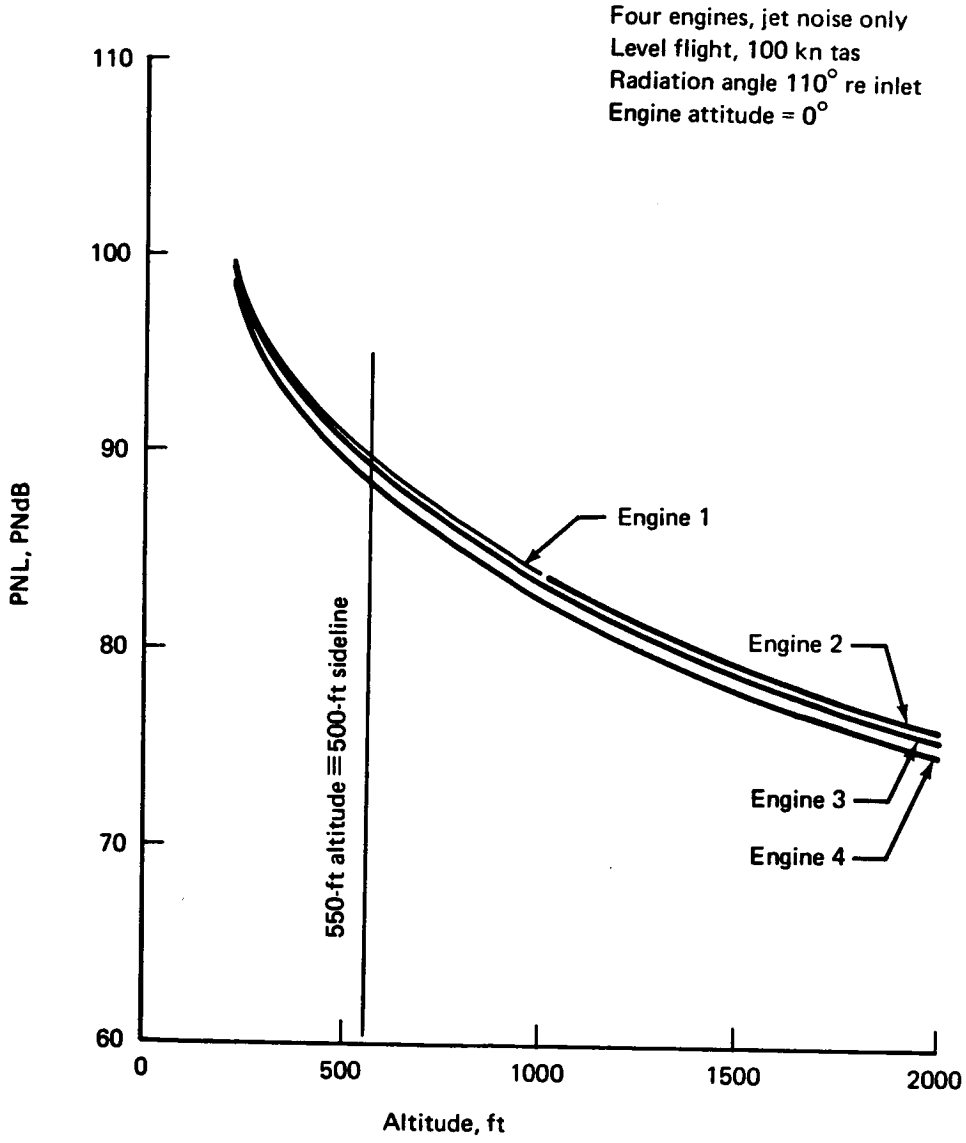

FIGURE 5-106.– PRIMARY JET NOISE VS ALTITUDE, ENGINES 1, 2, 3, AND 4

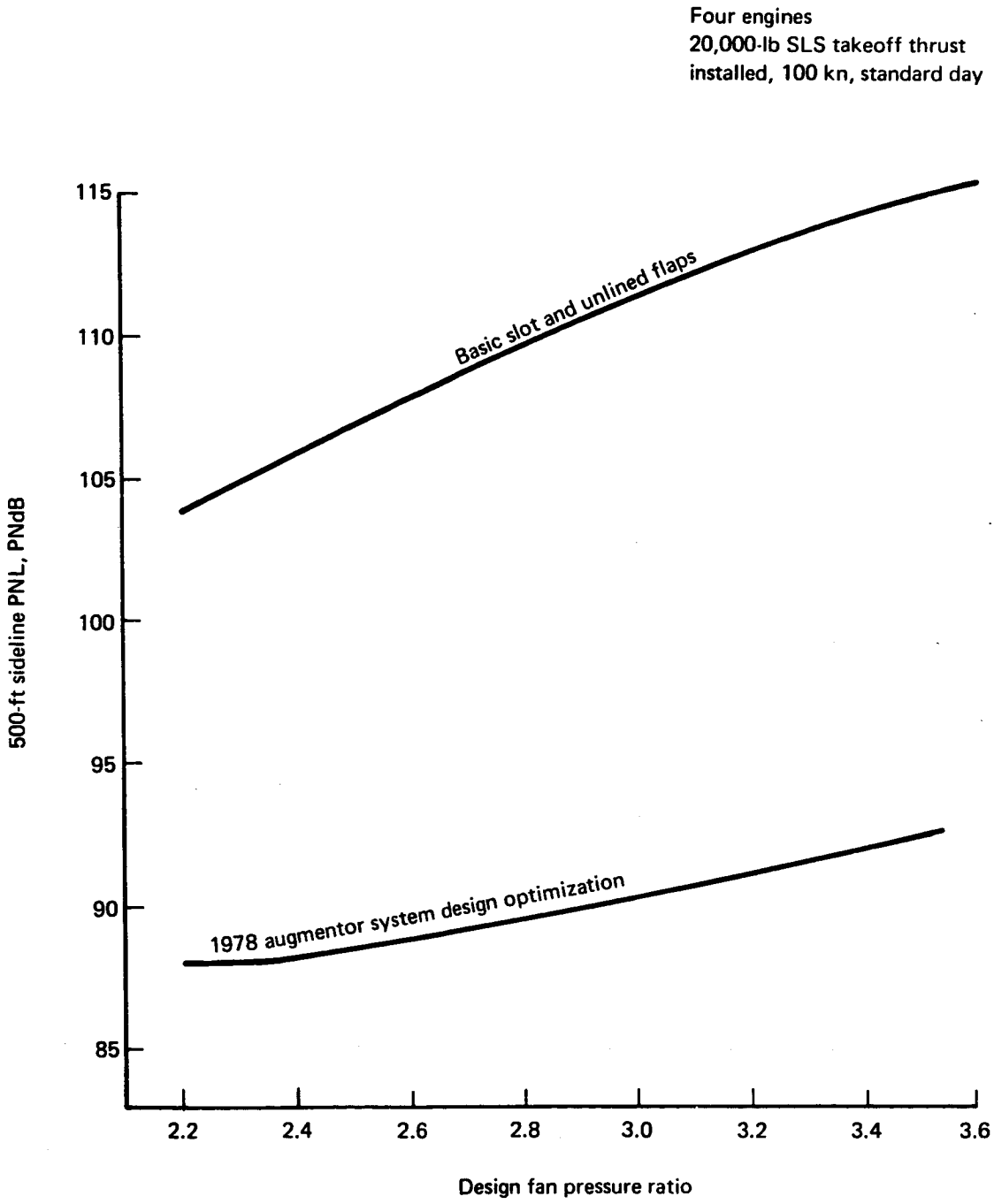

FIGURE 5-107.—AUGMENTOR NOISE VS DESIGN FAN PRESSURE RATIO, ENGINES 1, 2, 3, AND 4

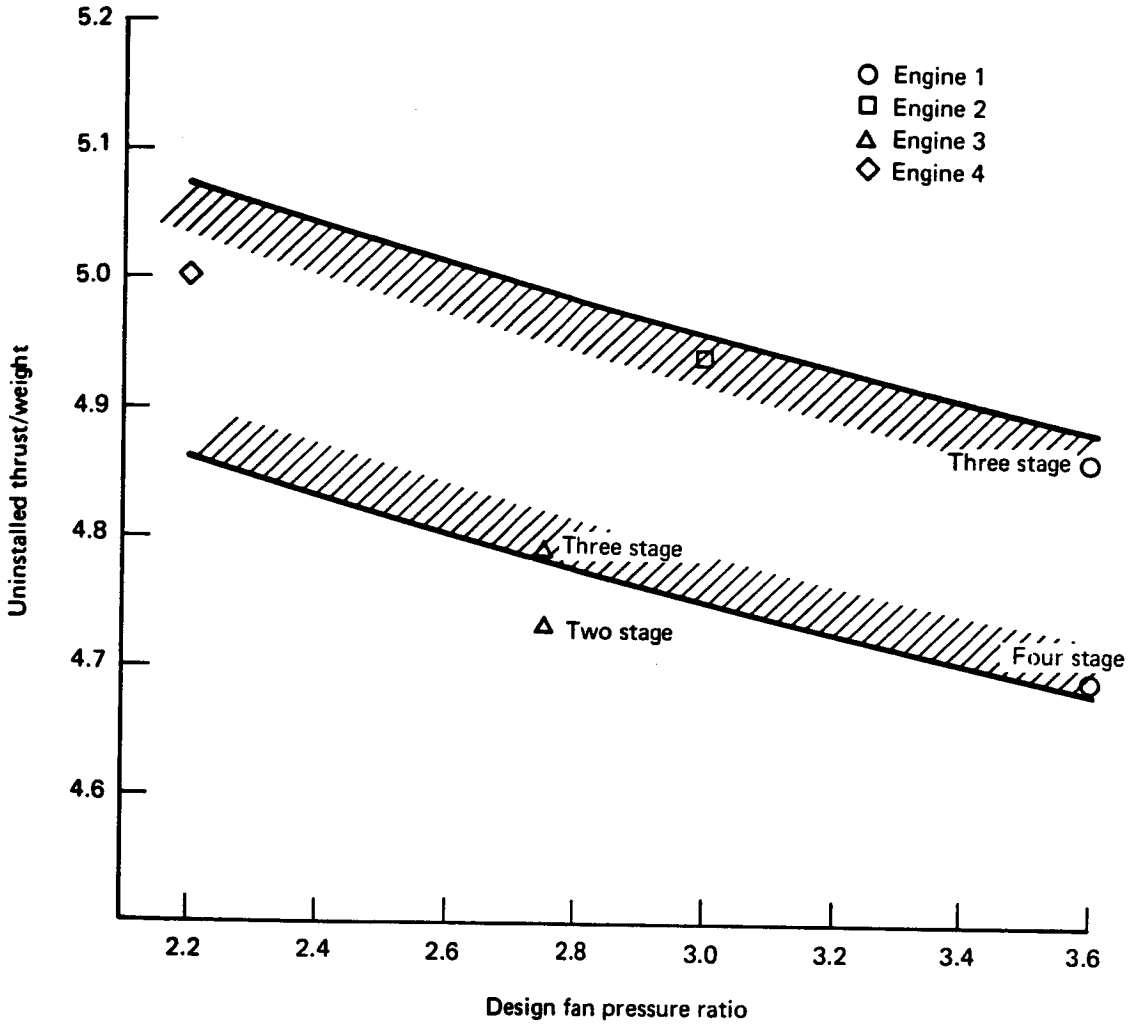

FIGURE 5-108.–UNINSTALLED THRUST/WEIGHT VS DESIGN FAN PRESSURE RATIO

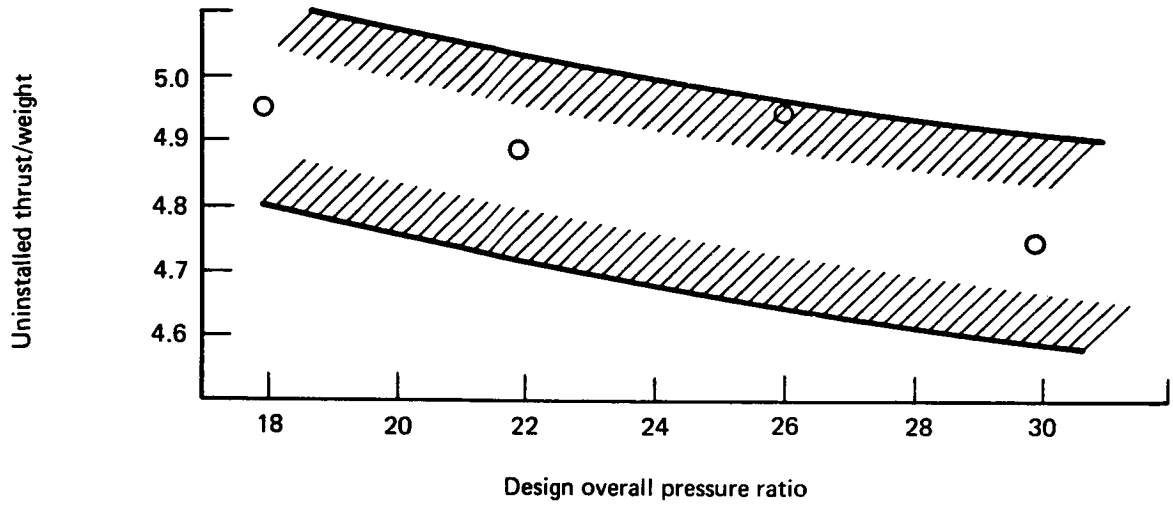

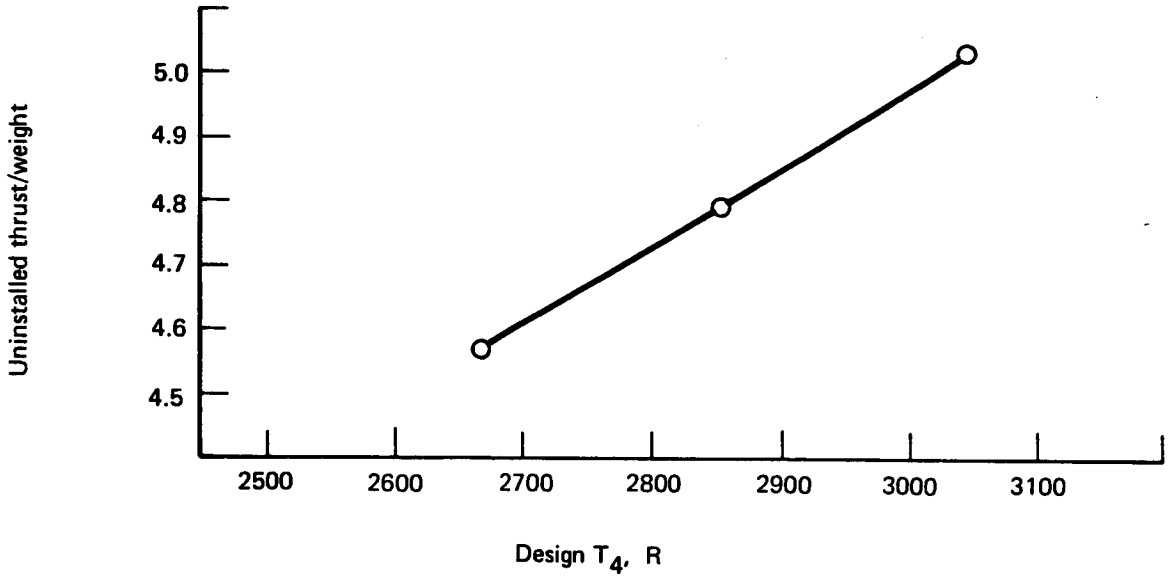

FIGURE 5-109.—UNINSTALLED THRUST/WEIGHT VS DESIGN OVERALL PRESSURE RATIO AND DESIGN T_4

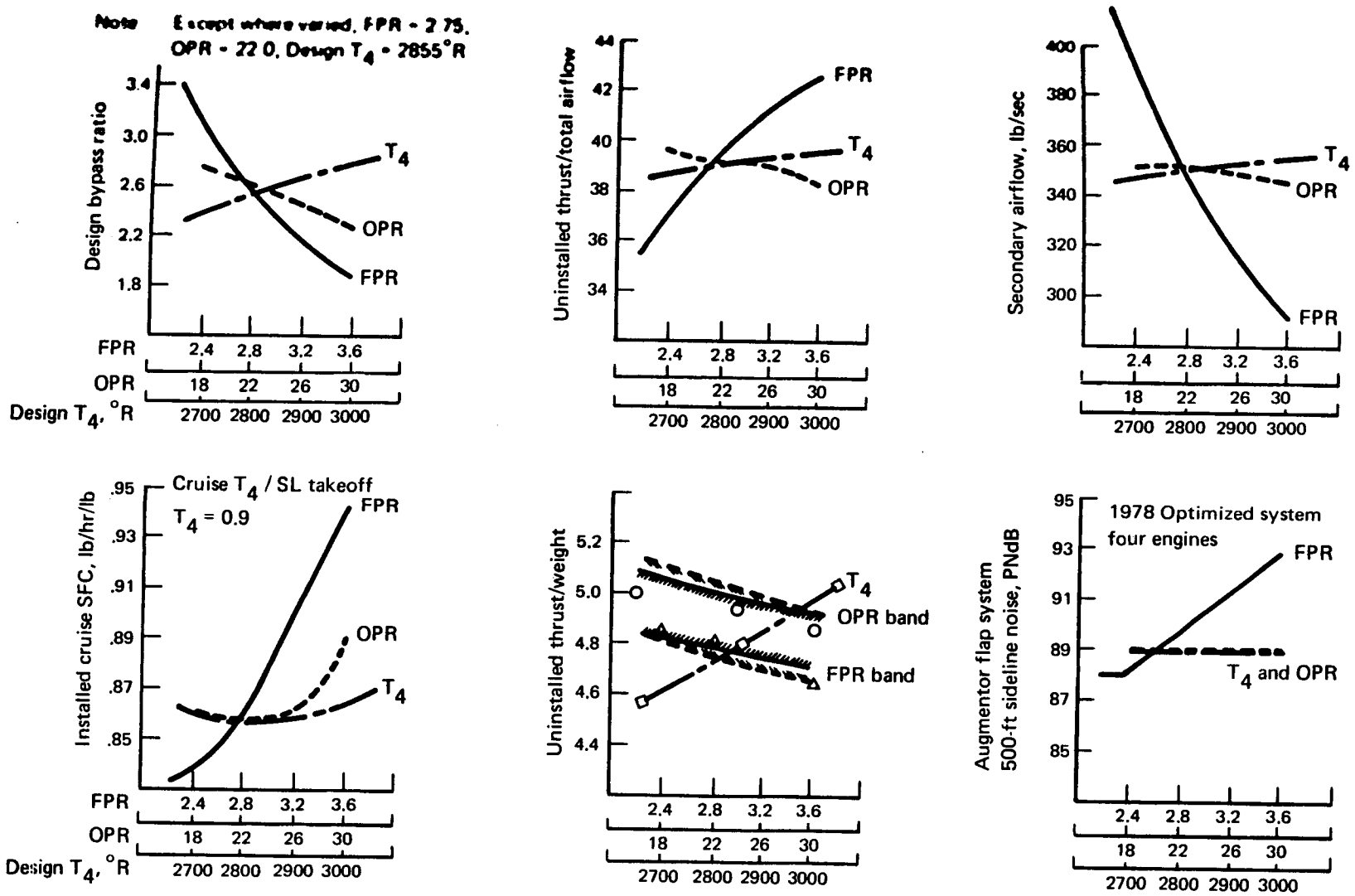

FIGURE 5-110.– SUMMARY OF PARAMETRIC STUDY RESULTS

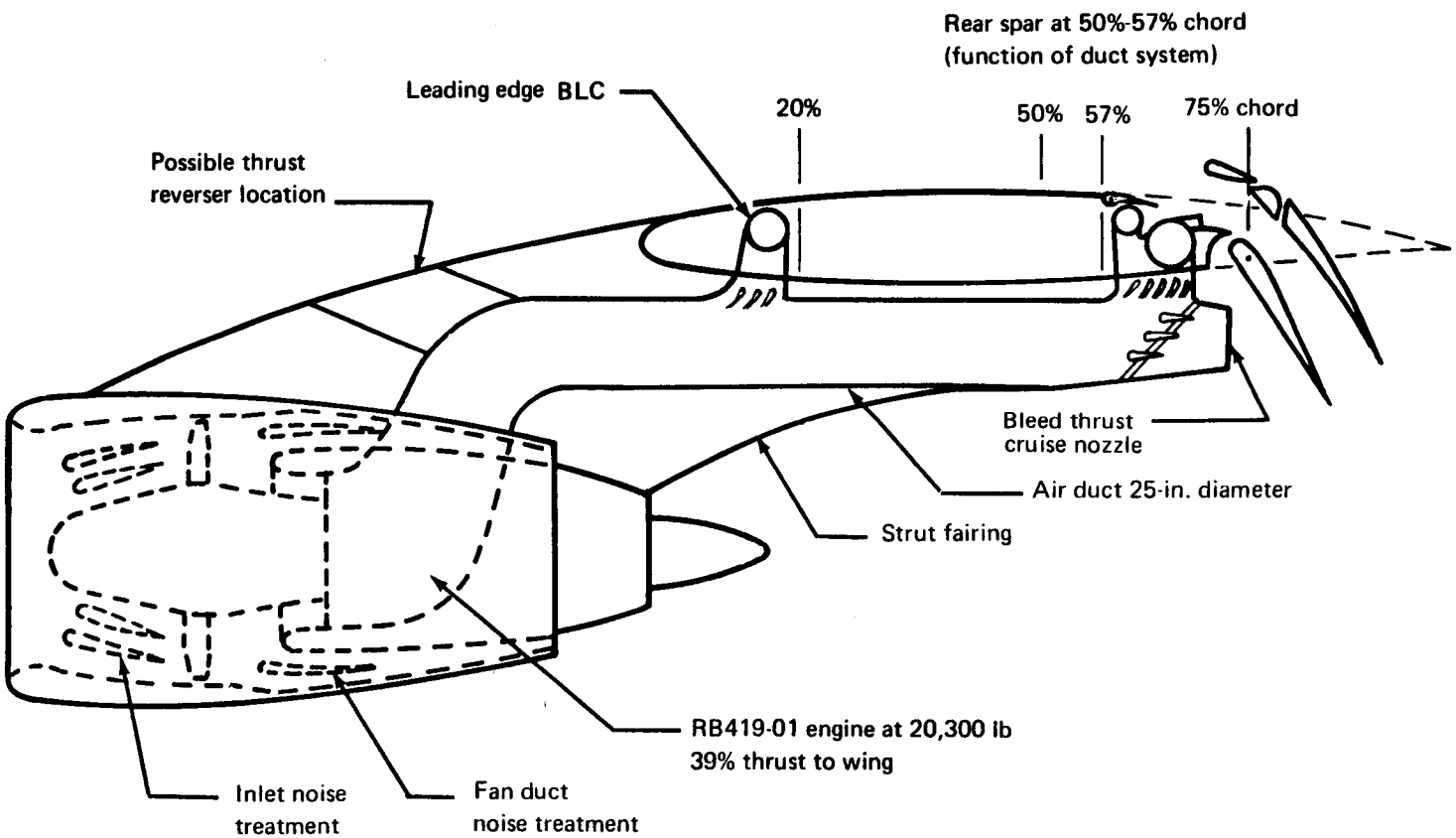

FIGURE 5-111.– ENGINE INSTALLATION–AUGMENTOR WING WITH THREE-STREAM ENGINE CYCLE

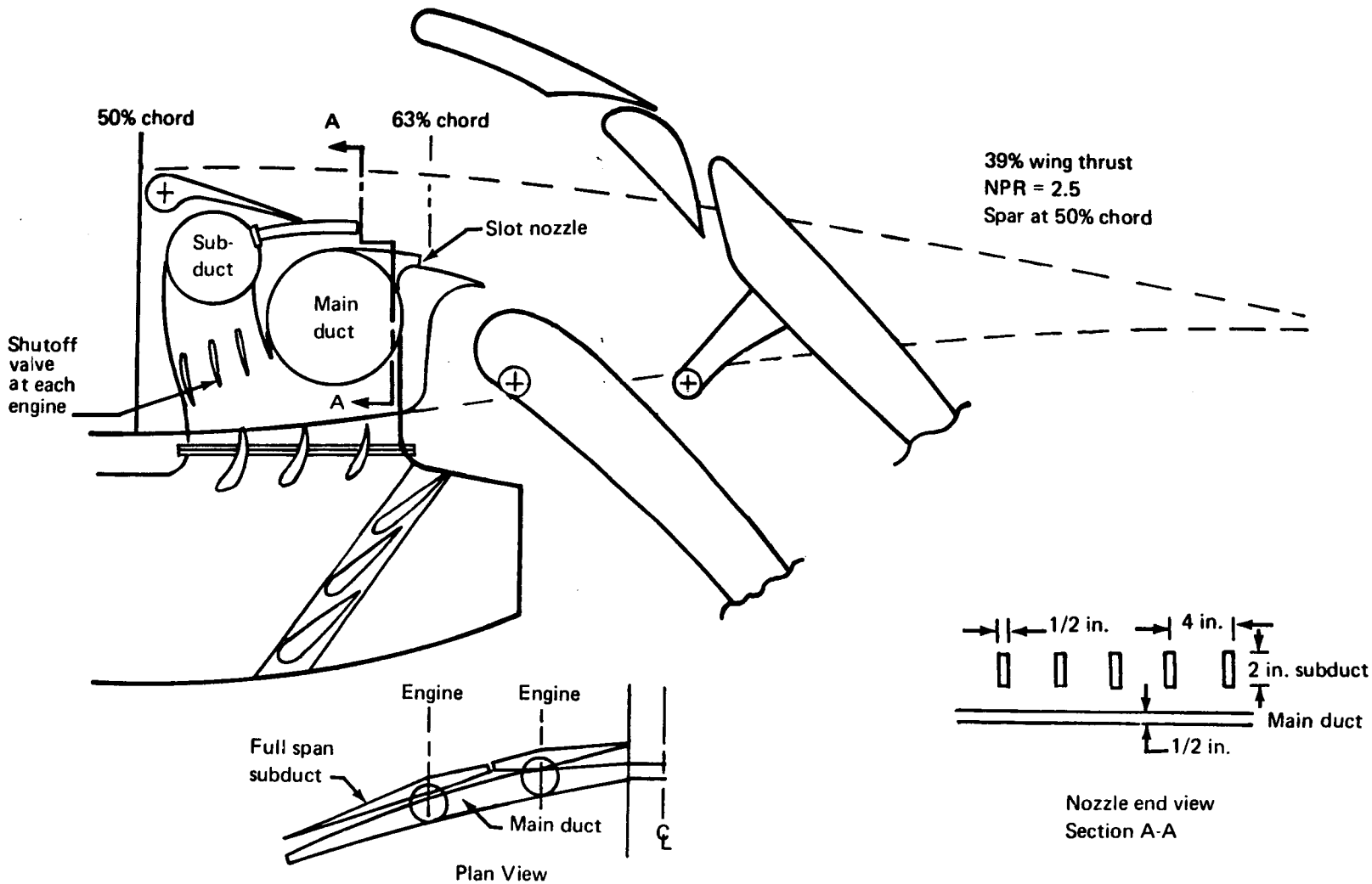

FIGURE 5-112.– THREE-STREAM AUGMENTOR PLENUM DUCT SYSTEM

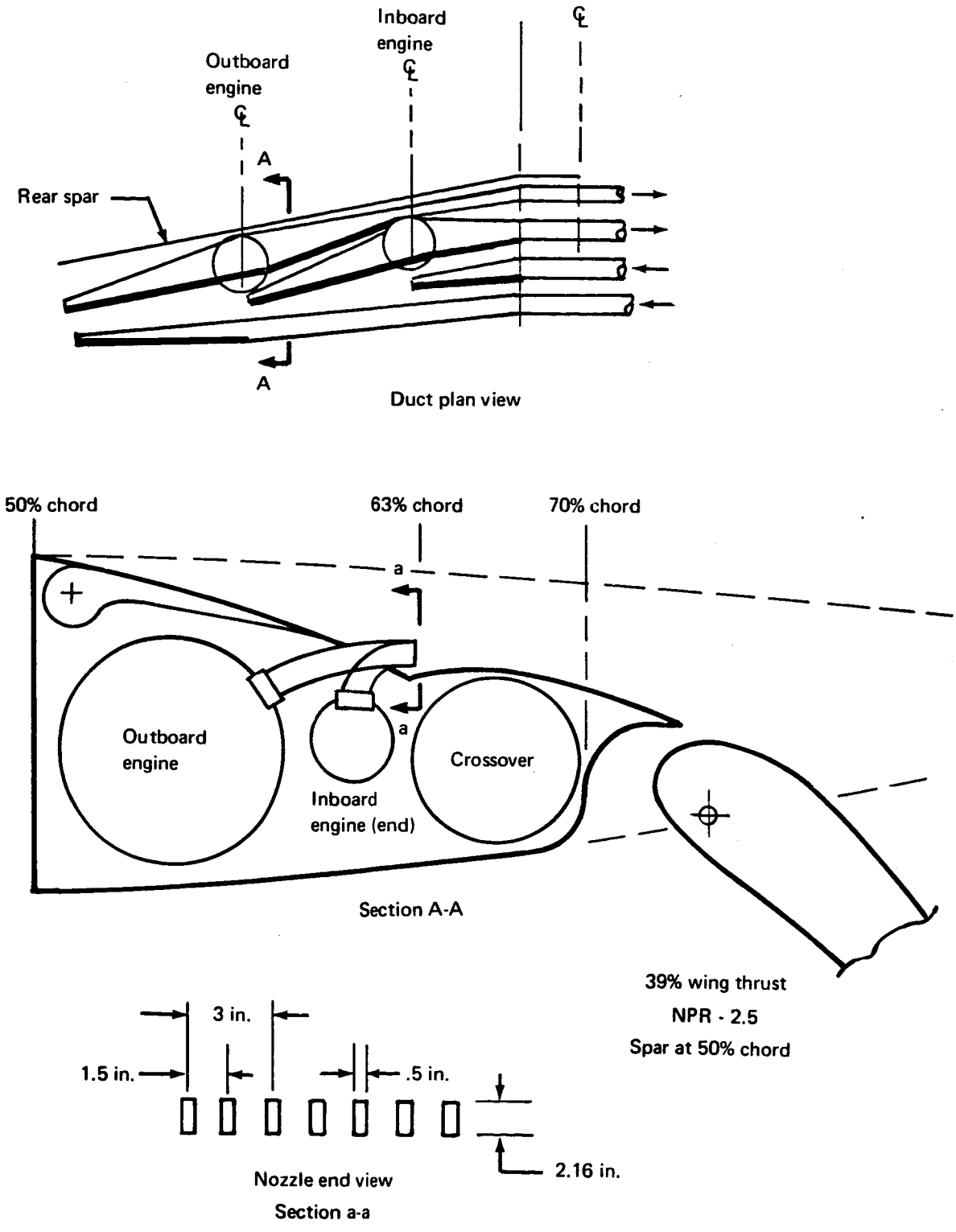

FIGURE 5-113.– THREE-STREAM AUGMENTOR INDEPENDENT DUCT SYSTEM

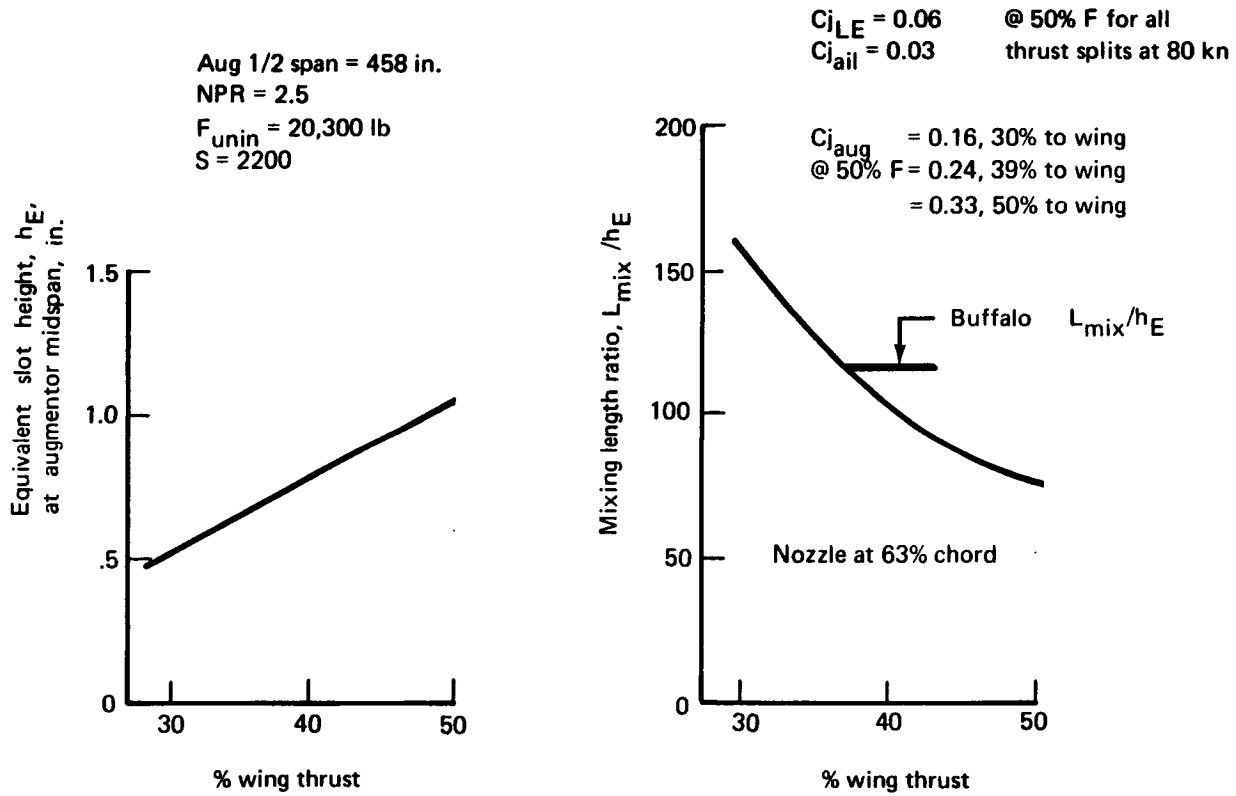

FIGURE 5-114.– THREE-STREAM AUGMENTOR–EQUIVALENT NOZZLE HEIGHT AND MIXING LENGTH RATIO

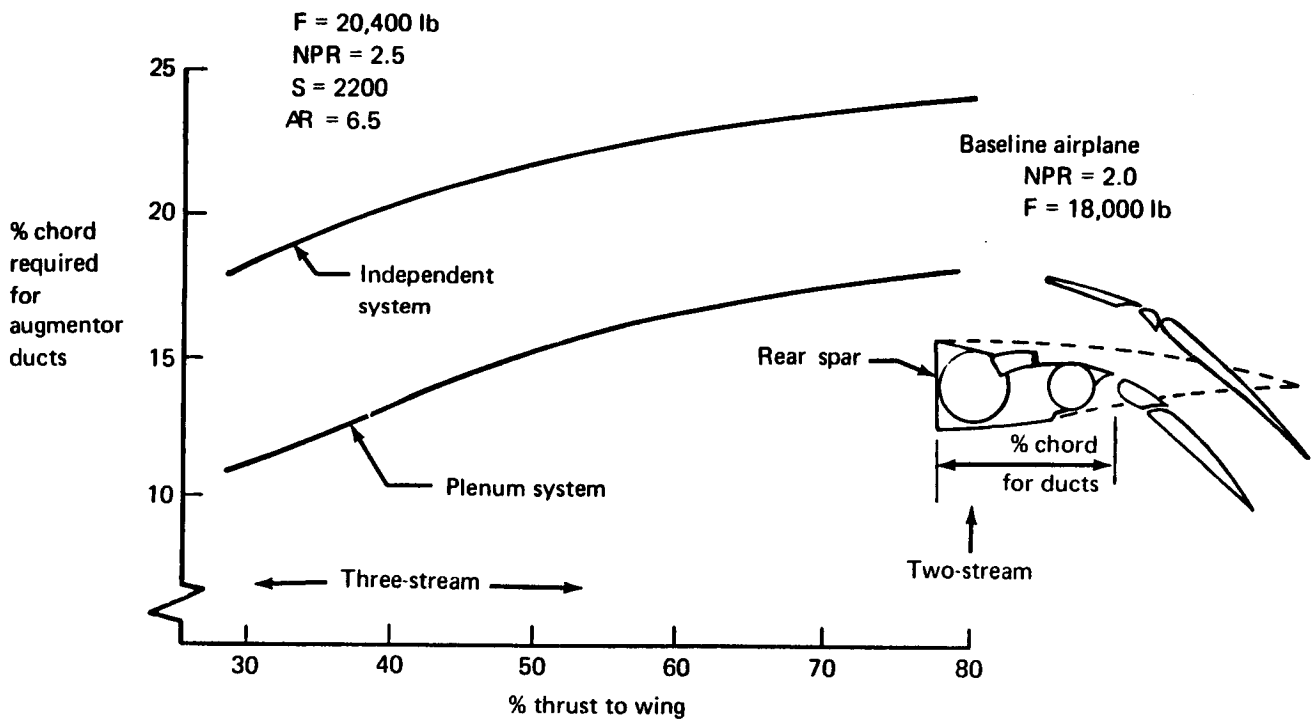

FIGURE 5-115.– COMPARISON OF DUCT VOLUME BETWEEN TWO- AND THREE-STREAM AUGMENTORS

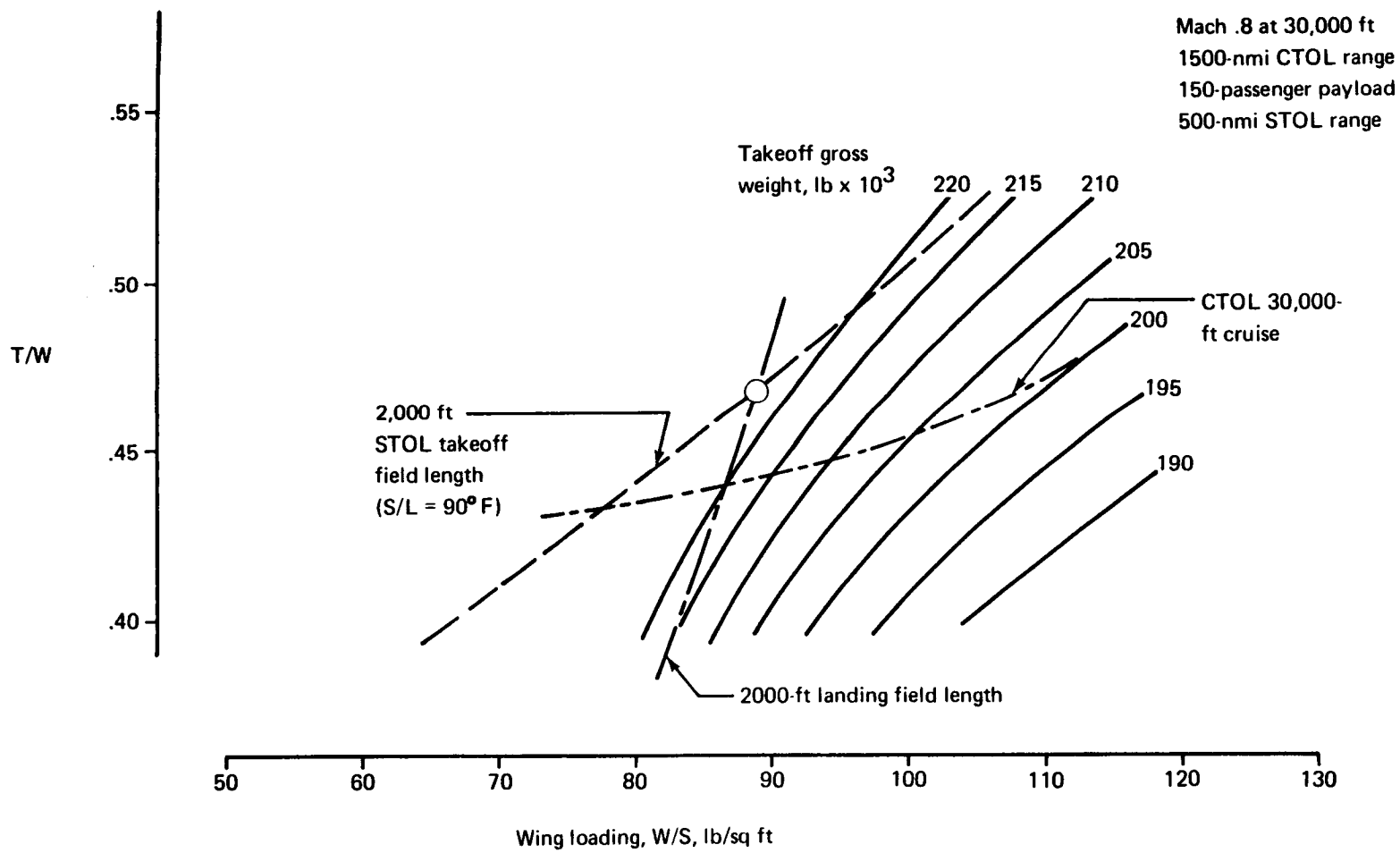

FIGURE 5-116.—AIRPLANE/ENGINE DESIGN RELATIONSHIP, THREE-STREAM AUGMENTOR WING, 30% BLOWING THRUST

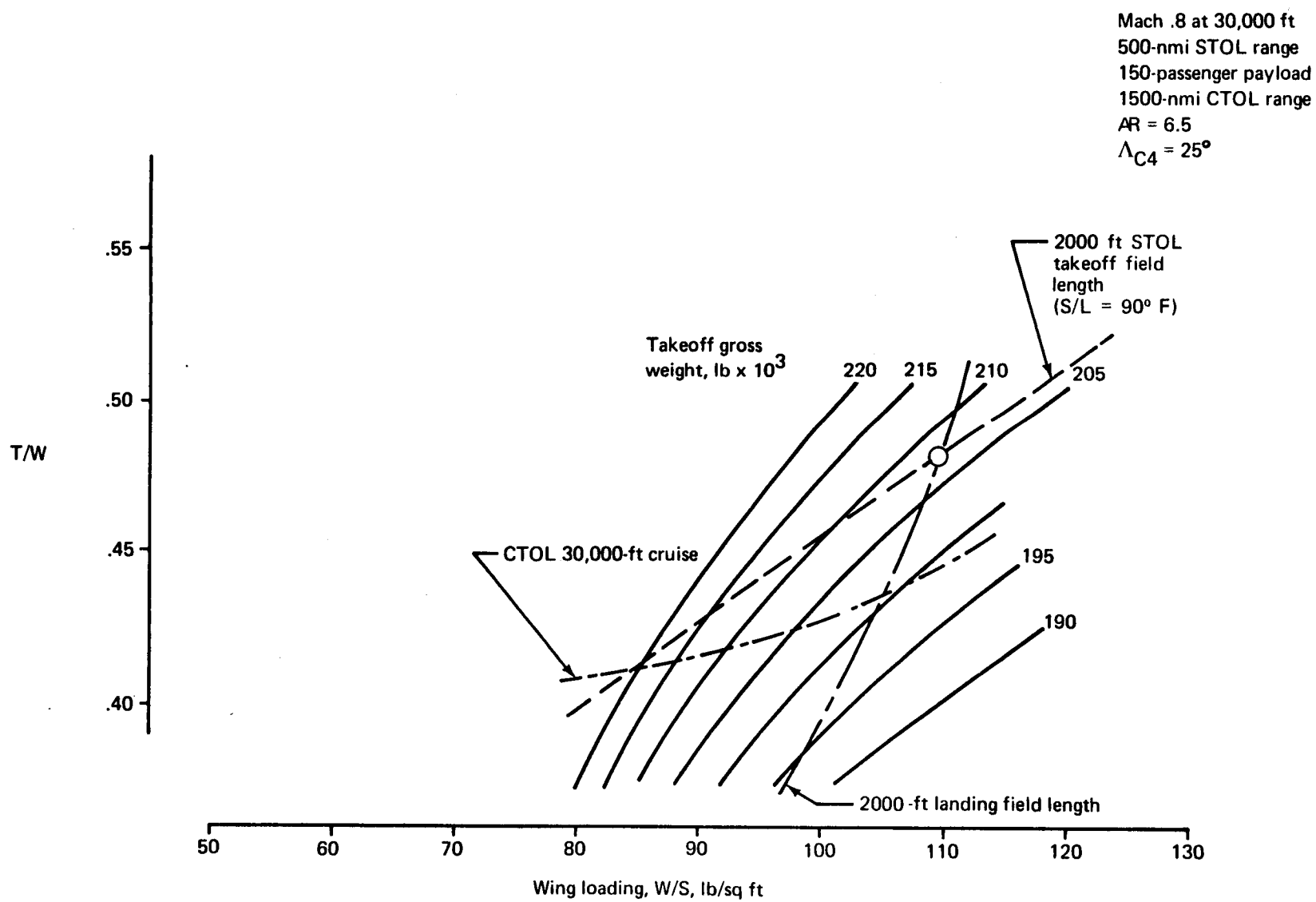

FIGURE 5-117.– AIRPLANE/ENGINE DESIGN RELATIONSHIP, THREE-STREAM AUGMENTOR WING, 50% BLOWING THRUST

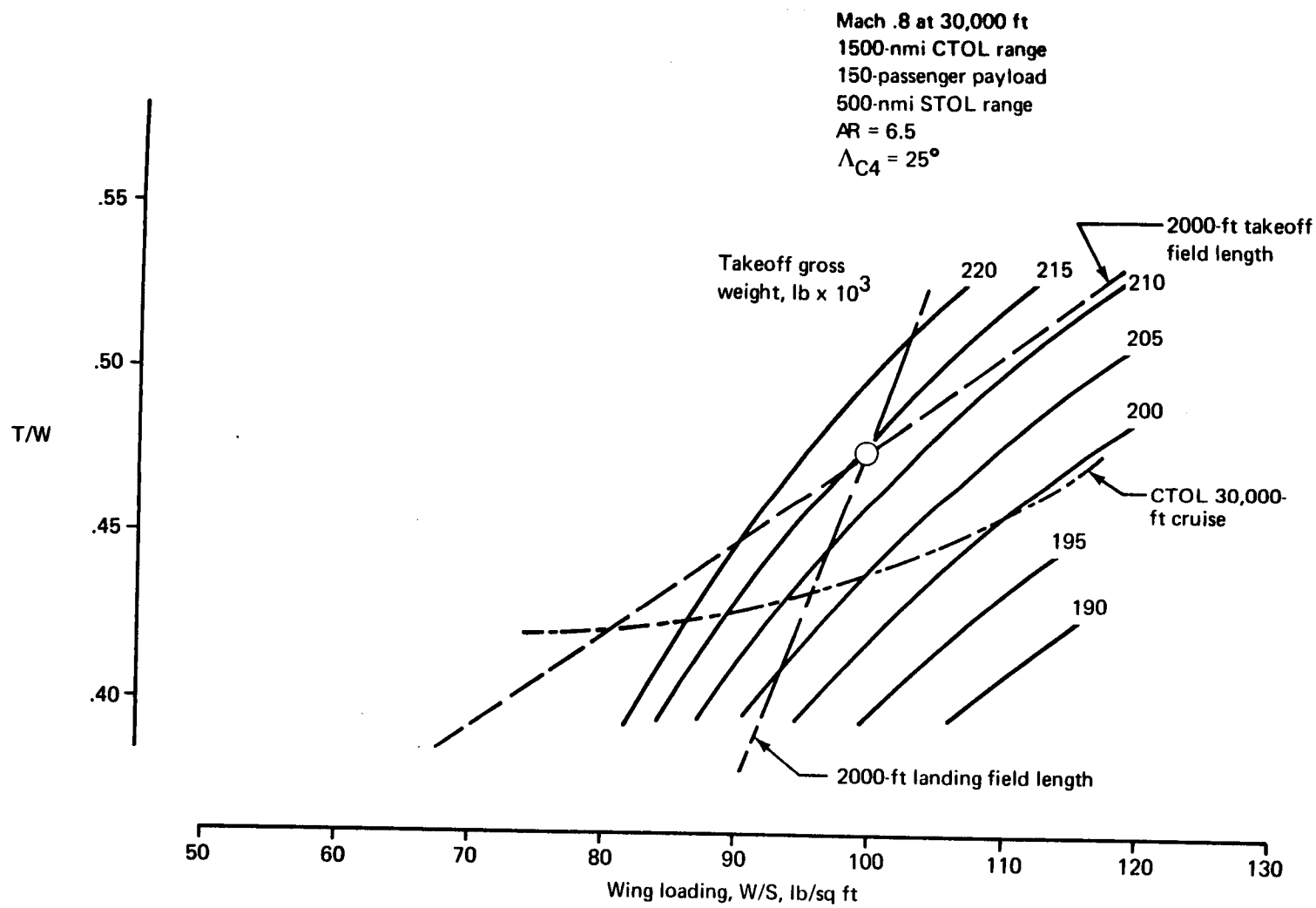

FIGURE 5-118.– AIRPLANE/ENGINE DESIGN RELATIONSHIP, THREE-STREAM AUGMENTOR WING, 40% BLOWING THRUST

6.0 STATIC RIG TEST PROGRAM

6.1 INTRODUCTION

Discussions of system analysis in section 5.0 have pointed out the feasibility and potential of a STOL aircraft that can operate from metropolitan STOLports without community annoyance due to noise. Limited field length associated with these STOLports makes thrust and lift augmentation very desirable. The augmentor wing is a promising device for lift and thrust augmentation and for noise suppression and control. At present, the full potential of this concept has not been determined with respect to achieving the noise suppression necessary to meet the 95-PNdB 500-ft sideline noise objective.

Noise reductions on the order of 20 PNdB are required, with respect to the baseline airplane, to meet the noise objective. This suppression must be obtained without significant configuration and performance compromises. A development test program is needed that will provide augmentor design information for a STOL configuration that meets the target noise level and also satisfies the propulsion and aerodynamic requirements.

6.1.1 Background

The test program definition was initiated by a thorough study of available theory and test data. Information presented below obtained from this study serves to identify noise suppression parameters and equations available for noise control and isolate the areas of uncertainty in design information that will require further testing.

Even though no complete theory for jet noise suppression exists, equations developed by Lighthill and Strouhal may be used to guide in the design analysis of noise suppressors. The works of Lighthill (and others) have shown that, in the jet velocity regimes of subsonic and low supersonic flow, jet noise radiation is dominated by sound generation of convected turbulence in the jet efflux. Lighthill expressed the acoustic power generated by turbulence in this regime as proportional to $K\rho^2AV^8$, where K is a constant related to the level of turbulence, ρ is jet density, A is nozzle area, and V is the jet velocity. This relation points out that the principal factor controlling the noise level of a jet operating in this regime is velocity (fig. 6-1). A large class of suppressors operates on the principle of entraining surrounding air into the jet flow to reduce the mean velocity gradients, which in turn reduces the noise level.

Research studies have shown that the source of noise in a jet stream is not located right at the jet nozzle but is actually distributed over a considerable distance downstream from the nozzle exit (fig. 6-2). It has been observed that the very high frequencies are produced close to the nozzle, and that the lower frequencies are produced further downstream from the jet nozzle. The distributed nature of the jet noise source is an important consideration when using an ejector as a suppression device.

The frequencies of the noise generated by convected turbulence scale with Strouhal number (fD/V), where D is the diameter of the total jet or jet element, f is the frequency, and V is the jet velocity (fig. 6-3). Strouhal relations are useful in guiding the shaping of the peak noise spectrum generated by the jet suppressor. Figure 6-4 shows the influence of

increasing velocity and decreasing nozzle diameter on frequency peak. As the nozzle dimension is decreased at a constant velocity, the peak frequency is increased. On the other hand, decreasing the velocity of a constant-dimensioned jet will decrease the peak frequency.

At higher supersonic flow, theoretical developments predict Mach wave radiation from the jet to dominate the radiation pattern. In this regime jet noise approaches a V^3 relationship (see fig. 6-1). An additional source of noise is the interaction between turbulence and the stationary shock pattern in supersonic jets (i.e., shock-induced noise). These types of noise sources tend to mask the turbulence noise which is related by Lighthill and Strouhal number and hence limit the usefulness of these relations in analysis of supercritical flow noise suppressors. Design and development of suppressor systems in these regimes have been predominantly empirical.

The lack of clear theoretical guidelines has forced the study of jet noise suppressors to rely heavily on parametric test investigations. Several NASA, Boeing, and other industry reports have contained discussions of augmentor wing concepts. Investigations have included a description of the noise and performance characteristics of slot nozzles, breakup nozzles, and associated jet flap hardware.

In 1957 NASA (ref. 6-1) reported results from a full-scale test of two slot nozzles: one with an aspect ratio of 14:1, the other with a 100:1 aspect ratio. Test results demonstrated the directional characteristics of the noise pattern from a high-aspect-ratio slot nozzle (fig. 6-5). There was very little total noise reduction, but noise spectrum correlations were observed. The frequency distribution was generally flatter for the slot nozzles than for a round convergent nozzle; reductions in noise energy were found at low to middle frequencies, and increases were found at the higher frequencies.

A report by Pratt and Whitney Aircraft (ref. 6-2) indicated that significant noise reduction can be obtained on the narrow side of a two-dimensional nozzle, the amount depending on the nozzle aspect ratio (fig. 6-6). Part of the noise suppression was attributed to increased perimeter of the slot nozzle. The noise reduction values were obtained by comparing the slot nozzle peak noise data with data from a standard nozzle; both were evaluated at a constant altitude. Results of this report are somewhat in conflict with the more conservative NASA results.

Test results from Rolls-Royce (ref. 6-3) show that the measured attenuation of a 24:1-aspect-ratio slot nozzle varies as much as 7 dB with orientation from broadside to endside (fig. 6-7). Such directional characteristics can be used to advantage when designing the augmentor wing for low takeoff noise levels. The increase of slot nozzle noise suppression with jet velocity is also illustrated in this graph.

A range of slot nozzle pressure ratios from 2.0 to 3.0 has been considered in system studies. Recent NASA test results (ref. 6-4) show that slot nozzle noise levels continuously increase with increasing pressure ratio (fig. 6-8), indicating selection of a low pressure ratio for low noise levels. An augmentor wing configuration was also tested, and the results indicated that further noise reduction is necessary to meet STOL noise objectives.

Boeing studies (ref. 6-5) have shown that shock-induced noise is a significant noise source when round convergent nozzles are operated at supercritical pressure ratios. Tests of convergent-divergent nozzles demonstrated measurable noise reduction at the design pressure ratio (fig. 6-9).

The effect of adding a nozzle lip to the slot nozzle is reported in reference 6-6. Results (fig. 6-10) indicate an increase in the low frequencies and a reduction in the high frequencies; this is beneficial with respect to annoyance considerations.

Results from tests on rectangular arrays of multilobe nozzles are presented in reference 6-7. Noise characteristics of an 18-section rectangular-lobed nozzle are shown in figure 6-11. The sound field is rotationally unsymmetrical, indicating the influence of aspect ratio. Noise spectrums for both the broadside and endside positions show a considerable decrease in low-frequency energy, with some increase of high-frequency energy. A method of establishing the premerging jet noise frequencies is presented using the Strouhal number relations, fD/V. The importance of lobe spacing to ensure the entrainment of ambient air into the jet flow, reducing the mean velocity, is also discussed.

Boeing studies related to the augmentor wing jet flap concept have included slot nozzle configurations with a flap ejector lined with sound-absorbing fiberglass material (ref. 6-8). Noise reductions associated with this concept (fig. 6-12) have demonstrated that a lined flap ejector produces significant additional noise reduction, especially at higher frequencies.

Results of extensive research to investigate noise suppressor concepts for SST jet engines are presented in reference 6-9. The data show the influence of nozzle area ratio, element number, and size on noise spectra (fig. 6-13). Increase in area ratio required wider spacing of the suppression elements, which reduced low-frequency noise. Decreased element size when used with adequate element spacing shifted the noise energy to the high frequencies.

6.1.2 Design Principles

There are a number of principles of jet noise suppressor design that are identified in the above and other reports. These include:

1) Increasing the perimeter of the nozzle by using high-aspect-ratio slot or breakup nozzles

2) Large area ratio (ratio of total suppressor discharge area to primary jet discharge area)

3) Small dimensions of individual jet discharge elements

4) Good ventilation (free access of secondary air to individual jet streams)

5) Shielding or absorption of high-frequency noise

6) Optimization of array geometry, i.e., choice of shape for maximum acoustic results. An example would be a high-aspect-ratio array as opposed to a radial array of suppressor elements.

Understanding of these principles is incomplete. They are all interrelated to some degree. Previous tests have served more to reveal their existence than to establish values for their application in an augmentor suppression system. In consequence, the effects of given changes in suppressor geometry can only be predicted in a general way. More precise knowledge of such effects would be invaluable in the design of all suppressors that utilize any of the same principles.

For the useful application of each of the suppression principles cited above, more information is required than is presently available. Some of the areas of uncertainty are discussed below.

It has been established that, for good low-frequency noise reduction, a large area ratio is necessary. Increasing area ratio results in spacing individual nozzle elements more widely. This produces less low-frequency noise, but the point is quickly reached at which the elements are so widely spaced that they behave like independent jets. The sum of their acoustic powers is then equal to that of a single consolidated jet having the same geometry as the elements, but at a higher frequency. There is no overall noise suppression attributable to the nozzle array, only a frequency shift. At the other extreme, crowding the elements together produces a consolidated jet with no breathing space between elements; again, there is no suppression except that due to the geometry of the consolidation. For an intermediate spacing, the total acoustic power generated may drop to only a fraction of the unsuppressed noise. Thus there appears to be an optimum spacing or area ratio. Stated more generally, the acoustic characteristic of an array can be substantially altered by changing the spacing and geometric arrangement of its elements.

There are many details about which there is little information. For example, how are area ratio effects influenced by changes in array geometry? Are the relationships for a radial array still valid for a high-aspect-ratio rectangular array of the same number of elements at the same spacing? Does this depend more on the number of elements or their arrangement?

The cross-sectional area needed for adequate secondary air access to divided nozzle elements can be estimated from consideration of jet mixing requirements or empirical information. However, the effects of "starvation" are known only in a qualitative way; base drag and high-frequency noise are both increased, but quantitative knowledge is lacking.

Although breakup of the jet stream into small units is required to achieve large amounts of suppression, there are many trades involved. For example, should the ultimate breakup be lobes or circular nozzles, or can a slot nozzle in combination with a tuned augmentor liner provide adequate suppression?

In tests of multitube arrays with the nozzle arranged in a line, it has been observed that adjacent nozzle wakes tend to shield the noise from neighboring wakes, with the result that less noise is radiated along the line of nozzles normal to the line. This phenomenon needs investigation to determine the effectiveness of shielding with array orientation, element spacing, and element shape.

None of the past work has led to augmentor wing systems that meet STOL noise objectives. However, the reports have identified the parameters available for noise control. These

parameters include slot aspect ratio, orientation, shock noise, pressure ratio, coanda lips, multi-element nozzle geometry, and augmentor lining. In order to develop an augmentor concept with a goal of 25 PNdB noise reduction, a complete investigation of these parameters is required. Emphasis should be placed on multi-element nozzles used with augmentor flap systems with noise suppression acoustic liners.

6.1.3 Test Objective

The objective of the task I static rig test program is to determine the noise, noise attenuation, and performance characteristics of selected high-aspect-ratio nozzle confiugrations which provide information relative to the design of a suppressor concept which meets the STOL noise performance objectives. More specifically, the test objective is to describe noise and performance characteristics of candidate nozzles as a function of key suppressor variables:—nozzle aspect ratio, pressure ratio, orientation and multi-element geometry. Important noise sources associated with candidate nozzle designs will be identified and a means of controlling them demonstrated. Jet wake characteristics will be related to the performance and noise variables. Information obtained from these tests will be used to develop nozzle design charts for noise suppression and to select candidate nozzle configurations for task II testing. Test results will also be utilized in evaluation of STOL configurations.

In the sections that follow, detailed descriptions are given of how the test program was developed, what facilities were used, what measurements were taken, and what the specific results were.

6.2 TECHNICAL APPROACH

The development of a logical test program for obtaining technology for the augmentor wing requires consideration of both the airplane and augmentor systems. These considerations have had a major influence on the test program. Task I models have been selected with the total system in mind. In the following discussion, augmentor wing components are related to a system design approach and a scale-model test program.

The augmentor wing provides the opportunity to develop a noise suppression system that can achieve large noise reductions for STOL airplanes. The suppressor system consists of a high-aspect-ratio slot primary augmentor nozzle, breakup of the slot flow with smaller dimension elements, and an augmentor lined with sound-absorbing material (fig. 6-14). Ability to attenuate shock noise and vary the nozzle pressure ratio provides further design flexibility.

A basic slot nozzle shifts the noise energy to a higher peak frequency relative to a round convergent nozzle. The multi-element nozzle is a spectrum-shaping device which attenuates low-frequency noise by element spacing, and shifts the frequency energy to a higher frequency by element sizing and spacing. The basic slot height provides fundamental spectrum shaping; the multi-element nozzle extends the spectrum-shaping capability of the slot nozzle to the extremes that may be required. When used in conjunction with a lined shroud, the large potential of the breakup nozzle lies in its ability to shape the noise spectrum of the jet in a manner that complements the suppression ability of the lined shroud. Even though the multi-element suppressor may not always show significant perceived noise

level suppression by itself, it will provide effective suppression when combined with the shroud. Emphasis in task I has been on designing a component of a suppression system and not solely a suppressor nozzle. The purpose of the task I test program is to evaluate the noise attenuation and performance capabilities of the type of nozzles mentioned above in a parametric fashion.

The candidate nozzle configurations were evaluated using scale model test and analysis. The scaled models lead to lower cost experimental facilities and test operation and also improve timing by making it possible to obtain experimental data early enough to influence augmentor designs. Performance evaluation of nozzles using scale models has been successful in the past and has a wide range of acceptance. A model noise source which is identical to a full-scale source (except in linear dimensions) has been used to scale the far-field noise to a reasonable accuracy (ref. 6-10). Full-scale values of Mach number, velocity, and density at the nozzle exit are required for accurate acoustic scaling. The size of the scale models is generally determined by the facility and air supply limits.

Accurate evaluation of the noise suppression and performance potential of scale-model nozzles requires careful nozzle design techniques. For high-aspect-ratio nozzles it is essential to be able to control and identify both the basic jet structures and the spanwise distribution of the flow. Uniform spanwise distribution of flow is obtained through proper design of plenum charging stations, and jet control is obtained by design and manufacture of the individual nozzle elements. It is important to identify trends that are associated with the nozzle geometry, rather than with anomalies of fit not associated with nozzle trades.

The choice of nozzle designs is influenced by trades involving a number of considerations. The best internal performance occurs in nozzles with accelerations very close to the nozzle exits. However, this causes steep closure for secondary flow leading to high losses in external flow. It also leads to steep nozzle angles with low discharge coefficients and unusual jet structures. In order to circumvent these problems, the nozzles are designed parallel, or with convergence angles less than 15°.

As the test program schedule developed, it became clear that model design decisions depend strongly on the constraints imposed by STOL airplane systems consideration. Although the majority of decisions were influenced by the baseline airplane study (sec. 5.0), all major decisions were made at the latest possible date, to be sure the most current thinking was involved in the model designs.

The augmentor wing nozzle systems all use very high aspect ratio nozzles. A series of scale-model slot nozzles were designed to determine the effect of aspect-ratio variation on noise and performance. The models are all of the same exit area with increasing aspect ratio and decreasing slot height, which, when scaled, is representative of typical augmentor slot heights. In addition, a convergent-divergent slot nozzle was designed to determine the effect of shock attenuation at supercritical pressure ratios on noise suppression. A design pressure ratio of 3.0 (representative of an upper limit augmentor wing pressure ratio) was selected for test.

Key geometric variables identified with multi-element nozzles are area ratio, element shape, number, and size. Nozzle area ratios as high as 4.0 were selected to provide the

necessary low-frequency noise suppression. Higher area ratios were not selected because of configuration constraints. Nozzle element shapes are convergent tubes and lobes. Element sizes were selected to provide a parametric study of decreasing element size on peak level frequency shift. Nozzle element size is ultimately limited by model construction problems and manufacturing costs.

These scale-model nozzles were tested over a range of nozzle pressure ratios (at ambient temperature) and orientations to determine the effect of these parameters on noise suppression. Acoustic test data are scaled to representative augmentor wing conditions to compare the relative merits of the various nozzle configurations in terms of noise suppression, spectrum change, and changes in the directionality pattern. Variables considered in the analysis included nozzle aspect ratio, pressure ratio, orientation, and multi-element nozzle geometry (i.e., area ratio, element shape, and size). Nozzle thrust measurements and rake profiles are used to establish the performance characteristics of the suppressors. Results are then used to verify initial augmentor wing airplane noise and performance predictions.

6.3 APPARATUS AND TEST PROCEDURES

The selection of a test facility, the establishment of model designs, and the implementation of test procedures were aimed at providing the most rapid and versatile test program, while exercising sufficient care to ensure confidence in the test results. It was desired to ensure a reasonable balance between model costs and testing time. Selection of the number and variety of task I nozzle configurations is based on a balance between model fabrication costs and the requirement for evaluating a representative number of slot nozzles and candidate noise suppression nozzles. The Boeing North Field Mechanical Laboratories in Seattle, Washington were chosen as the appropriate test location. The laboratories have a facility especially suitable for large-scale combined acoustic and thrust performance test programs. The augmentor thrust is measured with a six-component, platform-type balance bridged with high-pressure air; the noise is measured in a 180° arc in an acoustic arena as shown in figure 6-15. The thrust stand accurately measures model forces using either warm (300° F) or ambient temperature air. Nozzle flow rates are determined with precision using ASME venturi flow meters calibrated against a Boeing standard nozzle. An acoustically treated muffler plenum, located on the balance platform upstream of the test nozzle plenum, prevents any noise generated by the air supply lines and control valves from reaching the test nozzles.

To acquire acoustic data of the highest quality, data were recorded only during a limited range of atmospheric conditions. In addition, the round convergent nozzle was tested periodically as a reference to establish repeatability. The test fixture was designed to allow quick interchange of nozzles. Because of the desired precision for acoustic measurements, and the very large volume of acoustic data expected, each component of the instrumentation system for noise measurement was carefully chosen and integrated. The basic noise measuring system consists of microphones, a tape recorder, and one-third octave band analysis instrumentation calibrated and operated over a frequency range of 200 to 80,000 Hz. The output is punched cards, which are used to make computer plots of one-third octave band level versus frequency and other calculations used in the analysis. Block diagrams and photographs of system components are shown in figures 6-16 through 6-20.

In the paragraphs that follow, important details of the test rig and procedures are discussed, along with the instrumentation and data reduction. In section 6.4, the key achievements in accuracy and repeatability of performance and acoustic measurements are discussed.

6.3.1 Performance Data Acquisition

Model forces and moments are measured with a six-component platform-type external wind tunnel balance that is bridged by two high-pressure air lines each with three flexure bellows. The flexure-bellows air line sections are designed to produce a minimum of restraint on the balance for all components through the full range of balance deflections under operating pressure. The interactions due to pressure on all of the balance components are measured to be less than 0.1% of maximum nozzle thrust through the operating pressure range of these test nozzles. Static calibrations of the installed balance demonstrated accuracy, repeatability, and linearity within 0.1% of the maximum nozzle thrust levels.

All pressure transducers were calibrated prior to the task I testing, and again midway during the program. The most critical ones (flow meters and nozzle pressure ratio) are check calibrated biweekly. These calibrations indicated that all transducers used by this test were repeatable and linear to within at least 0.2% of the full-scale range of the transducer.

To obtain good performance measurements, the airflow rate, in addition to the thrust, must be accurately measured. This is done by using carefully calibrated ASME venturi flow meters in both air supply lines. The flow meters are calibrated as installed for absolute level, by operating them in series with a Boeing standard reference nozzle. ASME C_D levels are adjusted accordingly and applied to the flow rate calculations in the data reduction computer program. Comparisons of the convergent reference nozzle performance levels with the Boeing standard levels are shown in figure 6-21. The venturi throat Mach number does not exceed 0.6.

The nozzle pressure ratio is monitored separately from the main data acquisition system and displayed on the test console as a means of setting and holding exact test conditions while recording acoustic and performance data (fig. 6-22). The performance data are recorded by a Boeing standard digital data system on punched paper tape at 10 channels per second. The punched paper tape is converted to magnetic tape and processed at the Boeing Computer Center for final data output. The performance data system is pictured in figure 6-23.

To investigate the jet velocity profiles at various distances downstream of the rectangular array nozzles (slot and multi-element), several nozzles were tested with external total pressure rakes installed downstream of the nozzle exits.

For reasons of time and economy, a manually operated rake system was chosen. Sixteen-probe total-pressure rakes (1/16-in. probe spacing) are used on the slot nozzle exit rake surveys, while 31-probe rakes (0.20-in. probe spacing) are used with the multi-element nozzles that produced a thicker jet sheet. Figure 6-24 shows these pressure rakes installed on [illegible] the test nozzles. Nozzle jet pressure data are recorded at $X/h_E = 0, 5, 10$, and 20. The rakes are also set at several span positions for the multi-element nozzles. Acoustic data are not recorded while the nozzle exit rakes are installed.

The ideal airflow and ideal velocity used in the nozzle performance calculations are calculated as functions of the total pressures and temperatures measured at the nozzle charging station (fig. 6-25).

6.3.2 Performance Data Reduction

Velocity coefficient C_V is defined as the ratio of measured nozzle thrust to the total thrust produced by a fully expanded nozzle passing the same mass flow, or

$$C_V = \frac{F_G \cdot g}{m\, V_I}$$

where:

$$V_I = \sqrt{\frac{2\gamma g R T_T}{\gamma - 1}\left[1 - (NPR)^{\frac{1-\gamma}{\gamma}}\right]}$$

$$\gamma = 1.40$$

Nozzle discharge coefficient C_D is defined here as the ratio of measured nozzle airflow to the theoretical nozzle airflow, or

$$C_D = \frac{m}{m_I}$$

where:

$$m_I = A\,(P_T)\sqrt{\left[\frac{2g\gamma}{R\,(\gamma - 1)\,T_T}\right]\left[\left(1 - \frac{P_T - P_\infty}{P_T}\right)^{2/\gamma} - \left(1 - \frac{P_T - P_\infty}{P_T}\right)^{(\gamma + 1)/\gamma}\right]}$$

Nozzle thrust coefficient C_G is defined here as the ratio of the measured nozzle thrust to the ideal thrust produced by a fully expanded nozzle passing the ideal flow rate. This parameter does not involve the measured nozzle airflow rate and is used in section 6.4 as an indication of facility thrust repeatability.

$$C_G = \frac{F_G}{F_I} = C_V \cdot C_D$$

The nozzle exit velocity ratios plotted versus the term $Y/\delta_{1/2}$ in section 6.5 are non-dimensionalized to provide a universal method for comparing the velocity profiles produced by rectangular array nozzles. If Y is taken as the distance from the center plane of the jet sheet, then $\delta_{1/2}$ is defined as the location in the Y direction where $V_J/V_M = 0.5$.

6.3.3 Acoustic Data Acquisition

The basic components of the acoustic data acquisition system are the microphone system, recording system, calibration system, and wind monitoring system.

Acquiring high-quality acoustic data from an outdoor test facility requires that data be recorded only during a limited range of atmospheric conditions. Data are recorded with the following limitations: wind speed less than 5 mph, certain combinations of ambient air temperature and humidity, and no visible fog or precipitation. The combinations of air temperature and humidity that are acceptable for the task I acoustic tests are shown in figure 6-26. The effect of wind on far-field microphones is shown in figure 6-27.

6.3.3.1 Microphone System

The microphone system for the propagated noise measurements consists of the following components:

1) Bruel and Kjaer Model 4135, 0.25-in. condenser microphone operated without protecting grid

2) General Radio Model 1560-P42 microphone preamplifier operated at 20-dB gain position

3) Boeing microphone preamplifier power supply with level equalization adjustment

A microphone rain shield, constructed with 0.5-in. Scottfelt covered with light plastic, is used to protect the microphone from light rain. Twelve-foot microphone stands are hinged to permit quick access to the microphones for installation and calibration. They are located at 10° intervals in relation to the jet exhaust (see figs. 6-28 and 6-29).

Measurements of noises were made inside of the ducting, the plenum, and the nuffler to identify sources of noise in the air lines. Flush-mounted 1/16-in. Kulite Model CPL-070-58 microphones were used.

6.3.3.2 Recording System

The 14-channel recording system includes the following components:

1) Adjustable gain (10 dB/step) amplifier, Dynamic Model 7950

2) Ampex Model FR 1800L tape recorder operated in direct record mode at 30 in. per second (ips)

3) Oscilloscopes and level meters for monitoring all microphone channels simultaneously

4) A 400-Hz signal generator for placing a calibrated reference tone on the tape and for signalling the start and stop of the established test condition

5) A time code generator for placing a time code on one tape channel for use in data reduction

6) A microphone for announcing conditions and amplifier gain settings on one tape channel

7) A switch for selecting microphones in groups of 12.

6.3.3.3 Calibration System

The system used for measuring the combined frequency response of the microphone cartridge, preamplifier, and cable is a Bruel and Kjaer electrostatic actuator, UA 0033, used in conjunction with a B&K Model 1013 beat frequency oscillator and Model 2305 level recorder.

A B&K pistonphone, Model 4220, is used in the field for establishing the output voltage of each microphone system at 250 Hz at a nominal sound pressure level of 124 dB (re: 0.0002 microbar).

Frequency response of the tape recording and playback system is accomplished with a B&K Model 1013 beat frequency oscillator and a Model 2305 level recorder.

6.3.3.4 Wind Monitoring System

Four anemometers used in conjunction with a direct writing oscillograph are used to monitor and record the wind speed at four representative microphone locations. Specific instrumentation is listed below.

Item	Manufacturer/Model
Cup and vane anemometer	Taylor/3105
Signal detecting and averaging circuitry	Boeing
DC amplifiers	Electron/S1126
Oscillograph	Honeywell/1508

6.3.3.5 Acquisition Procedures

Frequency response calibrations of the microphones, recording, and playback systems are made in the acoustics laboratory prior to starting the test series, and periodically thereafter. Individual B&K microphone cartridges are selected so that the 0° incidence free-field response, obtained by combining the pressure response (from electrostatic actuator calibration) and the free-field correction (from B&K 4135 Instruction Booklet), is flat within ±1.5 dB in the range from 200 to 80,000 Hz. The combined response of the microphone and tape recorder system is generally maintained within ±2 dB, although in a few cases it has

exceeded this. One-third octave band corrections in steps of 1.0 dB are applied in the data reduction process to compensate for the deviations from flat response.

The pistonphone, which is used for establishing a reference level in the field, is calibrated by the Boeing metrology laboratory. These calibrations are traceable to the National Bureau of Standards by means of Western Electric 640-AA microphones, which are used to calibrate the pistonphone within ±0.5 dB. For field calibrations the pistonphone, which generates a nominal level of 124 dB (re: 0.0002 microbar) is applied to each microphone while the microphone preamplifier output is read on a voltmeter. All microphone outputs are adjusted to -5.0 dB ±0.3 dB (re: 1.0 V) by means of the attenuators in the microphone power supply. In practice, the pistonphone calibrations are made immediately before and after the model jet measurements for the day. After the initial level adjustment is made for a particular microphone system, it is seldom necessary to make additional adjustments to maintain the ±0.3 dB tolerance. If repeated adjustments are necessary, the microphone or preamplifier is questioned, and the components are replaced.

At the beginning and end of each reel of magnetic tape, a -5 dB (re: 1.0 V) 400-Hz calibration signal is applied simultaneously to each recording channel. This signal represents the pistonphone sound pressure level for use in playback.

The rain shields (see Figs. 6-28 and 6-29) used to protect the microphones from moisture were developed specifically for this program. The effect of this shield on the response was determined by measuring the noise from a 1-in. nozzle air jet with and without the rain shield. The configuration selected has one-third octave band deviations up to 0.6 dB in the frequency range of interest. Deviations in full-octave response are within ±0.3 dB. No corrections have been applied to account for these small deviations. The time of day for making runs is selected on the basis of low ambient noise and low wind. In addition, however, the wind monitoring system is used to determine the best time to start the data recording period. If before the recording interval is completed, the wind at any of the four monitoring positions appears excessive, or a noticeable ambient noise (e.g., airplane flyover) temporarily appears, the recording is continued until a sufficient data sample is obtained during calm and quiet conditions. In some cases the run has to be terminated and repeated at a later time.

6.3.4 Acoustic Data Reduction

The one-third octave data reduction system consists of an analog tape recorder, one-third octave spectrum analyzer, card punch, time code reader, and associated control and interface circuitry as listed below.

Item	Manufacturer/Model
Magnetic tape recorder	Ampex/FR 1800L
Spectrum analyzer	General Radio real time analyzer/1921
Card punch	IBM/526

Item	Manufacturer/Model
Time code reader	EECO/851A
Card punch interface	Boeing
Oscilloscope	Tektronix/RM 503
RMS voltmeter	Fluke/910AR/Z
Random noise generator	Allison/65D-4
Oscillator	Bruel & Kjaer/1013

Recorded data tapes are reproduced on the tape recorder operated in direct mode at 30 ips. The analyzer simultaneously breaks the analog signal down into one-third octave bands and then converts these to time averaged one-third octave band sound pressure levels in decibels in digital form. These values are transferred to the IBM card punch through the card punch interface. The punched cards are used in the CDC 6600 computer for follow-on plotting and computations.

The General Radio 1921 spectrum analyzer consists of (1) a bank of 24 parallel one-third octave filters with center frequencies of 200 to 80,000 Hz, (2) a provision for manually introducing system frequency response corrections, and (3) a multichannel RMS detector with true (linear) integration and variable integration time.

The narrow band data reduction system consists primarily of (1) a Federal Scientific Ubiquitous spectrum analyzer UA-6A, with digital averager option 129 B, and (2) a Honeywell X-Y recorder, Model 530 T. The analyzer has a selectable bandwidth, frequency range, and integration period. For this program, typical settings used are 80-Hz bandwidth, 0- to 40,000-Hz frequency range, and 25 sec integration period.

6.3.5 Acoustic Data Reduction Processing

The integration period selected for data reduction generally is 16 sec, although in a few cases 8 or 32 sec is used. The 16-sec period was arrived at after consideration of various factors such as:

1) Maintaining adequate statistical degrees of freedom

2) Minimizing effects of short gusts of wind (i.e., low-frequency noise generation, and altering the jet noise pattern).

3) Minimizing time for recording and data reduction.

4) Working between conditions of excessive ambient noise.

Oscillograms of wind velocity versus time are visually inspected for a suitable period with low wind. Selections are made separately for each of four microphone groups using data from the anemometer located closest to the applicable microphone. In some cases the wind is at a minimum at all anemometer stations simultaneously; however, frequently the minima occur at slightly different times. The undesirable effect of even a mildly gusty condition on the low-frequency noise data has made this procedure worthwhile.

One-third octave band data reduction is accomplished as follows:

1) Using the frequency response information obtained during calibration for each separate microphone recording channel, corrections are applied by means of one-third octave band attenuators, which are set manually.

2) Identification information is entered on the IBM cards through the keyboard.

3) The desired data sample to be analyzed is located on the tape using IRIG time signals, start and stop tones, and voice announcements.

4) After entering the record gain into the card interface, the operator starts the tape and initiates the start of the nominally 16 sec integration of the data sample. The General Radio 1921 analyzer, after completing the analysis, automatically transfers the stored data through the interface onto IBM cards.

   The completed data cards are sorted by microphone channel and conditions, and then printed in tabular form. The tabulated data are visually inspected for 1) proper order of condition sequence and 2) trends of overall level versus pressure ratio and microphone angle. Any apparent discrepancies are checked.

   The data cards are then processed through the CDC 6600 computer and SC 4020 plotting system. The results displayed on one 8-1/2 by 11 in. sheet are one-third octave band sound pressure level versus frequency for a given microphone at typically five pressure ratios. In this form the data are visually inspected for any anomalies in curve shape, trend in level versus pressure ratio, or angular location. The plotted data are also compared with typical background noise for the particular gain setting used during the recording.

6.3.5.1 Error Analysis

Estimated errors for the complete measuring system (microphone to tabulated one-third octave band) after application of instrumentation corrections are tabulated below.

	Absolute Error		Relative Error	
	Max (dB)	RSS (dB)	Max (dB)	RSS (dB)
Below 1 kHz	±2.1	±0.9	±1.0	±0.6
80 kHz	±3.9	±1.6	±3.3	±1.4

The assessment of absolute errors contains all components of the measuring system, including the absolute calibration of the pistonphone traceable to the National Bureau of Standards, whereas the relative errors exclude the pistonphone accuracy and the effect of rain shield because these are identical for all measurements. Maximum error is the addition of the individual error assigned to each part of the calibration and measuring system. The root-sum-square (RSS) error is the square root of the sum of the squares of the individual errors, as an indicator of probable error.

Ambient noise measurements were made and analyzed to ensure that the recorded jet noise data were above the electrical and background noise of the measuring system and the acoustical ambient noise of the arena.

Anomalies are handled in the following manner:

1) Curves showing moderate discrepancy in level are checked and reanalyzed. In the few cases when this has occurred, errors have been readily detected and corrected.

2) High-frequency portions of some curves that are too close to background are corrected by extrapolating the established downward trend with frequency and by comparing slopes with data from other pressure ratios, or from microphones at different angular locations. Corrections of this type are usually limited to the bands above 50,000 Hz, and particularly when testing the reference round nozzle which requires a large dynamic range. Mostly the need for this correction results from background random noise from the electronics or tape, but it occasionally results from feedthrough of the 60,000 Hz bias oscillator located in the microphone preamplifier.

3) Low-frequency portions of some curves that appear irregular in shape and do not fit into the five-curve pressure ratio family are corrected by drawing a best-fitting curve by examining trends from other microphones and pressure-ratio conditions. This low-frequency correction is required to eliminate the effect of wind on the microphone, particularly for the low jet noise conditions, i.e., at low pressure ratio. Improvements in procedure for wind monitoring during the run and selection of calm periods for analysis are reducing the number of times that this type correction is necessary.

Where corrections are required, the punched cards are repunched using data from the corrected curves. It is important to note that the above-described conditions have only a minor effect on the overall or perceived noise levels, and that they are performed more as a refinement than as a means for grossly changing the results. There is usually sufficient information from adjacent microphones or other pressure-ratio conditions to clearly establish an approximate correction.

6.3.6 Model Description

Five slot nozzles and four multi-element nozzles were tested for acoustic and thrust performance in task I. A reference nozzle was also tested to verify the consistency of facility performance. It is an axisymmetric convergent nozzle of 15° half angle, shown mounted on

the plenum in figure 6-30. The reference nozzle performance levels are directly comparable to convergent nozzle performance levels measured at the Boeing Propulsion Laboratories nozzle calibration facility. It is also useful to compare AWNP noise measurements with SAE prediction procedures. The reference nozzle thrust and acoustic performance data recorded during task I are presented in section 6.4.

The four convergent slot nozzles with nominal aspect ratios of 400, 250, 100, and 50, as shown in figure 6-31, were tested to determine both the relationship of slot height versus characteristic frequency, and the slot nozzle friction loss as a function of aspect ratio. Evidence of nozzle exit area growth during operation is indicated by analysis of the nozzle discharge coefficient data from the initial tests of these nozzles. Analyses show that the nozzle area growth effect could be corrected by the installation of bolts spaced evenly along the span of the nozzles upstream of the nozzle lips. Area control bolts were installed in the 100:1 aspect ratio convergent and convergent-divergent nozzles (fig. 6-32).

To evaluate potential noise reductions associated with shock attenuation in the jet, a convergent-divergent (C-D) slot nozzle (AR = 100) with the same throat area as the AR = 100 slot nozzle but a throat-to-exit area ratio of 1.095 was tested. A sketch of the C-D nozzle is shown in figures 6-32 and 6-33.

Four multi-element nozzles, two multitube and two multilobe, were built and tested (fig. 6-34). These four nozzles are all of AR = 100 and are designed with the same nominal exit area. The 140-tube nozzle and the 70-tube nozzles are designed with area ratios of 4.0 and 3.5, respectively; the 70-tube nozzles are designed with area ratios of 4.0 and 2.5. These breakup nozzles are designed to produce significant noise reductions by breaking up the slot flows into a large number of individual primary jets. To maintain high thrust performance with these sound-suppression nozzles, the internal Mach numbers are kept low and accelerations are made near the nozzle exit, minimizing friction losses. The nozzle array design also provides good secondary flow ventilation resulting in low base drag losses.

To fabricate the multi-element nozzles inexpensively, while providing dimensionally accurate models, two construction methods were employed. The tube nozzles were formed by a swaging process and the lobe nozzles were die formed and jig welded. The critical dimensions of the multi-element nozzles are shown on figures 6-35 and 6-36. To minimize the lobe nozzle exit area growth during operation, one small strut was installed in each lobe aligned in a streamwise direction.

All slot nozzles have internal static taps as shown in figure 6-25. The four multi-element nozzles incorporate both internal and external pressure instrumentation with the static tap locations indicated in figures 6-37 through 6-40.

The slot nozzle plenum, shown installed on the test facility in figure 6-31, is designed to accommodate all the slot nozzles and multi-element nozzles as shown in figure 6-41. The plenum is designed to provide uniform pressure distribution at the entrance to the nozzles by keeping internal Mach numbers low and using turbulence removal screens as shown in figure 6-25. It is also designed to rotate about an axis perpendicular to the plane of the nozzle exits. With the acoustic microphones arranged in a horizontal plane (fig. 6-15), this

rotation, β, provides the capability for simulating airplane flyover and sideline noise measurements. Flap deflection can be varied during task II by rotating the slot plenum about its own axis.

6.3.7 Test Variables

The test variables selected are based on system analyses made during the early part of task I. The nozzle acoustic and thrust performance data were recorded at nozzle total pressure ratios (NPR) of 1.6, 2.0, 2.3, 2.6, and 3.0. The reference nozzle was also operated at pressure ratios of 1.4 and 1.8, and the C-D nozzle was tested at two additional pressure ratios of 2.8 and 3.2. Nozzle total pressure exit rake data were recorded at pressure ratios of 2.0 and 3.0. Ambient temperature air was used during all task I runs except for a few checkout runs with the reference nozzle operating with 300° F air. Acoustic data were recorded at β rotation angles of 0°, 30°, 60°, and 90° although some configurations were tested at 0° and 90° only. A test run is defined as a series of pressure ratios with a given model configuration at one β rotation angle.

6.4 DATA ACCURACY AND REPEATABILITY

It is extremely important to provide acoustic and performance test data that can be used with confidence. Good data accuracy and repeatability will help establish this confidence; the task I tests have demonstrated excellent accuracy and repeatability.

6.4.1 Performance Measurements

Summary plots of the reference nozzle performance, measured at several intervals during the task I tests, are presented in figures 6-42 and 6-21. Both long-term and short-term repeatability for thrust and airflow are presented in these figures. The plot of mean thrust coefficient level, C_G, in figure 6-42, which includes data from five sets of reference nozzle runs, indicates that the maximum variation in measured thrust is ±0.4% throughout task I. Velocity coefficient data from four reference nozzle runs, also shown in figure 6-42, represent typical short-term repeatability for combined thrust and airflow.

Mean C_D and C_V levels from several sets of reference nozzle runs showing the facility long-range repeatability of both airflow, C_D, and combined thrust and airflow, C_V are shown in figure 6-21. The maximum variations experienced with these parameters during task I are ±0.3% and ±0.5%, respectively. The mean C_D and C_V levels produced by a convergent nozzle of identical geometry on the Boeing nozzle calibration facility are also shown in figure 6-21. Comparison of these levels provides a means for evaluating the absolute accuracy of the performance data. It would be possible to adjust the performance levels of the configurations tested between two reference nozzle runs by the amount required to adjust the mean of the reference nozzle runs; however, the adjustment was not made for this report.

All configurations except the reference nozzle were installed and tested on the slot nozzle plenum. During the initial facility checkout runs, the total pressures at the charging station probes were recorded through the full range of model flow conditions. The

percentage deviation from the average total pressure along the span of the plenum is shown in figure 6-43. A 1% deviation in total pressure represents only about a 7-ft/sec deviation in velocity; the total pressure variations demonstrate that the slot plenum has very uniform spanwise flow characteristics.

6.4.2 Acoustic Data Measurements

The probable error for the acoustic measurements lies between 1.5 and 2.5 dB. It is difficult to make a better estimate of acoustic accuracy since no physical standard is available for direct comparison. For jet noise the $f(V_R)$ curve from SAE ARP 866 (ref. 5-11) is sometimes regarded as a standard, and a comparison of the normalized mean of the measured baseline data is plotted in figure 6-44. This comparison indicates offset errors of 2 to 8 dB; however, it must be recalled that this "standard" curve is based upon data taken from hot jet flow. Cold-flow jet noise lies well below the "standard" curve, references 5-11 and 5-15. The lower estimate of probable error (1.5 dB) is derived by assuming that the errors in the electronic data acquisition and reduction system are significantly larger than errors from any other source. The higher estimate (2.5 dB) is derived by assuming that errors produced in the construction and operation of the nozzles, and errors produced by the medium through which the sound travels, are of a value equal to that of the receiver. The true value of probable error probably lies closer to the lower end of the range.

6.4.2.1 Acoustic Repeatability

The standard deviation 1σ of the acoustic data is less than 0.4 PNdB (5.0%). This figure is based on an analysis of six baseline (round convergent nozzle) runs. The data were scaled (6.4/1), corrected to standard day conditions (59° F and 70% relative humidity) and extrapolated to a 500-ft off-axis distance. At each of the five engine conditions the mean OASPL and mean PNL and their standard deviations were calculated. The results of these calculations are shown in figure 6-45. In addition, a mean spectrum (at NPR = 2.3) was calculated together with the standard deviation of each one-third octave band. The results of these calculations are shown in figure 6-46. Assuming that the suppressors would show the same repeatability, the standard deviation in suppression will be less than 0.55 PNdB (7%).

6.4.2.2 Ground Reflection Effects

Acoustic measurements made in the augmentor wing test facility are essentially unaffected by reflected acoustic energy (see refs. 6-11 and 6-12). The distortion of a point source spectrum in the presence of a perfectly reflecting ground plane is shown in figure 6-47. To reduce this effect, washed beach rock of an average diameter of 2 to 3 in. was laid on the ground in the acoustic arena, and a significant improvement occurred (compare a) and b) of fig. 6-47). The round convergent nozzle is a good approximation to a point source; therefore, curve b) would be applicable to the measurements made on the round convergent nozzle. It indicates less than 1 dB increase in OASPL and no change in PNL. Curve c) of figure 6-47 (see ref. 6-13) is applicable to measurements made on a slot or breakup nozzle; it indicates no change in OASPL or PNL due to ground reflection effects.

6.5 RESULTS

A primary task I objective is to establish reliable trades between noise suppression and performance. The design of practical nozzle systems with minimum performance loss is desired, particularly for the multi-element nozzles. In section 6.4, the accuracy and repeatability were shown to be very good for both performance and noise measurements. Thus, the trends shown by the noise suppression data may be reliably related to the performance measurements. For convenience, performance and noise results are discussed independently.

6.5.1 Performance Results

A summary of the more pertinent performance results is given in figure 6-48. The velocity coefficient is given as a function of the primary nozzle pressure ratio for all nozzles of 100:1 aspect ratio, and as a function of the nozzle perimeters. The Boeing Standard and the AWNP reference nozzle tests are included for comparison. The performance of the individual nozzles changes very little with pressure ratio, except for the convergent-divergent nozzle. As expected, the best performing nozzle was the slot nozzle; the breakup nozzles were generally not quite as good.

The slot and breakup nozzle performance was generally higher than in previous studies of suppression systems using breakup nozzles in cylindrical ejectors. The main reason for this is the flexibility of nozzle designs permitted by the augmentor wing configurations. Internal accelerations can be reasonably controlled, and external flow areas present less critical design problems (sec. 6.3). The present designs probably provide close to maximum performance for each configuration. The maximum expected performance for designs similar to those of task I can be estimated from a curve of C_V against nozzle perimeter, figure 6-48. (See section 6.6.) There is a direct correlation that is independent of nozzle type; thus, if similar control of accelerations is maintained, and if the same ground rules exist for external flow considerations, the maximum primary nozzle performance can be predicted. The Buffalo comparable C_V was about 0.935 at a pressure ratio of 2.6, and 0.925 at 1.6; the nozzle perimeter was about 390 in. This result is consistent with task I results.

6.5.1.1 Slot Nozzles

The primary purposes of the slot nozzle testing are to determine the effect of aspect ratio on noise and to identify performance changes. The performance measurements are successful in identifying performance changes, but the expected trend of velocity coefficient with aspect ratio is not established.

The value of C_V should systematically decrease with increasing aspect ratio for the slot nozzles tested, since the internal nozzle lines are identical, and the perimeters increase with aspect ratio. However, the measured trend (fig. 6-50) is not as expected. The primary reason for the trend is associated with model structural design, and not with aspect ratio effects.

The principal effect of the model structural design was expansion or "bulging" of the nozzle exits. The slot nozzles are built with smooth elliptical internal contours and parallel exits. However, due to internal nozzle pressures, considerable expansion of the nozzle exits occurred. The resulting change in nozzle area is seen in the measured discharge coefficient

curves for the nozzles, figures 6-49 and 6-51 through 6-53. The C_D curves indicate variable expansion with pressure ratio, with area growths up to 12% at nozzle pressure ratio 3 for the 400:1-aspect-ratio nozzle. (This is why the abscissa for fig. 6-50 is called nominal aspect ratio).

A review of the nozzle design stress calculations indicates that the underlying assumptions involved in the nozzle exit deflection calculations were oversimplified. Additional calculations were made, and it was determined that some moments were overlooked. The moments account not only for the expansion indicated by the C_D measurements, but for an actual outward rotation of the nozzle lips. This rotation of the lips causes the internal lines of the nozzles to have a convergent-divergent effect. This C-D effect is reflected in reduced performance (fig. 6-50) for the 100-, 250-, and 400-aspect-ratio nozzles. There is a fairly marked increase in C_V performance with pressure ratio for the 100- and 400:1-aspect-ratio nozzles (figs. 6-51 and 6-53), which is characteristic of C-D nozzles. A check of internal static pressures for the 400-, 250-, and 100-aspect-ratio nozzles indicated near-sonic or supersonic internal Mach numbers, a further indication that the nozzles were C-D. The C_D curve, (fig. 6-53) for the 400-aspect-ratio nozzle shows, for example, an area growth of about 12%. The nozzle C_V tends to peak at a pressure ratio near 2.9. This would correspond to a C-D effect associated with an 8% increase in area from a throat to exit, which is quite possible with the 12% growth.

The C-D effect is responsible for reduced C_V, particularly at lower pressure ratios. To check this, the 100-aspect-ratio slot nozzle was modified to prevent deflection of the nozzle exit. There is a definite resulting increase in measured performance (stable exits on figs. 6-50 and 6-54). Furthermore, the "stable" 100-aspect-ratio nozzle C_V fits smoothly with the breakup and reference nozzles on the perimeter correlation, figure 6-48. The fact that C_D for the 100-aspect-ratio nozzle is greater than 1.0 reflects inability to measure the exit area precisely. As a result of these determinations, all breakup nozzles are designed with 10° to 15° convergence at the exit, so if expansion occurs the nozzle remains convergent.

It is worth noting that the difficulties with slot nozzle design and manufacture at model scale would also occur in airplane designs. Precise area control of slot nozzles is difficult, although performance losses can be avoided by maintaining convergent exits.

Not all of the anomalies of figure 6-50 are connected with the C-D effect, however. The 50- and 250-aspect-ratio nozzles show very little change in C_V with pressure ratio, even though they also show C-D deflections. The 100- and 400-aspect-ratio nozzles differ in the side plate designs for the nozzle edges, in that the sideplates extend downstream. The 50- and 250-aspect-ratio nozzle sideplates are designed to be flush with the nozzle exit; however, when the nozzles expand with pressure ratio, they tend to extend beyond the sideplates, and flow bends away from the thrust line at the sideplates. At higher pressure ratios, sonic or supersonic flows occur in the approaches to this region, and Prandtl-Meyer turning around the end plates increases with pressure ratio. This causes more losses with increasing pressure ratio. Calculations indicate that this effect is large enough to counteract the upward C_V trend with pressure ratio for the C-D effect in the 50- and 250-aspect-ratio nozzles.

The conclusions are that the slot nozzle measurements should not be used to determine slot nozzle performance. Rather, the performance should be determined by the perimeter correlation of figure 6-50; these C_V values can be obtained by designing nozzles that avoid

the problems outlined above. Also, the aspect ratio noise data may contain anomalies associated with the phenomena discussed above; the best noise correlations should be with the 100-aspect-ratio nozzle (which, incidentally, has the same span and area as the breakup nozzles) with the stable exits, and the poorest with the 250-aspect-ratio nozzle. The 50- and 400-aspect-ratio nozzle correlations would fall between these two.

6.5.1.2 Convergent-Divergent Nozzle

The purpose for testing the convergent-divergent nozzle is to investigate suppression gains available from the attenuation of shocks associated with the nozzle jets. A C-D slot nozzle was designed for pressure ratio 3 at 100 aspect ratio. The design for shock-free isentropic flow requires a carefully contoured internal geometry with a throat-to-exit area increase of about 9%. Contours were developed using transonic and supersonic flow analyses. There was great difficulty in fabricating and maintaining the necessary precise area distribution and contours. As a consequence, the jet probably still contained some shocks during the testing. However, the measured performance of the nozzle (fig. 6-55) shows the usual increase in C_V with pressure ratio for this type nozzle. The peak C_V level is a few tenths percent less than the corresponding 100-aspect-ratio (stable) slot nozzle. The small gain obtained from the nozzle divergence is offset by the skin friction due to additional length. This is in agreement with the general practice in the use of C-D nozzles; such nozzles are not generally used for performance gains at nozzle pressure ratios below 4 to 6.

The shape of the C_V curve for the C-D nozzle is similar to the 400-aspect-ratio nozzle measurements. This clearly shows the C-D effect caused by expansion of the 400-aspect-ratio nozzle.

6.5.1.3 Multi-element Nozzles

The use of multi-element breakup nozzles (multitube or multilobe) for noise suppression generally causes performance losses. However, in addition to the noise advantages, these nozzles offer advantages when they are used in ejector systems. The noise suppression capabilities of these nozzles generally increase with the amount of breakup, while the C_V performance generally decreases. Consequently, it is necessary to carefully establish the performance penalties associated with the noise suppression.

Multitube nozzles can be built with smaller internal performance losses for a given amount of breakup than can multilobe nozzles. The tubes generally have smaller total perimeters, and do not have corner losses. They are also easier to build, and are less subject to expansion. However, proper ventilation for external flow is more difficult than with lobes when they are used in an ejector or augmentor system. Jet sheets from tube arrays may be more difficult to turn in augmentor wing systems than are either slot or lobed nozzles. Trades involving secondary losses and augmentor turning will be determined during task II augmentor system static testing.

The augmentor primary tube nozzle performance is shown in figures 6-56 and 6-57 There is a difference of about 1% to 1.5% in performance between the 140- and 70-tube nozzles of 100 aspect ratio, and the C_V is 0.97 or above for both for pressure ratios of 2.3. There is considerable room for additional breakup using even twice as many tubes in 100-aspect-ratio nozzles.

Multilobe nozzles generally have lower internal thrust performance than others, but they are expected to have slightly better suppression characteristics. The performance of the lobed nozzles is given in figures 6-58 and 6-59. There is considerable expansion of the nozzle exit indicated by the slope of the C_D curve for the area ratio 4 thin-lobe nozzle. Since internal performance is critical, it is necessary to minimize wall thickness on this nozzle to provide the best combination of external ventilation and internal performance. Consequently, the wall is designed thin with internal struts, and deflection is purposely permitted. The possible loss of performance from a C-D effect caused by expanding of the nozzle exit was counteracted by converging the sidewalls of the nozzle exit.

The lobe nozzles are expected to turn more readily than tube nozzles in augmentors; this will be determined in task II testing for STOL-oriented configurations. The margin available in internal performance for increasing the number of elements in lobe nozzles is not as great as with tube nozzles, but C_V performance for the nozzles is still 0.96 or above for pressure ratios above 2.3.

6.5.1.4 Nozzle Lip Extensions–Preliminary Results

Some preliminary results of performance measurements involving nozzle lip extensions are shown in figure 6-60. The data show that the addition of the lips causes additional losses of 1% to 3% in C_V.

The nozzle lip extensions are spanwise flat surfaces extended from the nozzle exit downstream for distances of $X/h_E = 5$ (about 2 in. short lip) and $X/h_E = 10$ (about 4 in., long lip). The primary purpose is to shield the high-frequency noise from under the flap and to help attenuate screech noise. Augmentor gains or penalties from these devices are not known.

6.5.2 Primary Nozzle Jet Profile

It is important that jet noise measurements be representative of jet noise source distributions associated with the actual geometry being tested, and not of anomalies from the test rig or models. This is particularly true of high-aspect-ratio nozzles for augmentor wing application.

The spanwise total pressure distribution is measured to be very even at the primary nozzle plenum charging station (sec. 6.3). The acceleration of the flow from the charging station to the nozzle exits is made as low-loss and smooth as possible for each design.

Jet velocity profiles are measured at several spanwise and several axial locations downstream from the nozzle exits. Comparisons are made of the jet profiles to identify anomalies in the high-aspect-ratio jet sheets. All nozzles show good similarity of the jet profiles at spanwise locations. The slot nozzles produce universal profiles similar to those measured by other investigators. The breakup tube and lobe nozzles show varied developments of jet velocity profiles, but their profiles become similar to the slot nozzle profiles further downstream.

Basic differences in jet structure are identified in the tube and lobe breakup nozzles. These are useful for understanding differences in noise measurements. During task II, attempts will be made to relate the augmentor thrust performance and flow turning capability to the structure of the jet sheet. Jet structures will also be examined in relation to high-frequency noise source location, lining placement, and screening of the noise with extensions of the primary nozzle lower lip.

6.5.2.1 Slot Nozzle Profiles

The test rig and models produce very good two-dimensional jet sheets. The jet profiles are examined in detail for two of the nozzles—the aspect ratio 400 and 100. The results for the 400-aspect-ratio nozzle are given in figures 6-61 through 6-65. Profiles are given for X/h_S = 3, 5, 7, 10, and 20 for all six spanwise rake positions. Velocity is nondimensionalized by dividing by V_M, the maximum velocity for the rake. The value of Y is divided by $\delta_{1/2}$, the distance from the jet sheet centerline to the value of Y where the local velocity is half the maximum. This forces the profile through the coordinates $V/V_M = 0.5$ at $Y/\delta_{1/2} = 1.0$.

The important thing to note is that there are very small spanwise differences between profile shapes even as far downstream as $X/h_S = 20$. It was shown in reference 6-14 that jet profiles from breakup nozzles of low aspect ratios tend to form profiles similar to round jets. The 400-aspect-ratio slot nozzle does not show this tendency up to $X/h_S = 20$ (about 9 in.). In fact, no effects of the nozzle edge are seen, even through some rakes are fairly close to the edge of the jet sheet. The jet sheet is essentially two dimensional in this region.

The two-dimensional core of the slot nozzles disappears near $X/h_S = 7$, which is in general agreement with previous tests. The profile shapes at varying distances downstream are summarized in figure 6-66. A comparison is made with the universal two dimensional jet profile. The agreement is close and within the errors of the data scatter; also, the compressibility effects of the present tests may contribute to some differences.

The results for the 100-aspect-ratio jet profiles are given in figures 6-67 through 6-70. Profiles are given up to $X/h_S = 10$. The same general observations and conclusions may be made as for the 400-aspect-ratio nozzles. The curves are summarized in figure 6-71.

6.5.2.2 Multi-Element Nozzle Profiles

The jet sheets from the breakup nozzles reflect the particular nozzle geometry close to the nozzle exits. Generally, the sharp profile features from tube and lobe nozzle exits rapidly disappear and the jet profiles assume shapes similar to the slot nozzle and universal profiles. However, while slot nozzle jets form the universal shape at $X/h_E \sim 7$, the breakup nozzle shapes become similar at $X/h_E \sim 20$. Note that all breakup nozzles have the same area per unit span as the 100-aspect-ratio nozzle; consequently h_E, the equivalent slot height for breakup nozzles, is the same as h_S for the 100-aspect-ratio nozzle. Thus, breakup nozzles require three times the mixing length to reach a universal profile.

This does not mean that the slot nozzles are better nozzles. The breakup nozzles will entrain more air at short distances downstream from the nozzle, and the jet sheet is wider at larger X/h_E stations. This causes the jet to have lower transverse velocity gradients and

lower shear further downstream in the region of noise sources for lower frequencies, and will cause suppression of these frequencies. On the other hand, at points very close to the nozzle exit there are larger regions of high-frequency noise sources relative to the slot nozzles.

The jet velocity profiles from the breakup nozzles were measured at numerous spanwise locations, and at $X/h_E = 5$, 10, and 20. The nondimensionalization is similar to that of the slot nozzles. However, because of the sparse number of probes near the nozzle exits, some details are lacking. Occasionally, because of calculation techniques, the profiles do not go through $V/V_M = 0.5$ at $\delta_{1/2}/h_E = 1.0$. However, the data give a clear indication of the types of profiles generated by the various nozzles.

The 140-tube-nozzle Y jet profiles are presented in figures 6-72 through 6-80. Each of the three spanwise rakes were positioned in similar relative locations within the arrays and tested at the three X/h_E locations. The Y profiles for rakes behind the centerline of two tubes vertically aligned from the jet sheet in the 140-tube nozzle are given in figures 6-73 through 6-74, the profiles behind a central tube are given in figures 6-75 through 6-77, and intermediate profiles are given in figures 6-78 through 6-80.

As might be expected, there are numerous and strong velocity gradients in the Y profiles at $X/h_E = 5$ (figs. 6-72, 6-75 and 6-78), indicating that very good entrainment characteristics may be expected from this nozzle. At $X/h_E = 10$, (figs. 6-73, 6-76, and 6-79), most of these gradients have disappeared; at $X/h_E = 20$, the profiles have become similar to the slot nozzle profiles, but the thickness of the jet is larger than that of the slot nozzles (see figs 6-81, 6-106 and 6-109).

Some spanwise Z profiles for the 140-tube nozzle are given in figures 6-82 and 6-83. At $X/h_E = 5$, the velocity varies by nearly 100%; at $X/h_E = 10$, the maximum variation is ±12%. At $X/h_E = 20$, this has been reduced to ±3% maximum, indicating that the profile is substantially uniform. Thus, considerable spanwise variation is seen in the jet sheet at $X/h_E = 5$; this is substantially reduced at $X/h_E = 10$, and insignificant at $X/h_E = 20$. The spanwise distribution of the noise sources will be relatively uniform at lower frequencies, and will be in 70 recurring patterns at higher frequencies. The microphone array will see the recurring patterns as essentially uniform spanwise noise sources.

Jet sheets from slot nozzles are, in general, easier to turn over coanda surfaces than are jet sheets from breakup nozzles. However, the data show that the 140-tube-nozzle jet sheet becomes similar in profile to a slot jet sheet at $X/h_E = 20$. It is tempting to conclude that the breakup nozzle jet sheet will turn as well as slot jet sheets if the coanda surface is placed in this region of the breakup nozzle jet sheet. This is probably not true because the ratio of the jet sheet thickness to the coanda radius is much larger than for the slot jet sheet.

For ejectors with breakup nozzles, some authors (for example, ref. 6-15) have shown that when diffusers are used, the best performance occurs when the primary nozzles are not aimed down the centerline of the ejector. Profiles in the diffuser entrance region of the higher performing ejectors were nonuniform, and higher velocities were concentrated near the diffuser walls, providing extra momentum to overcome the diffuser pressure gradients. Turning the flow in the augmentor causes acceleration along the lower wall and deceleration

along the upper wall, the effect being that the lower wall must eventually diffuse through a larger pressure gradient. It might be desirable to create a profile such as that of figure 6-73 and place the coanda side of the augmentor throat at the location in the jet sheet at the peak velocity. (This is for an illustration only; the profile in the figure is not the same at all other spanwise locations.) Such a profile would provide more momentum along the coanda surface than would the profile in figure 6-74, for example.

It is important to understand the relationship between the primary nozzle jet sheets and augmentor performance. What is said here is somewhat speculative. During task II, such breakup nozzle jet sheets will be placed in augmentors, and more will be learned about their relationship to performance and noise. Profiles near the throat and exit of the augmentor will be measured and compared with augmentor performance and the primary nozzle profiles measured in task I.

The 70-tube-nozzle jet sheet has many of the same general features as that of the 140-tube nozzle. The velocity profiles are shown in figures 6-84 through 6-89. The 70-tube-nozzle profiles take longer (larger X/h_E) to mix to a universal type profile than the 140-tube nozzle profiles since breakup is not as complete. The data indicate (figs. 6-86 and 6-89) that mixing is more complete at pressure ratio 3 than at pressure ratio 2 for $X/h_E = 20$. The spanwise profiles (fig. 6-90) show results similar to those of the 140-tube nozzle, except that they show slower mixing characteristics.

The thin-lobe-nozzle Y jet profiles are presented in figures 6-91 through 6-96. The nozzle jet sheet mixes quite rapidly, perhaps slightly more rapidly than the 140-tube nozzle. Spanwise profiles (fig. 6-97) also reflect the rapid mixing. The thick-lobe nozzles (figs. 6-98 through 6-103) show jet sheets that are similar to those of the thin-lobe nozzles. Similarly, figure 6-104 shows the spanwise profiles for the thick-lobe nozzles.

6.5.2.3 Jet Velocity Decay and Jet Spreading

Measurements of the augmentor primary nozzle jet velocity decay and spreading are shown in figures 6-105 through 6-114. For the 400-aspect-ratio slot nozzle (figs. 6-105 and 6-106), six spanwise rake positions are plotted. The data indicate that the jet sheet velocity decay and spreading are very uniform spanwise for this nozzle.

The jet velocity decay and spreading for the 100-aspect-ratio augmentor primary nozzle at four spanwise rake positions are given in figures 6-107 and 6-108. The velocity decay differs only slightly from that of the 400-aspect-ratio nozzle. The jet spreading is consistently wider for the 400-aspect-ratio nozzle. Each jet also spreads wider at higher pressure ratios.

Velocity decay and jet spreading curves for the 140-tube nozzle at three positions within a given array pitch are given in figures 6-109 through 6-114. The maximum velocities in the 140-tube-nozzle jet sheet decay more rapidly than the slot nozzle jet sheets for $X/h_E < 10$; however, for $10 < X/h_E < 20$, the situation reverses; and the effect is that the maximum velocities at $X/h_E \sim 20$ are nearly the same. The 140-tube nozzle jet spreading is greater, being 25% wider at $X/h_E \sim 20$. This means that the entrainment is significantly greater in the region near the nozzle exit, and probably not as good further downstream. It

also means that the velocity gradients are lower at $X/h_E \sim 20$ (about 8.5 in.) and the noise generation for lower frequencies associated with this scale will be reduced, while those higher frequencies near the 140-tube nozzle exit will increase in level relative to slot nozzles. There is a small increase in jet spreading with pressure ratio but the velocity decay is unaffected by pressure ratio.

The decay and spreading of the 70-tube augmentor primary nozzle (figs. 6-115 through 6-118) follow the same general pattern as those of the 140-tube nozzle, except for one important difference: the velocity decay of the jet sheet is less rapid. This indicates that the entrainment properties are not quite as good, and the noise differences from the slot nozzle should not be as marked. There is also a slight difference in the jet width at $X/h_E \sim 20$.

The curves for the thin-lobe augmentor primary nozzle are given in figures 6-119 through 6-122. The characteristics of this nozzle resemble most closely those of the 140-tube nozzle, but the spreading is a little less at $X/h_E \sim 20$. The same general observations otherwise apply.

The thick-lobe-nozzle jet curves (figs. 6-123 through 6-126) show slightly faster initial decay and a smaller spreading rate than the 70-tube jet.

The jet spreading and velocity decay results are summarized in table 6-1 and compared with thrust performance results. Since the results were taken from arbitrarily selected profiles, the numbers may change if all data are considered.

Table 6-1.—JET SPREADING AND VELOCITY DECAY RESULTS

	Nozzle				
	400 AR slot	140 Tube	70 Tube	Thin lobe	Thick lobe
[a] $\delta_{1/2}/h_E$ at $X/h_E = 10$	1.2	1.9	1.0	1.7	1.25
$\delta_{1/2}/h_E$ at $X/h_E = 20$	2.0	2.5	2.6	2.1	1.8
[a] V_M/V_J at $X/h_E = 10$	0.86	0.71	0.92	0.70	0.88
V_M/V_J at $X/h_E = 20$	0.65	0.58	0.60	0.62	0.70
C_V $P_{Tap}/P_\infty = 2$	[b]0.959	0.966	0.980	0.959	0.974
C_V $P_{Tap}/P_\infty = 3$	[b]0.970	0.972	0.982	0.965	0.980

[a]All values of $\delta_{1/2}$ and V_M/V_J are at $P_{Tap}/P_\infty = 2.0$

[b]Expanded exit

6.5.3 Acoustic Results

Noise suppressors in general divide the jet exhaust into segments and spread the wake to an overall cross-sectional area considerably larger than that of a single circular jet having the same nozzle-exit area. This technique employs the principle of increasing the perimeter of a jet nozzle to reduce the noise level.

Tests of multitube arrays have shown that adjacent nozzle wakes shield the noise of neighboring wakes, with the result that less noise is radiated along the line of the nozzles than normal to the line. Thus, for a single rectangular nozzle it can be reasoned that turbulent flow regions shield the noise from adjacent regions. Because of greater shielding, noise generated within the flow cannot travel across the long dimension of the wake as readily as across the short dimension, with the result that less noise is radiated off the short ends than off the long sides of the wake—hence, the elliptical noise patterns of high-aspect-ratio slot nozzles.

6.5.3.1 Slot Nozzles

Applications of these noise suppression mechanisms are used to guide the investigation of AWNP high-aspect-ratio slot nozzles. It is necessary to determine the effects of slot aspect ratio, slot height, and nozzle pressure ratio to develop accurate trades with respect to slot nozzle design. Four different aspect ratio convergent slot nozzles (fig. 6-31) were tested at pressure ratios of 1.6, 2.0, 2.3, 2.6, and 3.0 at ambient total temperature. Previous discussion of high-aspect-ratio slot nozzles has indicated the noise patterns to be unsymmetrical. For this reason, each configuration was tested at four orientation angles to provide the necessary noise pattern definition (fig. 6-127). Model data are scaled to a 770-sq in. flow area representative of augmentor wing configurations and evaluated at a 320-ft radius. Results from the 250:1-aspect-ratio slot are considered unacceptable due to nozzle exit geometry expansion during testing. Therefore, only data results for the aspect ratio 50, 100, and 400 nozzles are discussed.

Noise level.—A comparison of the noise levels for the different aspect-ratio slot nozzles (fig. 6-128) shows very little change in noise with increasing aspect ratio (decreasing slot height). This is in agreement with the results of reference 6-1, which also noted only a small noise level reduction with increase in nozzle aspect ratio from 14 to 100. Very little PNL reduction of any magnitude was calculated because of the shift of the peak level frequency to the frequency region adversly weighted by the PNL unit (Noy).

The influence of nozzle pressure ratio is evident in this set of data. As the pressure ratio is increased to supersonic flow conditions a favorable reduction with aspect ratio increase is observed. At the lower pressure ratios, however, there is an increase in noise with decreasing aspect ratio. Mechanisms which cause these shifts in data trends are not identifiable at this time. The most important observation to make is that noise reduction capabilities of slot nozzles are pressure ratio dependent.

The directional properties of the high-aspect ratio slot nozzle are illustrated by the decrease in noise levels with change in nozzle orientation from $\beta = 0°$ (broadside) to $\beta = 90°$ (endside). This variation is only slightly affected by slot aspect ratio and pressure ratio. The most rapid change occurs between $\beta = 60°$ and 90°.

OASPL and PNL increase continuously with nozzle pressure ratio from 1.6 to 3.0. Shock-induced noise has a dominant effect on noise levels (especially PNL) at pressure ratios above 2.0.

Noise directionality patterns.—Noise directionality patterns are used to identify the angle with respect to the engine inlet (or jet axis) at which the maximum noise level occurs, and also how the noise varies with angle. Since noise suppression and peak sideline noise are determined by peak levels, it is important to understand the method of determining this peak and its relation to adjacent levels. Effective suppressor design requires that the peak level occur at an angle such that distance to the sideline is a maximum (i.e., the further the distance the noise radiates the more it is attenuated). Knowledge of the directivity patterns is especially important when the nozzle (or flap) undergoes a series of rotations on engine attitude adjustments. The shape of the directivity pattern provides information as to the benefit of specific attenuation at certain angles. If the pattern has very little change in level with angle, any improvement in suppression will require a noise reduction over a wide range of angles. A flat directivity pattern is also penalized for its "duration correction" in the EPNL weighting system. Comparison of directionality patterns generally provides verification as to the changes in noise spectra for different suppressors. It has been observed in the comparative study of suppressors that a significant shift in the frequency of noise energy is generally accompanied by measurable shifts in the noise directionality patterns. Changes in nozzle exit condition (temperature and pressure ratio) also produce shifts in the directionality patterns.

OASPL and PNL directionality patterns for the broadside orientations (fig. 6-129) show that the maximum noise levels are produced at about 40° from the jet axis. Very little change in the shape of the directivity pattern with aspect ratio is observed. A simple lowering of the noise level occurs. With respect to a round convergent nozzle there is a measurable OASPL reduction attributed to slot nozzles at the angles near the jet axis. An increase in PNL of the slots relative to the RC nozzle is observed for most angles.

Directional distribution of the noise levels presented in figure 6-130 shows a decrease in noise with increasing nozzle orientation from broadside to endside. The difference becomes larger as the aspect ratio is increased. A definite change occurs between the 60° and 90° orientation. At $\beta = 90°$, the peak level shifts to an angle very close to the jet axis. Most of the change has occurred at the lower angles. The highest angles (160° to 170°) are dominated by the low-frequency noise generated downstream of the slot nozzle exit where the initial rectangular flow profile has become more uniform. The large dimensions of the symmetrical wake and the reduced velocity of the jet produce a diminished noise level, dominant low frequency, and uniformly radiating jet.

As the aspect ratio is decreased, the effects of orientation on directivity and level are diminished. In the limit as the aspect ratio approaches one, the directionality patterns will become symmetrical with orientation.

An increase in the slot nozzle pressure ratio produces a continuous increase in the magnitude of the directionality patterns (fig. 6-131). A small shift of the peak level to a smaller angle occurs. This shift may be attributed to the increase in the amount of shock-induced noise and the general shift in peak Strouhal frequency, S_N, with increasing velocity.

Previous data plots were presented on a 320-ft polar arc basis. It is also important to analyze directionality pattern on a sideline basis and observe any changes in the peak noise angles and effects of slot nozzle rotation. In figure 6-132 directionality patterns for a 500-ft altitude distance are presented. The peak noise level is now observed to be near the 100° angle, a shift of 40° with respect to the polar data. Upon rotating the nozzle 45° (i.e., $\delta = 45°$) the peak level is again observed to occur in the 130° to 140° range. This angle of rotation is considered typical for augmentor wing airplane takeoff conditions. These data illustrate the imporatance of defining the "evaluation" distance and configuration geometry in evaluating the noise characteristics of suppressor nozzles.

Symmetry of the noise pattern radiated above and below the slot nozzle is illustrated in figure 6-129.

Noise spectra.—Based on a Strouhal analysis ($S_N = fD/V$) a shift in the noise spectrum to the higher frequencies was predicted. Evidence of this shift is found in figure 6-133 noise spectra. A decrease in the low frequency of up to 15 dB is measured relative to a round convergent nozzle. This reduction is due to the large perimeter of the slots, resulting in lower downstream velocity. There is, however, a corresponding increase in the higher frequencies, resulting in an increase in the PNL. An increase in OASPL is also noted. The dominant characteristic of the slot nozzle is its ability to shift the frequency spectrum.

The influence of nozzle orientation is shown in figure 6-134. A decrease in the mid- and high-frequency energy occurs as the nozzles are oriented from broadside ($\beta = 0°$) to end-side ($\beta = 90°$). This reduction is attributed to the noise-shielding properties of high-aspect-ratio arrays. The low-frequency noise levels are generated in the downstream region of the jet. The jet wake profile is symmetrical, and the resulting noise pattern is also symmetrical with orientation. Hence, the low-frequency noise is not influenced by nozzle orientation. The slot nozzle directionality characteristics are influenced mostly by the amount of dominant high-frequency energy in the spectrum.

As the noise radiation angle, θ, approaches the jet axis there is an increase in the low- and mid-frequency energy (fig. 6-135). This is consistent with the understanding that a major part of the low-frequency noise is generated downstream of the jet exit and radiated at angles close to jet axis. High-frequency noise is shown to decrease slightly with increasing angle.

A continuing rise in the noise spectrum is observed with increasing pressure ratio (fig. 6-136). At pressure ratios of 2.3 to 3.0, shock-induced noise is in evidence. This phenomenon is discussed in section 6.5.3.2.

Noise suppression.—Noise suppression is defined in this report as the difference in peak noise level between a suppressor and a reference nozzle when both are operated at the same pressure ratio and evaluated at the same distance. The slot nozzles are compared to a round convergent nozzle in figure 6-137. These data show the slot nozzles to be more annoying than conventional round convergent nozzles for the $\beta = 0°$ orientation. The spectra presented in figure 6-133 show that decreasing the low frequencies and increasing the high frequencies usually results in an increase in noise annoyance, especially for increases in frequencies in the range of greatest sensitivity of the ear.

The ability of the slot nozzles to suppress low-frequency noise is illustrated in the bottom graphs of figure 6-137. Data for these graphs are obtained by comparing the 125-Hz one-third octave band data at the 140° noise radiation angle.

The best suppressor is observed to be the 400:1-aspect-ratio slot nozzle, especially with respect to OASPL and 125-Hz band data. Suppression is also increased as the nozzle is oriented to the 90° position.

Both PNL and OASPL suppression decrease above a pressure ratio of 2.3. Shock-induced noise is known to influence the supersonic jet noise spectrum. The harmonic and broadband noise contribution of shock-induced aerodynamic resonance and turbulence interaction occurs near the peak level of the turbulence spectrum, which increases both the OASPL and PNL relative to the round convergent nozzle.

Quite possibly, the operation of the slot nozzles at such low velocities (900 to 1300 ft/sec) also limits the suppression potential of slot nozzles. Tests are planned with 300° F heated flow, which will increase the jet velocity at the same pressure ratio and possibly improve the suppression potential.

Noise suppression relative to the 100:1 slot (fig. 6-138) illustrates the improvement in suppression with aspect ratio increase to 400.

Normalized data.—To summarize the data trends for high-aspect-ratio slot nozzles, several normalized curves were constructed. These curves show the influence of slot nozzle orientation, pressure ratio, and aspect ratio on OASPL and PNL (figs. 6-139 through 6-141). The dependence of orientation effects on nozzle aspect ratio is illustrated in figure 6-139. The data curves are referenced to the broadside orientation ($\beta = 0°$). The influence of pressure ratio on noise levels shown in figure 6-140 has been referenced to a pressure ratio of 2.0. Both the orientation and aspect ratio (fig. 6-141) graphs are constructed using pressure ratio 2.0, 2.3, and 2.6 test data.

Slot nozzle peak noise spectra are normalized using Strouhal number in figure 6-142. Pressure ratio 1.6 and 2.0 data are used. Shock-induced noise associated with the other pressure ratio caused data points to scatter, detracting from the resolution. These data are being given further study. Only data reduction for the broadside orientation ($\beta = 0°$) is complete. Scaled slot height was used as the dimension parameter. Data from the round convergent nozzle are presented for reference.

The peak Strouhal number is observed to shift to a lower value as the slot aspect ratio is increased. Lowering of the peak Strouhal number will diminish the influence of a smaller slot height to shift the peak level to a higher frequency. Hence, the spectrum shift is not as great as would be expected if the Strouhal number remained constant.

Conclusions.—The noise-suppressing capabilities of a slot nozzle are confined primarily to changes in the directivity and frequency of the noise. Low-frequency noise reductions in the order of 10 to 15 dB are observed when compared to a round convergent nozzle. The low-frequency noise reduction increases with increasing aspect ratio. The increased frequency of the slot nozzles results in actual increases in PNL for some configurations,

although OASPL was always reduced. The noise level increases continuously as nozzle pressure ratio increases from 1.6 to 3.0. Shock-induced noise is identified as a significant noise source for supersonic pressure ratios. The directionality patterns are changed as the nozzle is oriented from broadside to endside. A 4- to 6-dB reduction on the endside is measured. When slot nozzle spectra are normalized in a Strouhal basis, a reduction in the peak Strouhal number with increasing aspect ratio is found. This diminishes the frequency-shifting capability of slot nozzles with decreasing slot height.

6.5.3.2 Convergent-Divergent Nozzles

The noise spectra of jets issuing from convergent nozzles operating at critical and supercritical pressure ratios contain discrete frequency components which cause a large rise in the noise level. The discrete frequencies are generated by a feedback loop created by the propagation upstream, to the jet exit, of sound waves generated by the interaction of turbulence with shock waves in the jet flow. On arriving at the jet exit plane, the sound waves affect the nozzle pressure ratio slightly, causing the jet to become self-stabilized. This condition sets up an aero-acoustic resonance that causes the jet to emit intense screech tones.

A method of approach for eliminating screech is the use of C-D nozzles operated at their design pressure ratios, thereby preventing the formation of the above-mentioned mechanism. This approach was used in this program to study the achievable noise attenuation when reducing shock-related noise.

The study was conducted using a C-D slot nozzle designed for shock-free operation at a nominal pressure ratio of 3.0. The nozzle has a throat aspect ratio of 100:1 (43 by 0.43 in.) followed by a divergent section 0.4-in. long. Static taps upstream and downstream of the throat were used to monitor the static pressure along the nozzle. The nozzle was operated over a range of pressure ratios from 1.6 to 3.2, and the resulting noise fields were measured.

Identification of screech frequency.—Presented in figure 6-143 is a typical narrow-band analysis (80 Hz) of the noise spectrum of a 100:1-aspect-ratio convergent slot nozzle at a pressure ratio of 3.0, illustrating the noise signature of screech. Powell, in reference 6-16, derived the following relationship for predicting the fundamental frequency of a screech tone:

$$f = \frac{a}{K\,d\,[(PR) - 1.89]^{1/2}} \qquad (1)$$

where K is a constant, a is the speed of sound, d is the nozzle characteristic dimension, and PR is the nozzle pressure ratio. On the basis of two-dimensional experimental data, Powell found that when K was taken as 5.2 and when the nozzle height was used for characteristic nozzle dimension, equation (1) fit his experimental points.

Using Powell's approach, the frequencies of the discrete tones observed in the spectra of the various aspect ratio slot nozzles tested in this program were plotted and found, as shown in figure 6-144, to agree well with Powell's relation for screech tones. This indicates that the discrete spikes are indeed caused by screech.

Since screech occurs as well for round convergent nozzles above the critical pressure ratio, Powell's method has been extended to the test results of the standard nozzle of this program, to the results of Simcox (ref. 6-19), and to those of Franklin (ref. 6-20). It is found, as shown in figure 6-144, that using the value of K = 2.8 and the nozzle diameter for characteristic dimension gives a good estimate of the frequency of screech for round convergent nozzles.

Noise levels.—Presented in figures 6-145 through 6-149 are the measured overall sound pressure levels (OASPL) and perceived noise levels (PNL) of both 100:1 aspect ratio convergent and C-D slot nozzles over a range of pressure ratios from 1.6 to 3.2. From these measurements it is seen that when the C-D nozzle is operated much below its nominal design pressure ratio of 3.0, the levels of its noise generation are considerably higher than those of the convergent nozzle. This is caused by the formation of a shock wave in the divergent section of the C-D nozzle. Although the presence of such a shock wave would tend to have a suppressing effect on the noise by reducing the velocity of the jet, it appears that the normal shock contributes considerably to the acoustic output.

As the pressure ratio is increased toward the design point of the C-D nozzle, the noise levels of the C-D nozzle become lower than those of the convergent nozzle. The largest noise attenuation, occurring at the C-D nozzle nominal design pressure ratio, is of the order of 5 dB in SPL and 5 PNdB in PNL when the nozzle is perpendicular to the plane of measurements (see figs. 6-145 and 6-146), and is of the order of 4 dB in SPL and 3 PNdB in PNL when the nozzle is in the plane of the measurements (see figs. 6-147 and 6-148). These attenuations are due to the fact that while the noise field of the C-D nozzle is primarily generated by the shear-induced turbulence effects, the noise field of the convergent nozzle is dominated by shock-related noise.

For pressure ratios between 3.0 and 3.2 the C-D nozzle exhibits a rather rapid rise in noise level. Although no noise measurements were taken beyond a pressure ratio of 3.2, references 6-5 and 6-17 have reported a continued rapid rise in noise levels when operating C-D nozzles at pressure ratios much higher than their design points.

Figure 6-150 presents a comparison of shock-related noise attenuation achieved by using a 100:1-aspect-ratio C-D nozzle designed for a nominal pressure ratio of 3.0, and the attenuations reported in reference 6-5 where four round C-D nozzles designed for pressure ratios of 2.4, 3.2, 4.3, and 5.7 were tested. Good agreement exists between the results, and advantage can be taken from these data for the purposes of design trade studies involving effects of pressure ratios and temperatures on shock-related noise.

Spectra.—To identify the mechanisms responsible for the generation of discrete tones in the measured noise fields of this study, narrow band analyses (80-Hz bancwidth) of the radiated noise spectra are examined for their frequency contents. Typical results of this analysis are presented in figures 6-151 and 6-152, illustrating the presence of spikes caused by aerodynamic phenomena which radiate discrete tones.The spikes of figure 6-151 are caused by the presence of a shock wave in the diffuser section of the C-D nozzle that cause a substantial rise in the noise radiated by the jet when the nozzle is operated much below its design pressure ratio. Figure 6-152 is the narrow-band spectrum of the C-D nozzle when operated at its nominal design pressure ratio of 3.0. The spikes in the spectrum indicate the

presence of shock-related noise caused by the fact that the actual pressure ratio for shock-free operation of the C-D nozzle is slightly less than 3.0 and seems to be between 2.8 and 3.0. The contribution of these spikes to the sound pressure levels is 1.5 dB. Thus, the achieved suppression caused by shock noise attenuation, shown in figure 6-150 could have been improved from 5 to 6.5 dB had the C-D nozzle been operated at its actual design pressure ratio.

Directivity.—From the data shown in figure 6-153, it is evident that the C-Dnozzle, when operating near the pressure ratio for shock-free operation, is quieter than the convergent slot nozzle at all angles of radiation.

Conclusions.—The results of this study indicate that for a jet operating at a particular supercritical pressure ratio, there is significant noise attenuation to be gained by using a C-D nozzle designed for that pressure ratio instead of a convergent nozzle. The largest attenuation achieved by C-D design in this study is of the order of 5 dB in SPL and PNL.

However, for jets operating over a wide range of pressure ratios, a noise penalty results when operating a C-D nozzle much below its design pressure ratio (over-expanded regime). Also, when exceeding the design pressure ratio (under-expanded regime) the noise level of a C-D nozzle rises at a more rapid rate than that of a convergent nozzle. There exists a range of pressure ratios, between the over-expanded and fully expanded regimes, where a moderate attenuation of the order of 2 dB is achieved.

6.5.3.3 Multi-Element Nozzles

Several basic types of jet noise suppressors have been recognized. These include the directional and mixing nozzle. A directional suppressor nozzle operates partly or completely on the principle of redirecting the acoustic radiation. A slot nozzle is an example. The multi-element nozzle belongs to the class of mixing nozzles. Mixing nozzles subdivide the jet exit flow into many element jets that have a total jet area approximately equal to the original circular nozzle area and distribute the element jets over a base area larger than the original jet. The noise reduction of this class of nozzles involves a frequency shift and a lowering of the velocity of the mixed jet. In the augmentor wing suppressor system the characteristics of both suppressor types are combined.

Previous test experience has been sufficient to give some indication of the mechanism by which multi-element suppressor nozzles function (ref. 6-9). A possible explanation is conjectured in figure 6-154. For the case of multiple elements (tubes or lobes), one can compute the noise to be expected from a number of separate element nozzles. The total noise level is the same as for a single element, but the spectrum is shifted to the right according to the Strouhal number relations where the characteristic dimension is the element dimension and the velocity is determined by the nozzle exit conditions. In most multi-element arrangements, the elements are relatively close together and there was a merging of the jet exhaust streams from the elements not far downstream from their exit plane. Between the exit plane and the merging plane, a great deal of external air was entrained, but in this region there was probably very little interference between the separate jets. Downstream of the merging plane, the flow can be expected to rapidly simulate the flow of a simple circular nozzle made up of the basic airflow plus the airflow entrained prior to the

merging plane. One can expect the noise produced downstream of the merging planes to be similar to that produced by a larger jet with a larger airflow but a slower velocity. Figure 6-154 shows hypothetically the amount of noise that might be produced downstream of the merging. This noise should be subject to computation if the amount of air entrained between the exit plane and the merging plane were known. The noise produced by the separate jets prior to reaching the merging plane will be less than that which these same jets would produce if they had not merged. The amount of this reduction will be very much dependent upon the spacing of the jets one from another or the area ratio of the nozzle. Thus, a high-area-ratio nozzle with large spacing between the jets should give little suppression of the high frequencies that are produced close to the exit plane. A lower area ratio with jets closer together and a shorter distance to the merging plane would be expected to generate less high-frequency noise. The model test data show similar trends. Hopefully, a theory of suppression can be developed in the near future.

The four multi-element nozzles (figs. 6-35 and 6-36) were tested at ambient total temperature over a range of nozzle pressure ratios from 1.6 to 3.0. Pictures of these nozzles are presented in Figure 6-33. A Brief physical description of each multi-element nozzle is tabulated in table 6-2 for reference.

TABLE 6-2.—MULTI-ELEMENT NOZZLE GEOMETRY

Configuration number	Element type	Element number	Area ratio[a]	Flow area,[b] sq in.	Span,[b] in.	Element dimension,[b] in.
6-1	Tubes	70	3.5	18.7	43	0.58
6-2	Tubes	140	4.0	18.7	43	0.41
5-1	Lobes	70	2.5	18.7	43	0.24 (lobe width)
5-3	Lobes	70	4.0	18.7	43	0.15 (lobe width)

[a]Area ratio (AR) $= \frac{\text{enclosed array area}}{\text{flow area}}$

[b]Model dimensions (full-scale dimensions are 6.4 times as large)

Noise characteristics of these nozzles were compared with those of a 100:1-aspect-ratio convergent slot nozzle of the same span (43 in.) and model flow area (18.7 sq in.) to determine noise suppression values.

Acoustic data have been scaled to a nozzle flow area of 770 sq in. (6.4 scale), which is representative of current augmentor span flow area. The data were evaluated at a 320-ft radius from the nozzle exit centerline plane.

Noise level.—A comparison of peak noise levels for the different multi-element nozzles with the 100:1-aspect ratio slot of the same span is presented in figure 6-155. The peak noise levels along a 320-ft arc were determined by examining the noise directionality patterns.

It is evident that these multi-element arrays are more efficient in lowering the overall sound pressure level than the perceived noise levels. This would imply that the peak noise spectrum was not significantly altered by multi-element geometry in the PNL-sensitive region. The noise level reduction is also shown to be sensitive to nozzle pressure ratio (and jet velocity). At the high pressure ratios, noise reductions of the order of 5 to 7 PNdB and 10 to 12 dB (OA) are observed. The ability of multi-element arrays to attenuate the shock-induced noise generated at pressure ratios above 1.89 may account in part for this effectiveness. Increased velocity is another factor; noise suppression in general improves with increase in velocity to about 2000 ft/sec. Low pressure ratio (1.6 to 2.0) operation of these nozzles produced only small values of PNL and OASPL reduction. Suppressor design principles appear to lose validity for overall noise reduction in the low velocity range. Spectrum-shaping capability in the lower frequencies is still maintained, however.

Lobe element arrays were the most effective suppressors. These nozzles had the smallest element dimensions (lobe width) of any of the suppressors and hence provided the greatest spectrum shift. Changing the area ratio produced essentially no change in the PNL. Doubling the number of the tube elements (and decreasing the element diameter) was effective in reducing the noise. Directivity characteristics associated with high-aspect-ratio arrays are still in evidence. Noise reduction potential of these suppressors remained relatively uniform with array orientation.

Noise directionality.—Typical noise directionality patterns (figs. 6-156 and 6-157) show the peak noise levels (PNL and OASPL) to occur between 130° and 140°. A peak noise radiation angle of 135° was assumed in the initial STOL predictions. This means that for the airplane flyover case ($\beta = 0°$) with the nozzle rotated 45° from the horizontal, the maximum noise is radiated almost straight down. Such a direct path provides no noise attenuation advantage with distance. It would be desirable to shift the peak energy to a higher angle (say 110°) in order to take advantage of the longer noise path for attenuation purposes. Heated flow may provide this favorable change in directivity.

The directionality patterns of the multi-element array are similar in the 100:1 convergent slot nozzle pattern; only a general reduction in noise level is noted. It is evident that multi-element nozzles produce very little change in the shape of the directionality patterns with respect to the reduction observed to increase with increasing nozzle pressure ratio.

Orientation of the arrays to the runway sideline configuration, figure 6-158, $\beta = 90°$ reduces the directionality and noise level range. Increasing the nozzle pressure ratio also produced a flattening of the directionality pattern, indicating an increase in the noise at the lower angles (fig. 6-159).

Noise spectra.—Multi-element nozzle noise spectra are compared with the 100:1-aspect ratio slot for two different pressure ratios in figures 6-160 and 6-161. At a pressure ratio of 2.0, one-third octave band noise reduction is found only in the low- and mid-frequency range. The higher frequency levels sensitive to annoyance do not appear to be influenced by element size reduction, shape change, number of elements, or area ratio. Hence, only a very small reduction in PNL is calculated. This trend is improved for the pressure ratio 2.6 operation. Improved noise performance with pressure ratio is not well understood; contributing factors are thought to be shock-induced noise attenuation and a favorable frequency shift determined by Strouhal number relations.

Increasing the 70-lobe array area ratio from 2.5 to 4.0 provided a desired decrease in the low-frequency energy. This is illustrated in figure 6-162, where 3 to 5 dB reduction is noted. In fact, both the area ratio 4.0 nozzles generate the same amount of low-frequency noise, even though one was a tube array and the other a lobe array (see fig. 6-160, $\theta = 150°$). Area ratio is a very important parameter in controlling low-frequency noise generation. Further reductions would be expected for an area ratio 6.0 array. The trend is maintained at other angles and pressure ratios. Noise reduction due to area ratio increase is very evident at the higher angles close to the jet axis where low-frequency noise energy is concentrated. There is an interesting correlation between the low-frequency noise and the downstream velocity profiles. Increasing the area ratio leads to an increase in rate of secondary air mixing. This results in a large-diameter, slower moving jet profile downstream of the nozzle exit. The large diameter produces a lower frequency noise from Strouhal relations, and the lower jet velocity results in a lowering of the noise level per Lighthill's relation.

Increasing the number of tube elements from 70 to 140 with only a slight change in area ratio (3.5 to 4.0) resulted in a favorable mid-frequency noise reduction (fig. 6-162). Further reductions in the noise would be expected for a 280-tube array. As the element number is increased for a constant area ratio array, the element dimensions become smaller, resulting in a higher peak frequency according to Strouhal relations. This produces noise reduction in a slightly higher frequency range. Previous studies pertaining to SST tubular suppressor designs (ref. 6-9) may be used to substantiate this trend (fig. 6-13). A similar effect with lobe-type geometry is expected but needs test verification.

It is evident from the above data that decreasing the nozzle element dimension produces a shift in the peak level frequency according to the Strouhal relation $[f_{max} = K(V_J/d)]$, where K is assumed to be 0.3 for the tubular elements and 0.15 for the lobe elements. Determination of this constant has been made from previous round convergent nozzle studies and the slot nozzle analysis presented in this report. Figure 6-163 shows the frequency increase of the peak level with decreasing element dimension (lobe width or tube diameter). Nozzle exit velocities determined from pressure ratio and total temperatures were used in these calculations.

As the nozzle pressure ratio is increased 1.6 to 3.0, a change in the noise spectrum profile is noted in figure 6-164. Part of the change may be attributed to shock-induced noise as is evidenced by the "rough" spectrum shapes. These phenomena are presented in narrow-band form in figure 6-165. Screech noise frequency prediction relations presented in section 6.5.2 were used to identify these sources.

It is interesting to observe that the low-frequency energy (approximately 125 Hz) increases at a more rapid rate than the high-frequency energy (1000 Hz). For higher pressure ratio operation it is therefore desirable to use a high-area-ratio nozzle to keep the low-frequency energy down. This may be attributed to the fact that as pressure ratio increases the area ratio becomes effectively smaller since expanded flow area is greater, hence less mixing and less low-frequency noise reduction occur. Note that the peak levels occurring near 1 kHz are about the same for both nozzles.

The rectangular array multi-element nozzles have been tested at four different orientations. Typical spectra (fig. 6-166) show very little change with orientation until the $\beta=90°$ orientation. This corresponds to a runway sideline condition during takeoff roll of the airplane. A flattening of the spectrum and a lowering of the PNL and OASPL are noted, confirming the shielding mechanisms associated with high-aspect-ratio arrays. The suppressor is most effective to the runway sideline. Lack of noise level change with orientation for the other orientations (0° to 60°) indicates a symmetrical noise radiation pattern for these angles. This should simplify noise contour plotting for the multi-element nozzle arrays. One other point should be made concerning the orientation effects. Note that the low-frequency energy is not affected by the orientation, even at 90°. This indicates a symmetrical jet downstream.

Area ratio, element shape, number, and size are effective in shaping and attenuating the noise spectrum. The shaping, however, has occurred mainly in the frequencies below 1000 Hz. There has been little reduction in the noise above 1000 Hz, hence very little reduction in the PNL (see fig. 6-162, for example). Perceived noise level is very sensitive to the noise energy in the 1000 to 10,000 Hz range. For increased suppression a device must be found that will be effective in reducing the higher frequencies. Previous testing has shown that a lined shroud should provide significant suppression. For the augmentor wing noise suppressor system, in-line arrays of elements have been used with selected spacing, element number, and shape to reduce the low- and mid-frequency energy and use of the lined shroud is planned to complement the total design by reducing the high frequencies. In this manner optimum use is made of each suppressor component design technique.

Noise suppression.—The multi-element configurations have been compared to the 100:1-aspect-ratio slot nozzle geometry to determine noise suppression. Figure 6-167 presents noise suppression as a function of pressure ratio, configuration geometry, and array orientation. Noise suppression is observed to increase with pressure ratio (and jet velocity). More OASPL reduction than PNL reduction was observed. Orientation appears to have little effect on suppression. The 70-lobe arrays provided the most noise reduction. Further improvements in suppression characteristics are also possible by increasing the area ratio and the number of elements with corresponding size reduction.

Distance effects.—Extrapolation of noise levels to distances greater than the measurement distance involves calculation of the attenuation of noise due to spherical divergence and atmospheric absorption. Spherical divergence results in a decrease in the intensity of sound with the square of the distance from the same. It is independent of frequency; doubling the distance reduces the noise 6 dB.

Two types of atmospheric absorption, "classical" and "molecular," are considered. Classical absorption is a function of frequency and temperature; molecular absorption is a function of frequency, temperature, and relative humidity. The reduction of noise energy per unit distance is significant for the high-frequency energy produced by jet engines. This is especially true for suppressor nozzles where the peak energy levels occur in the high frequencies.

In figure 6-168 the effects of these absorption parameters with distance are presented for the 70-lobe area ratio 4.0 array. An average reduction of 8 PNdB and 7 dB for doubling of distance is observed. The dashed lines representing round convergent nozzles show slightly less reduction with doubling of distance, indicating less significant high-frequency energy and hence less effective attenuation by atmospheric absorption.

Conclusions.—Selection of a multi-element nozzle for testing with a lined flap configuration is now possible using information presented in this report. The curves of figure 6-167 indicate that the best suppressors tested to date are the 70-element lobe arrays. Area ratio difference between these two arrays made little difference in the PNL and OASPL characteristics. However, spectrum analysis (see fig. 6-162) shows significant reduction in the low-frequency noise as the area ratio is increased from 2.5 to 4.0. It is important to select a multi-element nozzle that will provide the best low-frequency suppression when PNL suppression characteristics are nearly equal, because the lined flap test results from previous programs have shown that flaps effectively attenuate high-frequency noise energy but have very little effect on low-frequency noise levels (fig. 6-12). The low-frequency noise reduction must therefore be obtained by the multi-element primary suppressor. For these reasons, the 70-lobe multi-element nozzle with an area ratio of four was selected as the initial primary suppressor nozzle to be tested in combination with the lined flaps.

Test results from rectangular arrays of multi-element nozzles have demonstrated that element number, shape, and area ratio are effective in shaping the noise spectrum and providing OASPL and PNL noise reduction. Increasing the nozzle pressure ratio produced a continuous increase in the OASPL but a flattening of the PNL at the higher pressure ratios (fig. 6-169). Orientation effects are still in evidence (fig. 6-170) for multi-element arrays. About 4 PNdB reduction in level is noted as the nozzle is oriented to the end side.

A comparison of the multi-element nozzle noise suppression and nozzle performance relative to the 100:1-aspect-ratio slot nozzle is summarized in figure 6-171.

6.6 APPLICATIONS

Augmentor wing noise estimates were made for a 150-passenger STOL airplane using the test data for the 100:1-aspect-ratio C-D slot, the 400:1 aspect-ratio slot, and the 70-lobe nozzles. Four 20,000-lb (static thrust) engines were used to power the aircraft. An aircraft velocity of 100 kn at 500-ft altitude was assumed. A noise path distance of 700 ft was also assumed in estimating the 500-ft sideline perceived noise levels. For a 45° flap/engine rotation, this implies that the noise path is nearly vertically down and to the side.

The noise was calculated by scaling the test data in the following manner. First, the 6.4 scale data (770 sq in. flow area) peak PNL was observed to occur near the 135° noise radiation angle. The peak noise level at a model pressure ratio which corresponded to the actual engine exhaust relative velocity was selected and corrected for engine density and area variations required to maintain a constant 40,000-lb engine thrust per span. The broadside noise level was adjusted to account for a 45° orientation geometry. Three dB was added to correct for the other wing span noise. Since scaling of the data by a factor of 6.4 resulted in slot heights very close to typical augmentor wing slot heights, and since the analysis results have also shown very small changes in PNL with slot height variations, no frequency corrections were made. Because of the limited velocity range of the test data, the augmentor wing STOL noise estimates at an engine pressure ratio of 3.0 were obtained by extrapolation procedures using previous trends and the Lighthill relations ($SPL - 10 \log \rho^2 A V^8$).

Augmentor wing noise estimates are compared to the initial prediction in figure 6-172. The scaled tests show good correlation with the initial predictions in the pressure ratio 2.0 range. At higher pressure ratios a wider range of levels somewhat higher than predicted was found. This difference has been attributed mainly to shock-induced noise. Further reductions of the multi-element nozzle noise are possible with increased area ratio, number of elements, and corresponding decrease in element size.

The thrust losses due to the internal friction of nozzles with similar internal flow acceleration, similar base drag effects, and the same exit areas can be correlated with nozzle wetted perimeter or hydraulic diameter. Velocity coefficients measured for six augmentor primary nozzles tested in task I were plotted versus equivalent hydraulic diameter for nozzle pressure ratios of 1.6 and 2.6 in figure 6-173. This relationship provides a method for estimating the nozzle performance of any suppressor nozzle of similar design selected for an airplane augmentor nozzle with knowledge of the hydraulic diameter after applying corrections for Reynolds number effects. A method for adjusting the velocity coefficient of a nozzle for Reynolds number effect is also shown in figure 6-173. The calculations involve turbulent, compressible boundary layer analysis suggested by B. S. Stratford (ref. 6-21).

The following example illustrates the estimation of performance of an airplane augmentor primary nozzle from model data: Using a suppressor nozzle selected for the airplane with an equivalent hydraulic diameter of 0.05 and operating at a pressure ratio of 2.6, the nozzle velocity coefficient is 0.961 uncorrected for Reynolds number effects. C_V at R_{N_2} is the airplane nozzle Reynolds number and the C_V at R_{N_1} is the model nozzle Reynolds number. The C_V correction is determined from the appropriate scale factor (R_{N_2}/R_{N_1}) if temperature effects on Reynolds numbers are neglected. At a model nozzle $C_V = 0.961$ and a scale factor of 4, the airplane nozzle C_V is = 0.970.

Also shown in figure 6-173 are two data points measured from the 0.7 scale model modified C-8A (Buffalo) augmentor flap tests conducted at Boeing. The model was a double slot nozzle with aspect ratios of approximately 700 for each slot. The slightly lower nozzle performance compared to the task I predicted performance levels is most likely due to turning vane losses.

The takeoff noise footprint (fig. 6-174) weredetermined with the help of a computer proprogram. The program flies the aircraft along the specified flight profile and extrapolates the peak noise produced by the aircraft. The noise is extrapolated to a grid of individual

observation points on the ground. The resulting grid and associated peak noise level is searched in an interpolative procedure which determines the location of the specified footprints. In addition, a numerical summing procedure totals the area, from the end of the runway to the footprint closure, within each specified footprint. Inputs for this program were obtained from figures 6-172, 6-175, and 6-176.

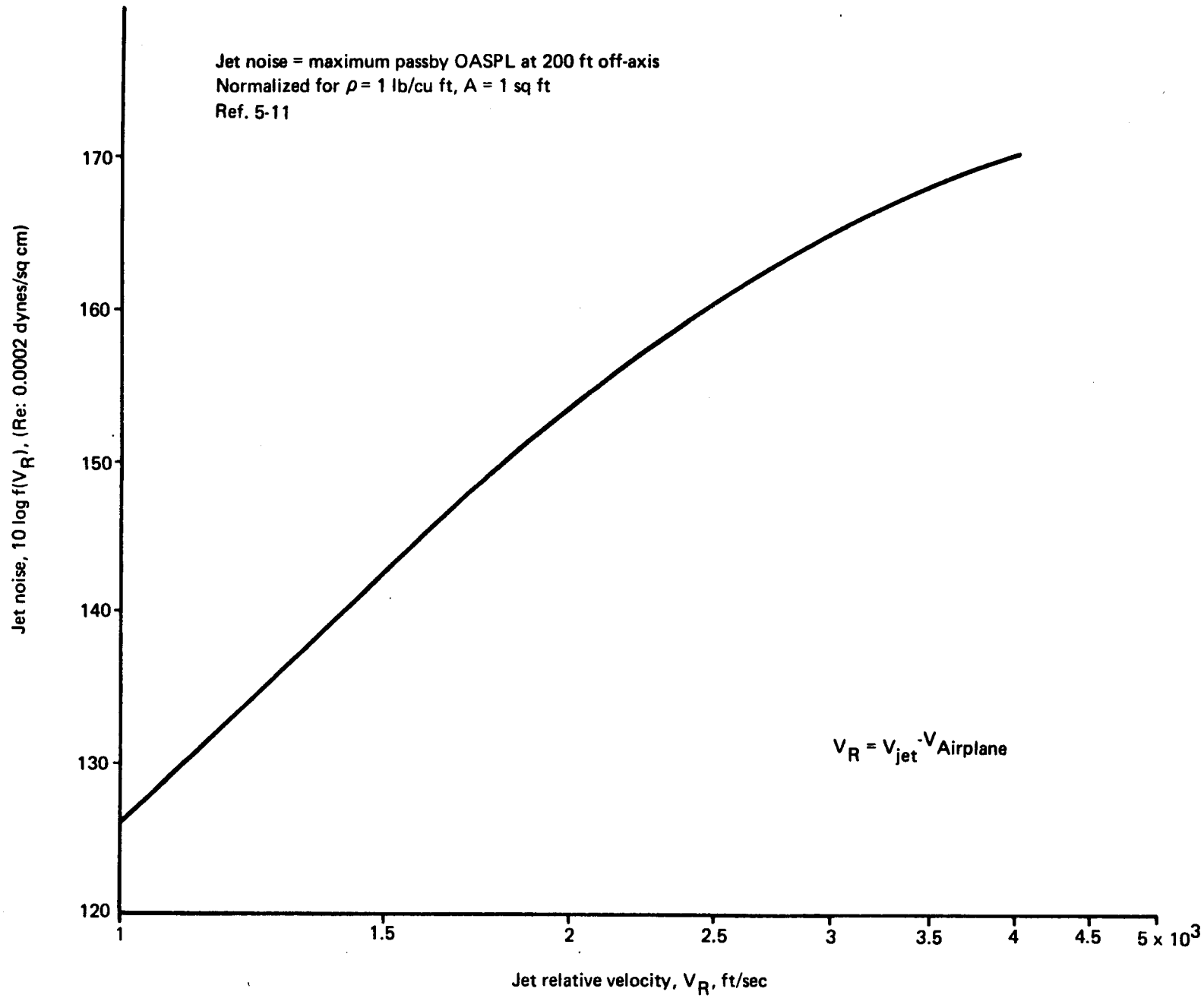

FIGURE 6-1.–NORMALIZED JET NOISE VS JET RELATIVE VELOCITY

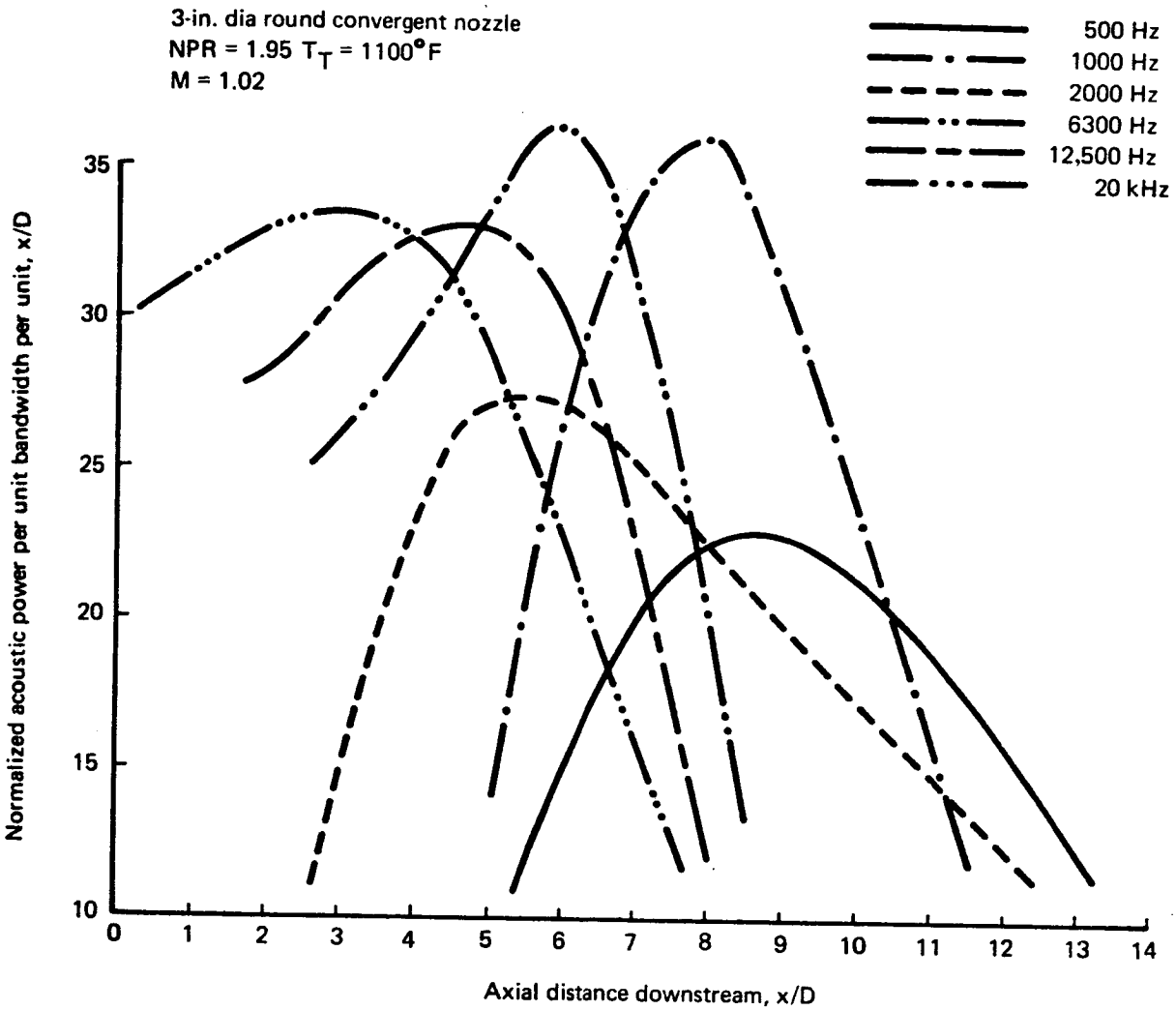

FIGURE 6-2.– NOISE SOURCE DISTRIBUTION WITH AXIAL DISTANCE DOWNSTREAM OF JET

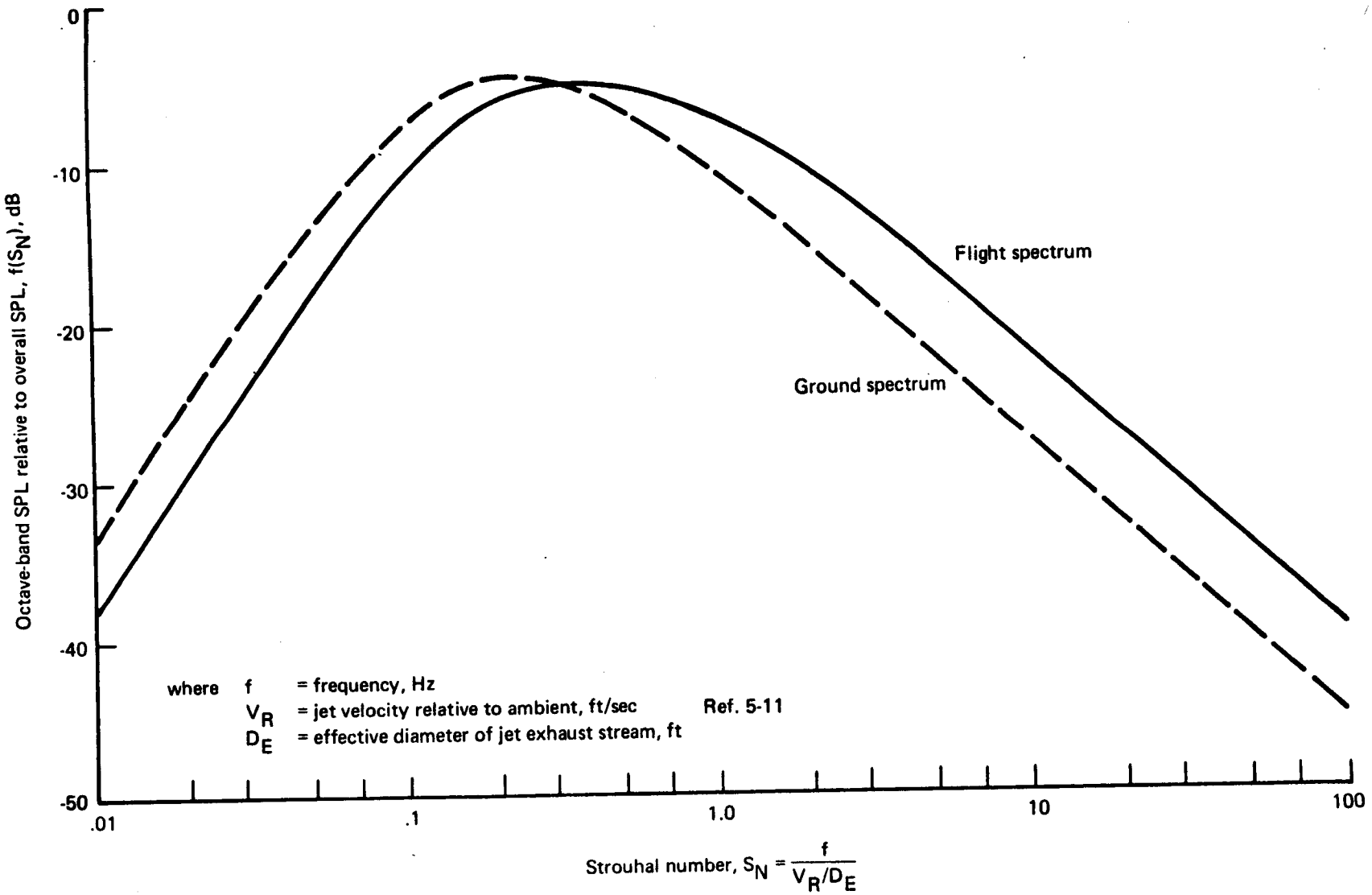

FIGURE 6-3.– OCTAVE-BAND JET NOISE VS STROUHAL NUMBER

Strouhal number relationships (S_N)

$$S_N = \frac{f^1 D_E}{V_R{}^*}$$

S_N = a nondimensional parameter
(0.22 for round nozzles)
(0.15 for slotted nozzles)
f^1 = peak frequency, Hz
V_R = relative jet velocity, ft/sec
D_E = round nozzle diameter, ft, or slot height, ft

$$\therefore \frac{S_N}{D_E} = \frac{f'}{V_R} \qquad \frac{S_N}{D_E} = K_{constant} \qquad V_R K = f^1$$

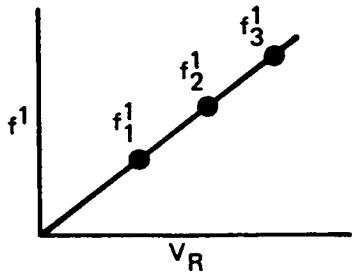

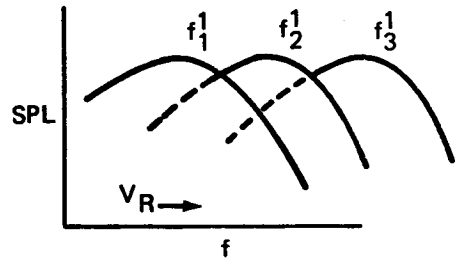

$^*V_R = (V_{jet} - V_{airplane})$

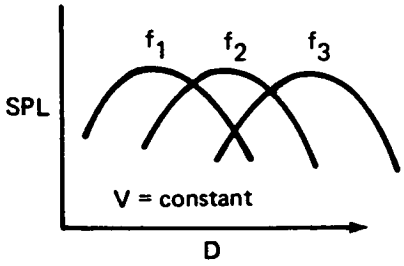

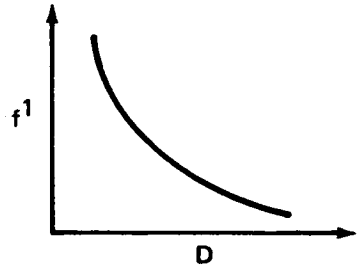

V_{jet} is a direct function of engine power setting, i.e.,
(1) Nozzle pressure ratio and temperature
(2) Thrust and mass flow

FIGURE 6-4.— JET NOISE PEAK SPECTRUM DESIGN VARIABLES

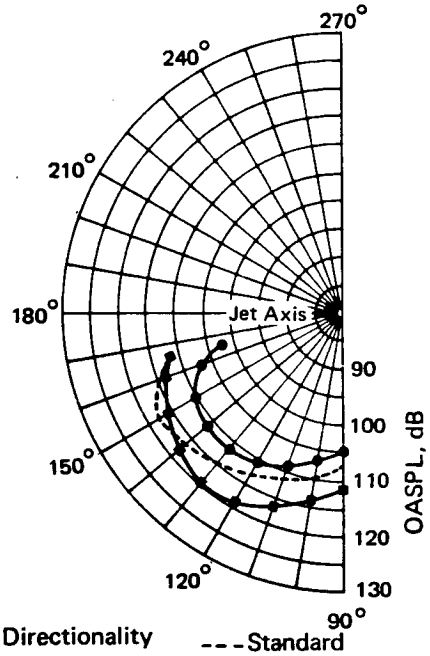

a) Directionality pattern, 14:1 slot nozzle (66 by 4.6 in.)

- - - Standard
● $\beta = 90°$
■ $\beta = 0°$

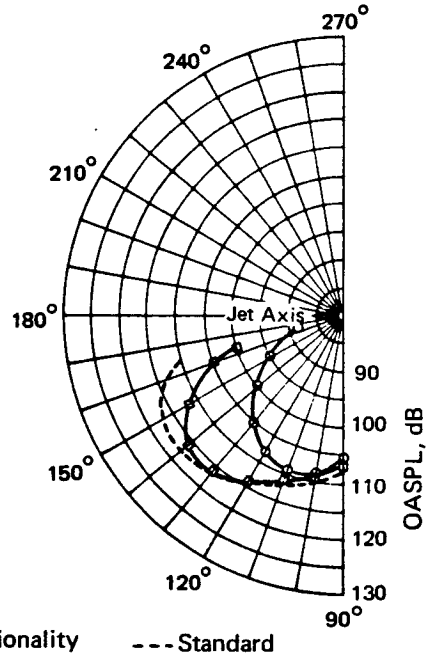

b) Directionality pattern, 100:1 slot nozzle (180 by 1.8 in.)

- - - Standard
○ $\beta = 90°$
□ $\beta = 0°$

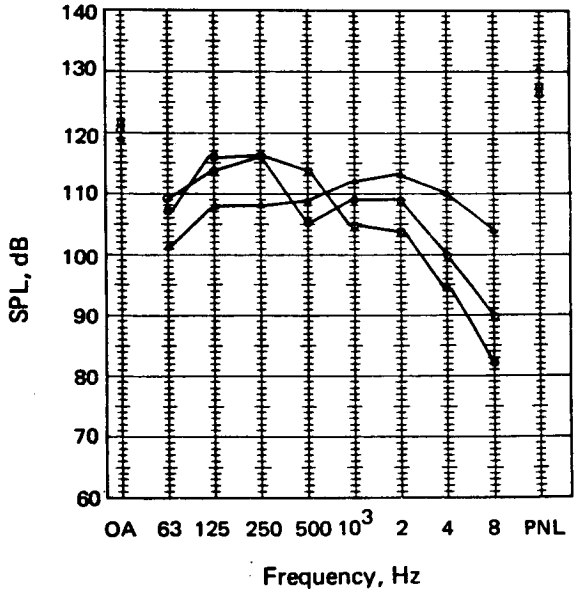

○ 14:1 slot nozzle $\beta = 0°$
▲ 100:1 slot nozzle
□ Standard

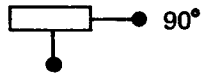

Orientation, $\beta = 0°$

T_T = 1735°R
NPR = 1.7
V_{ji}* = 1600 ft/sec
A = 2.1 sq ft
Taken from figures 6 and 7, ref. 6-1

*Effective velocity

FIGURE 6-5.— COMPARISON OF 14:1 AND 100:1 SLOT NOZZLES

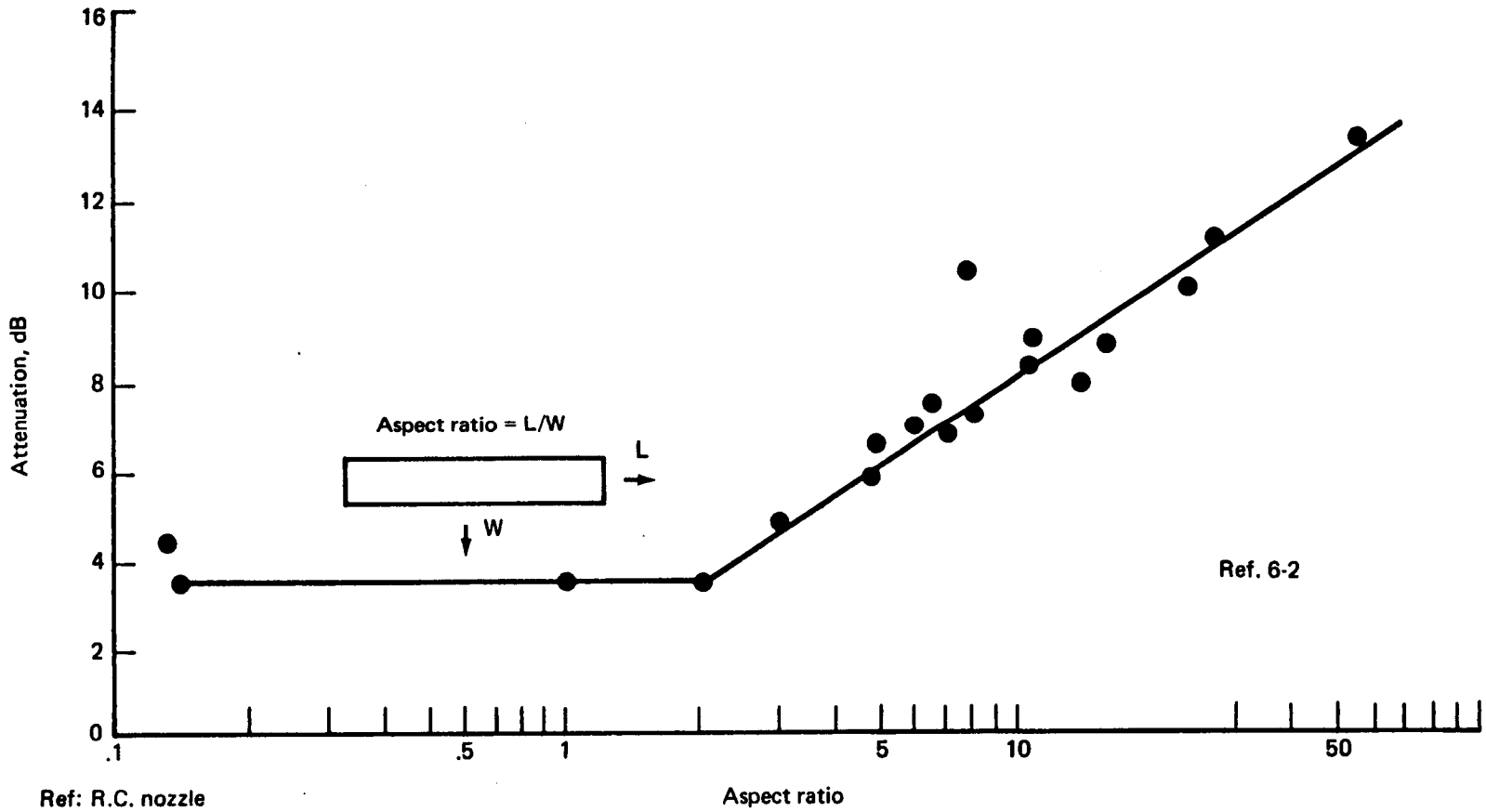

FIGURE 6-6.– EFFECT OF ASPECT RATIOS

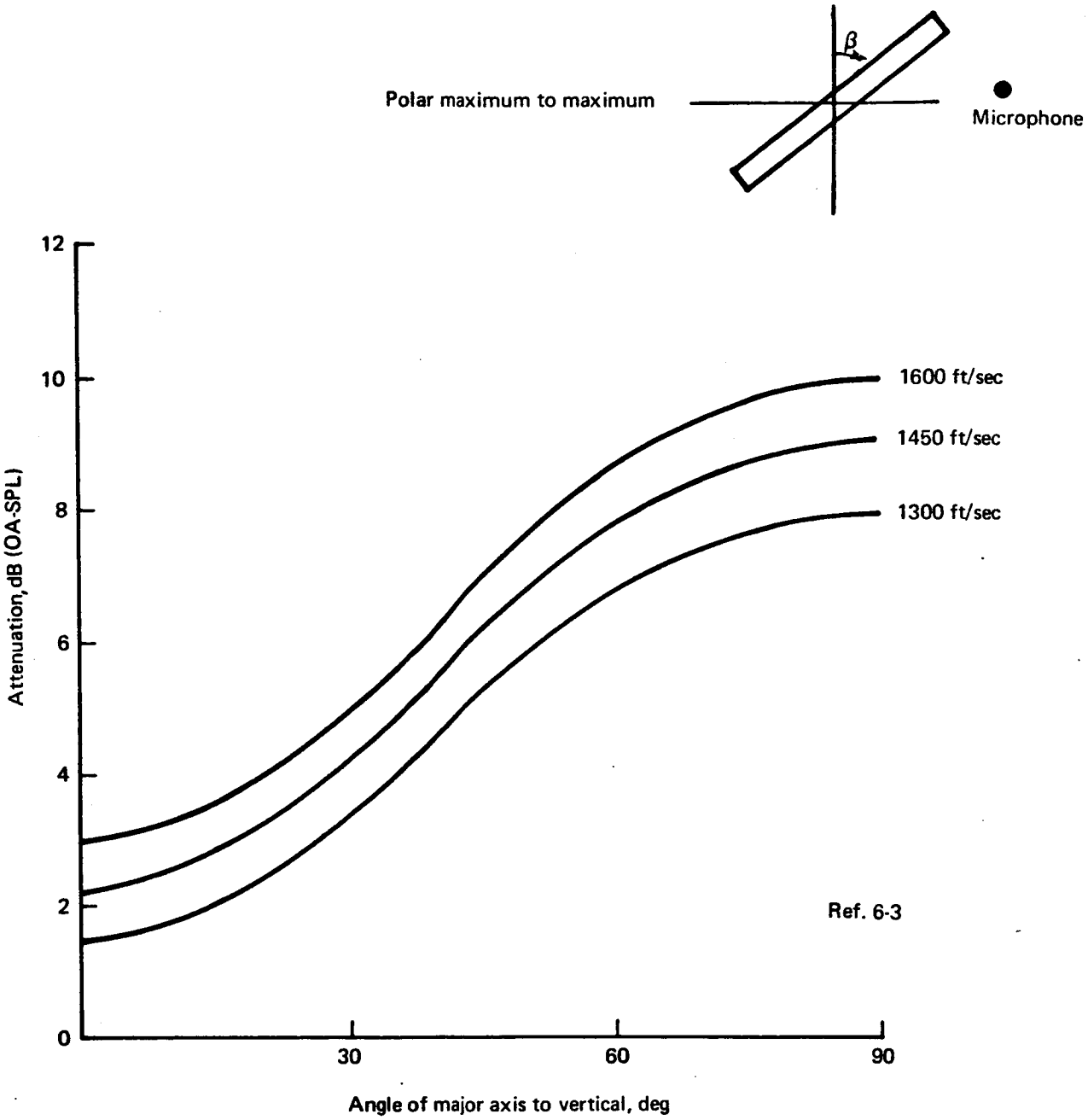

FIGURE 6-7.– EFFECT OF ORIENTATION

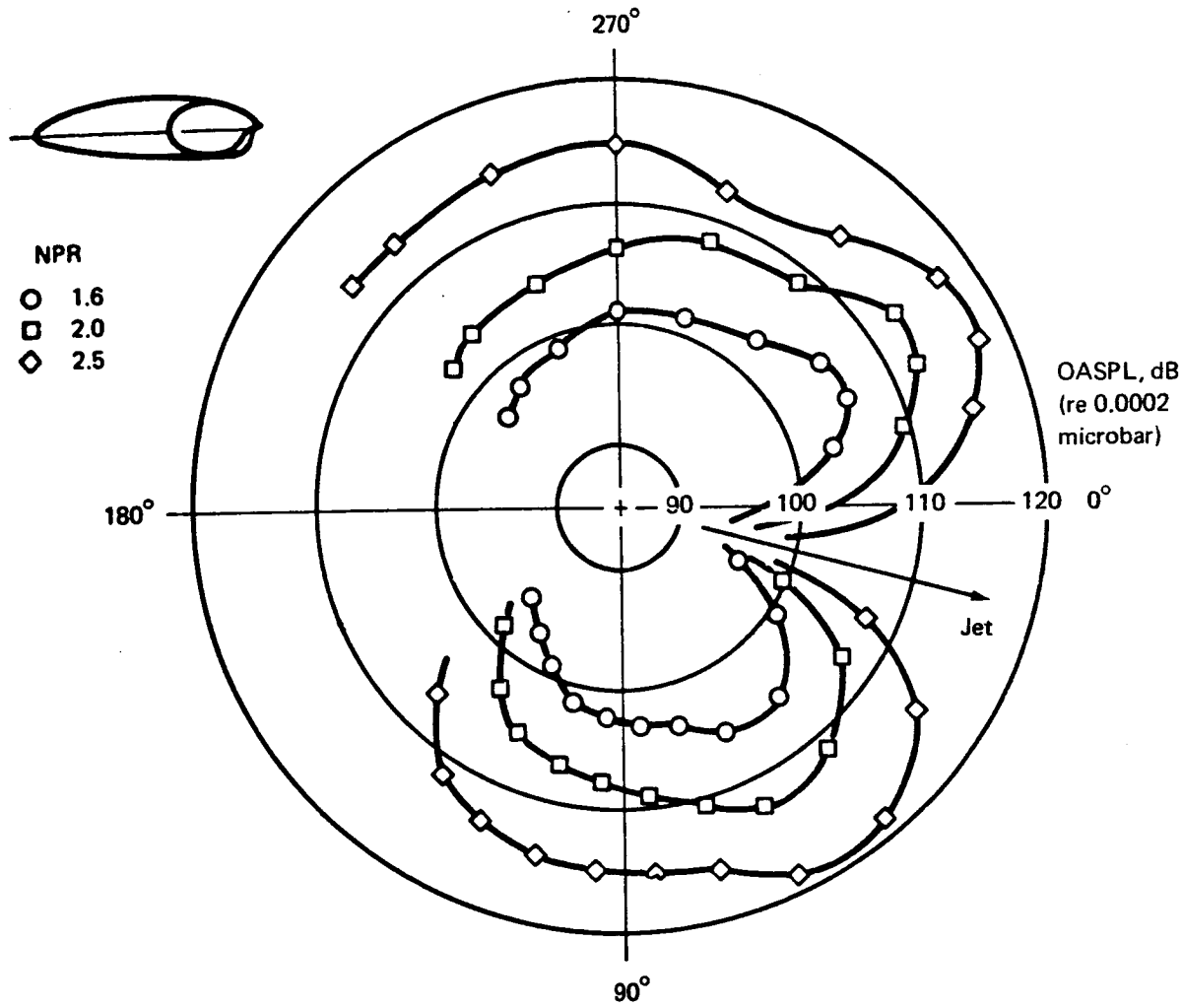

Direction pattern for augmenter wing slot-nozzle noise (flaps removed). Slot height, 0.68 in.; microphone radius, 50 ft

Ref. 6-4

FIGURE 6-8.— EFFECT OF NOZZLE PRESSURE RATIO ON NOISE

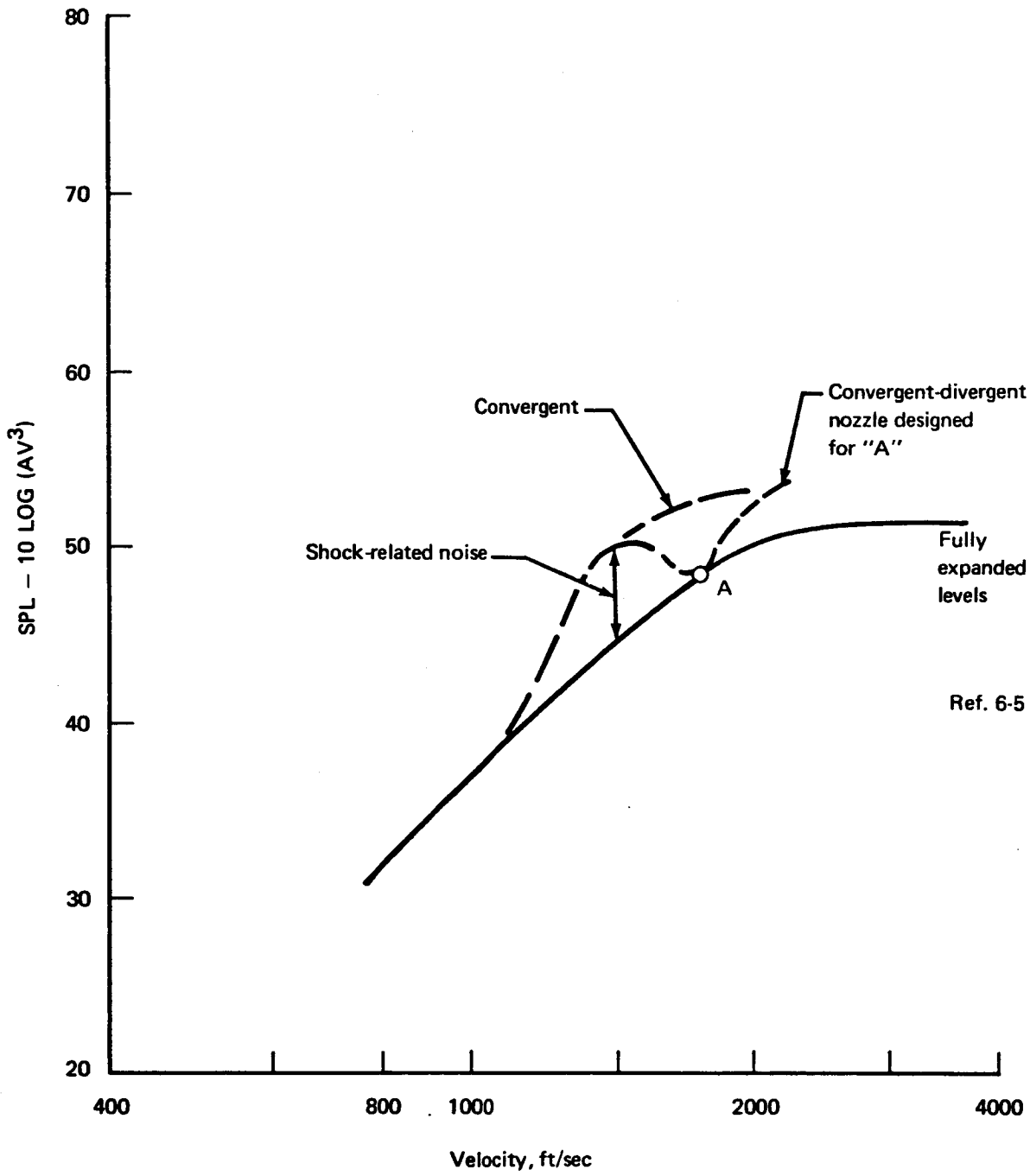

FIGURE 6-9.– SHOCK-RELATED NOISE, NOZZLE SHAPING

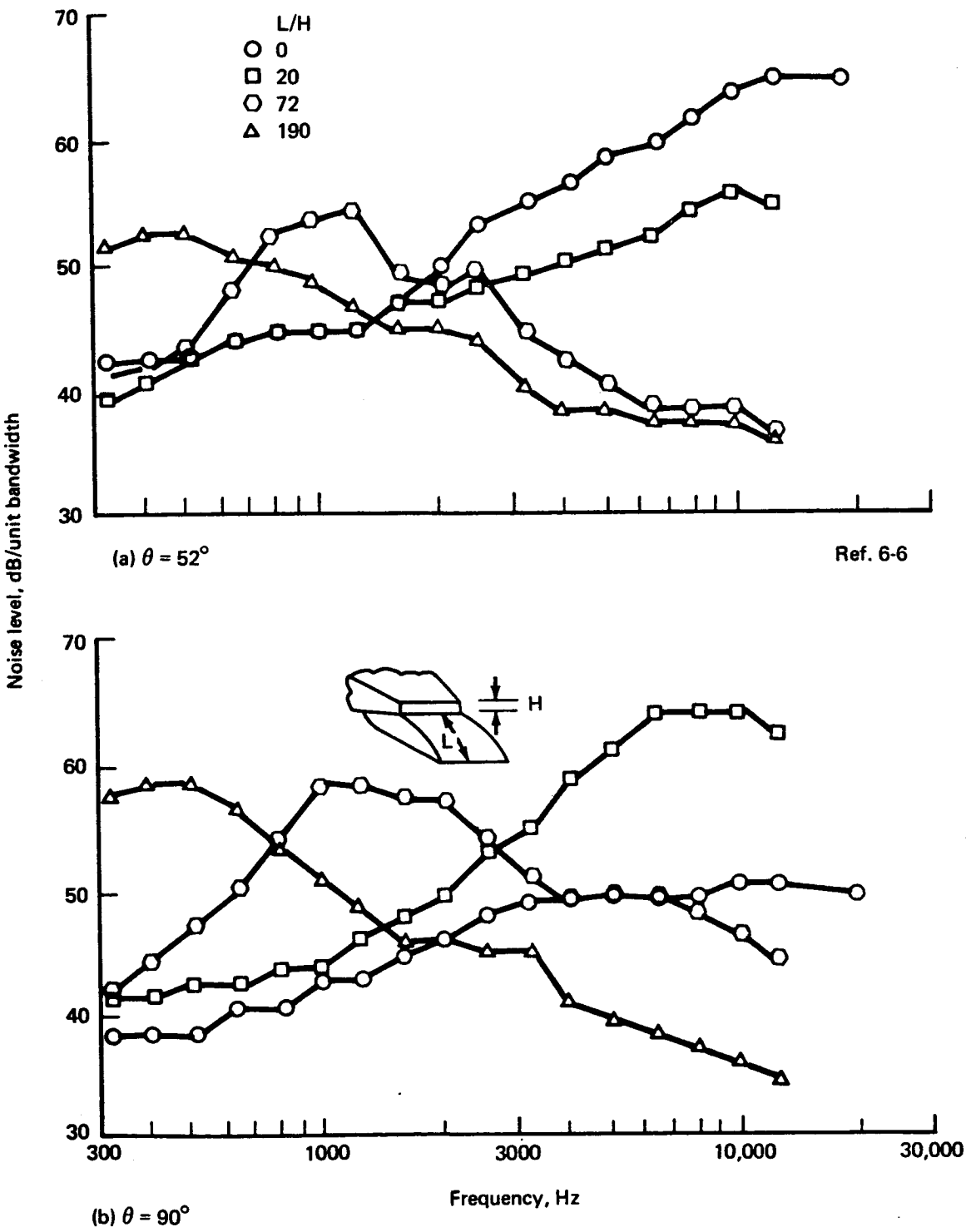

FIGURE 6-10.– EFFECT OF NOZZLE LIP LENGTH

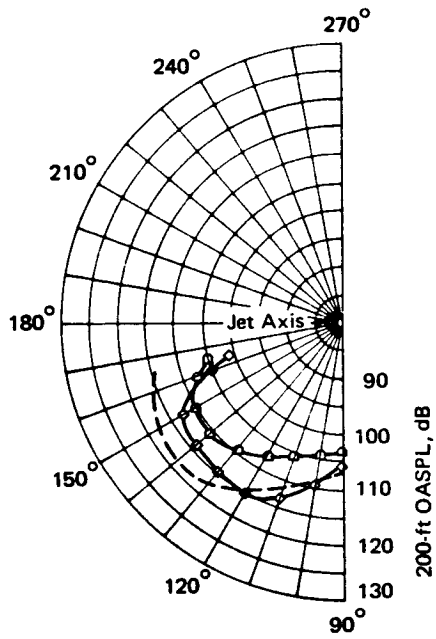

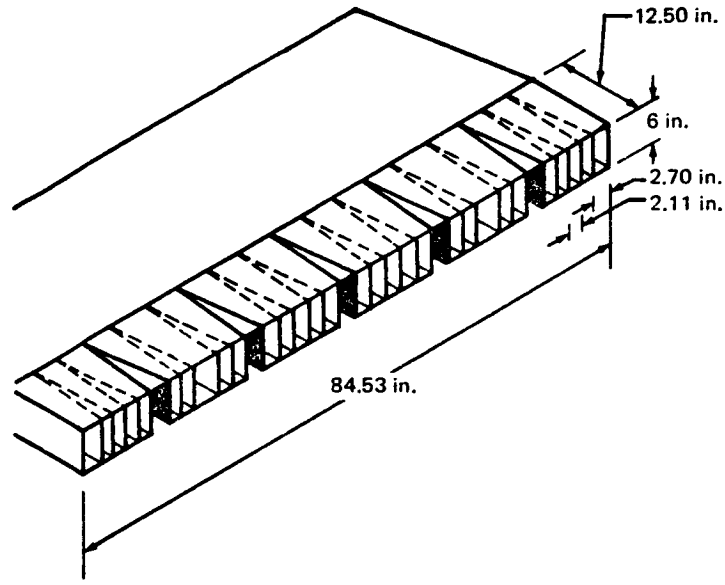

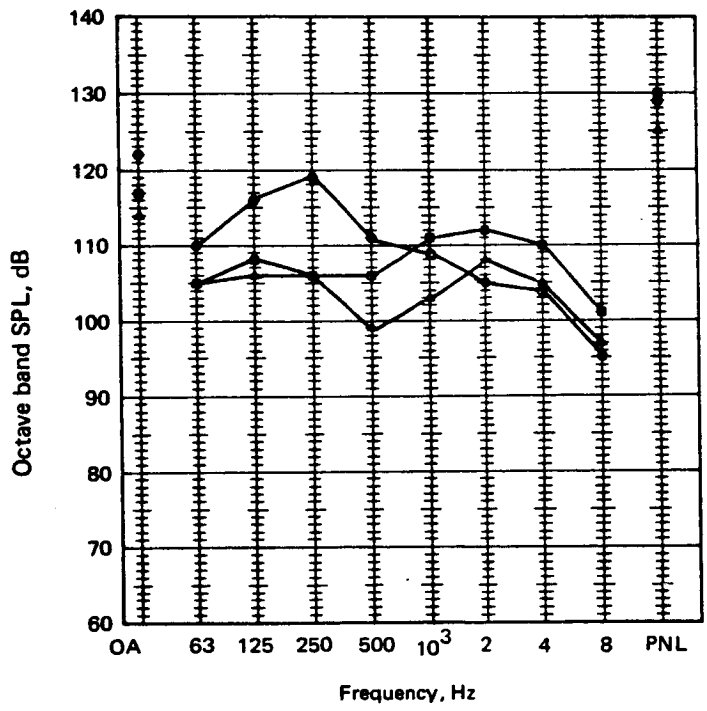

NPR ≅ 1.7
T_T ≅ 1640°R
V_{ji} ≅ 1730 ft/sec
A = 2 sq ft

Taken from Figure 13 of ref. 6-7

○ Standard
△ $\beta = 90°$
□ $\beta = 0°$
} Spectra plot

Horizontal ($\beta = 90°$)
◇ Vertical ($\beta = 0°$)
— — Standard nozzle
} Directivity plot

Θ = 150°

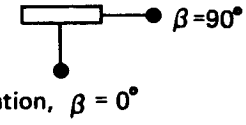

Orientation, $\beta = 0°$

FIGURE 6-11.– MULTI-ELEMENT NOZZLE NOISE CHARACTERISTICS

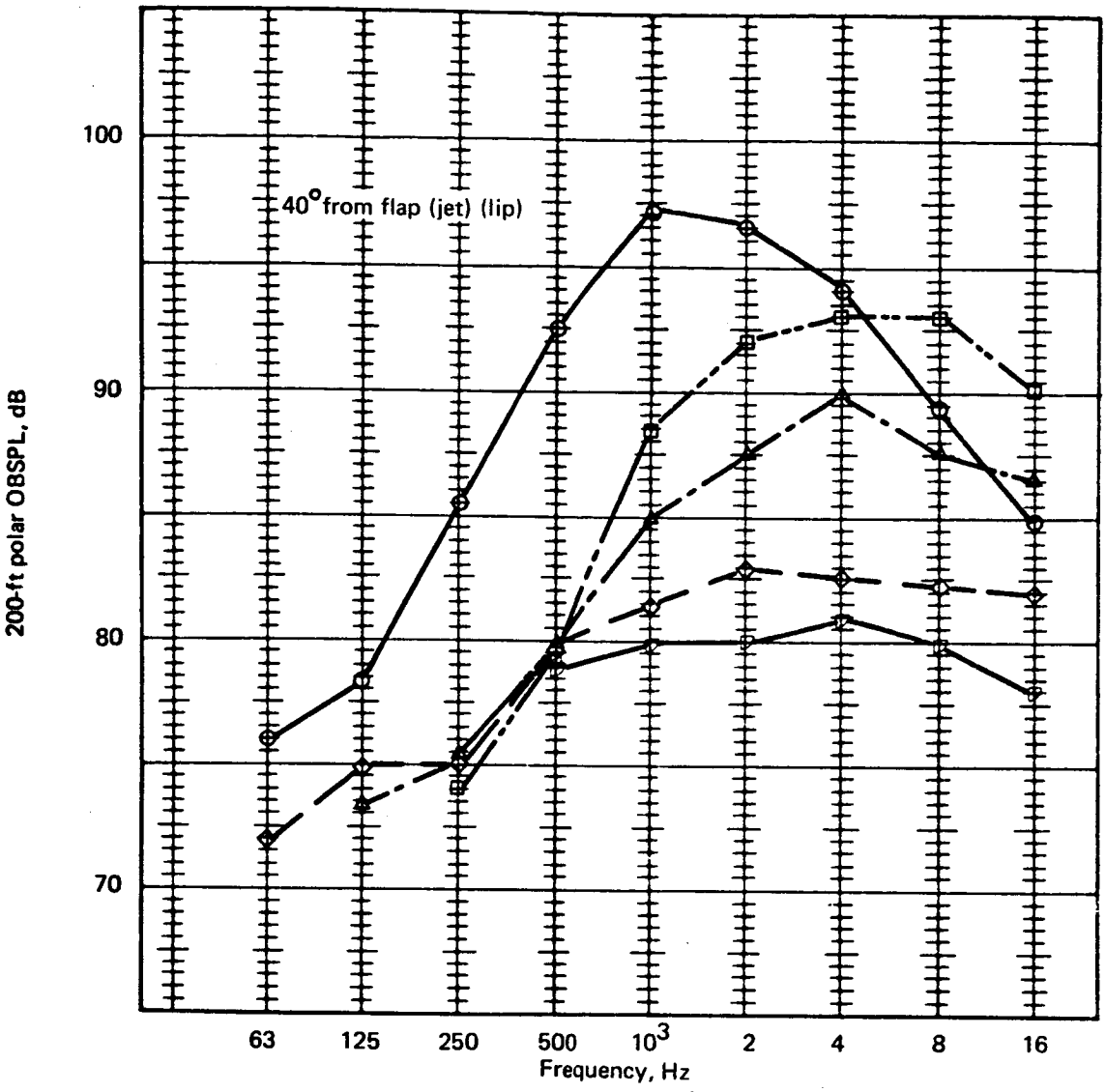

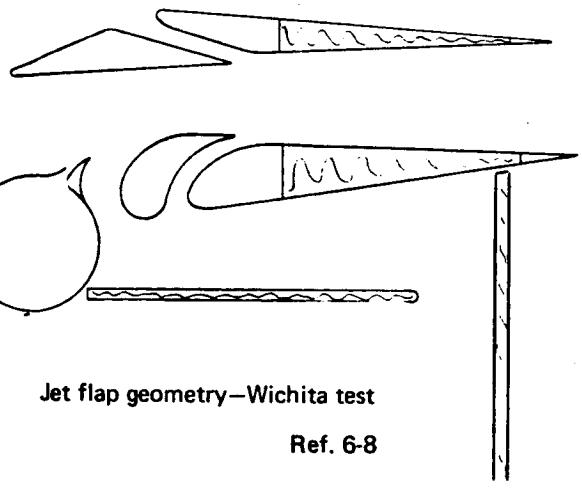

○ Round convergent nozzle
□ 75:1 aspect ratio slot with short lip
△ Unlined flaps
◇ Lined flaps
▽ Lined flaps with shield

Slot NPR = 2.5
Slot T_T = 240° F
A = 12 sq in.

Jet flap geometry—Wichita test

Ref. 6-8

FIGURE 6-12.— EFFECT OF LINED AND UNLINED FLAP ON SPECTRUM

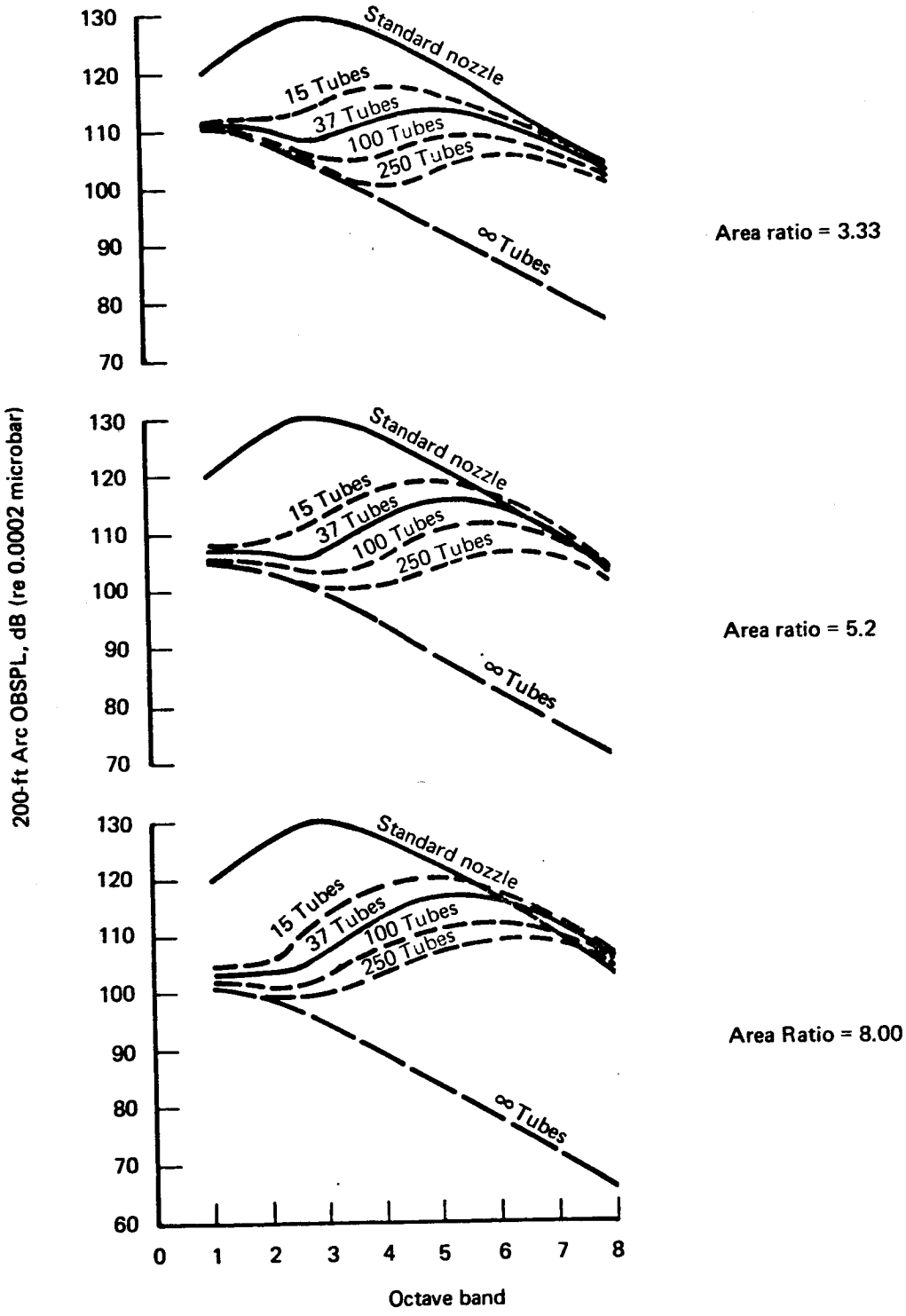

NPR = 3.0 T_T = 1500°F Ref. 6-9

FIGURE 6-13.– SPECTRA OF VARIOUS PLAIN-ENDED MULTITUBE NOZZLES

Basic system elements =

Modified primary nozzle + Lined shroud = Suppressor system

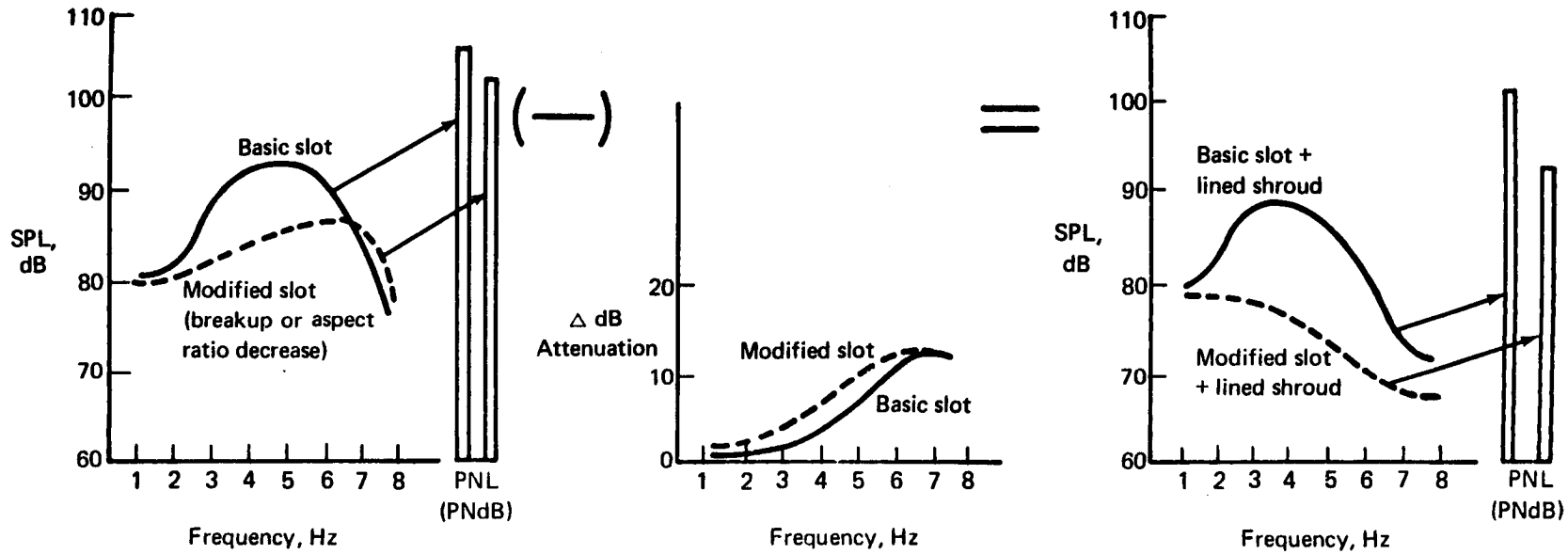

1. A modified slot nozzle produces a lower initial unshrouded noise level and will use the shielding and sound adsorbing properties of the shroud more efficiently.
2. The advantages of the modified slot lie in its ability to
   a) Provide a lower overall noise due to more efficient mixing.
   b) Shift the noise energy to a higher frequency and closer to the jet exit which complements the lined shroud capability.
3. The suppression capability is limited by:
   a) Configuration constraints
   b) Interaction effects and leakage

FIGURE 6-14.– AUGMENTOR WING JET FLAP NOISE SUPPRESSOR SYSTEM

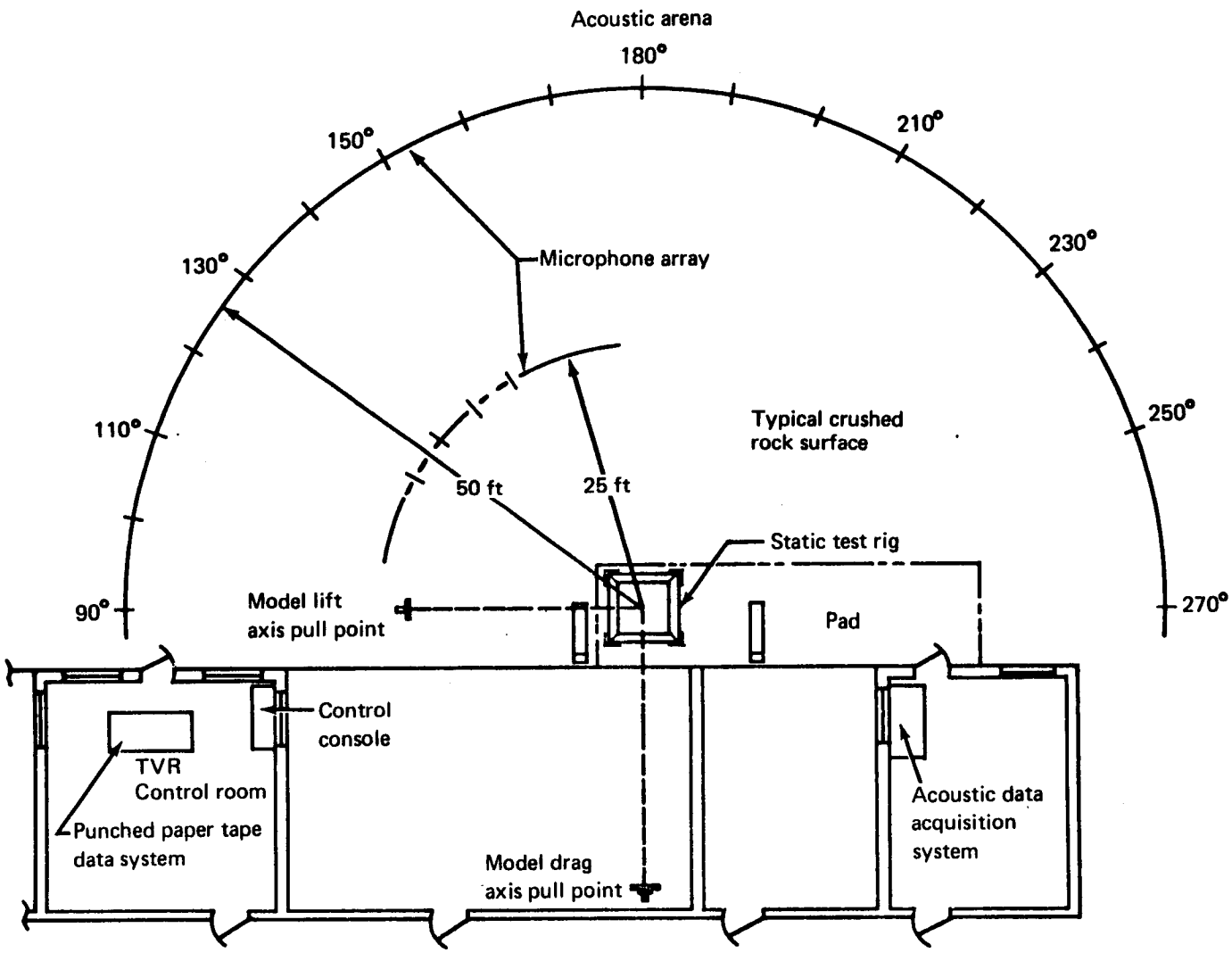

FIGURE 6-15.– STATIC TEST RIG TEST AREA INSTALLATION

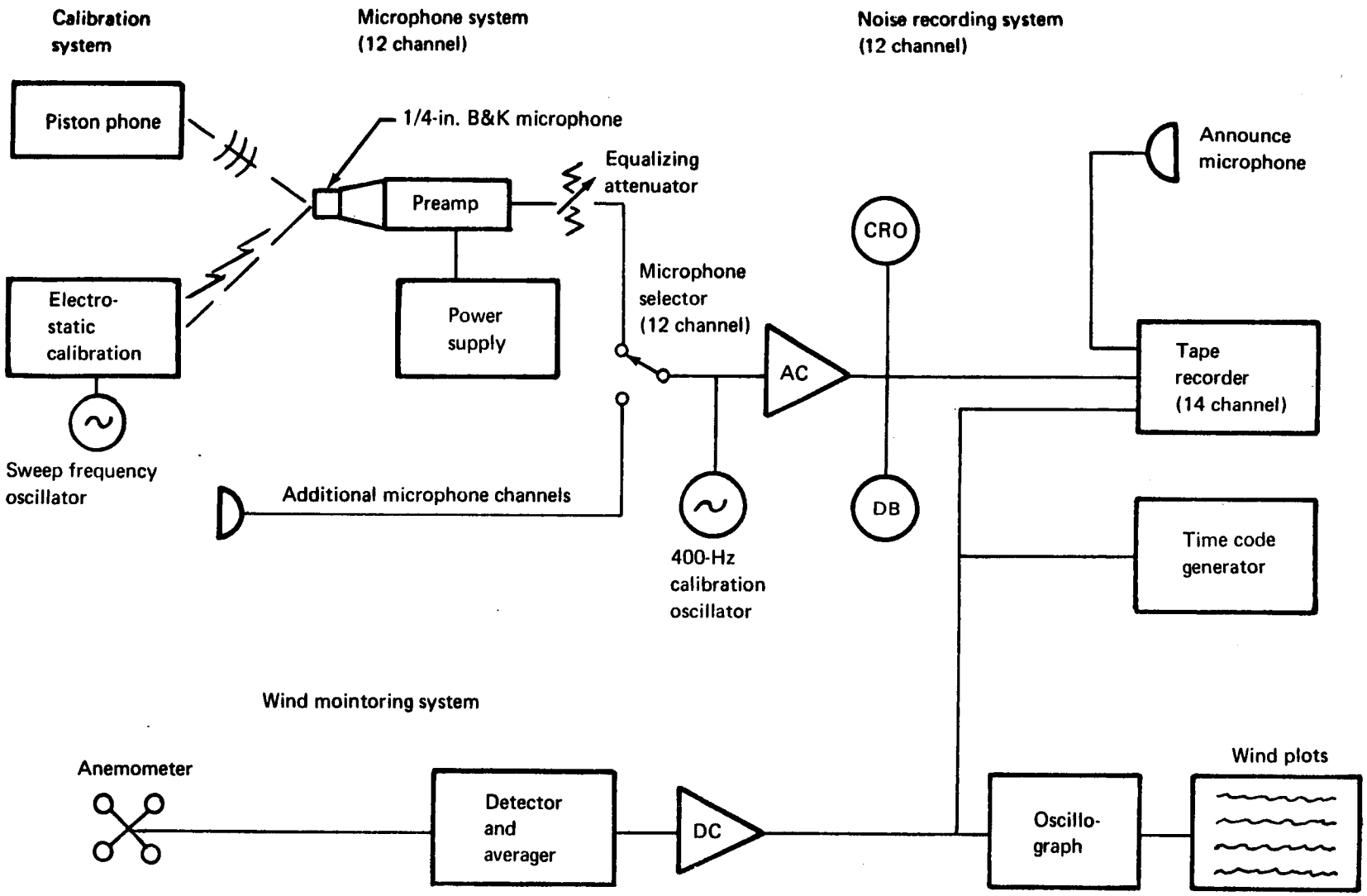

FIGURE 6-16.– ACOUSTIC DATA ACQUISITION SYSTEM

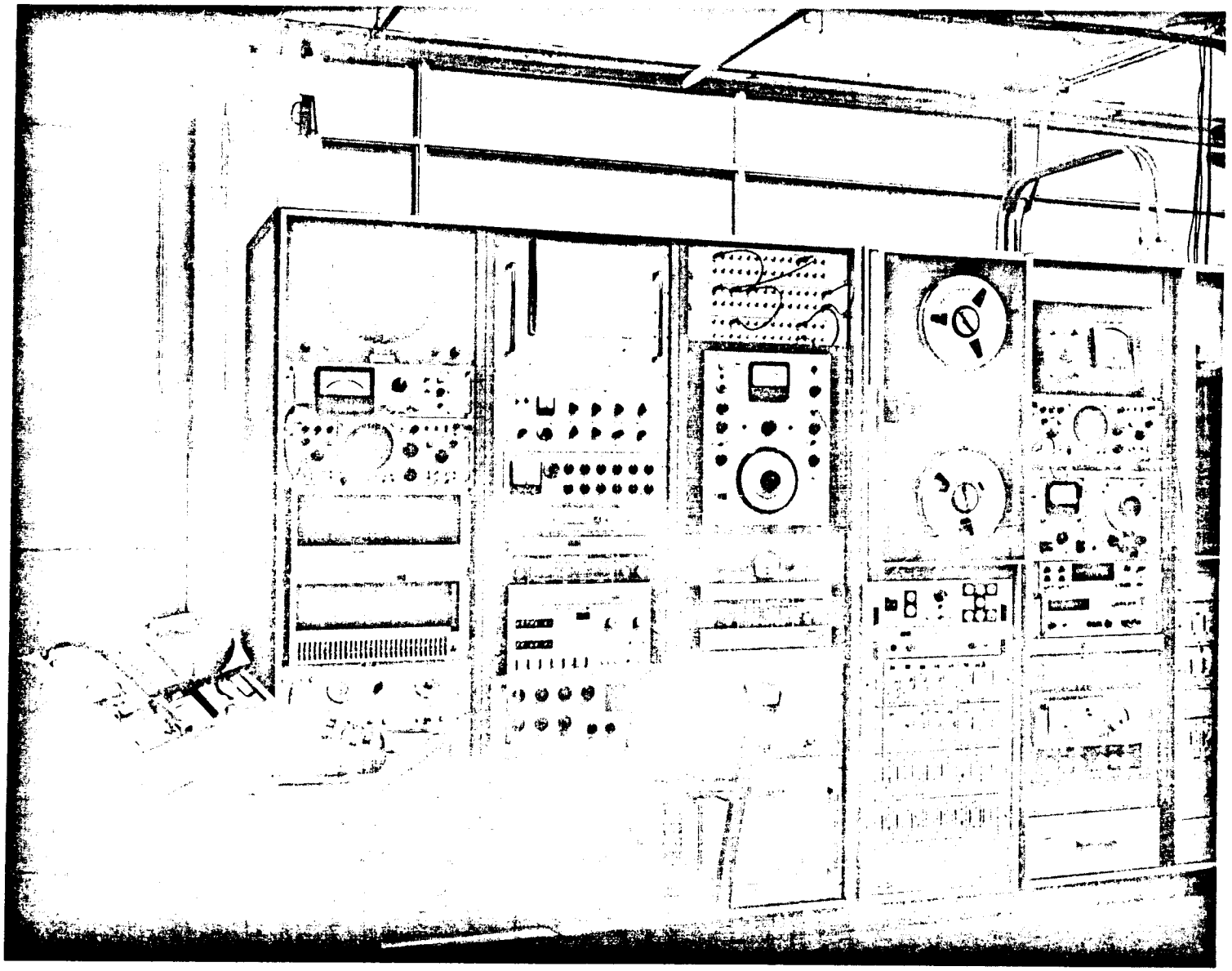

FIGURE 6-17.—THIRD-OCTAVE BAND DATA REDUCTION SYSTEM

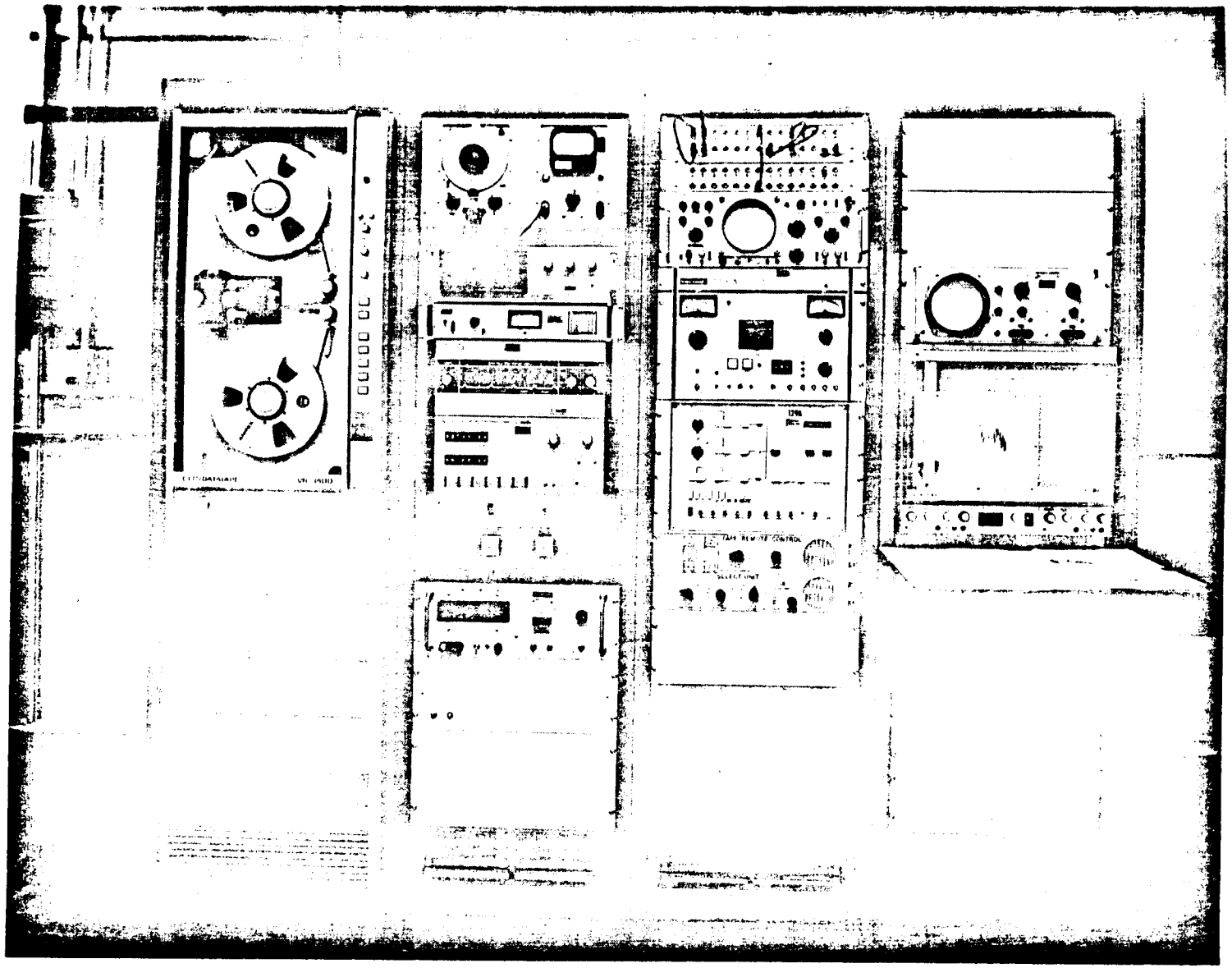

FIGURE 6-18.—NARROW-BAND DATA REDUCTION SYSTEM

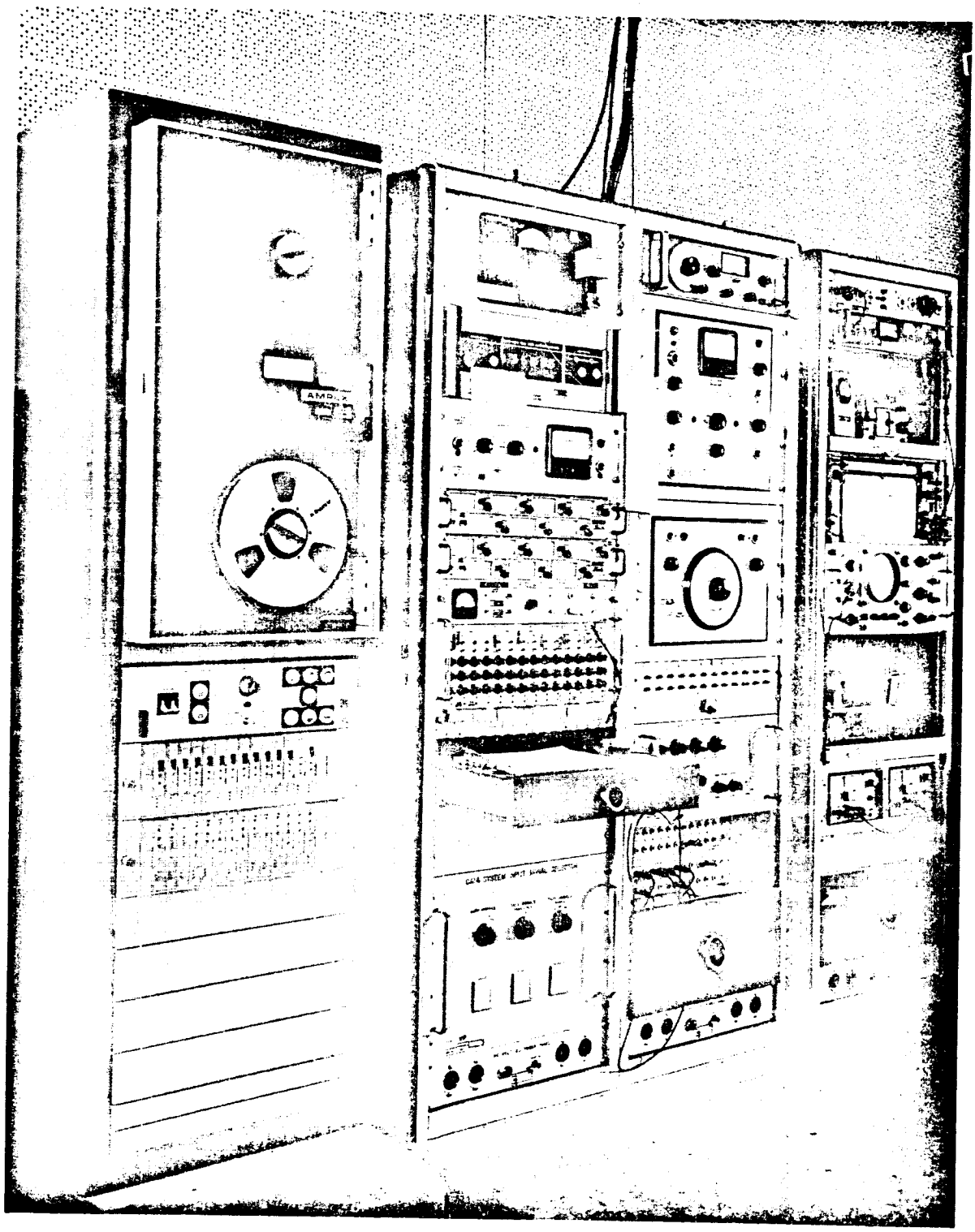

FIGURE 6-19.—ACOUSTIC DATA ACQUISITION SYSTEM

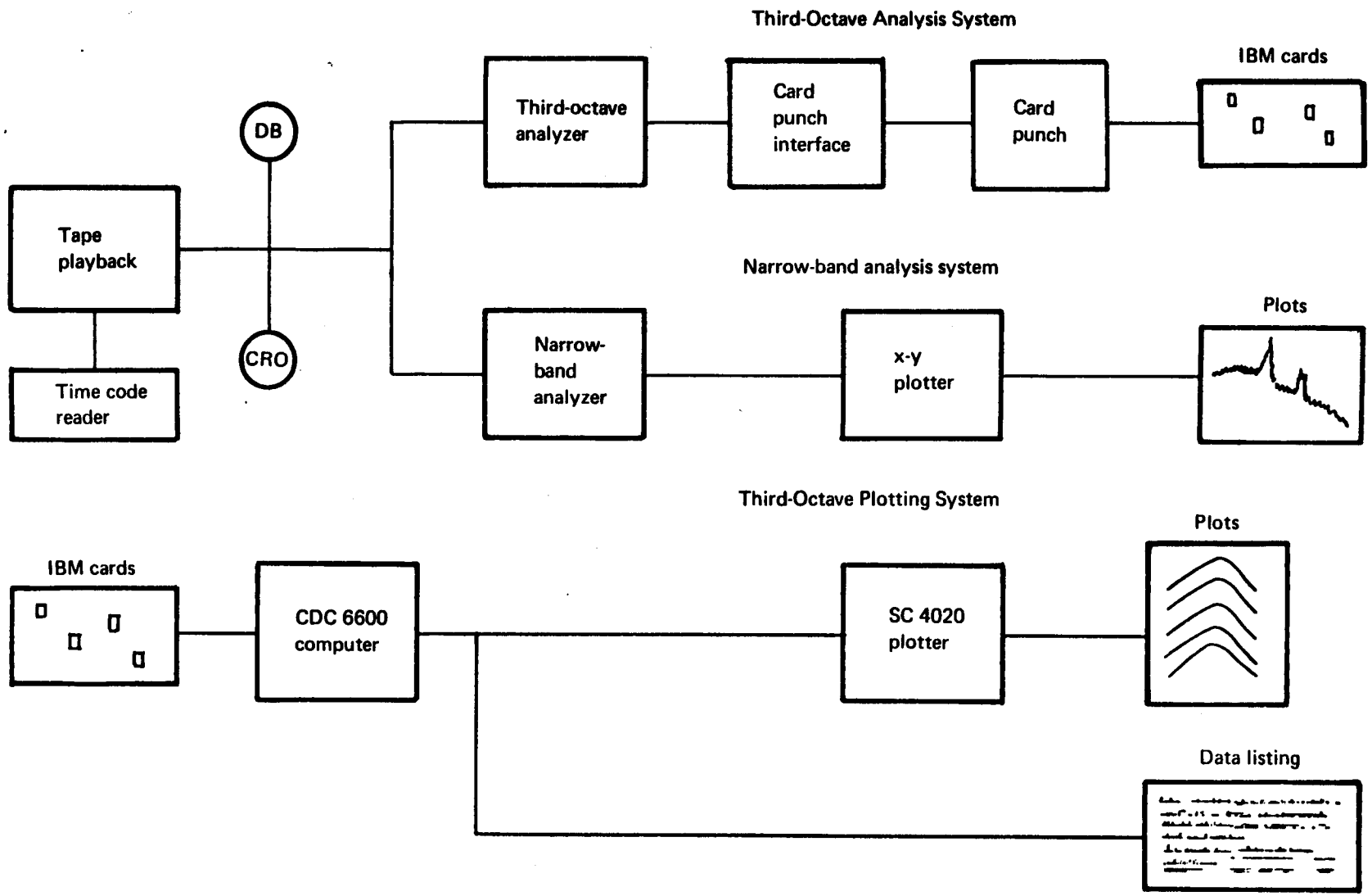

FIGURE 6-20.– ACOUSTIC DATA REDUCTION SYSTEM

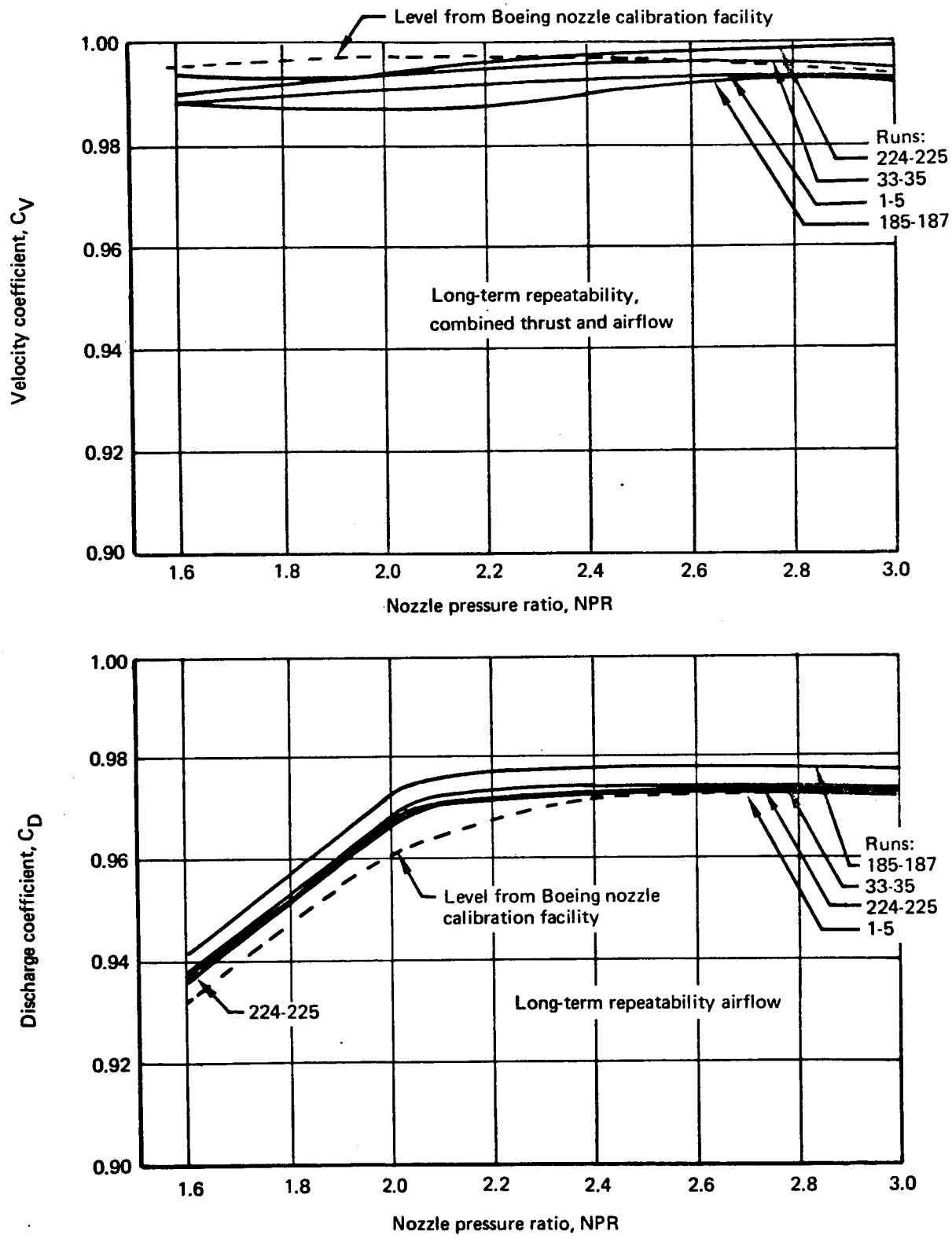

FIGURE 6-21.– REFERENCE NOZZLE PERFORMANCE REPEATABILITY

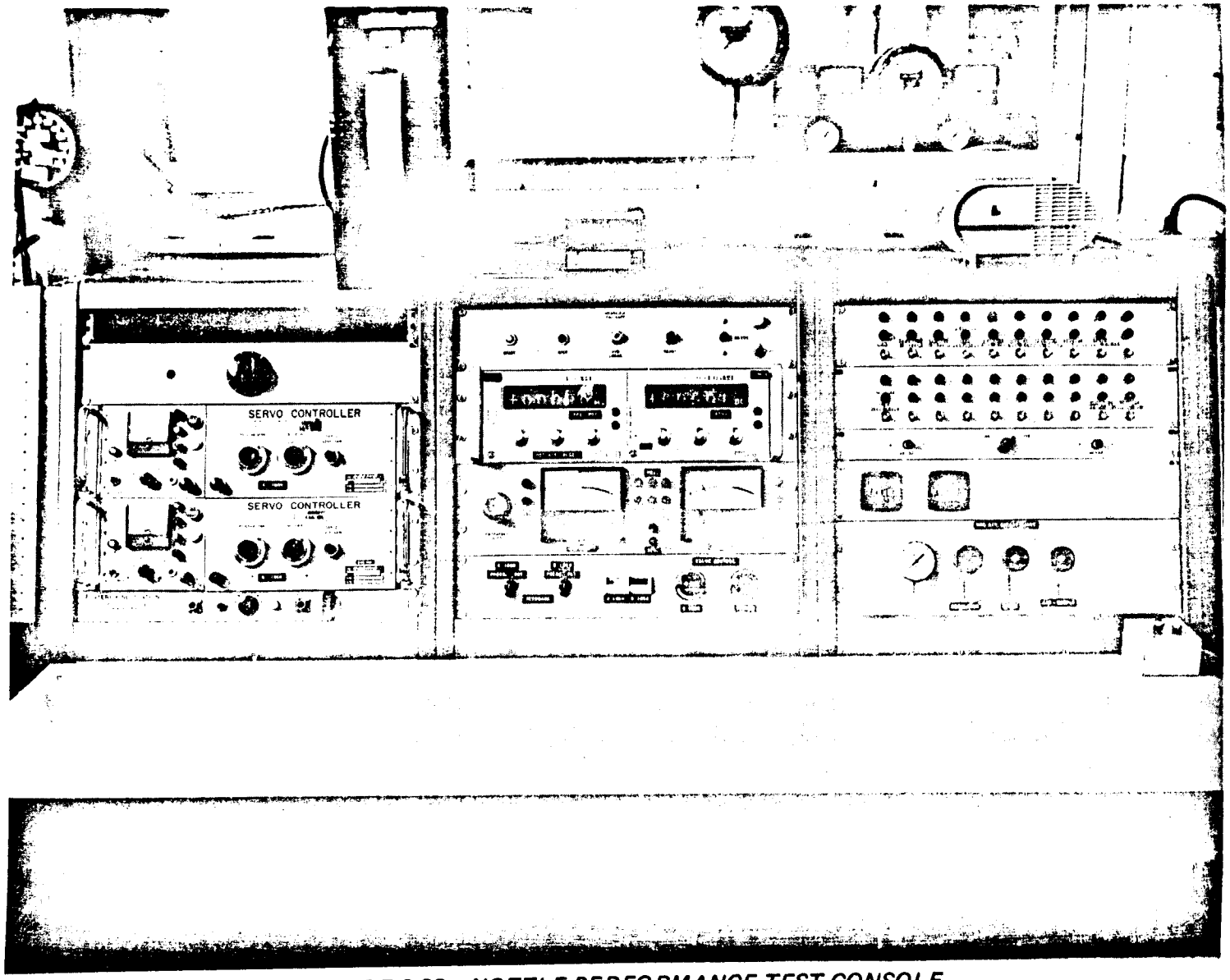

FIGURE 6-22.—NOZZLE PERFORMANCE TEST CONSOLE

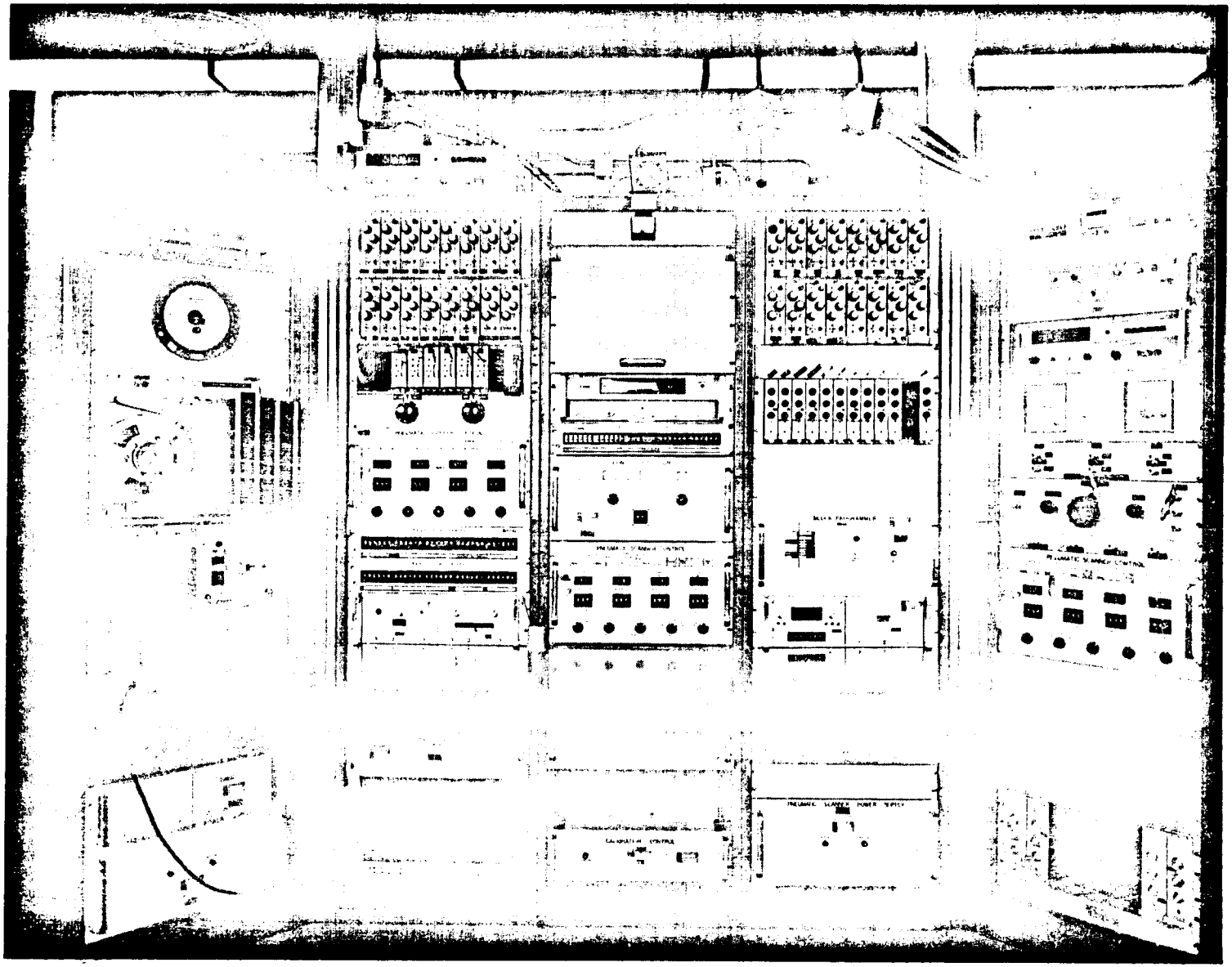

FIGURE 6-23.—NOZZLE PERFORMANCE DATA ACQUISITION SYSTEM

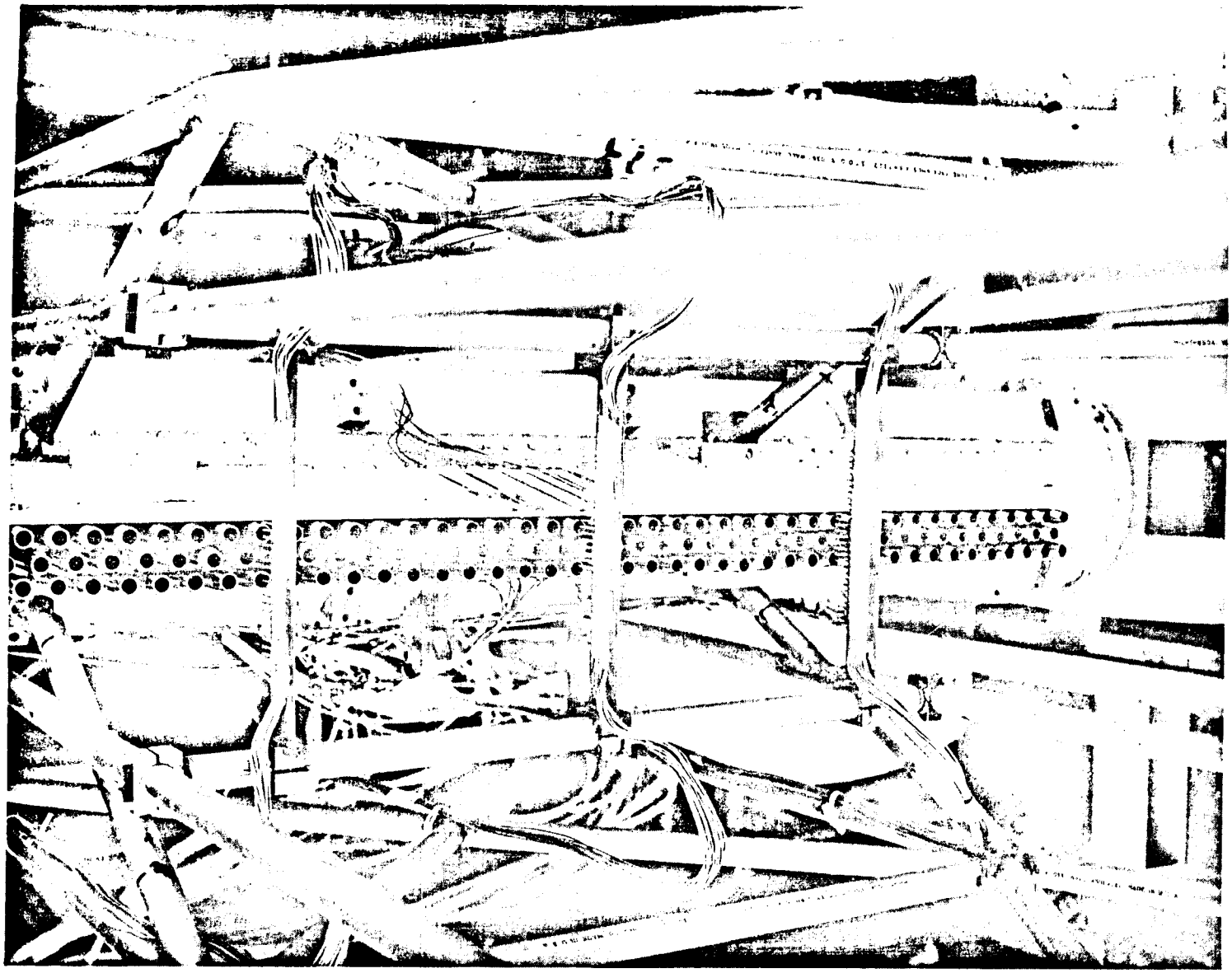

FIGURE 6-24.—JET WAKE TOTAL PRESSURE PROFILE RAKE

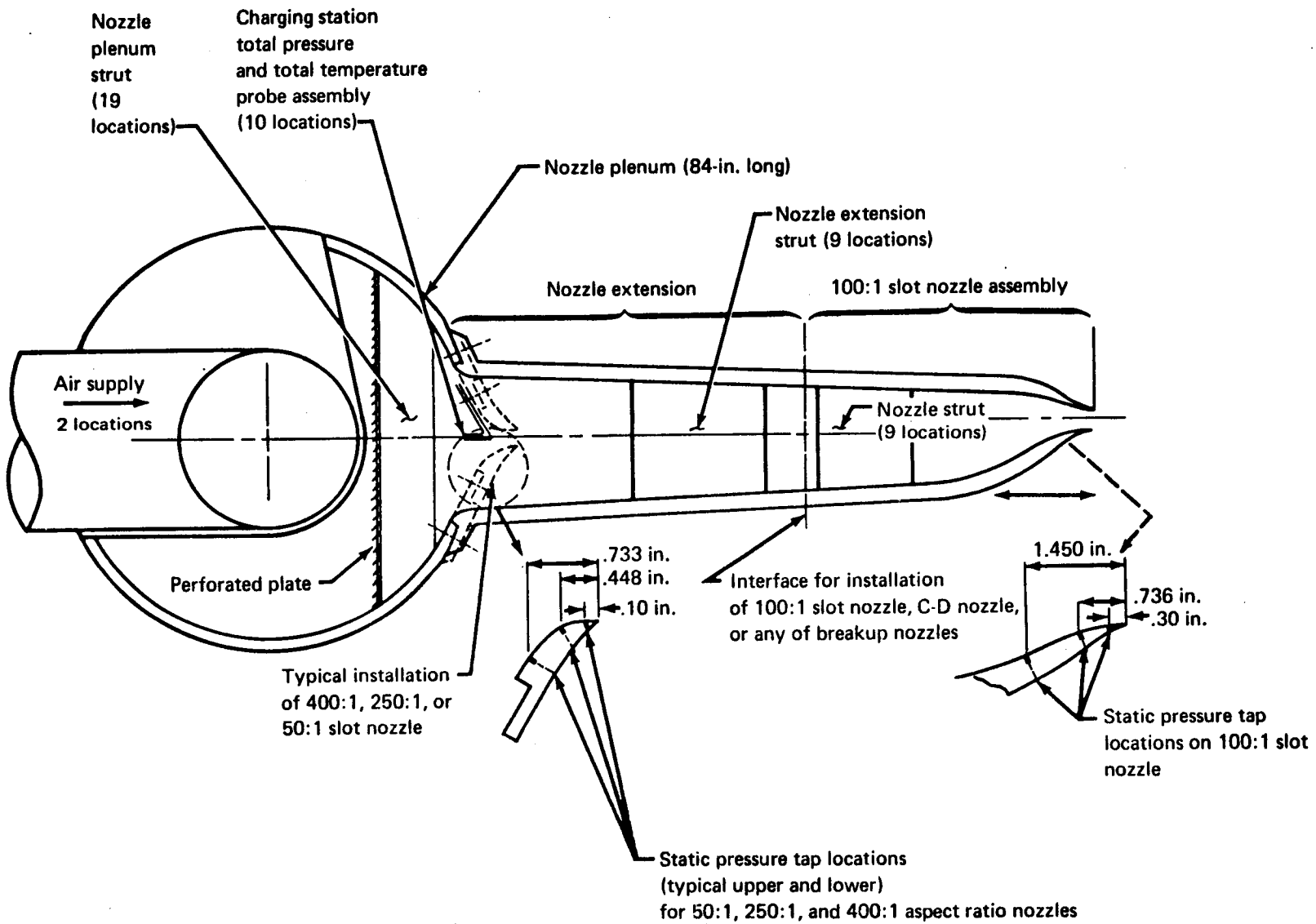

FIGURE 6-25.— TYPICAL SECTION OF NOZZLE PLENUM, EXTENSION, AND 100:1 NOZZLE

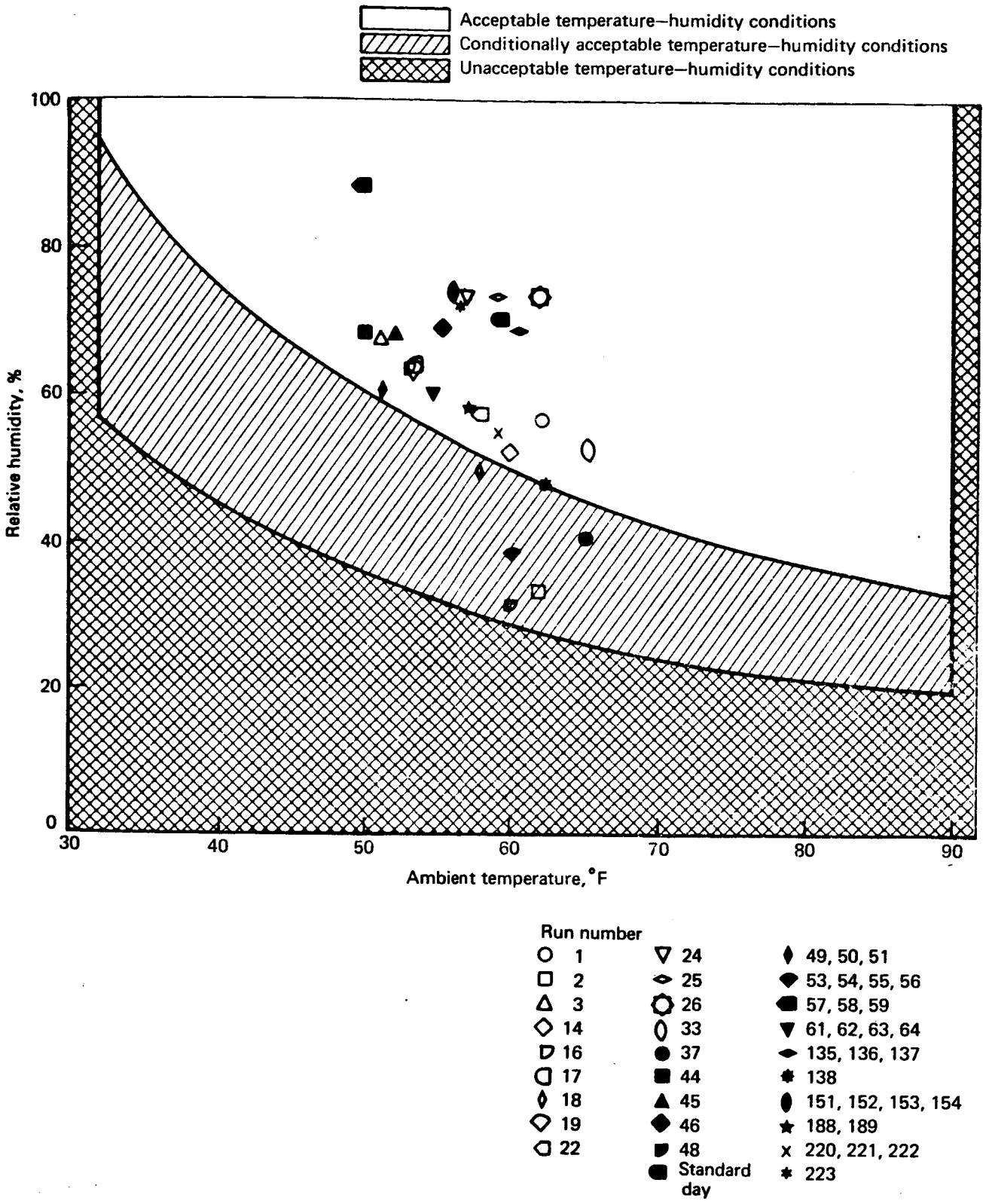

FIGURE 6-26.—RECORD OF AMBIENT CONDITIONS FOR ACOUSTIC RUNS THROUGH RUN 223

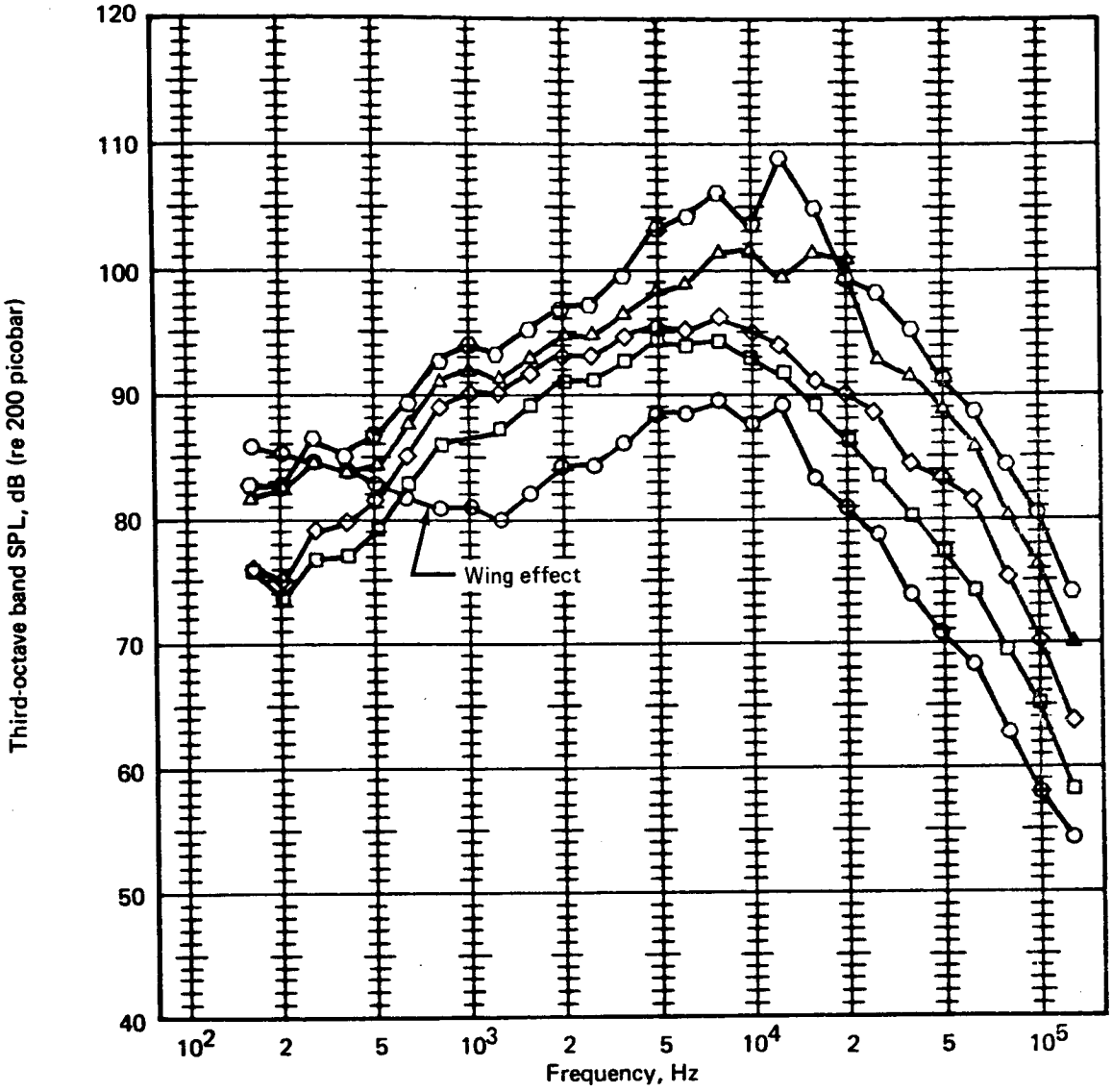

Run number 16
Angle re inlets 150°
Observer at 50 ft
Polar location

	Pressure ratio	Overall SPL, dB
○	1.60	98.5
□	2.00	102.9
◇	2.30	105.1
△	2.60	109.8
○	3.00	114.2

FIGURE 6-27.–EFFECT OF WIND ON MEASUREMENTS

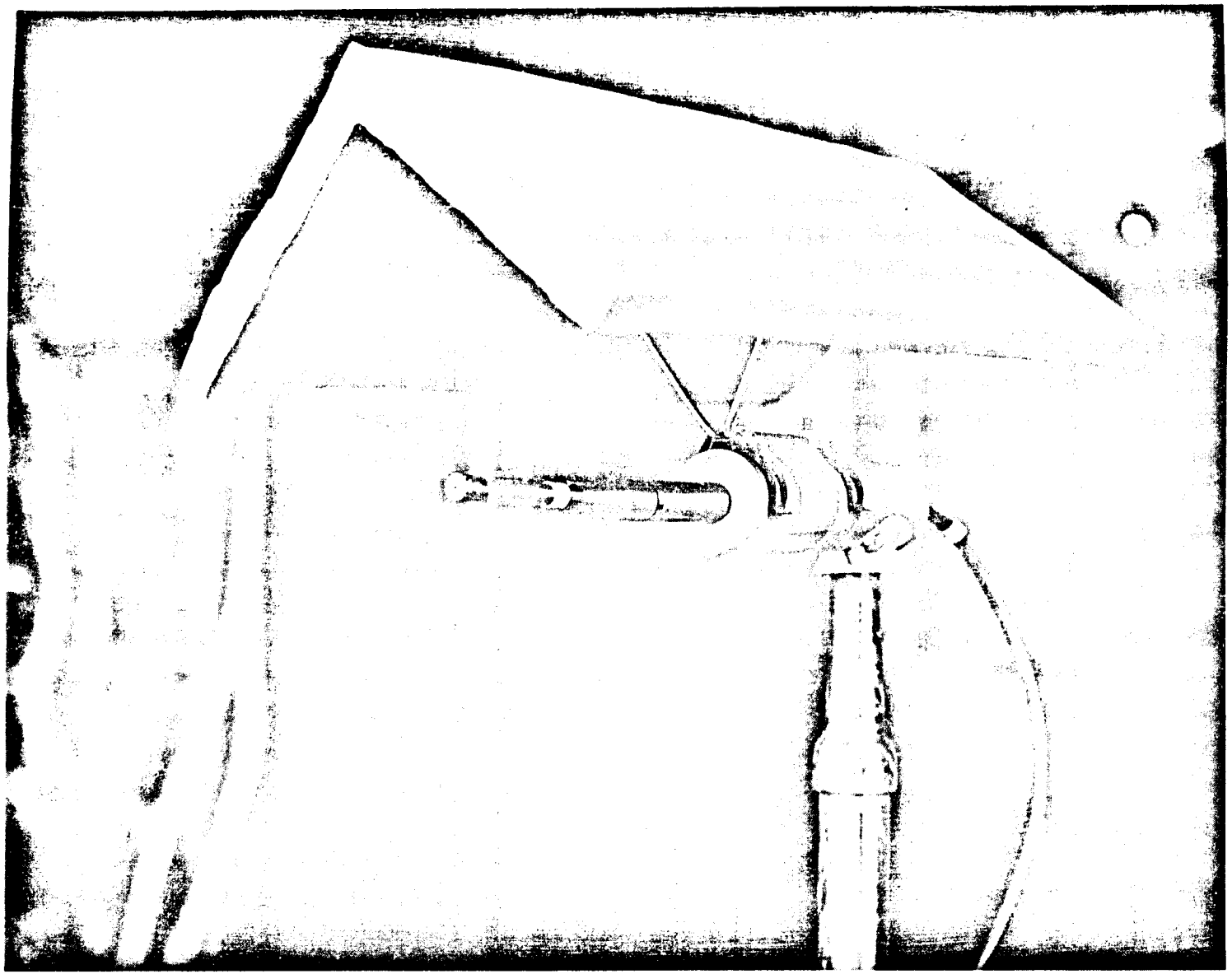

FIGURE 6-28.—MICROPHONE WITH RAIN SHIELD

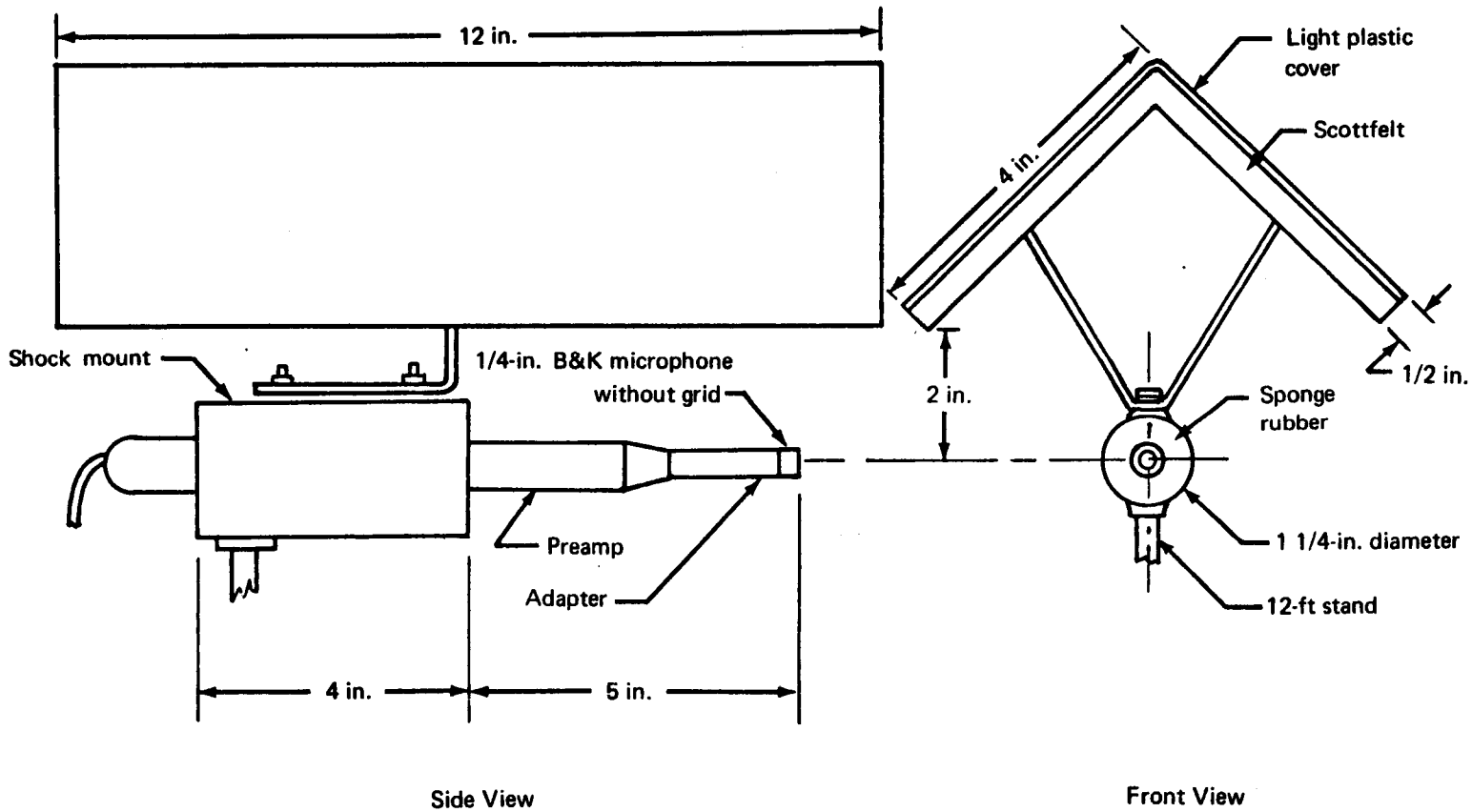

FIGURE 6-29.– MICROPHONE MOUNT AND RAIN SHIELD

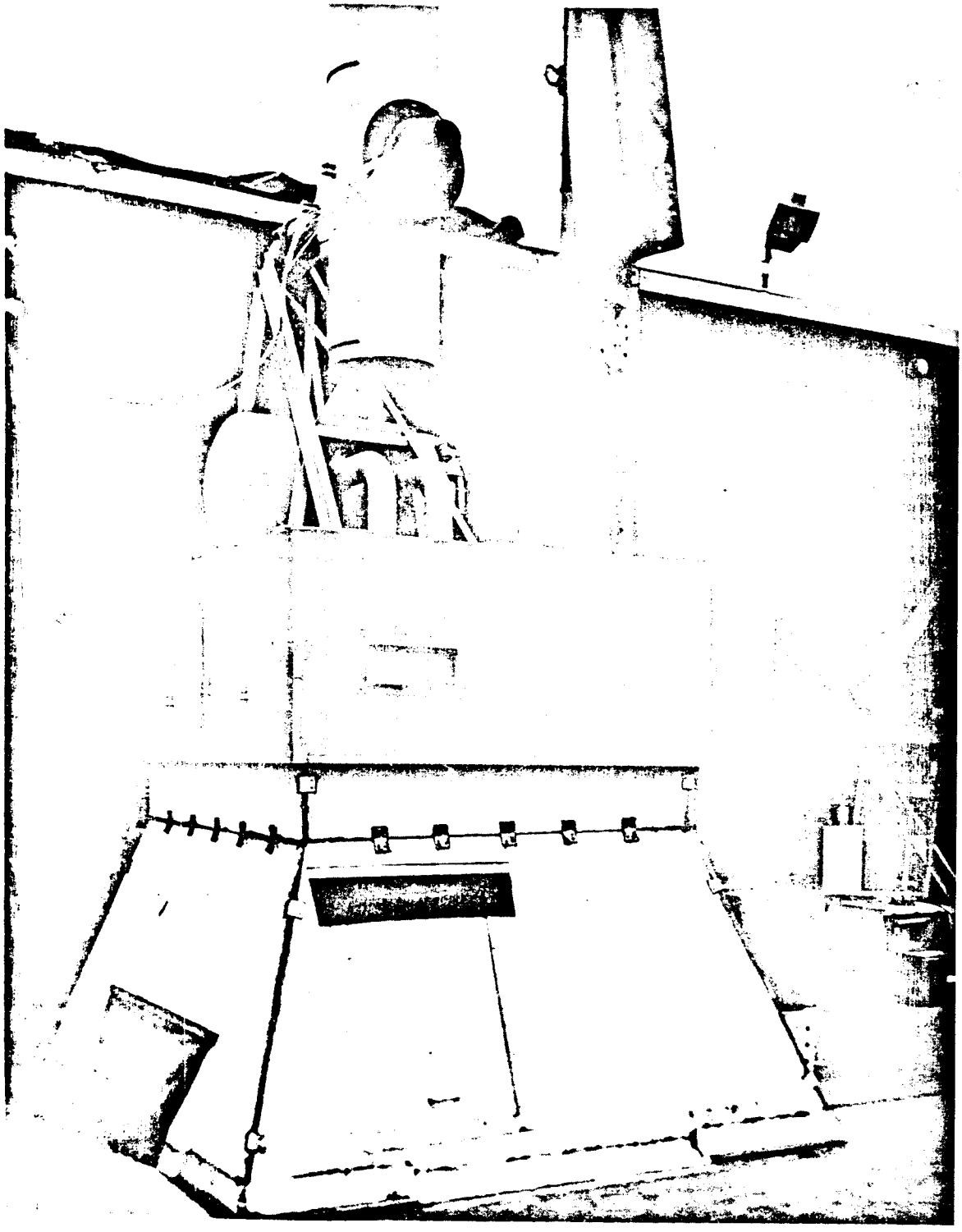

FIGURE 6-30.—BASELINE CONVERGENT NOZZLE MODEL

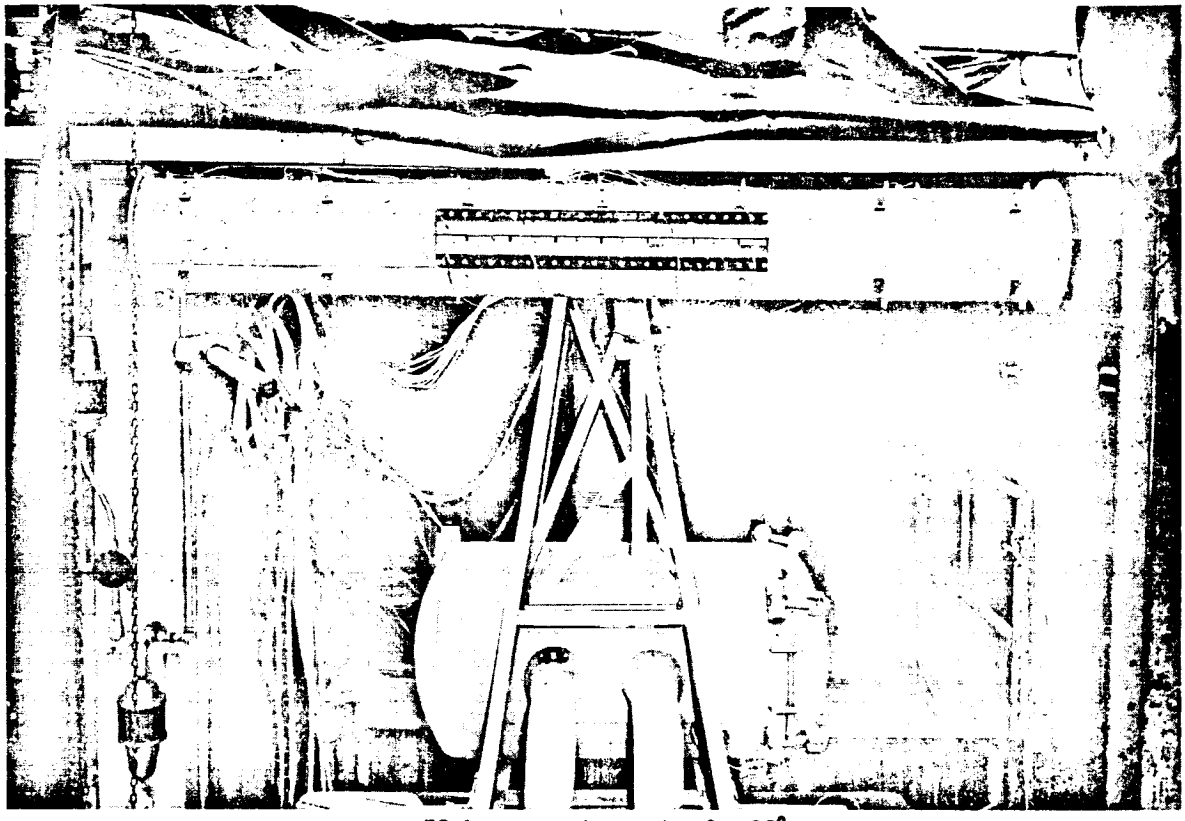

50:1-aspect-ratio nozzle, $\beta = 90°$

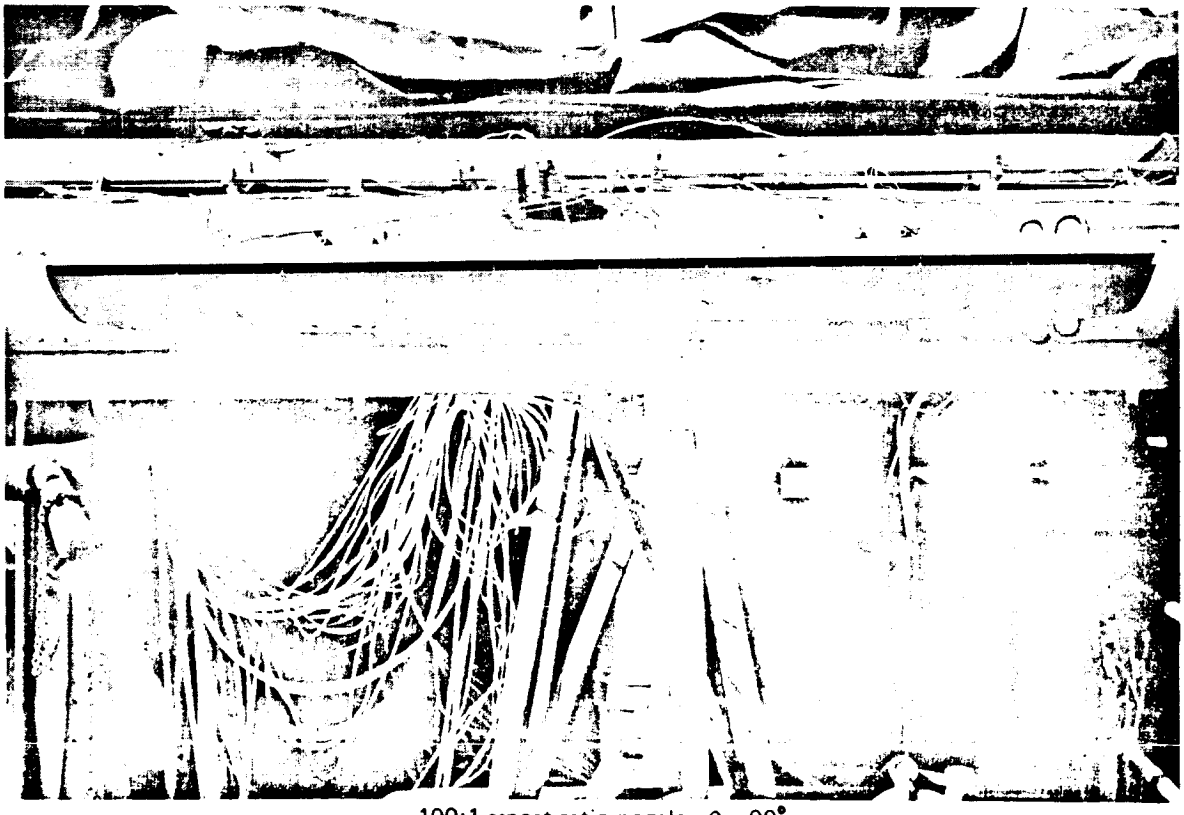

100:1-aspect-ratio nozzle, $\beta = 90°$

FIGURE 6-31.—CONVERGENT SLOT NOZZLES

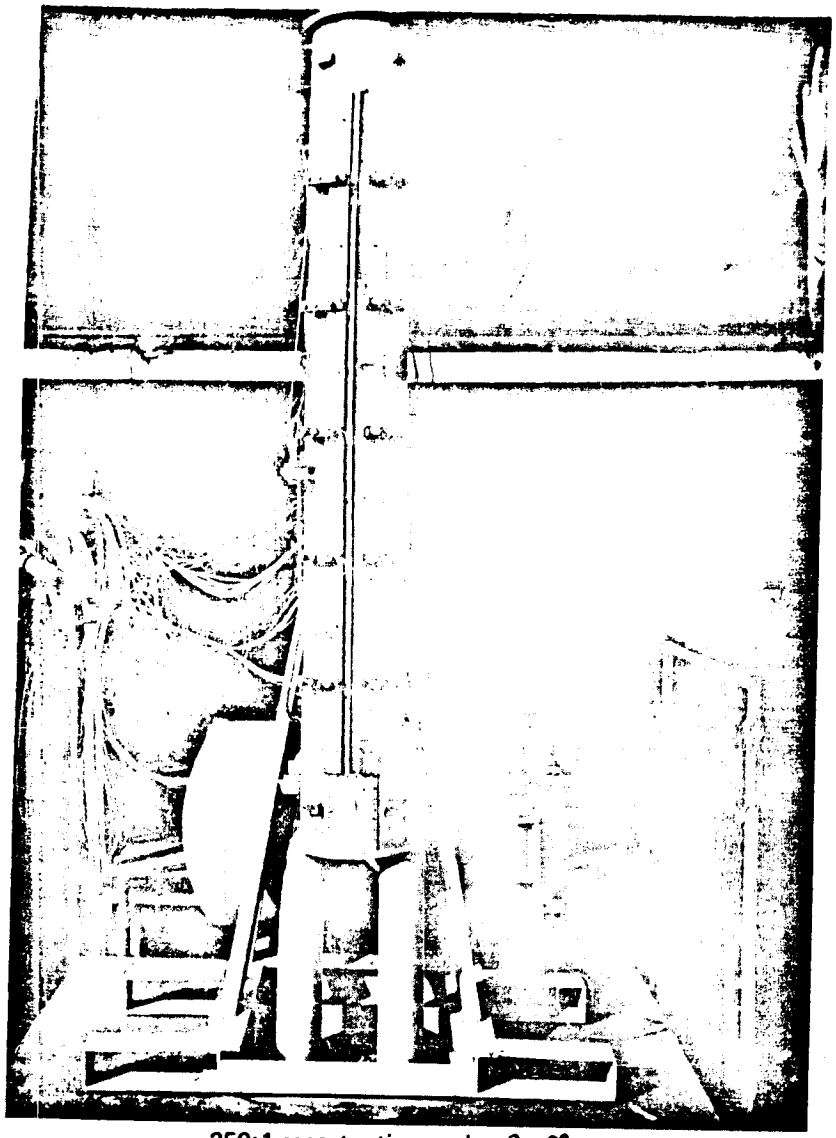

250:1-aspect-ratio nozzle, $\beta = 0°$

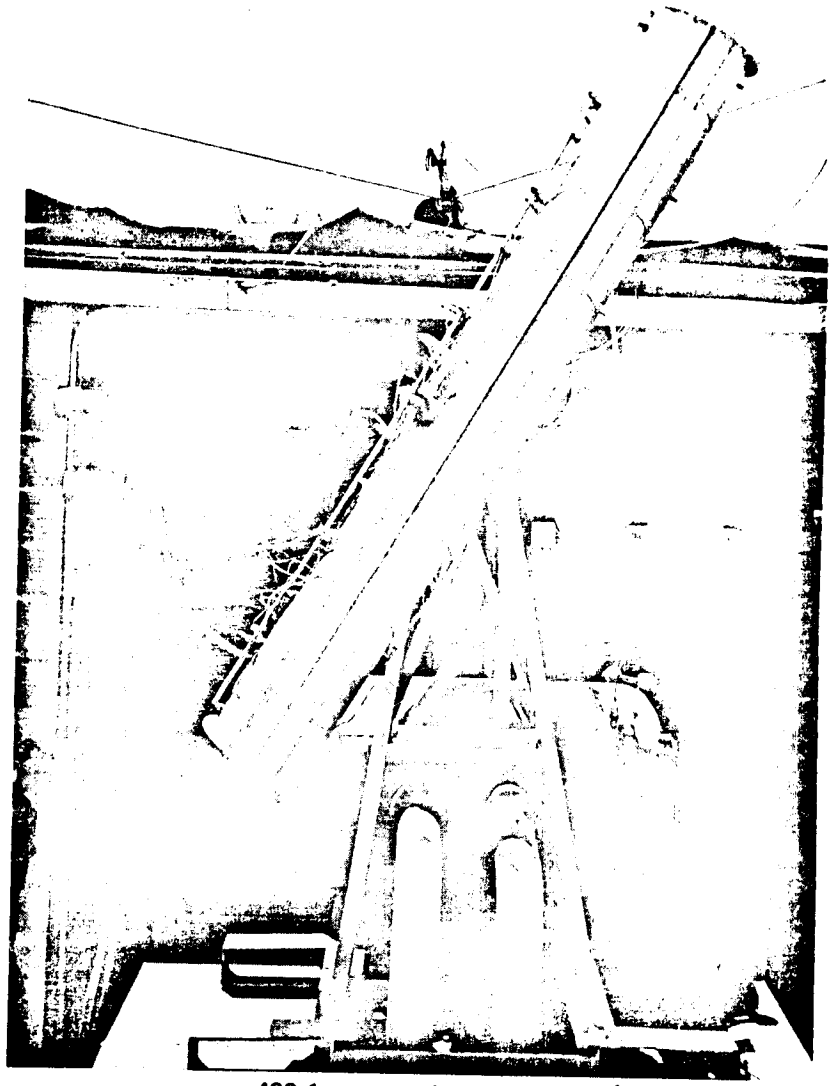

400:1-aspect-ratio nozzle, $\beta = 30°$

FIGURE 6-31.—CONCLUDED

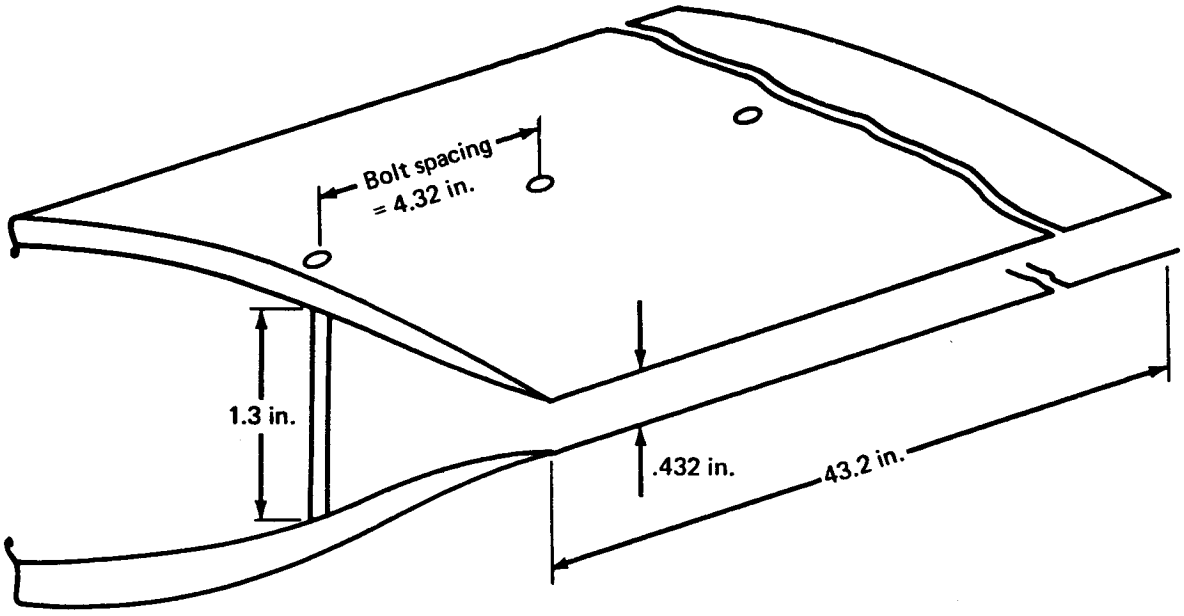

Convergent Nozzle

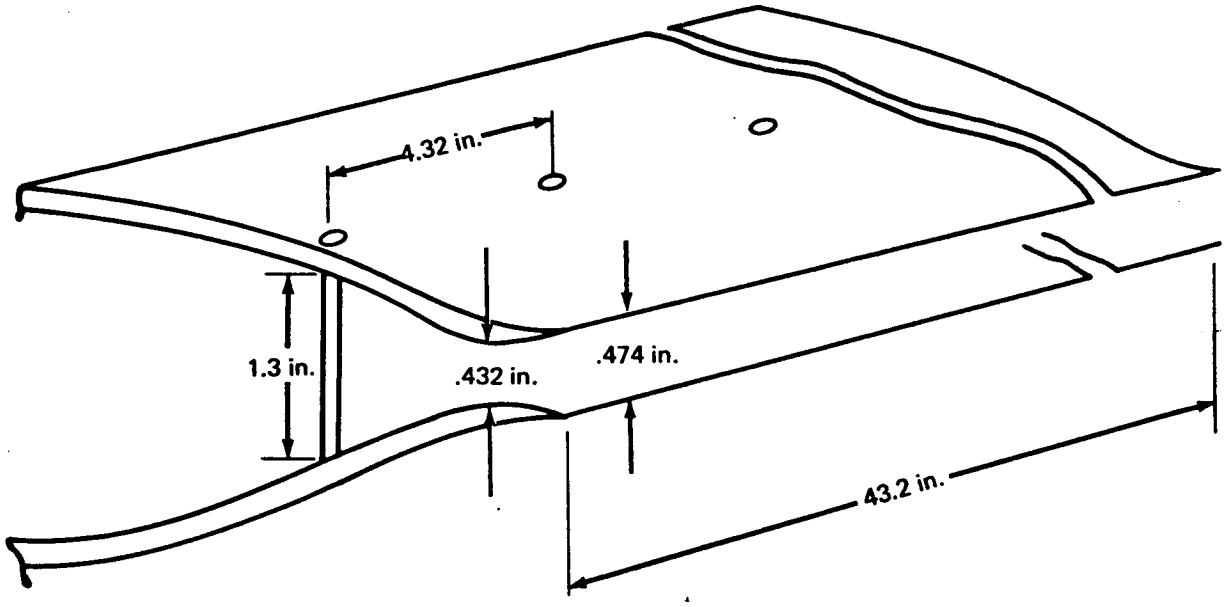

Convergent-Divergent Nozzle

FIGURE 6-32.– TEST CONFIGURATIONS–100:1 SLOT NOZZLES

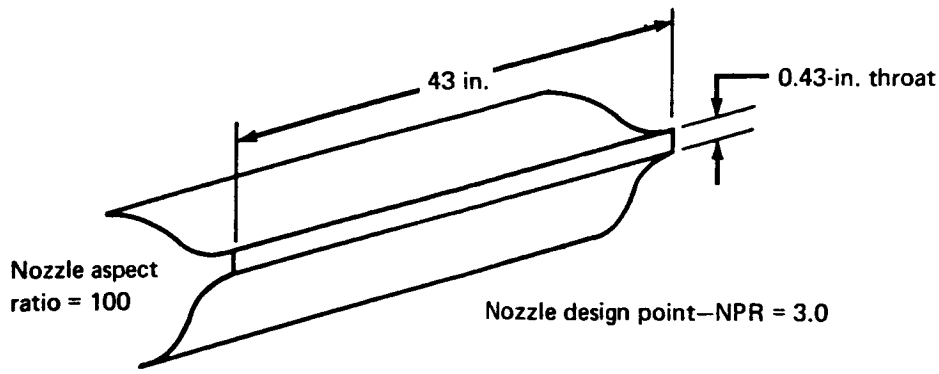

PURPOSE: DETERMINE QUANTITATIVE ACOUSTIC EFFECTS OF CONVERGENT-DIVERGENT NOZZLE GEOMETRY ON THE 3-D AP NOISE PATTERN FOR THE DESIGN AND OFF-DESIGN NPR i.e.,

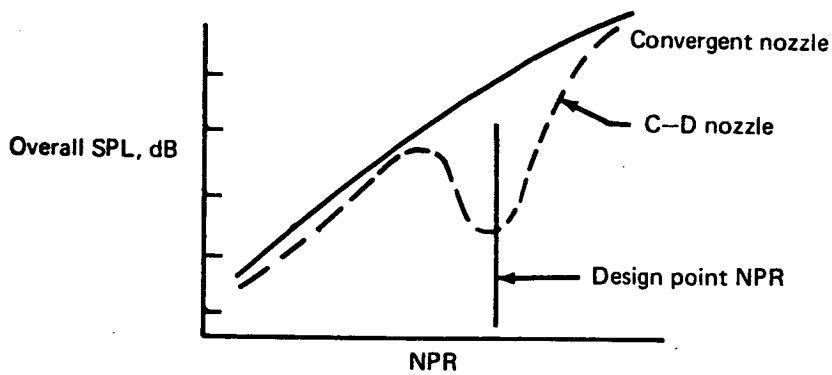

Test conditions: NPR = 2.0, 2.6, 2.8, 3.0, 3.2
T_T = ambient, 350° F

Data output: Noise levels (OASPL, PNL)
Spectra (third-octave band SPL)
Directivity (θ)
Thrust performance

FIGURE 6-33.—TEST CONFIGURATIONS—C-D SLOT NOZZLE

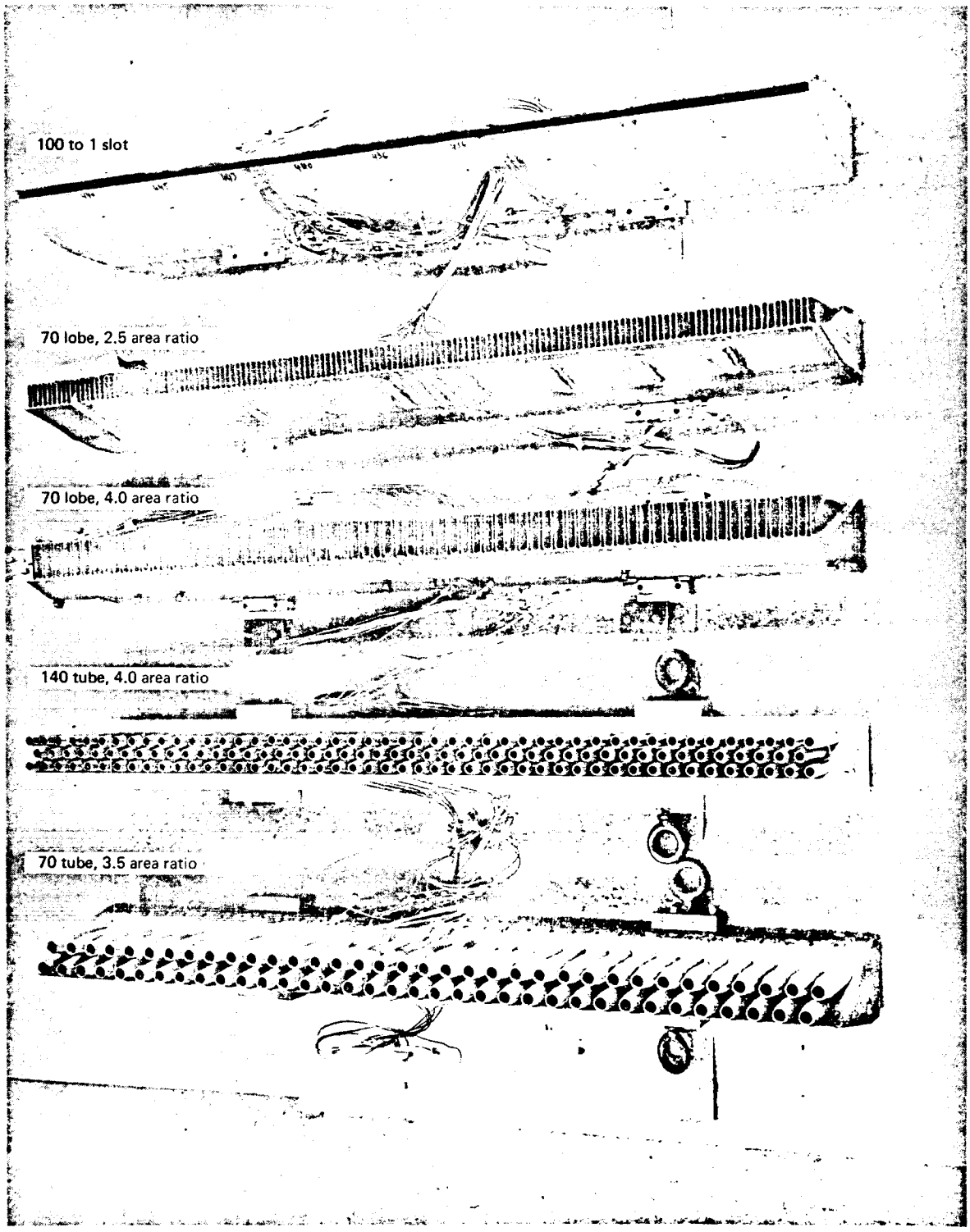

FIGURE 6-34.—SLOT AND MULTI-ELEMENT NOZZLES

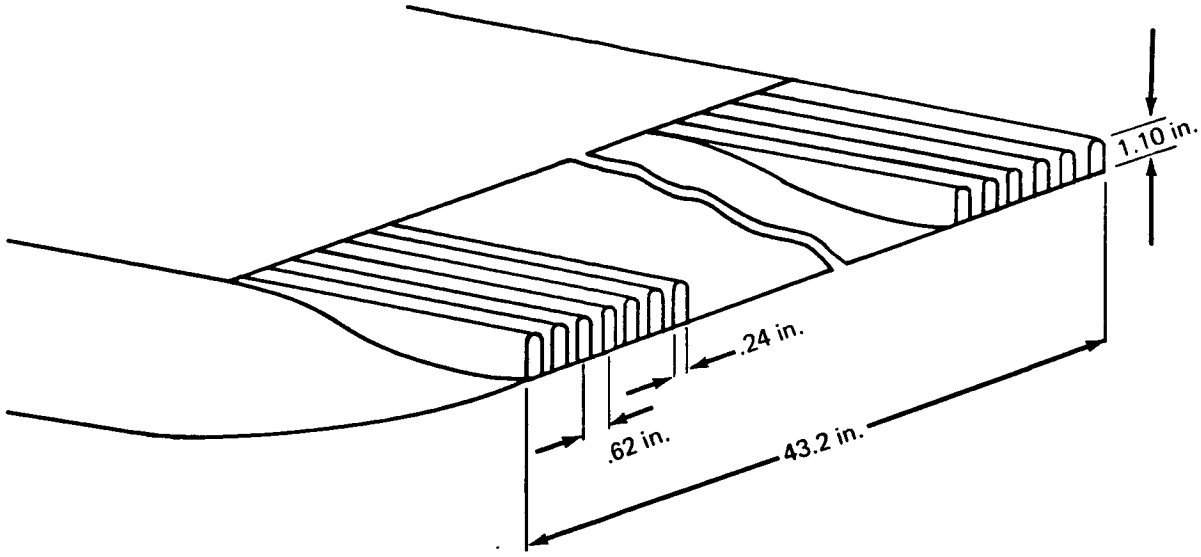

70-lobe nozzle
Spacing ratio = 2.5
Nozzle area = 18.7 sq in.

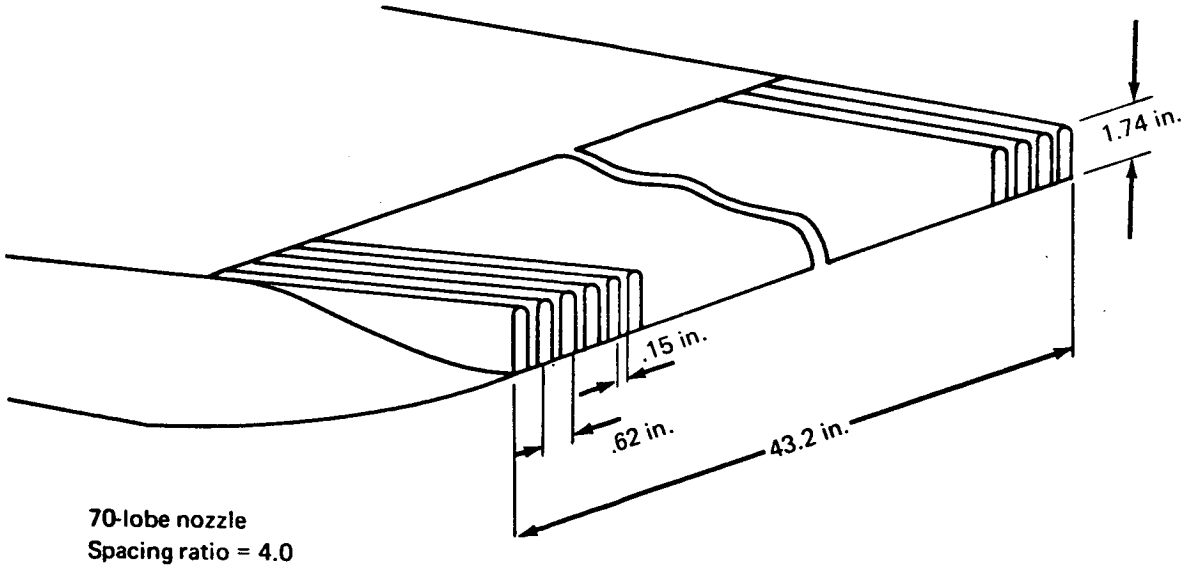

70-lobe nozzle
Spacing ratio = 4.0
Nozzle area = 18.7 sq in.

FIGURE 6-35.— TEST CONFIGURATIONS—LOBE NOZZLES

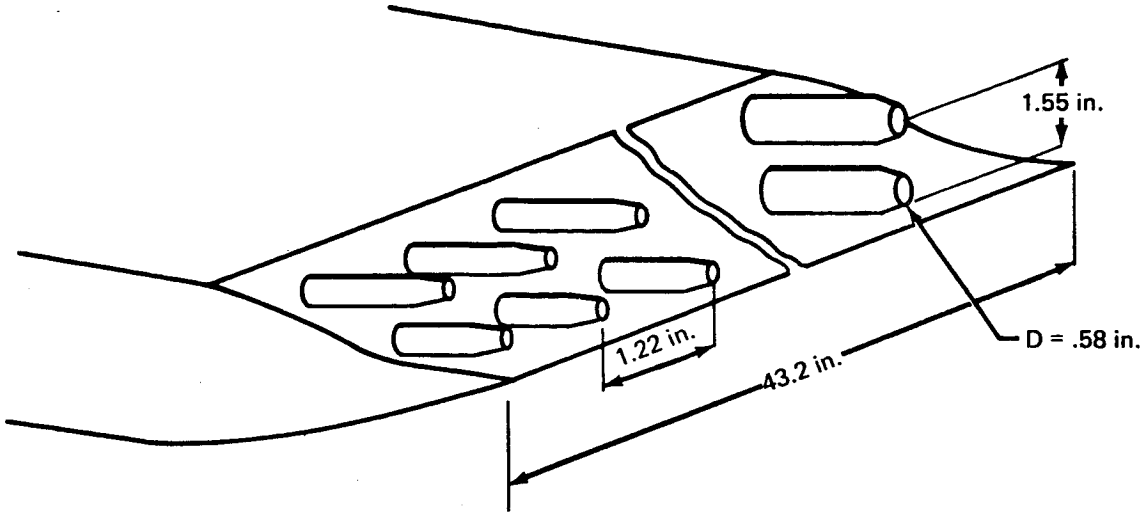

70-tube nozzle
Area ratio = 2.5
2 rows
Nozzle area = 18.7 sq in.

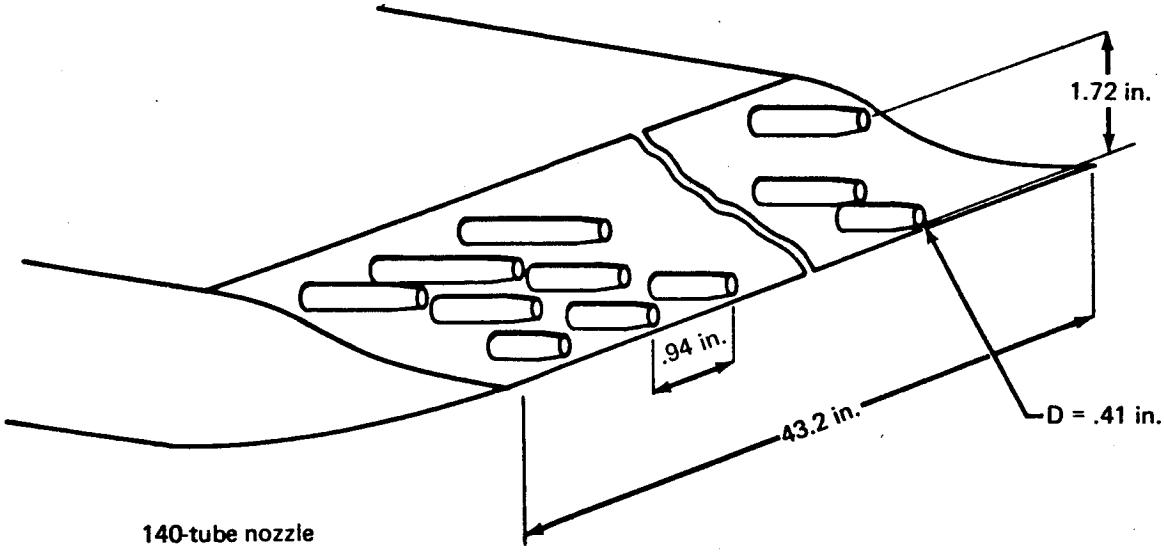

140-tube nozzle
Area ratio = 4.0
3 rows
Nozzle area = 18.7 sq in.

FIGURE 6-36.—TEST CONFIGURATIONS—TUBE NOZZLES

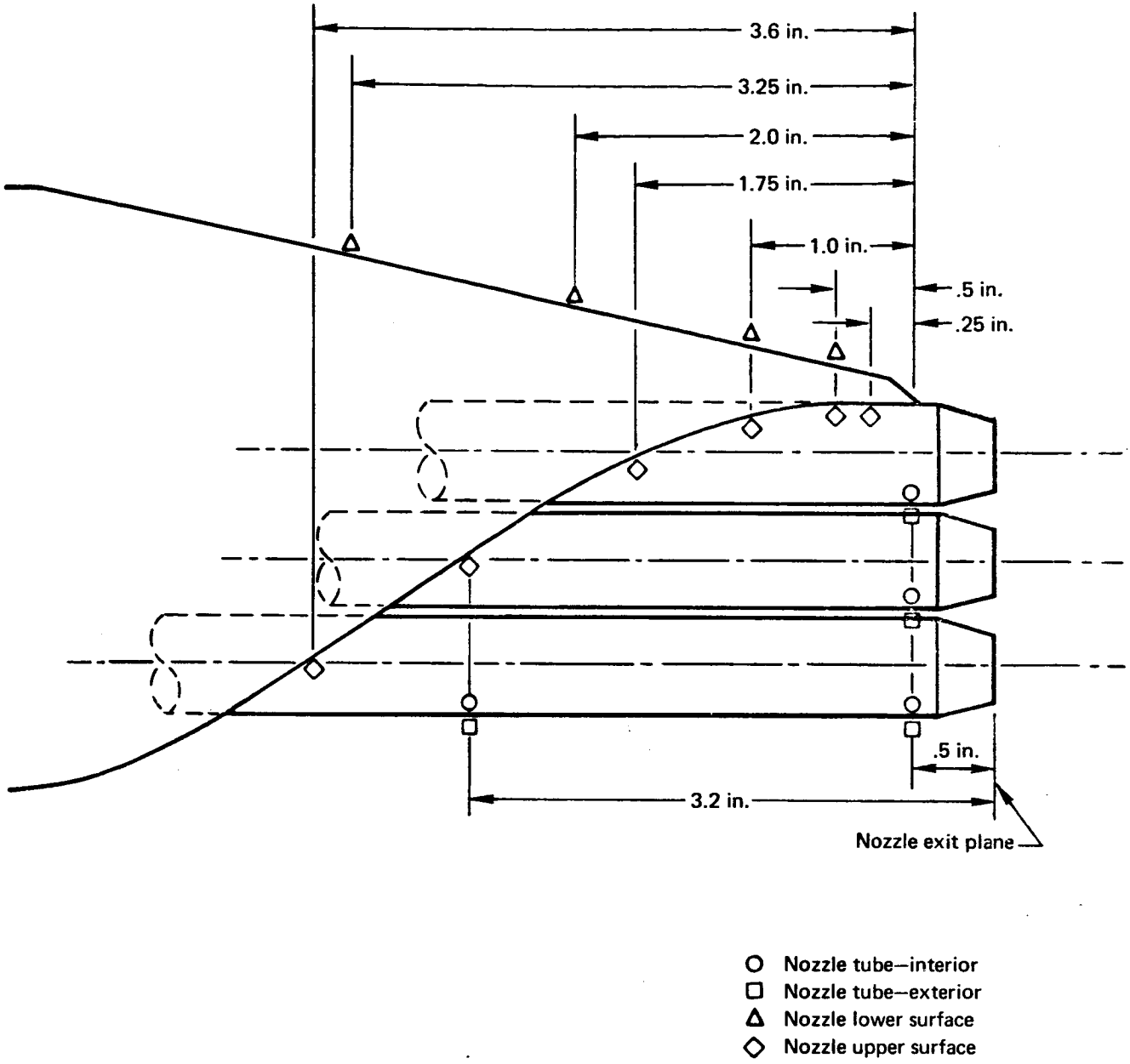

FIGURE 6-37.—STATIC PRESSURE TAP LOCATIONS 140-TUBE, 4.0 AREA RATIO NOZZLE

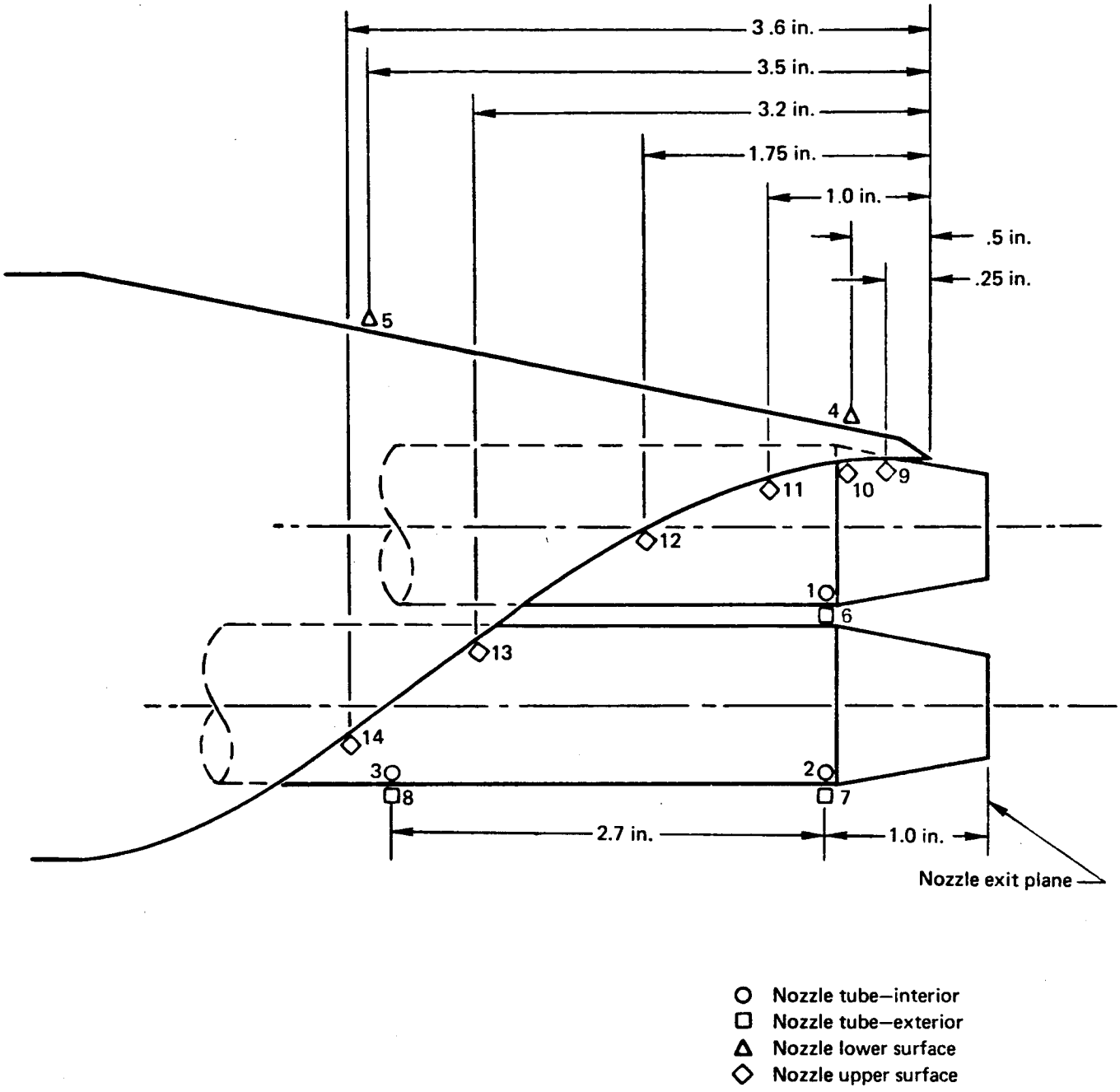

FIGURE 6-38.—STATIC PRESSURE TAP LOCATIONS—70-TUBE, 3.5 AREA RATIO NOZZLE

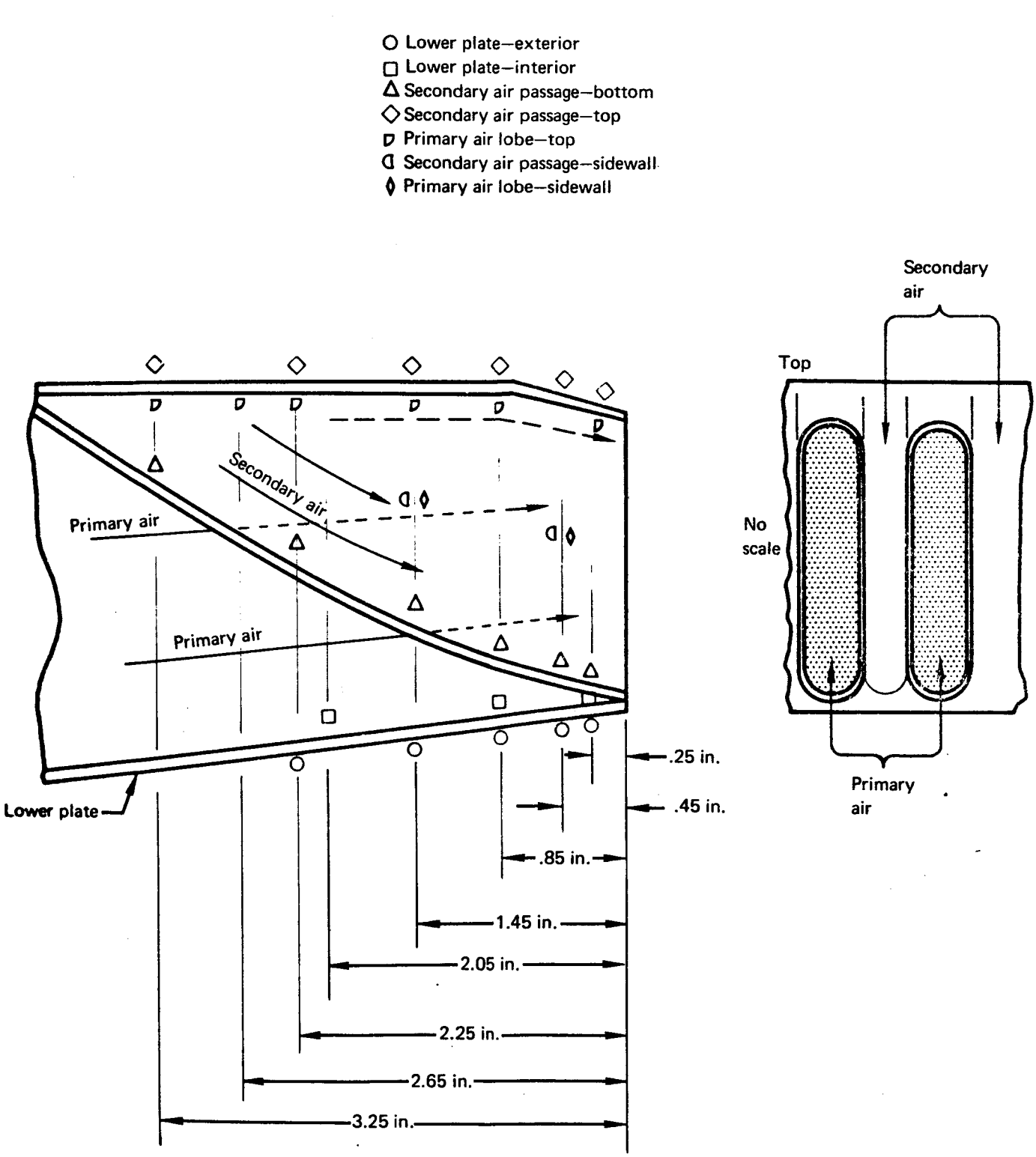

FIGURE 6-39.—STATIC PRESSURE TAP LOCATIONS—70-LOBE, 2.5 AREA RATIO NOZZLE

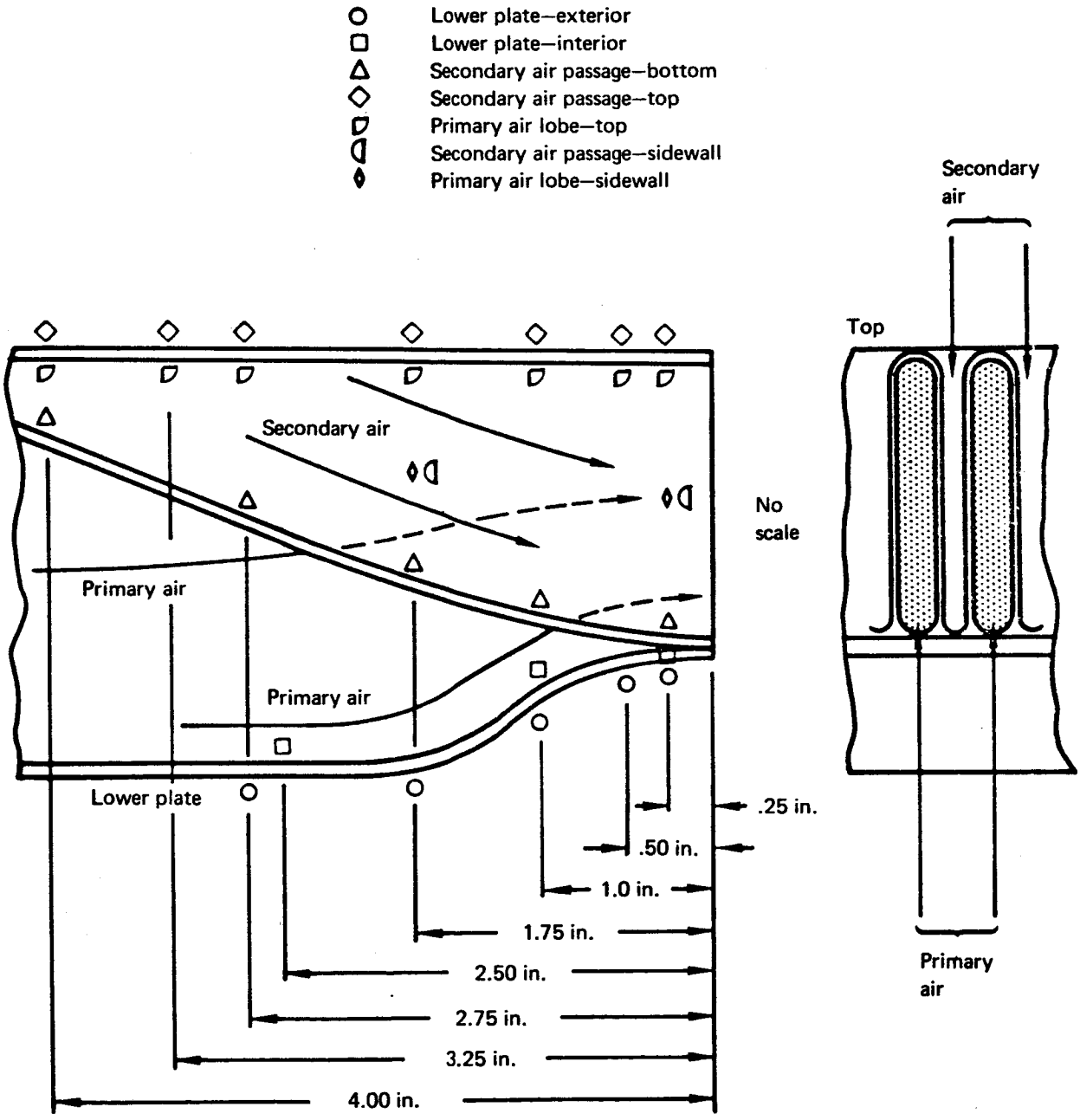

FIGURE 6-40.—STATIC PRESSURE TAP LOCATIONS—70-LOBE, 4.0 AREA RATIO NOZZLE

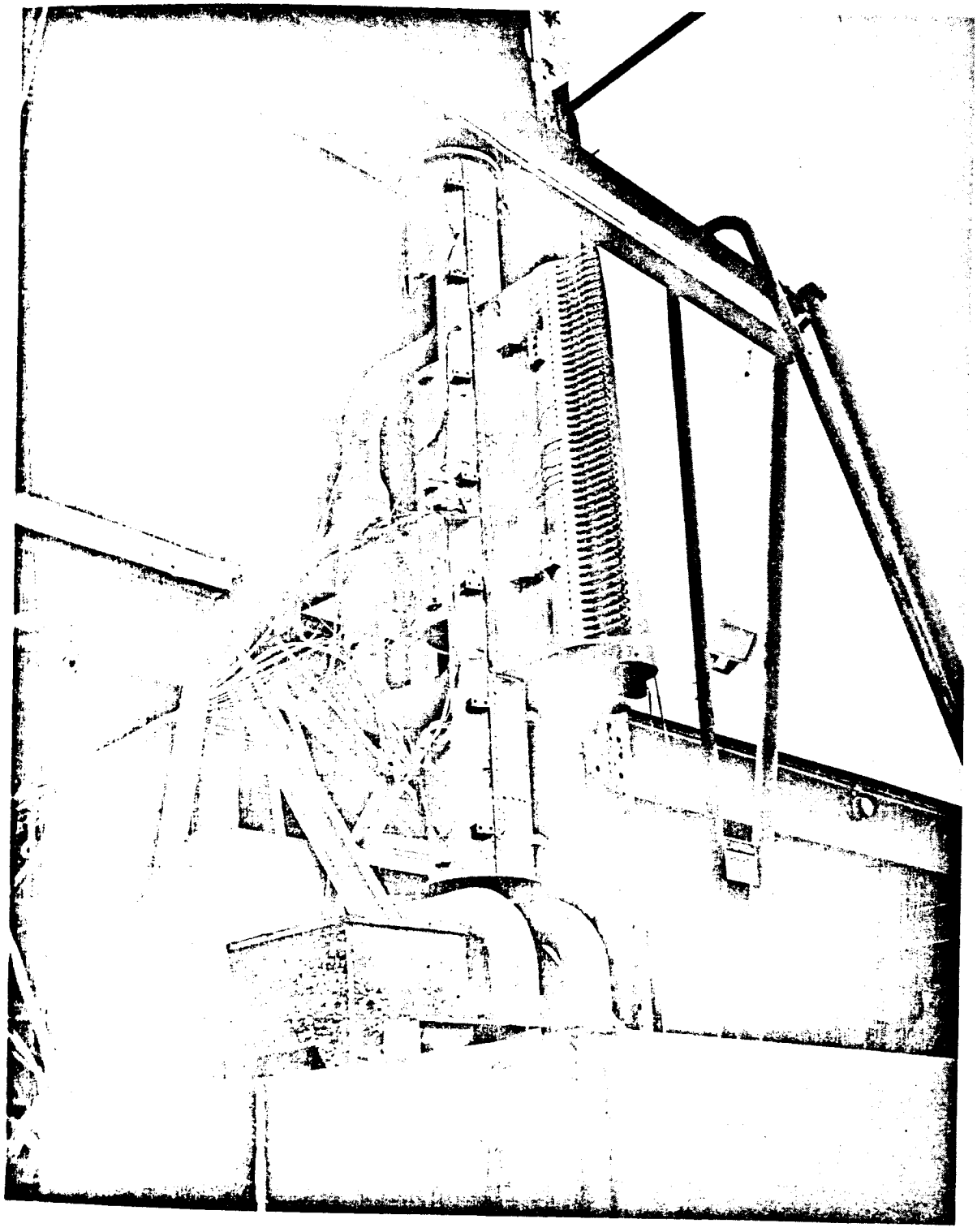

FIGURE 6-41.—140-TUBE BREAKUP NOZZLE

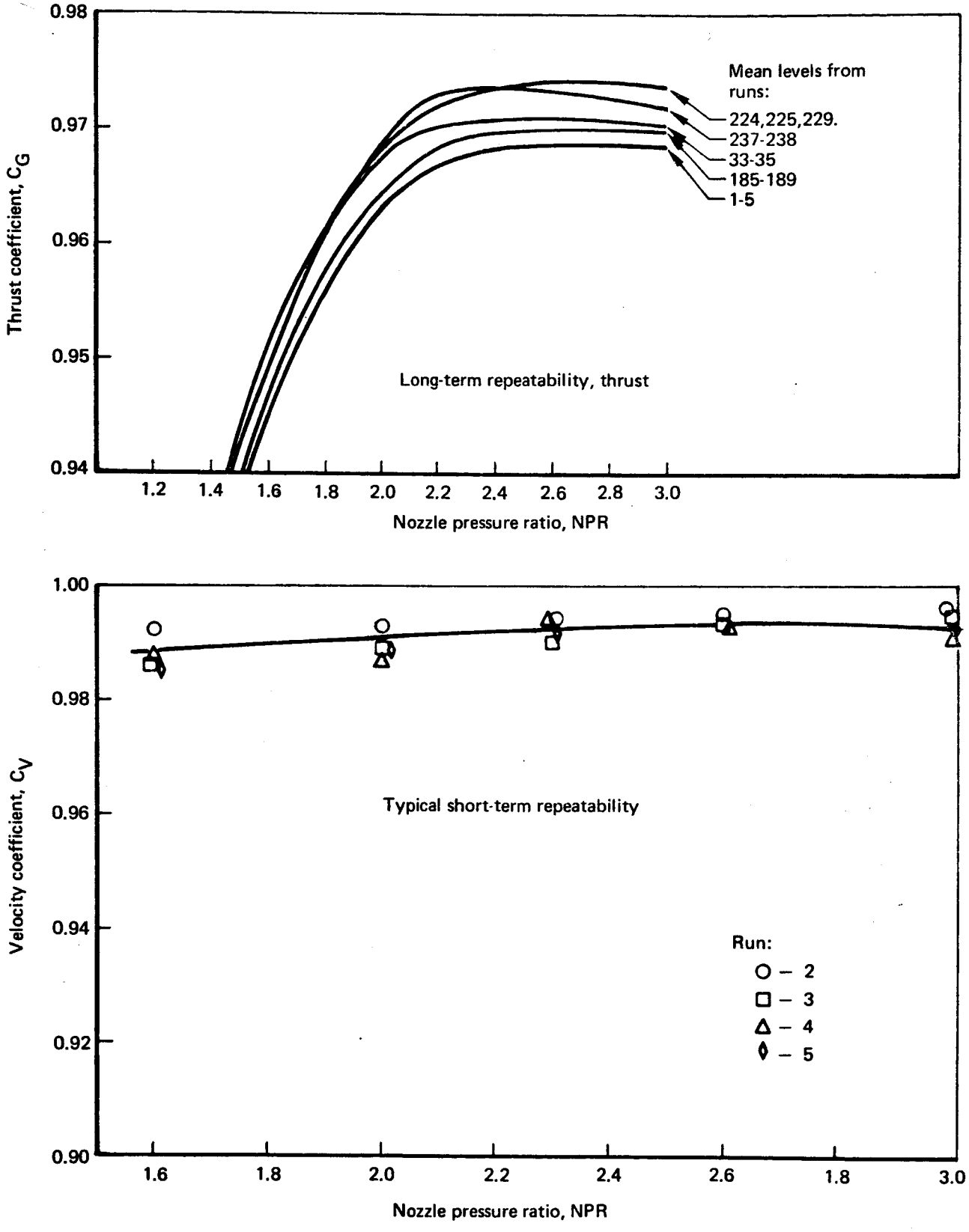

FIGURE 6-42.– REFERENCE NOZZLE PERFORMANCE REPEATABILITY

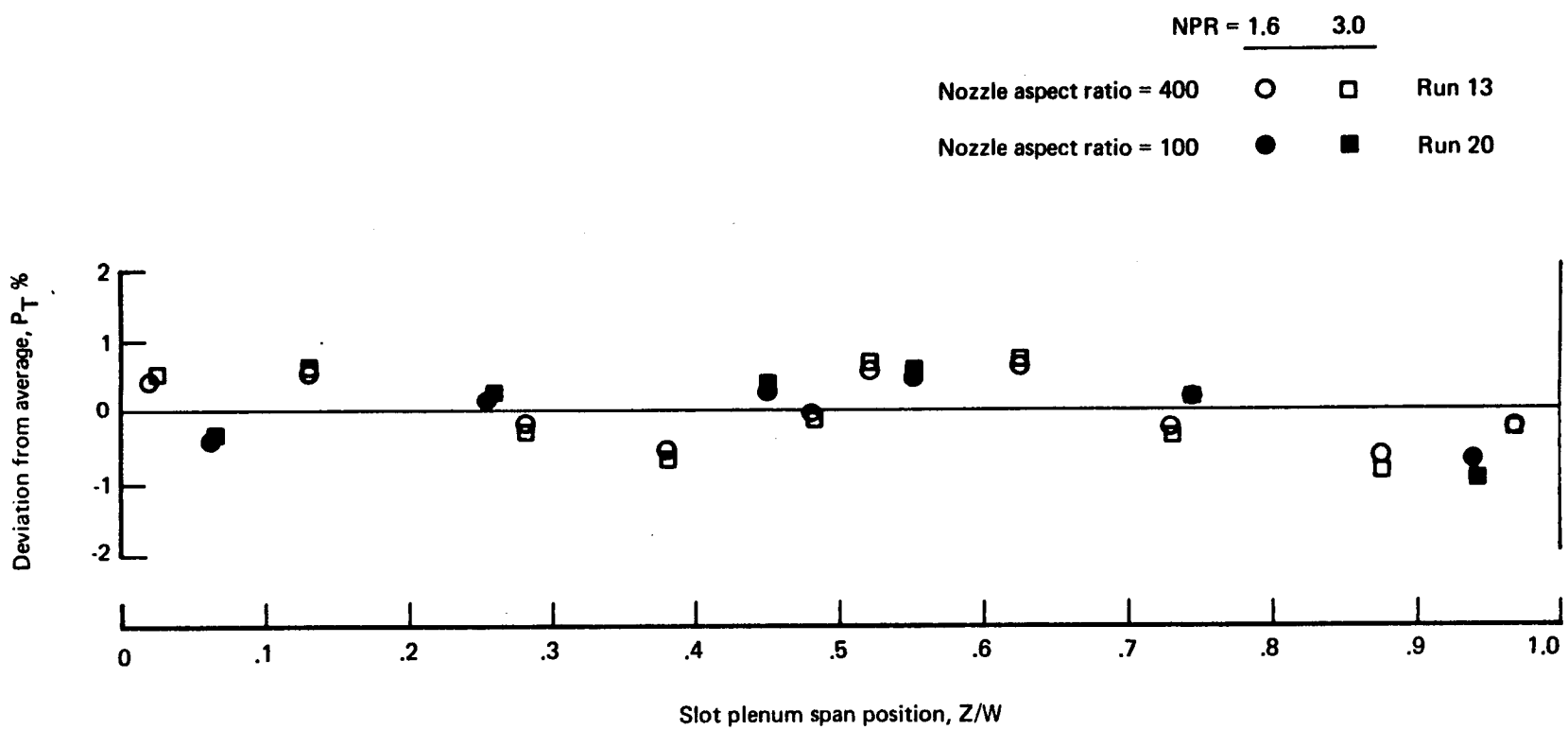

FIGURE 6-43.– SPANWISE TOTAL PRESSURE DEVIATION–SLOT NOZZLE PLENUM CHARGING STATION

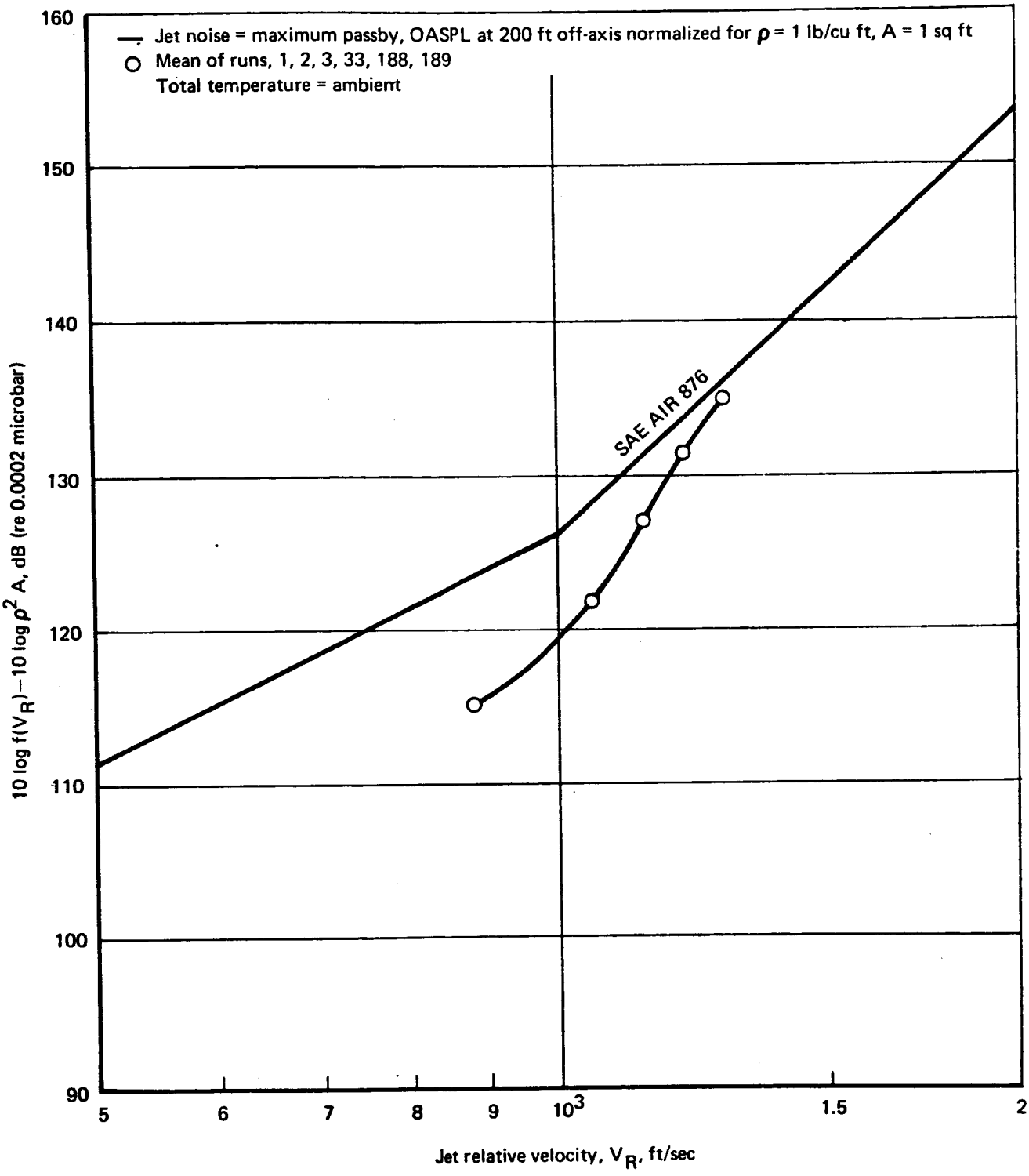

FIGURE 6-44.– NORMALIZED MEAN OASPL

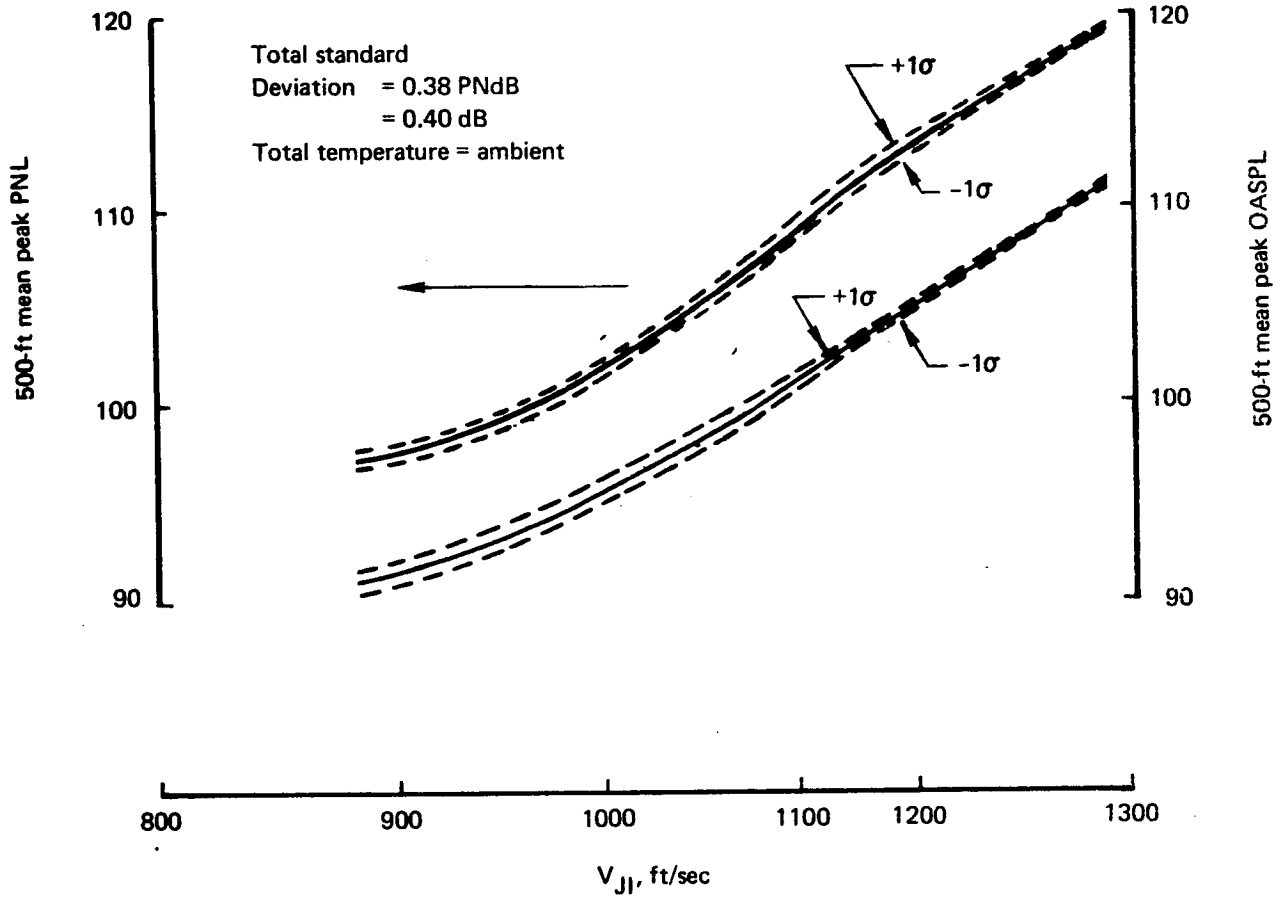

FIGURE 6-45.—MEAN PEAK OASPL AND MEAN PEAK PNL WITH THEIR STANDARD DEVIATIONS FOR RUNS 1, 2, 3, 33, 188, and 189

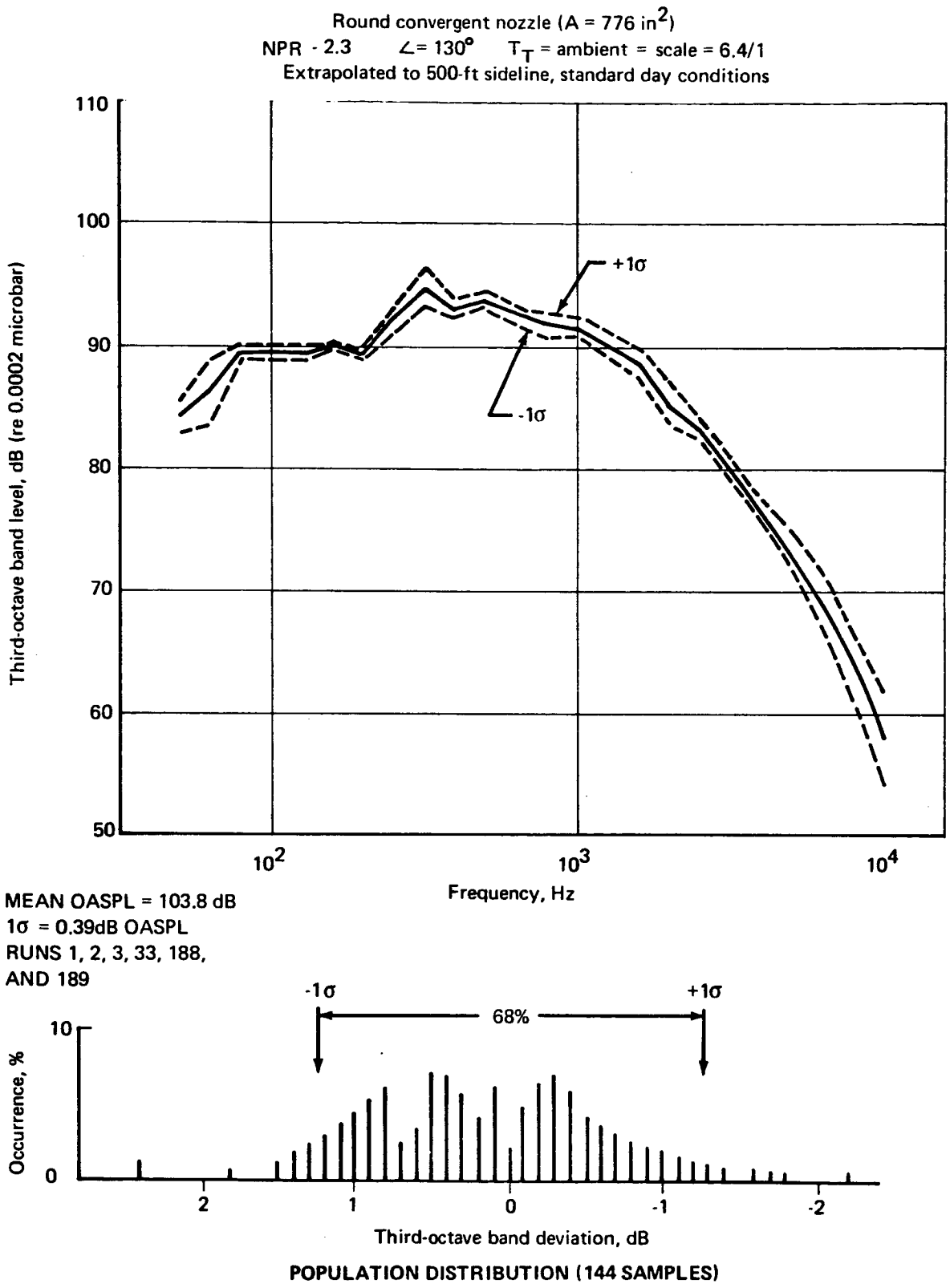

FIGURE 6-46.– MEAN SPECTRUM WITH STANDARD DEVIATIONS

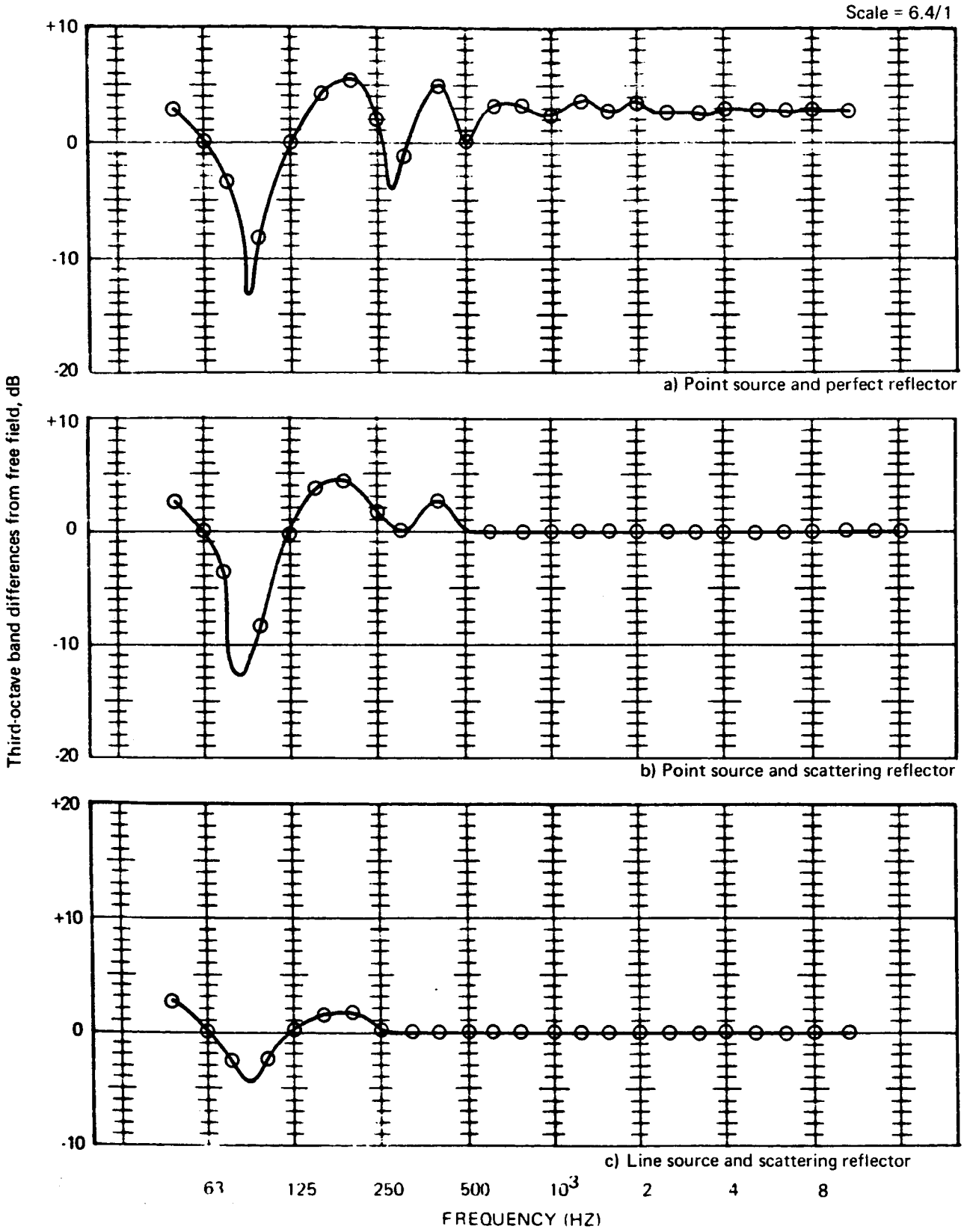

FIGURE 6-47.– REFLECTION EFFECTS

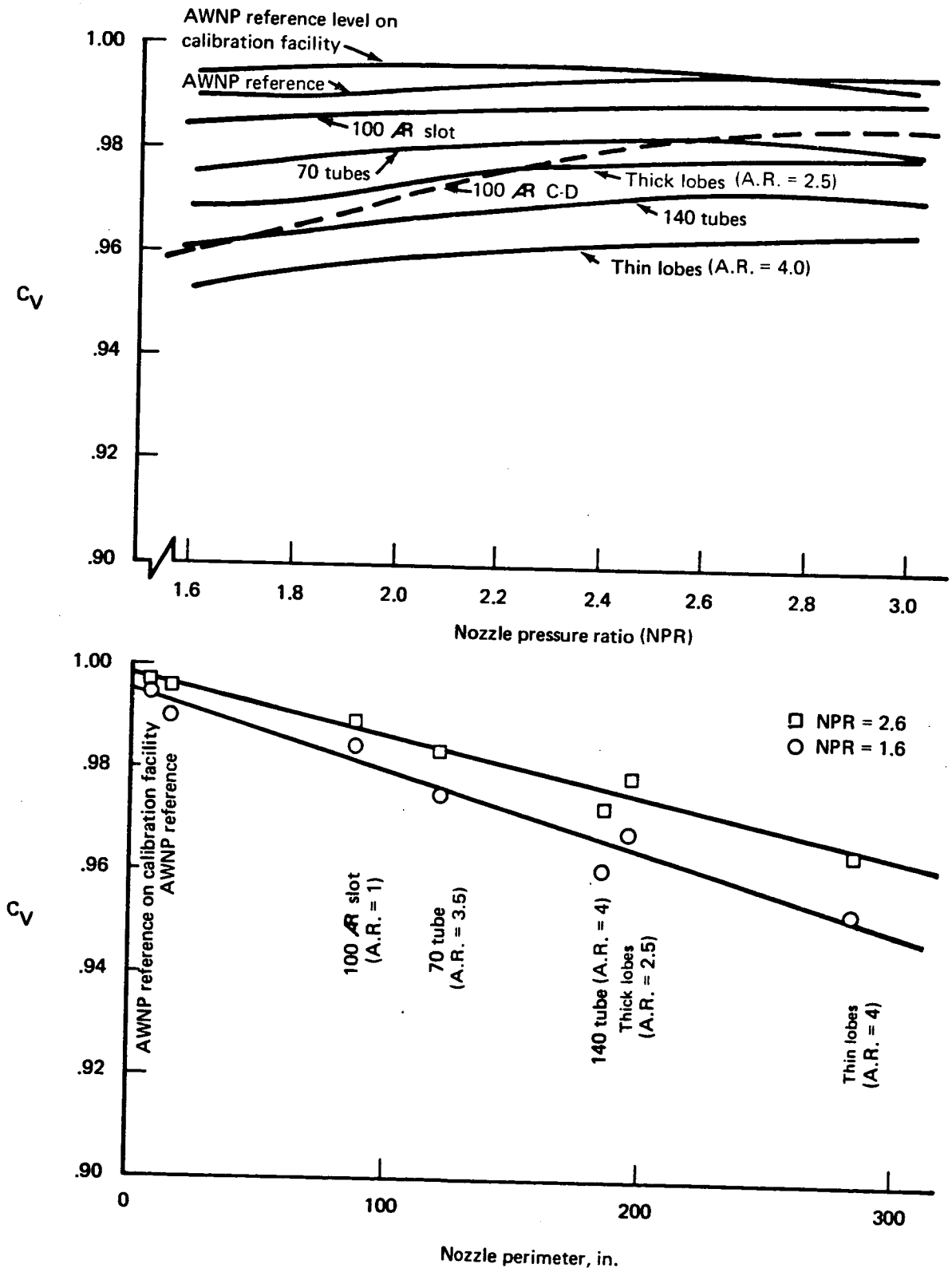

FIGURE 6-48.– PRIMARY NOZZLE PERFORMANCE

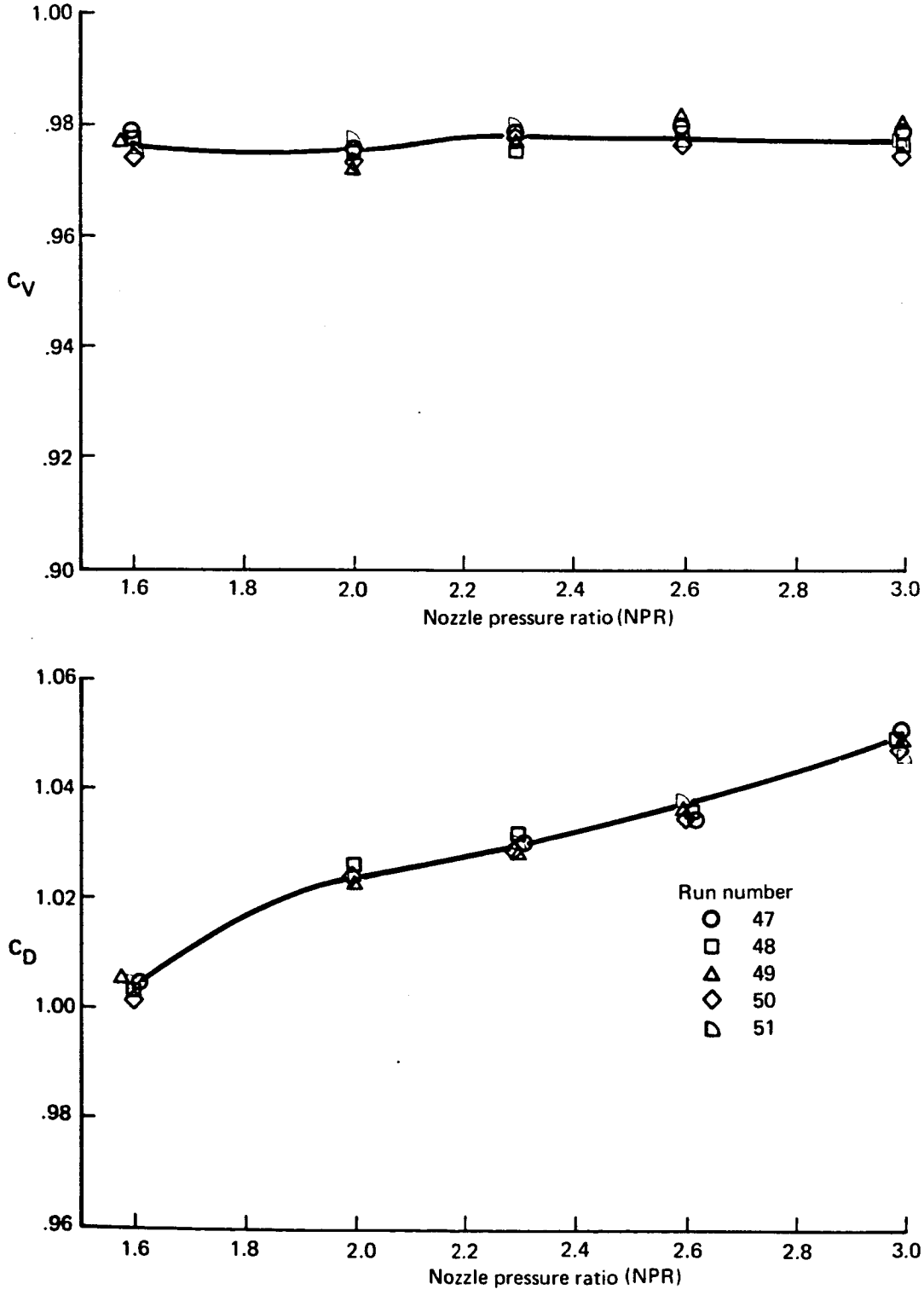

FIGURE 6-49.—SLOT NOZZLE PERFORMANCE, AR = 50 (EXPANDED EXIT) RUNS 47-51, 5/14/71

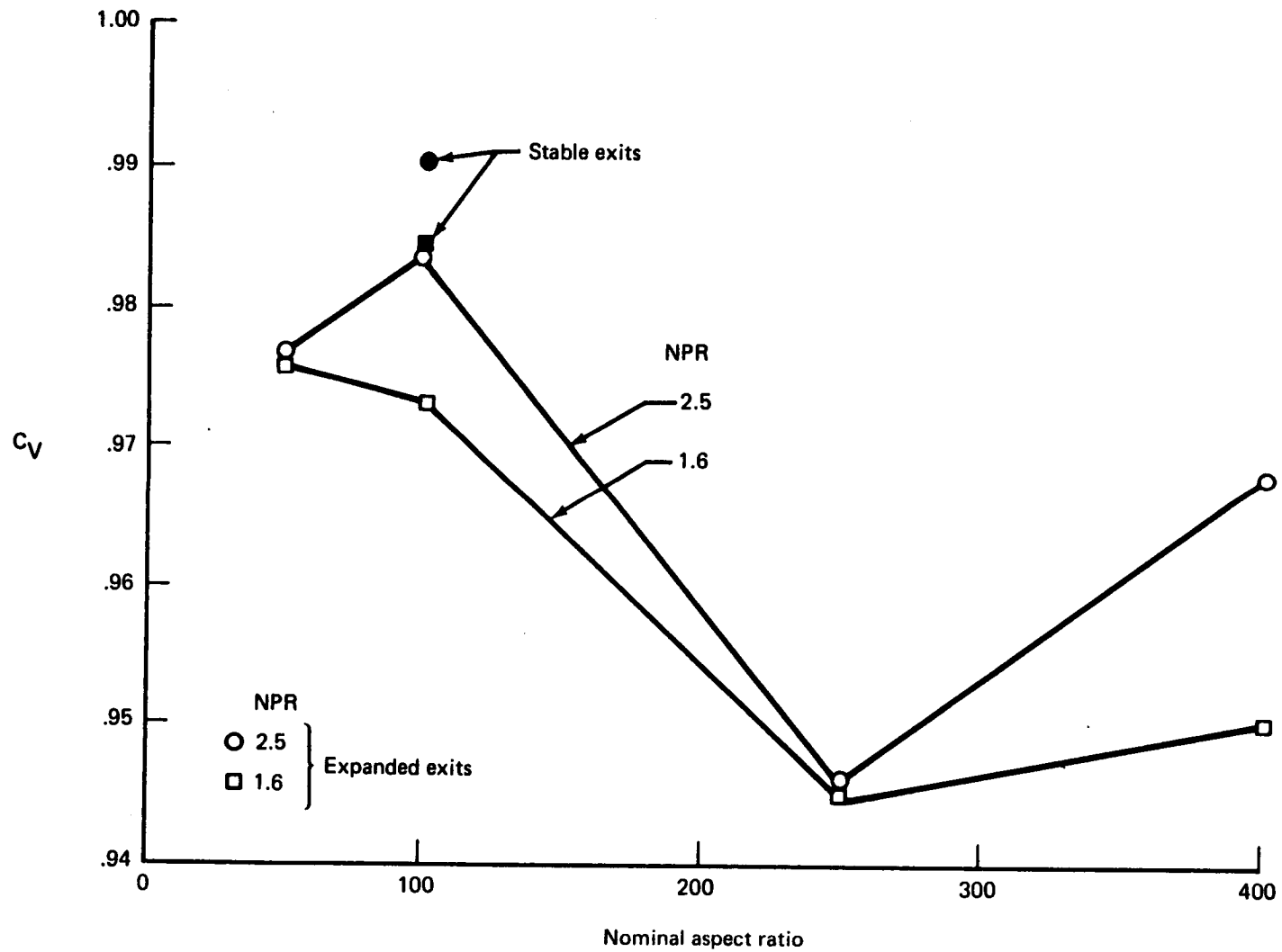

FIGURE 6-50.—MEASURED PERFORMANCE TRENDS FOR SLOT NOZZLE ASPECT RATIO EFFECTS

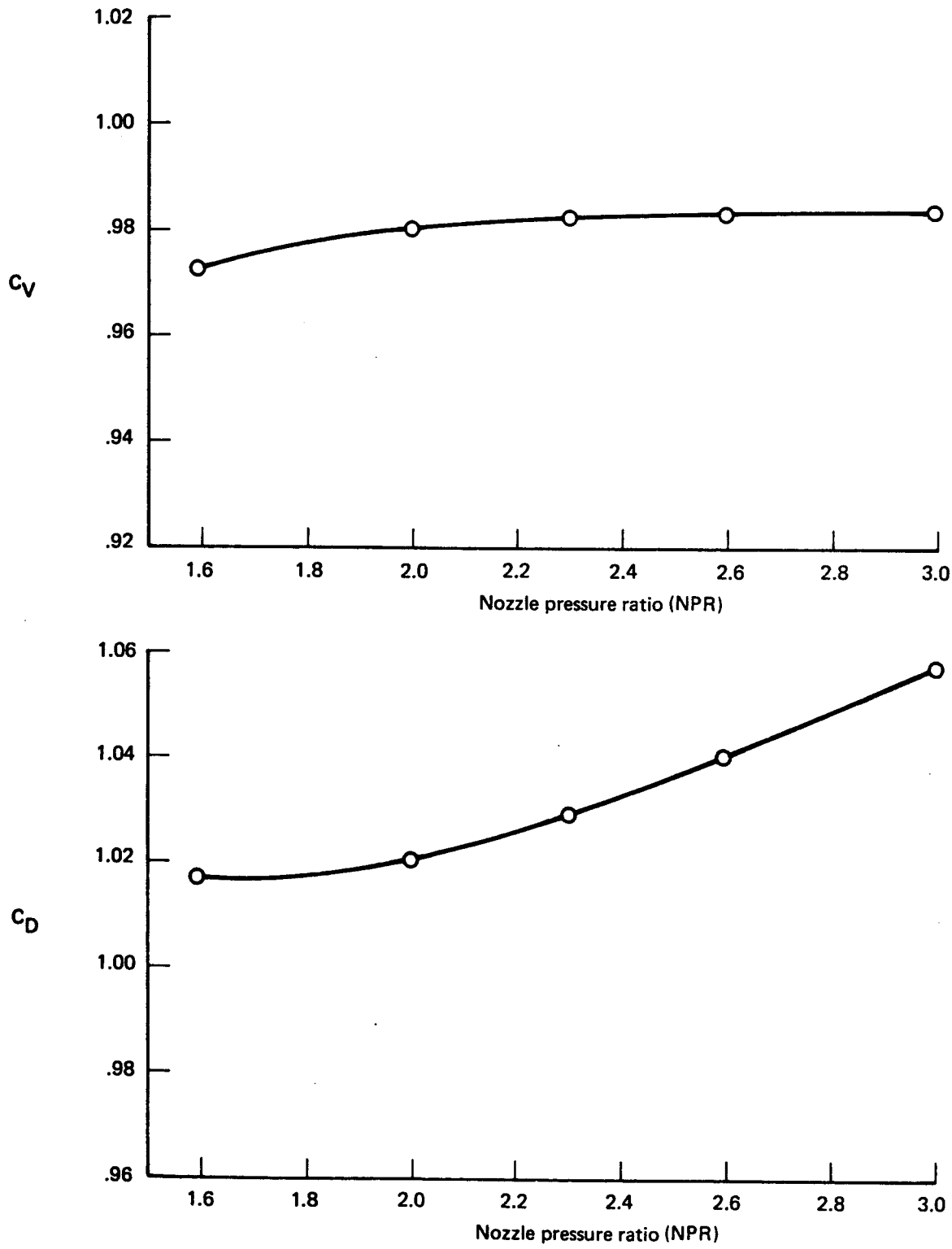

FIGURE 6-51.—SLOT NOZZLE PERFORMANCE, $\mathcal{R}$ = 100 (EXPANDED EXIT), RUN 19, 5/5/71

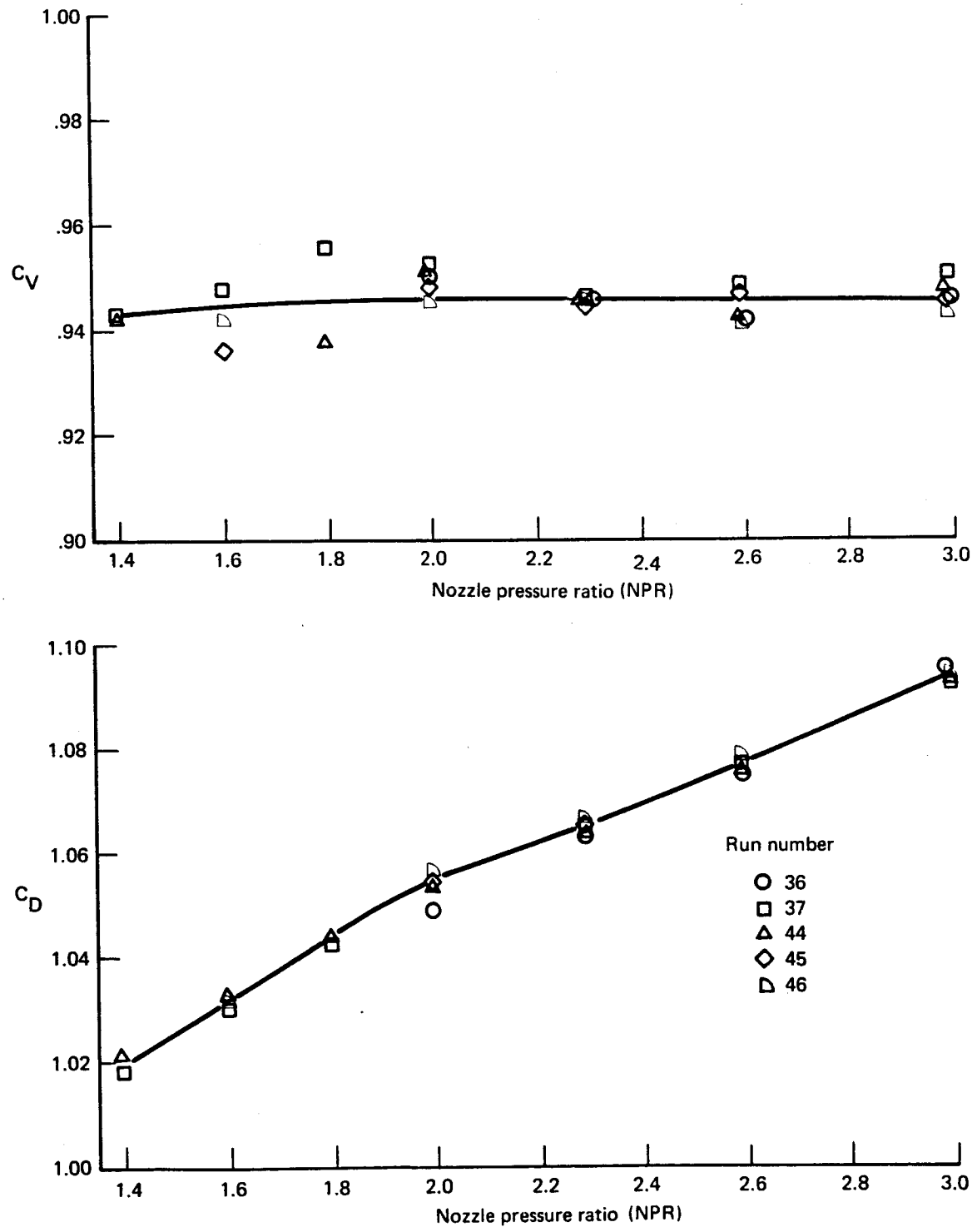

FIGURE 6-52.—SLOT NOZZLE PERFORMANCE, $\mathcal{A}R$ = 250 (EXPANDED EXIT), RUNS 36-37, 44-46, 5/12/71 AND 5/14/71

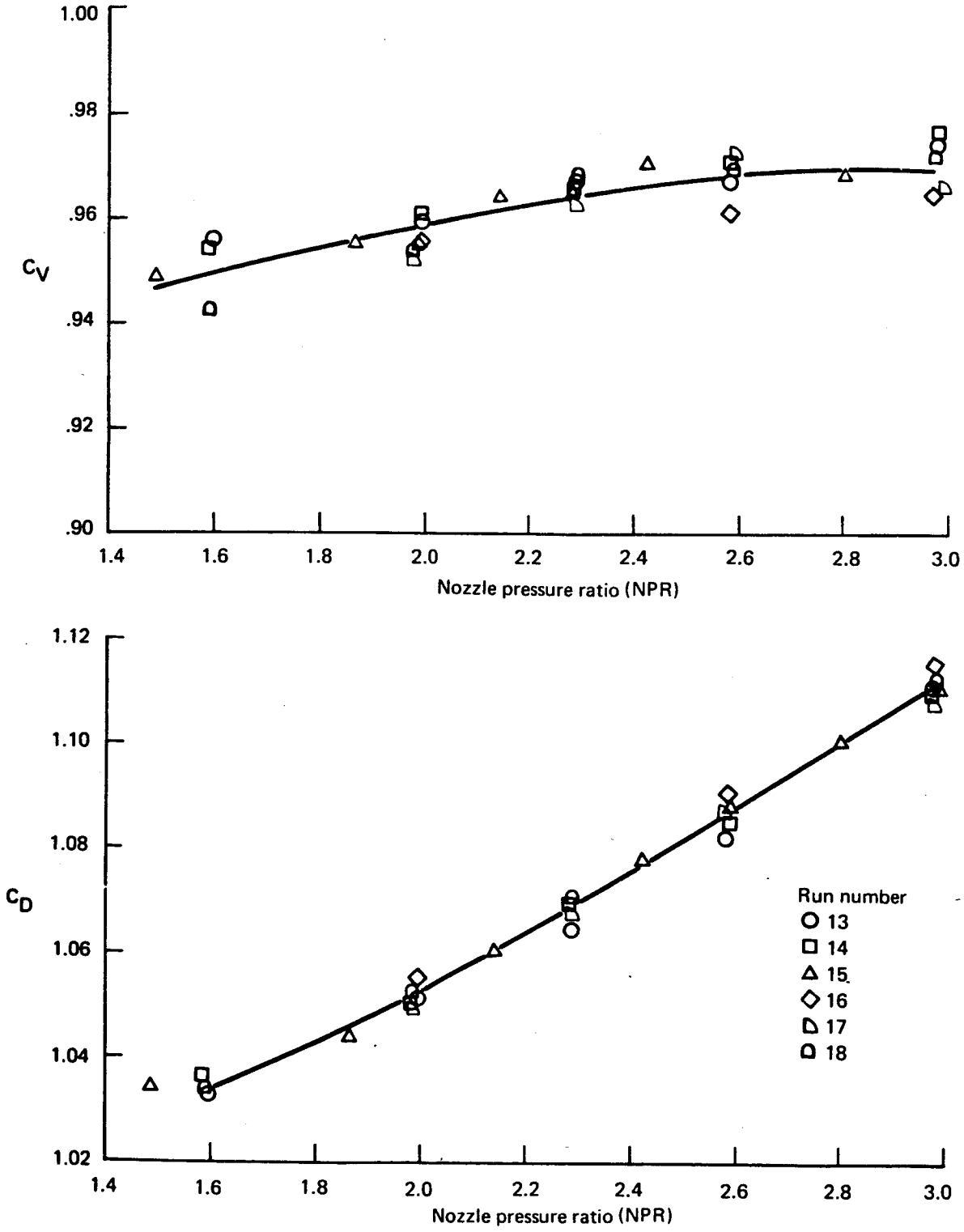

FIGURE 6-53.—SLOT NOZZLE PERFORMANCE, AR = 400 (EXPANDED EXIT), RUNS 13-18, 4/28/71 AND 4/29/71

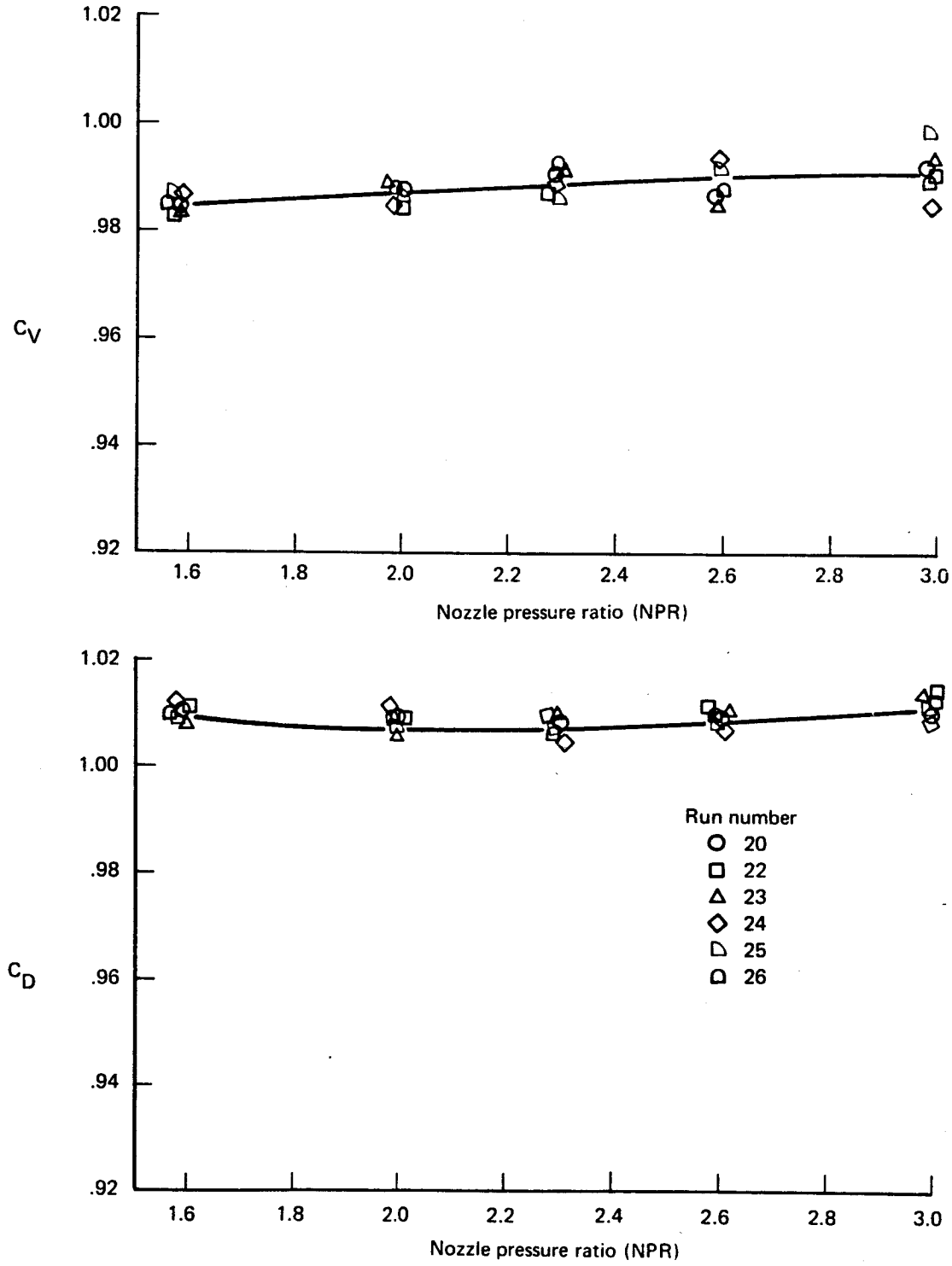

FIGURE 6-54.– SLOT NOZZLE PERFORMANCE, $\mathcal{A}R$ = 100 (STABLE EXIT), RUNS 20-26, 5/6/71 AND 5/7/71

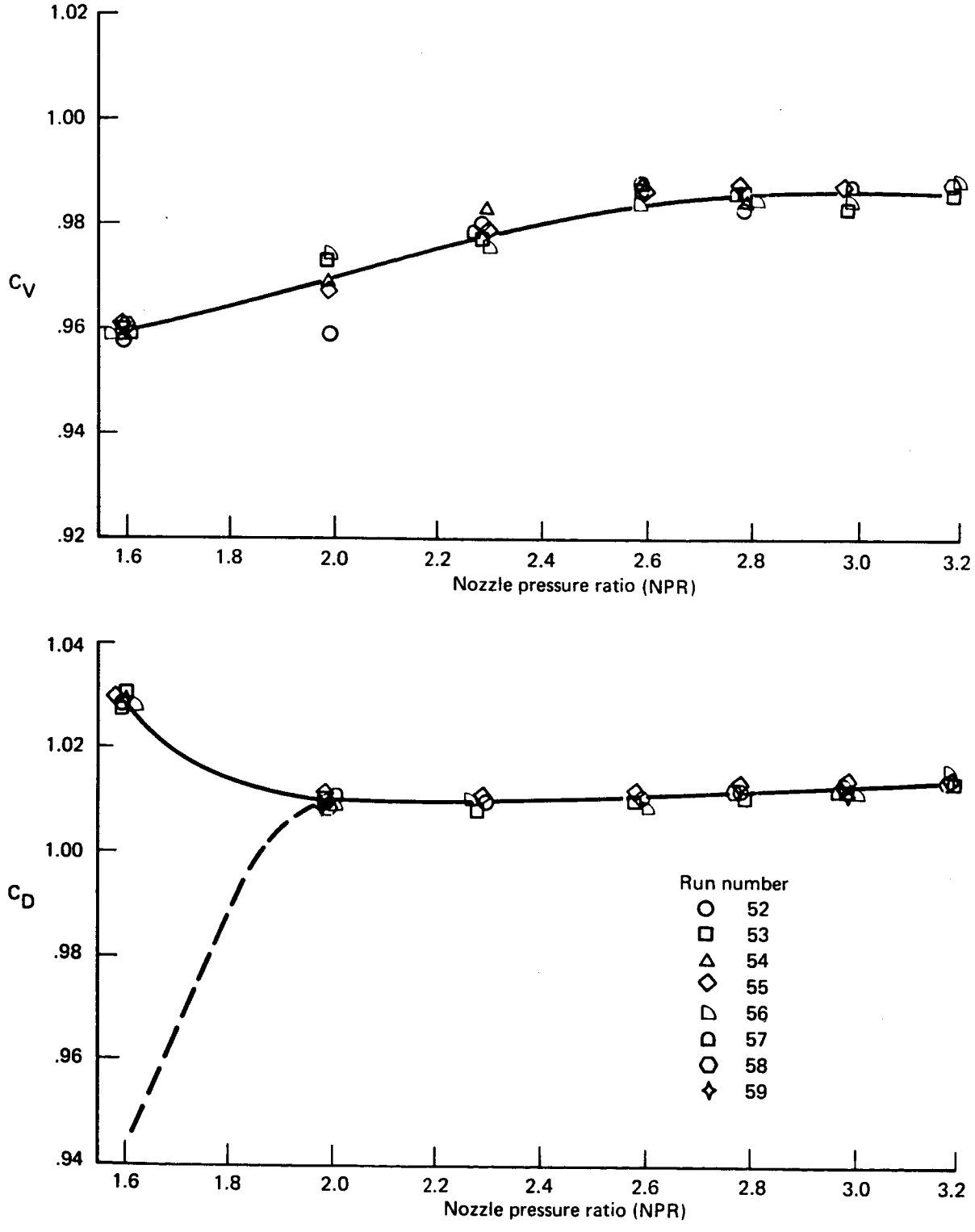

FIGURE 6-55.—CONVERGENT-DIVERGENT SLOT NOZZLE PERFORMANCE, DESIGN PRESSURE RATIO 3.0, RUNS 52-59, 5/18/71 AND 5/19/71

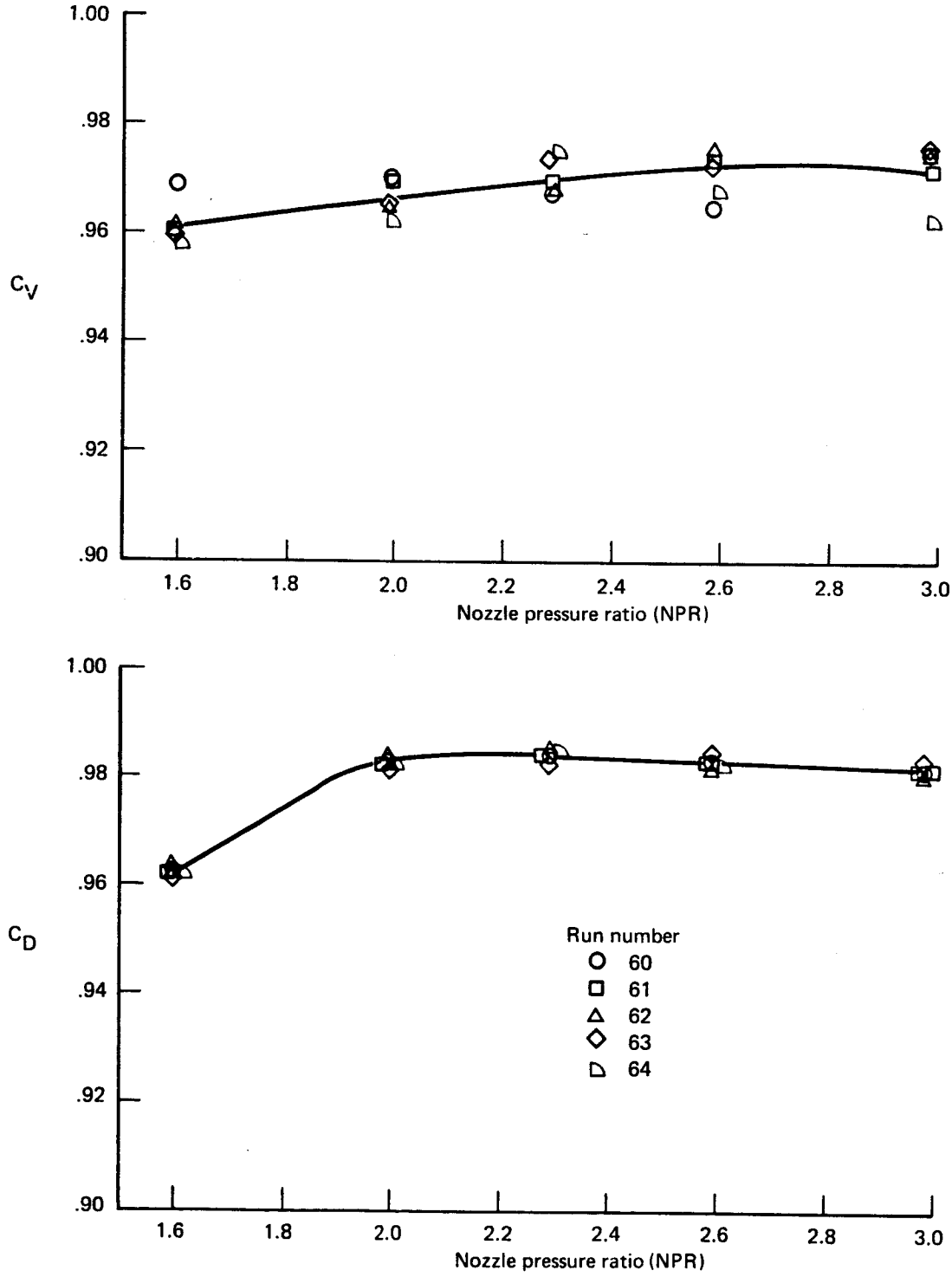

FIGURE 6-56.—140-TUBE (AREA RATIO 4) NOZZLE PERFORMANCE, RUNS 60-64, 5/20/71

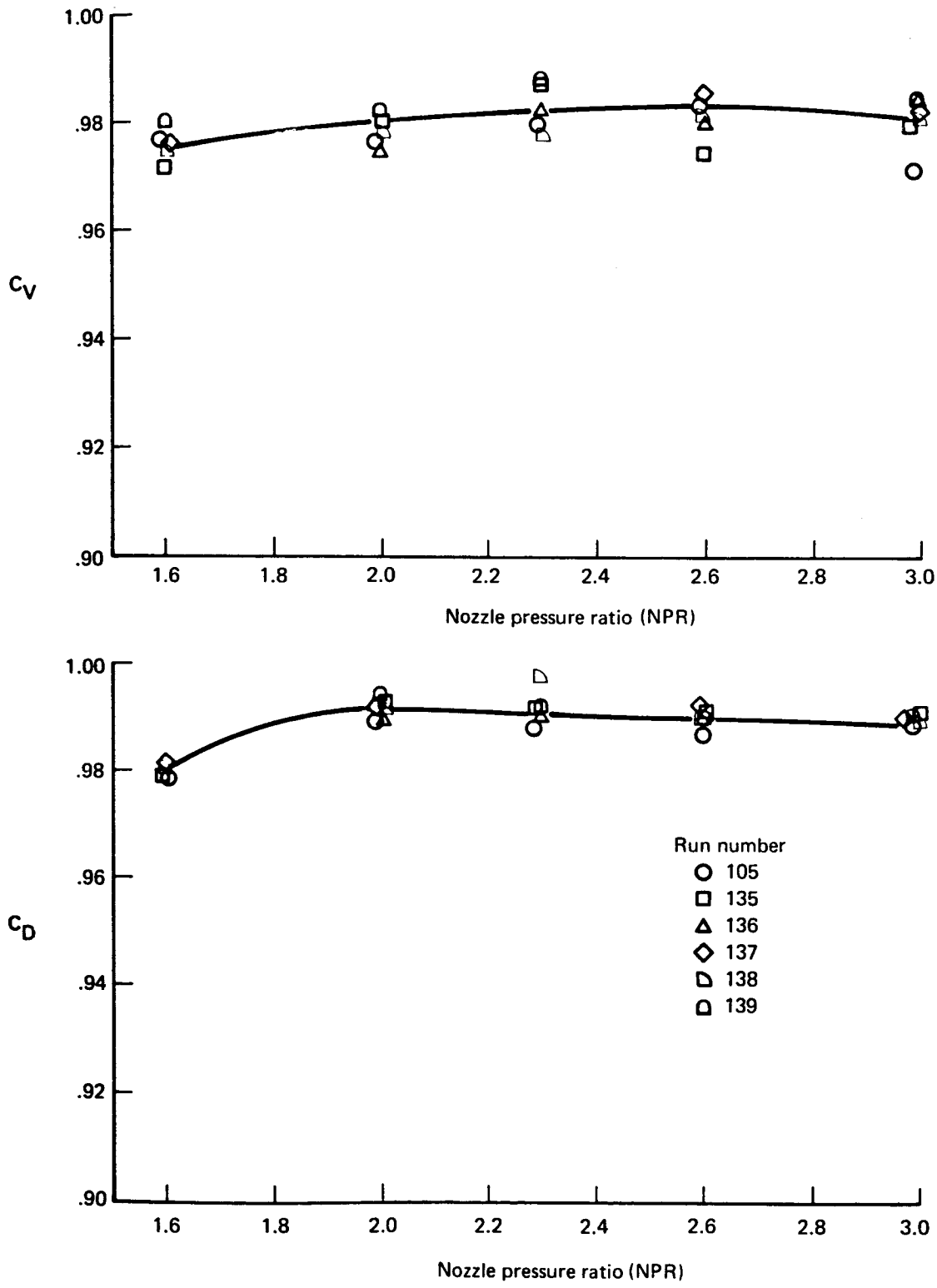

FIGURE 6-57.—70-TUBE (AREA RATIO 3.5) NOZZLE PERFORMANCE, RUNS 105 AND 135-139, 5/26/71 AND 5/28/71

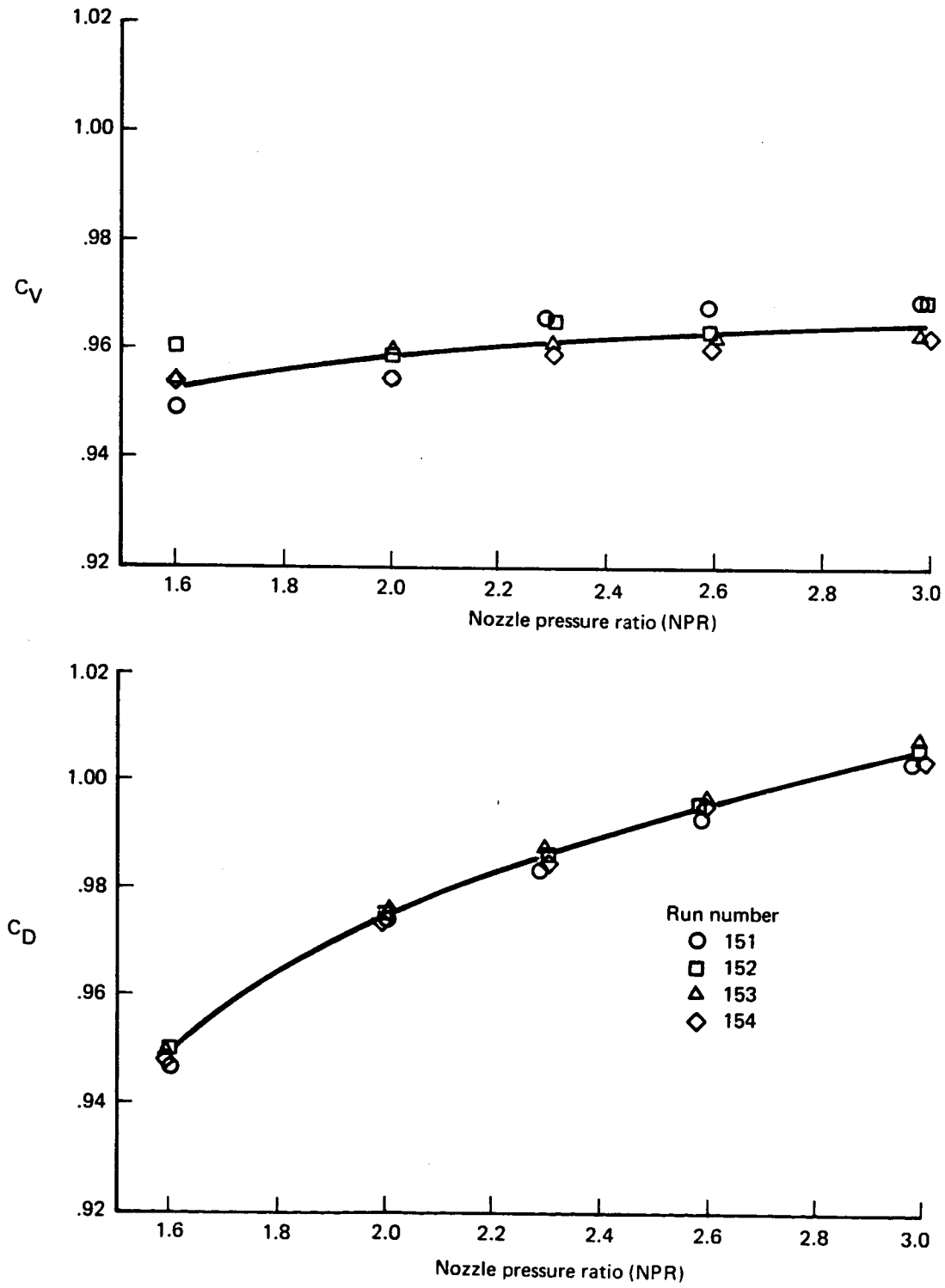

FIGURE 6-58.—70-LOBE (AREA RATIO 4) NOZZLE PERFORMANCE, RUNS 151-154, 6/2/71

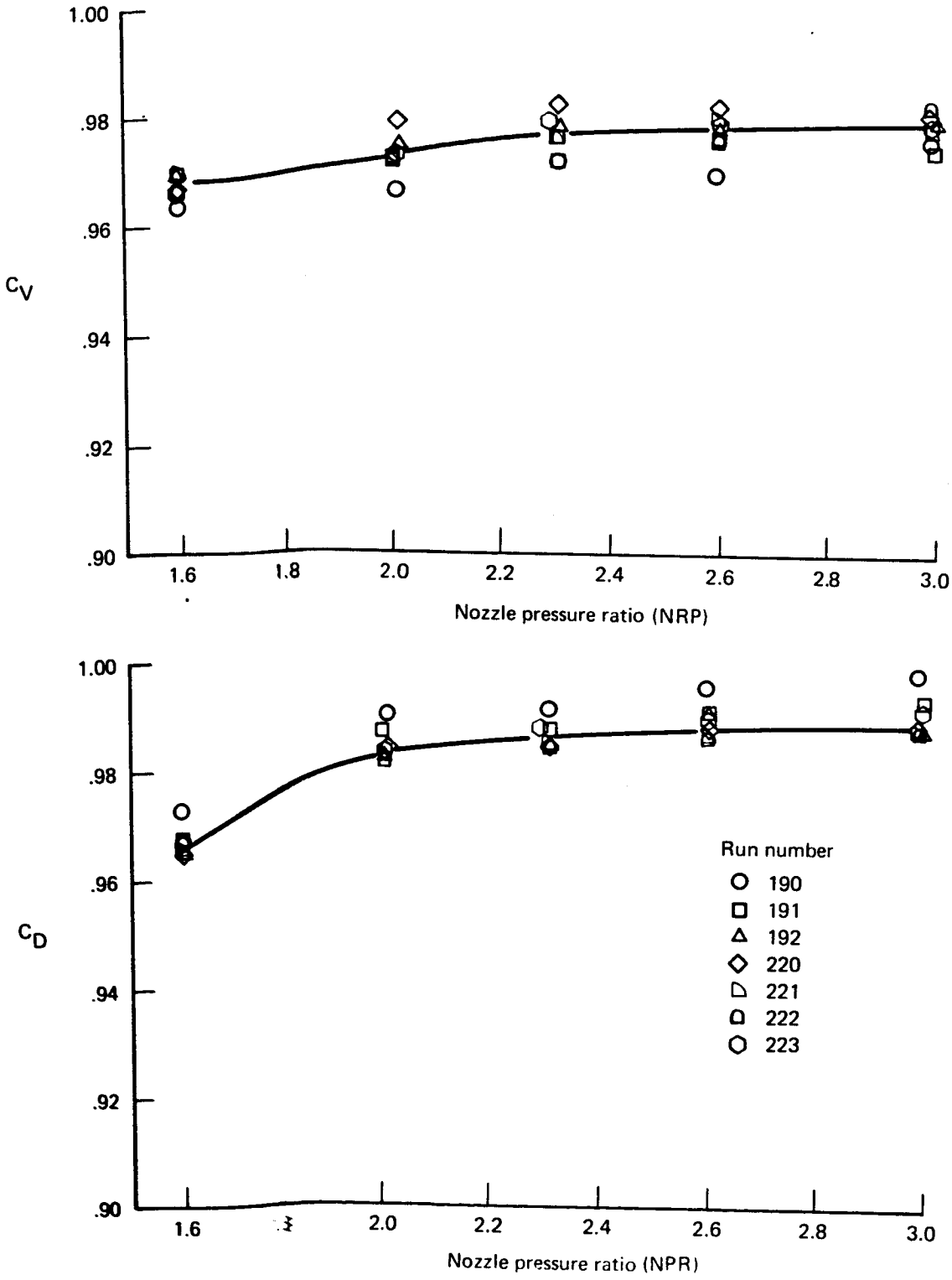

FIGURE 6-59.– [illegible] (AREA RATIO 2.5) NOZZLE PERFORMANCE, [illegible] 190-192 and 220-223, 6/9/71 AND 6/11/71

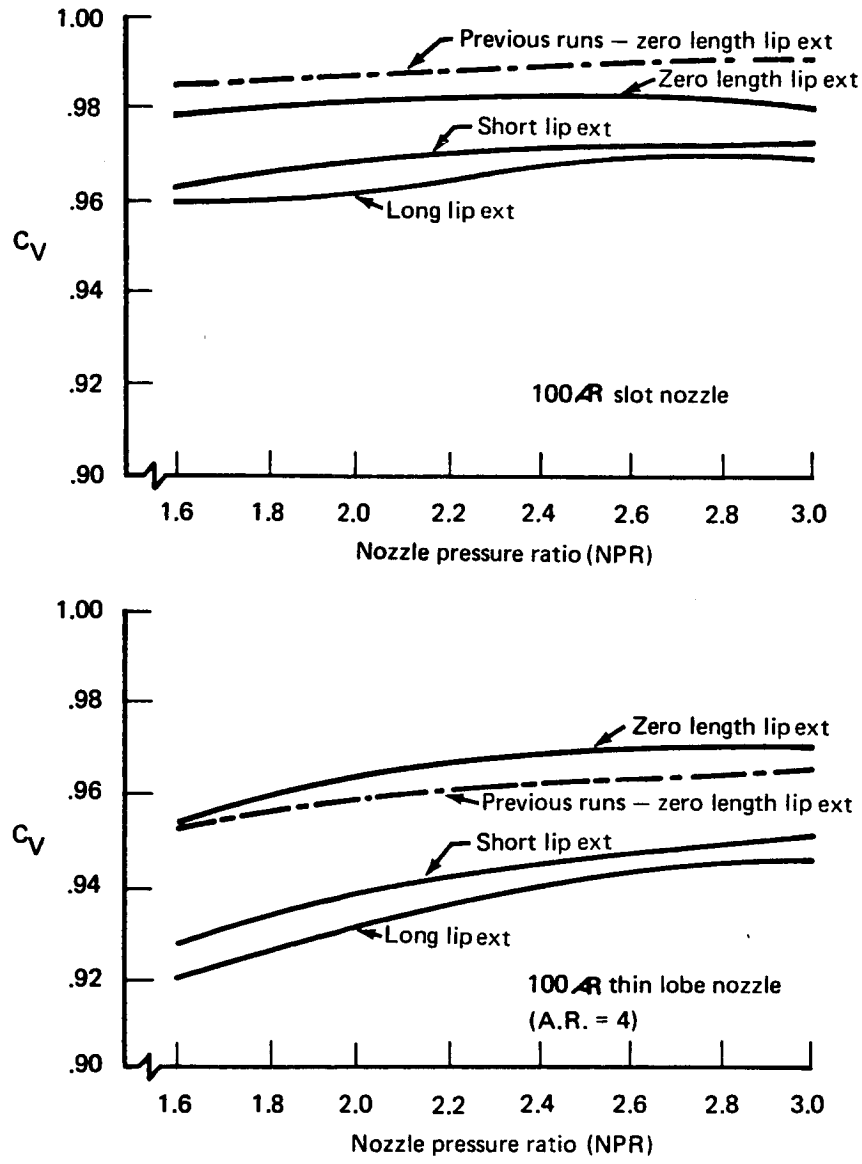

FIGURE 6-60.–PERFORMANCE CHANGES FOR NOZZLE LIP EXTENSION (PRELIMINARY)

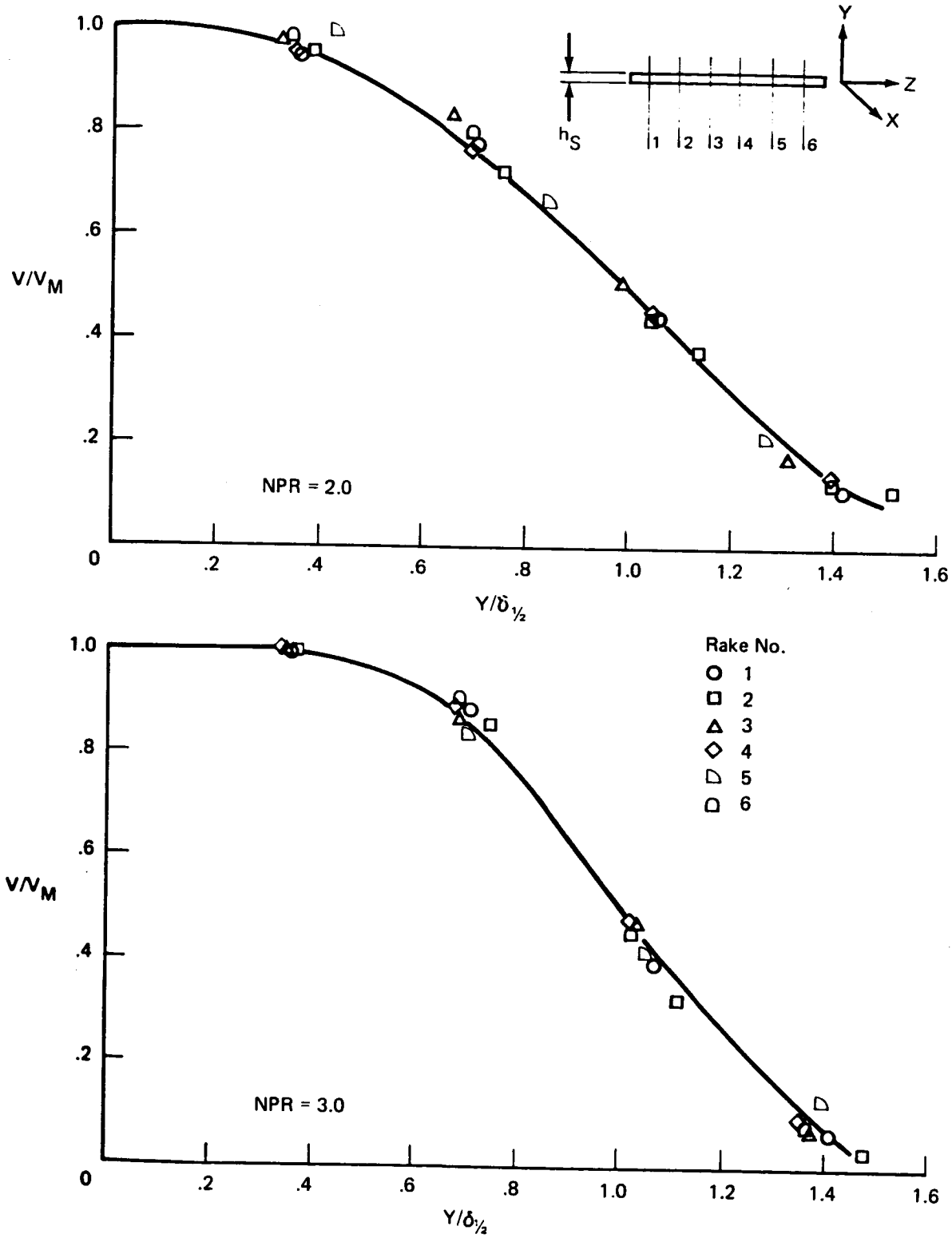

FIGURE 6-61.– SLOT NOZZLE JET VELOCITY PROFILES, AR= 400, X/h_S = 3, RUN 8, 4/28/71

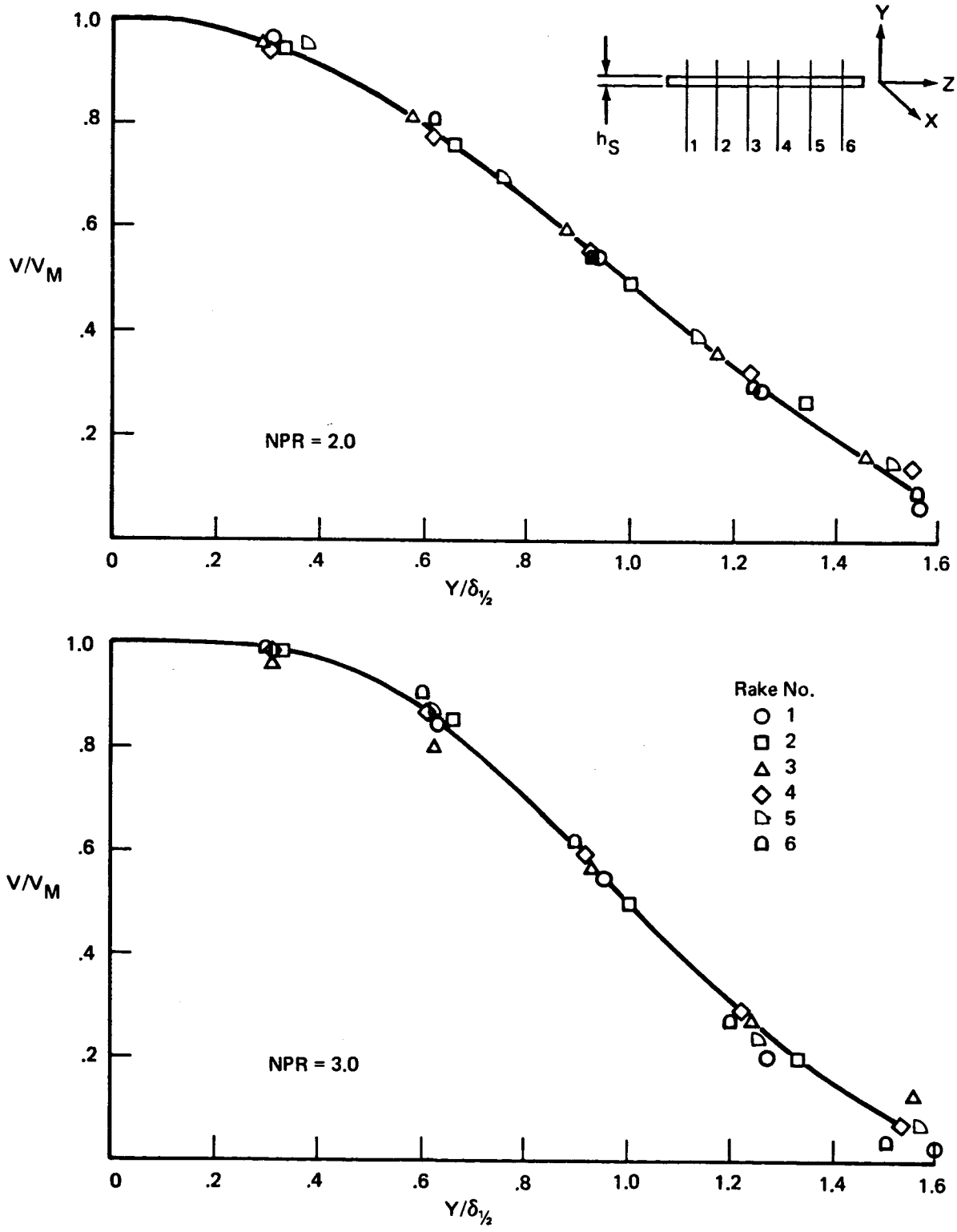

FIGURE 6-62.—SLOT NOZZLE JET VELOCITY PROFILES, AR = 400, $X/h_S = 5$, RUN 9, 4/28/71

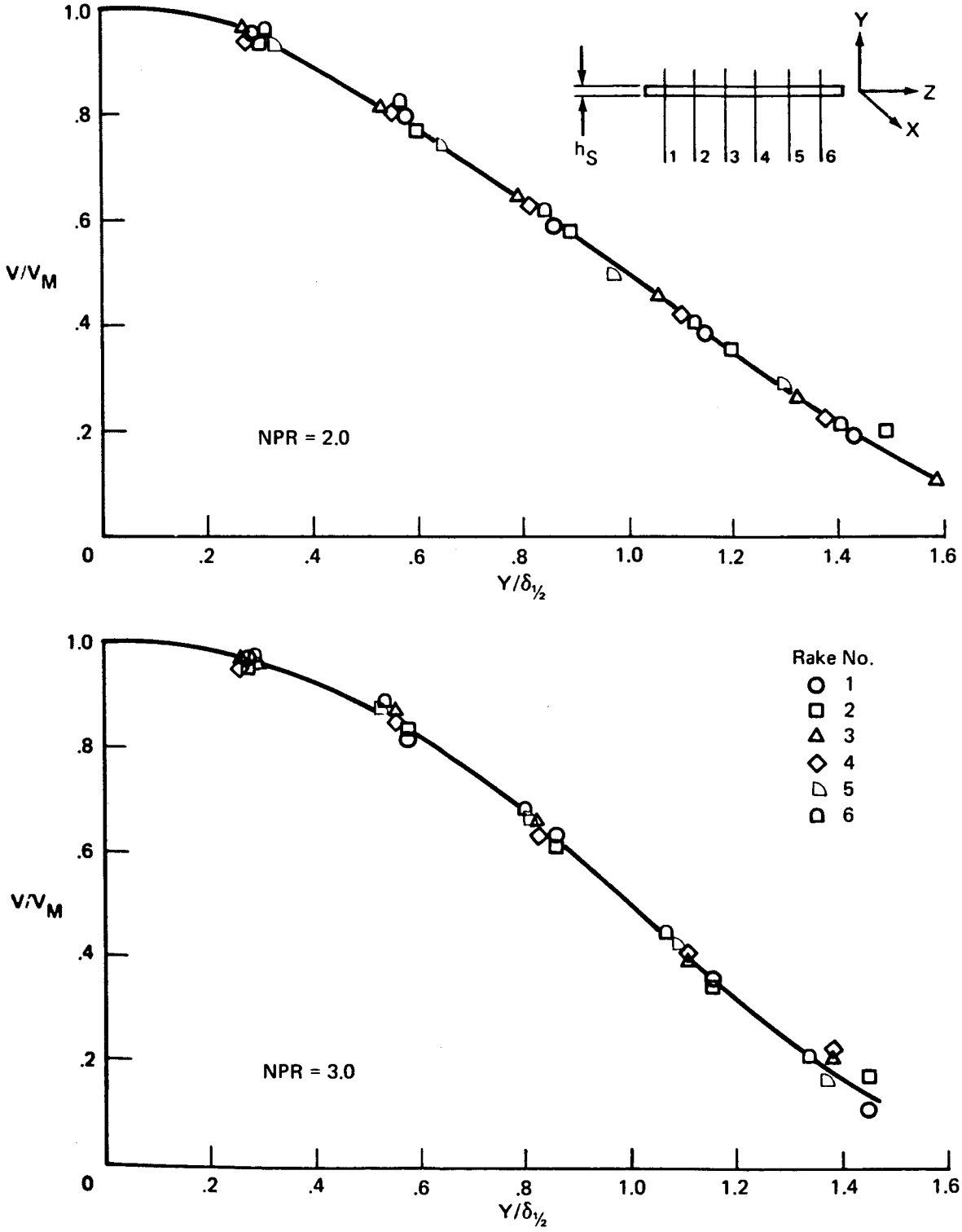

FIGURE 6-63.–SLOT NOZZLE JET VELOCITY PROFILES, AR = 400, X/h_S = 7, RUN 10, 4/28/71

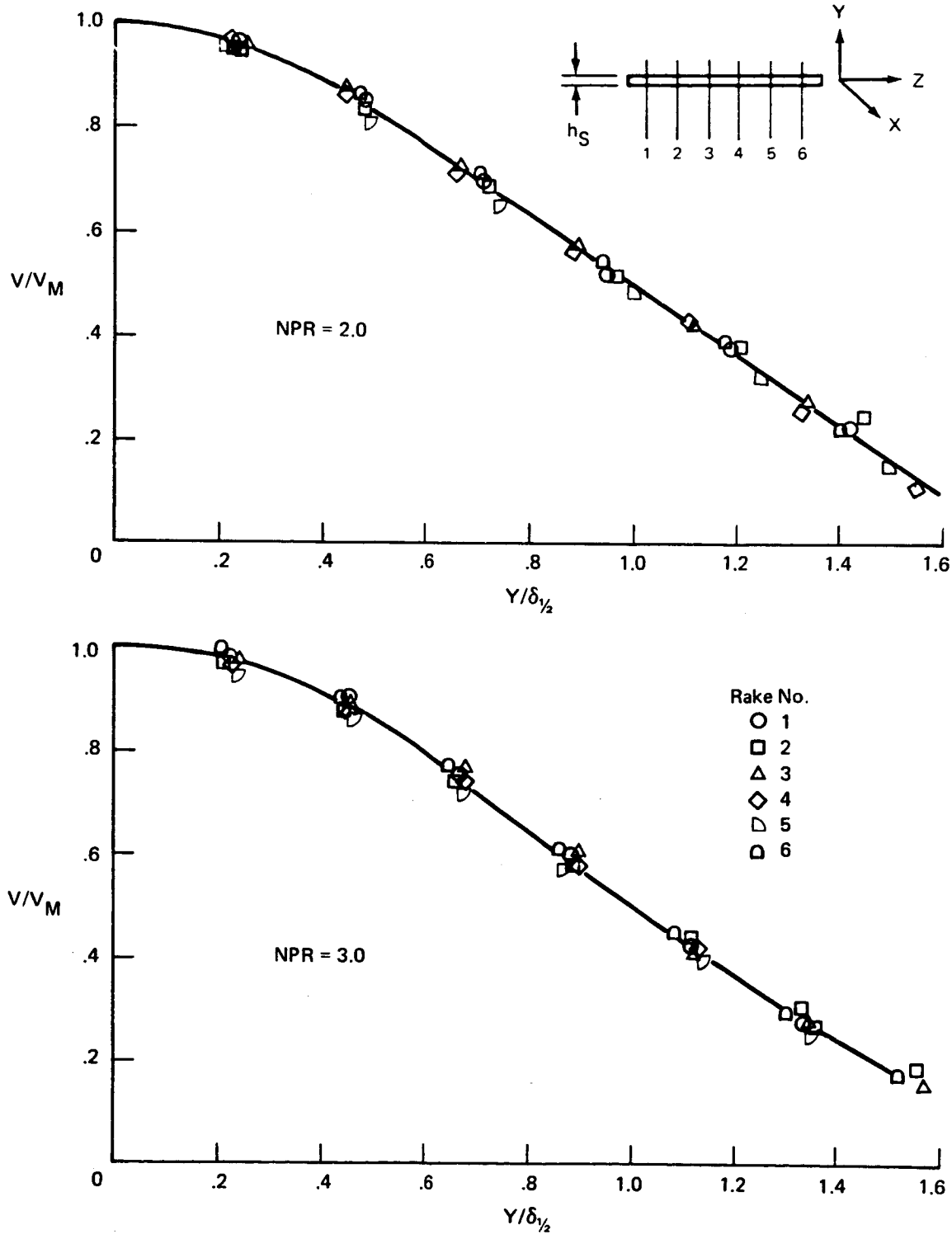

FIGURE 6-64.--SLOT NOZZLE JET VELOCITY PROFILES, $\mathcal{R} = 400$, $X/h_S = 10$, RUN 11, 4/28/71

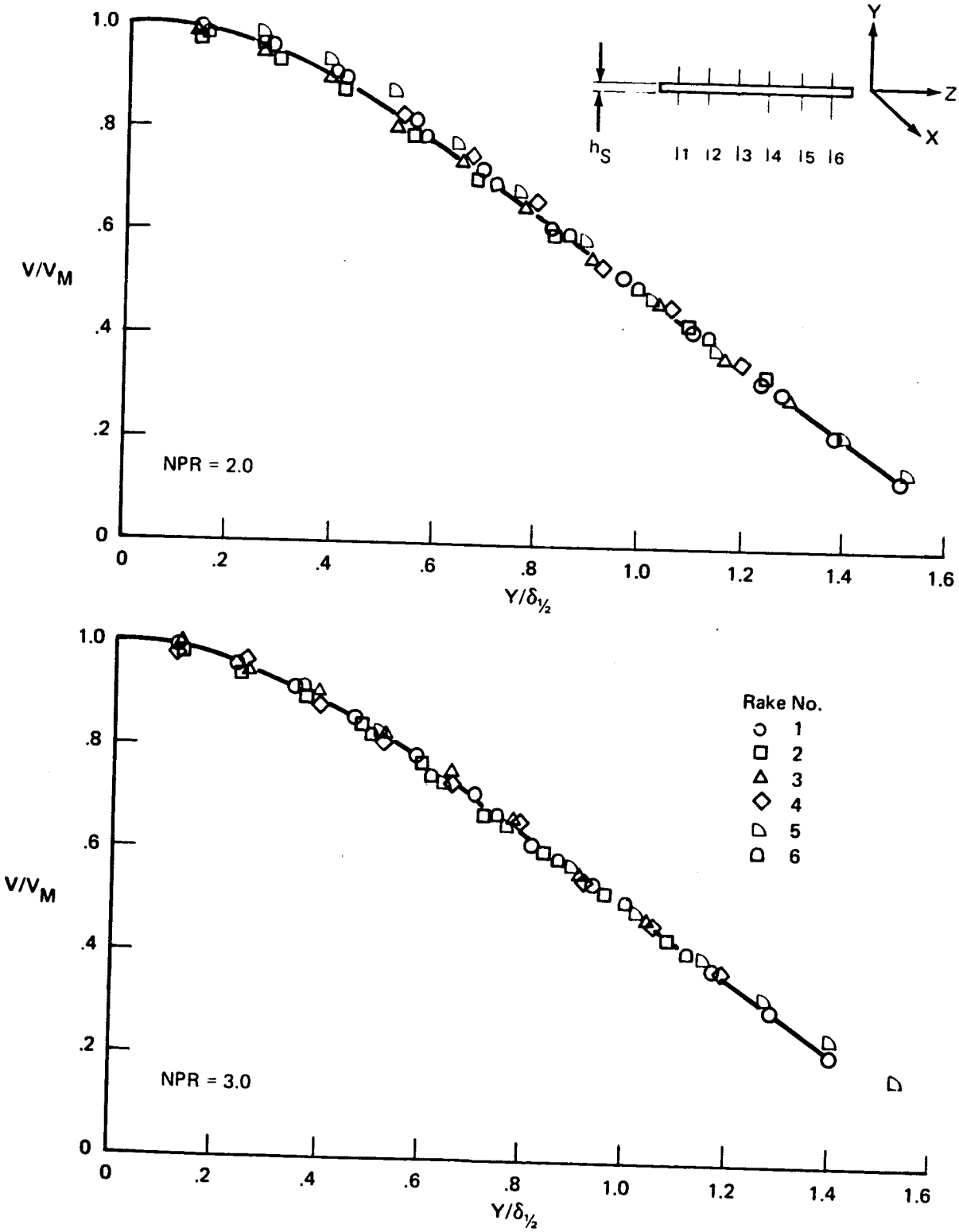

FIGURE 6-65.– SLOT NOZZLE JET VELOCITY PROFILES, AR = 400, X/h_S = 20, RUN 12, 4/28/71

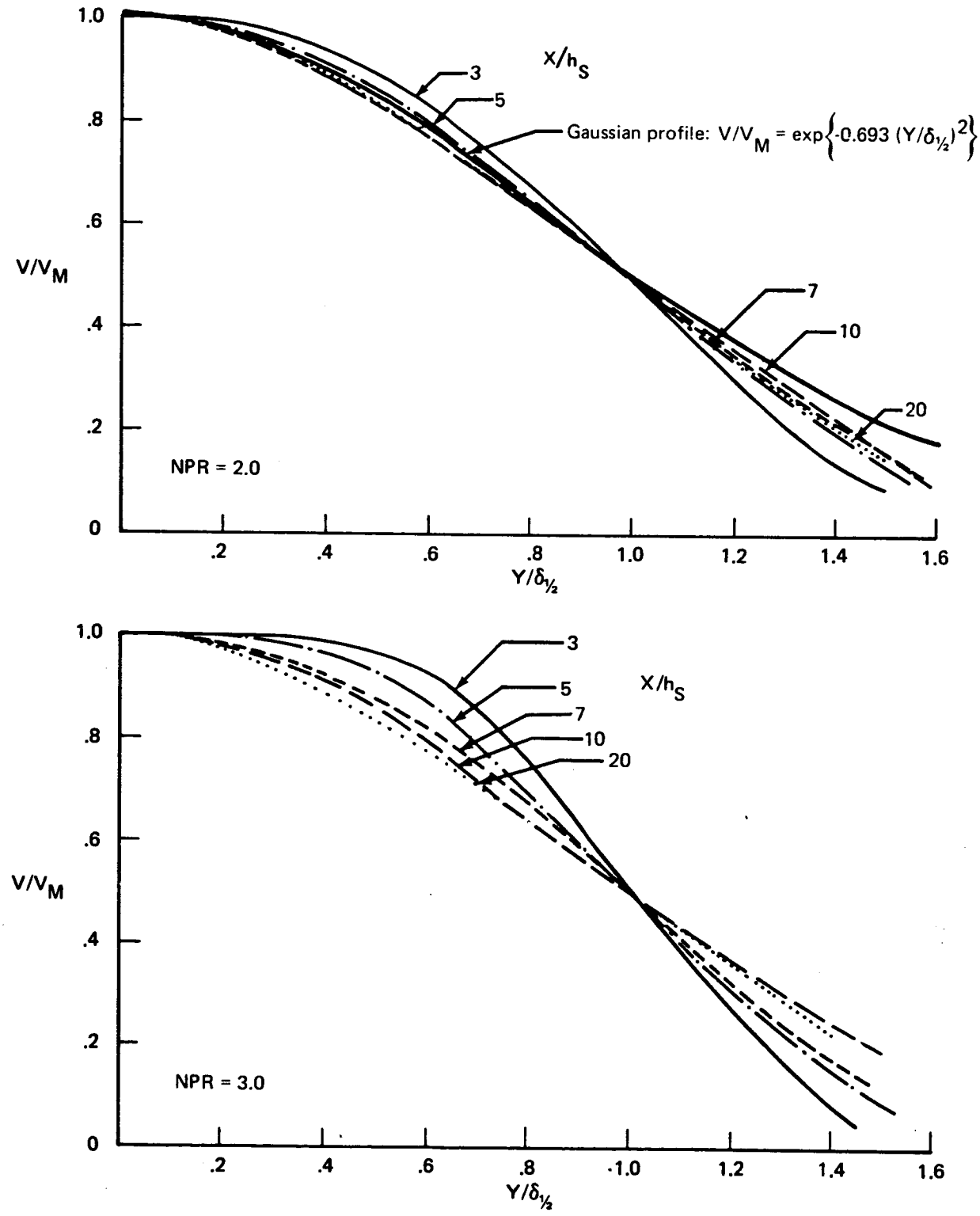

FIGURE 6-66.—SLOT NOZZLE JET VELOCITY PROFILES, AR = 400 SUMMARY CURVE

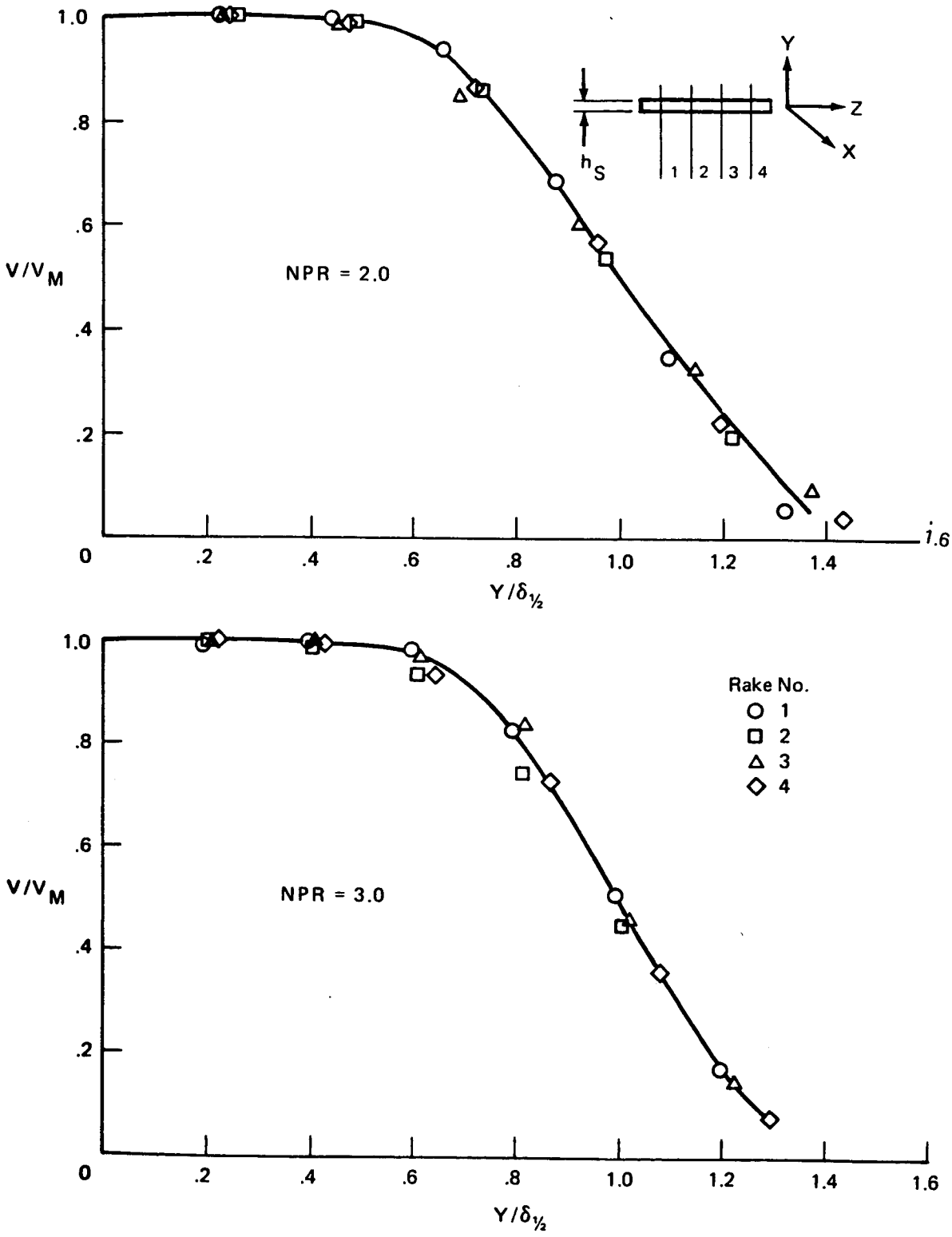

FIGURE 6-67.–SLOT NOZZLE JET VELOCITY PROFILES, AR= 100, X/h_S = 3, RUN 27, 5/7/71

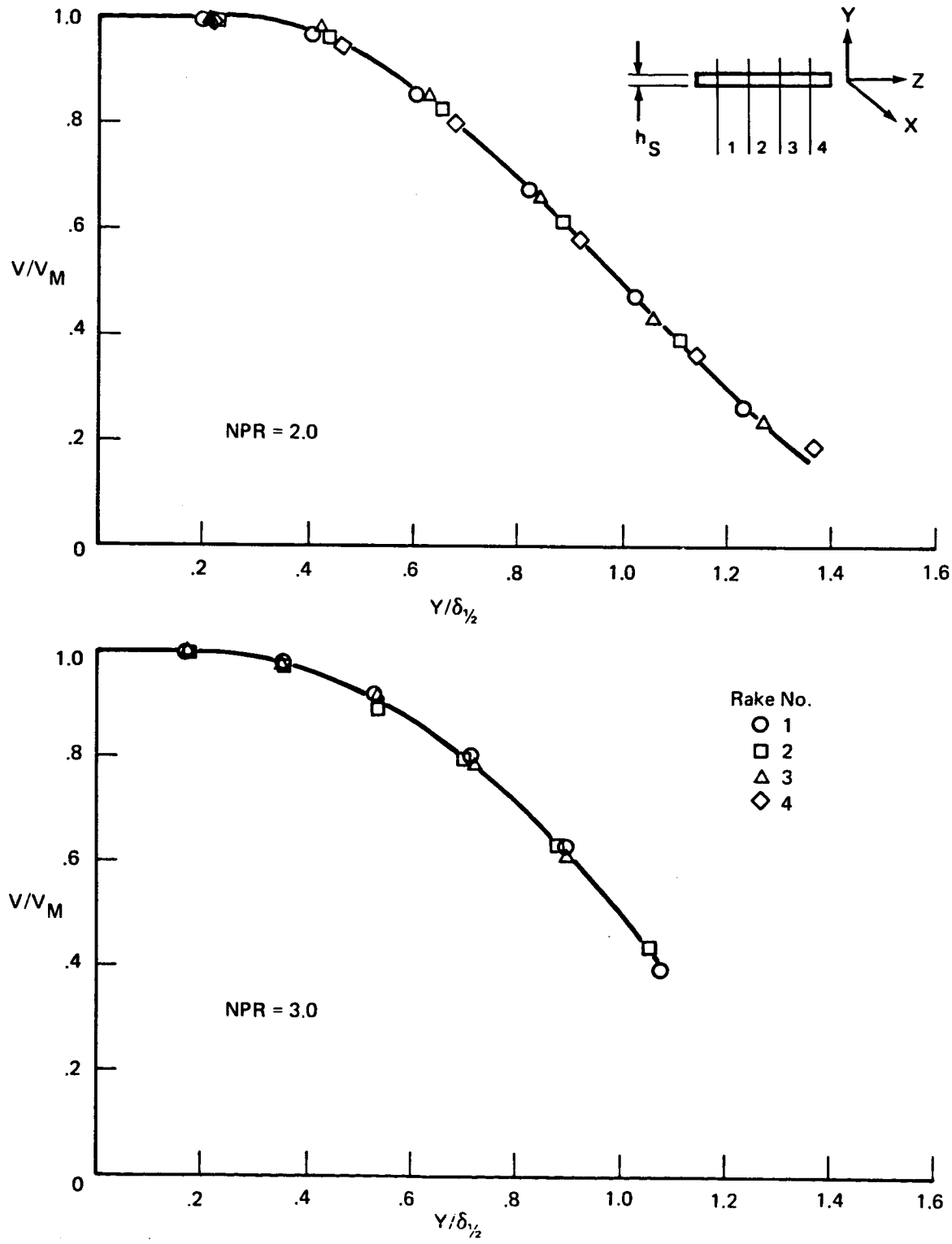

FIGURE 6-68.—SLOT NOZZLE JET VELOCITY PROFILES, AR = 100, X/h_S = 5, RUNS 29 AND 32, 5/7/71

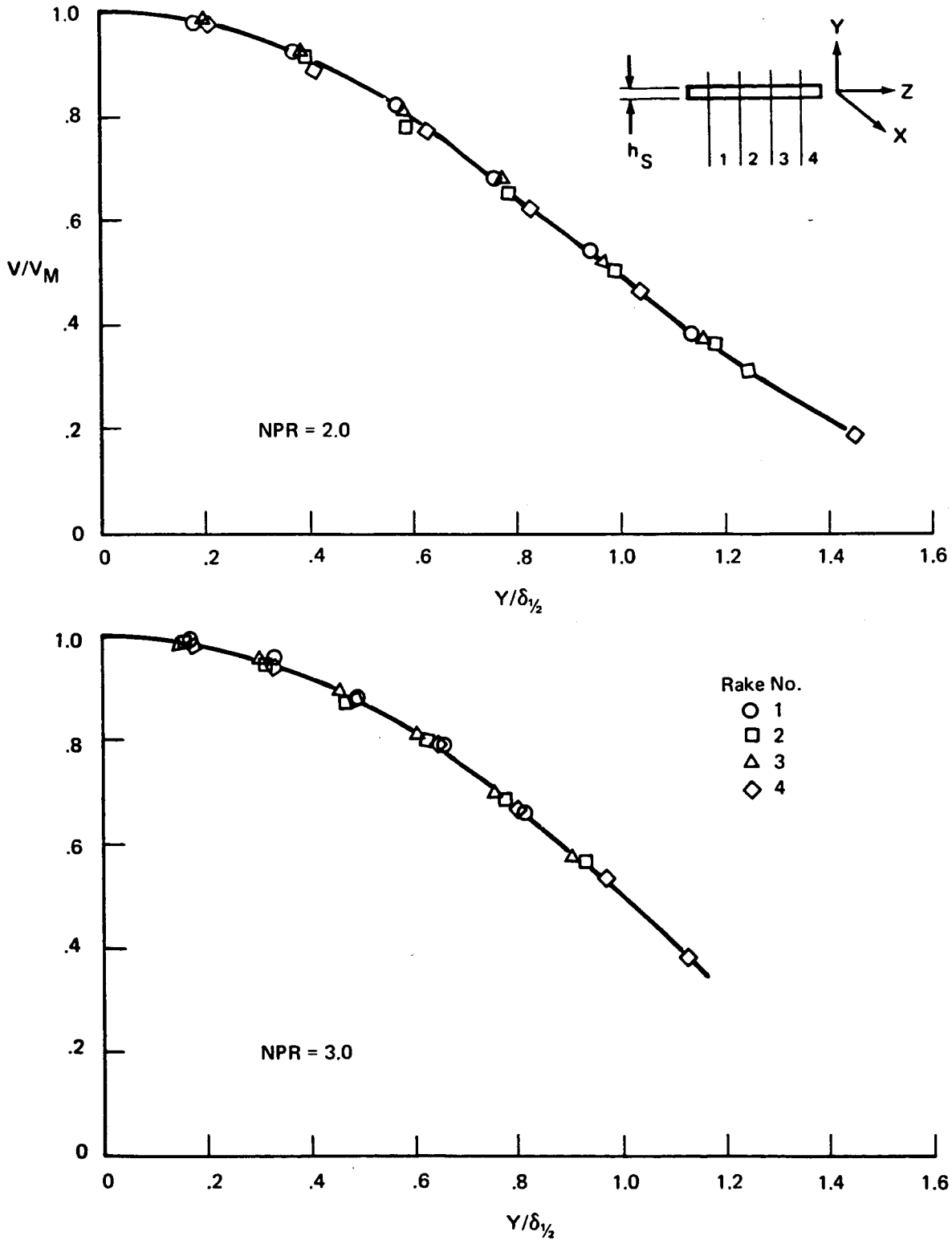

FIGURE 6-69.—SLOT NOZZLE JET VELOCITY PROFILES, AR = 100, X/h_S = 7, RUN 30, 5/7/71

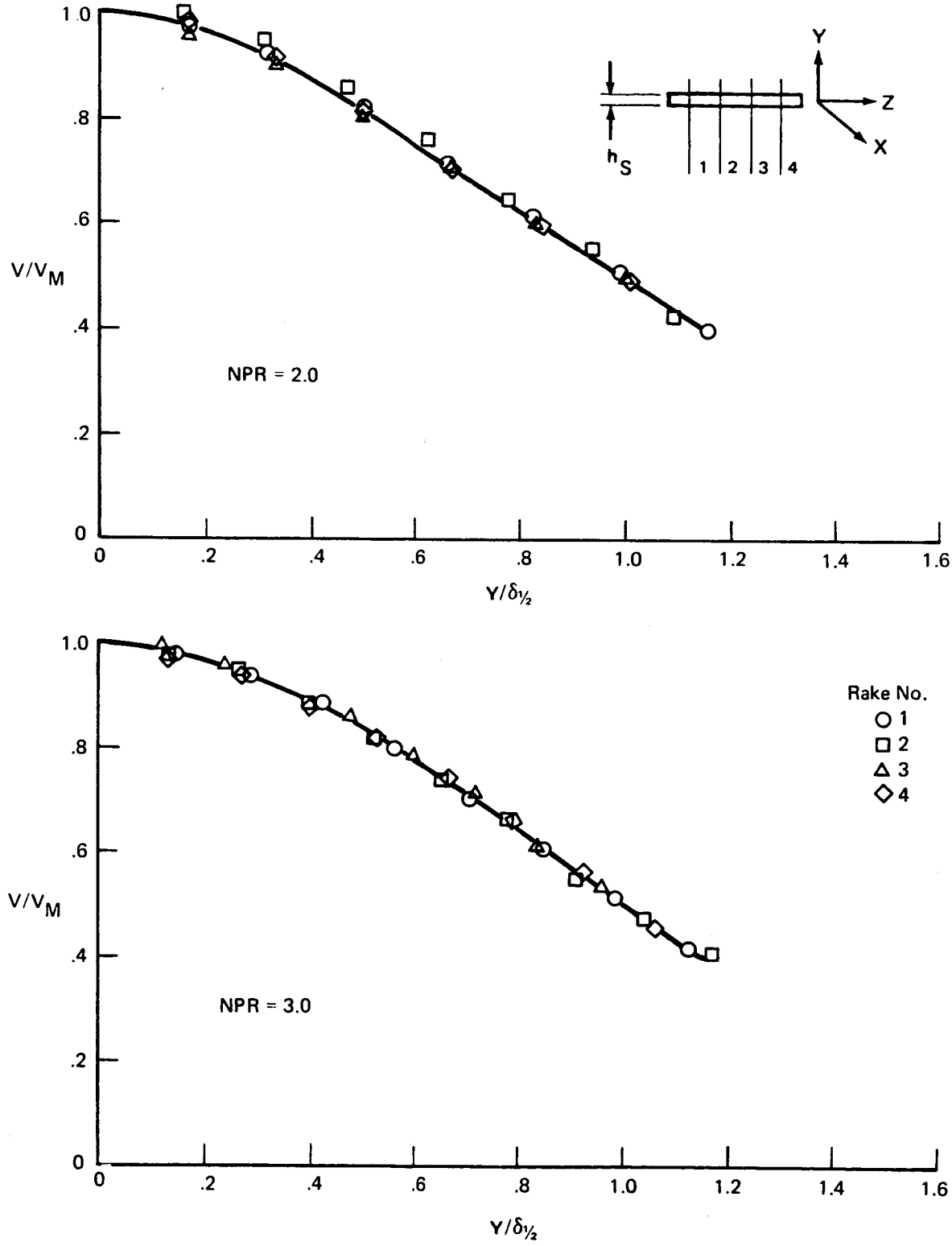

FIGURE 6-70.– SLOT NOZZLE JET VELOCITY PROFILES, AR = 100, X/h_S = 10, RUN 31

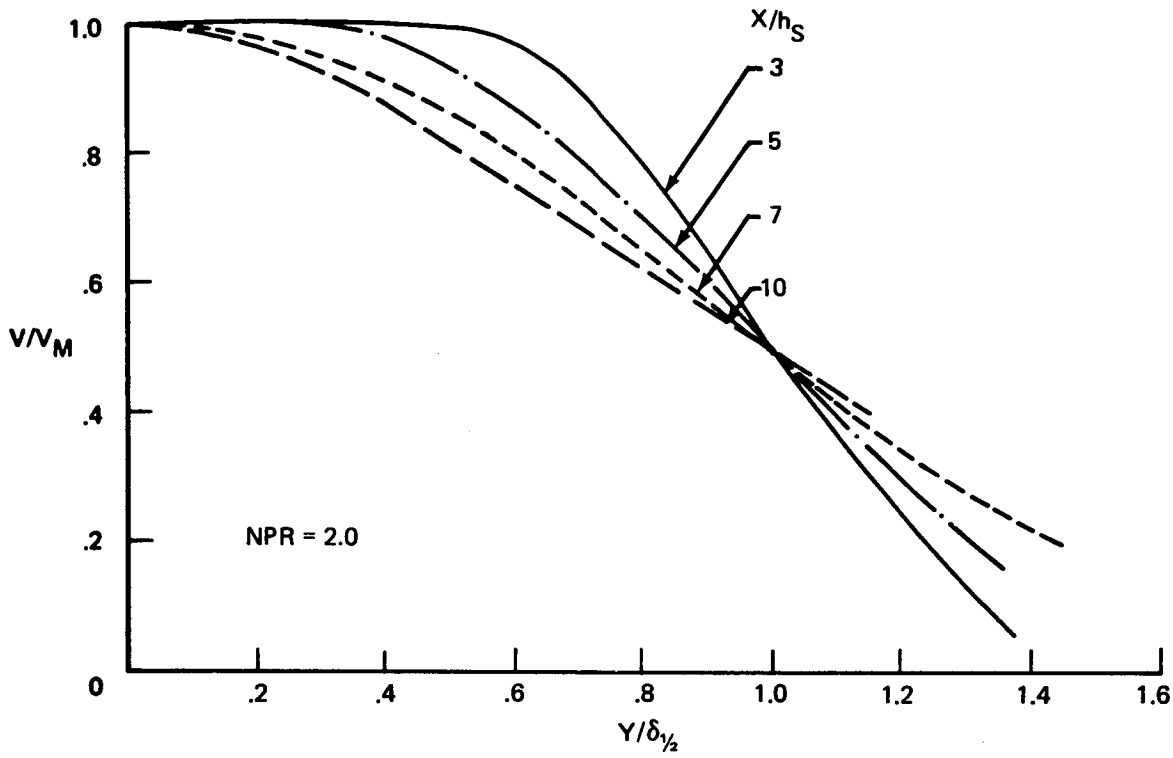

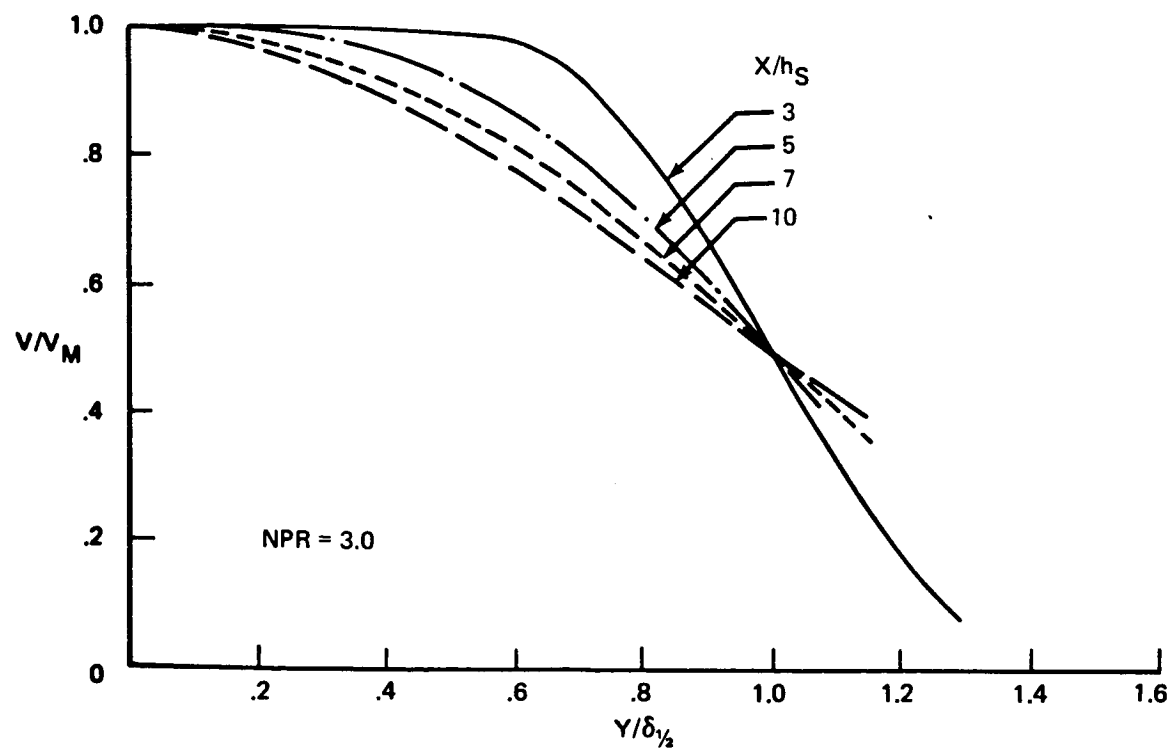

FIGURE 6-71.– SLOT NOZZLE JET VELOCITY PROFILES, AR = 100 SUMMARY CURVE

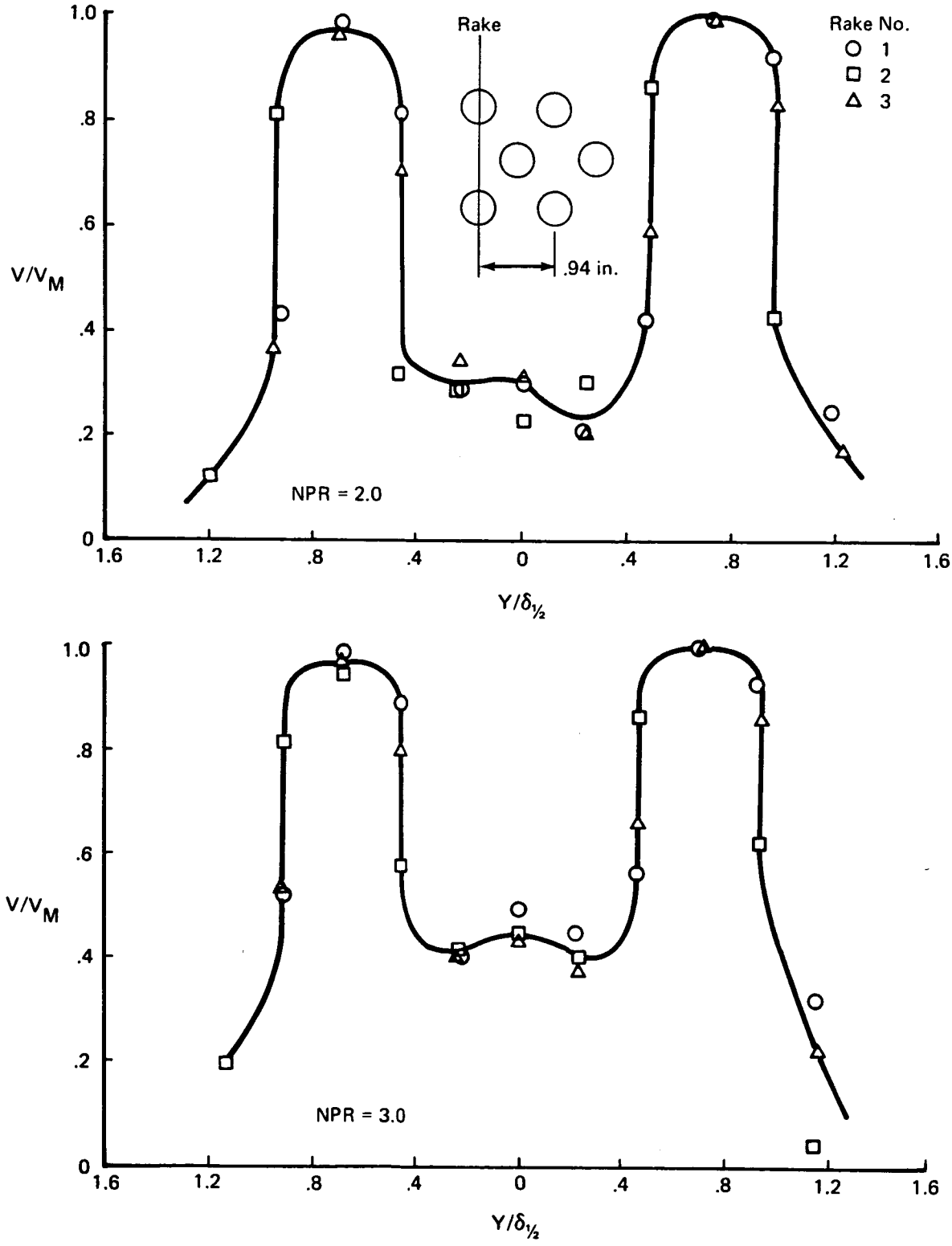

FIGURE 6-72.– JET VELOCITY PROFILES, 140-TUBE NOZZLE, X/h_E = 5, RUN 78

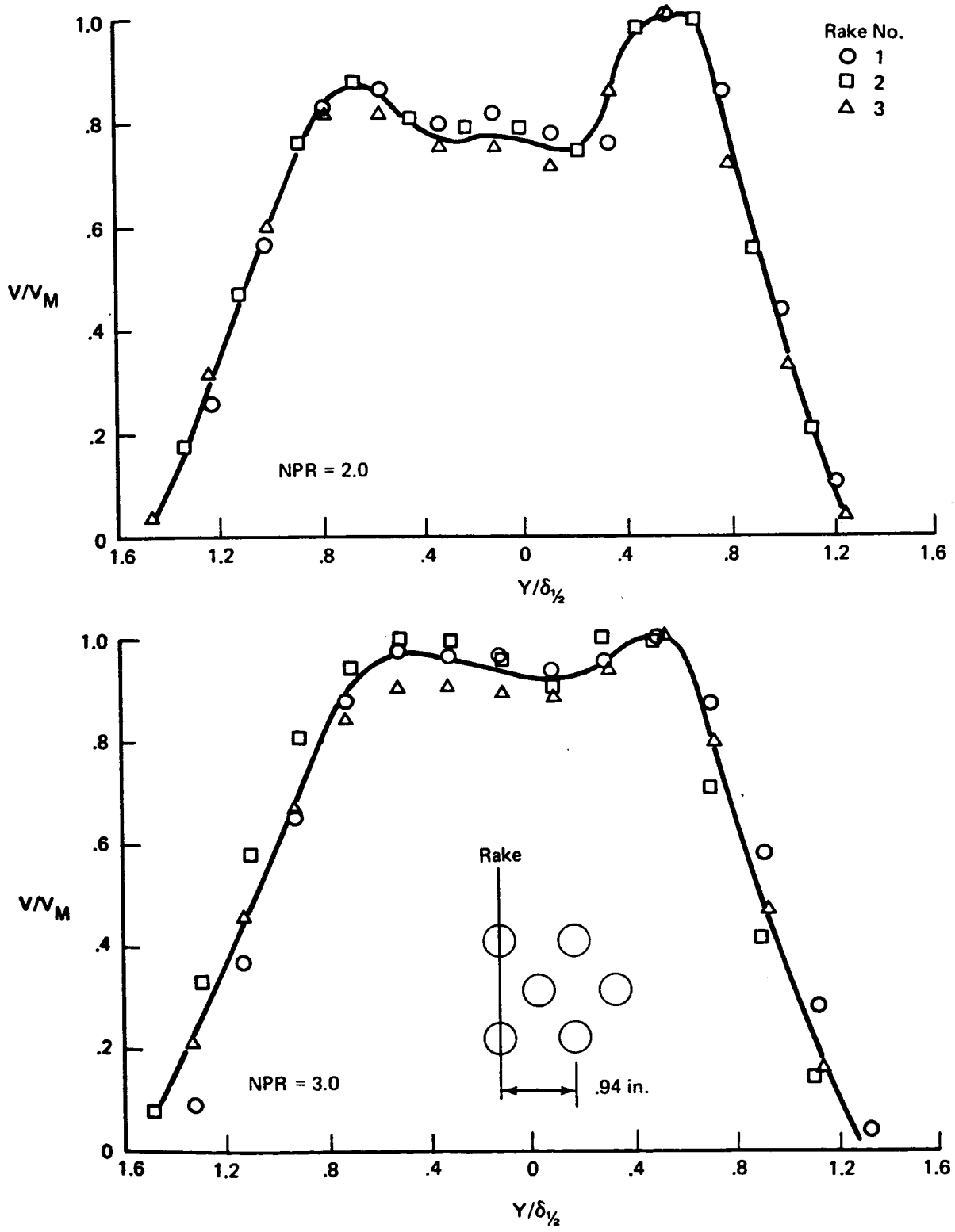

FIGURE 6-73.– JET VELOCITY PROFILES, 140-TUBE NOZZLE, X/h_E = 10, RUN 91

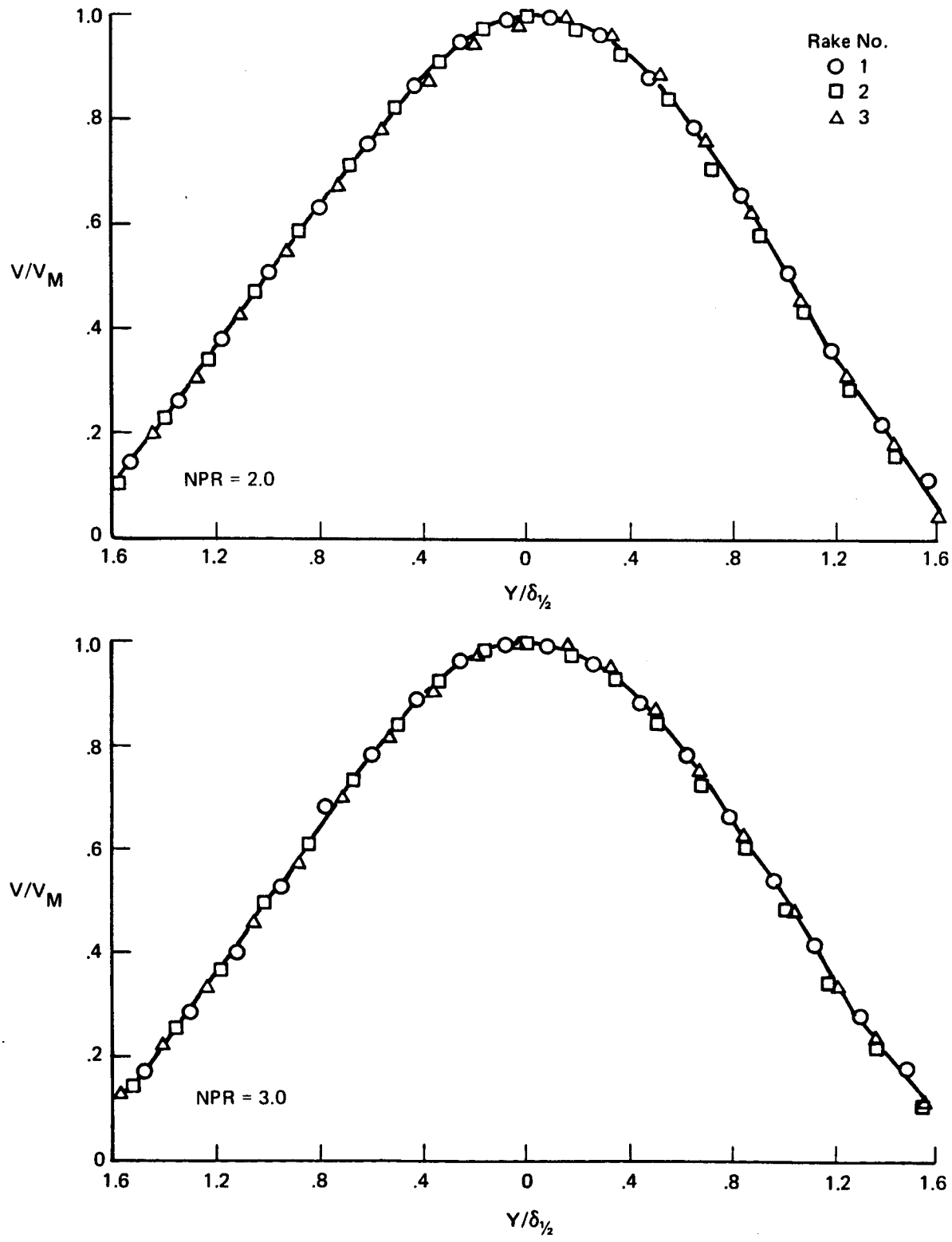

FIGURE 6-74.—JET VELOCITY PROFILES, 140-TUBE NOZZLE, $X/h_E = 20$, RUN 98

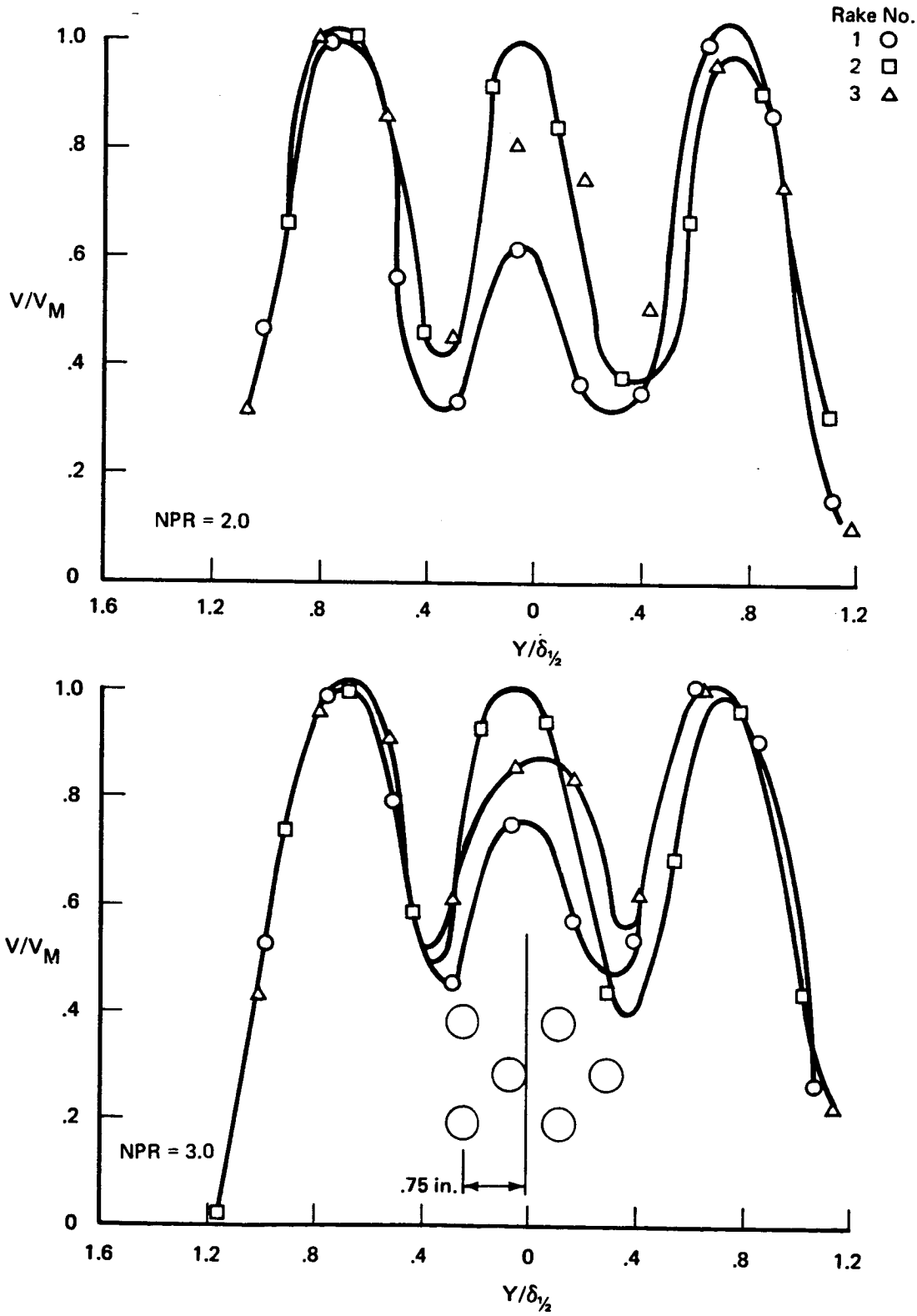

FIGURE 6-75.– JET VELOCITY PROFILES, 140-TUBE NOZZLE, $X/h_E = 5$, RUN 88

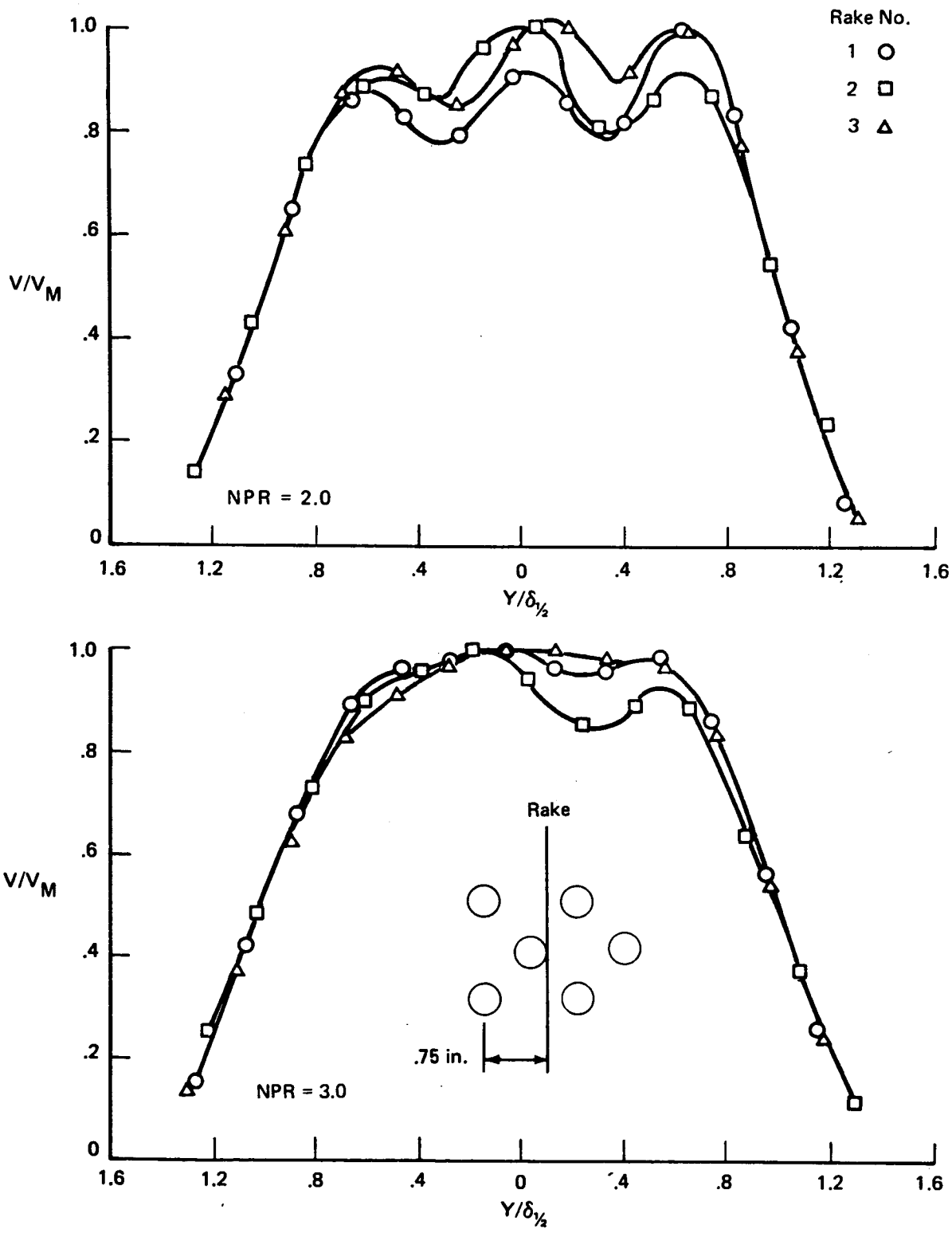

FIGURE 6-76.– JET VELOCITY PROFILES, 140-TUBE NOZZLE, X/h_E = 10, RUN 96

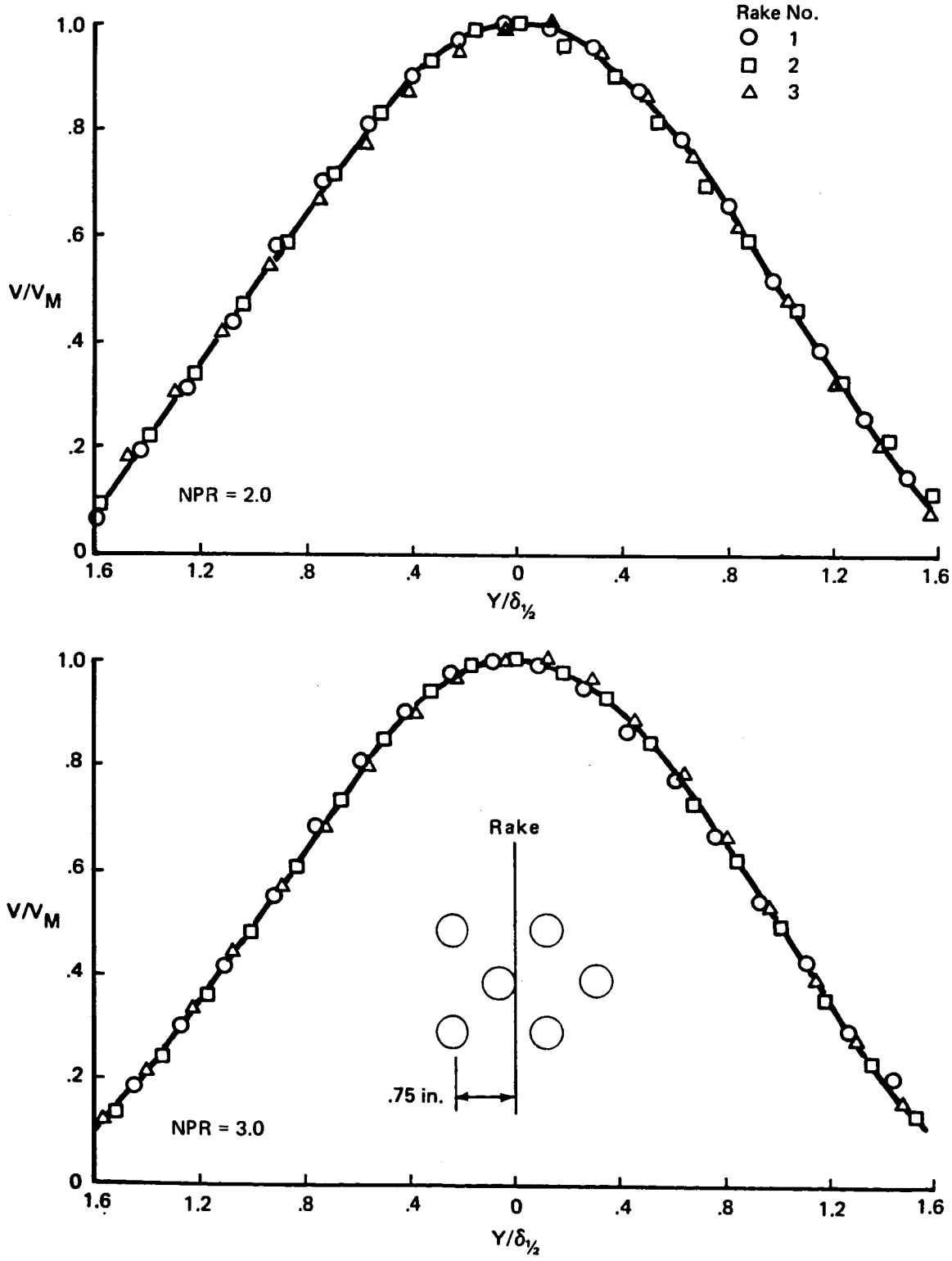

FIGURE 6-77.—JET VELOCITY PROFILES, 140-TUBE NOZZLE, $X/h_E = 20$, RUN 103

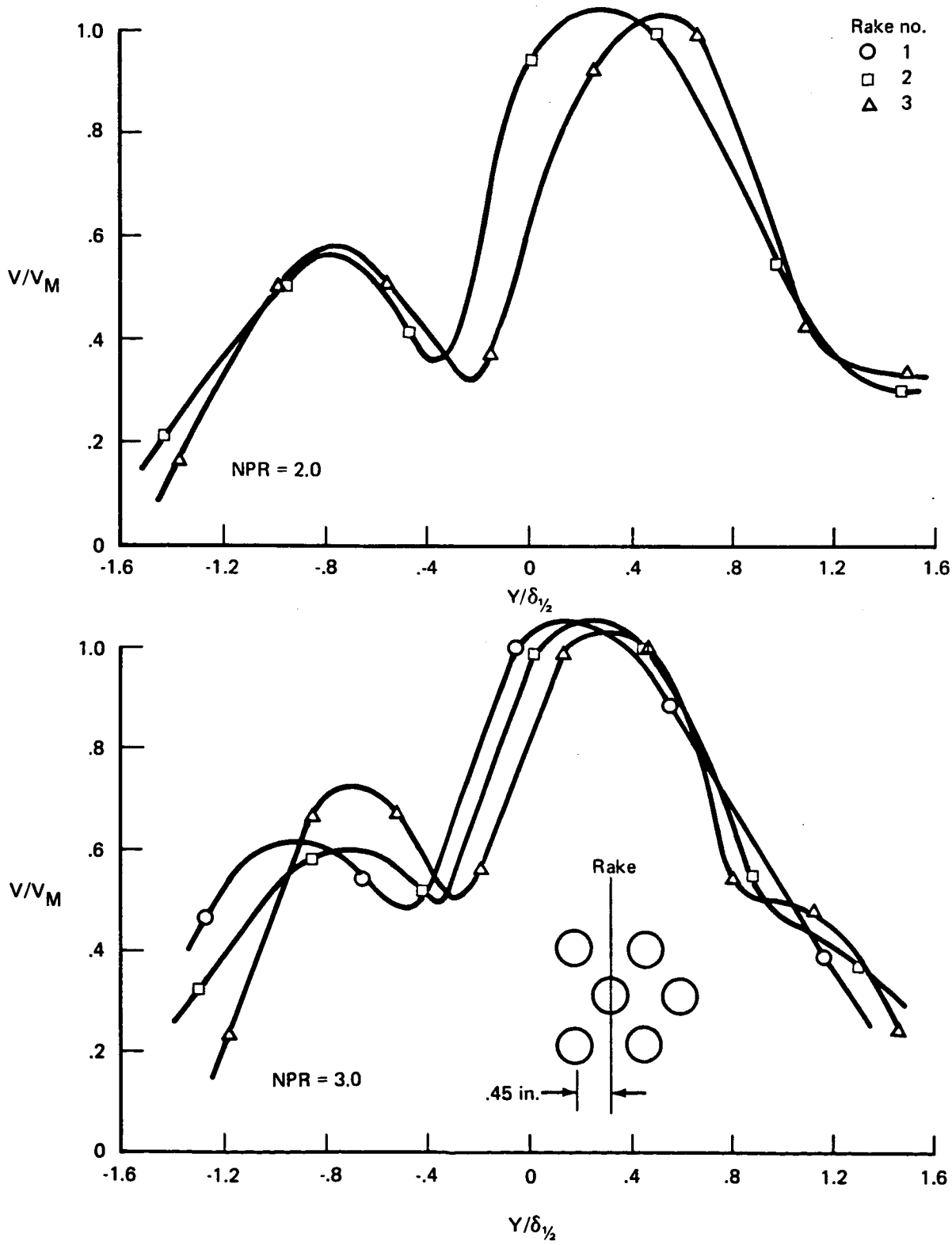

FIGURE 6-78.– JET VELOCITY PROFILES, 140-TUBE NOZZLE, $X/h_E = 5$, RUN 84

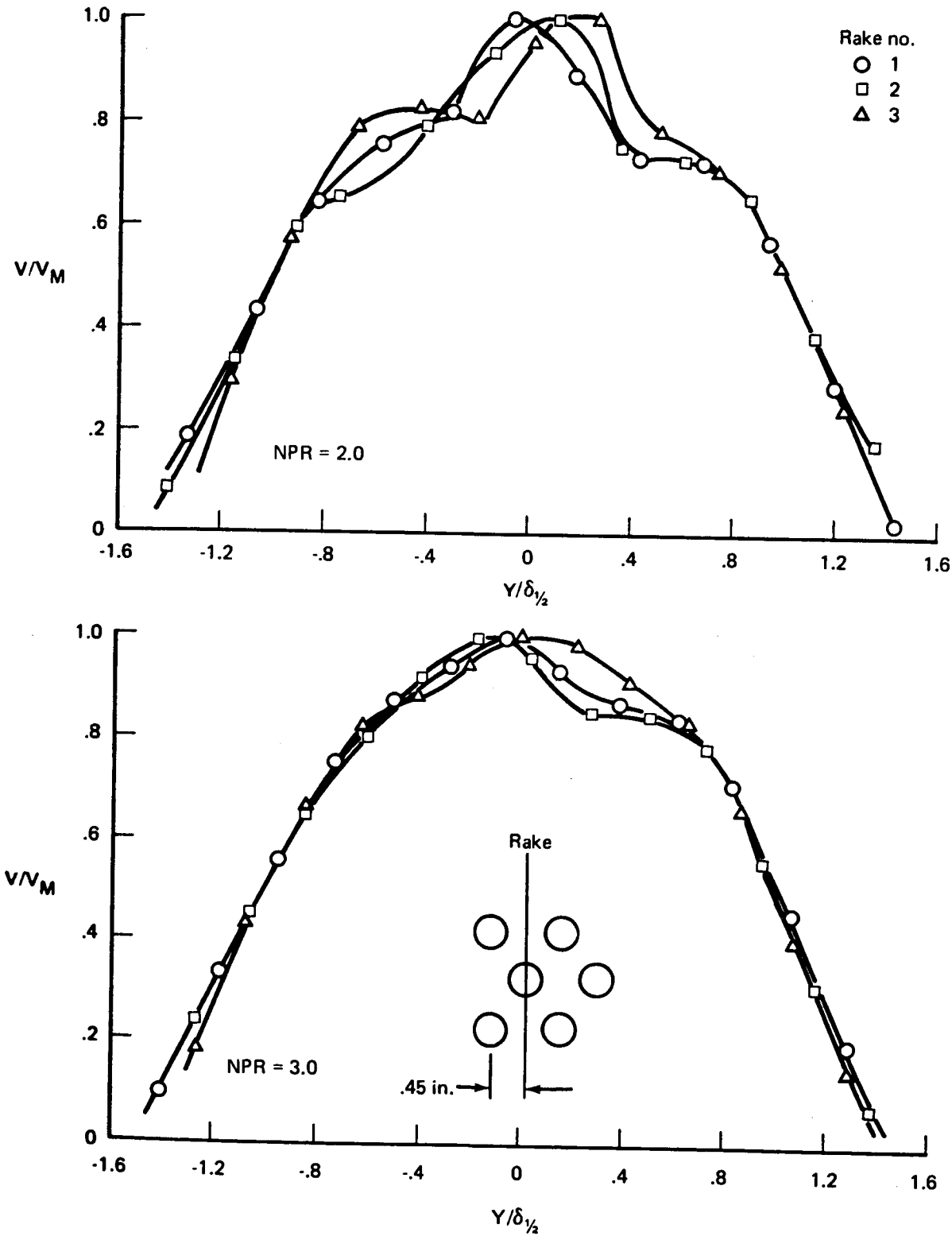

FIGURE 6-79.—JET VELOCITY PROFILES, 140-TUBE NOZZLE, $X/h_E = 10$, RUN 94

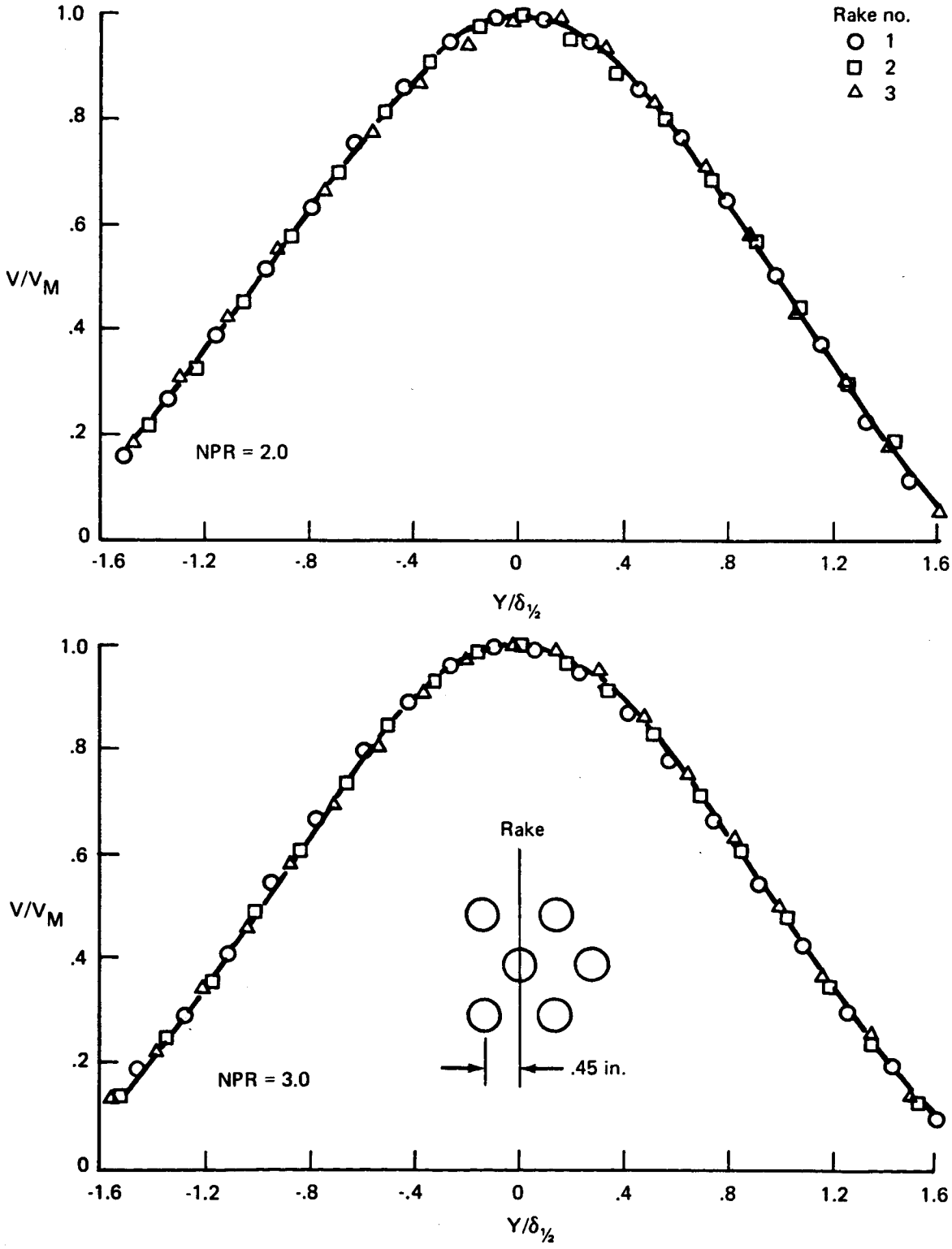

FIGURE 6-80.—JET VELOCITY PROFILES, 140-TUBE NOZZLE, $X/h_E = 20$, RUN 101

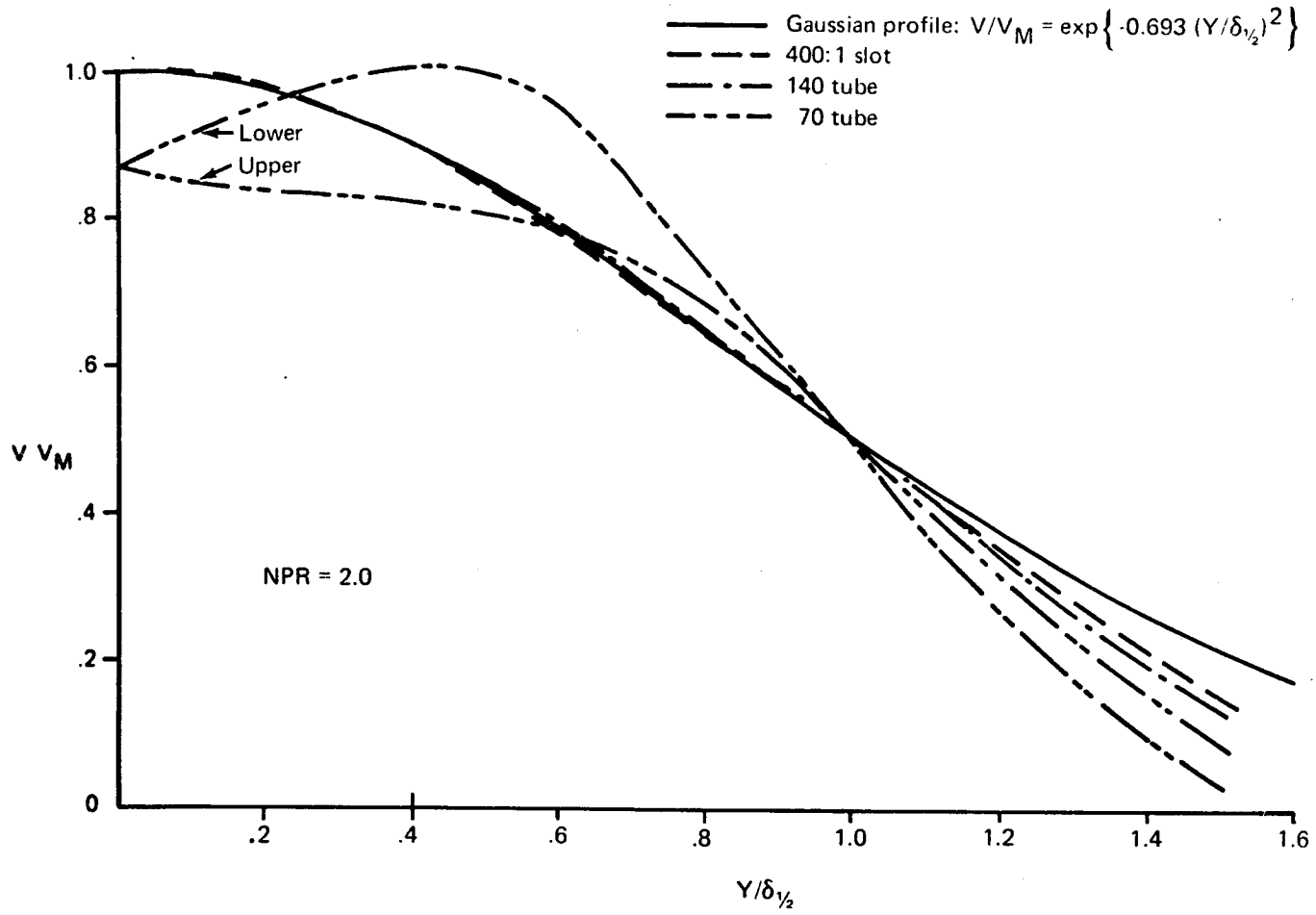

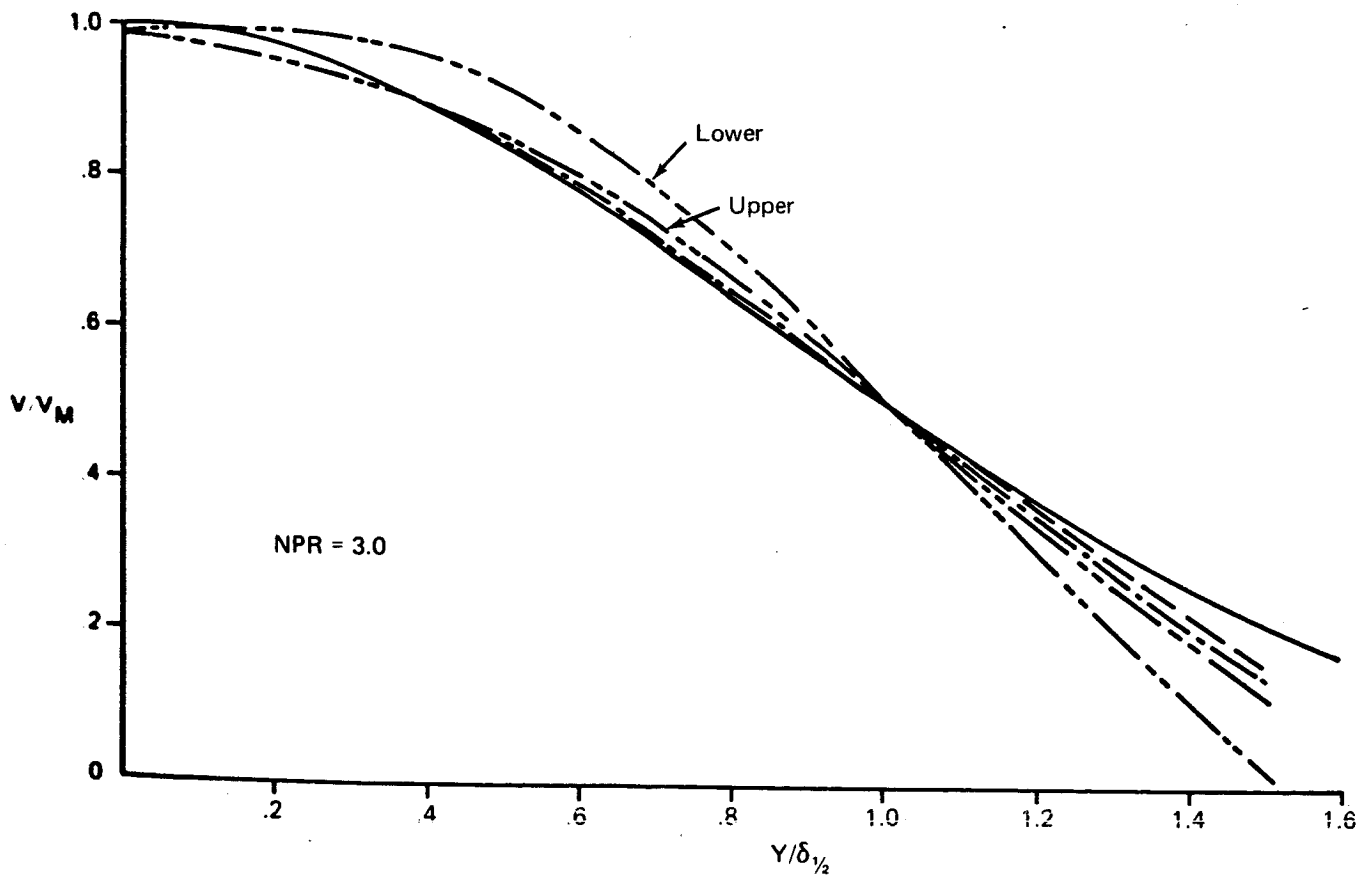

FIGURE 6-81.–PRIMARY NOZZLE VELOCITY PROFILES

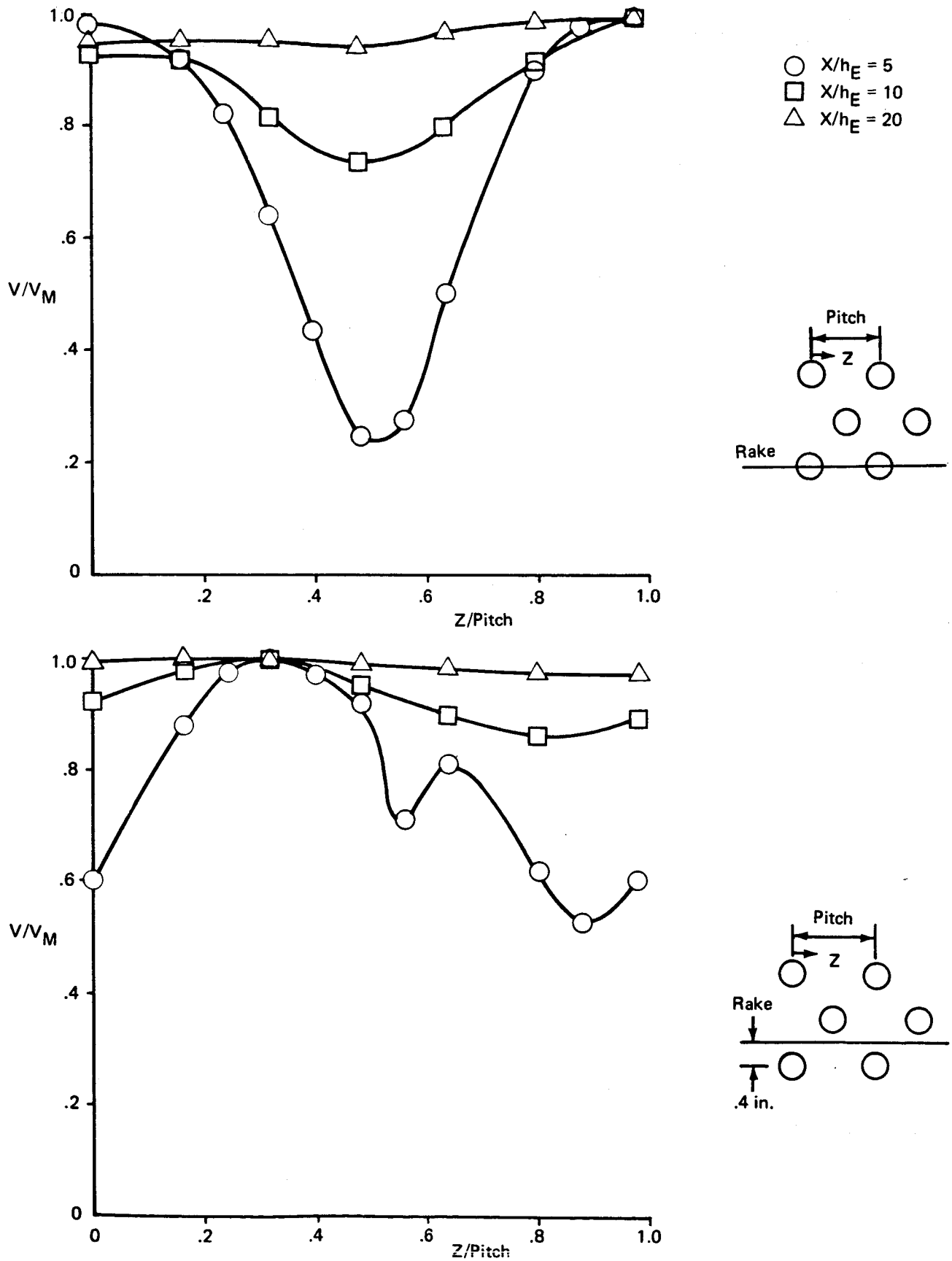

FIGURE 6-82.—SPANWISE VELOCITY PROFILES, 140-TUBE NOZZLE

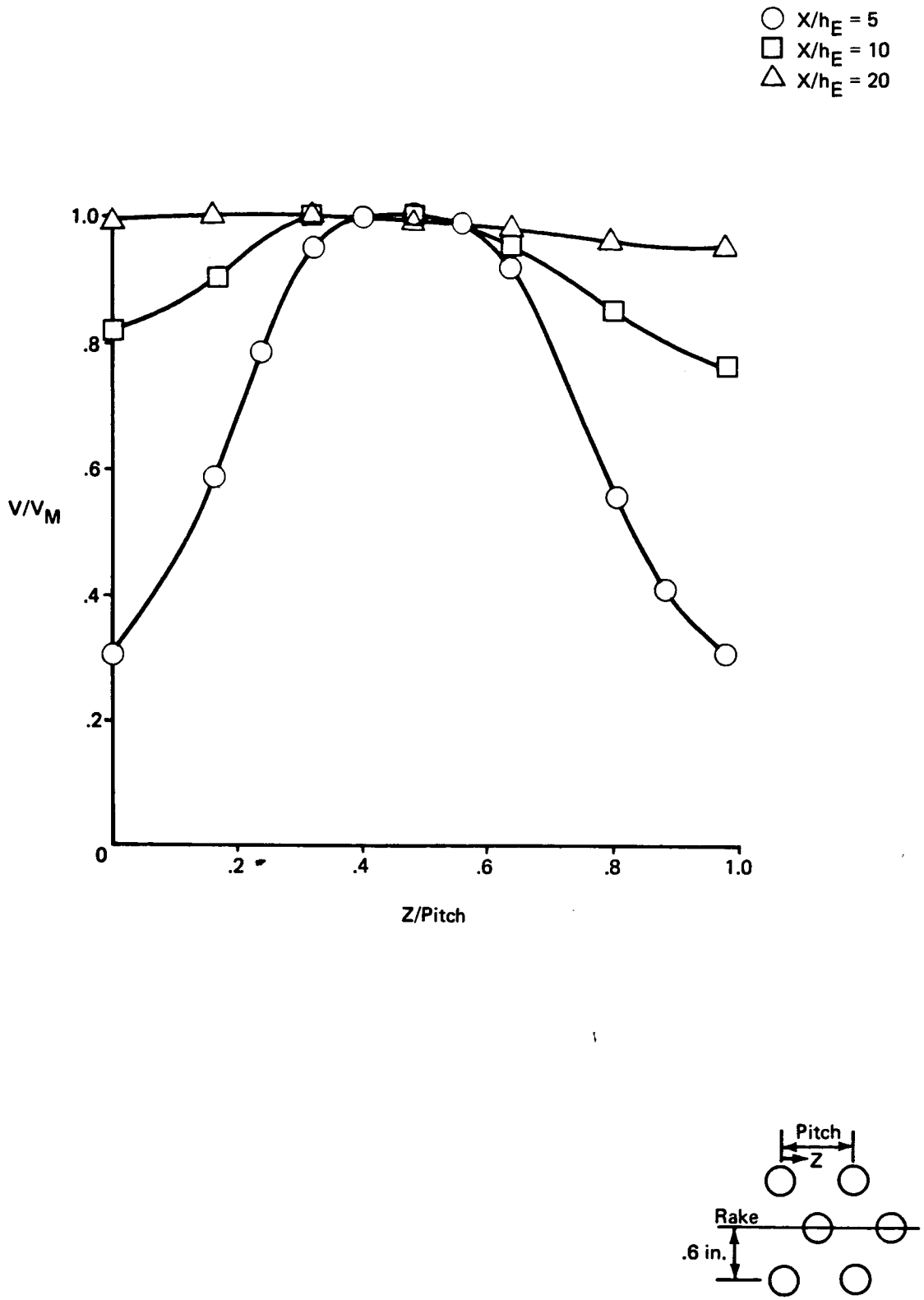

FIGURE 6-83.—SPANWISE VELOCITY PROFILES, 140-TUBE NOZZLE

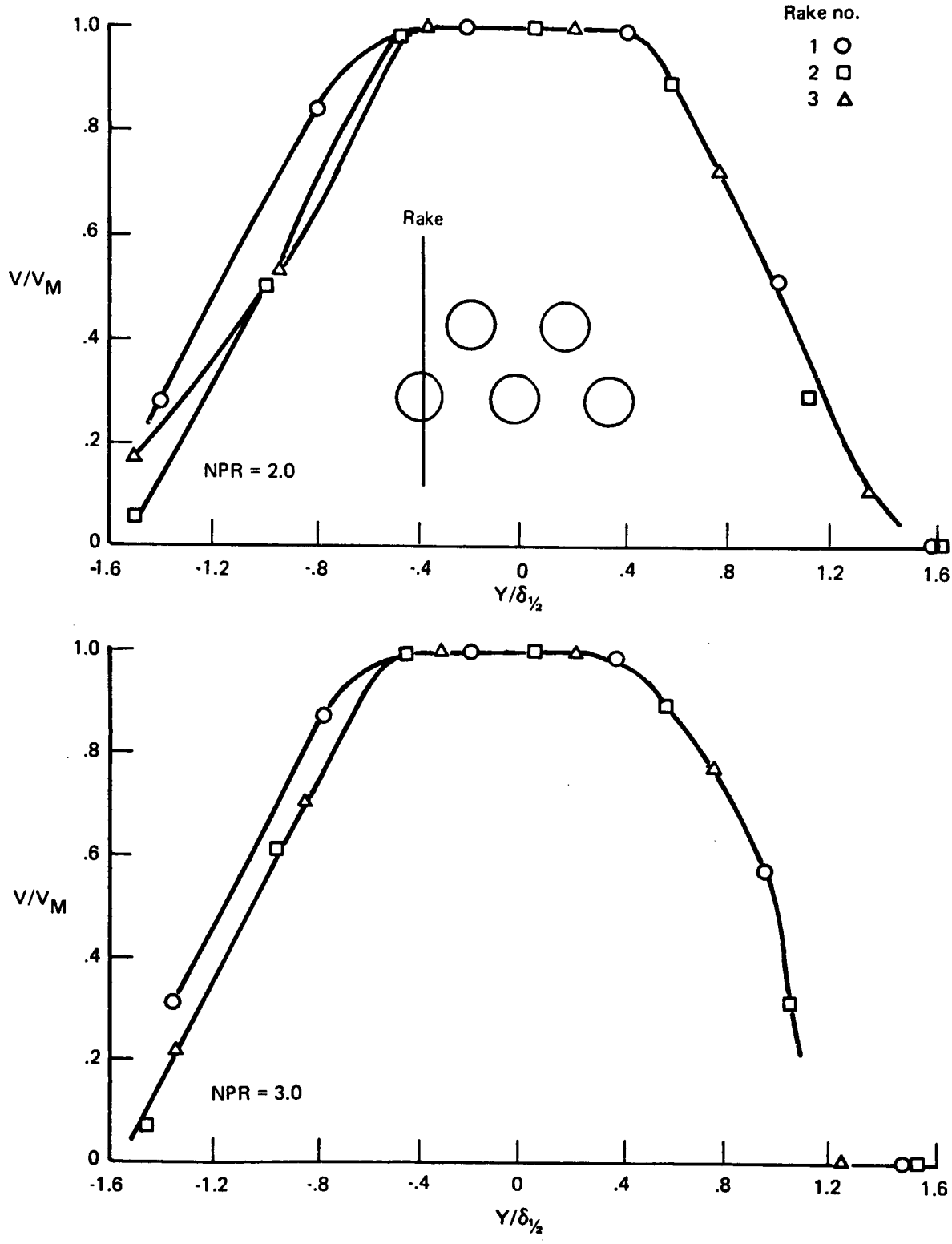

FIGURE 6-84.—JET VELOCITY PROFILES, 70-TUBE NOZZLE, $X/h_E = 5$, RUN 119

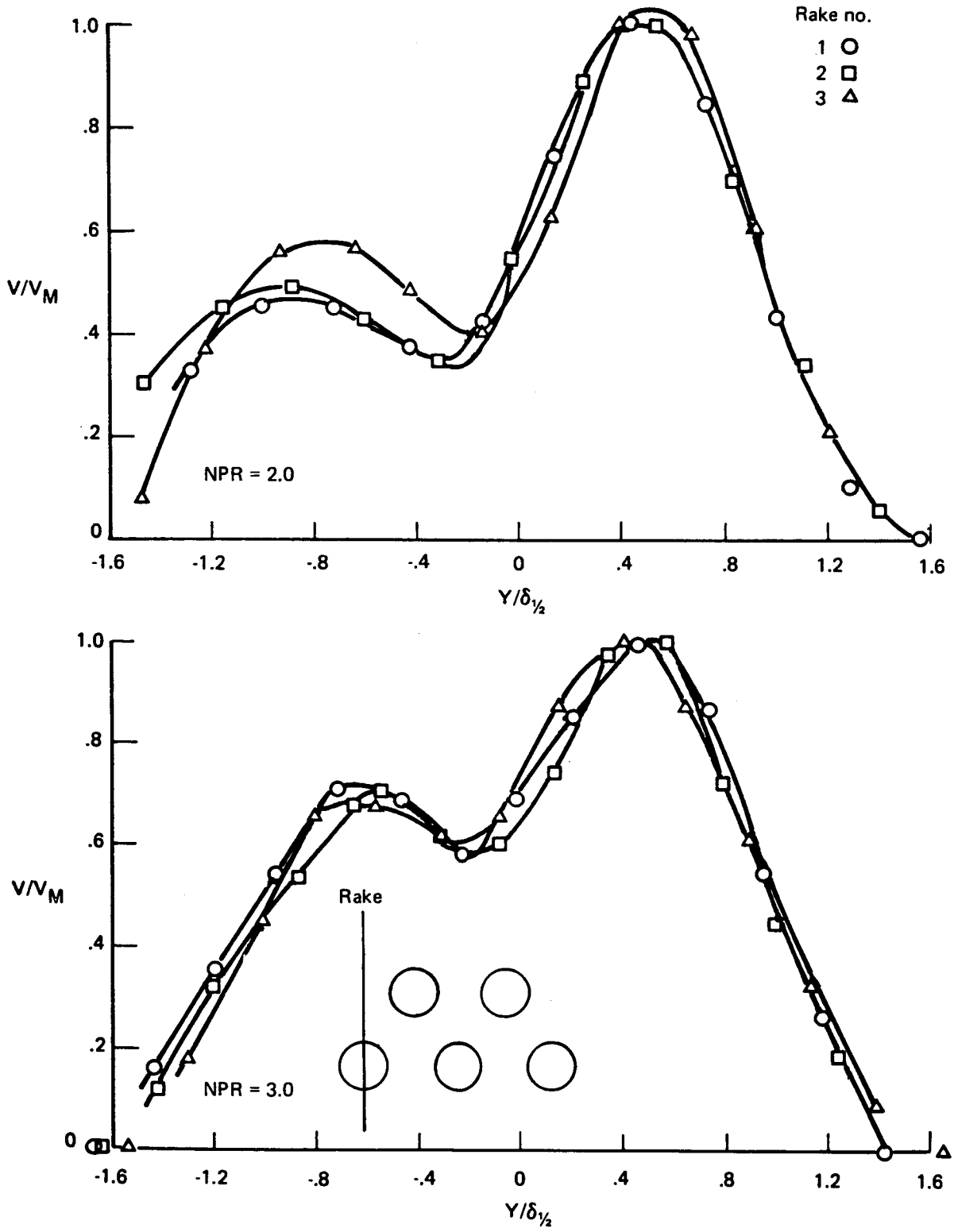

FIGURE 6-85.—JET VELOCITY PROFILES, 70-TUBE NOZZLE, $X/h_E = 10$, RUN 132

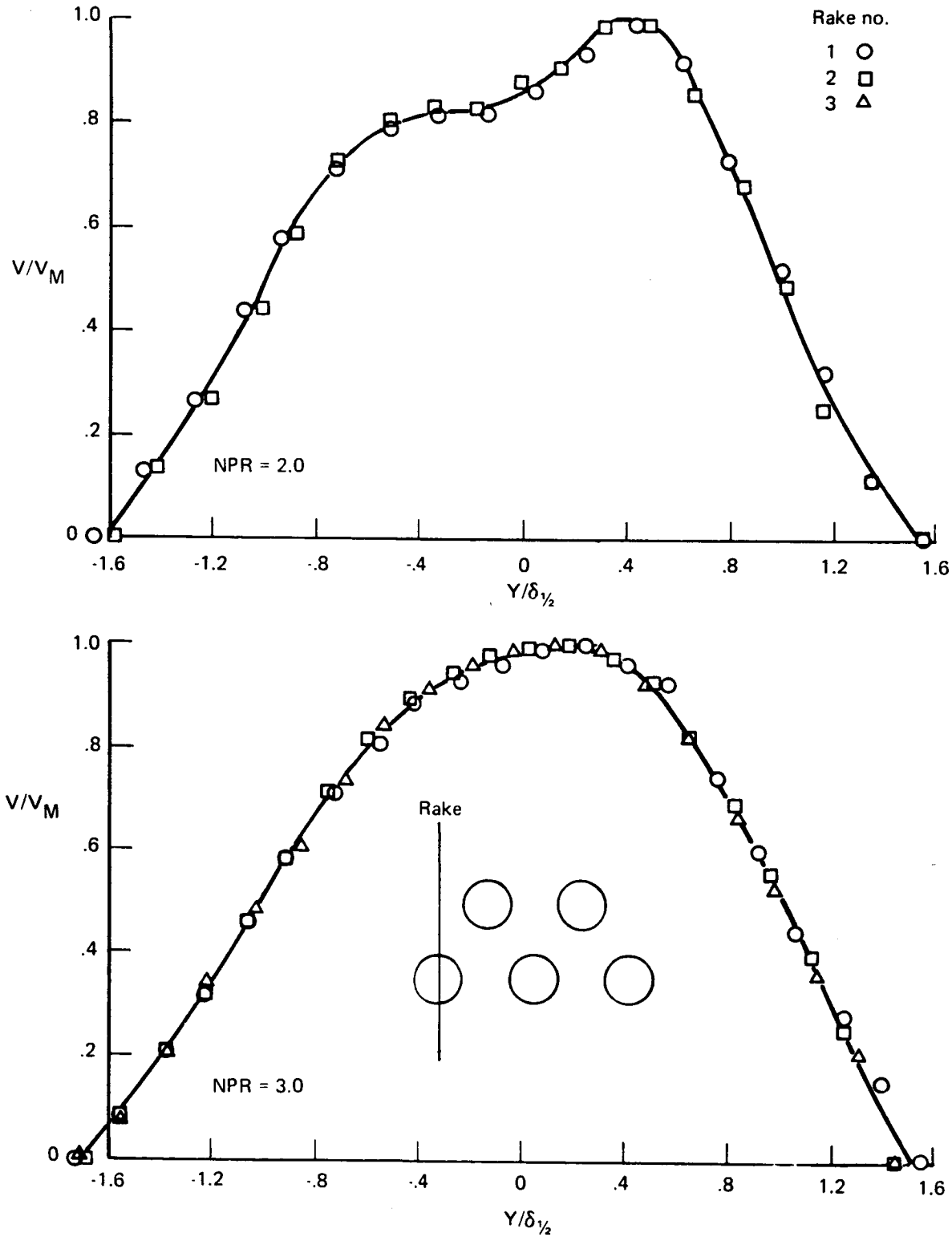

FIGURE 6-86.–JET VELOCITY PROFILES, 70-TUBE NOZZLE, X/h_E = 20, RUN 144

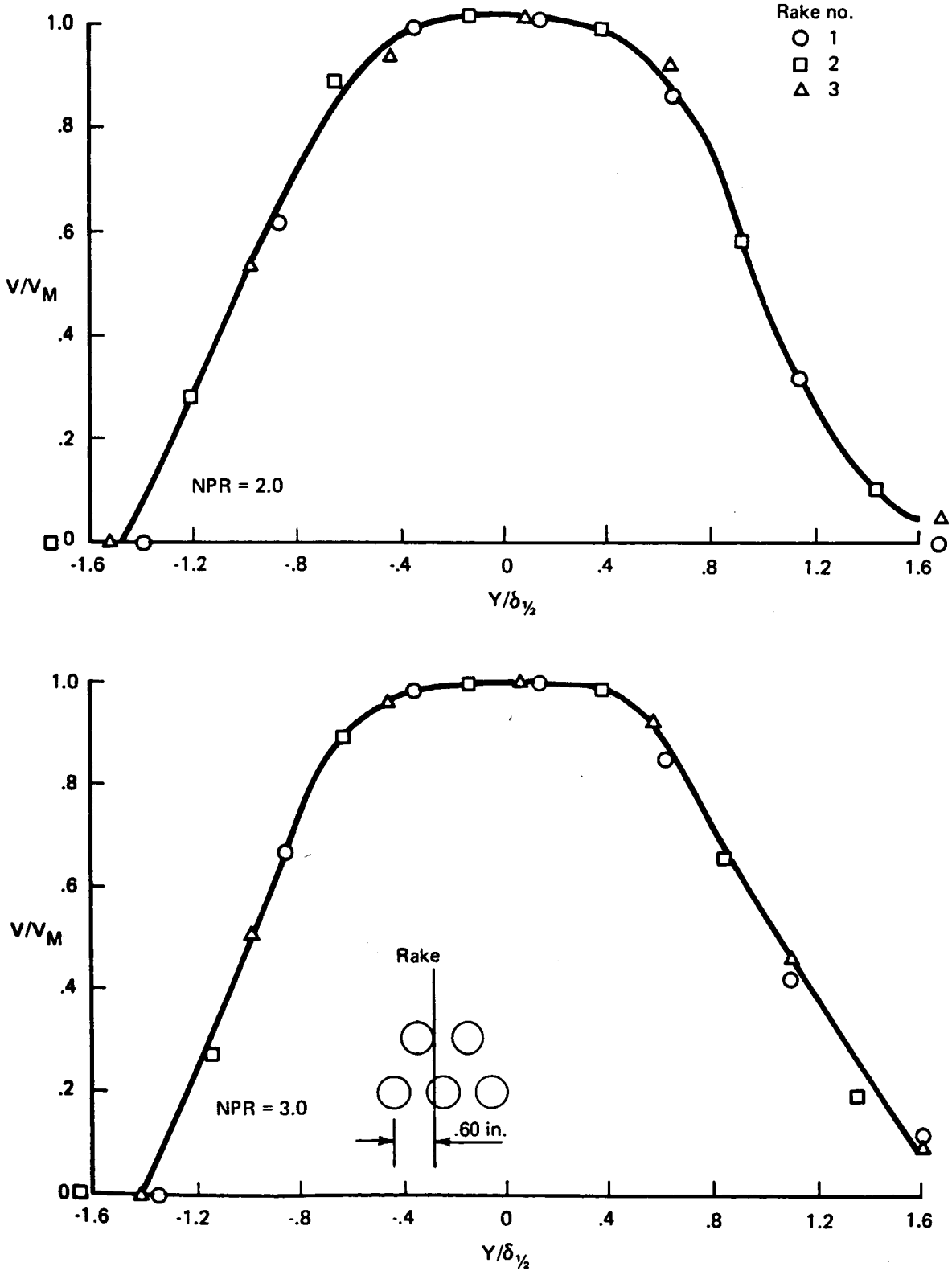

FIGURE 6-87.—JET VELOCITY PROFILES, 70-TUBE NOZZLE, $X/h_E = 5$, RUN 125

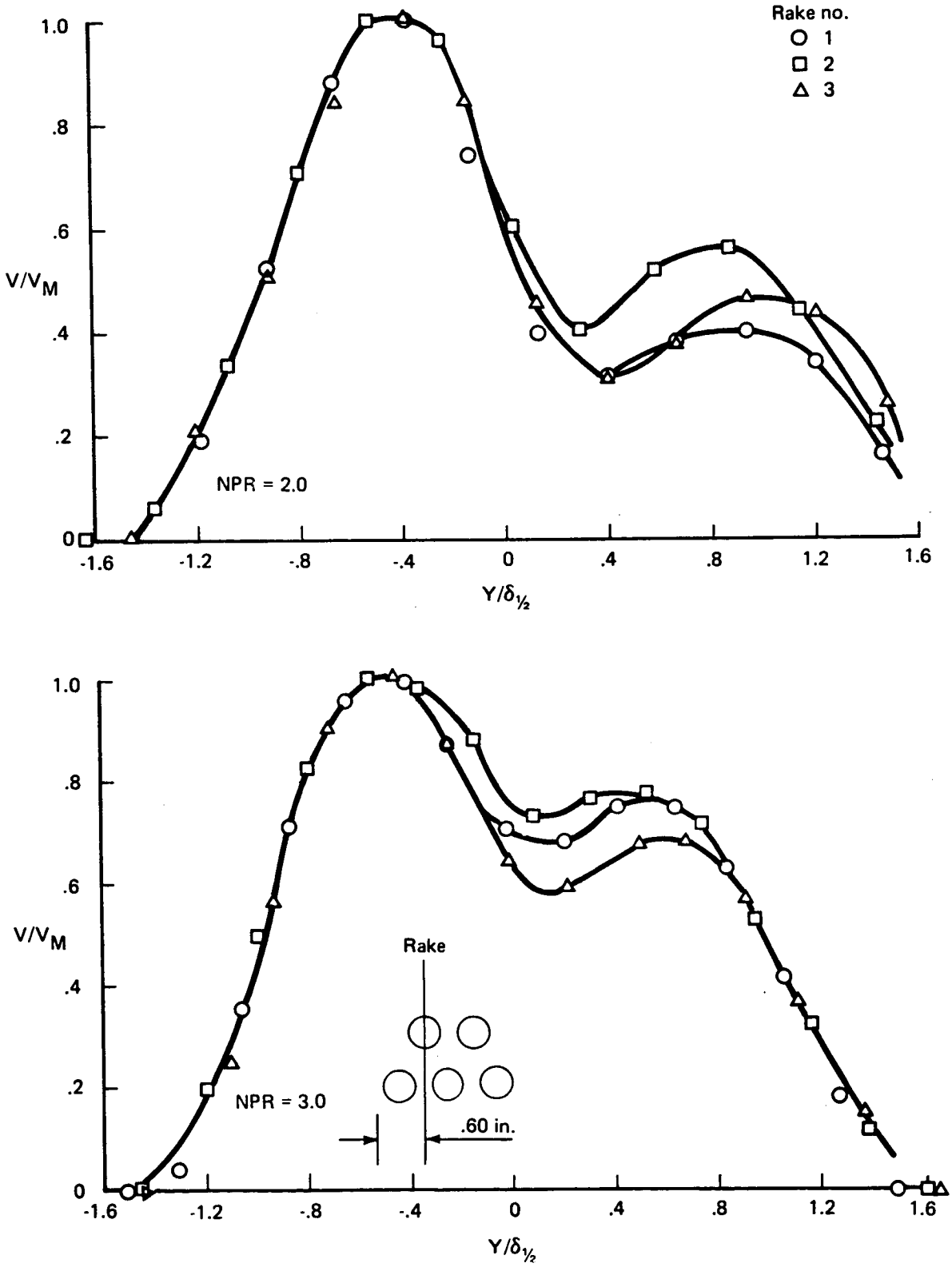

FIGURE 6-88.—JET VELOCITY PROFILES, 70-TUBE NOZZLE, $X/h_E = 10$, RUN 140

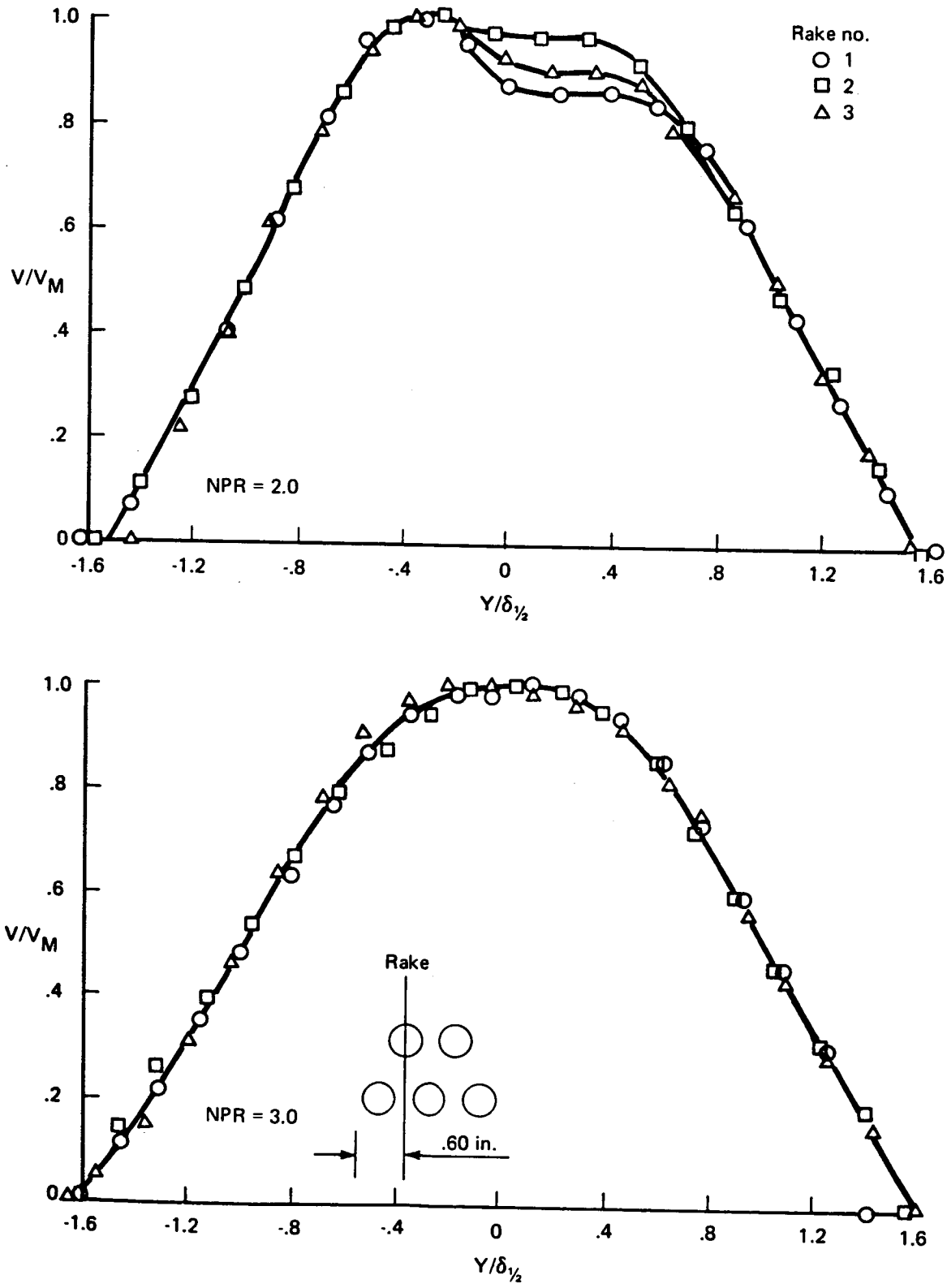

FIGURE 6-89.—JET VELOCITY PROFILES, 70-TUBE NOZZLE, $X/h_E = 20$, RUN 147

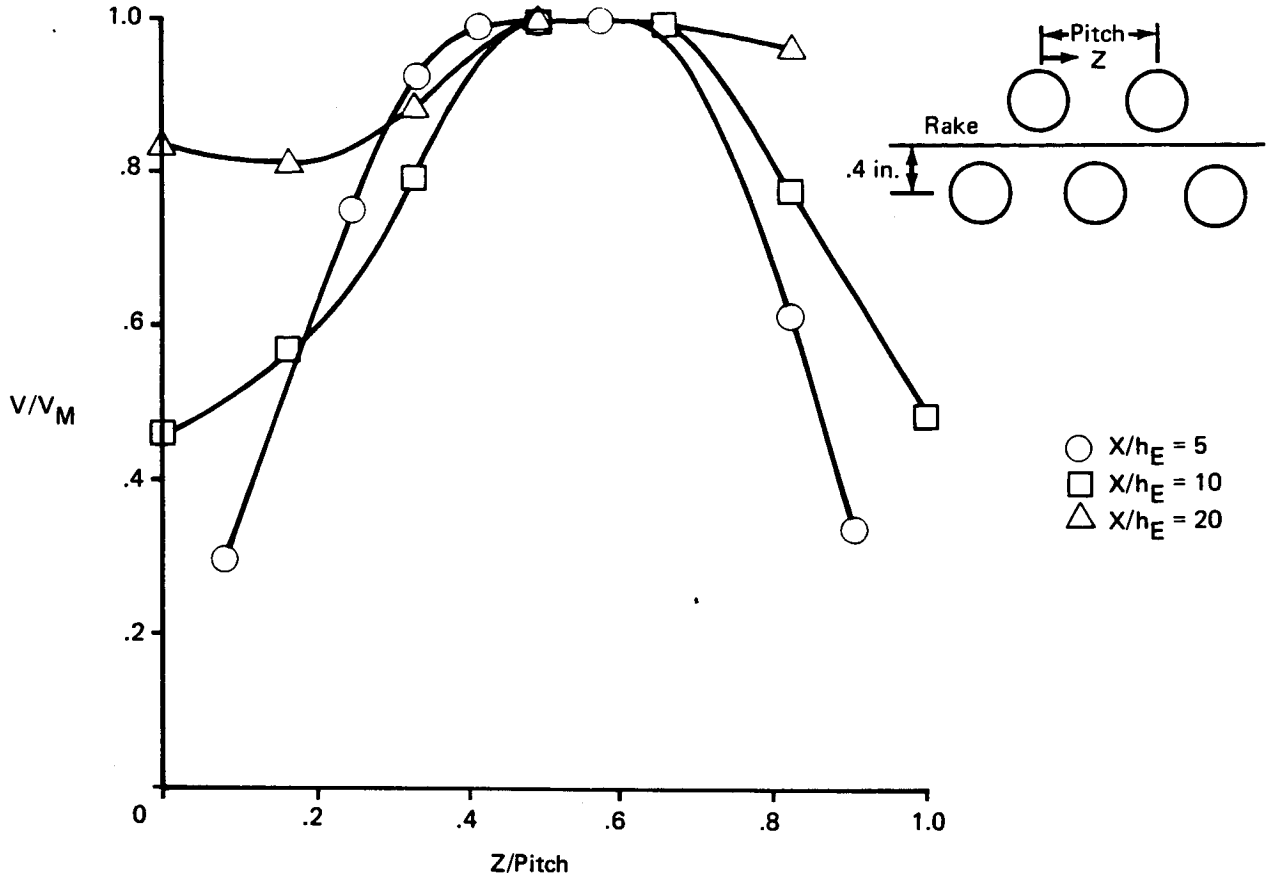

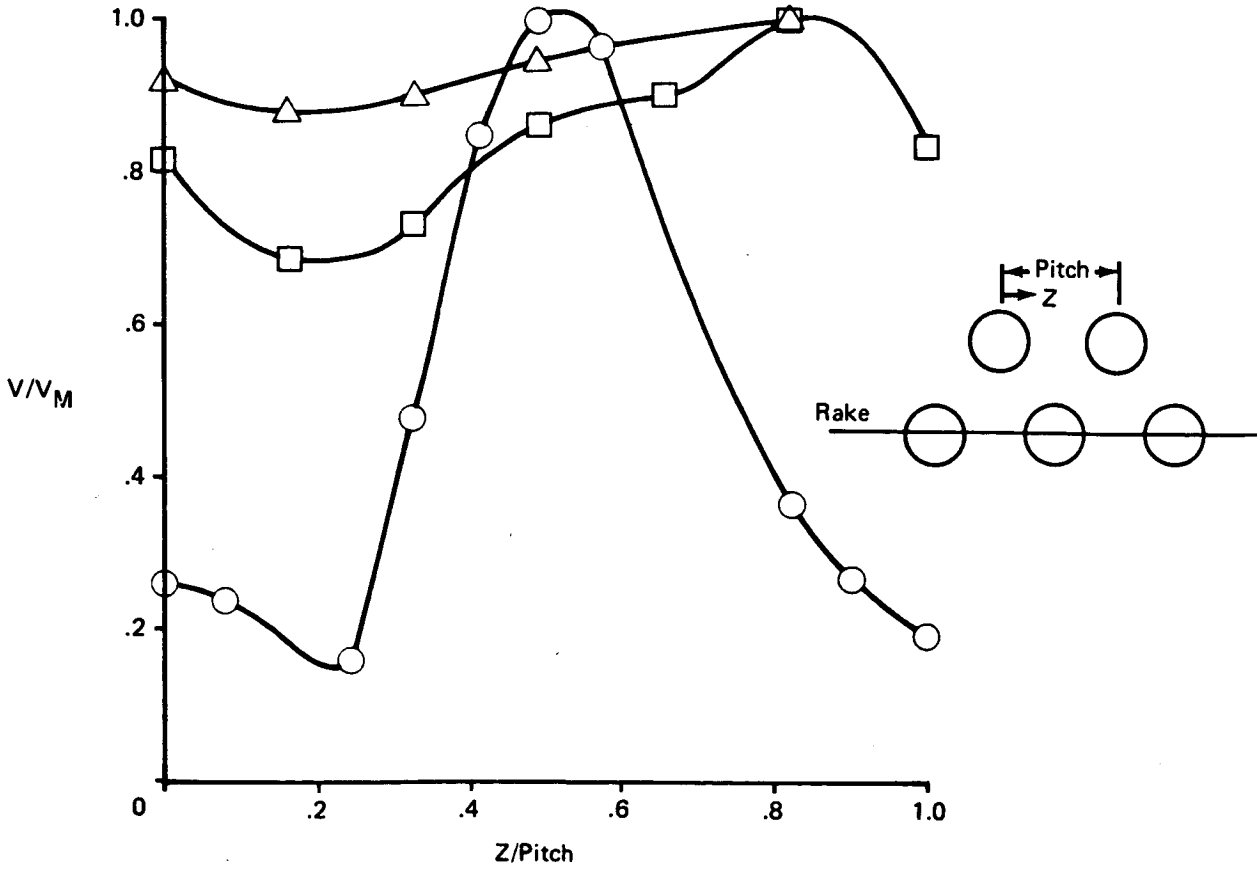

FIGURE 6-90.—SPANWISE VELOCITY PROFILES, 70-TUBE NOZZLE

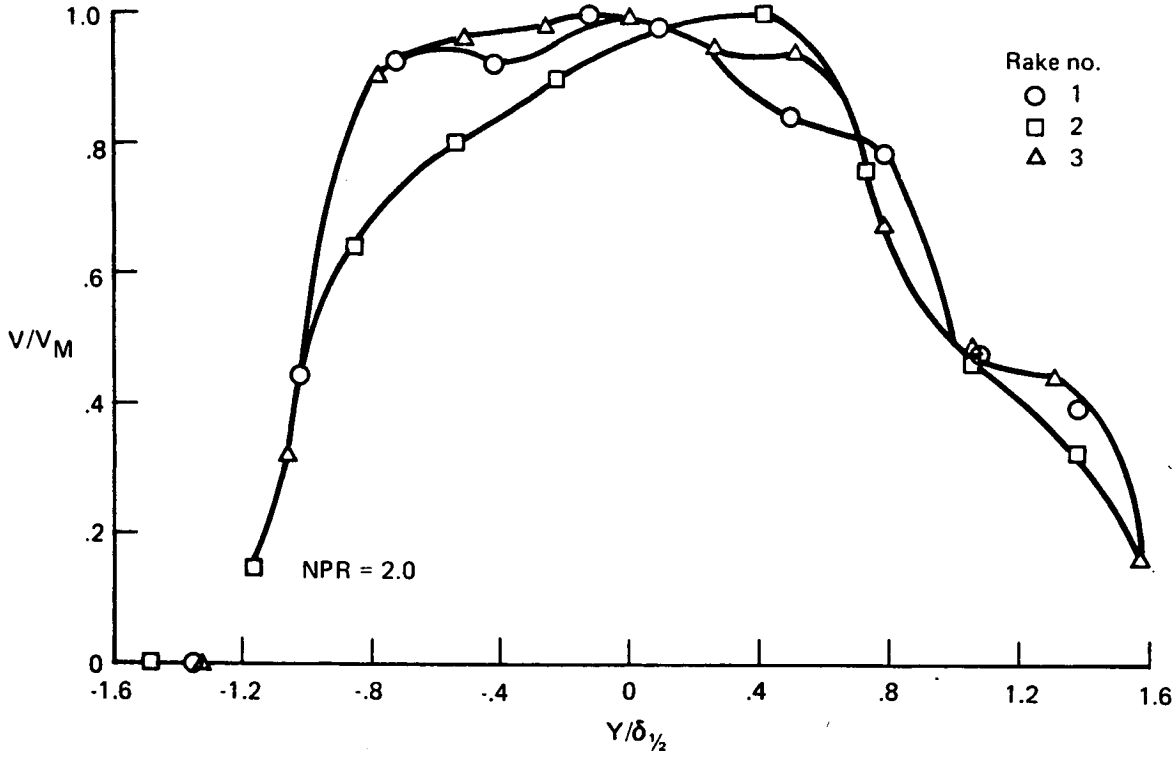

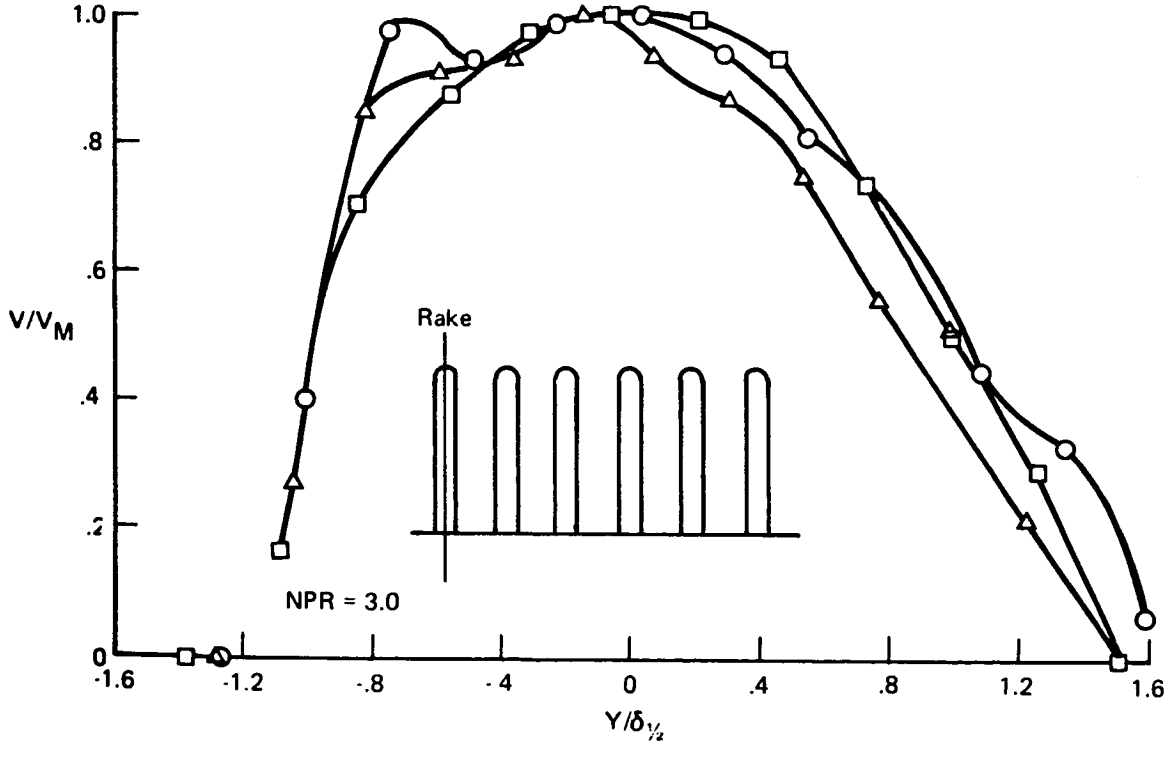

FIGURE 6-91.—JET VELOCITY PROFILES, THIN-LOBE NOZZLE, $X/h_E = 5$, RUN 159 (A.R. = 4.0)

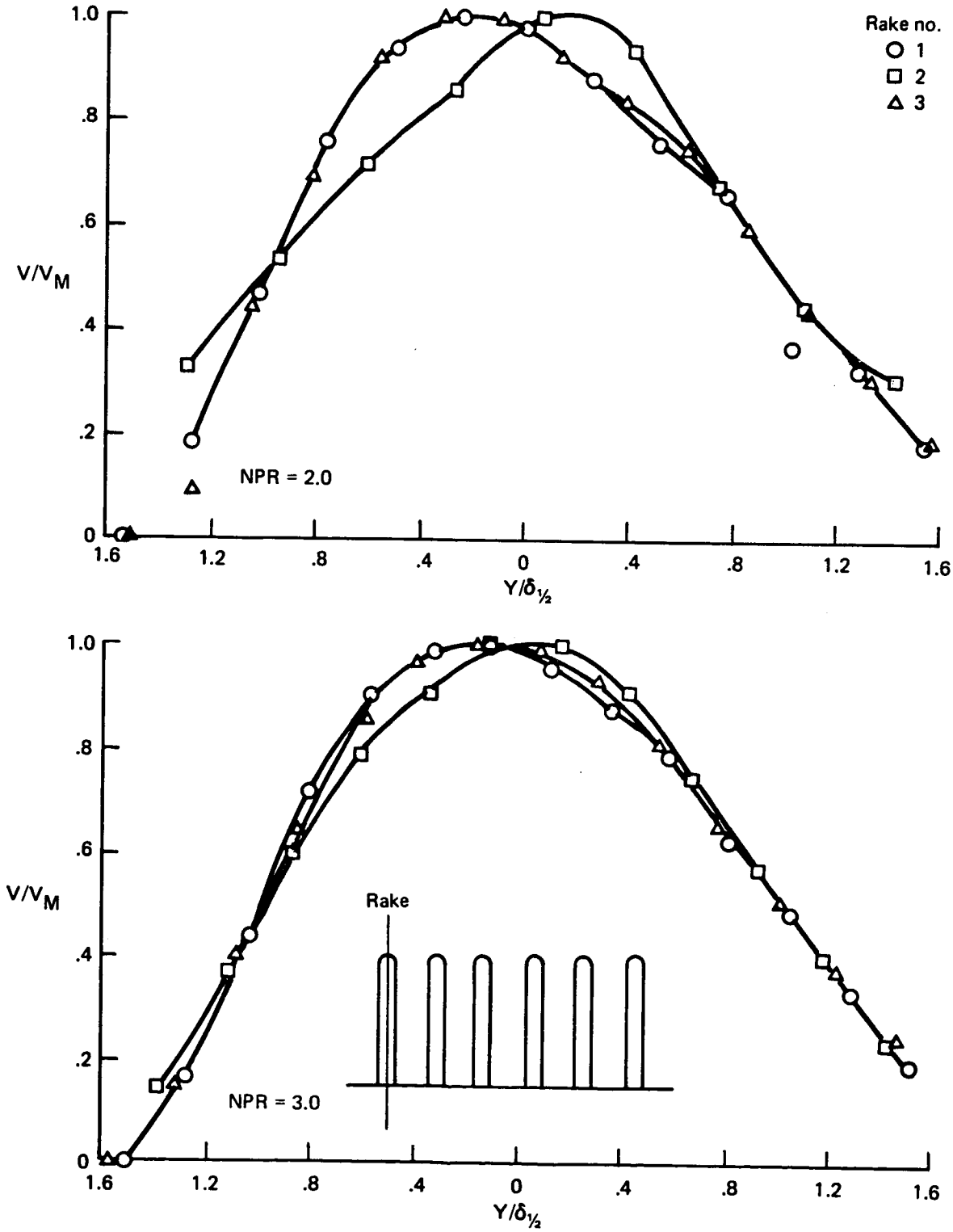

FIGURE 6-92.–JET VELOCITY PROFILES, THIN-LOBE NOZZLE, X/h_E = 10, RUN 170 (A.R. = 4.0)

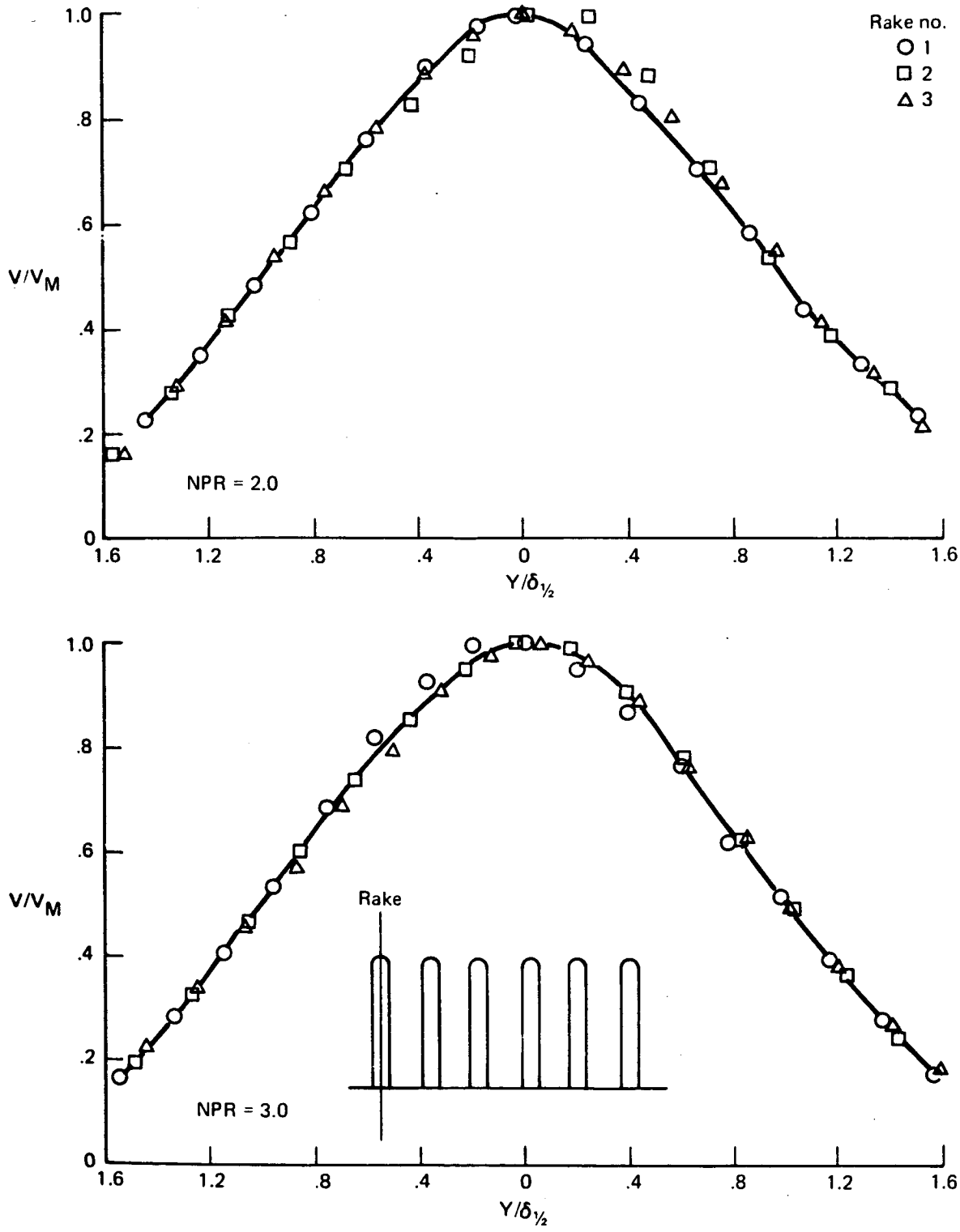

FIGURE 6-93.—JET VELOCITY PROFILES, THIN-LOBE NOZZLE, $X/h_E = 20$, RUN 177 (A.R. = 4.0)

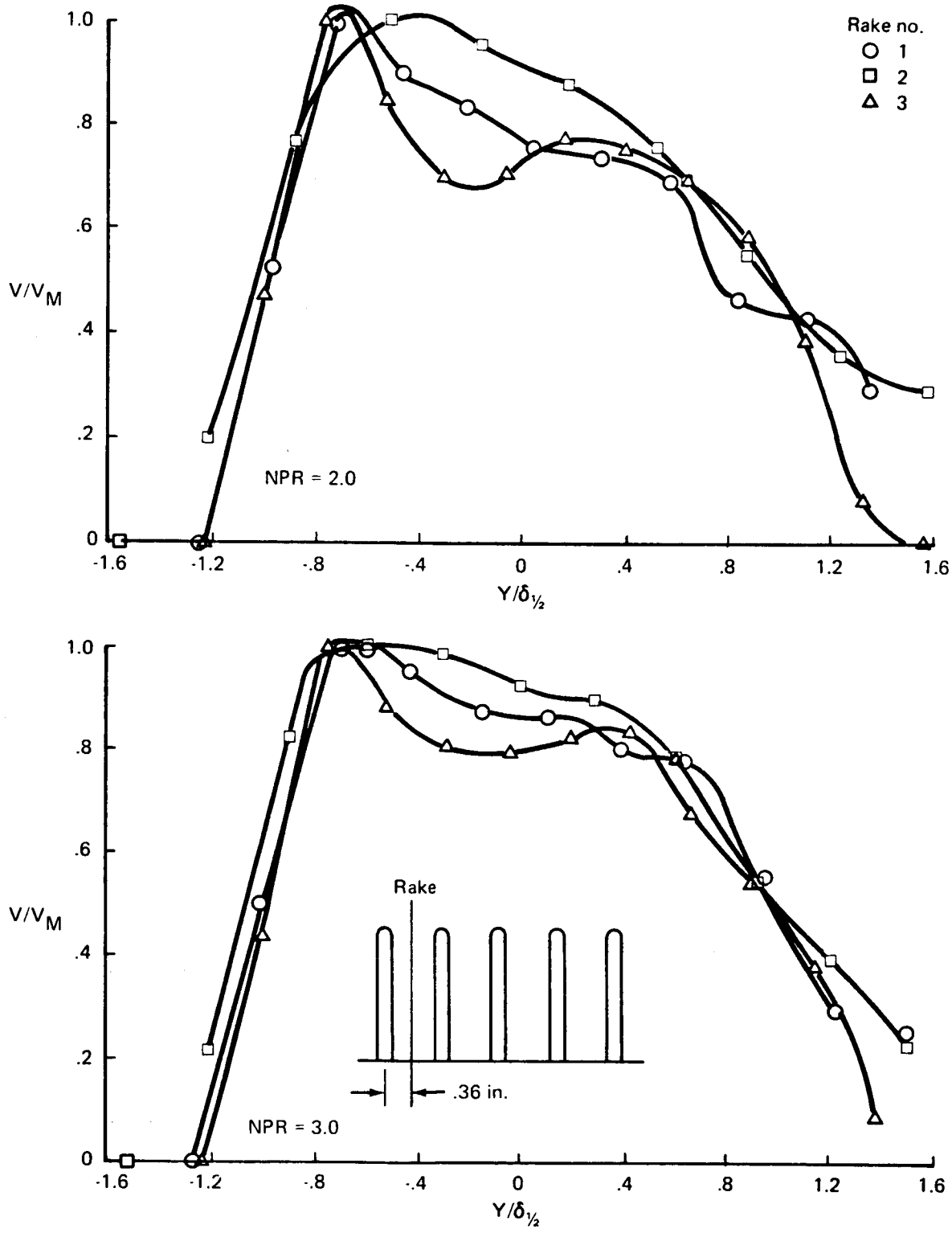

FIGURE 6-94.– JET VELOCITY PROFILES, THIN-LOBE NOZZLE, X/h_E = 5, RUN 165 (A.R. = 4.0)

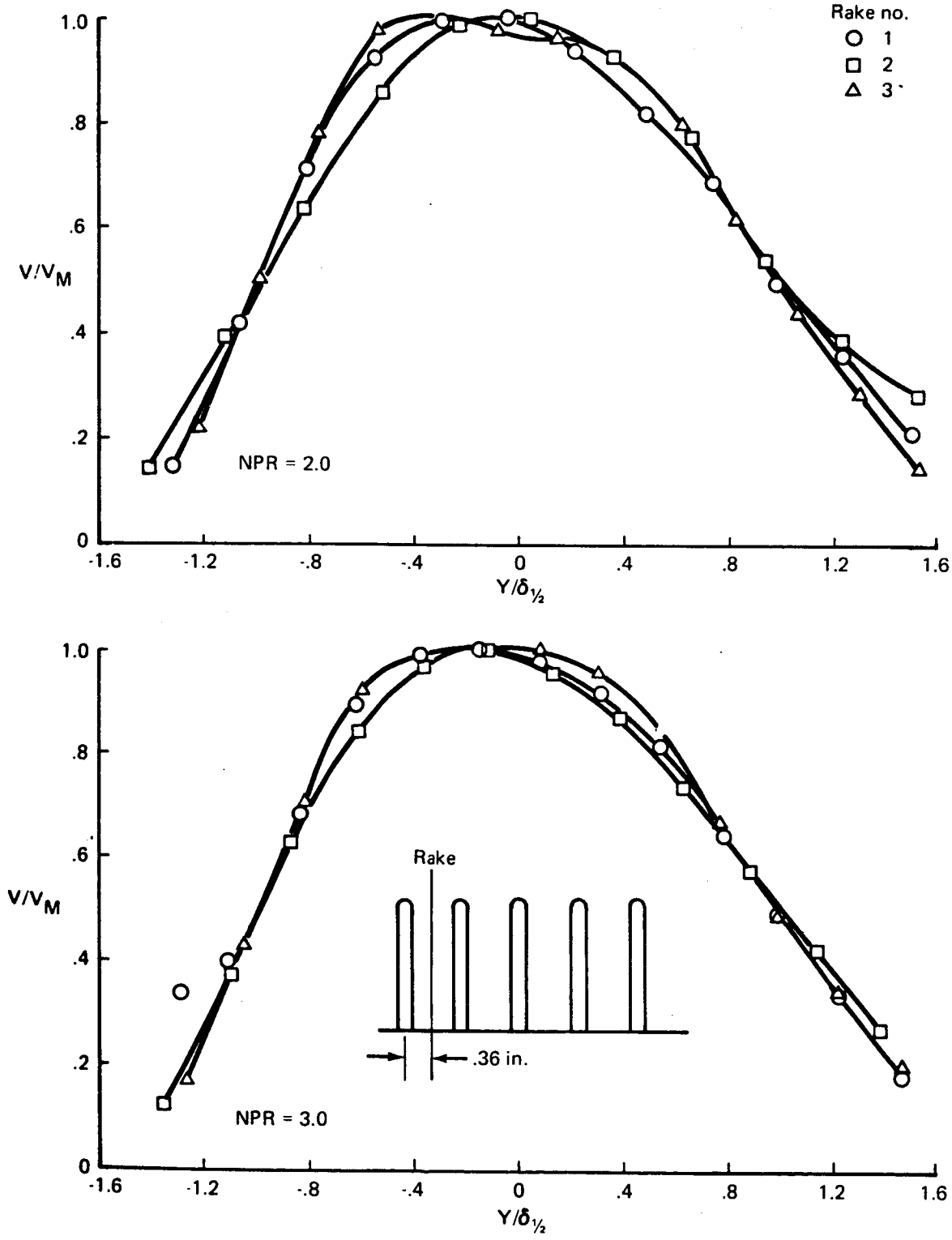

FIGURE 6-95.– JET VELOCITY PROFILES, THIN-LOBE NOZZLE, $X/h_E = 10$, RUN 173 (A.R. = 4.0)

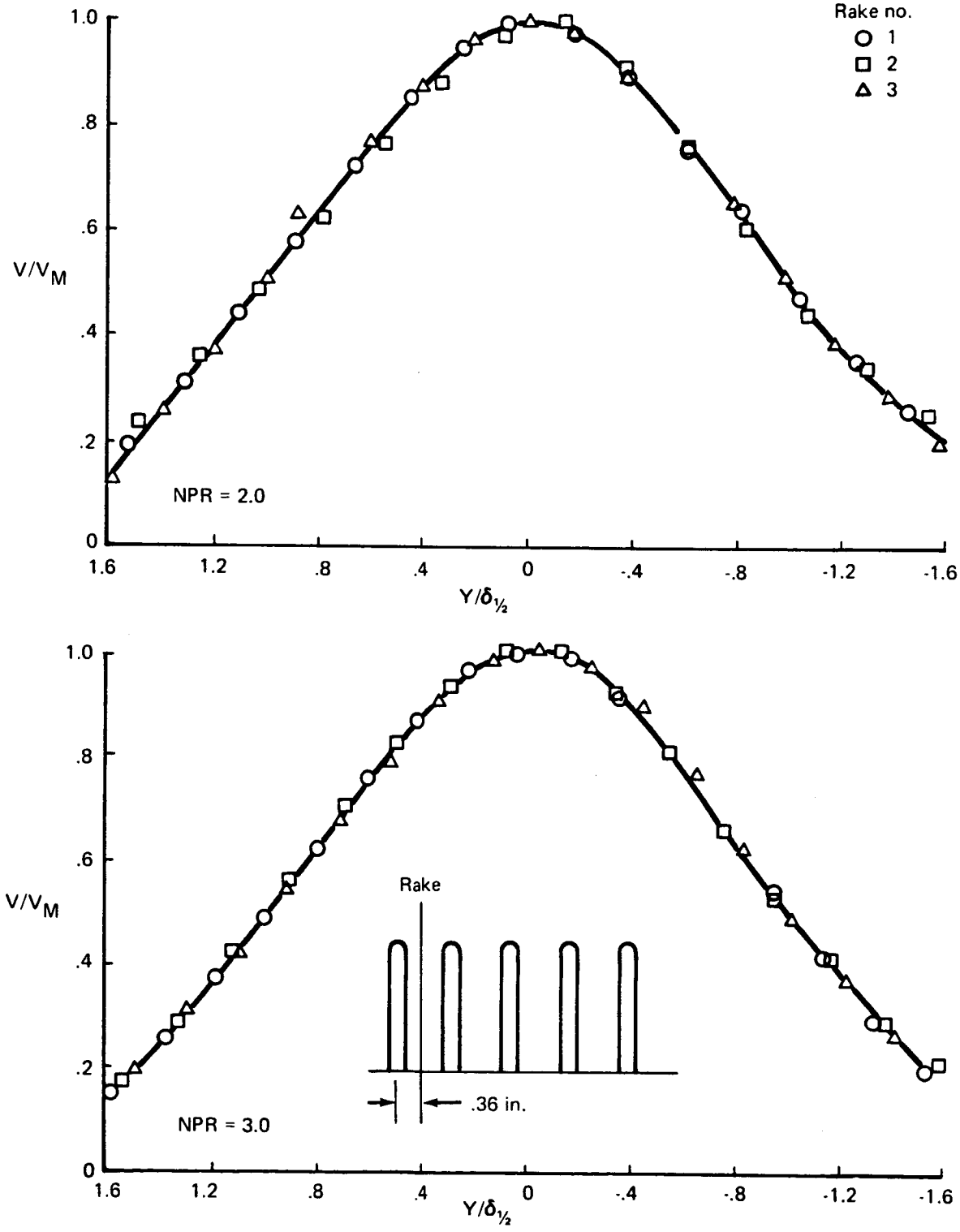

FIGURE 6-96.—JET VELOCITY PROFILES, THIN-LOBE NOZZLE, $X/h_E = 20$, RUN 180 (A.R. = 4.0)

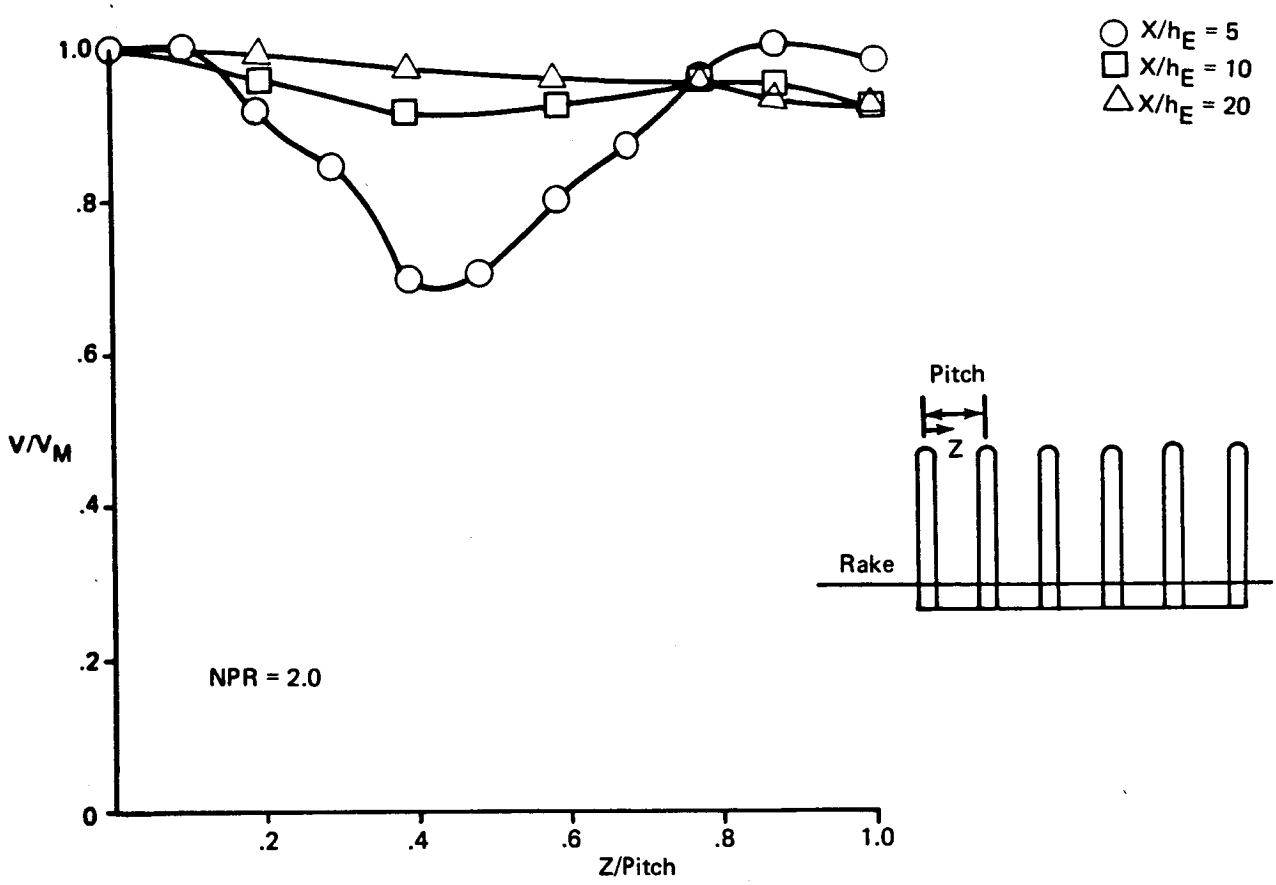

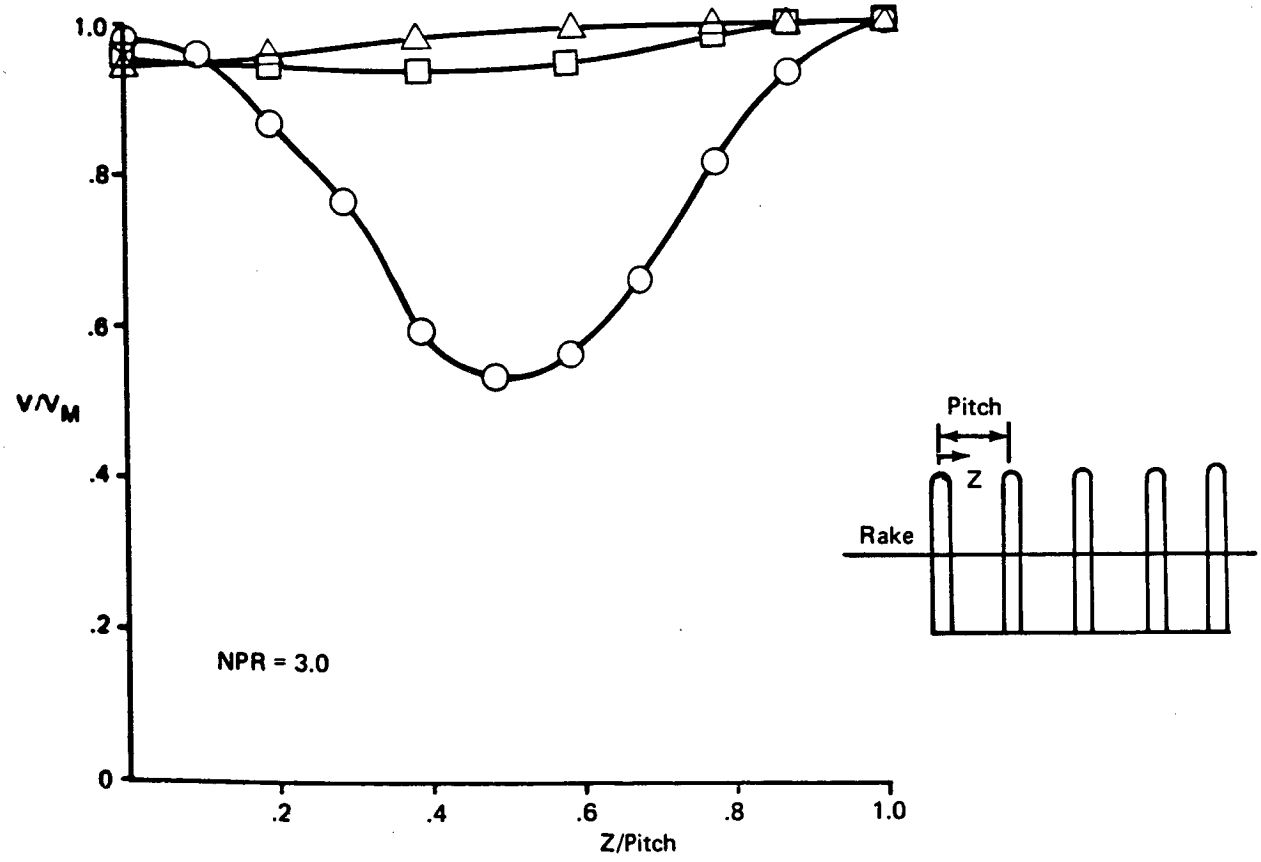

FIGURE 6-97.—SPANWISE VELOCITY PROFILES, THIN-LOBE NOZZLE (A.R. = 4.0)

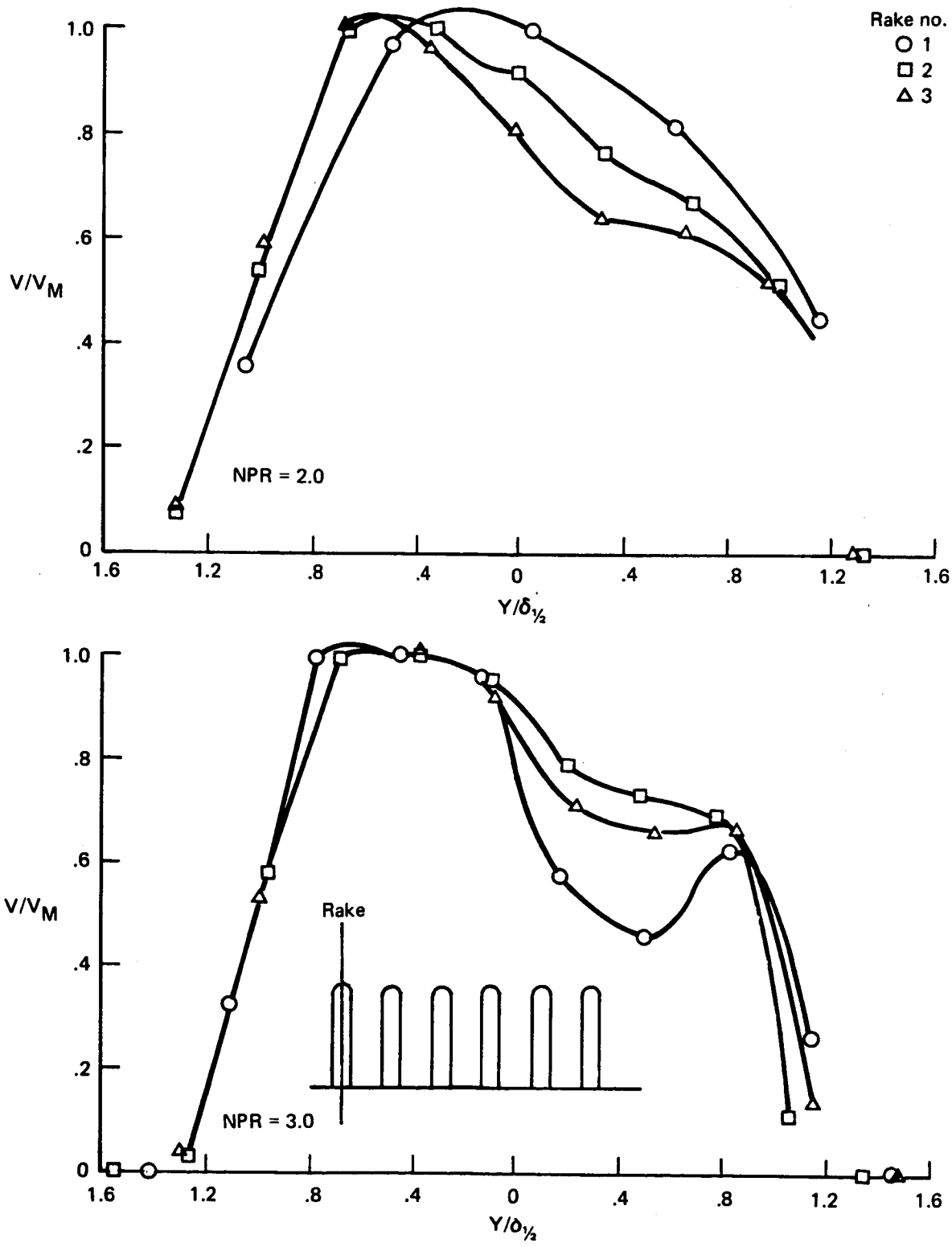

FIGURE 6-98.—JET VELOCITY PROFILES, THICK-LOBE NOZZLE, $X/h_E = 5$, RUN 198 (A.R. = 2.5)

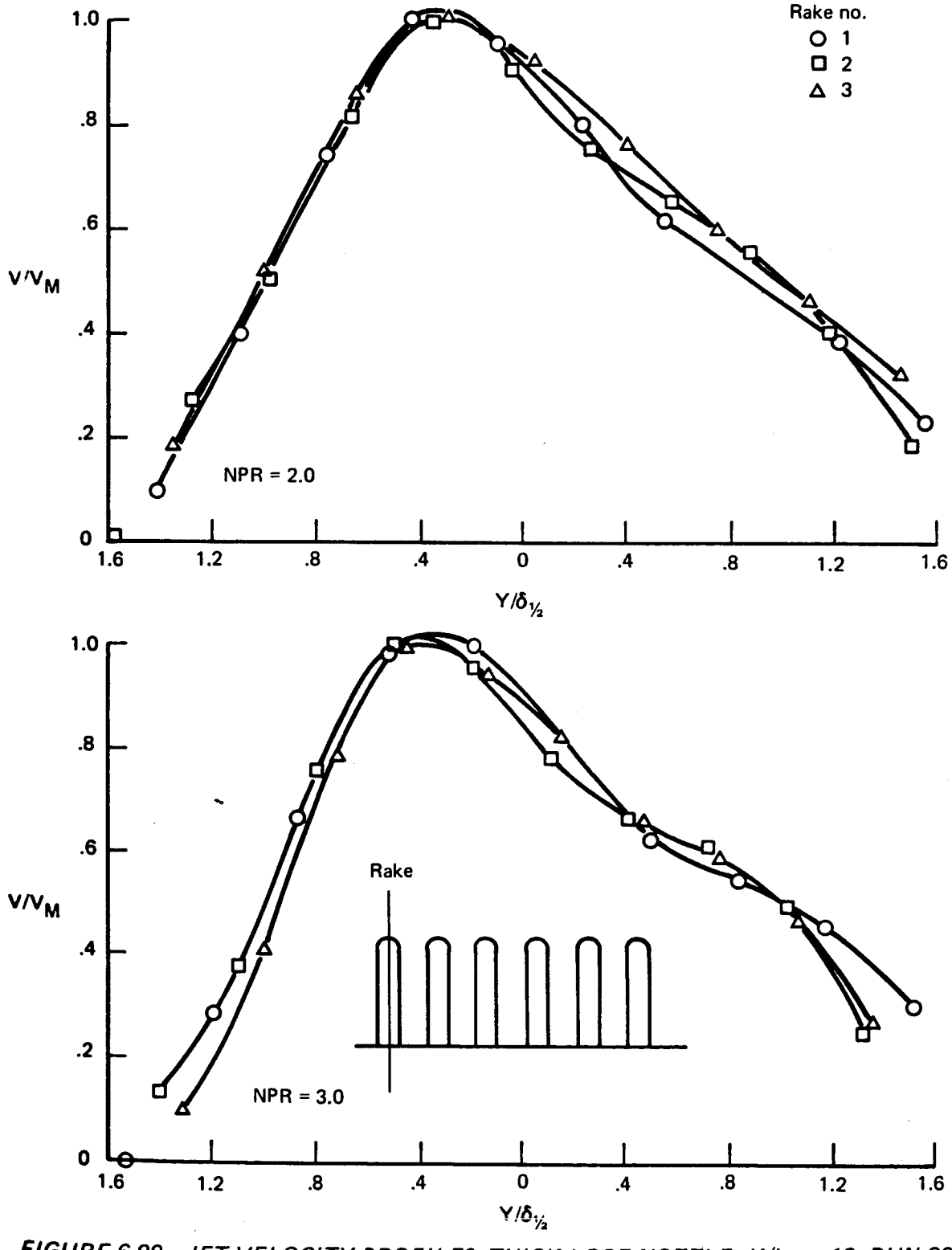

FIGURE 6-99.—JET VELOCITY PROFILES, THICK-LOBE NOZZLE, $X/h_E = 10$, RUN 208 (A.R. = 2.5)

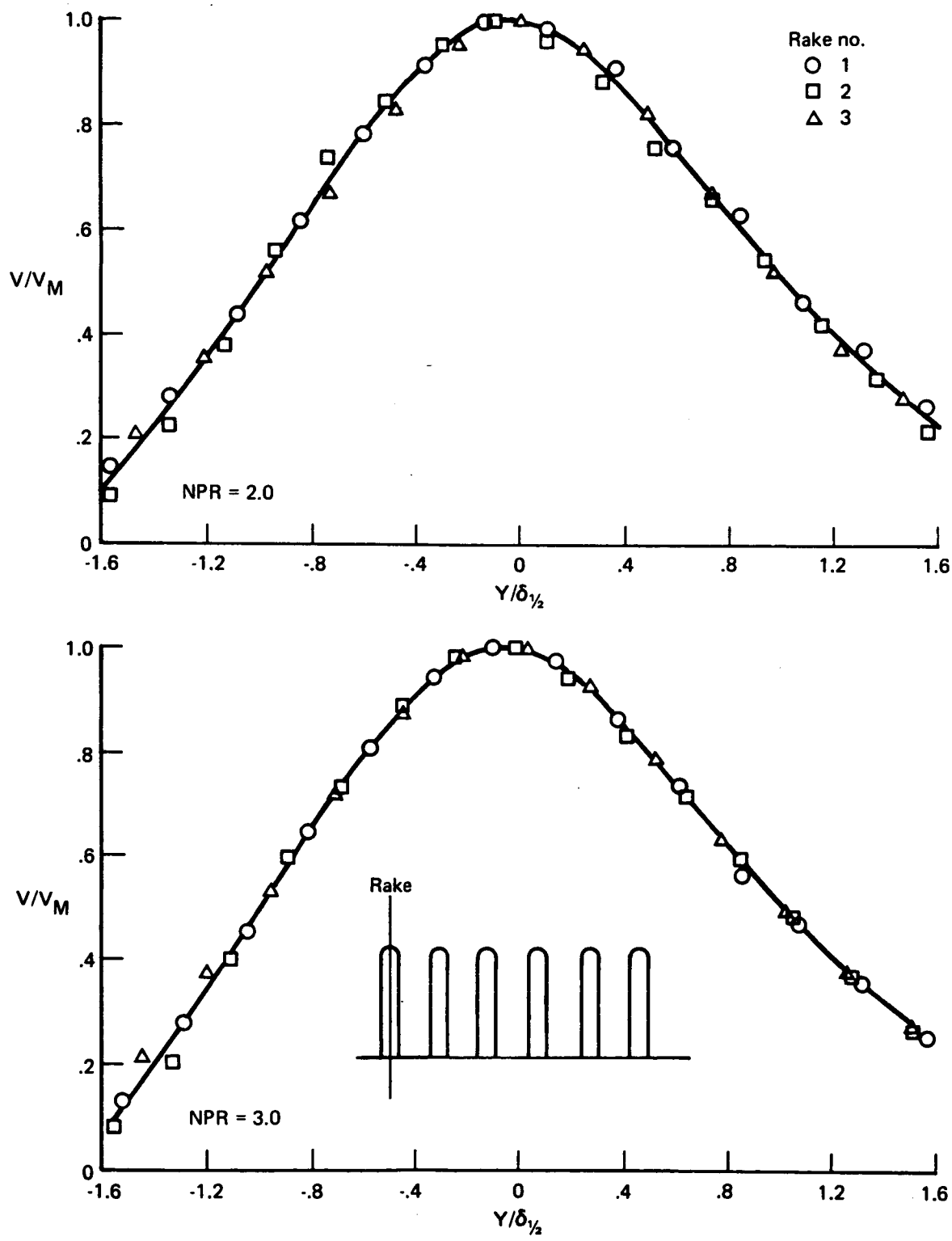

FIGURE 6-100.—JET VELOCITY PROFILES, THICK-LOBE NOZZLE, $X/h_E = 20$, RUN 214 (A.R. = 2.5)

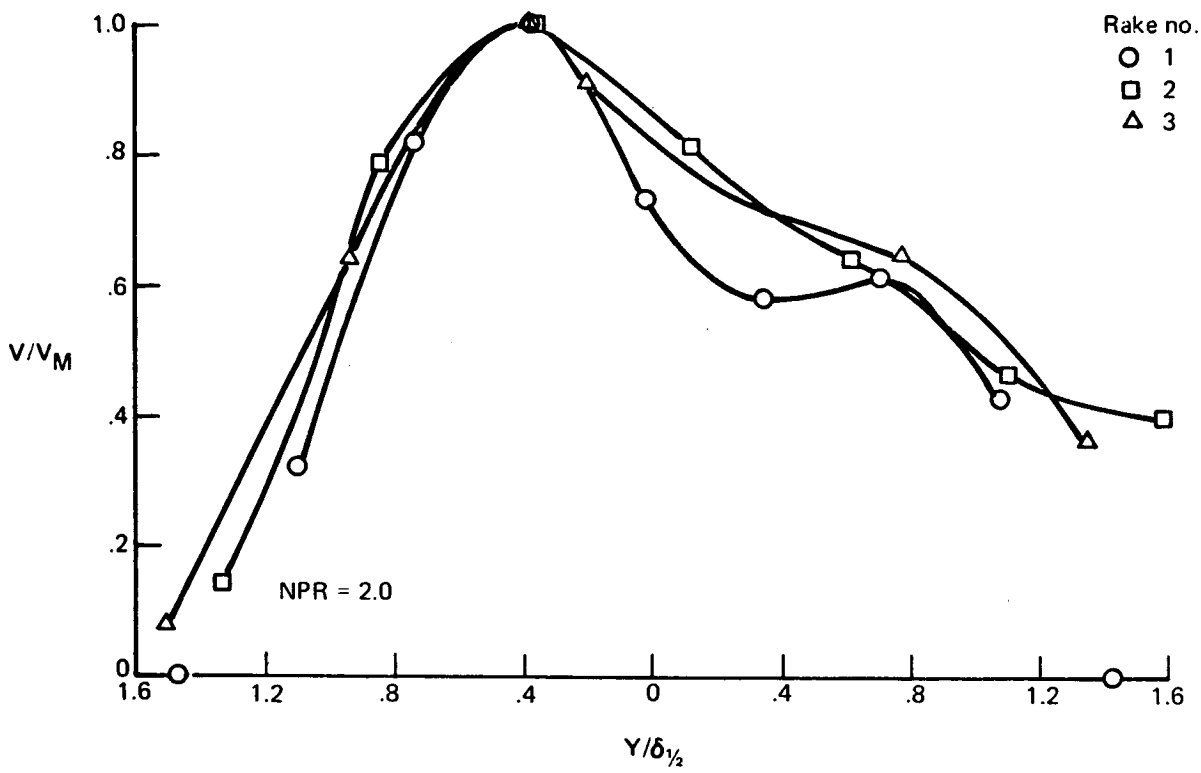

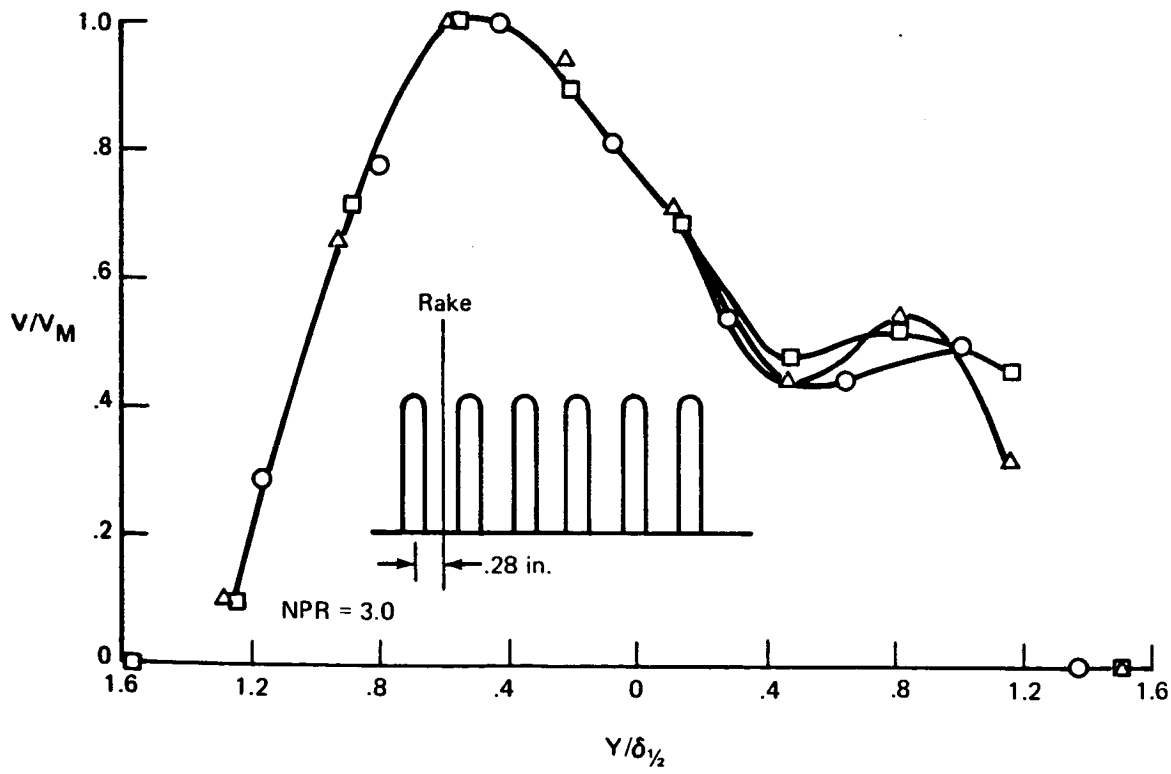

FIGURE 6-101.—JET VELOCITY PROFILES, THICK-LOBE NOZZLE, $X/h_E = 5$, RUN 202 (A.R. = 2.5)

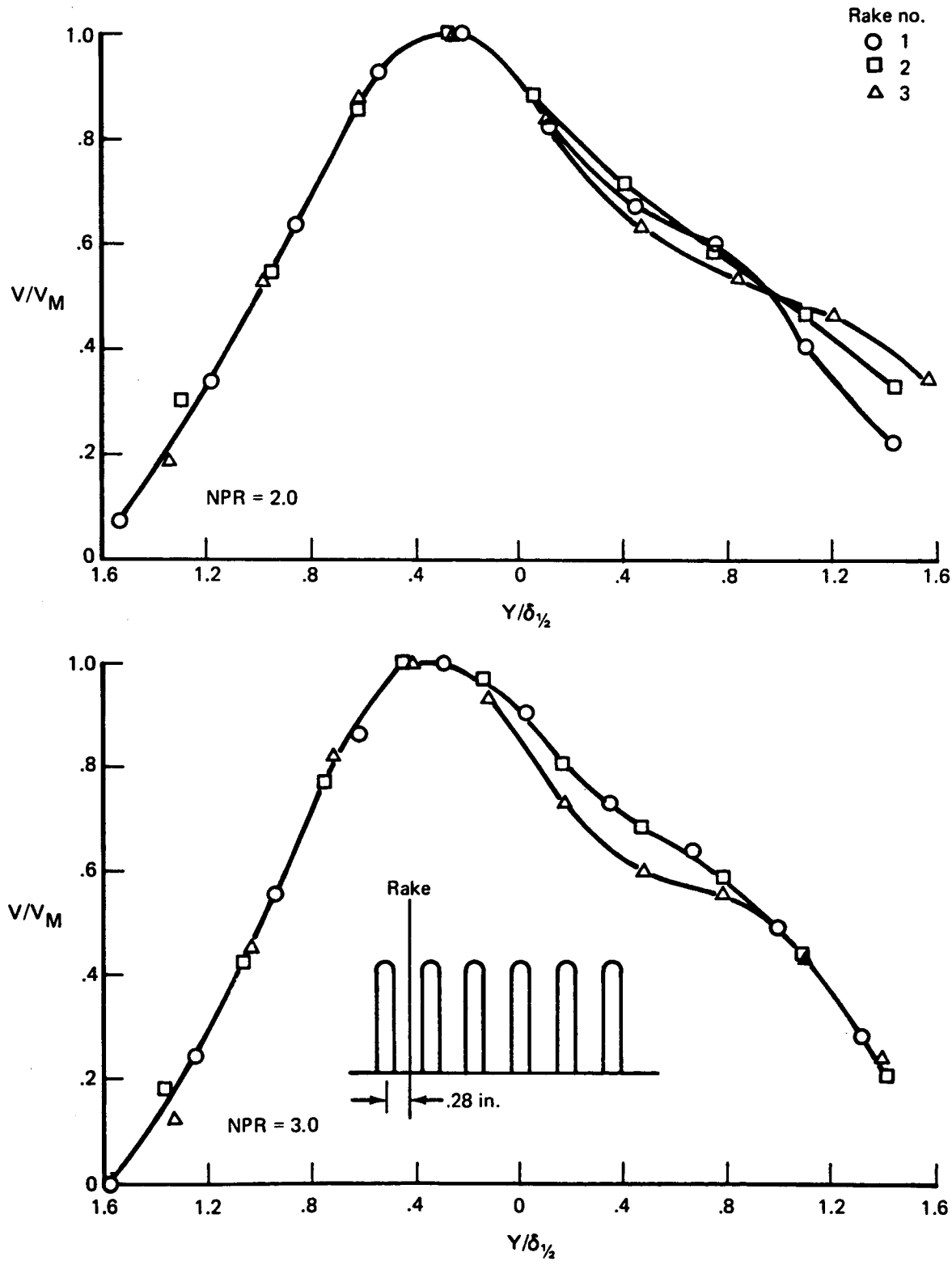

FIGURE 6-102.—JET VELOCITY PROFILES, THICK-LOBE NOZZLE, $X/h_E = 10$, RUN 210 (A. R. = 2.5)

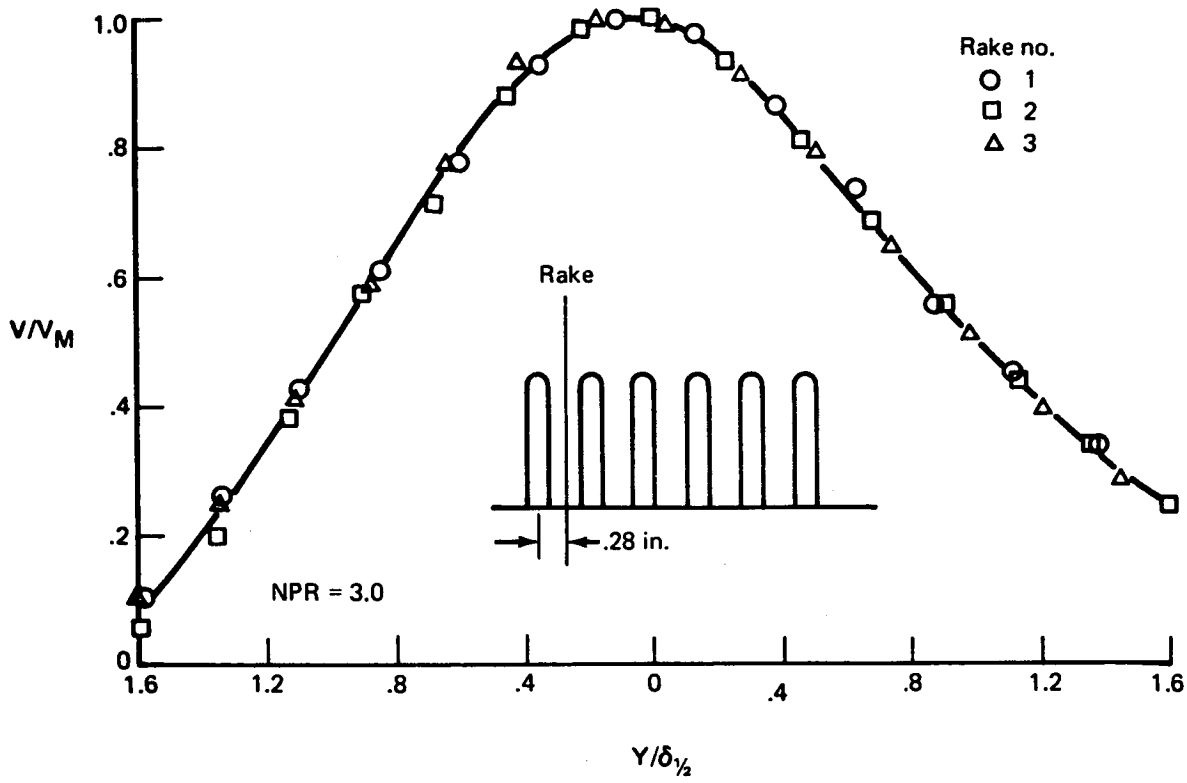

FIGURE 6-103.—JET VELOCITY PROFILES, THICK-LOBE NOZZLE, $X/h_E = 20$, RUN 216 (A.R. = 2.5)

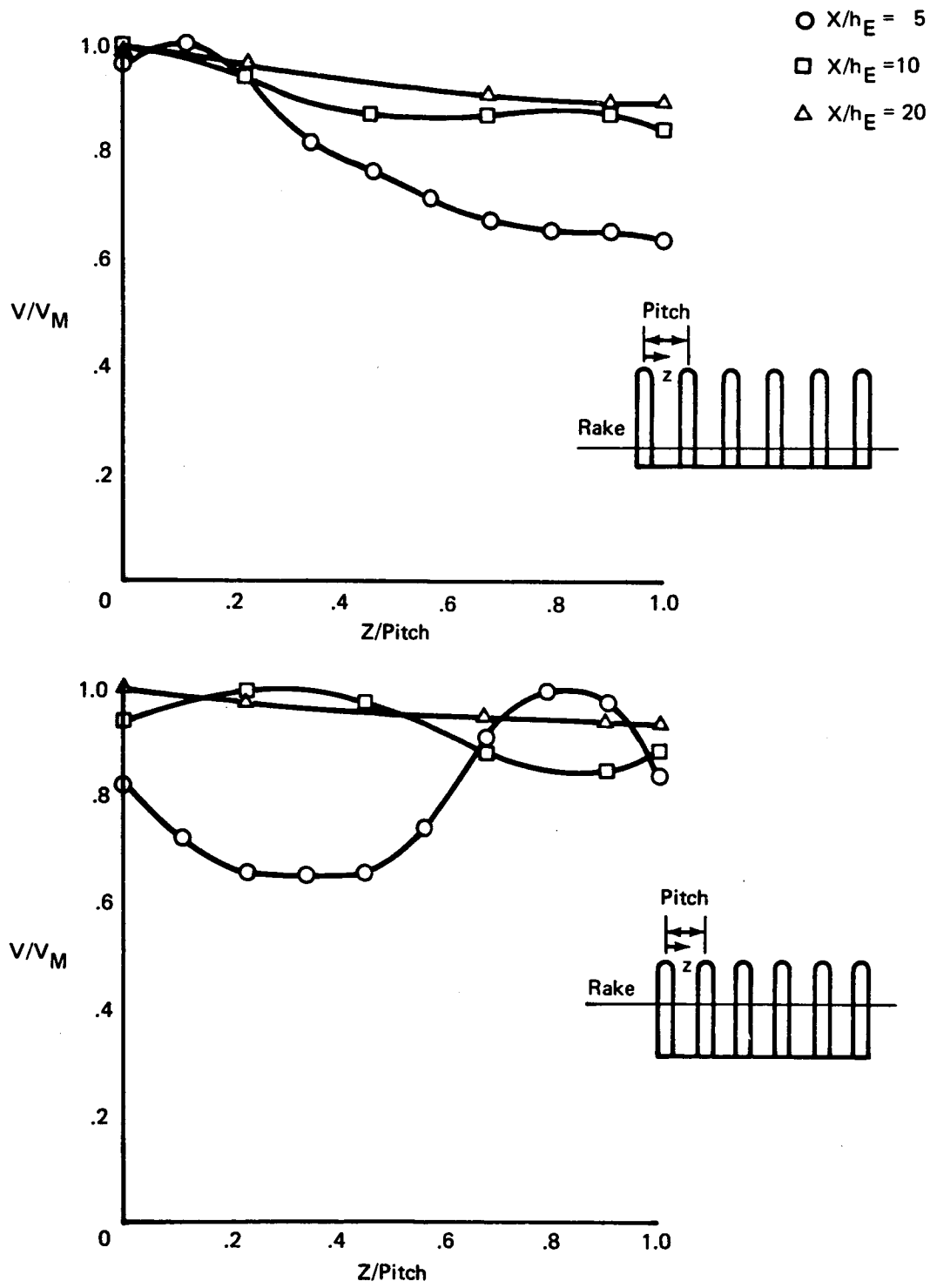

FIGURE 6-104.—SPANWISE VELOCITY PROFILES, THICK-LOBE NOZZLE (A.R. = 2.5)

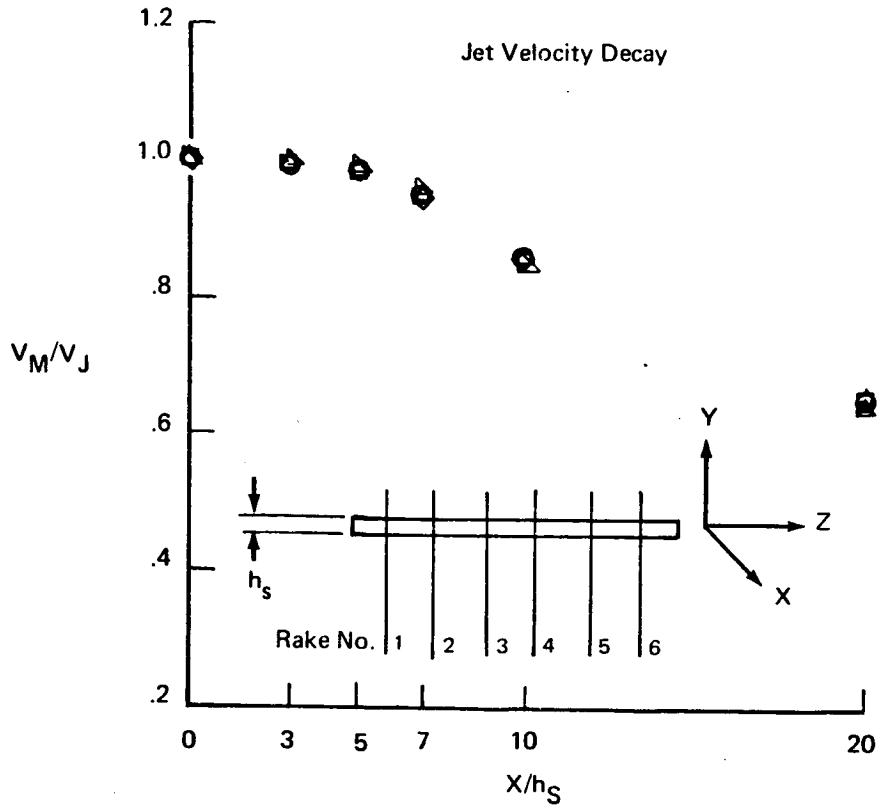

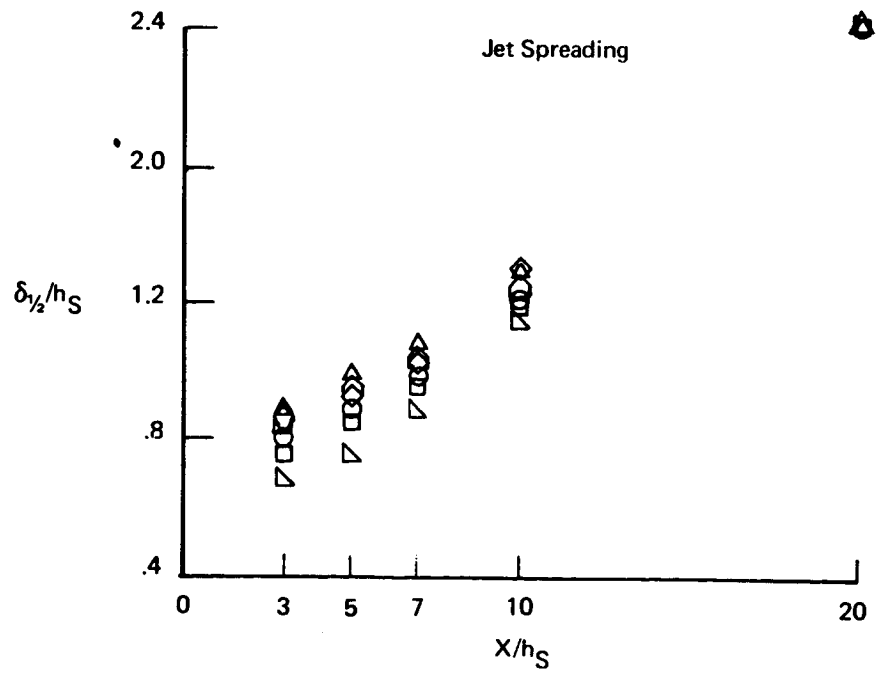

FIGURE 6-105.—JET VELOCITY DECAY AND JET SPREADING FOR 400:1 SLOT NOZZLE, NPR = 2.0

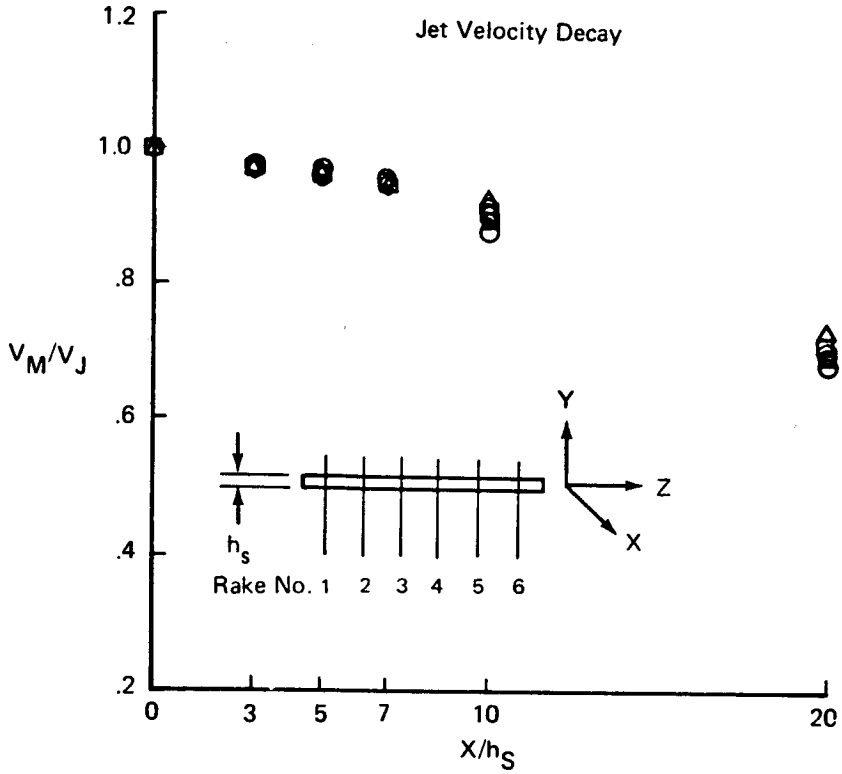

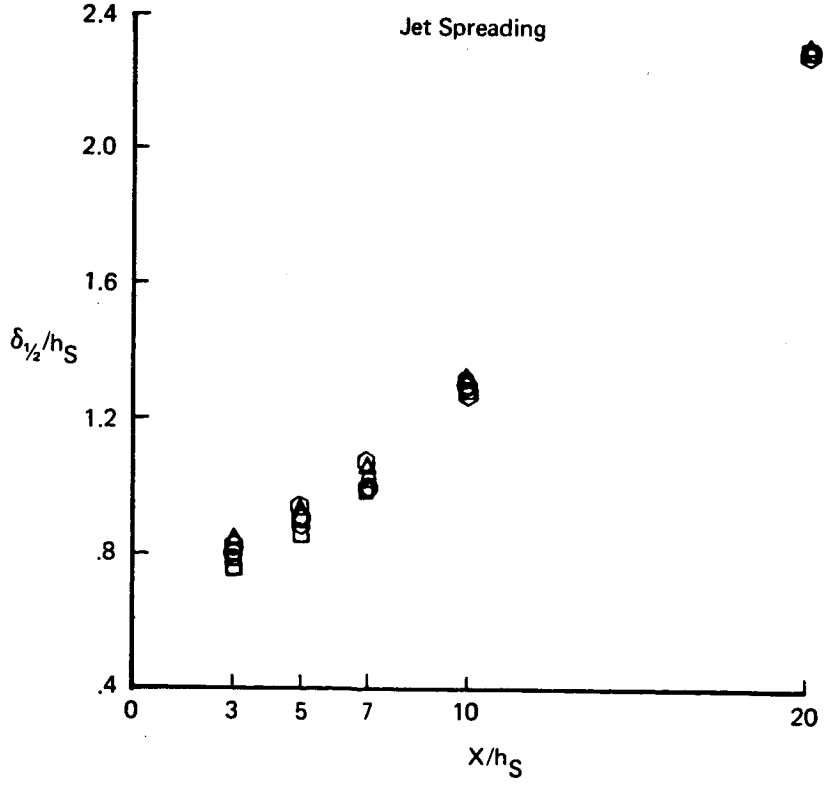

FIGURE 6-106.–JET VELOCITY DECAY AND JET SPREADING FOR 400:1 SLOT NOZZLE, NPR = 3.0

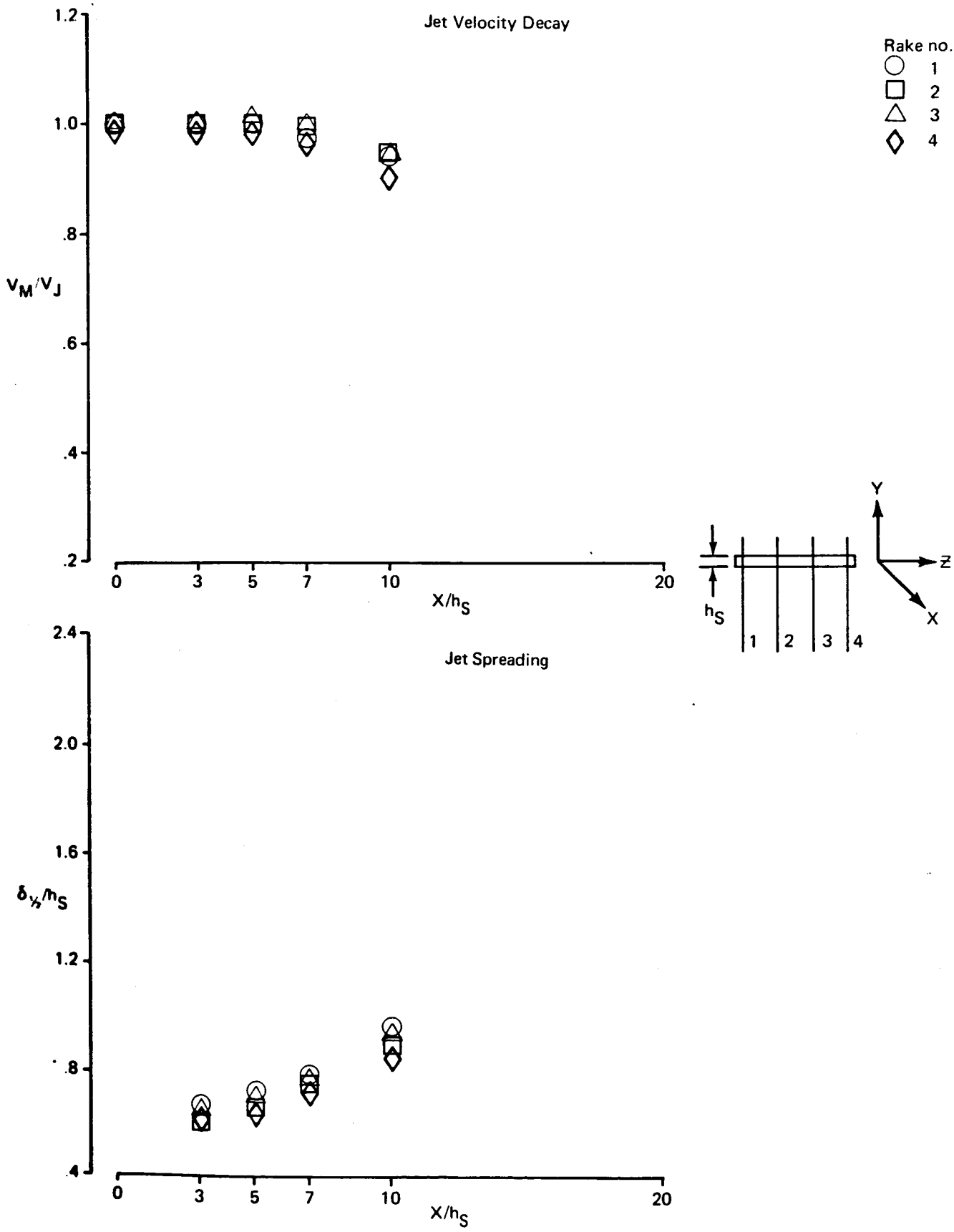

FIGURE 6-107.—JET VELOCITY DECAY AND JET SPREADING, 100:1 SLOT NOZZLE, NPR = 2.0

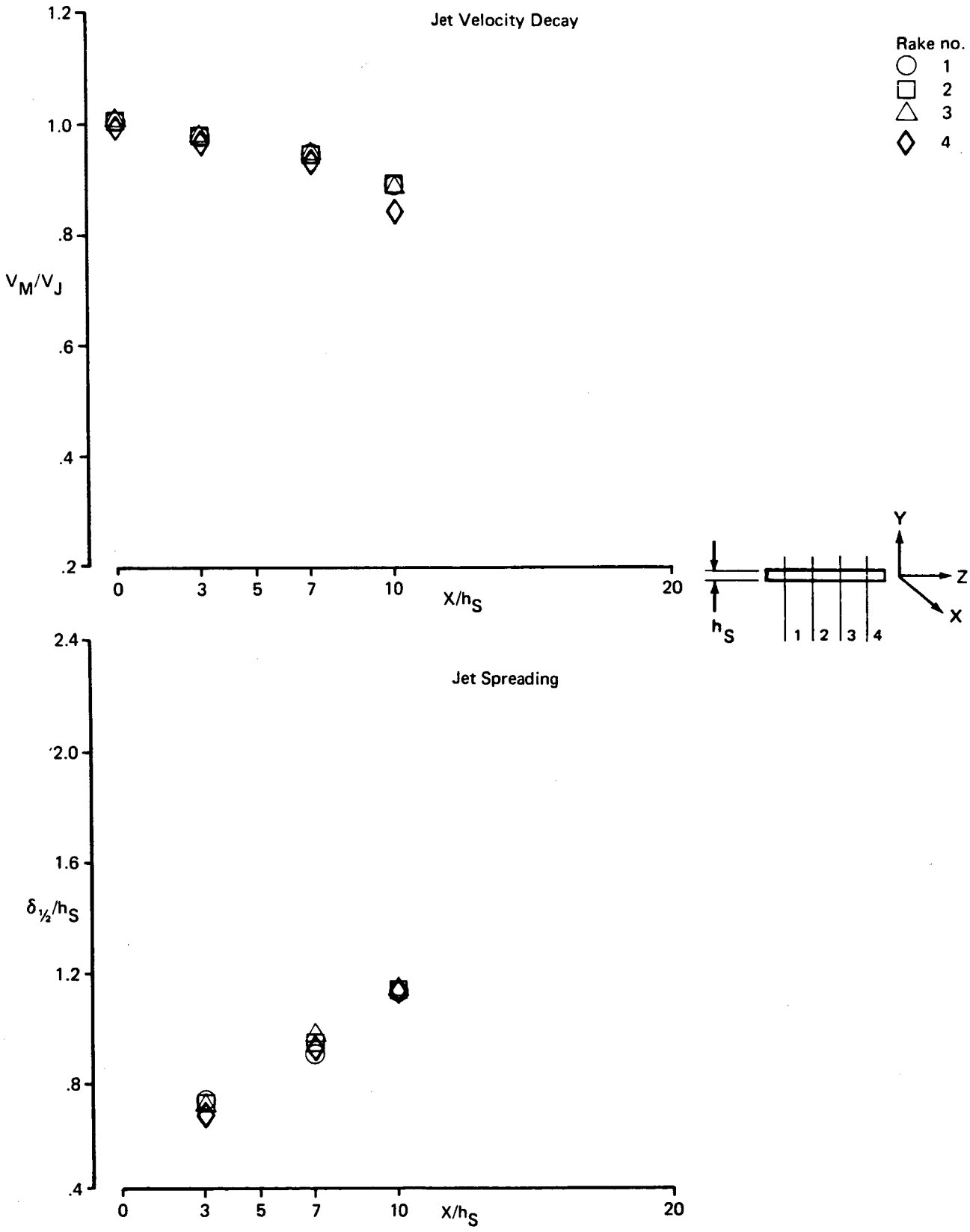

FIGURE 6-108.–JET VELOCITY DECAY AND JET SPREADING, 100:1 SLOT NOZZLE, NPR = 3.0

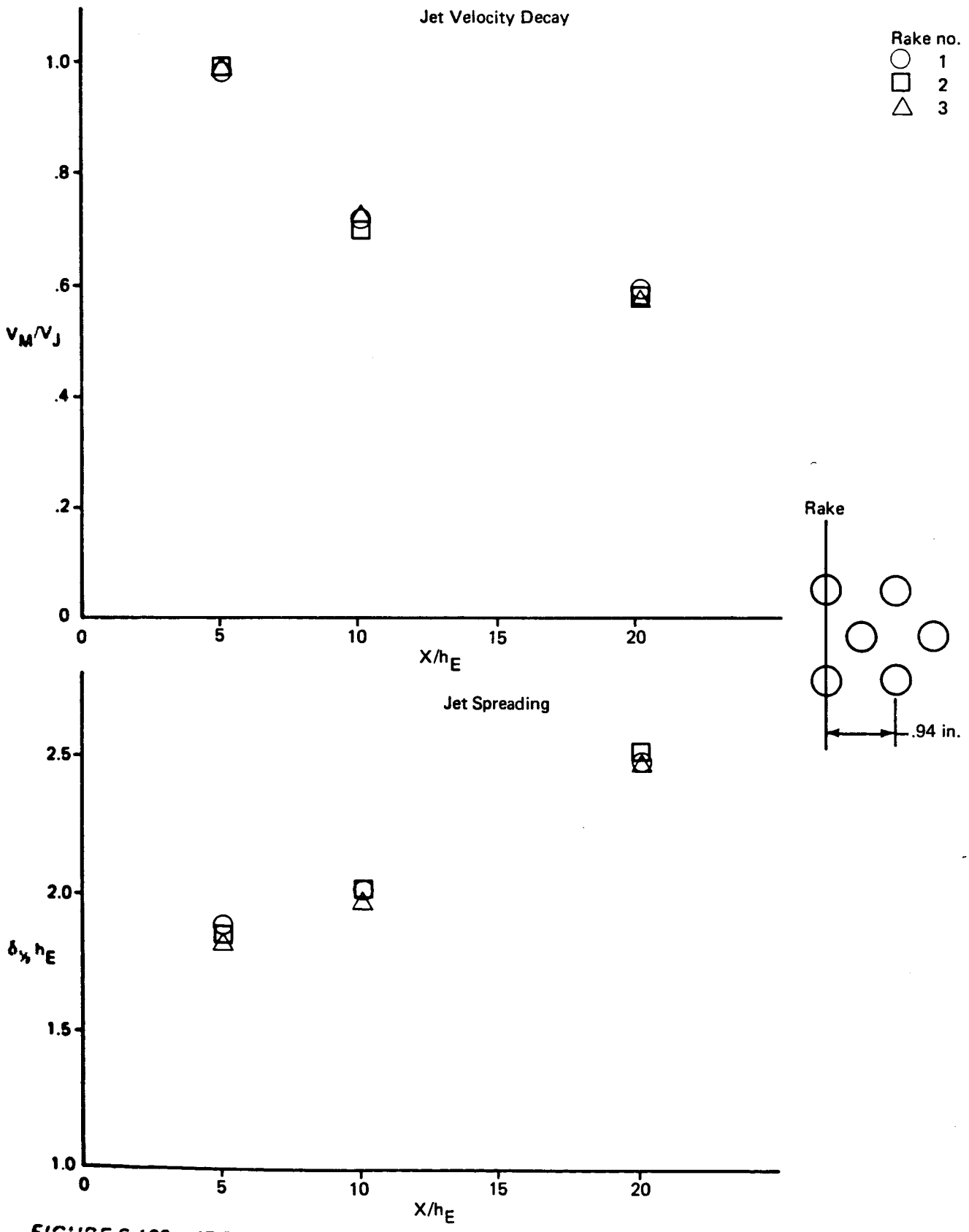

FIGURE 6-109.—JET VELOCITY DECAY AND JET SPREADING, 140-TUBE NOZZLE, NPR = 2.0

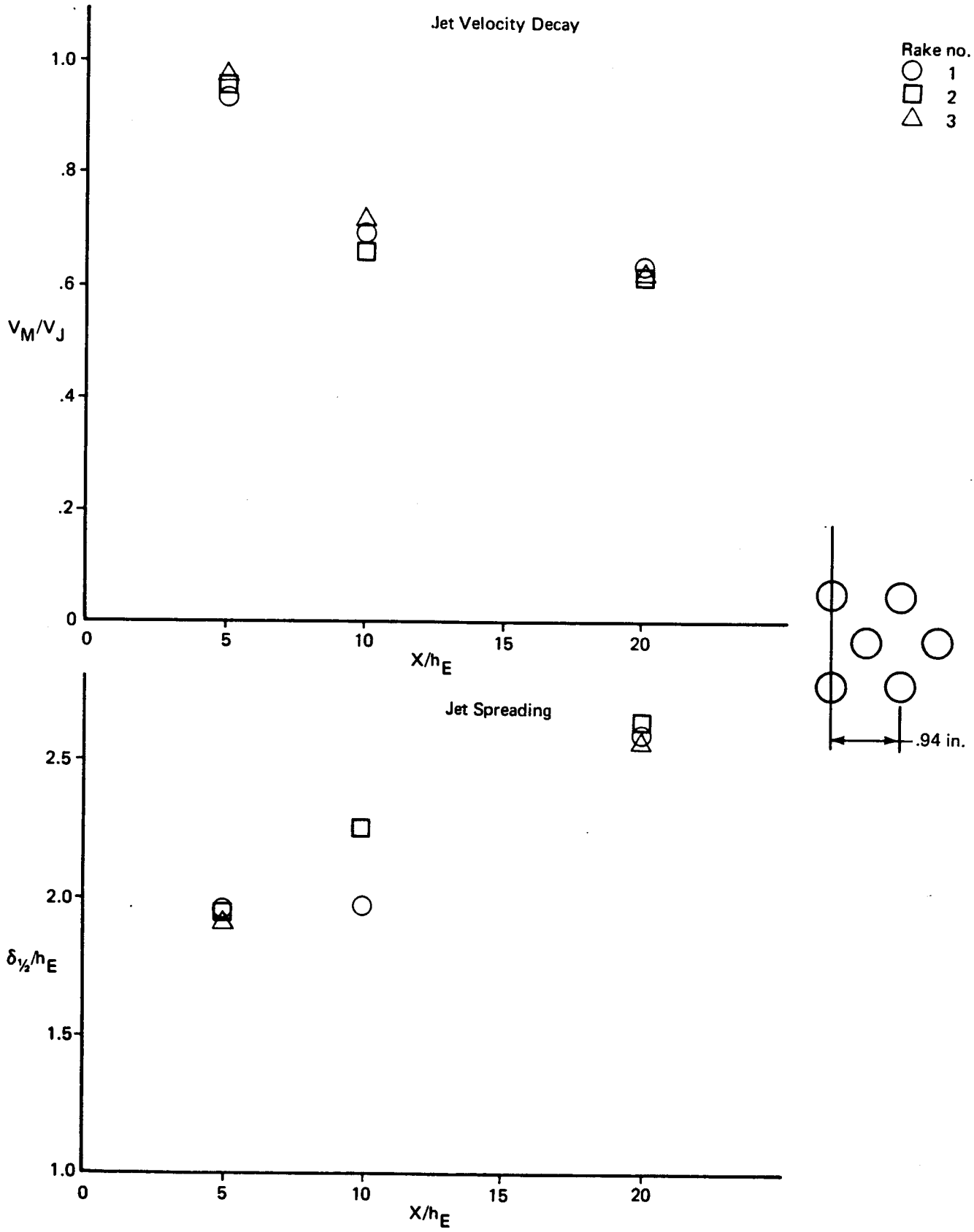

FIGURE 6-110.—JET VELOCITY DECAY AND JET SPREADING, 140-TUBE NOZZLE, NPR = 3.0

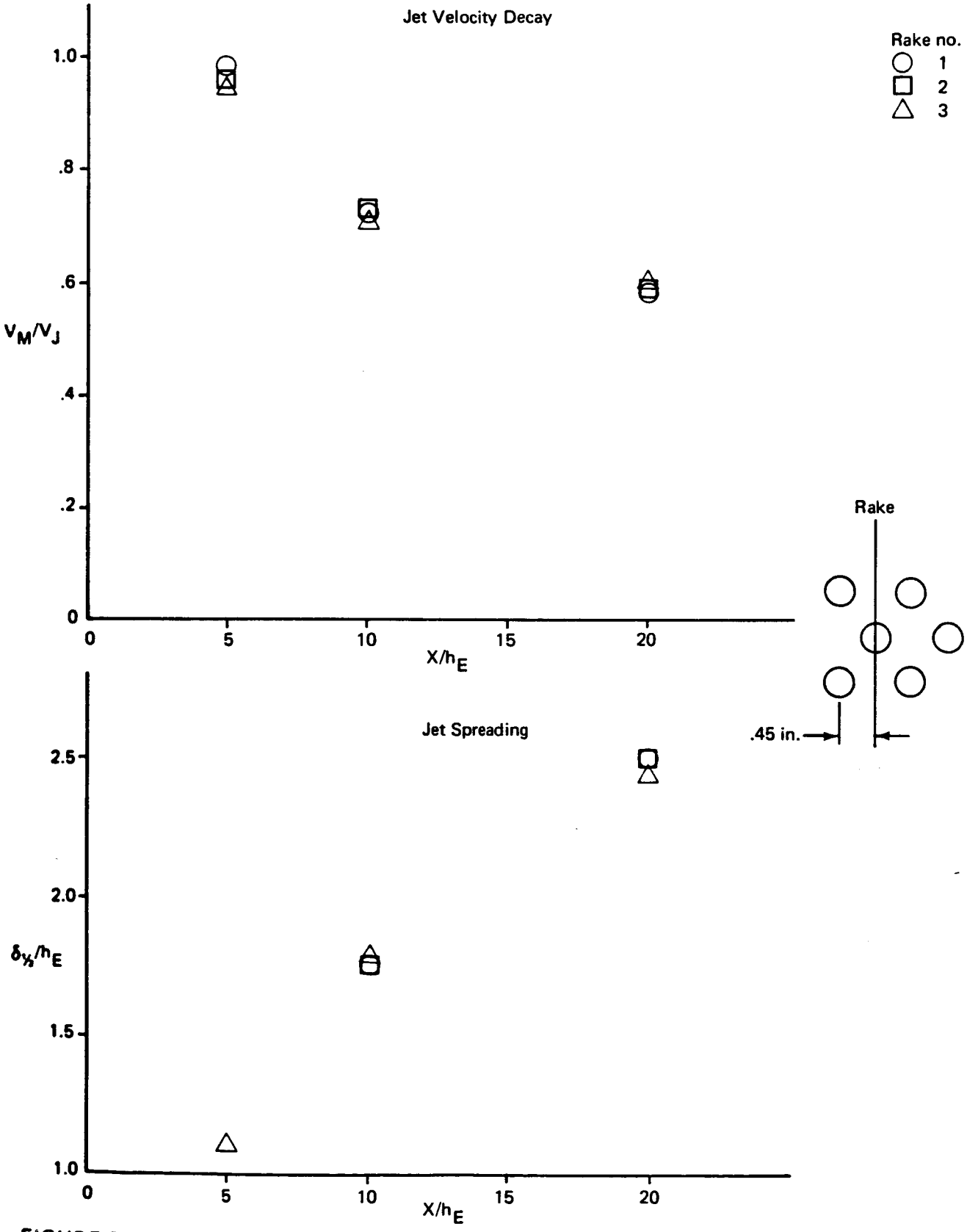

FIGURE 6-111.—JET VELOCITY DECAY AND JET SPREADING, 140-TUBE NOZZLE, NPR = 2.0

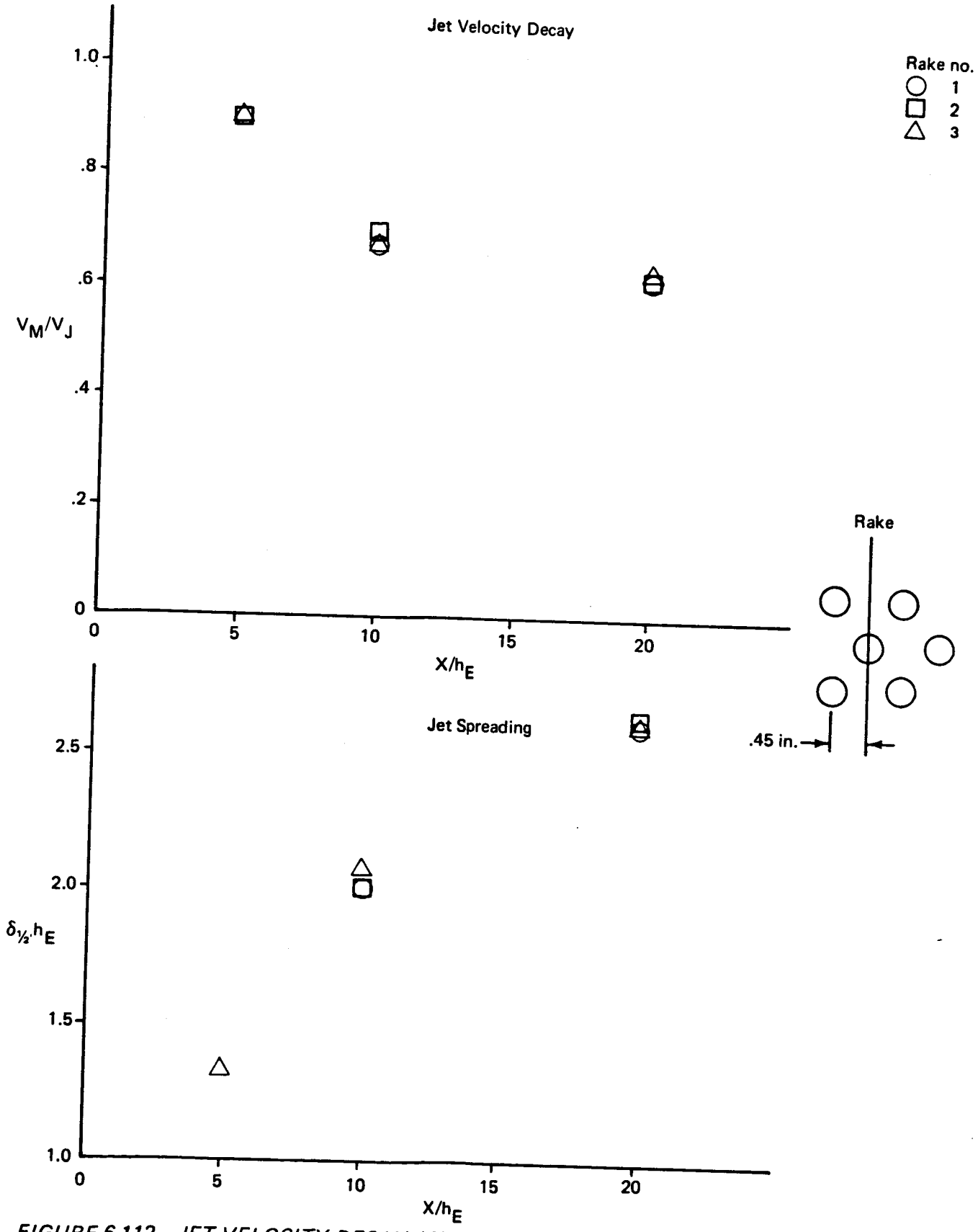

FIGURE 6-112.—JET VELOCITY DECAY AND JET SPREADING, 140-TUBE NOZZLE, NPR = 3.0

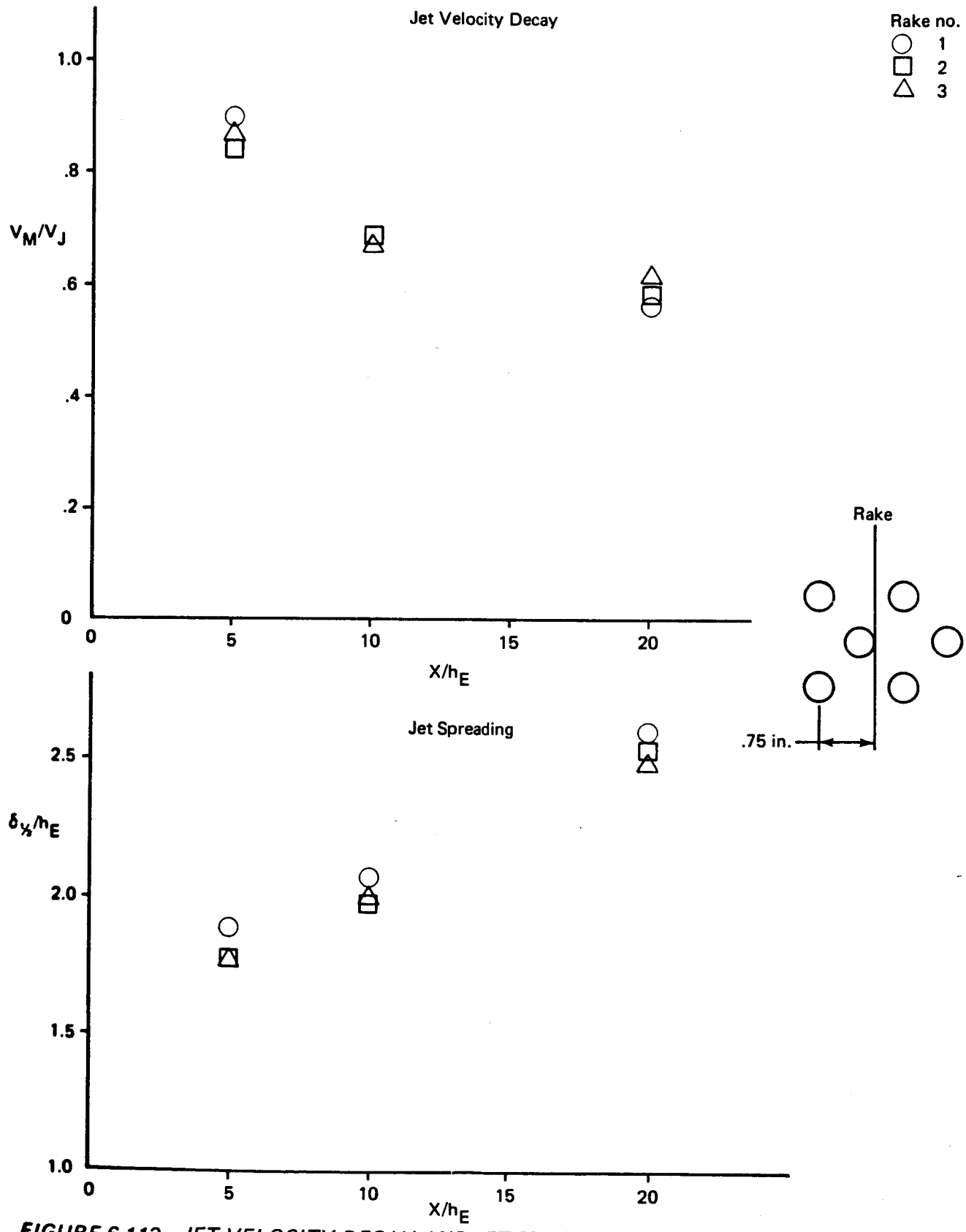

FIGURE 6-113.—JET VELOCITY DECAY AND JET SPREADING, 140-TUBE NOZZLE, NPR = 2.0

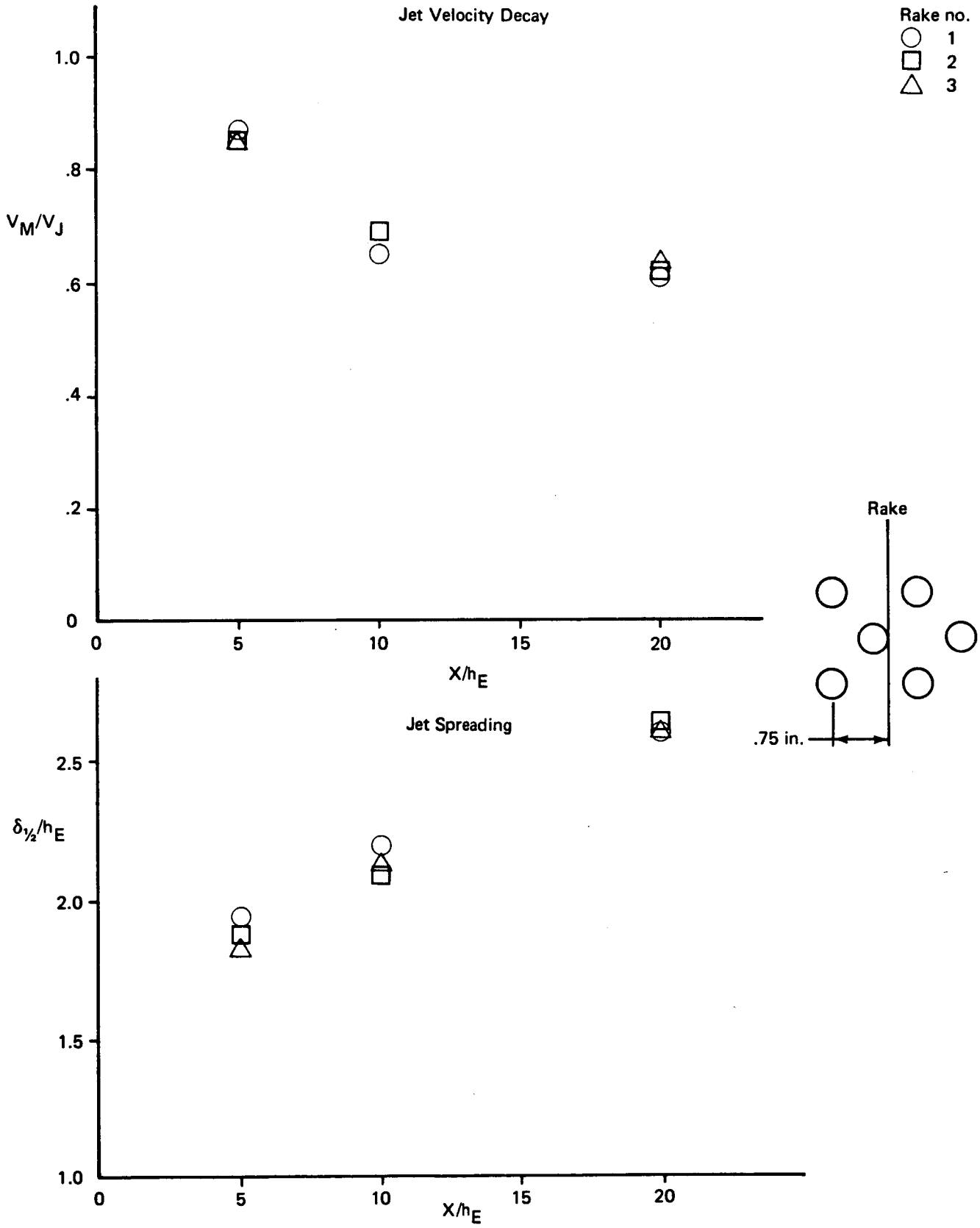

FIGURE 6-114.—JET VELOCITY DECAY AND JET SPREADING, 140-TUBE NOZZLE, NPR = 3.0

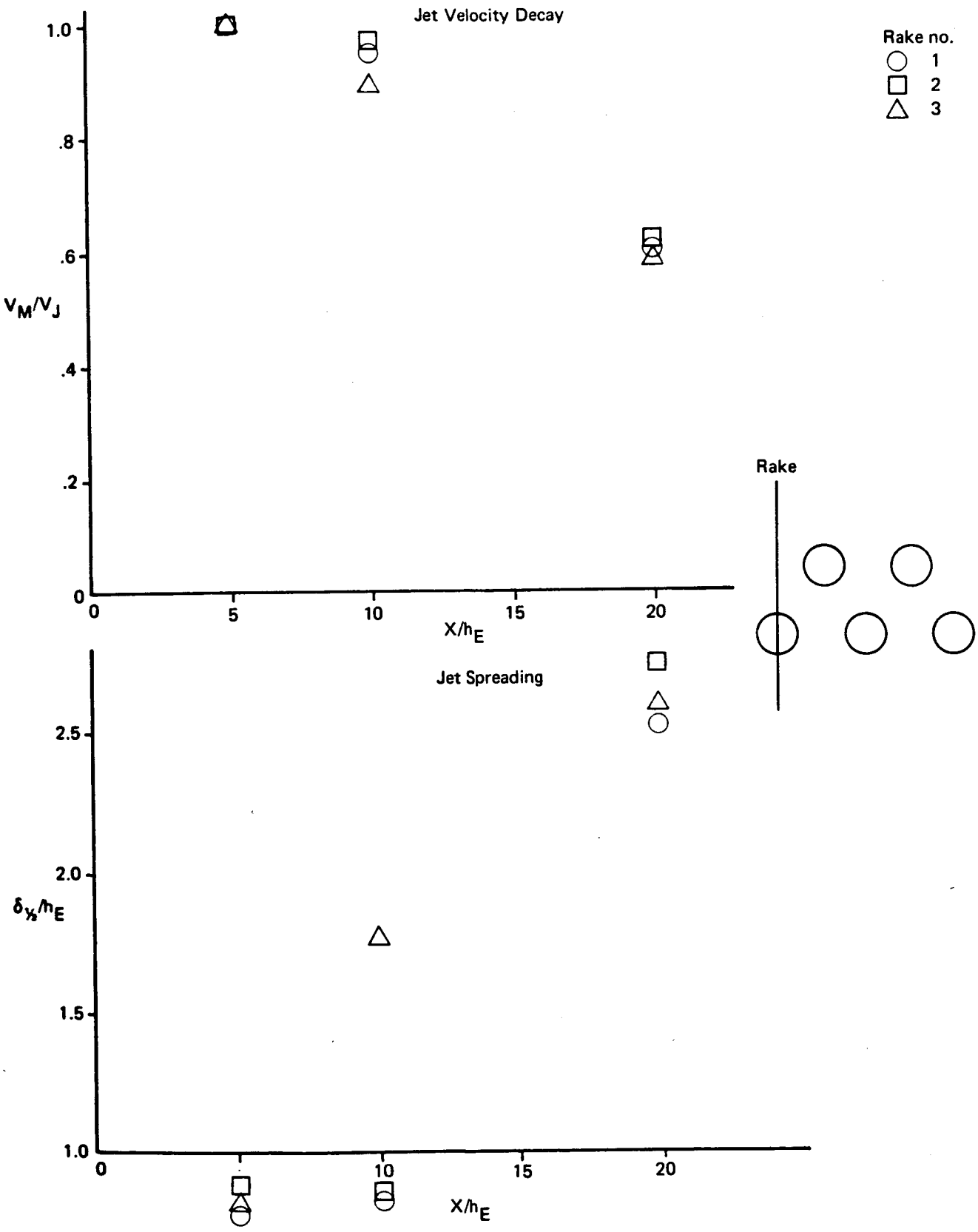

FIGURE 6-115.—JET VELOCITY DECAY AND JET SPREADING, 70-TUBE NOZZLE, NPR = 2.0

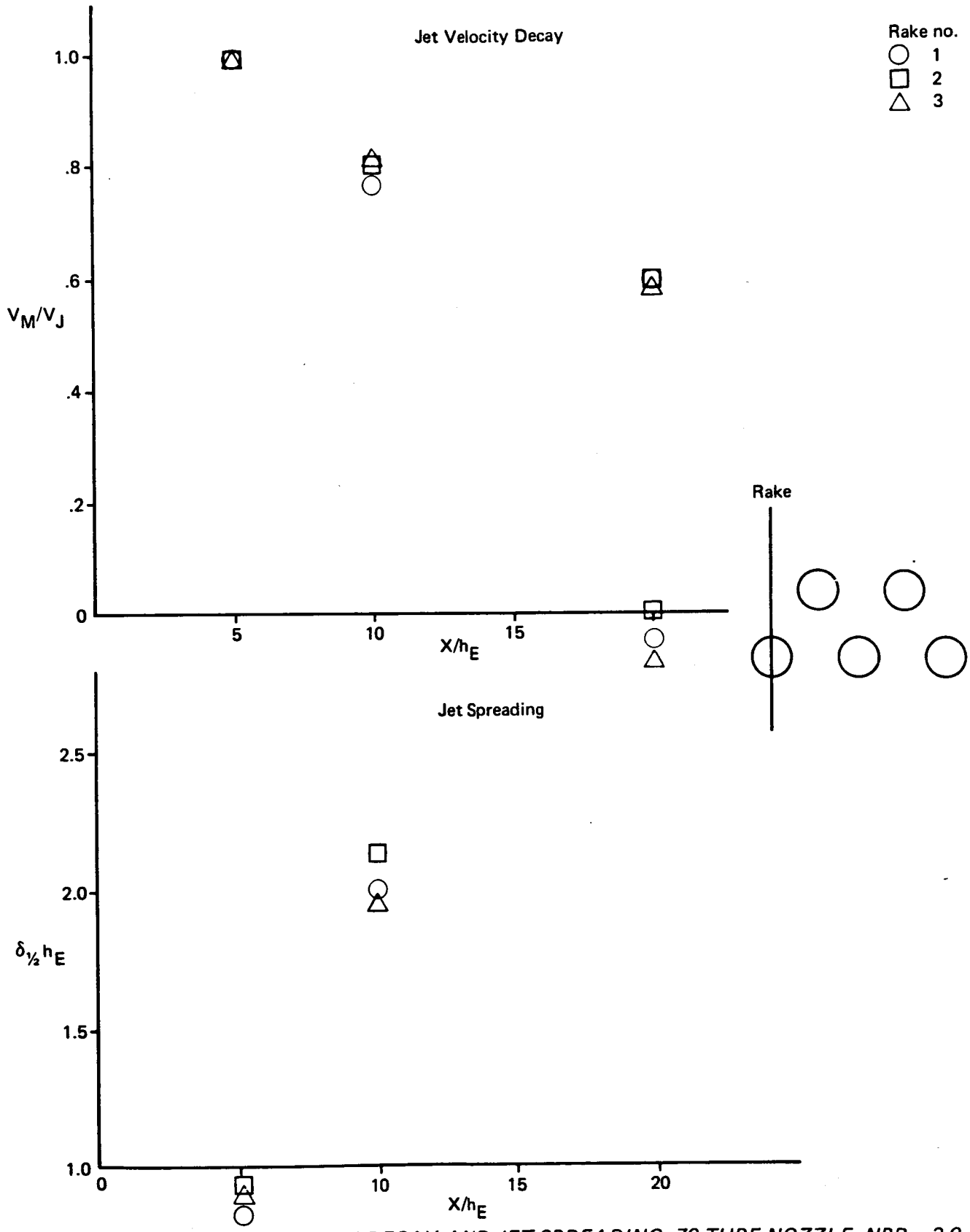

FIGURE 6-116.—JET VELOCITY DECAY AND JET SPREADING, 70-TUBE NOZZLE, NPR = 3.0

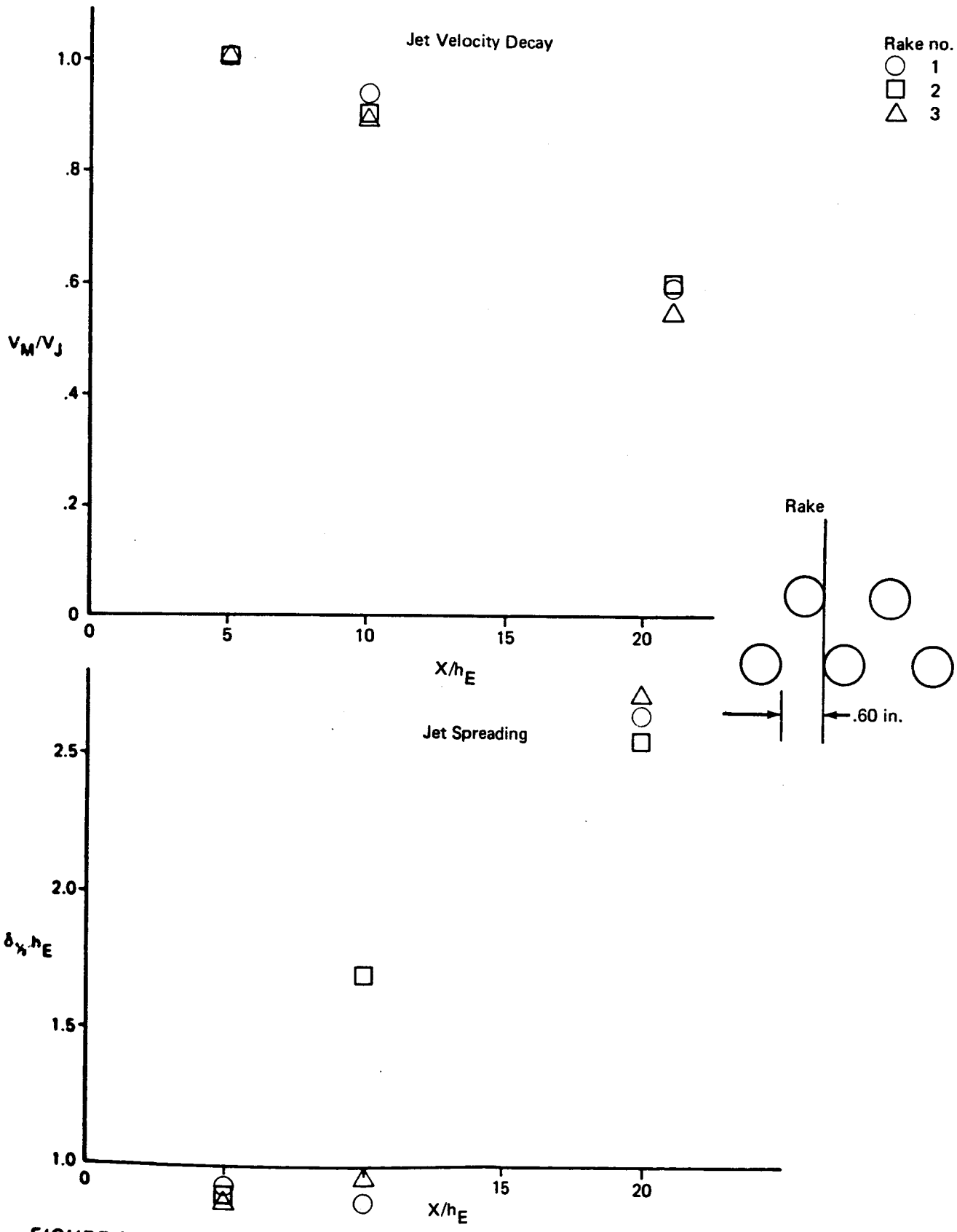

FIGURE 6-117.—JET VELOCITY DECAY AND JET SPREADING, 70-TUBE NOZZLE, NPR = 2.0

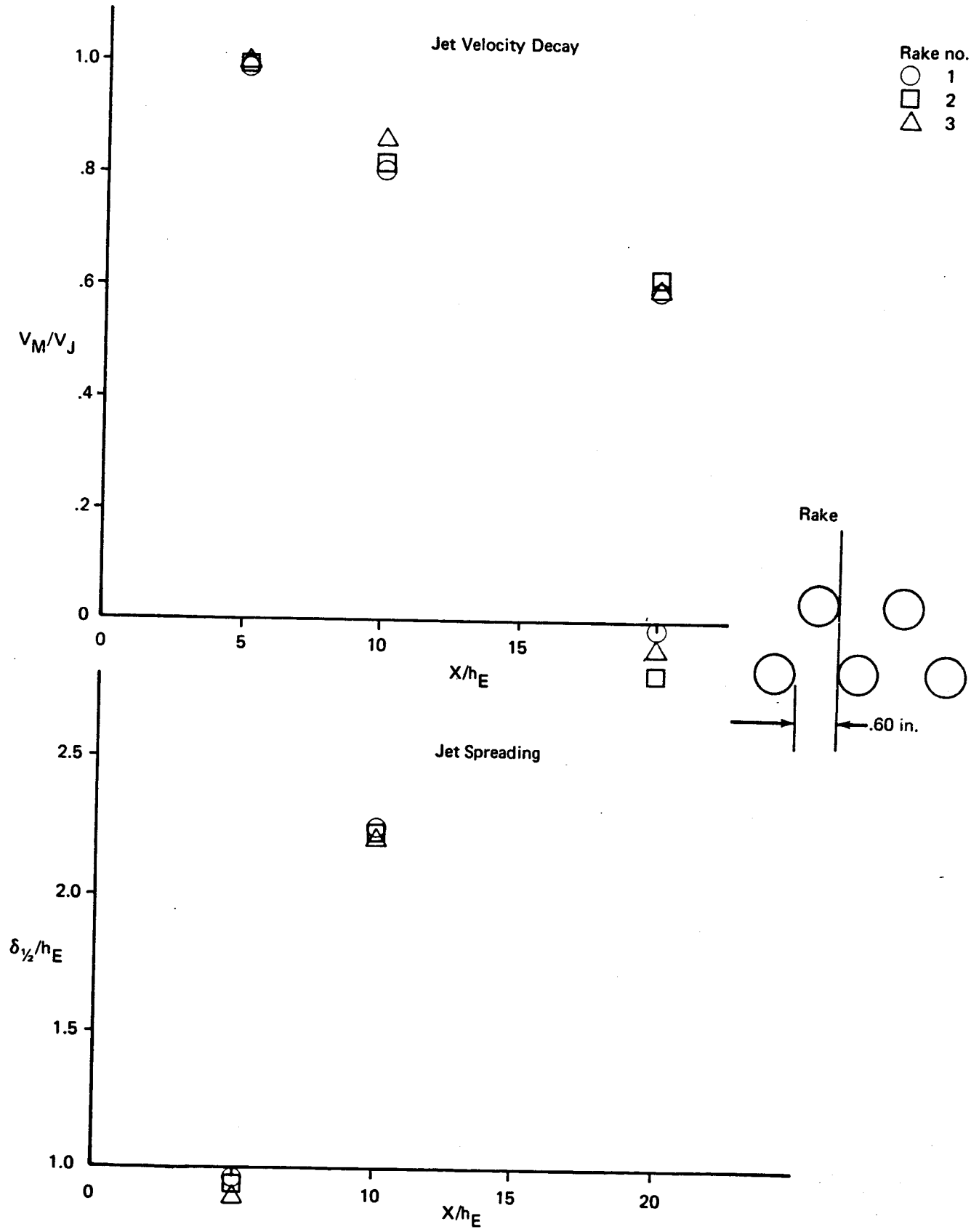

FIGURE 6-118.—JET VELOCITY DECAY AND JET SPREADING, 70-TUBE NOZZLE, NPR = 3.0

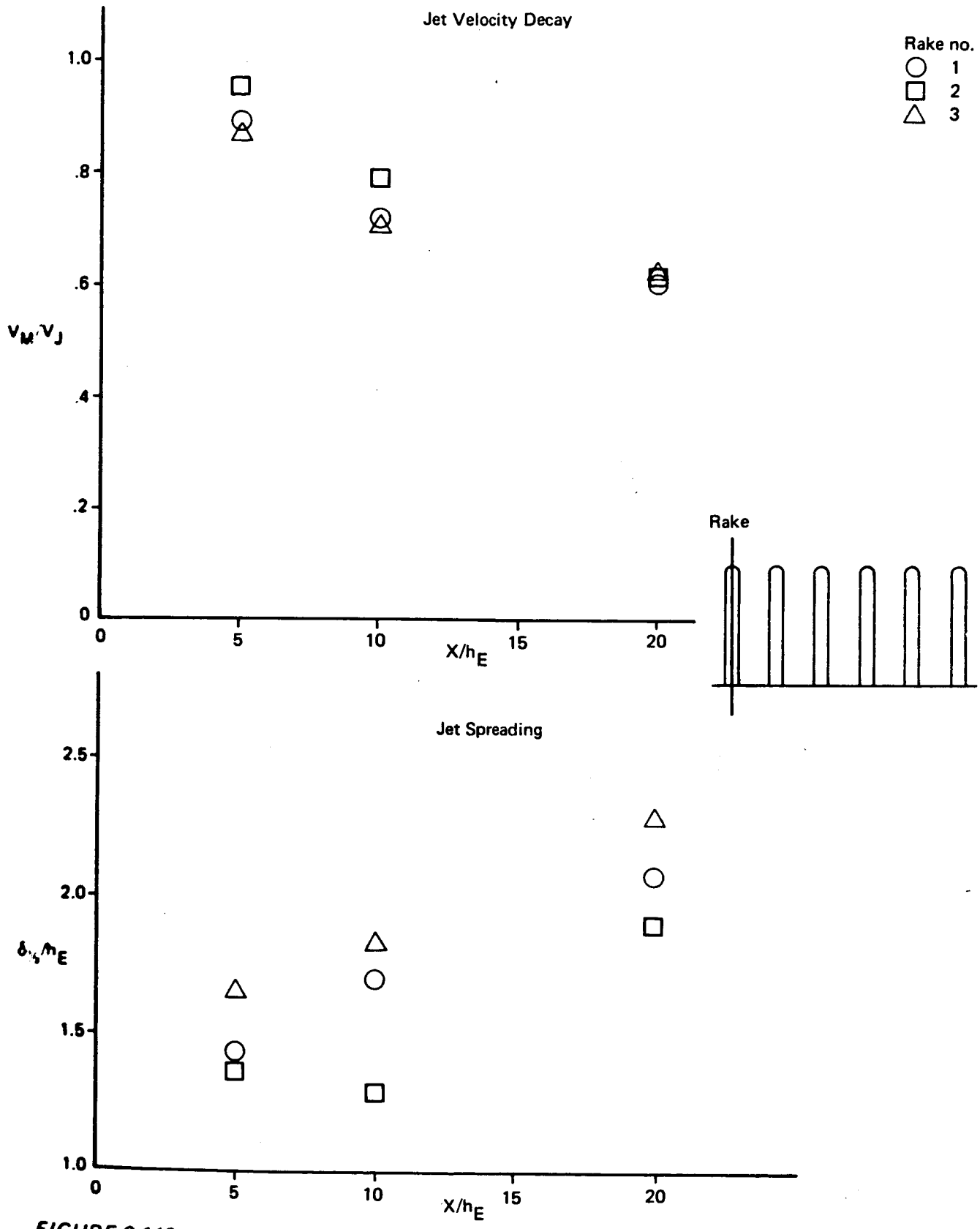

FIGURE 6-119.—JET VELOCITY DECAY AND JET SPREADING, THIN LOBE NOZZLE, NPR = 2.0 (A.R. = 4.0)

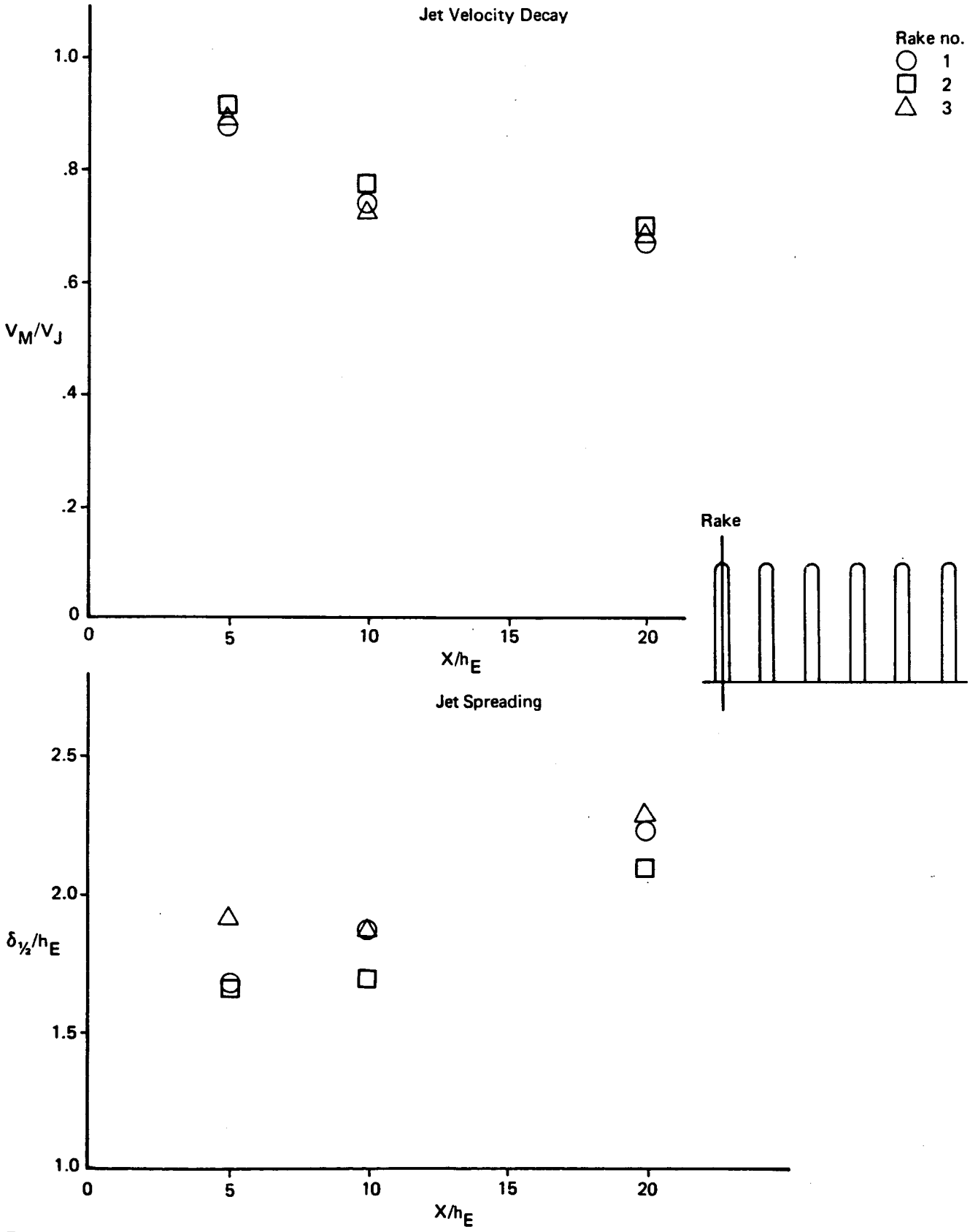

FIGURE 6-120.—JET VELOCITY DECAY AND JET SPREADING, THIN LOBE NOZZLE, NPR = 3.0 (A.R. = 4.0)

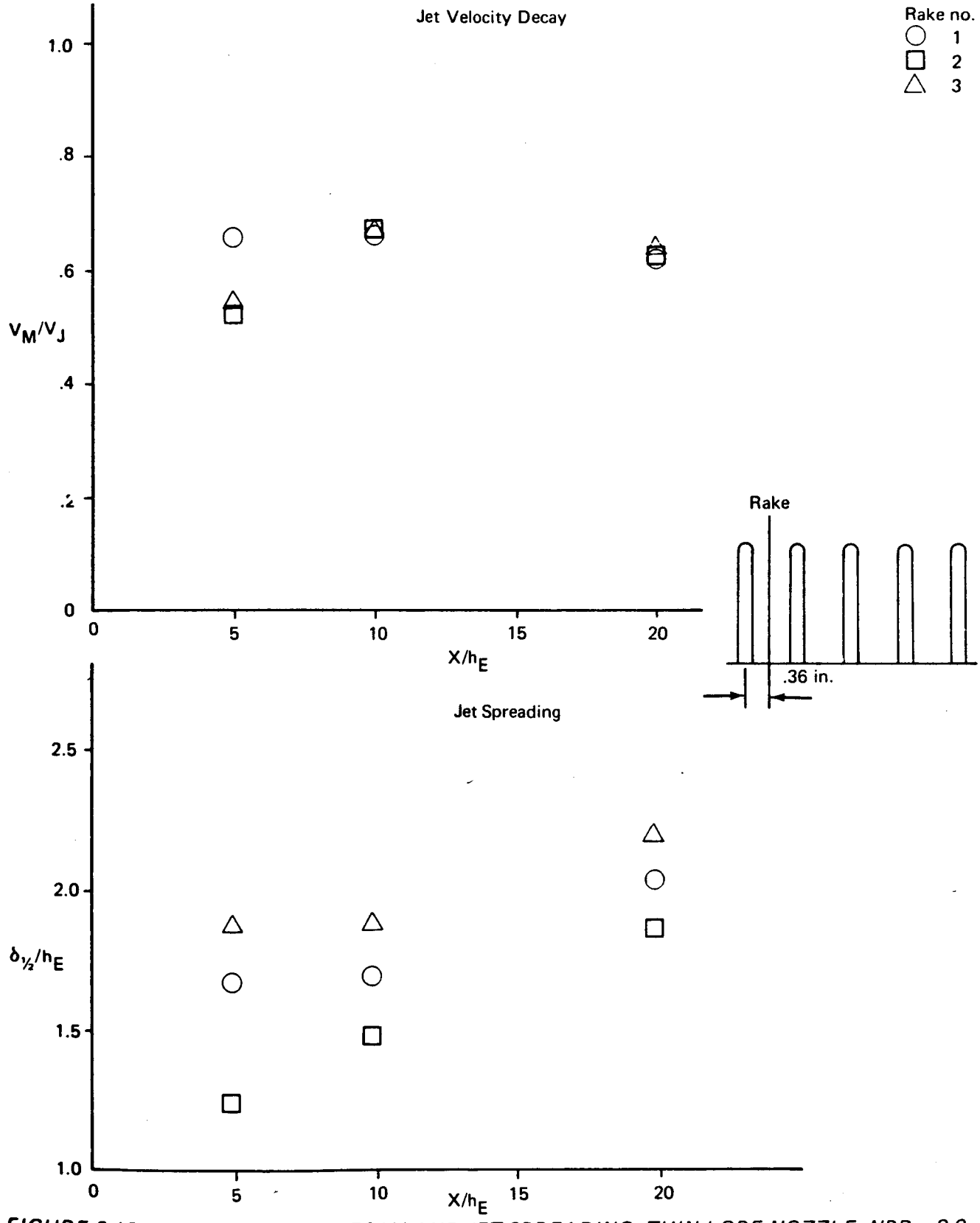

FIGURE 6-121.—JET VELOCITY DECAY AND JET SPREADING, THIN LOBE NOZZLE, NPR = 2.0 (A.R. = 4.0)

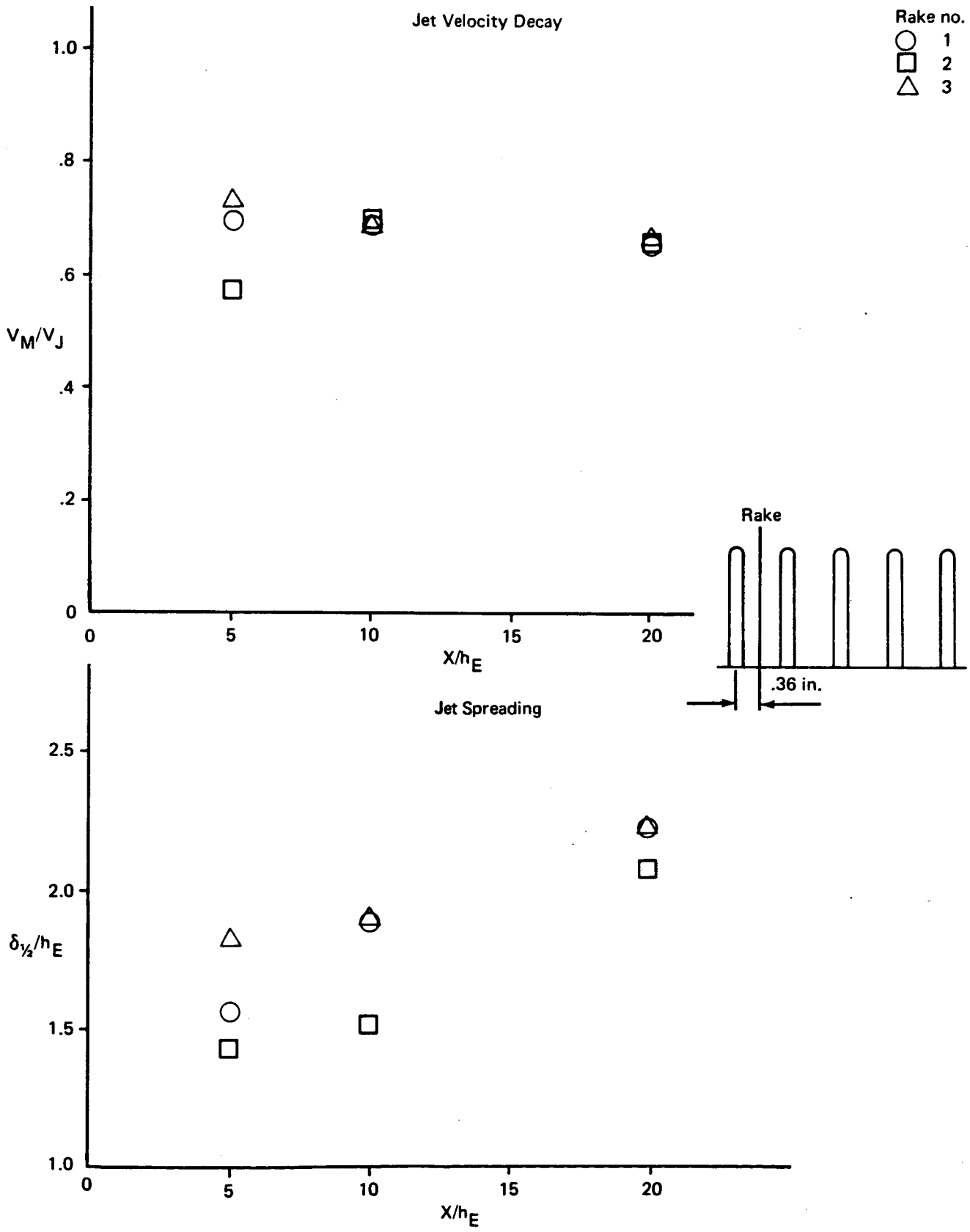

FIGURE 6-122.–JET VELOCITY DECAY AND JET SPREADING, THIN LOBE NOZZLE, NPR = 3.0 (A.R. = 4.0)

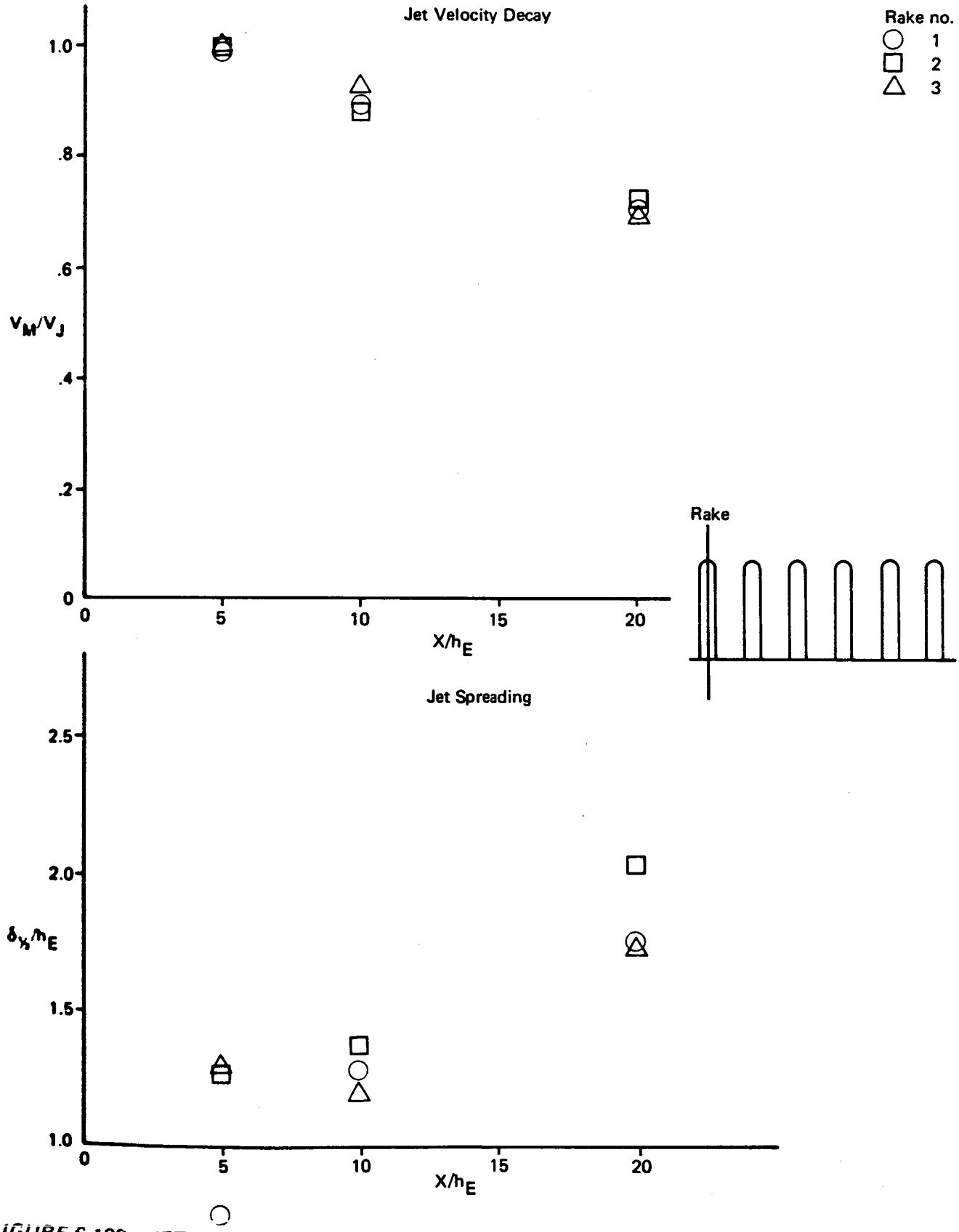

FIGURE 6-123.—JET VELOCITY DECAY AND JET SPREADING, THICK LOBE NOZZLE, NPR = 2.0 (A.R. = 2.5)

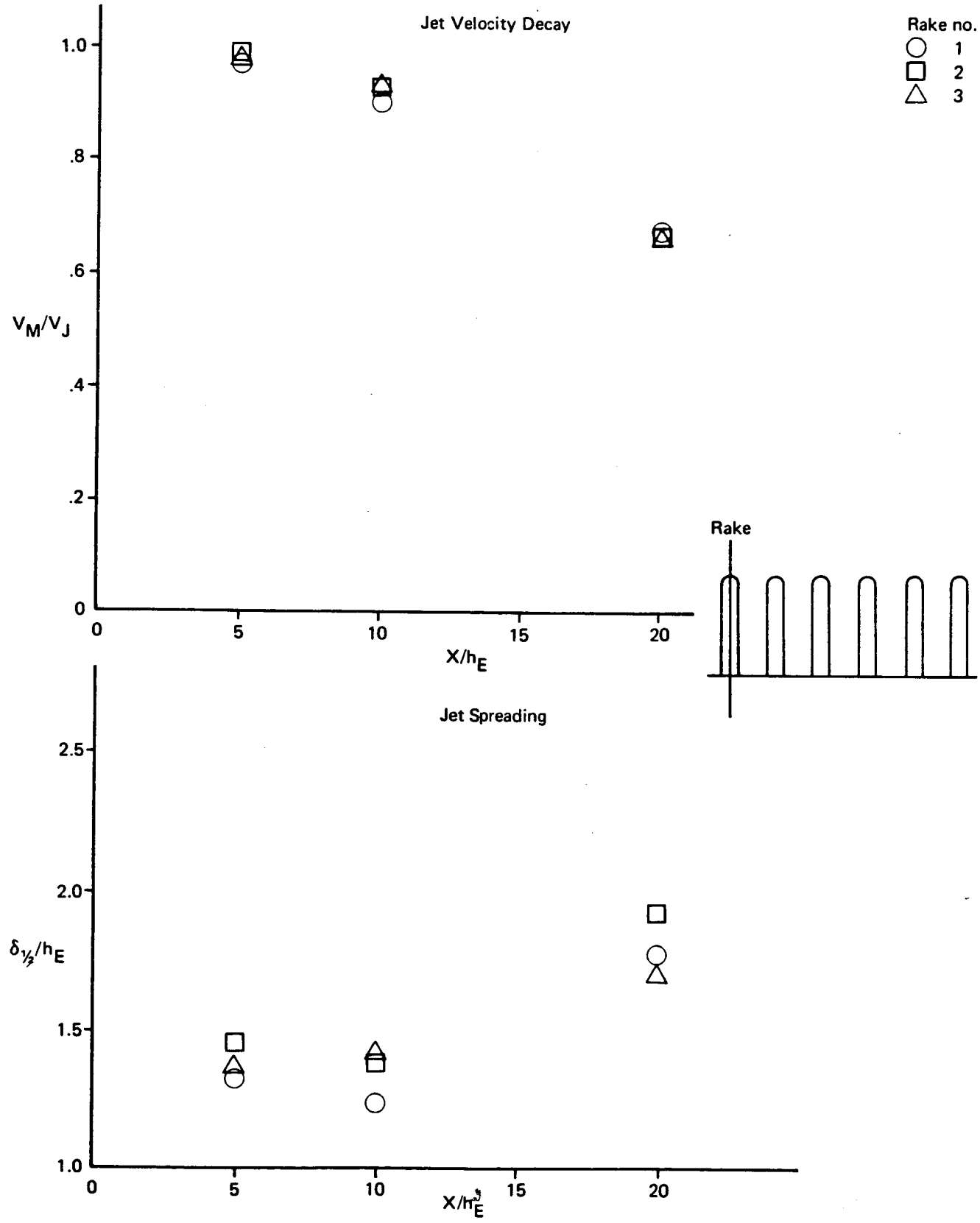

FIGURE 6-124.—JET VELOCITY DECAY AND JET SPREADING, THICK LOBE NOZZLE, NPR = 3.0 (A.R. = 2.5)

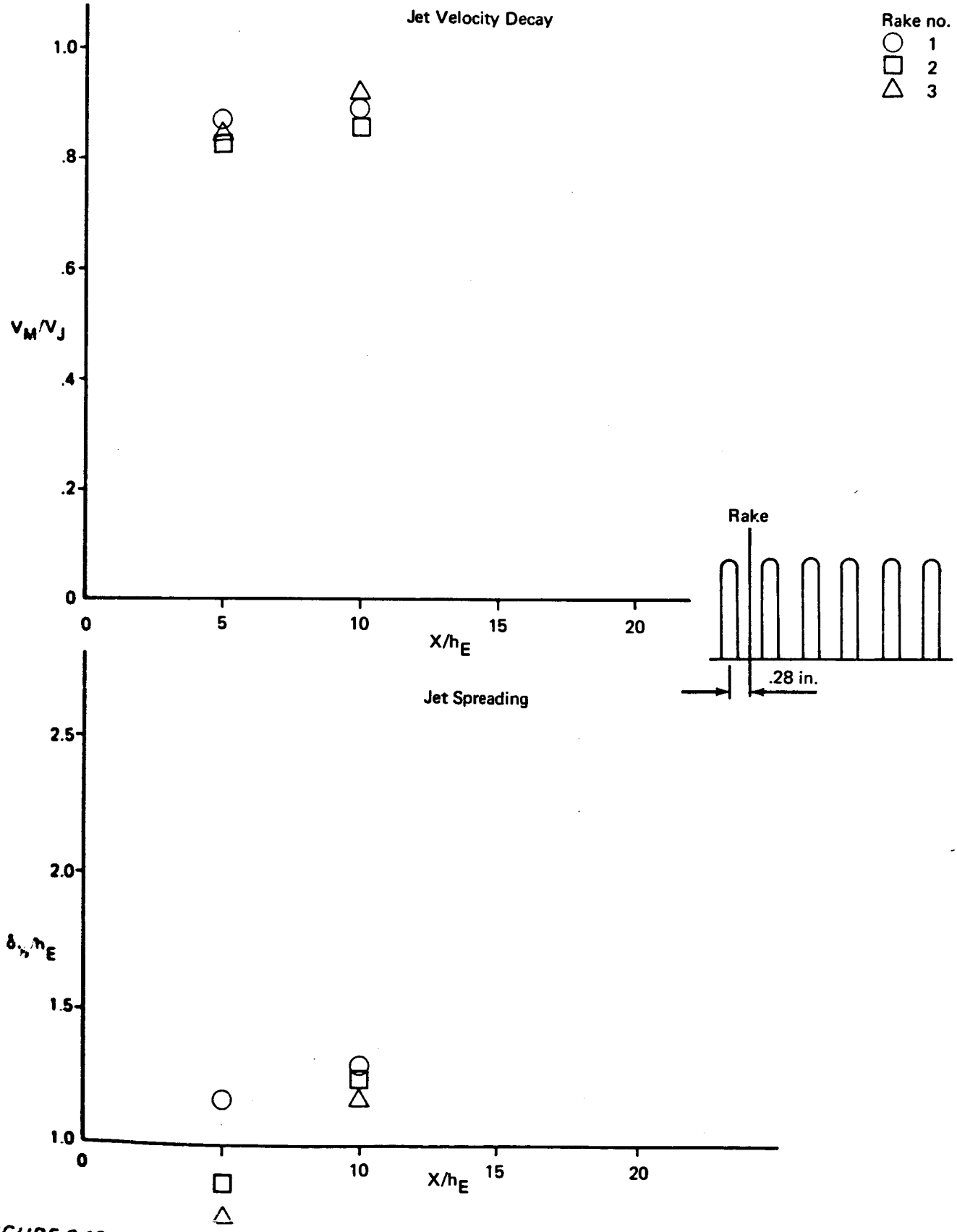

FIGURE 6-125.—JET VELOCITY DECAY AND JET SPREADING, THICK LOBE NOZZLE, NPR = 2.0 (A.R. = 2.5)

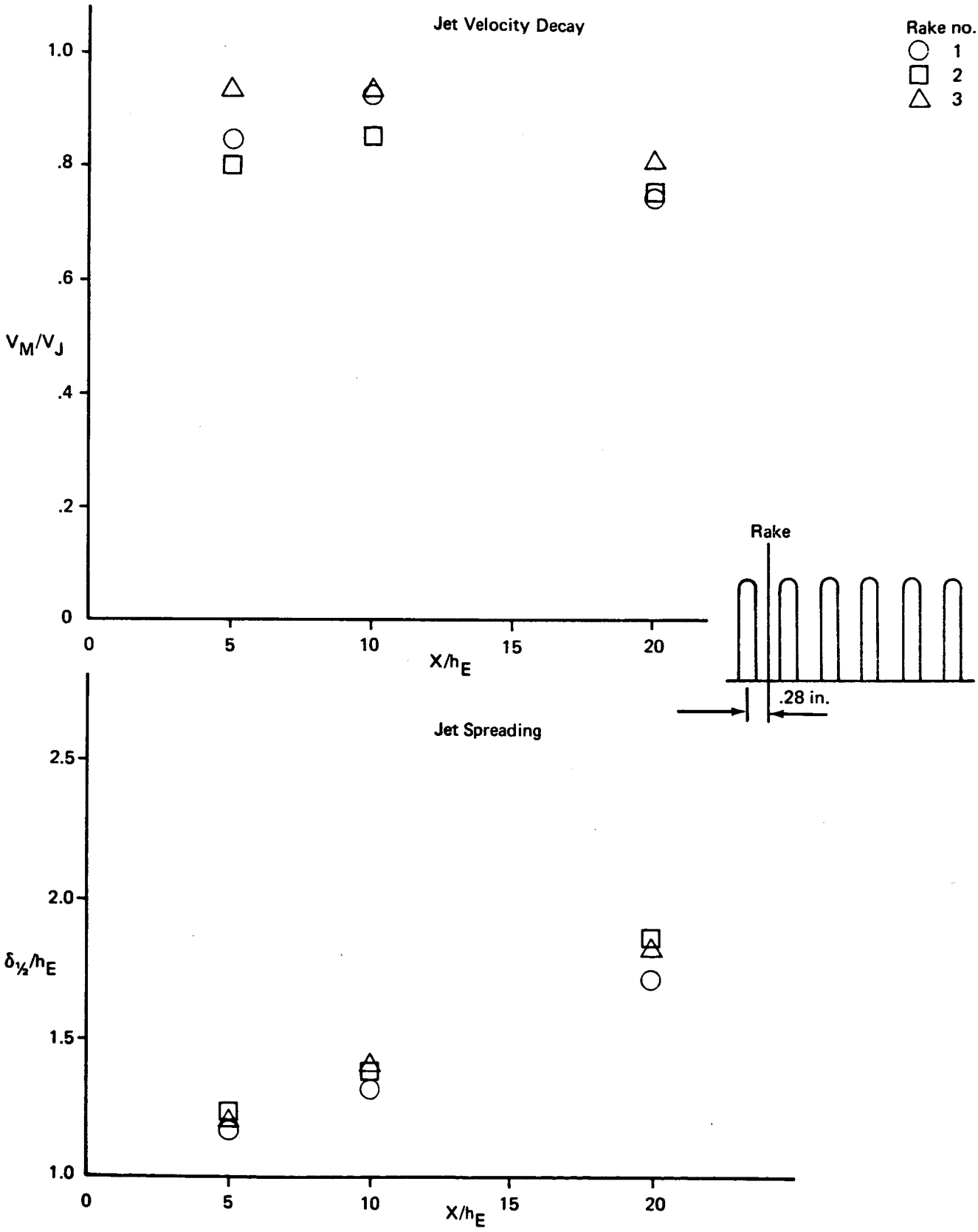

FIGURE 6-126.—JET VELOCITY DECAY AND JET SPREADING, THICK LOBE NOZZLE, NPR = 3.0 (A.R. = 2.5)

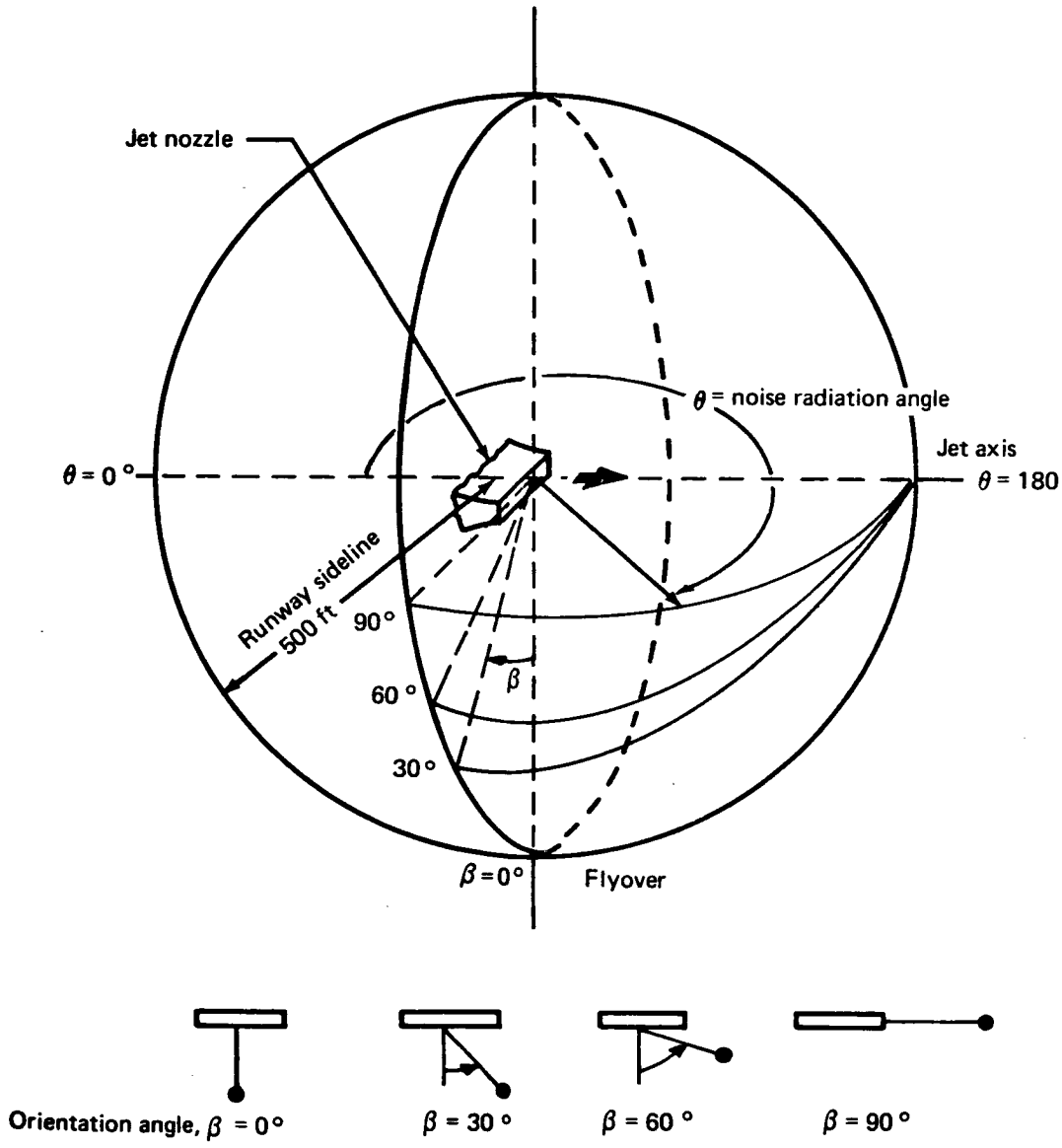

FIGURE 6-127.– COORDINATE SYSTEM USED FOR NOISE SURVEYS

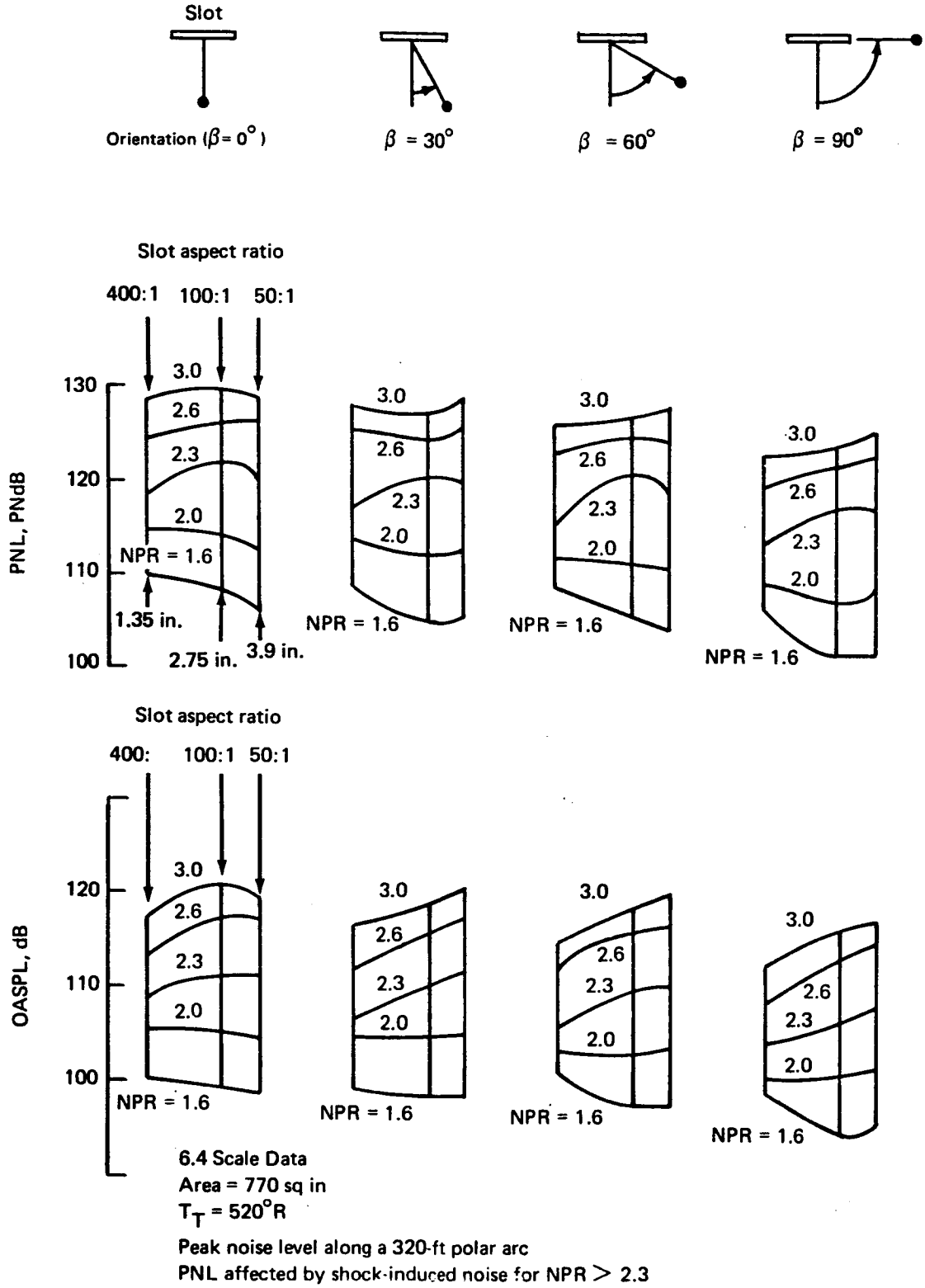

FIGURE 6-128.— SLOT NOZZLE PEAK NOISE LEVELS AS A FUNCTION OF PRESSURE RATIO, ASPECT RATIO, AND ORIENTATION

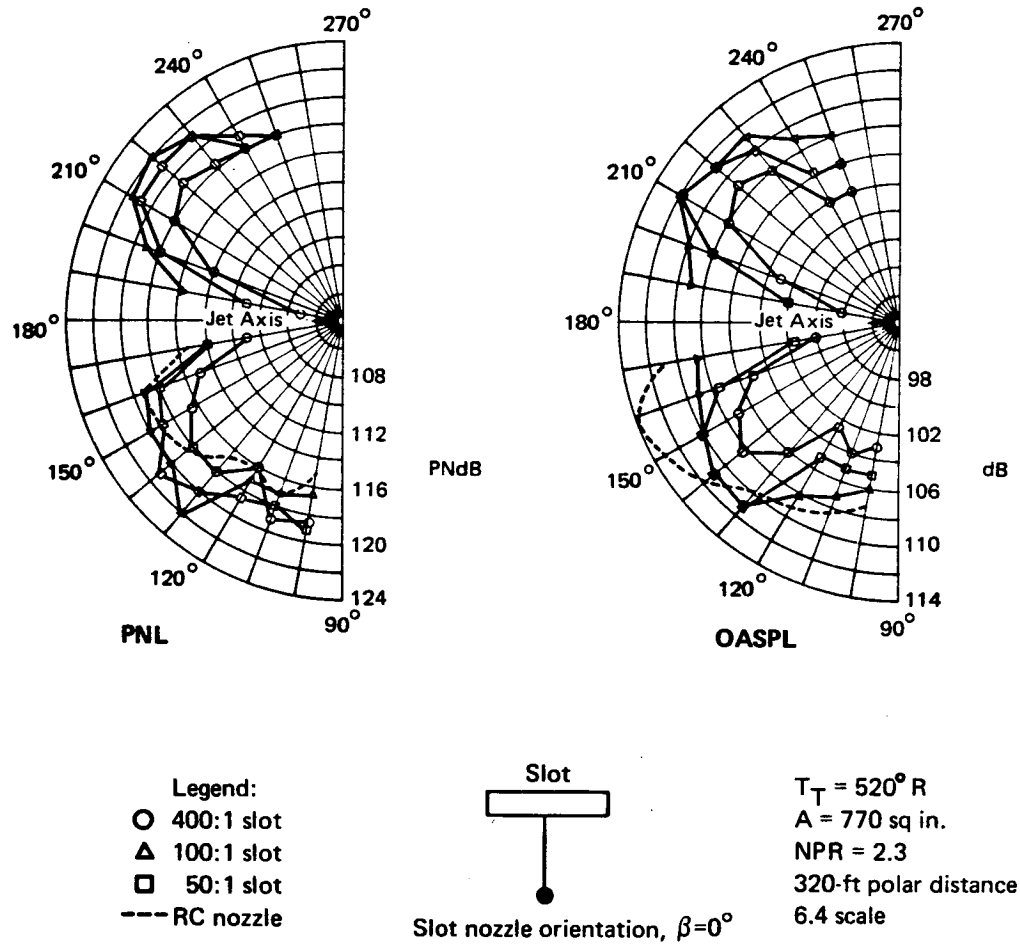

FIGURE 6-129.– EFFECT OF SLOT NOZZLE ASPECT RATIO ON DIRECTIONALITY PATTERNS

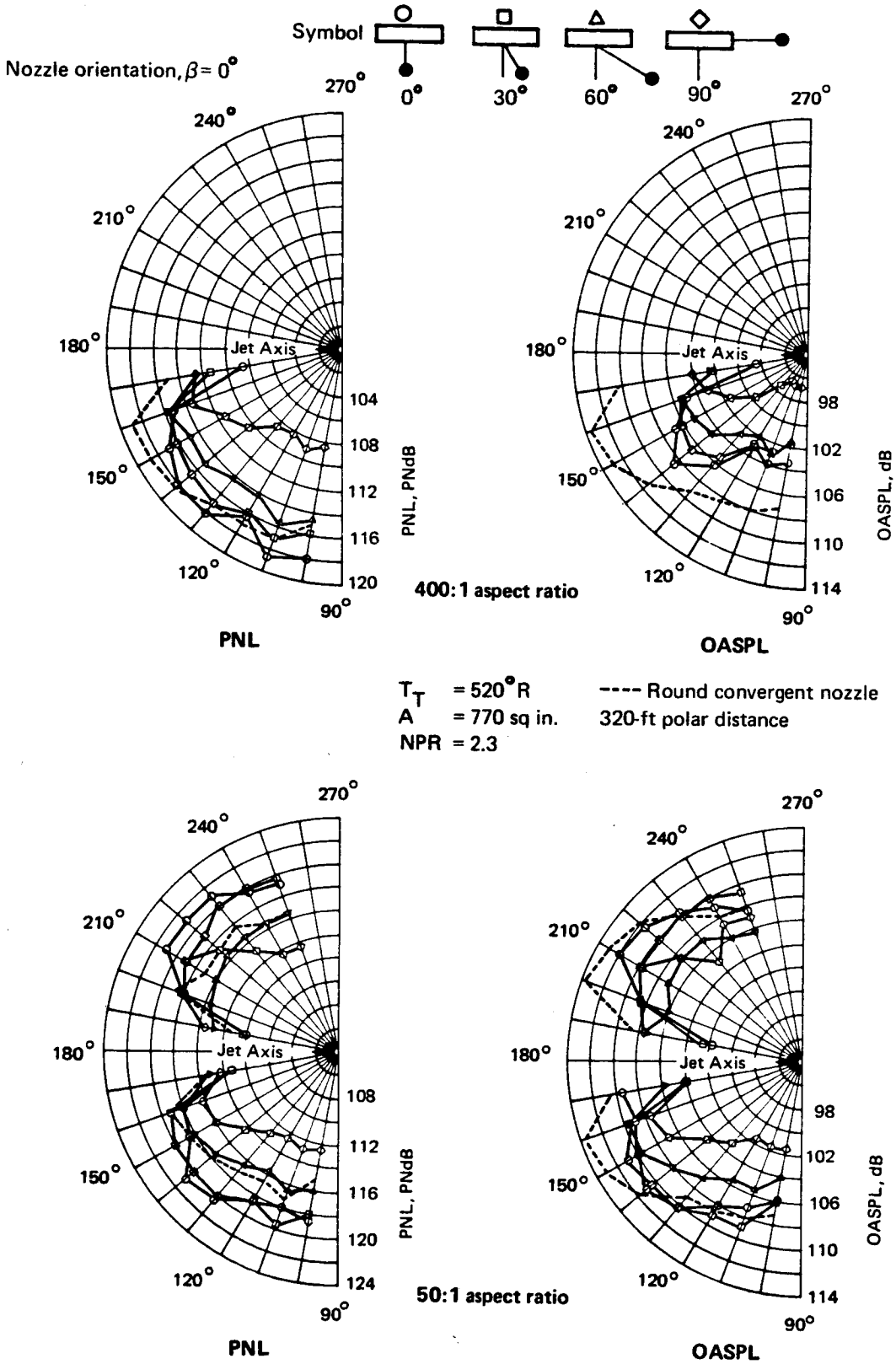

FIGURE 6-130.– EFFECT OF SLOT NOZZLE ORIENTATION ON DIRECTIONALITY PATTERN

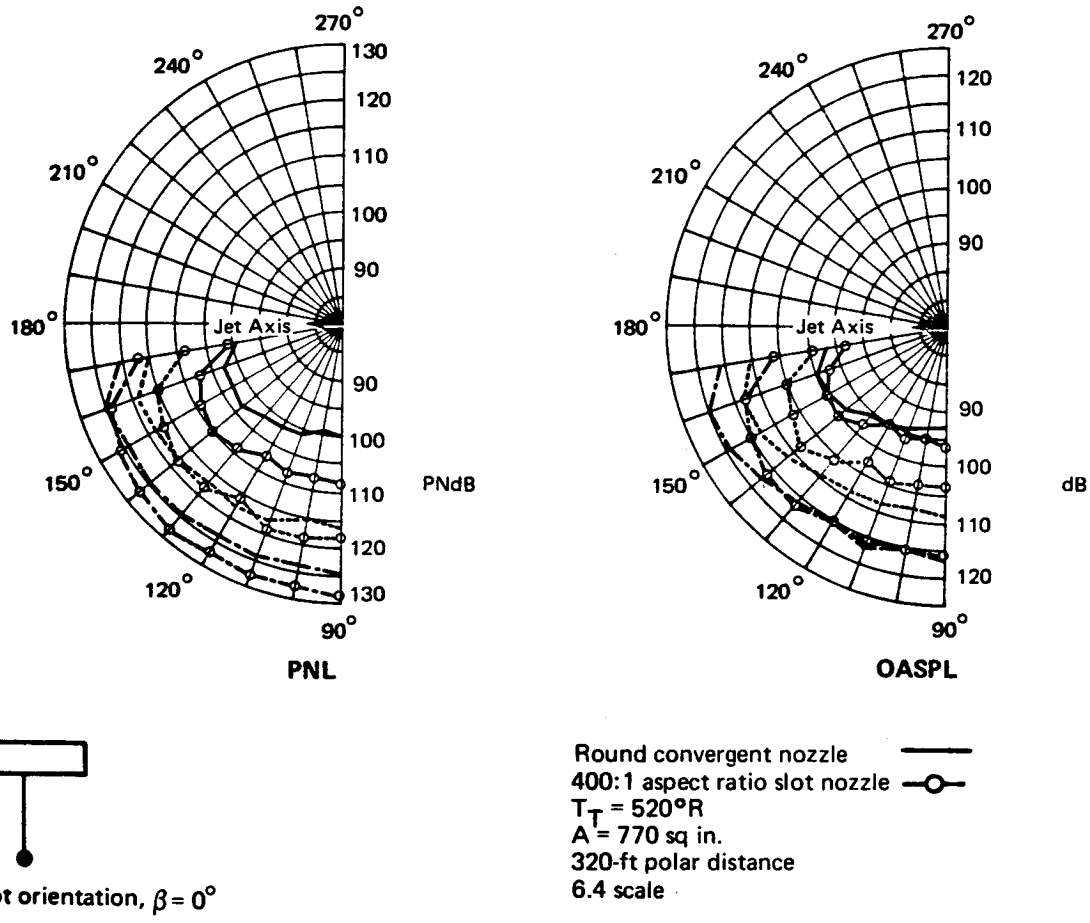

FIGURE 6-131.— EFFECT OF SLOT NOZZLE PRESSURE RATIO ON DIRECTIONALITY PATTERNS

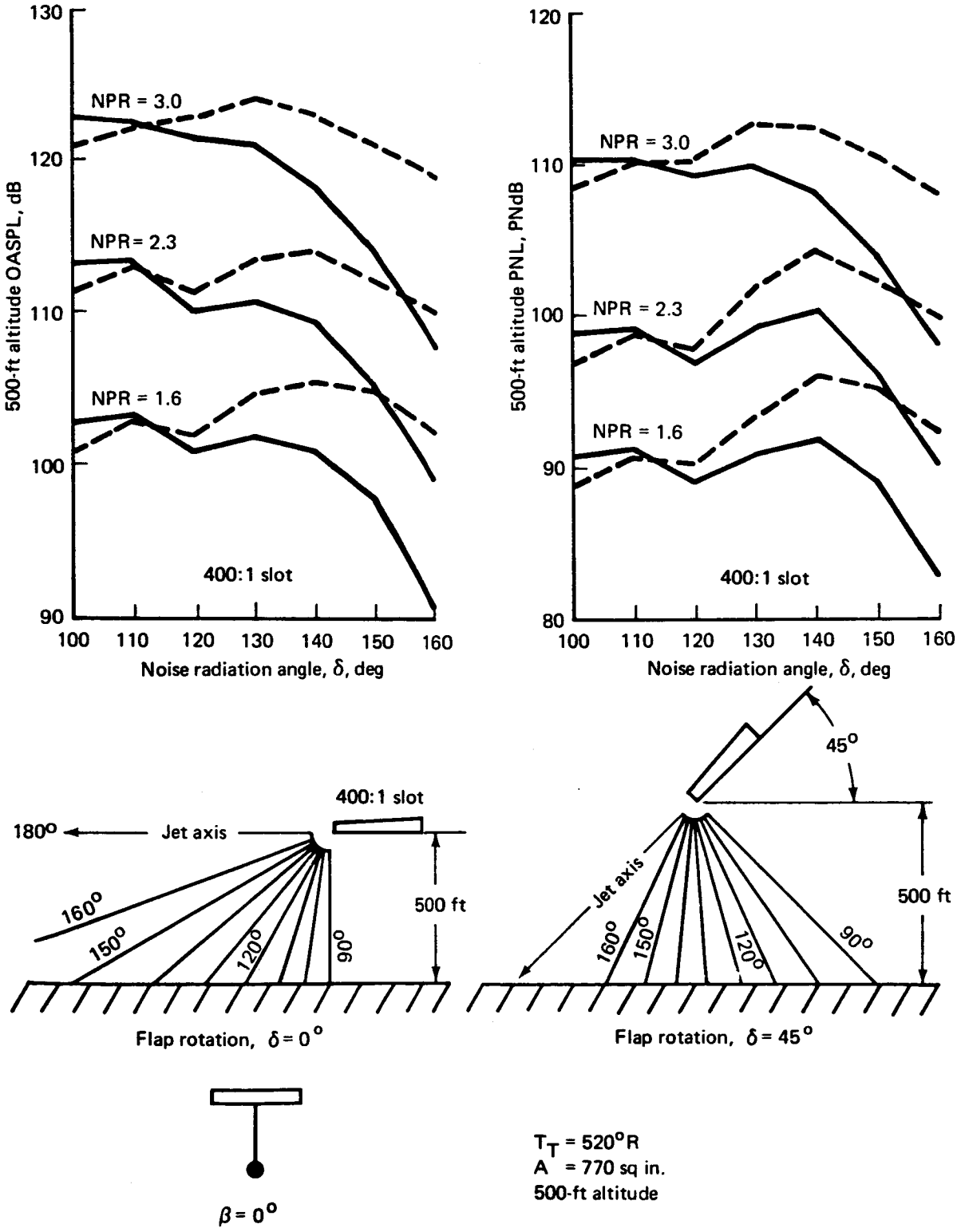

FIGURE 6-132.– EFFECT OF SLOT NOZZLE ROTATION, δ, ON FLYOVER NOISE LEVELS

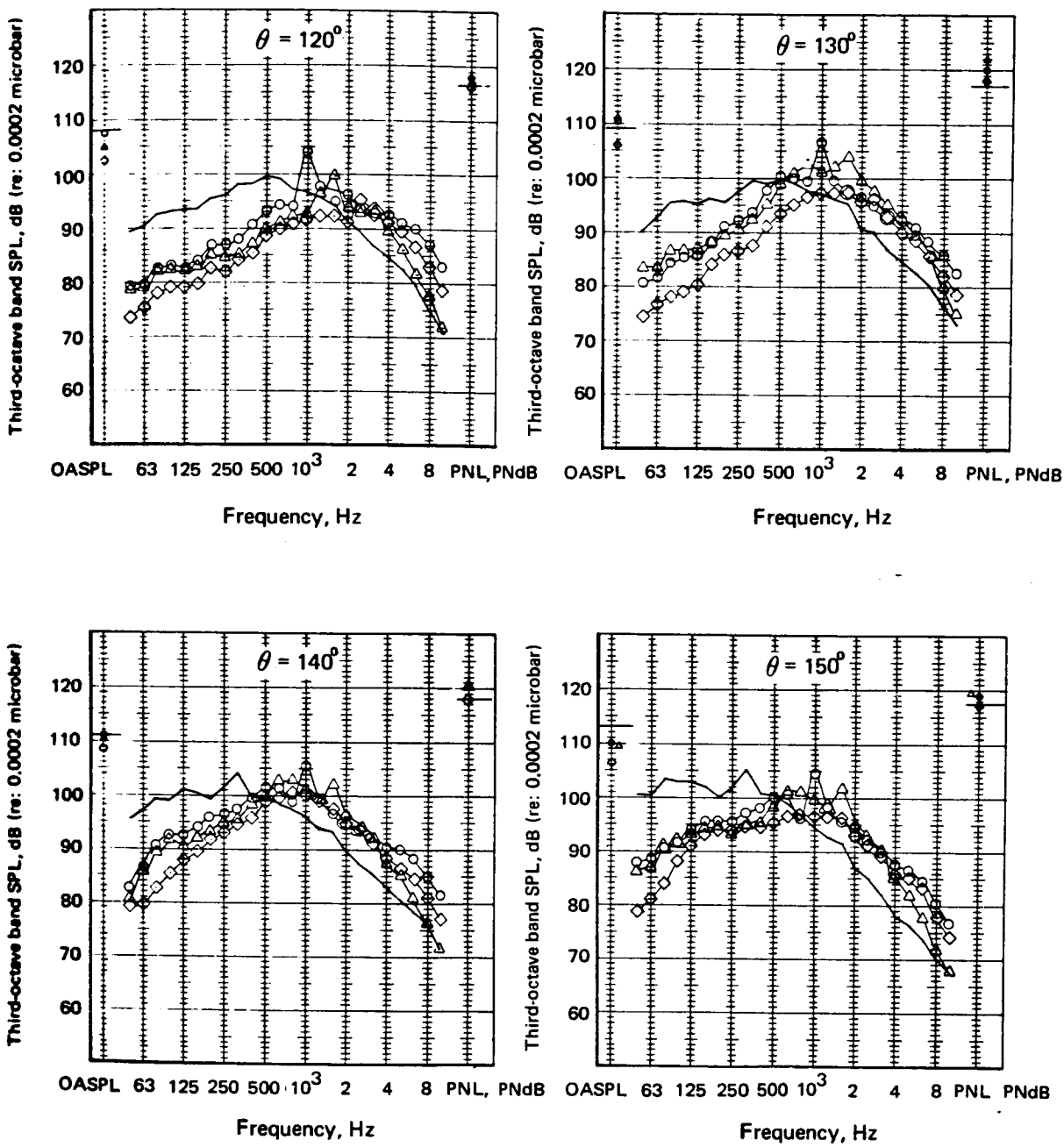

320-ft polar noise spectra

— Standard nozzle
○ 50:1 slot nozzle
△ 100:1 slot nozzle
◇ 400:1 slot nozzle

NPR = 2.3
T_T = ambient
A = 770 sq in.

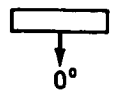

Slot nozzle orientation ($\beta = 0°$)

FIGURE 6-133.—NOISE SPECTRA FOR DIFFERENT ASPECT RATIOS ($\beta = 0°$)

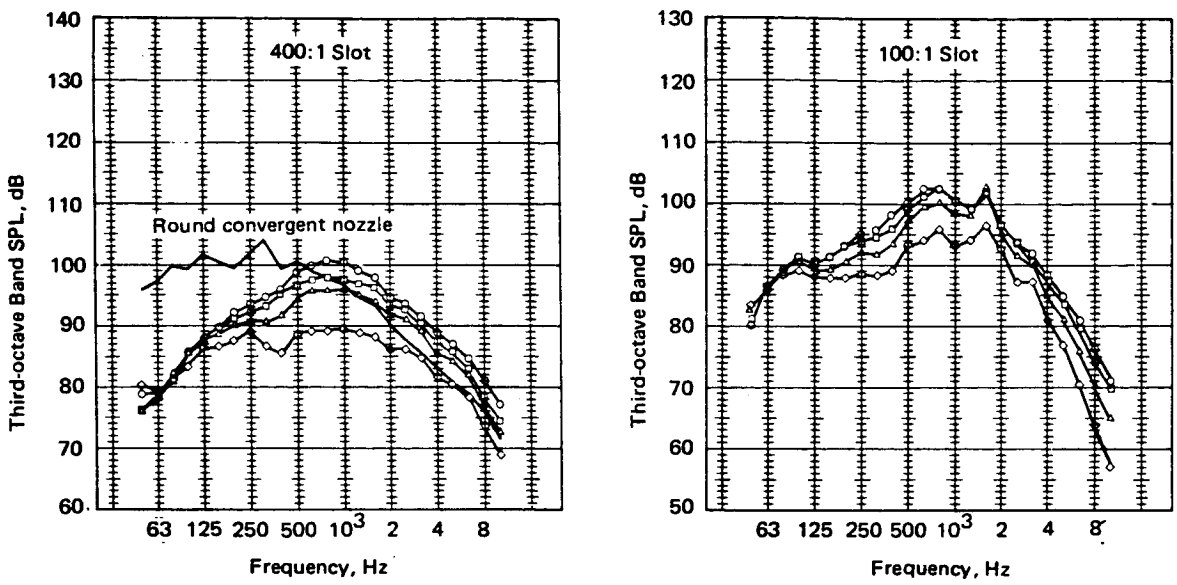

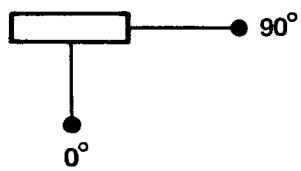

Slot nozzle orientation, $\beta = 0°$

○ $\beta = 0°$
□ $\beta = 30°$
△ $\beta = 60°$
◇ $\beta = 90°$

PR = 2.3
$T_T = 520°$ R
A = 770 sq in.
320-ft polar distance

FIGURE 6-134.—NOISE SPECTRA FOR DIFFERENT NOZZLE ORIENTATIONS

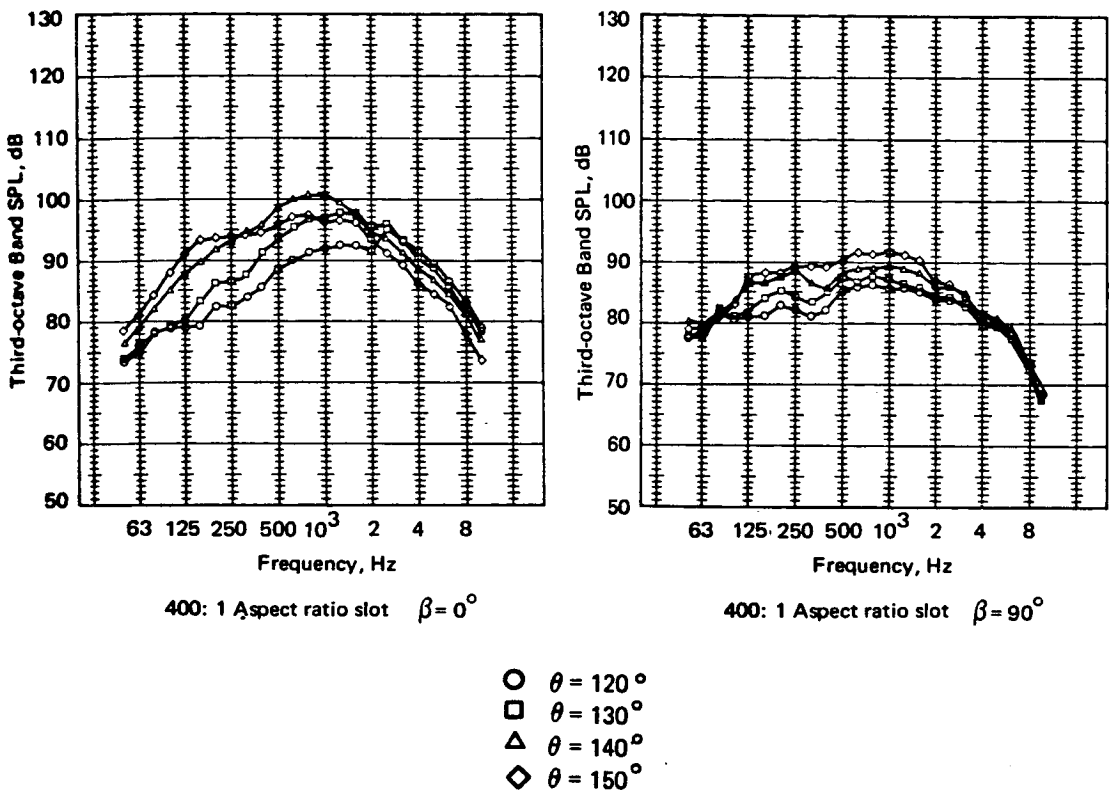

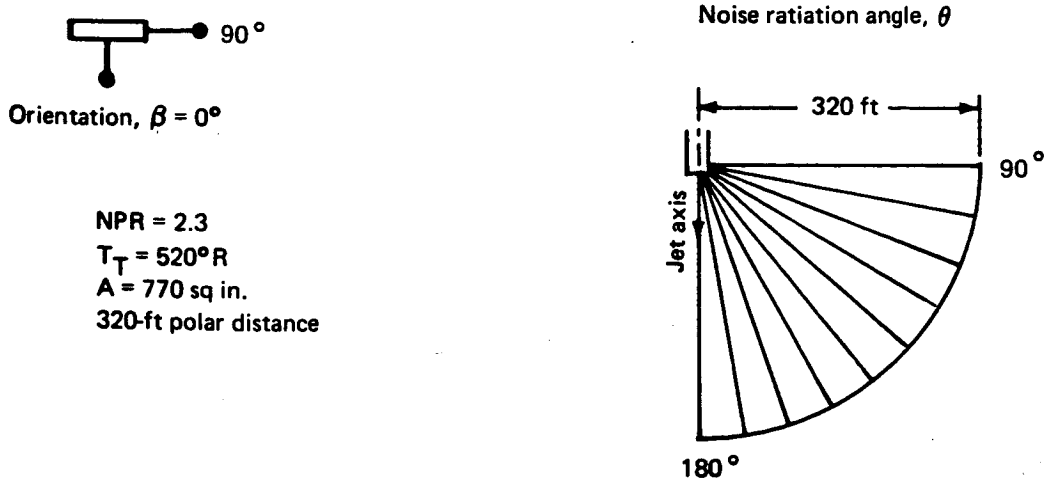

FIGURE 6-135.—NOISE SPECTRA AT DIFFERENT NOISE RADIATION ANGLES

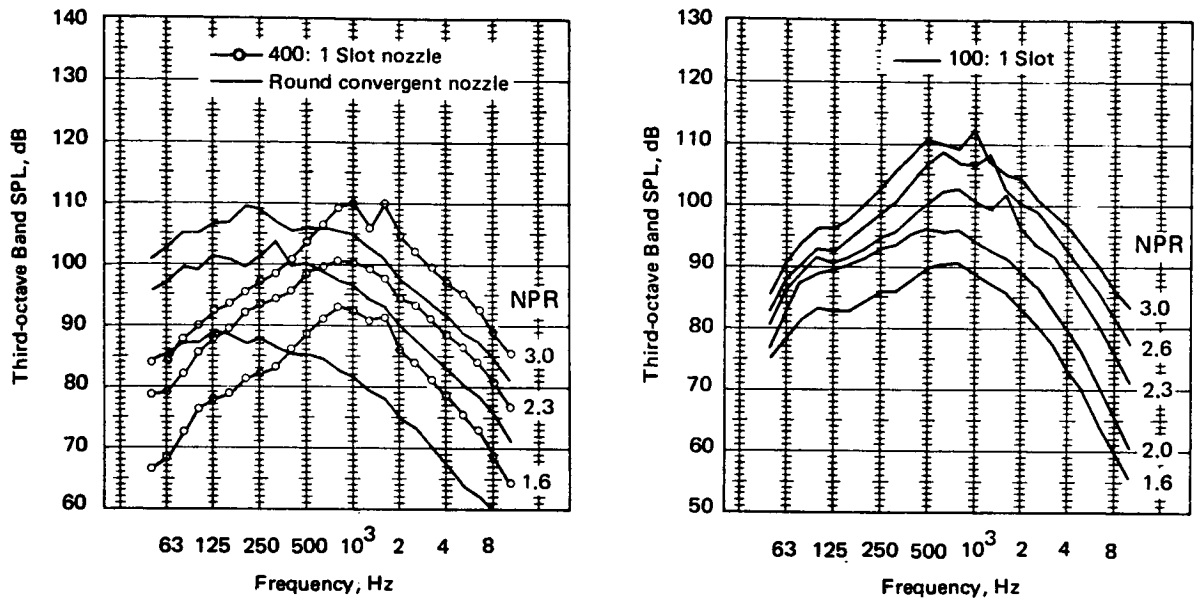

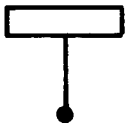

Slot nozzle orientation, $\beta = 0^\circ$

$T_T = 520°R$
A = 770 sq in.
320-ft polar distance
6.4 scale

FIGURE 6-136.—NOISE SPECTRA AT DIFFERENT SLOT NOZZLE PRESSURE RATIOS

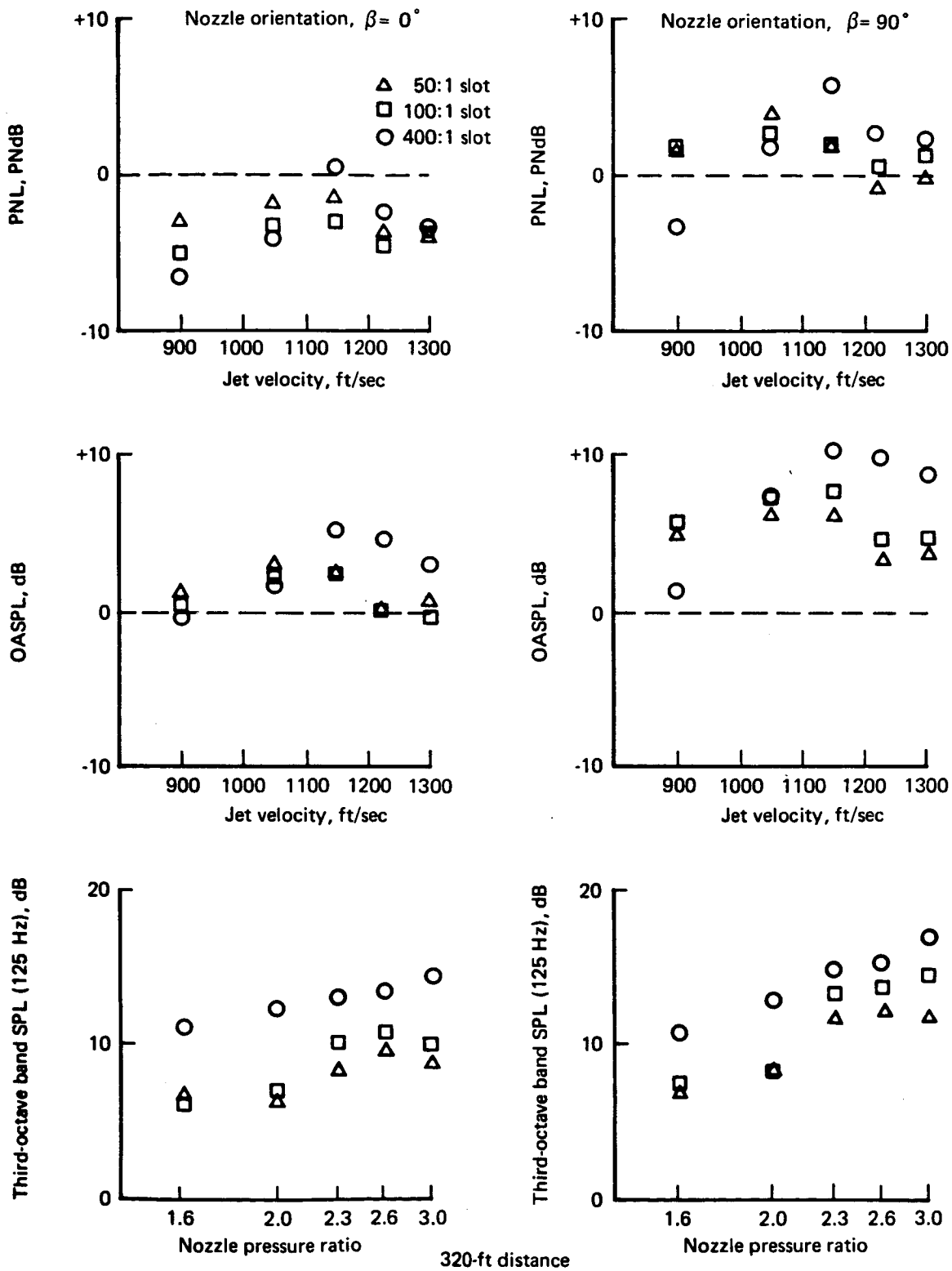

320-ft distance
A = 770 sq in.
T_T = ambient
Suppression relative to round convergent nozzle

FIGURE 6-137.—SLOT NOZZLE SUPPRESSION RELATIVE TO ROUND CONVERGENT NOZZLE

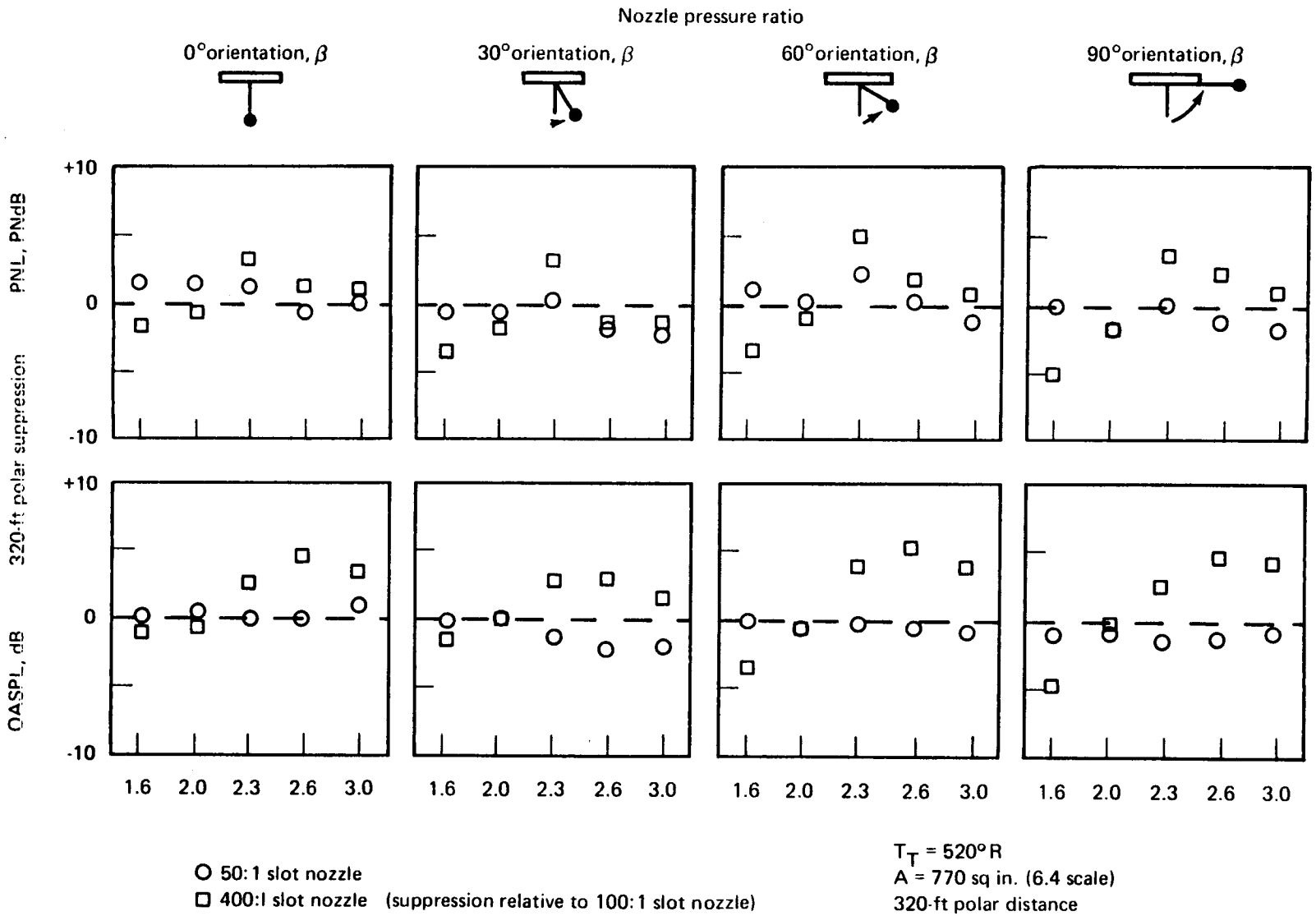

FIGURE 6-138.–SLOT NOZZLE NOISE SUPPRESSION RELATIVE TO THE 100:1 ASPECT RATIO SLOT NOZZLE

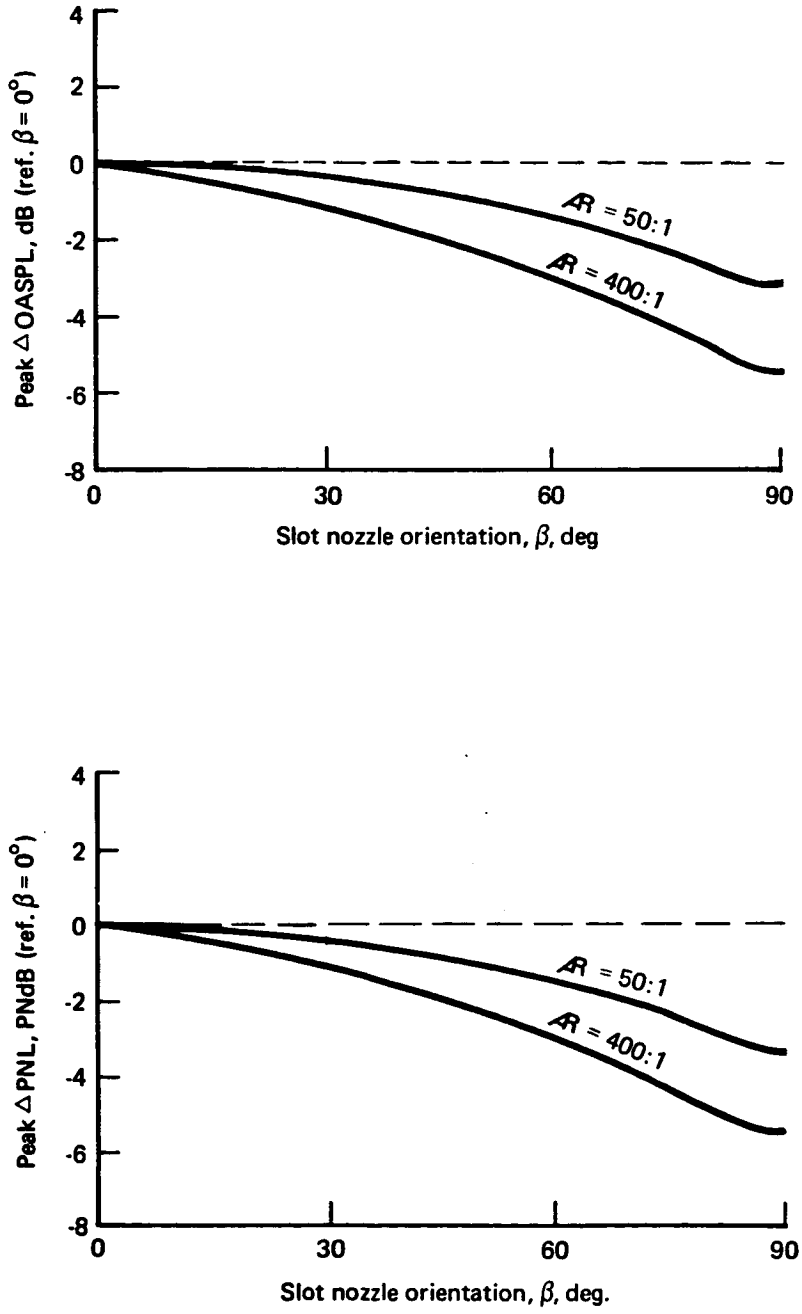

FIGURE 6-139.—EFFECT OF NOZZLE ORIENTATION ON NOISE

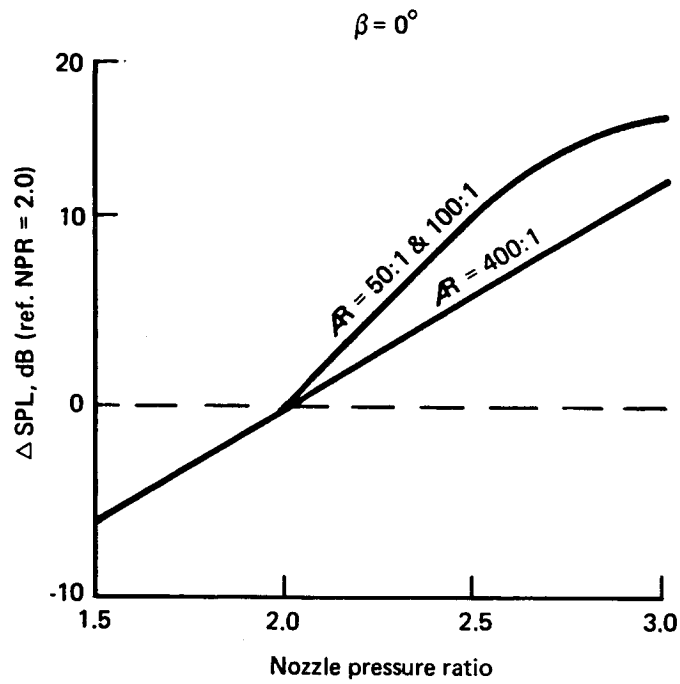

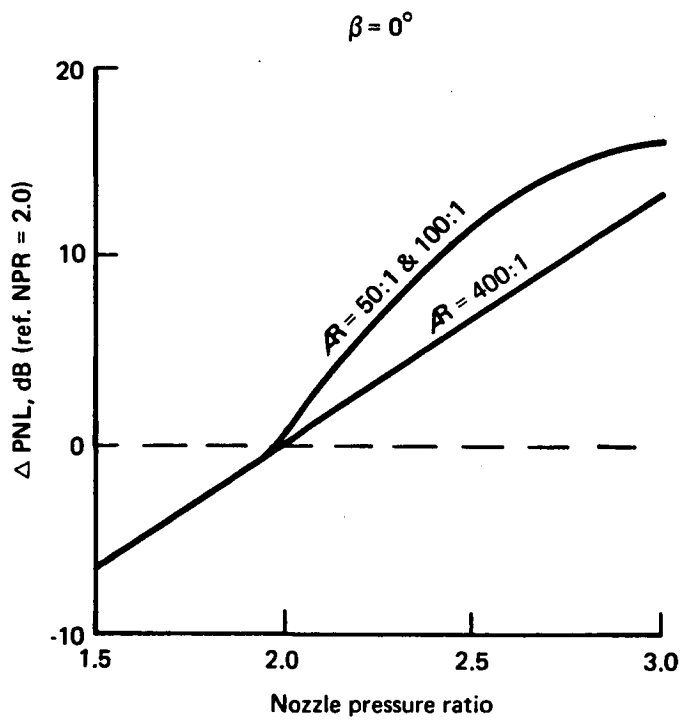

FIGURE 6-140.—EFFECTS OF PRESSURE RATIO AND ASPECT RATIO ON NOISE

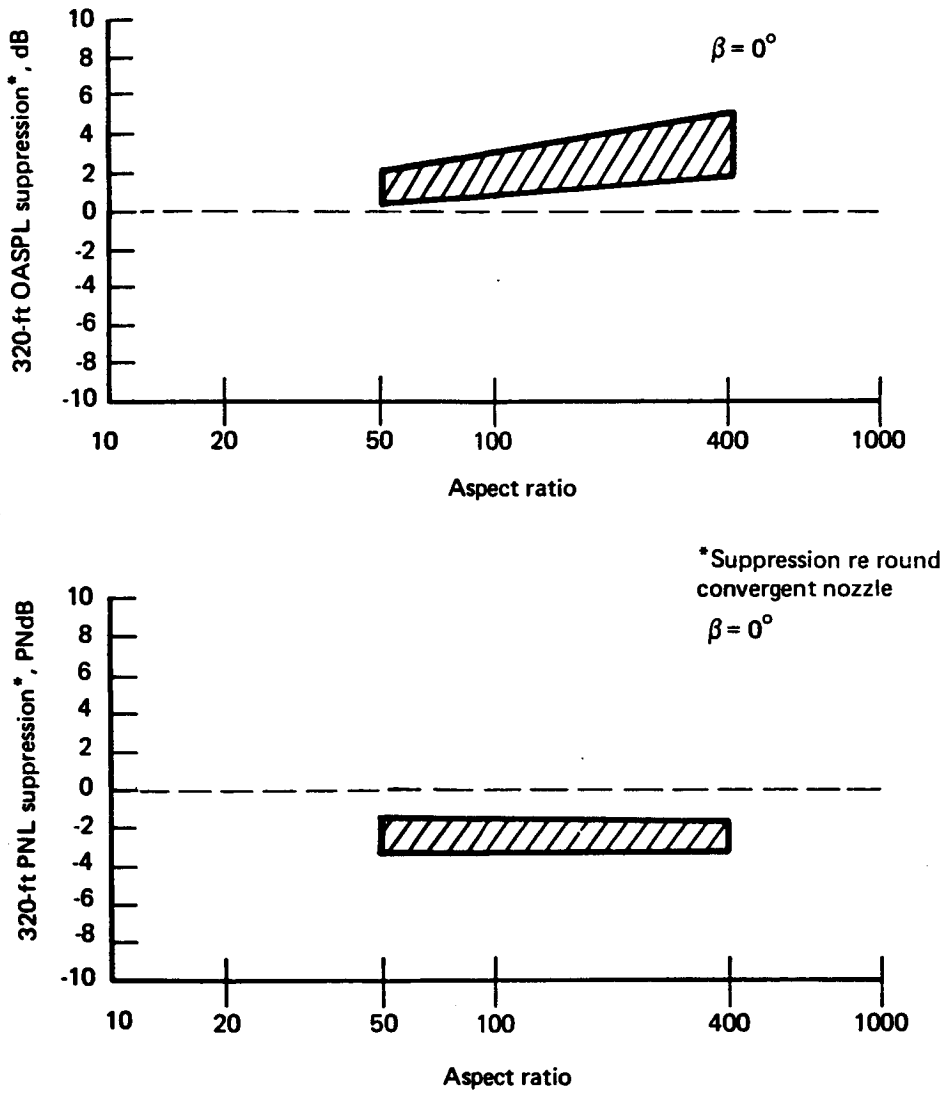

FIGURE 6-141.– EFFECT OF ASPECT RATIO ON SUPPRESSION

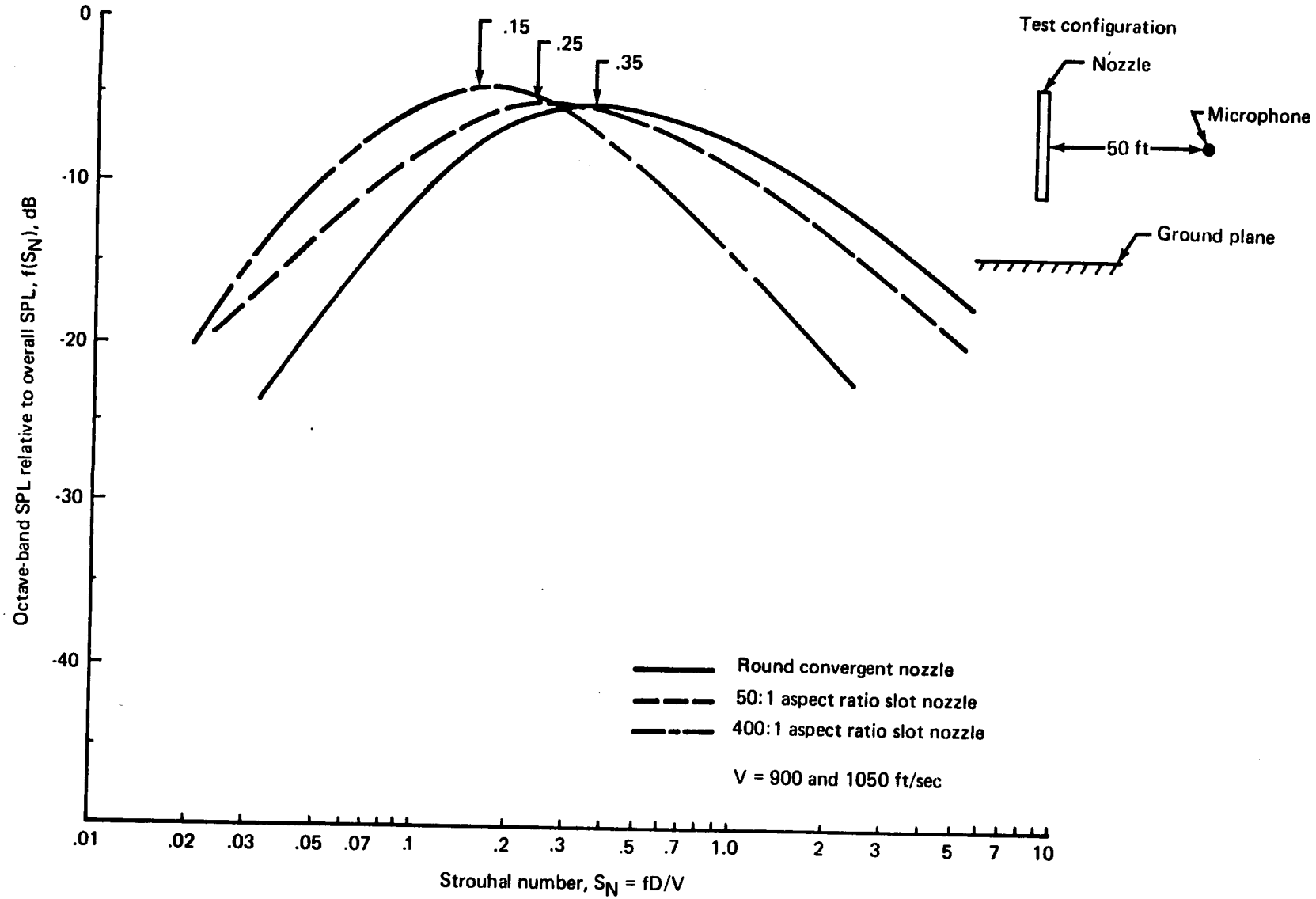

FIGURE 6-142.– EFFECT OF ASPECT RATIO ON PEAK STROUHAL NUMBER

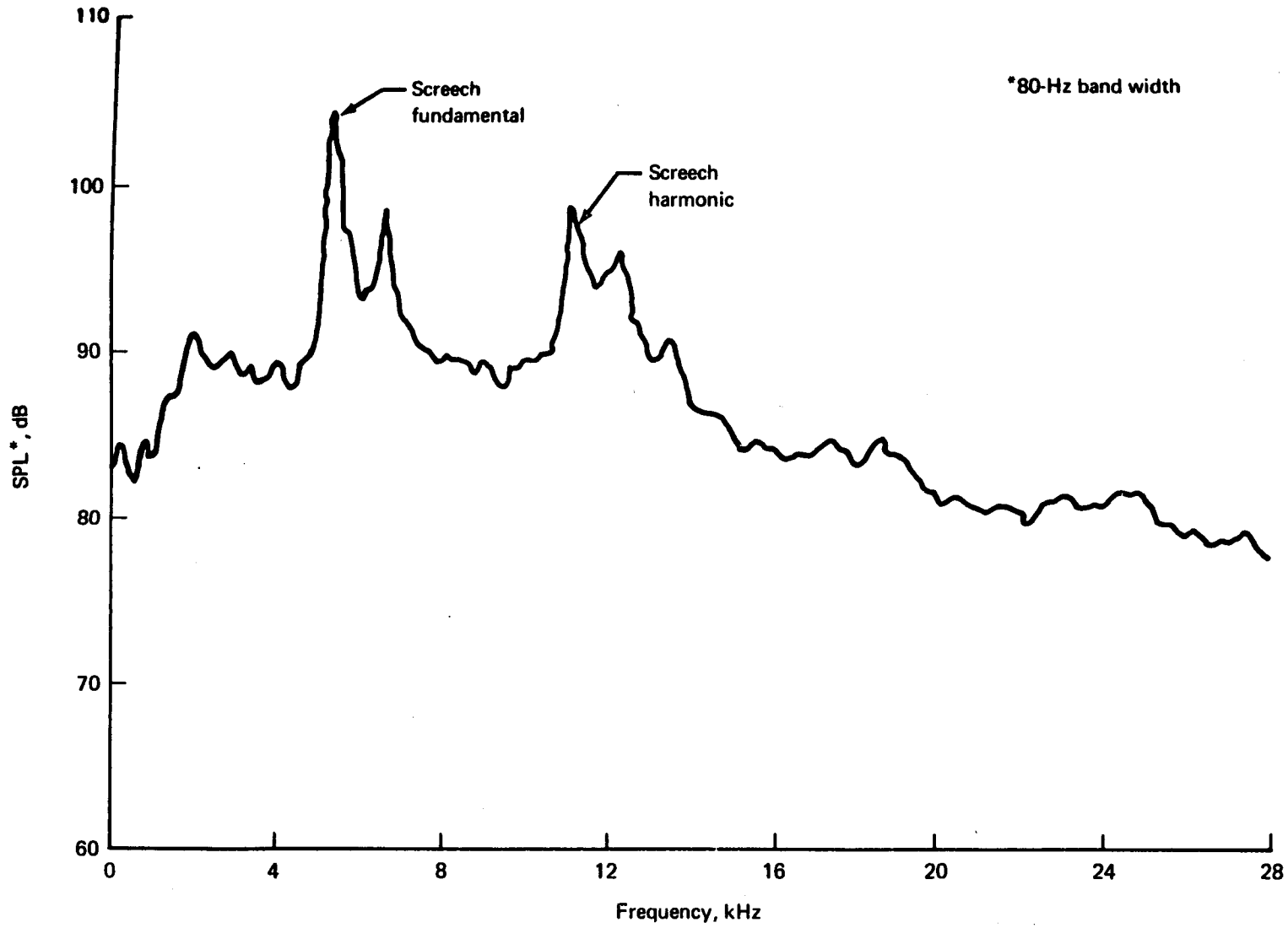

FIGURE 6-143.—NOISE SPECTRA OF CONVERGENT NOZZLE AT NPR = 3

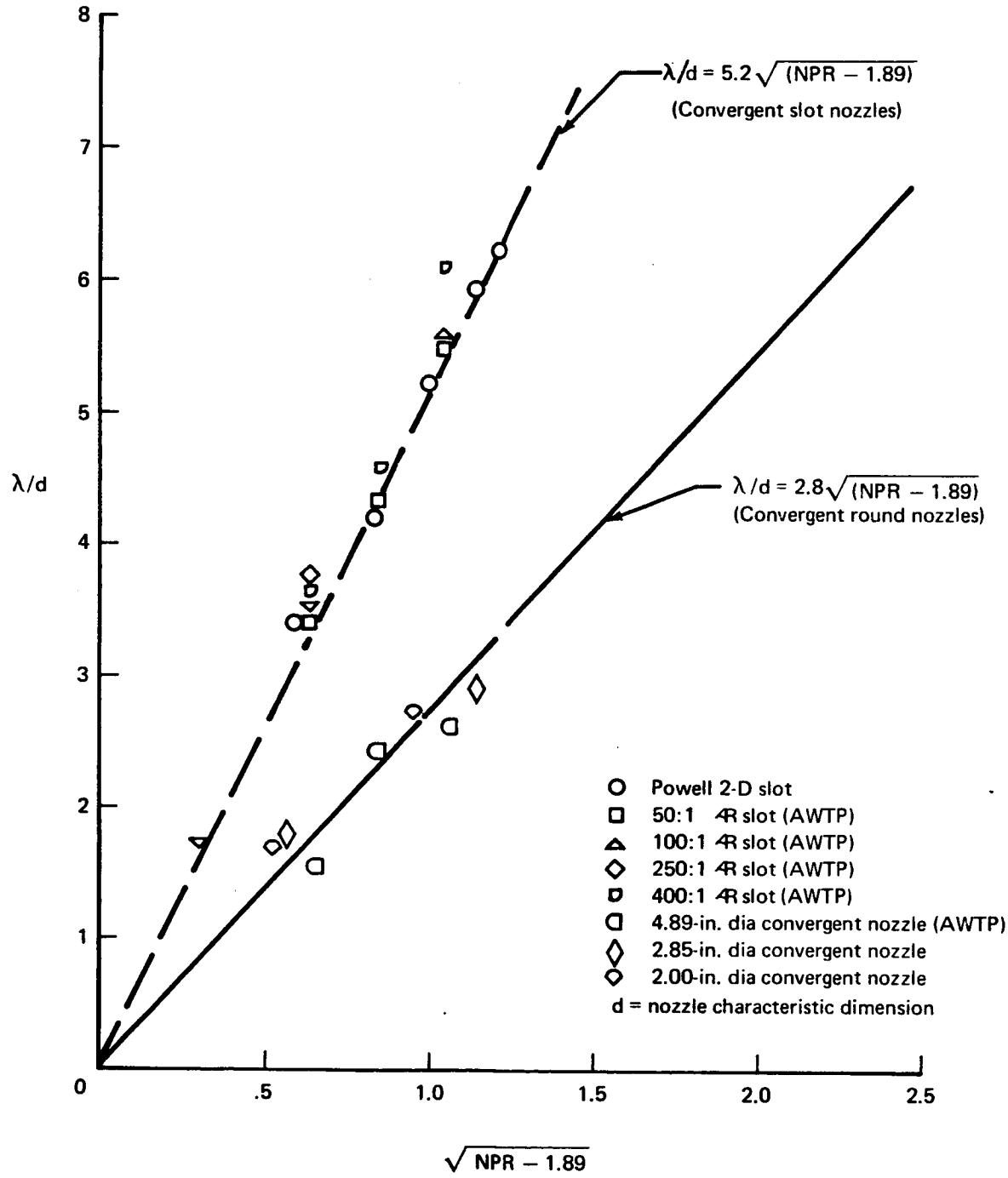

FIGURE 6-144.– NONDIMENSIONAL WAVE LENGTH OF SCREECH

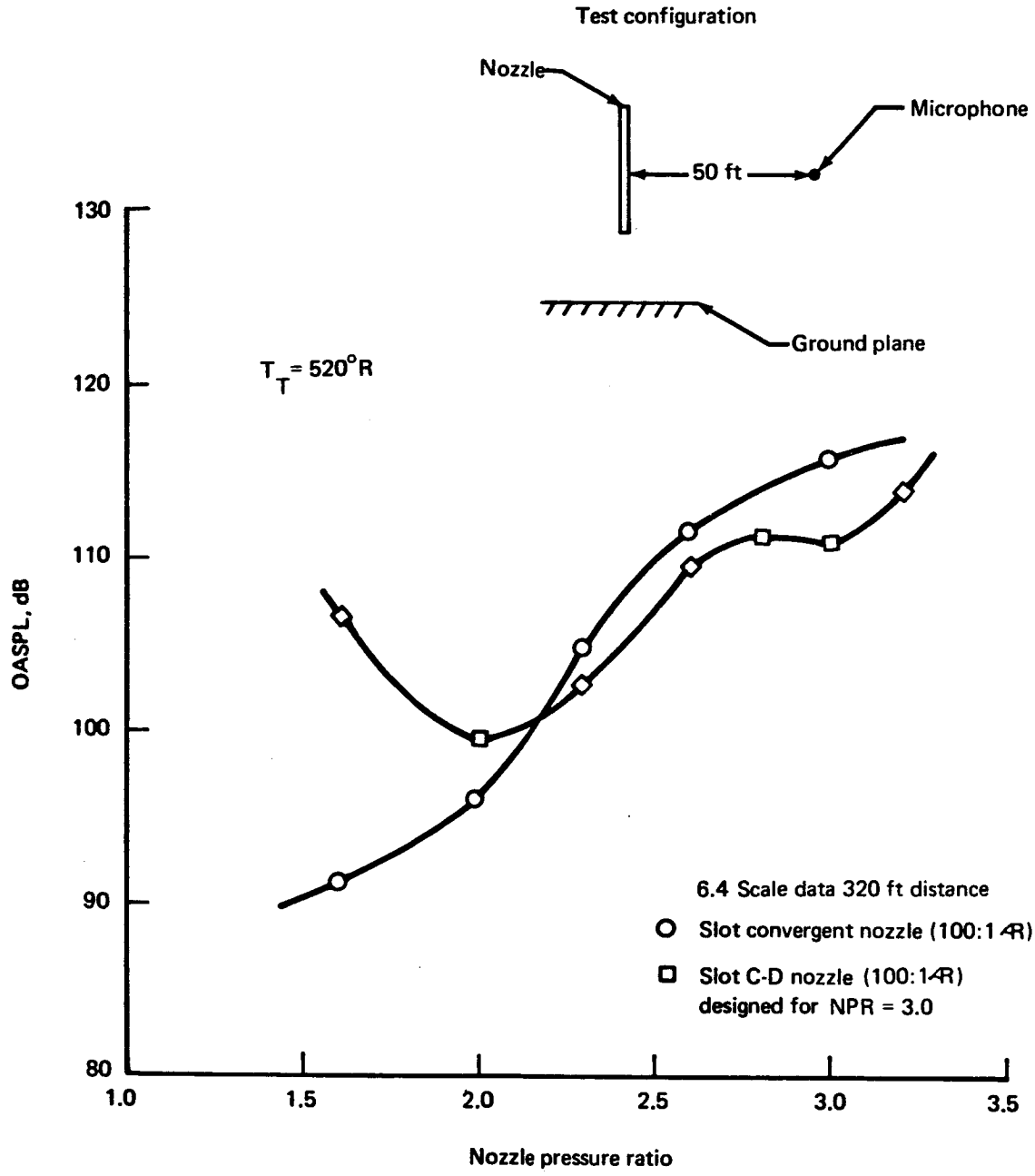

FIGURE 6-145.—OASPL COMPARISON OF CONVERGENT AND CONVERGENT-DIVERGENT SLOT NOZZLES AT 50 FT AND 90° FROM NOZZLE CENTERLINE, $\beta = 0°$

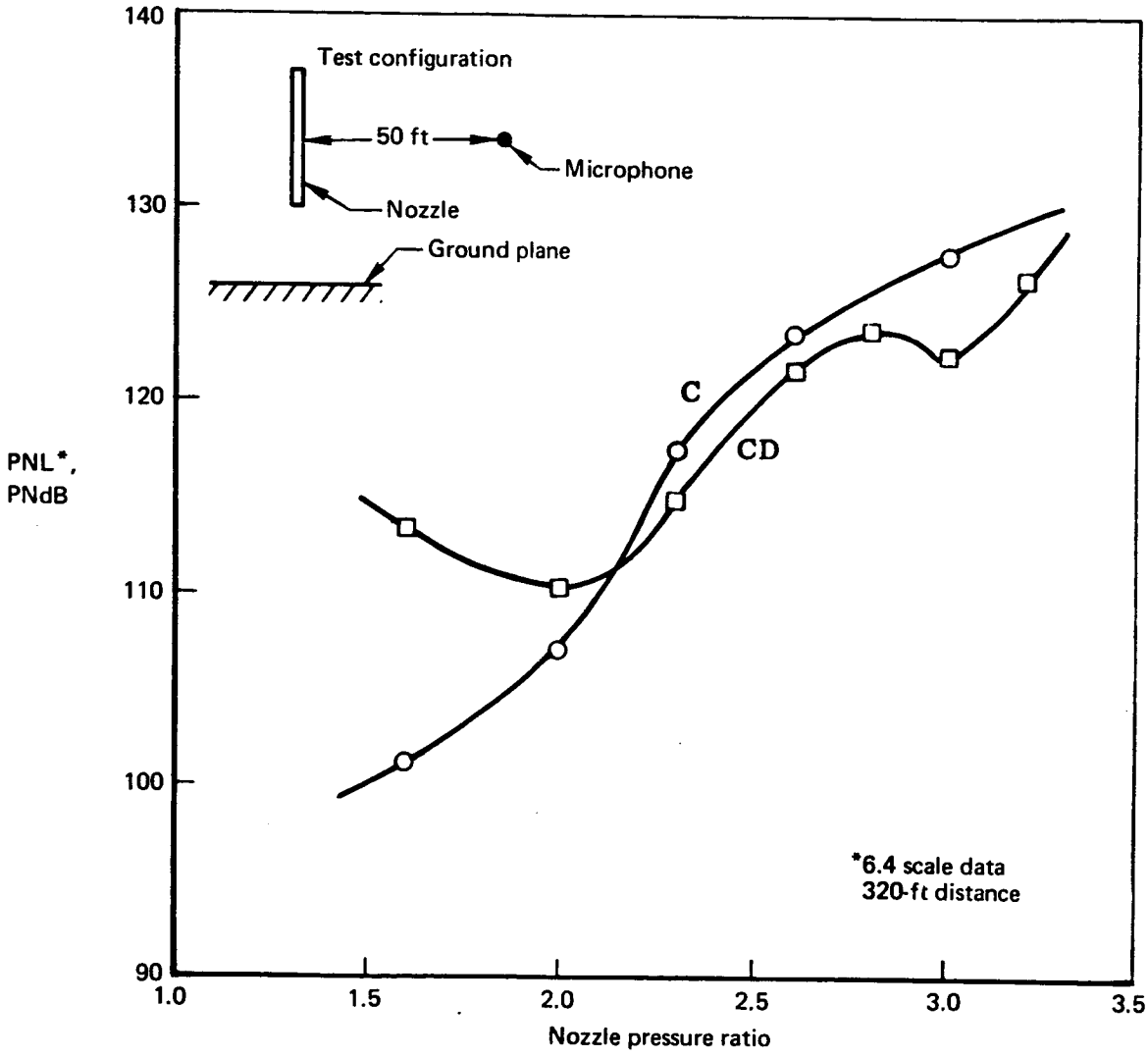

FIGURE 6-146.– PNL COMPARISON OF CONVERGENT AND CONVERGENT-DIVERGENT SLOT NOZZLES AT 50 FT AND 90° FROM NOZZLE CENTERLINE, $\beta = 0°$

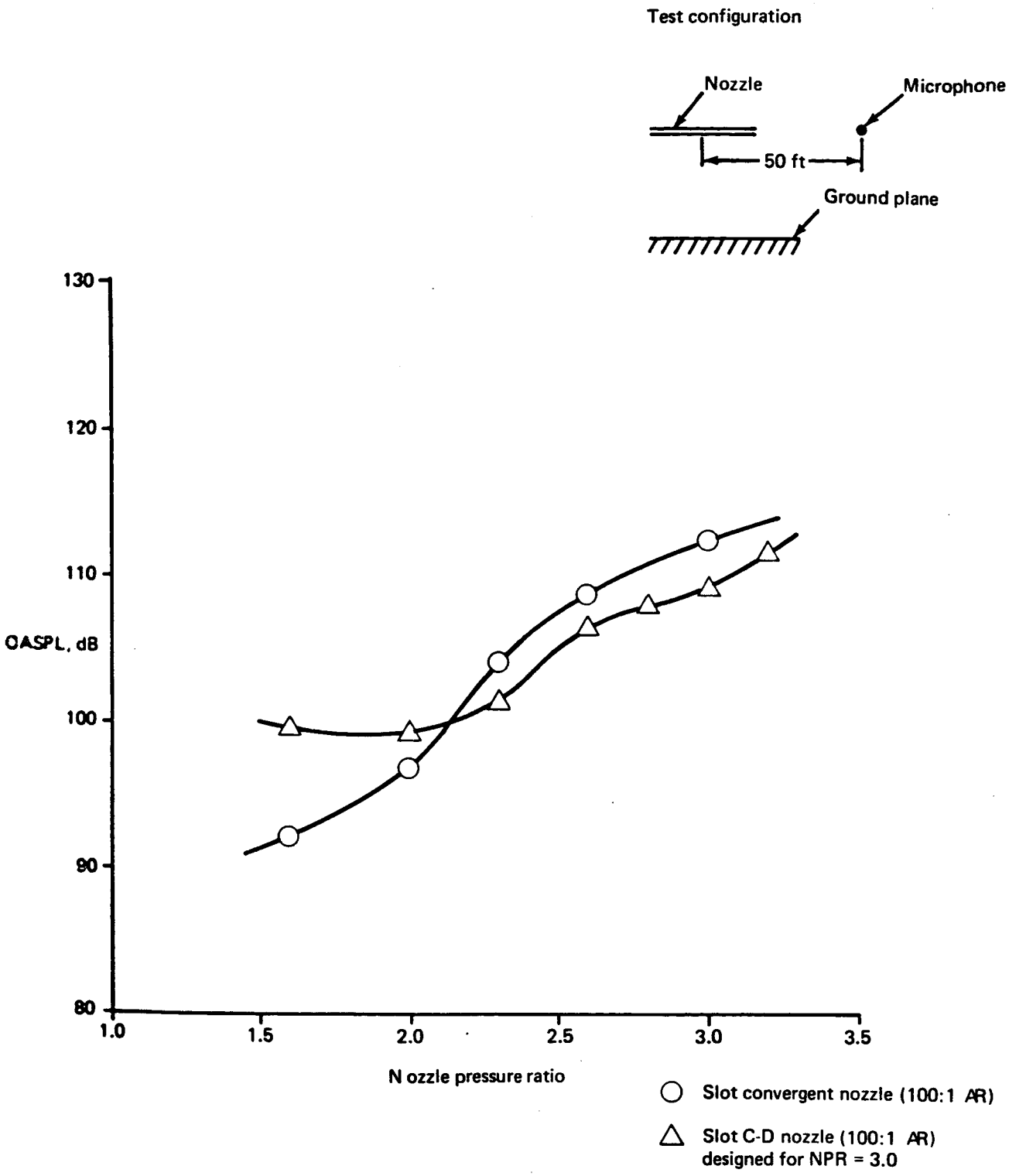

FIGURE 6-147.– OA SPL COMPARISON OF CONVERGENT AND CONVERGENT-DIVERGENT SLOT NOZZLES AT 50 FT AND 90° FROM NOZZLE CENTERLINE, $\beta = 90°$

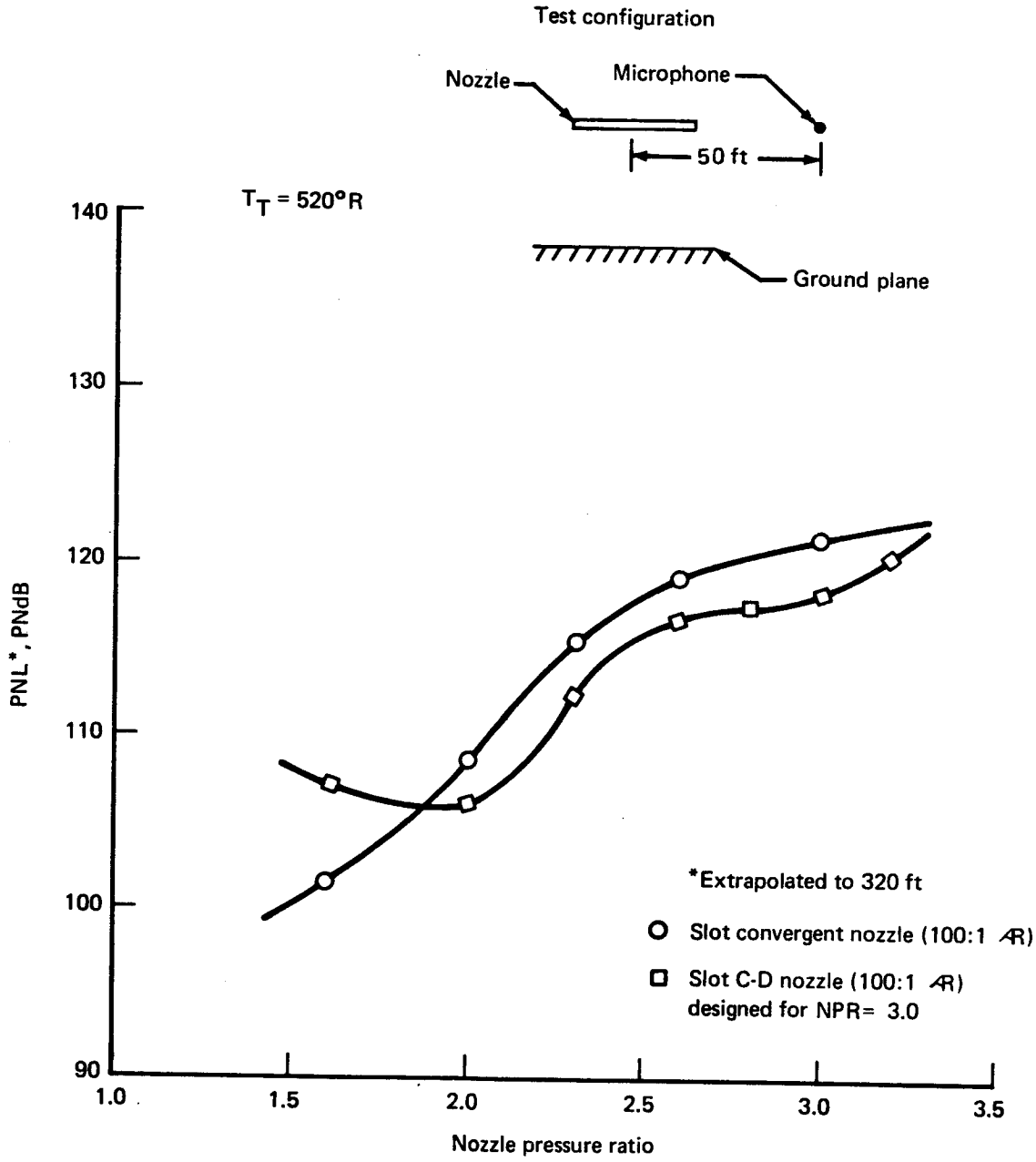

FIGURE 6-148.–PNL COMPARISON OF CONVERGENT AND CONVERGENT-DIVERGENT SLOT NOZZLES AT 50 FT AND 90° FROM NOZZLE CENTERLINE, $\beta = 90°$

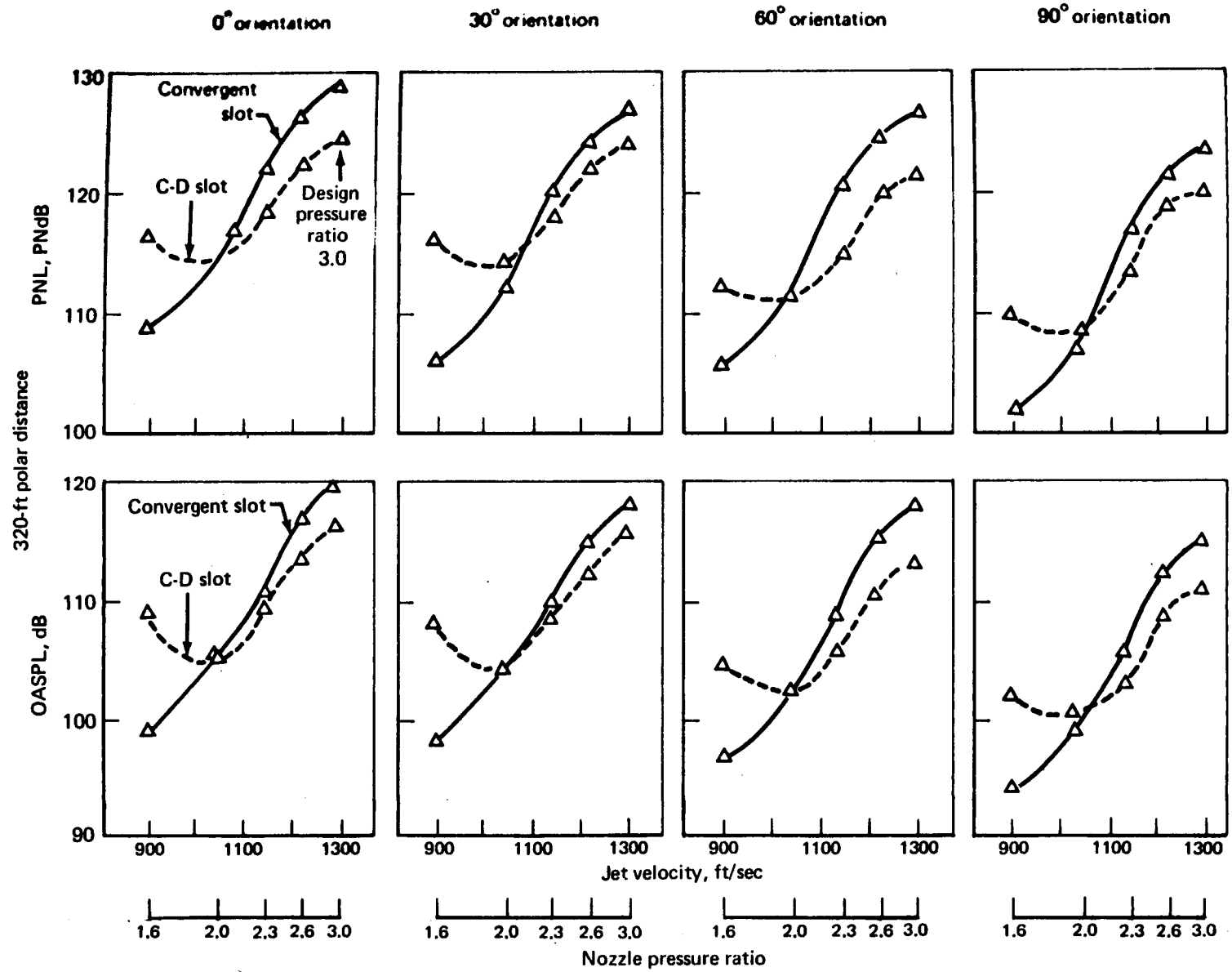

100:1 slot
100:1 C-D slot

FIGURE 6-149.– 100:1 SLOT NOZZLE PEAK NOISE LEVELS–300-FT POLAR DISTANCE

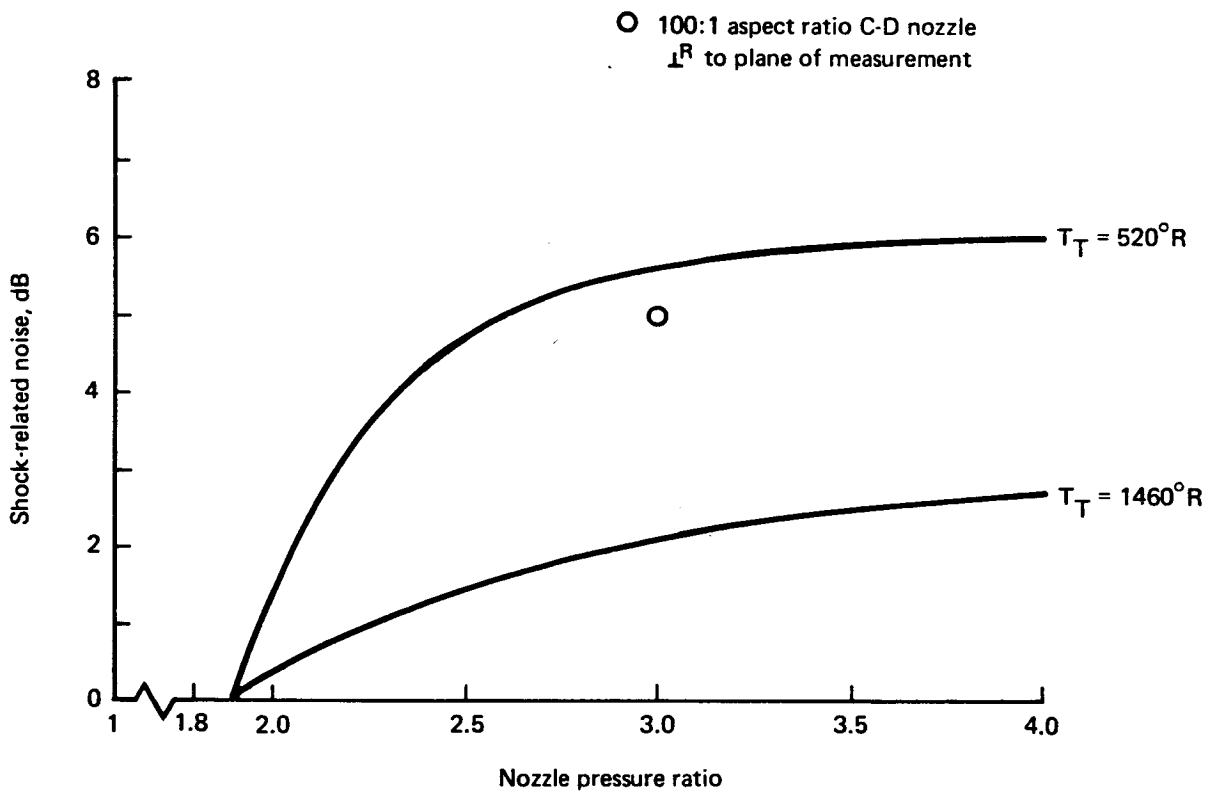

FIGURE 6-150.– OASPL SUPPRESSION CAUSED BY ATTENUATION OF SHOCK NOISE

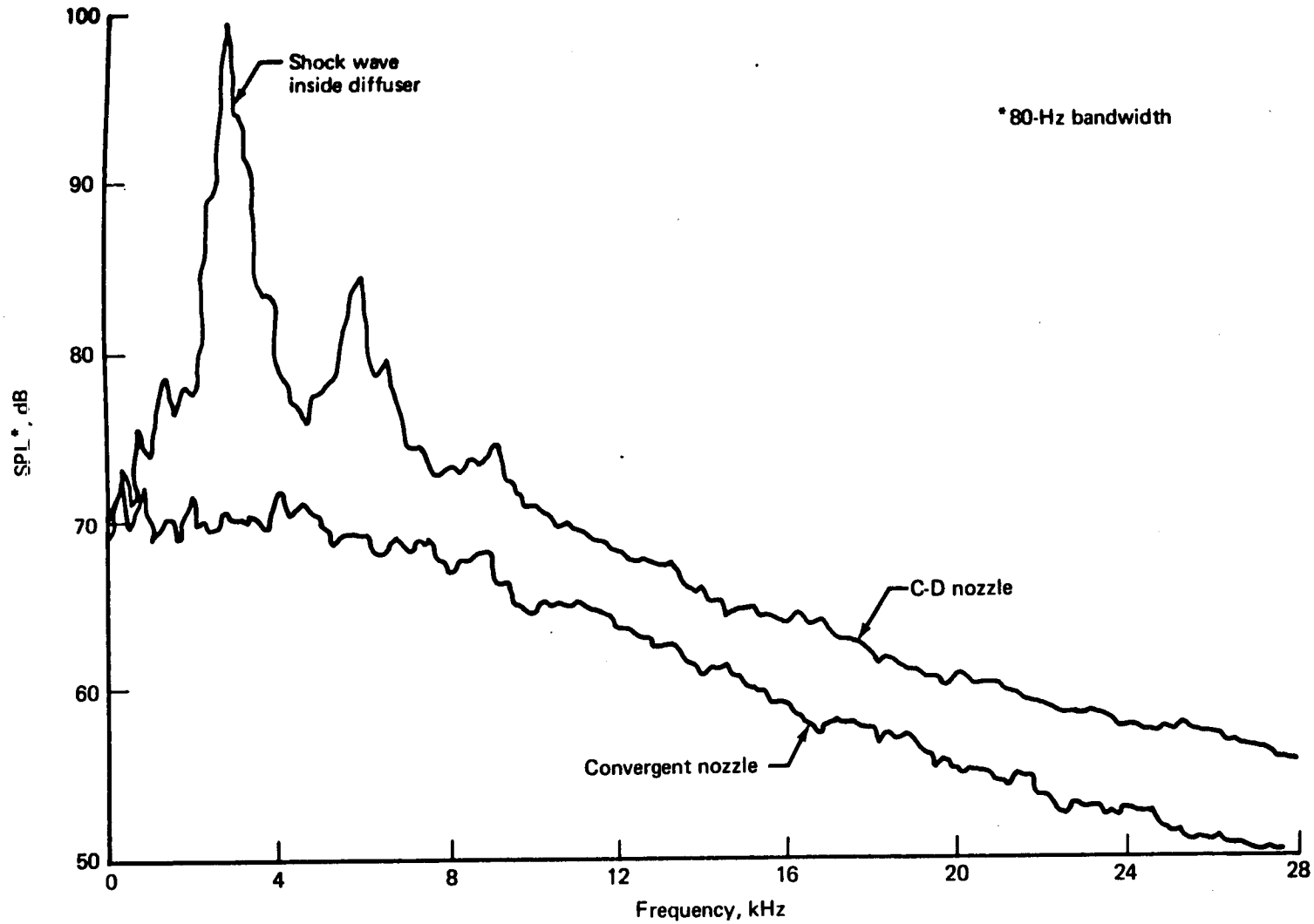

FIGURE 6-151.—NOISE SPECTRA OF CONVERGENT AND CONVERGENT-DIVERGENT NOZZLES AT NPR = 1.6

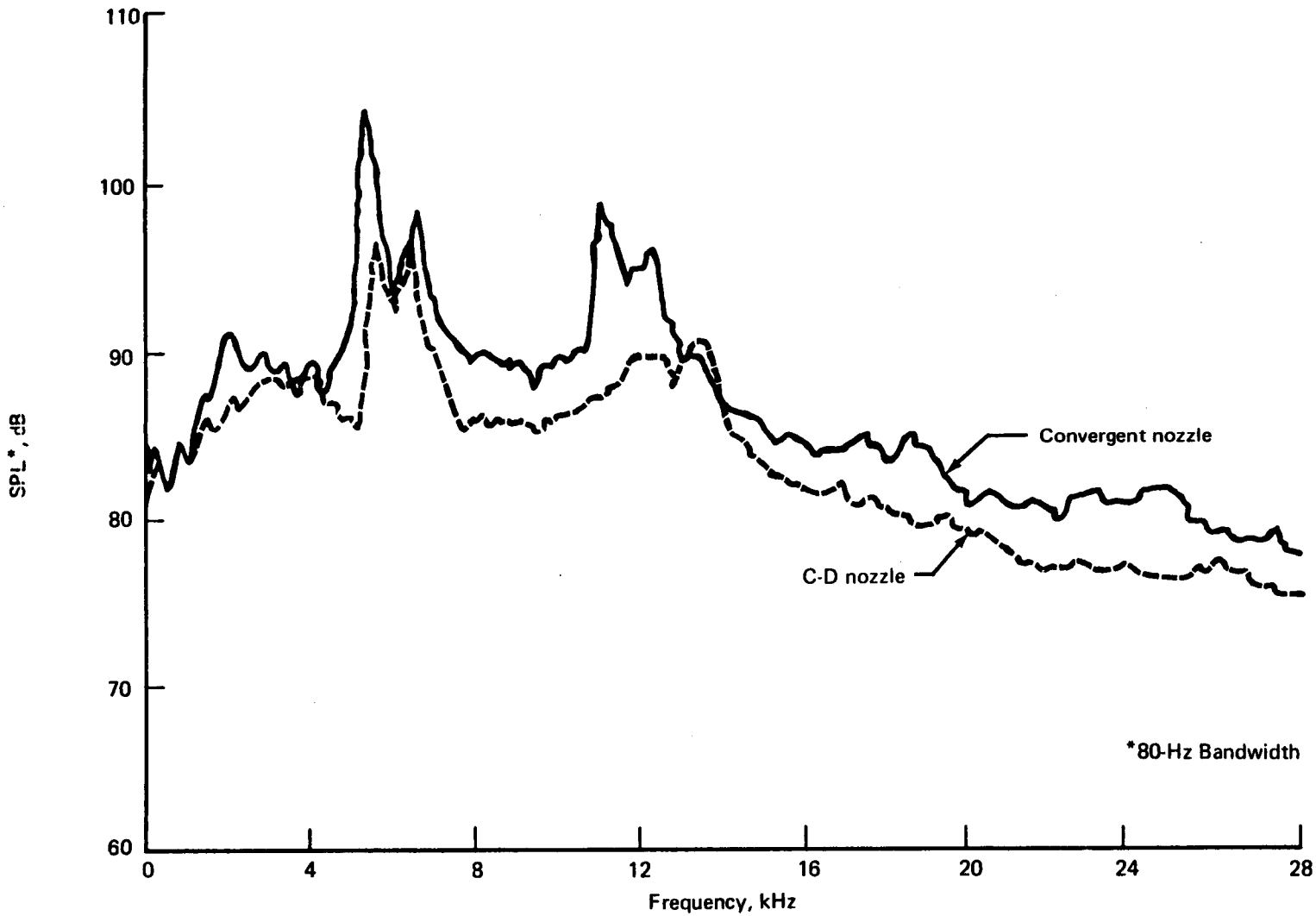

FIGURE 6-152.– COMPARISON OF NOISE SPECTRA OF CONVERGENT AND CONVERGENT-DIVERGENT NOZZLES AT NPR = 3

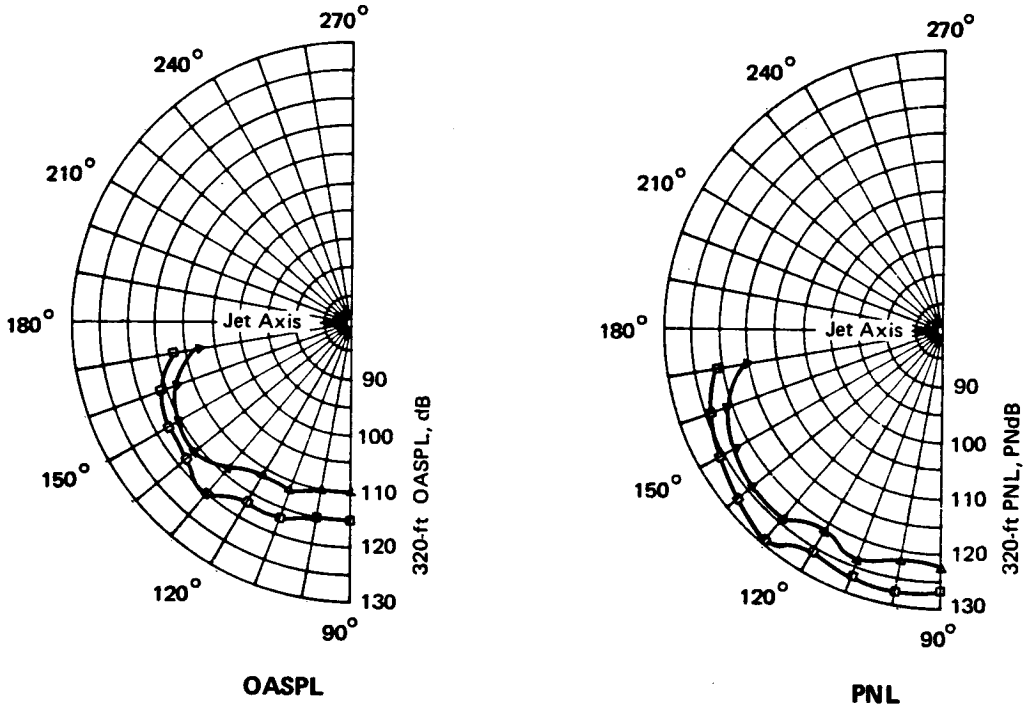

Nozzle orientation, $\beta = 0^\circ$
NPR = 3.0
T_T = Ambient
A = 770 sq in.
320-ft polar distance

□ Convergent nozzle
△ C-D nozzle

FIGURE 6-153.– NOISE DIRECTIONALITY PATTERNS OF CONVERGENT AND CONVERGENT-DIVERGENT NOZZLES

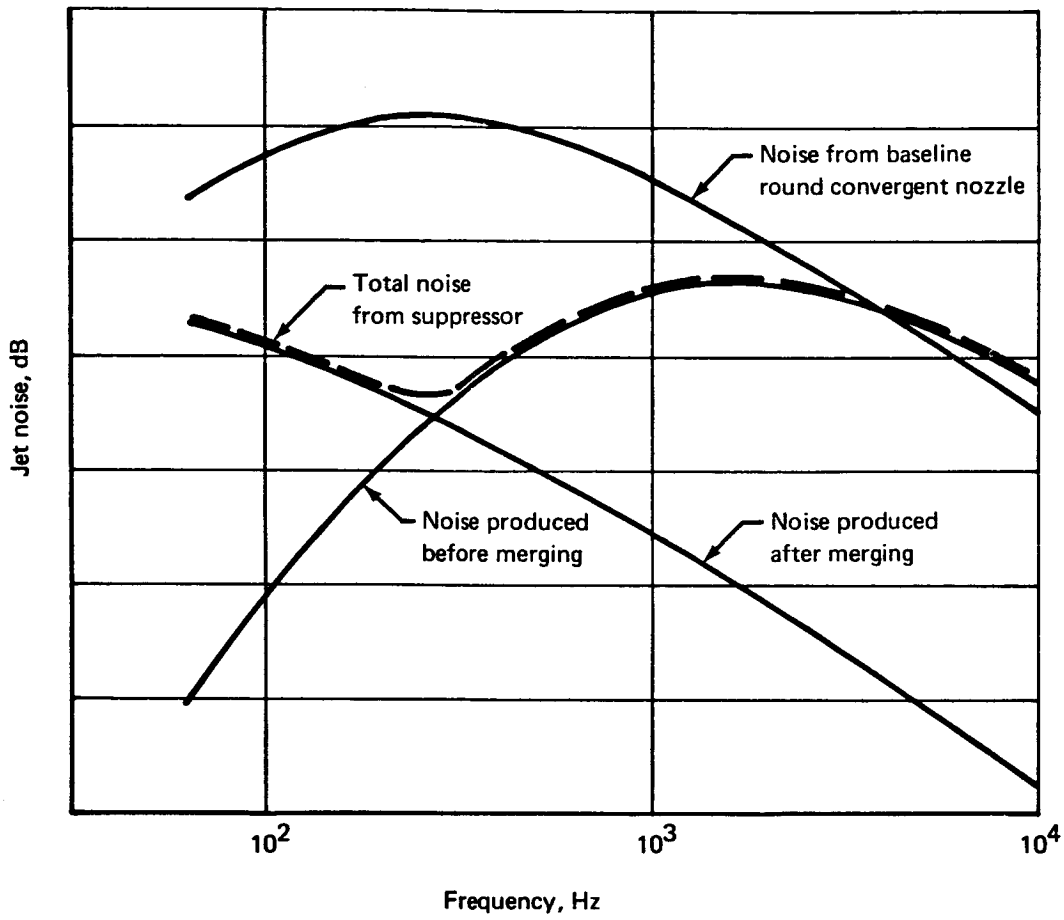

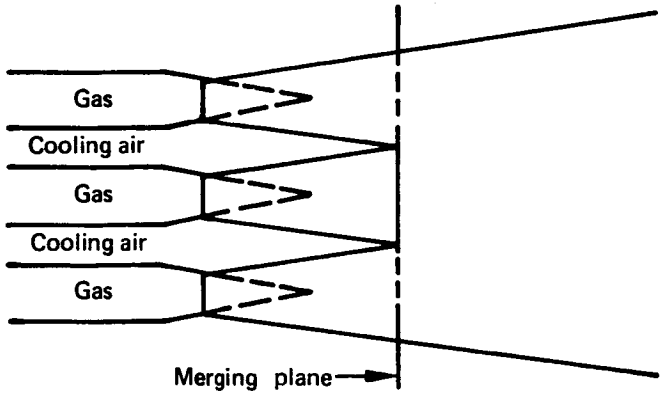

Multitube Nozzle

FIGURE 6-154.– BREAKDOWN OF NOISE FROM MULTITUBE NOZZLES INTO HIGH- AND LOW-FREQUENCY COMPONENTS

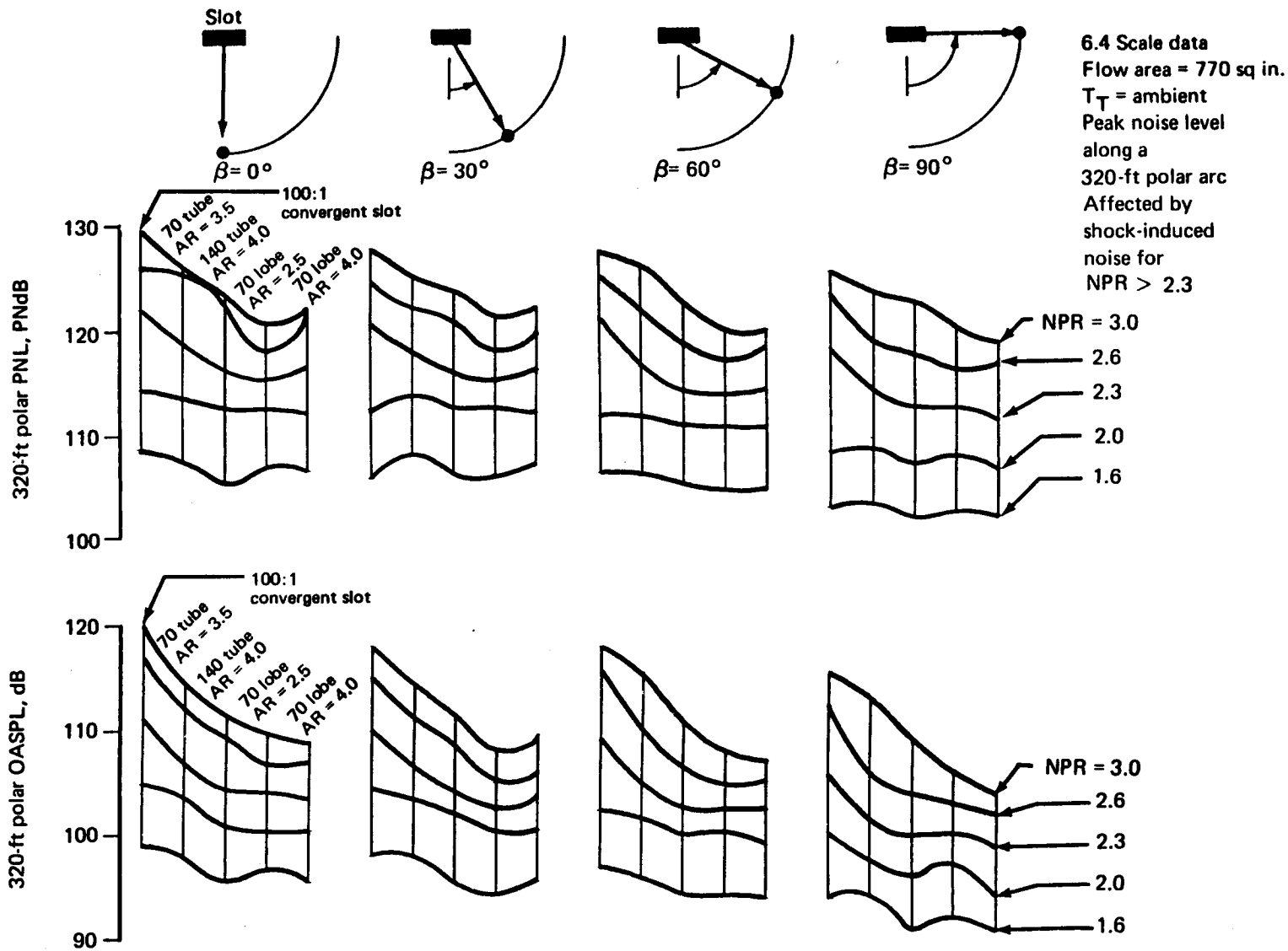

FIGURE 6-155.– MULTI-ELEMENT PEAK NOISE LEVELS AS A FUNCTION OF PRESSURE RATIO, CONFIGURATION, AND ORIENTATION

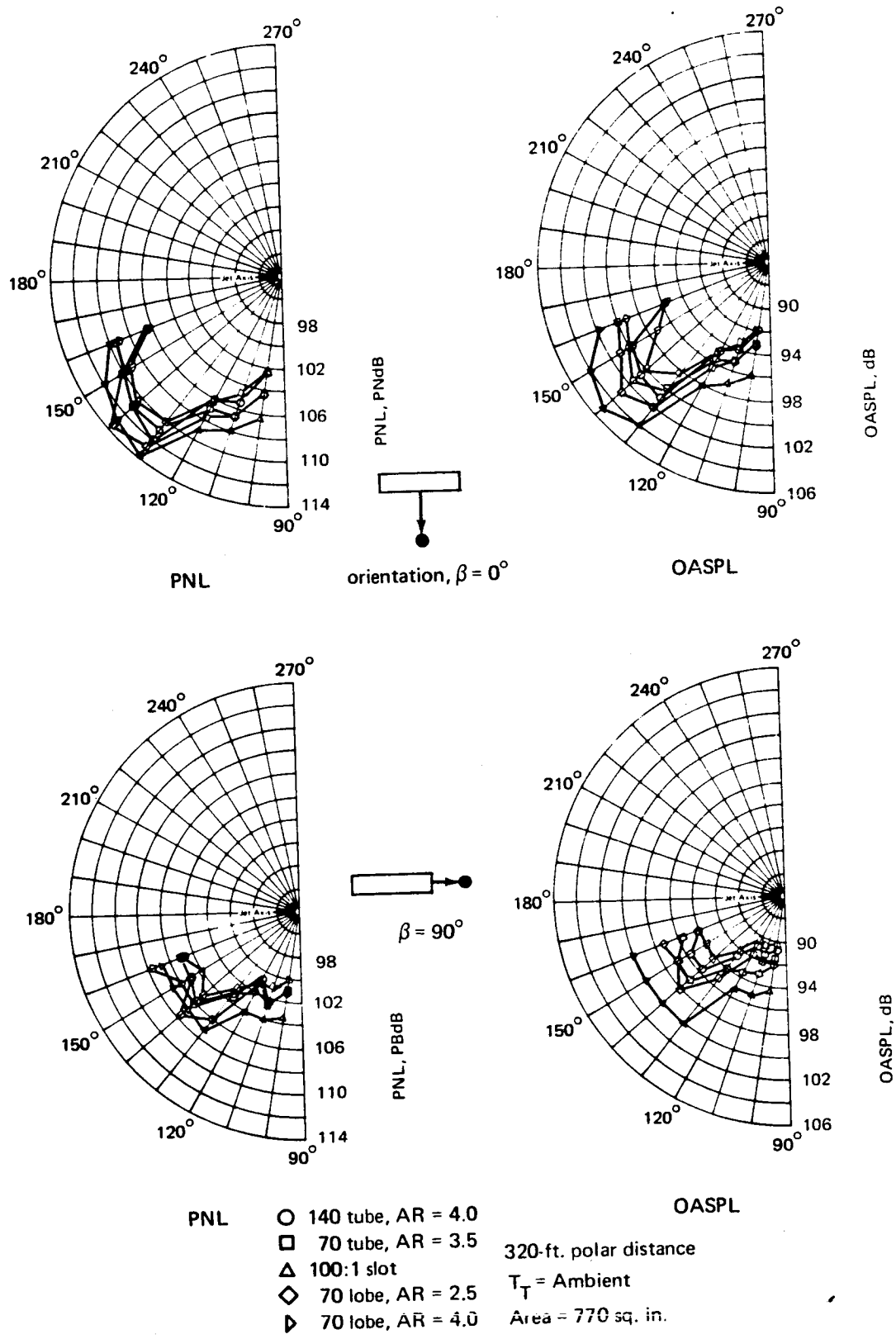

FIGURE 6-156.– MULTI-ELEMENT NOZZLE NOISE DIRECTIONALITY PATTERNS, NPR = 2.0

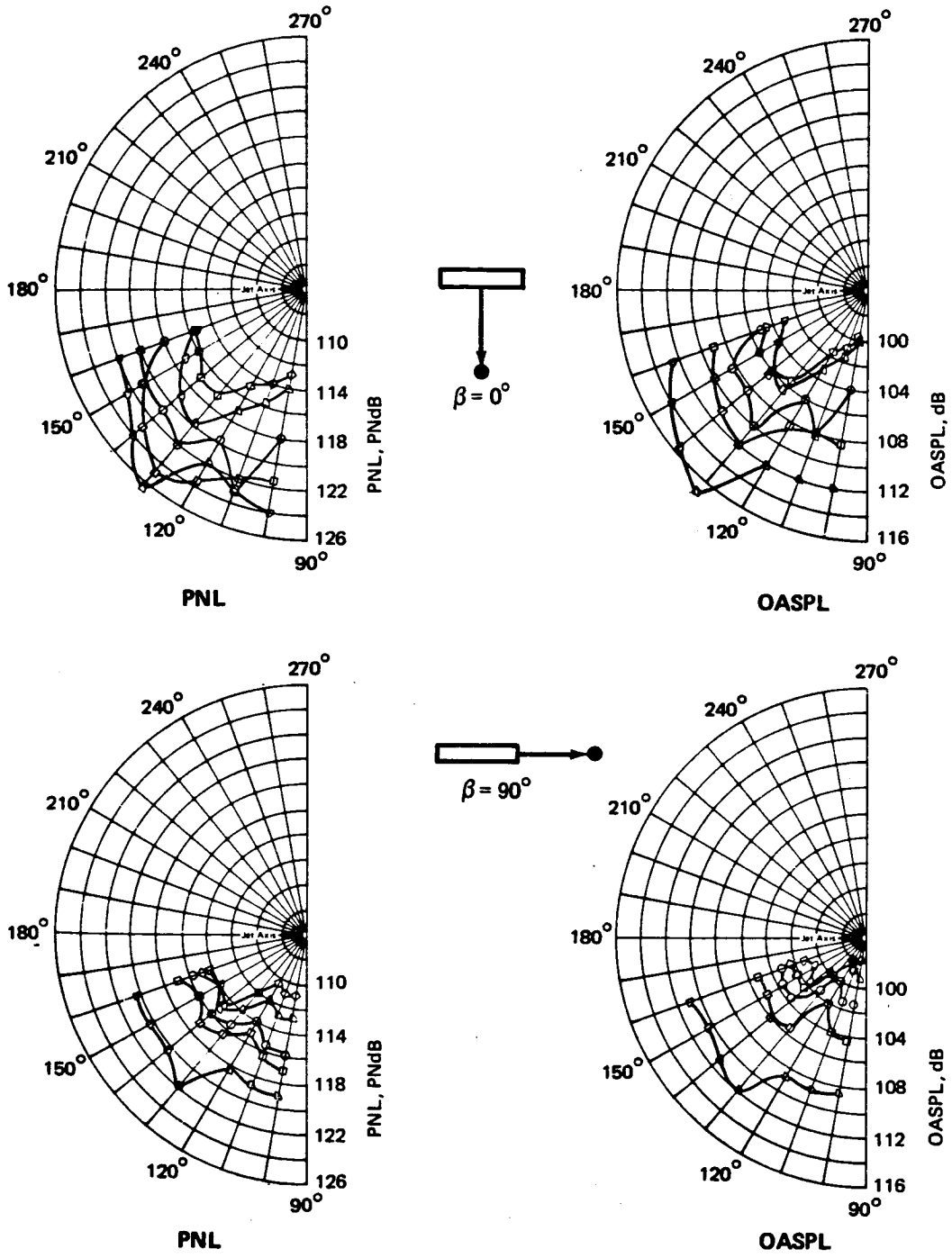

320-ft polar distance
T_T = Ambient
Area = 770 sq in.

- ○ 140 Tube, AR = 4.0
- □ 70 Tube, AR = 3.5
- △ 100: 1 Slot
- ◇ 70 Lobe, AR = 2.5
- ◺ 70 Lobe, AR = 4.0

FIGURE 6-157.— MULTI-ELEMENT NOZZLE NOISE DIRECTIONALITY PATTERNS, NPR = 2.6

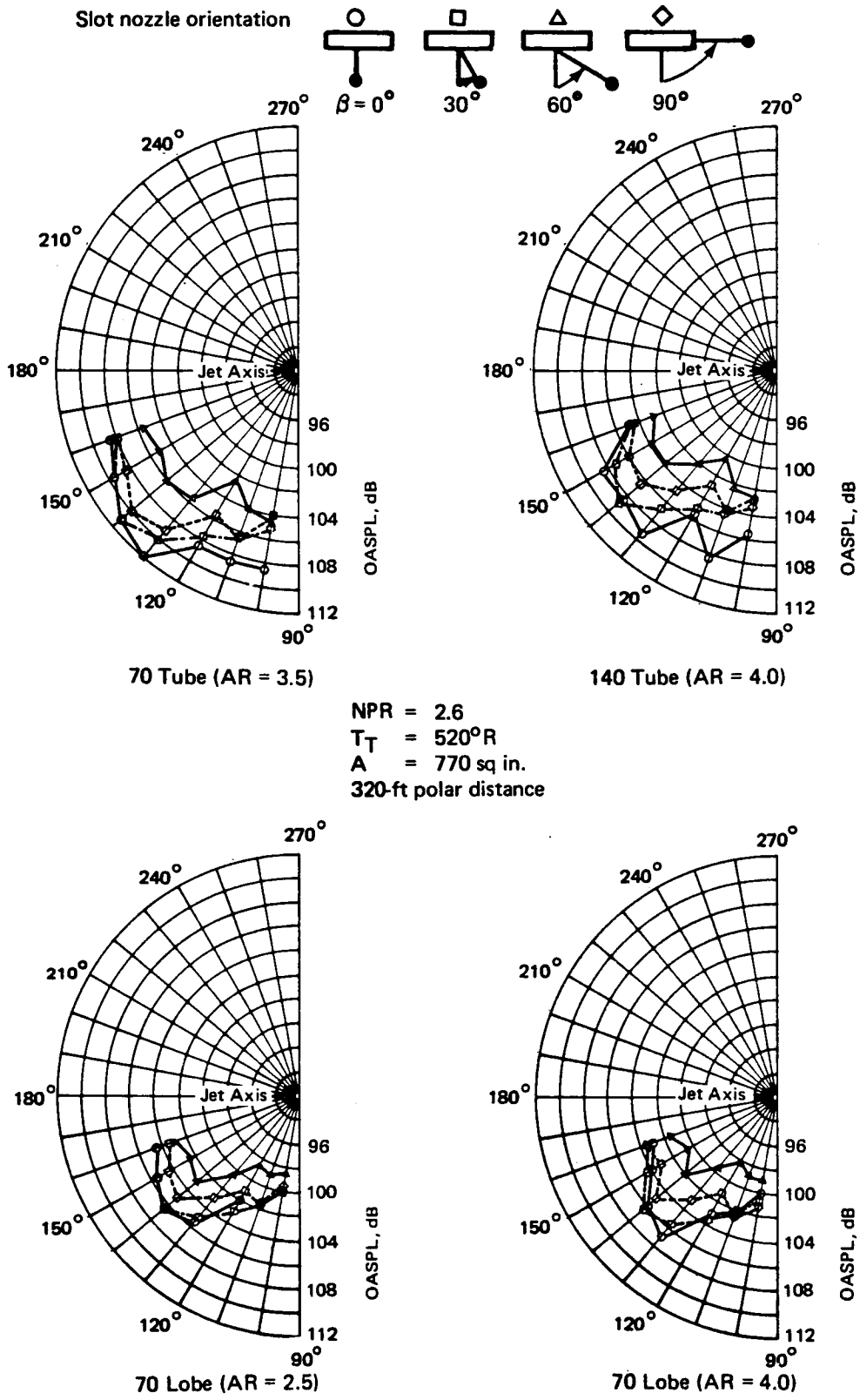

FIGURE 6-158.—EFFECT OF NOZZLE ORIENTATION ON NOISE DIRECTIONALITY PATTERNS

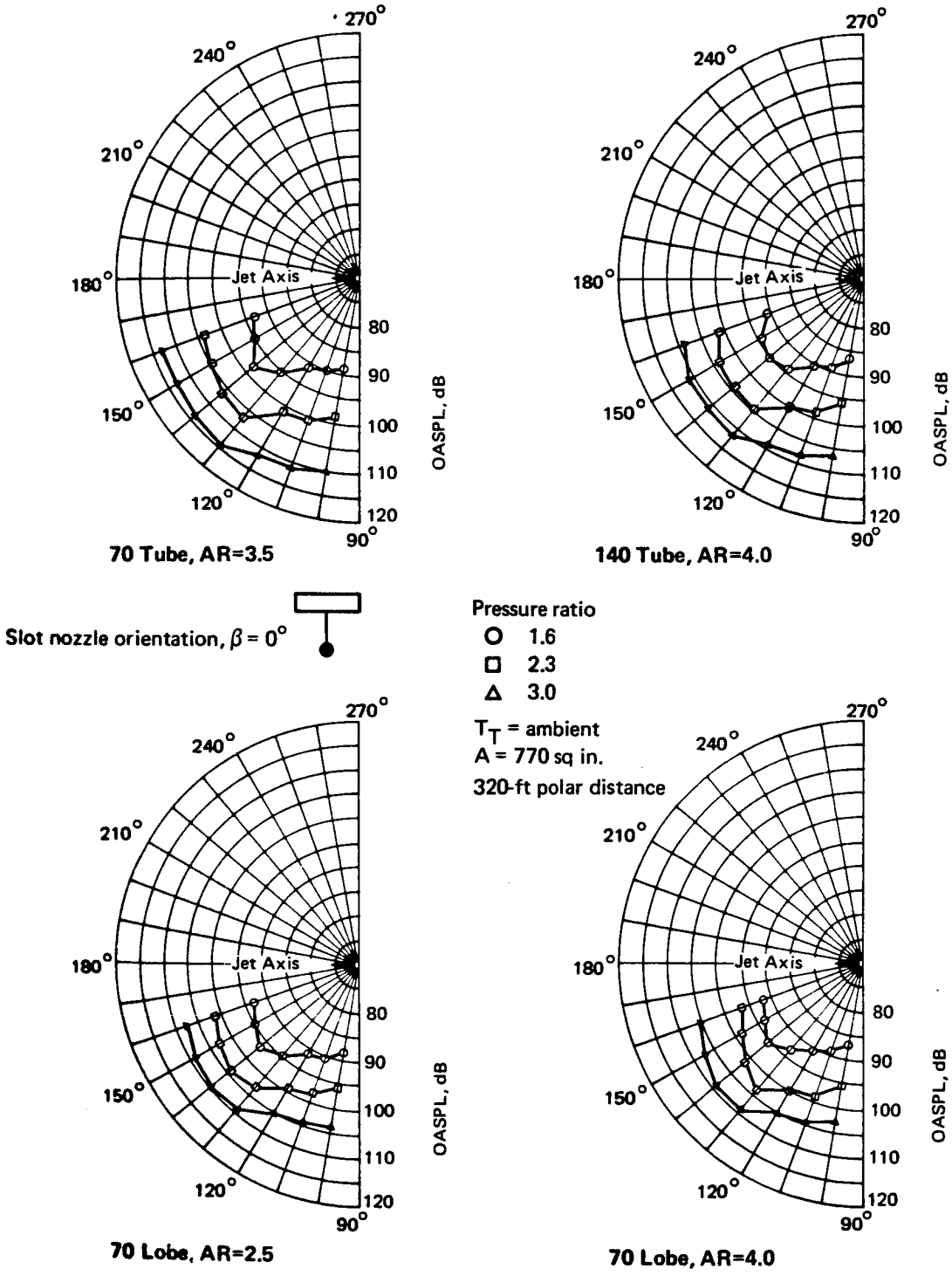

FIGURE 6-159.—EFFECT OF PRESSURE RATIO ON NOISE DIRECTIONALITY PATTERNS

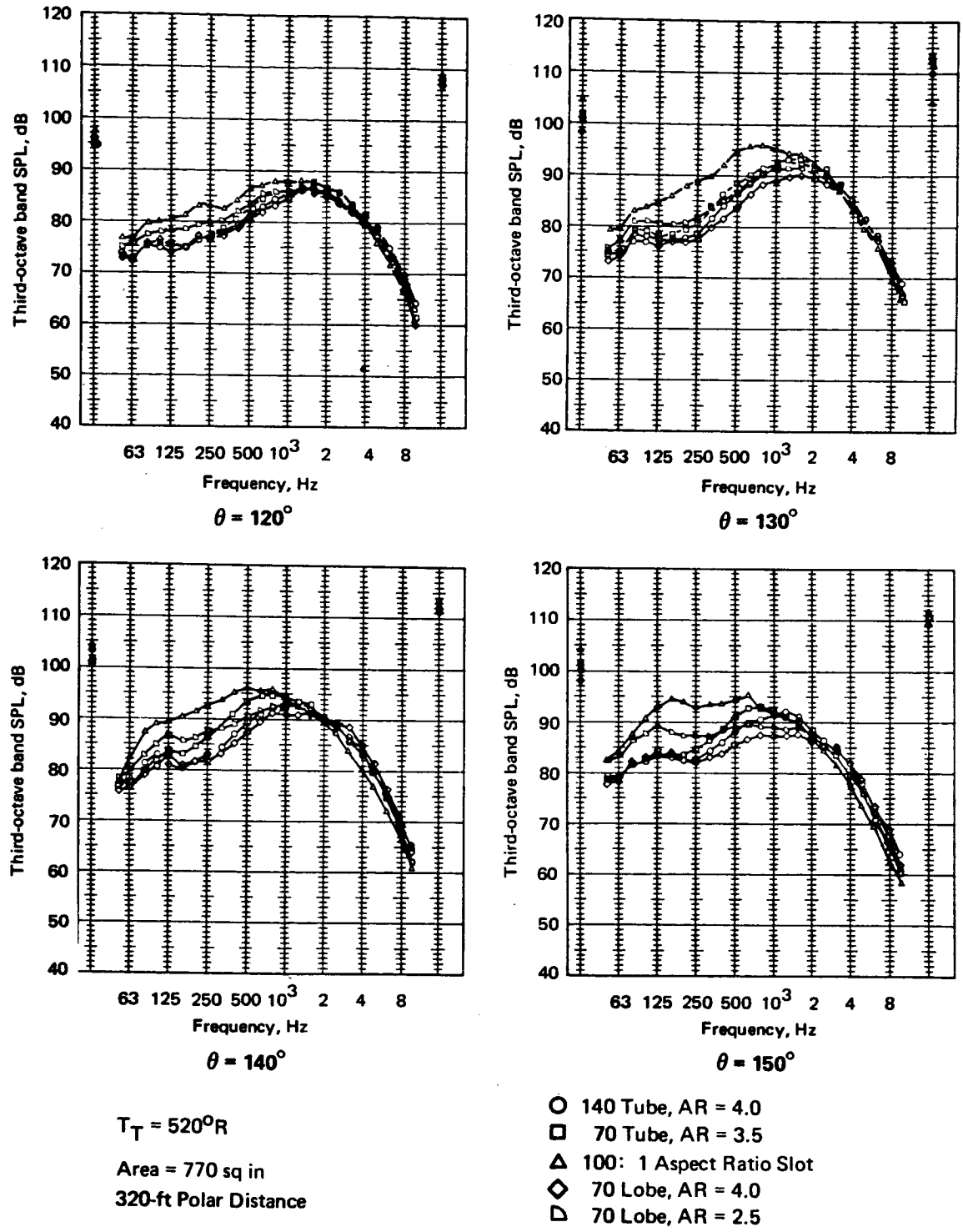

FIGURE 6-160.— MULTI-ELEMENT NOZZLE NOISE SPECTRA, NPR = 2.0

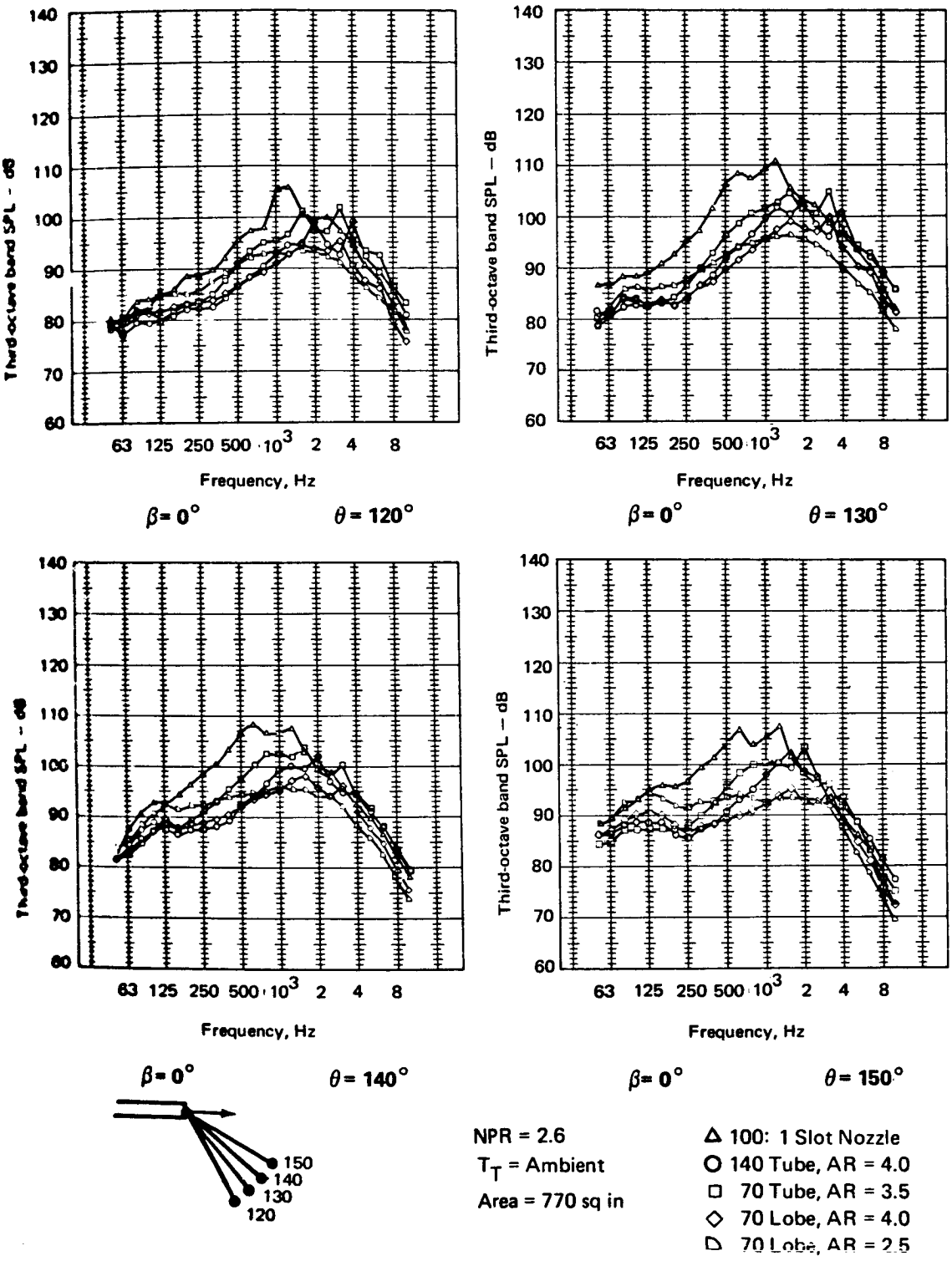

FIGURE 6-161.– MULTI-ELEMENT NOZZLE RECTANGULAR ARRAY NOISE SPECTRA

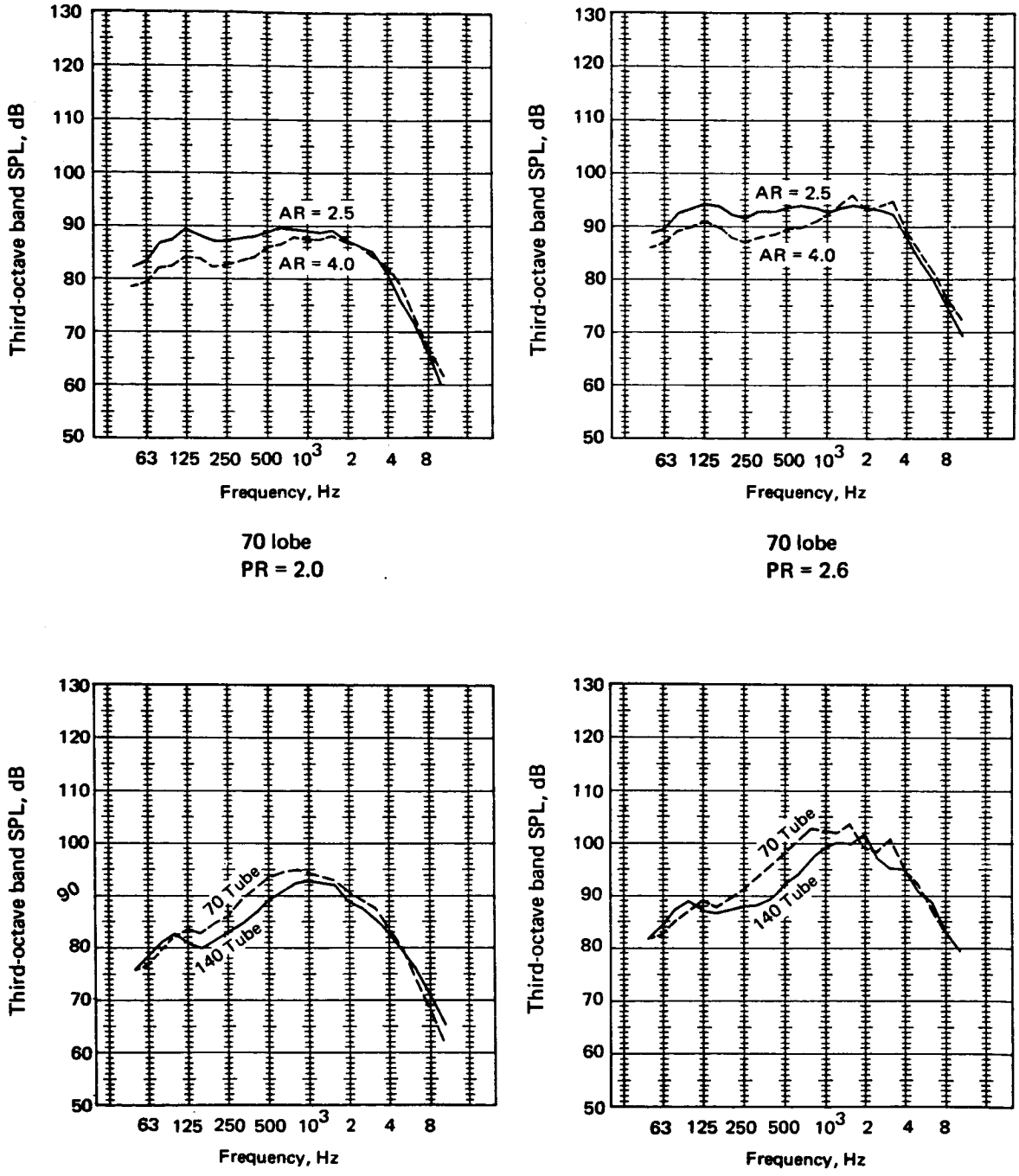

70 lobe
PR = 2.0

70 lobe
PR = 2.6

140 tube, AR = 4.0
70 tube, AR = 3.5
NPR = 2.0

140 tube, AR = 4.0
70 tube, AR = 3.5
NPR = 2.6

FIGURE 6-162.—EFFECT OF AREA RATIO AND ELEMENT NUMBER ON NOISE SPECTRA

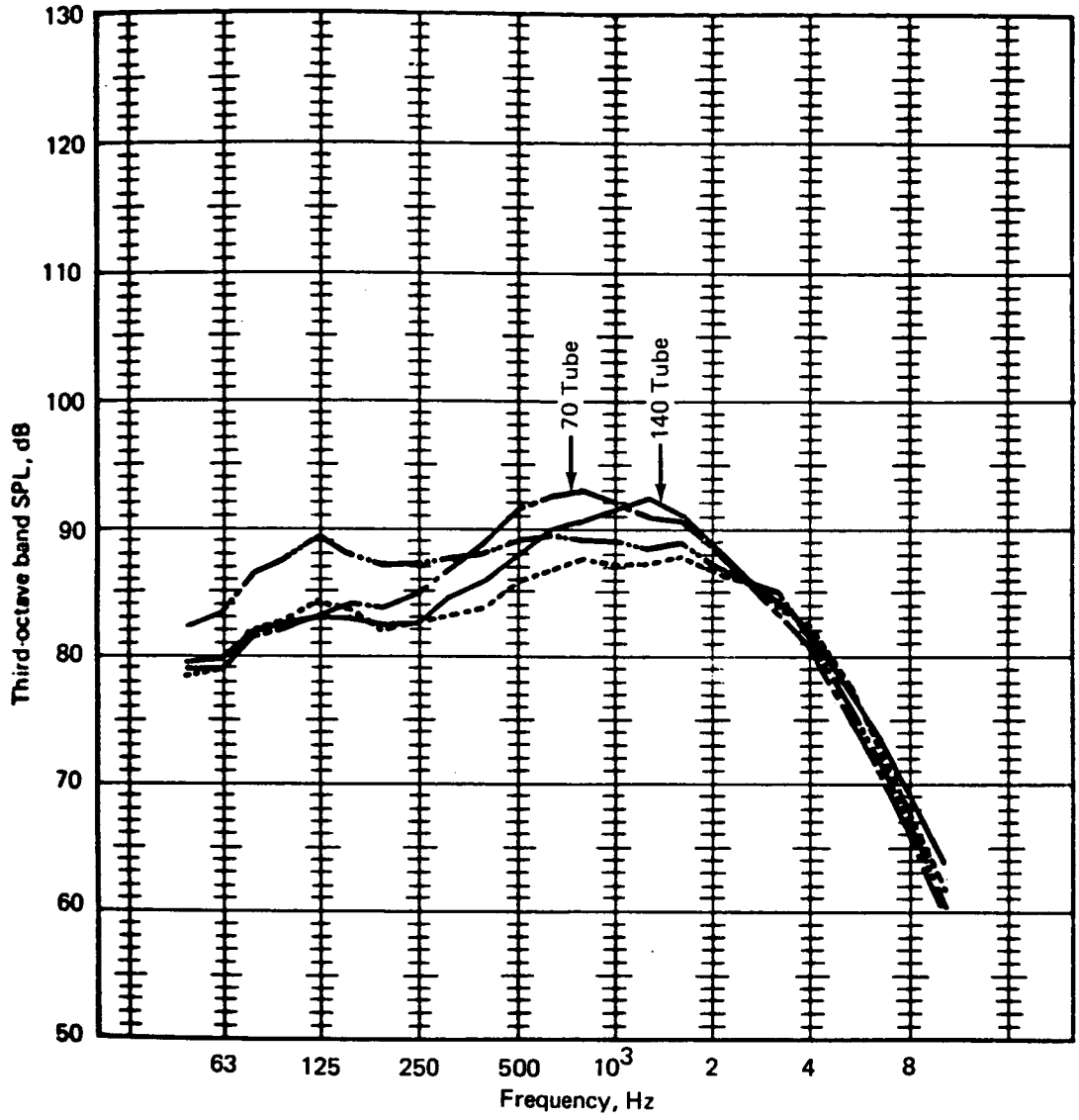

70 lobes, AR = 2.5
70 lobes, AR = 4.0
70 tubes, AR = 3.5
140 tubes, AR = 4.0

NPR = 2.0
T_T = 520° R
θ = 150°
A = 770 sq in.
β = 0°
320-ft polar distance

FIGURE 6-163.– EFFECT OF ELEMENT DIMENSIONS ON PEAK LEVEL FREQUENCY

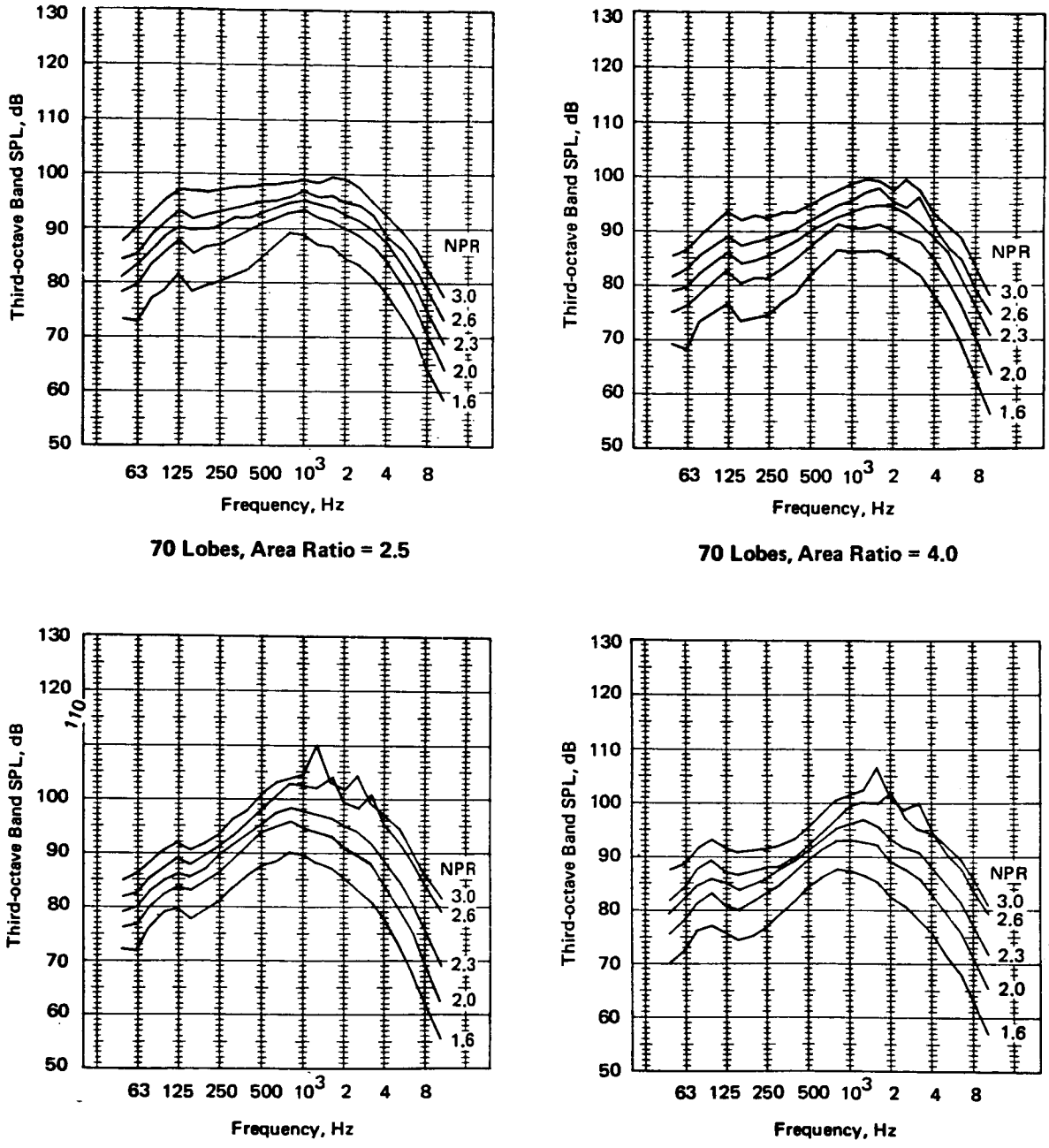

320-ft polar distance
Array orientation, $\beta = 0^\circ$
Noise radiation angle = 140°
A = 770 sq in.
$T_T = 520^\circ R$

FIGURE 6-164.– EFFECT OF PRESSURE RATIO ON MULTI-ELEMENT NOZZLE NOISE SPECTRA

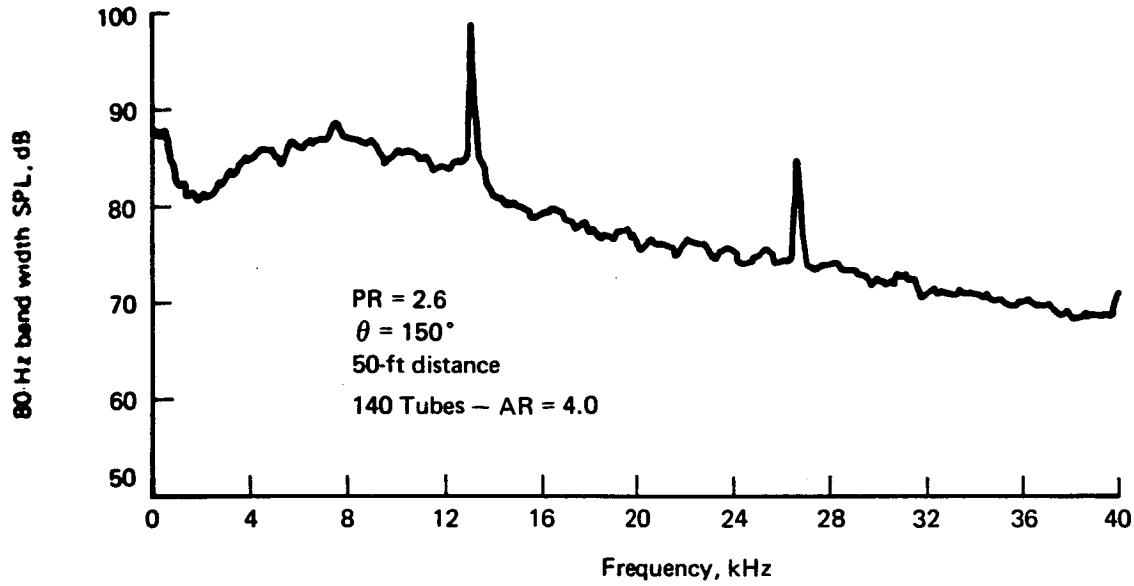

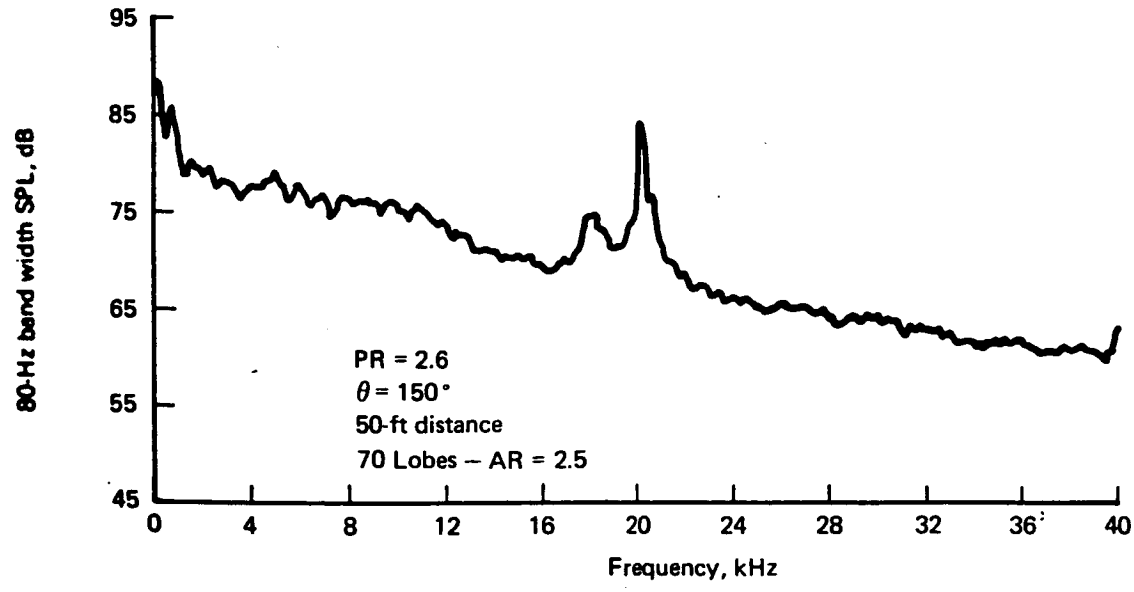

FIGURE 6-165.— MULTI-ELEMENT NOZZLE SHOCK-INDUCED NOISE

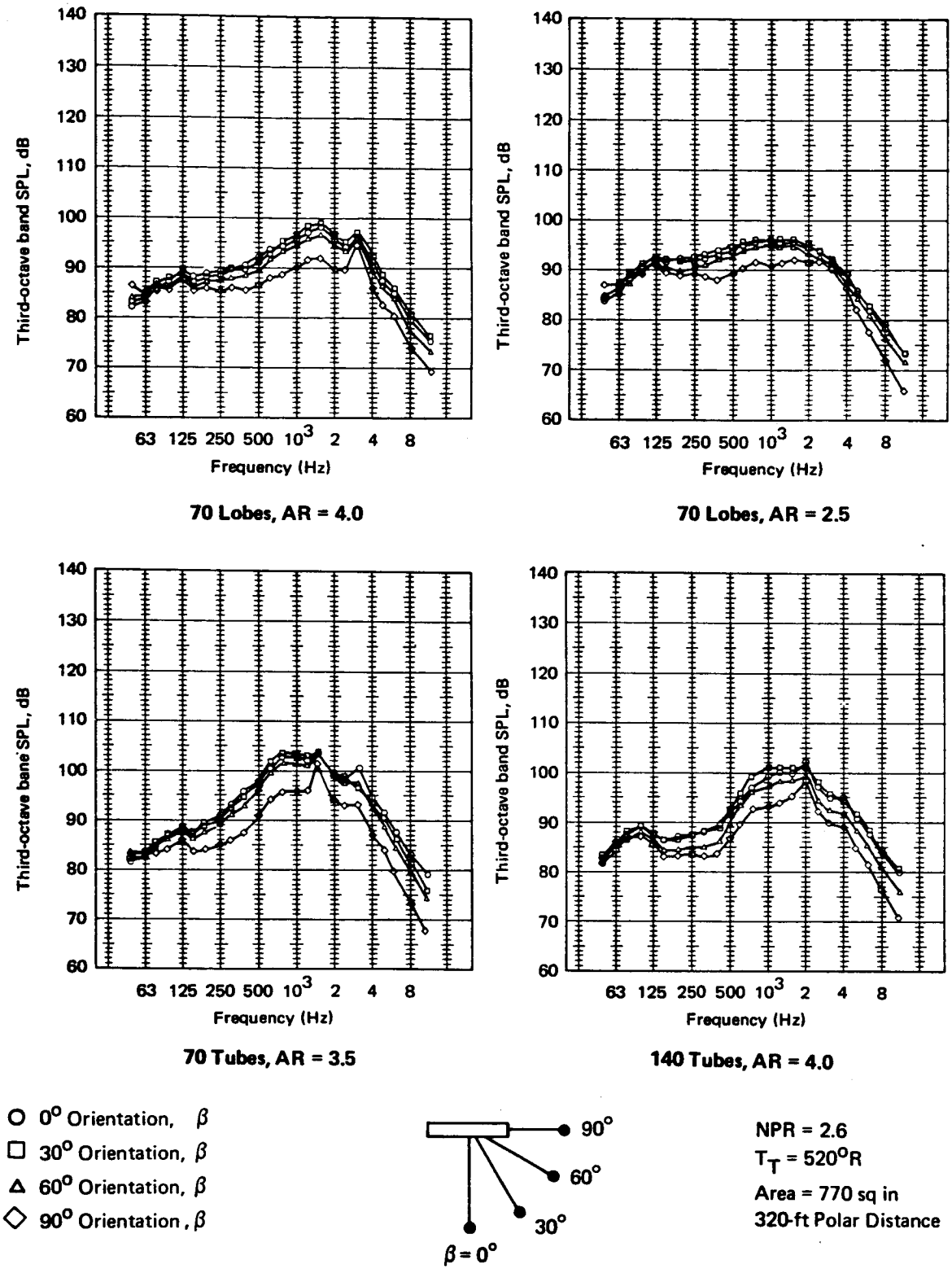

FIGURE 6-166.— EFFECT OF ARRAY ORIENTATION ON NOISE SPECTRA

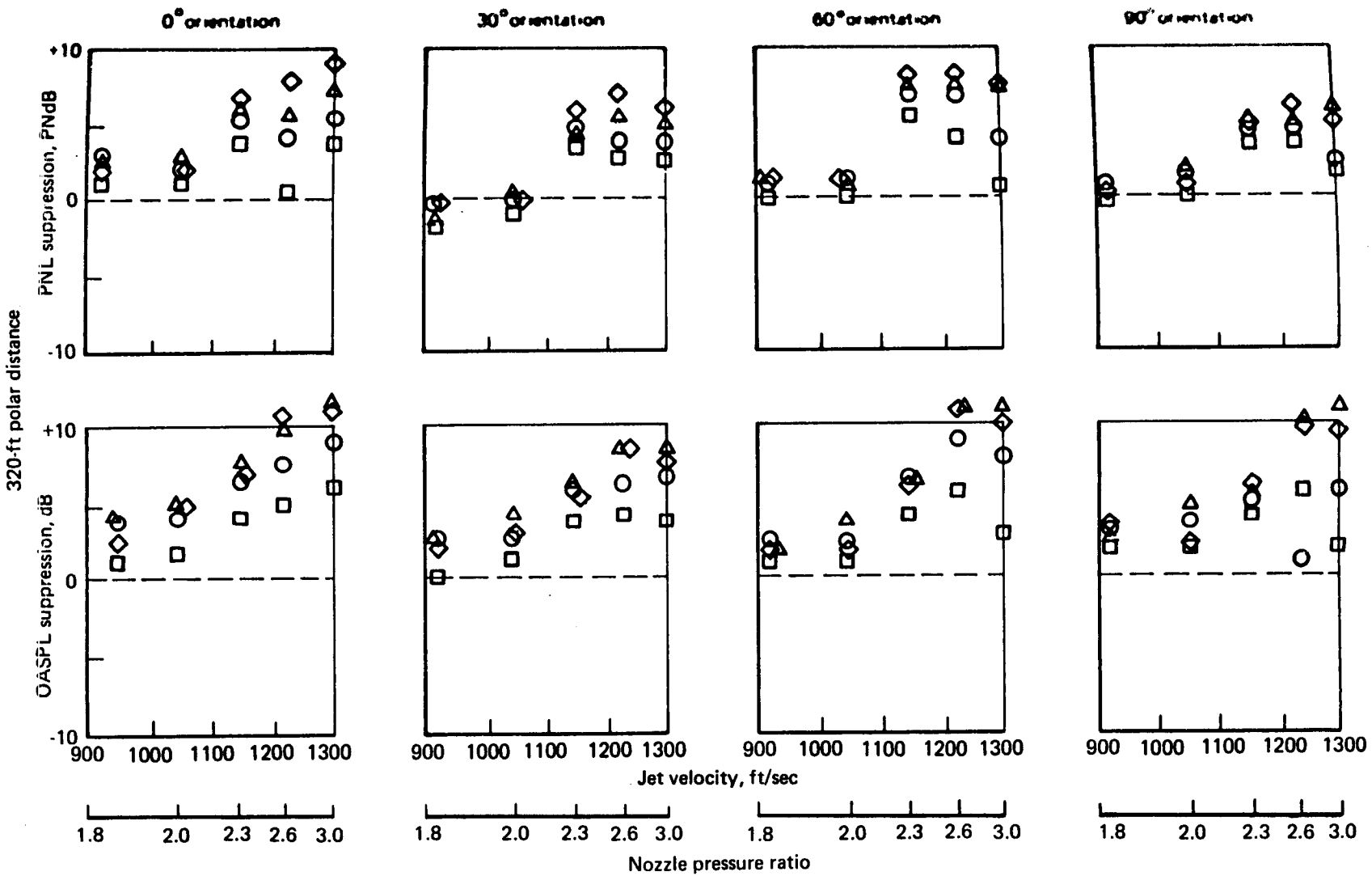

○ 140-tube rectangular array, AR = 4.0
□ 70-tube rectangular array, AR = 4.0
◇ 70-lobe rectangular array, AR = 4.0
△ 70-lobe rectangular array, AR = 2.5
6.4 scale
Area = 770 sq in.
Suppression relative to a 100:1 aspect ratio convergent slot

FIGURE 6-167.— MULTI-ELEMENT NOZZLE NOISE SUPPRESSION

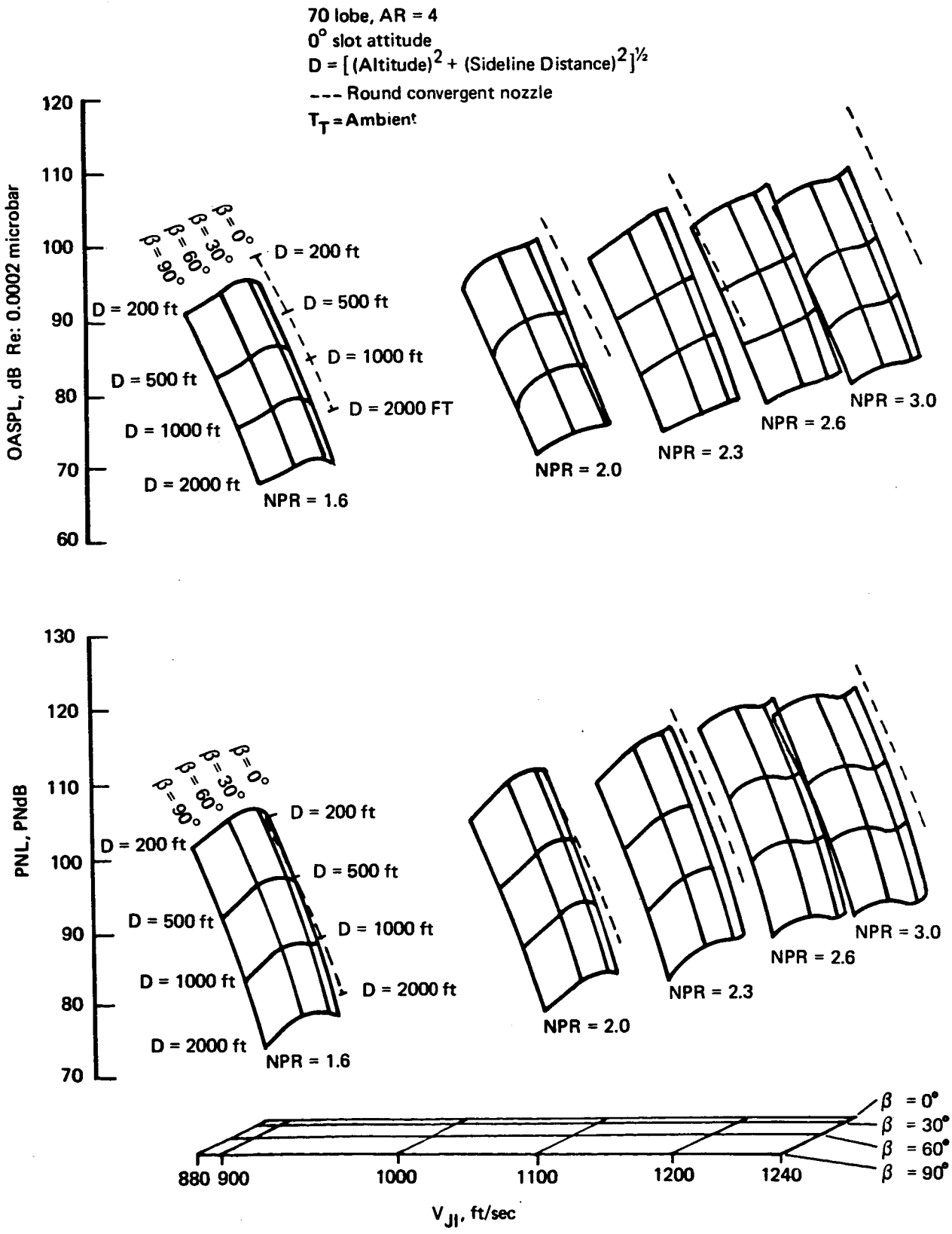

FIGURE 6-168.— DISTANCE EFFECTS

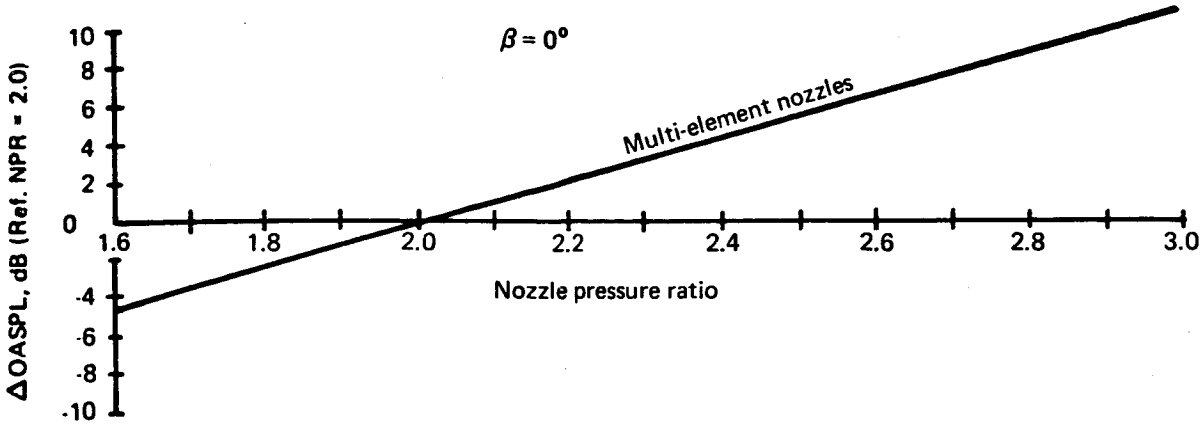

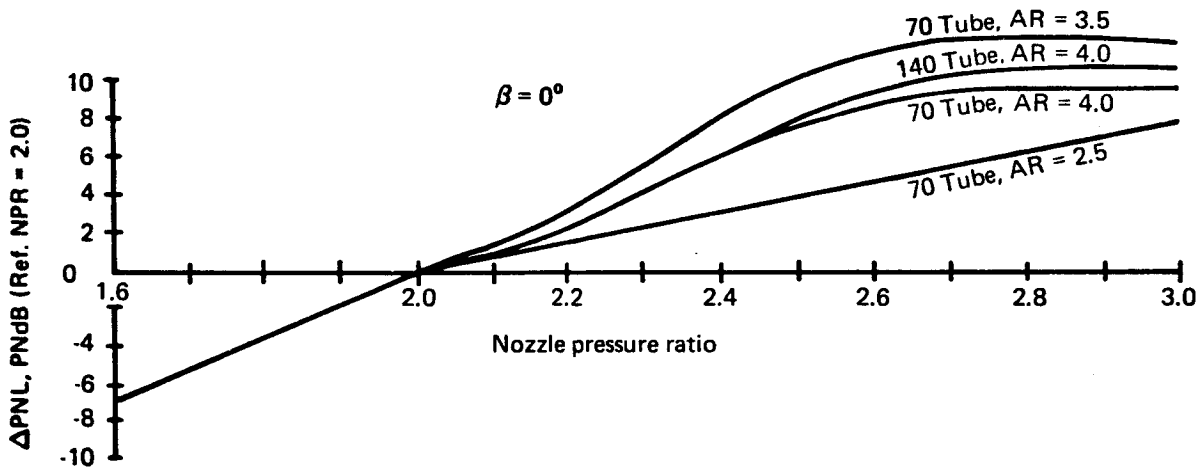

FIGURE 6-169. EFFECT OF PRESSURE ON NOZZLE BREAKUP

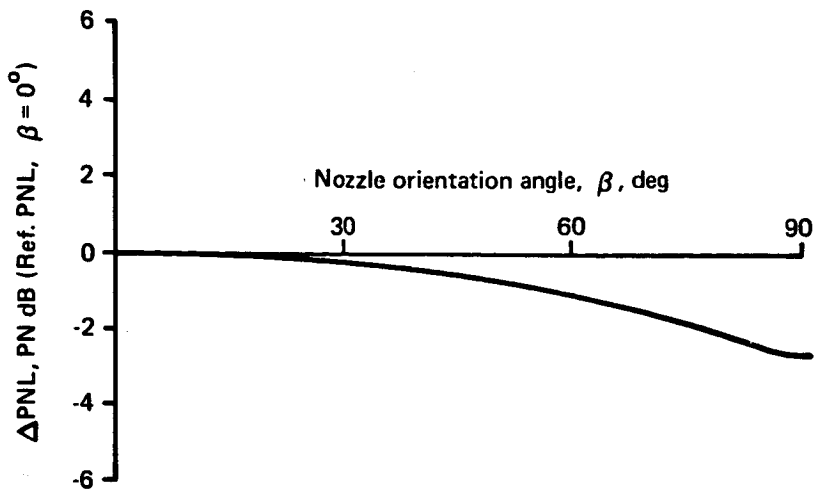

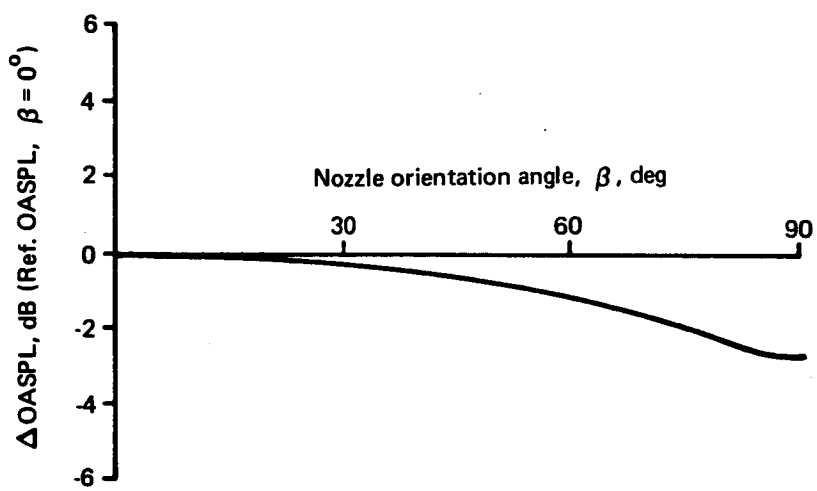

FIGURE 6-170.– MULTI-ELEMENT NOZZLES, NORMALIZED ORIENTATION

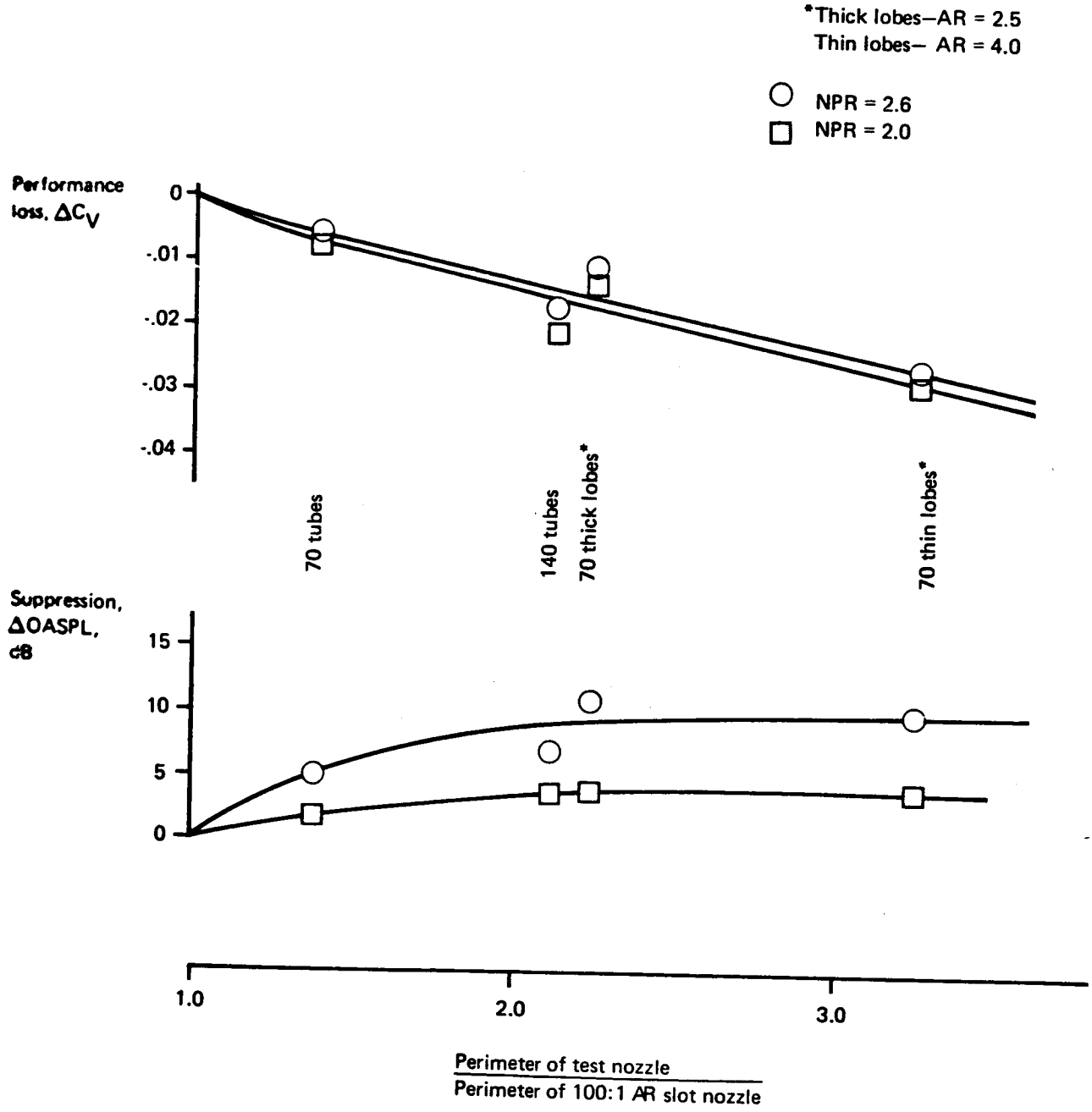

FIGURE 6-171.–BREAKUP PERFORMANCE AND SUPPRESSION RELATIVE TO 100:1 AR SLOT NOZZLE

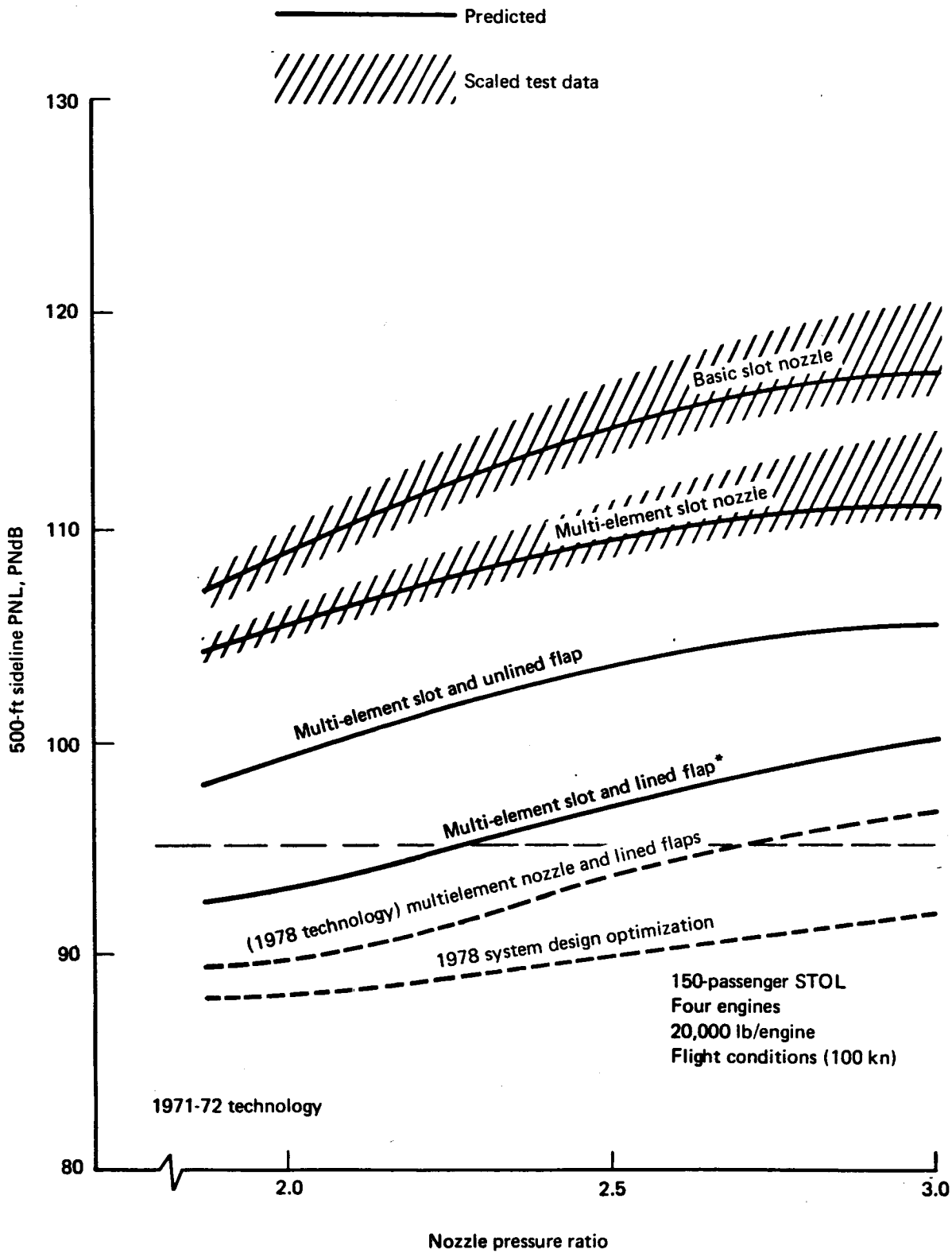

FIGURE 6-172.– AUGMENTOR WING JET FLAP NOISE COMPONENTS

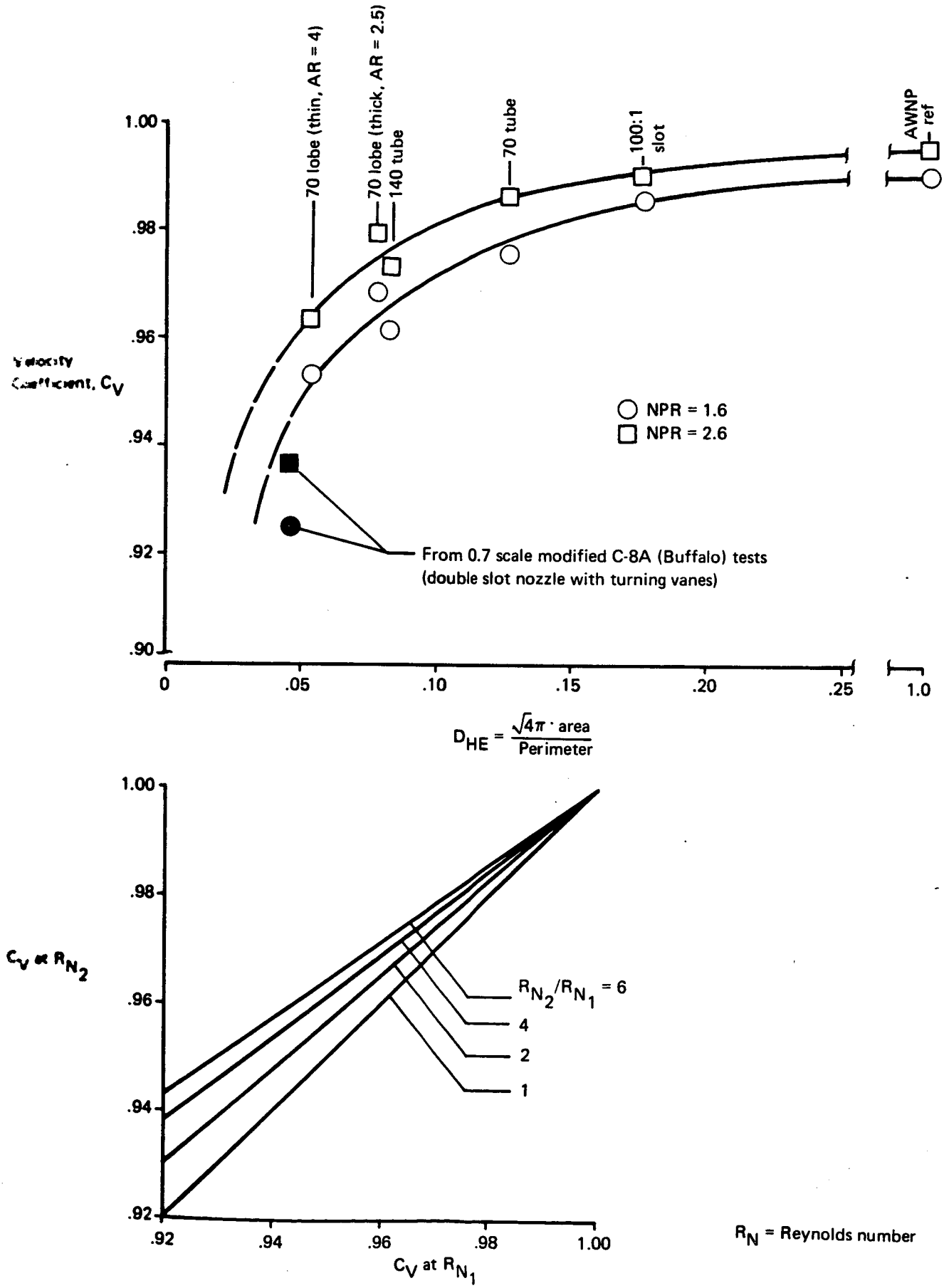

FIGURE 6-173.—CORRELATION AND SCALING FOR TWO-DIMENSIONAL, HIGH-ASPECT-RATIO SUPPRESSOR NOZZLES

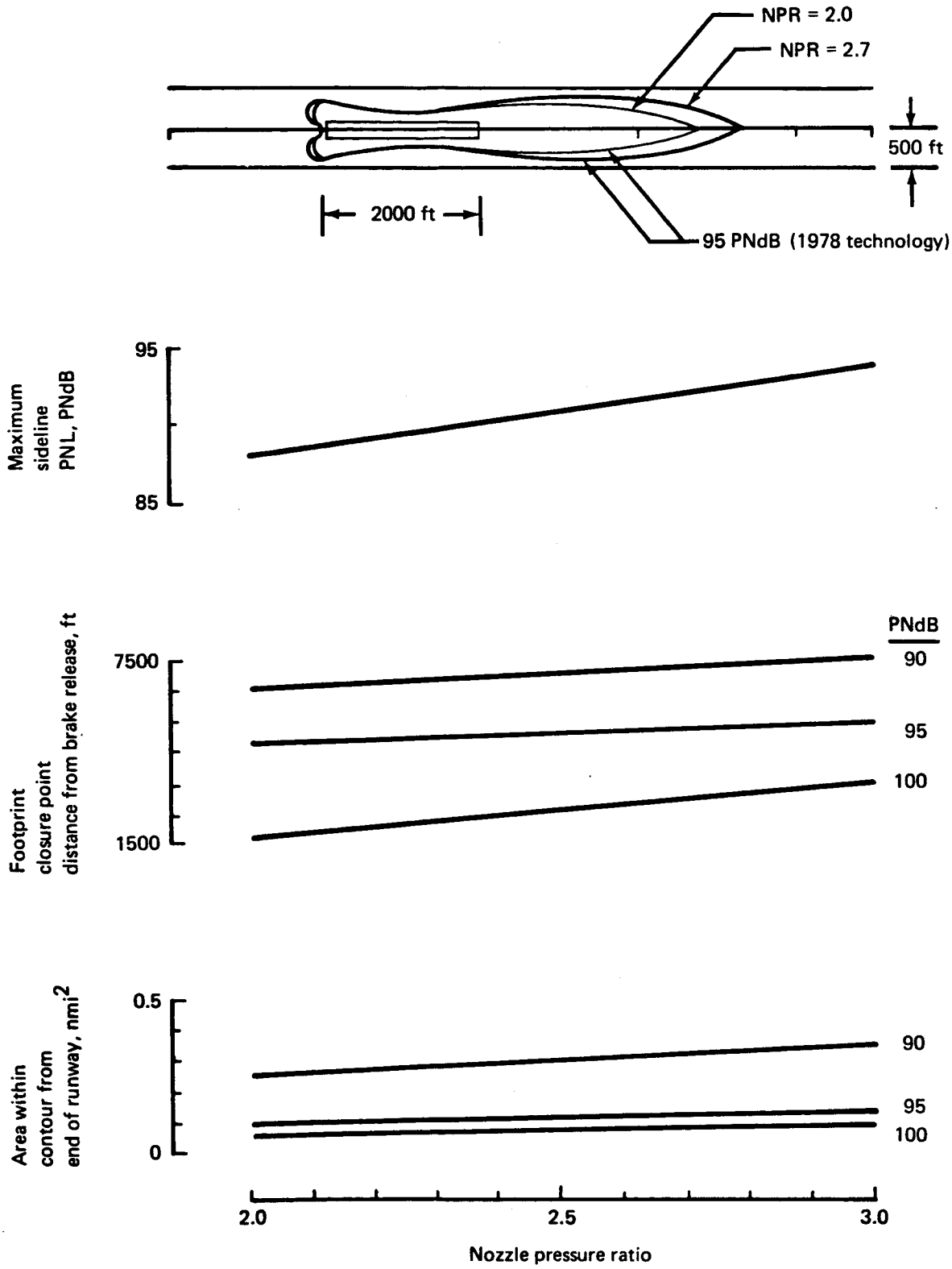

FIGURE 6-174.—STOL-AW AIRPORT AND COMMUNITY NOISE TAKEOFF OPERATION

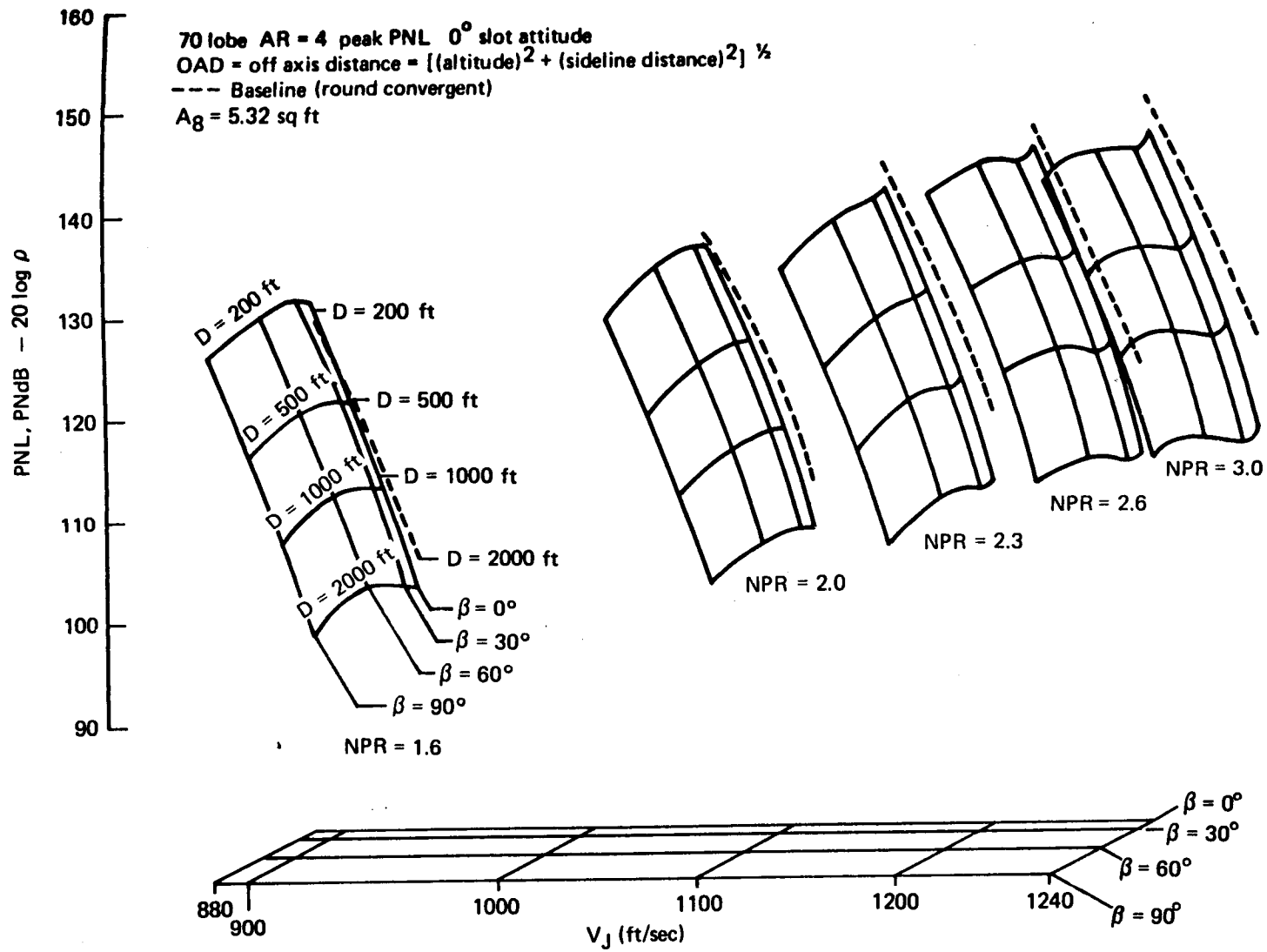

FIGURE 6-175.—DISTANCE EFFECTS

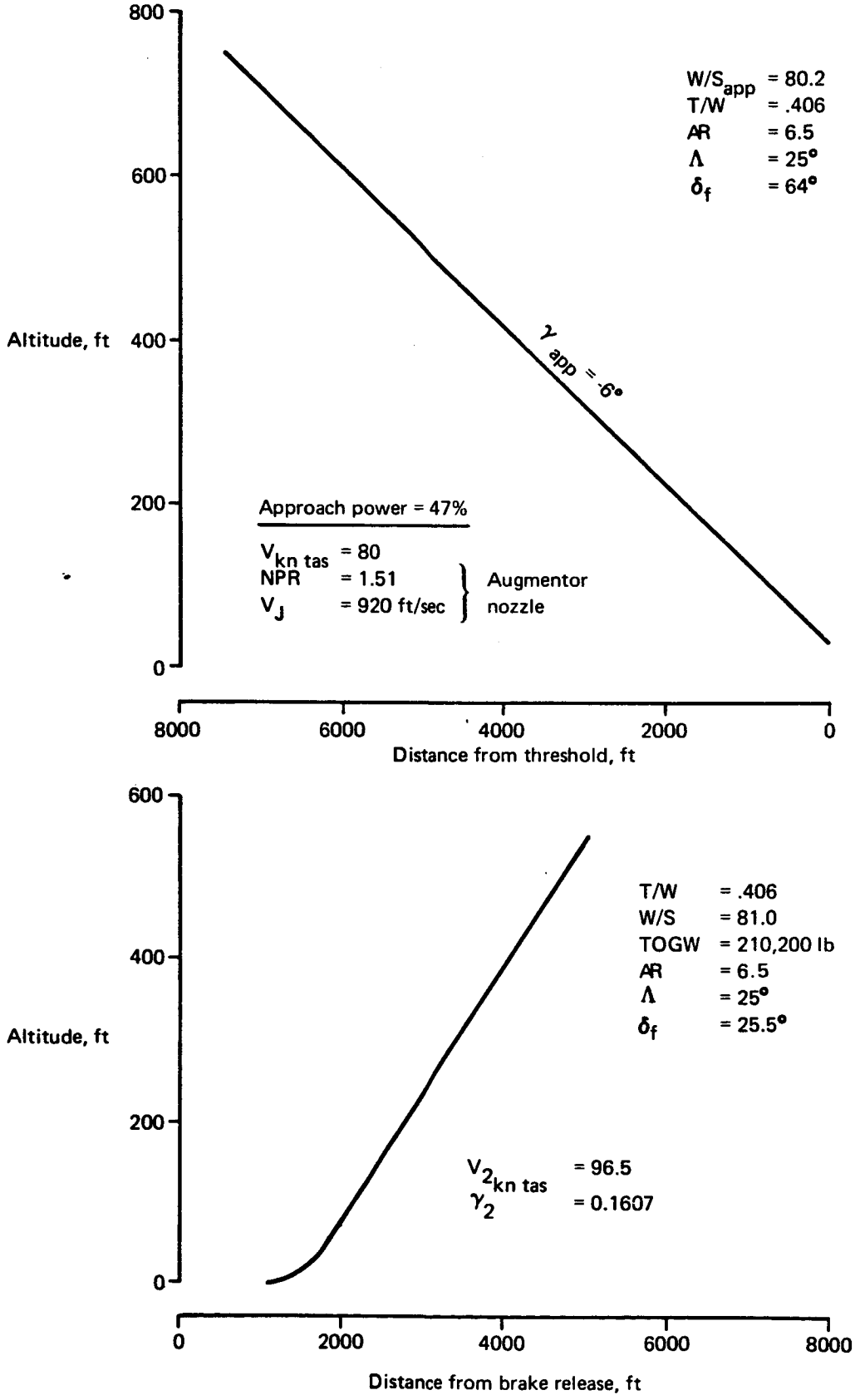

FIGURE 6-176.—AUGMENTOR WING APPROACH AND TAKEOFF

7.0 AERODYNAMIC DESIGN OF AUGMENTOR WING SECTION

7.1 INTRODUCTION

An augmentor wing consists of a jet flap issuing from an ejector. The aerodynamic design and analyses of such a wing section at a high-lift condition must account for boundary layer effects, ejector characteristics, jet mixing, and jet displacement. The complete theoretical solution of such a turbulent, viscous flow problem is unattainable at present. By drawing upon semi-empirical results from ejector and augmentor wing studies, as well as observations of certain jet characteristics, a useful design and analysis method has been formulated during task I of the present program. It consists of simulating the essential features of the flow around an augmentor wing by potential flow singularities. The singularity representation was developed in the present program, and solutions were obtained using an existing potential flow analysis method (ref. 7-1).

Lift, pitching moment, pressure distribution, and streamlines can be calculated for a given augmentor wing geometry, jet momentum coefficient, and assumed jet entrainment rate based on estimated ejector performance. A procedure was also developed to allow the designer to modify the shape of the augmentor wing segments to improve the pressure distribution.

Since the potential flow analysis method, in the form of a computer program, was not developed under the present contract, only a brief description of it is given in this section. This method has been used to design a new augmentor configuration known as flap "A," and to analyze a streamwise wing section of the NASA Ames phase VI augmentor swept wing model. The results are discussed in this section.

7.2 DESIGN AND ANALYSIS METHOD

7.2.1 Description of Existing Potential Flow Analysis Computer Program

The computer program uses the method of singularities to find the forces, moments, pressure distributions, and streamlines on a multi-element airfoil in two-dimensional potential flow. The surface of the wing section is represented by vortex polygons. The strengths of these vortices are unknown and have to be determined subject to boundary conditions. These conditions, in the simple cases without jet or boundary layer simulation, are: no flow through the airfoil surface and the Kutta condition at the trailing edge of each airfoil segment. These boundary conditions and the unknown vorticities yield a simultaneous system of linear equations that are solved by matrix inversion. Computed vorticities agreed well with exact solutions in numerous check cases. An example is shown in figure 7-1.

For a jet-flapped airfoil, the jet sheet is represented by a line of unknown vortices and treated in a manner similar to an airfoil. The final shape of the jet sheet is arrived at through an iterative process in the program such that the pressure difference across the jet sheet is proportional to the curvature and the rate of jet momentum flux. The lift calculated for a thin jet-flapped airfoil is shown in figure 7-2 in comparison with Spence's linearized theory (ref. 7-2).

To increase the versatility of this analysis method, the program also allows one to specify known and unknown singularities and additional boundary conditions in the flow field to model various physical flow problems.

7.2.2 Application of the Program to Augmentor Wing

The mathematical model of the augmentor wing consists of the usual vortex polygon representation of the airfoil and jet sheet plus a distribution of line sinks of known strength to account for jet entrainment in the ejector and a source/vortex barrier of unknown strength across the ejector exit to control the exit jet width. Figure 7-3 shows the special singularity representation of the augmentor flap and typical calculated streamlines and jet sheet.

The line sinks simulating jet entrainment are located along an estimated jet path (locus of maximum velocity point) in the ejector. The total entrained air flow is based on semi-empirical ejector theory. The sink distribution shown in figure 7-3 is based on incompressible free jet data (see ref. 7-3).

The source/vortex barrier at the ejector exit consists of two closely spaced lines of vortices and sources. The source barrier is on the exit side of the barrier and is used to fill in the exit flow field, satisfying prescribed flow direction behind the flap and shroud trailing edges. The vortex barrier is used to control the flow past the ejector exit. The vortex sheet simulating jet flap begins at the ejector exit and follows the estimated jet path within the ejector. The appropriate specification of singularities at the ejector exit is important to obtain a reasonable solution, i.e., no flow around the flap and shroud trailing edge plus the rapid convergence of the jet sheet iterations.

To reduce computer time, the number of unknown vortices representing the airfoil is reduced during jet sheet iteration. Once the jet flap solution is obtained, both the jet sheet and source/vortex barrier are input as known singularities, and the airfoil vortices are enriched to obtain well-defined surface pressure distributions. Minor modifications of airfoil shape to improve the pressure distributions can also be made without changing the jet flap solution. This procedure allows the refinements to augmentor aerodynamic design to be made in a reasonable time.

The method of modeling the augmentor jet flap configuration described above presents a reasonable facsimile of the flow, as evidenced from the streamlines presented in figure 7-3. This is especially true when one considers the simplicity of a potential flow model used for a configuration that actually involves some very complicated viscous interactions. As is true with all mathematical models of flow phenomena, the model is subject to improvement, based on experience gained from the analysis of applicable experimental data.

7.3 FLAP "A" DESIGN

The preliminary results of system design studies indicated that the projected airplane will have a flap chord to primary nozzle slot height ratio of only about half that on the modified C-8A Buffalo airplane (ref. 7-4), or the NASA-Ames phase IV model (ref. 7-5).

This means that the projected augmentor will have a smaller ejector area ratio (secondary to primary) and shorter mixing length than the Buffalo configuration and consequently a loss in thrust augmentation ratio (ref. 7-6). Therefore, the primary aim in flap "A" design is to achieve high thrust augmentation at the takeoff flap settings.

The design conditions and constraints, chosen based on system design studies, are as follows:

1) Main wing (nozzle lip) trailing edge located at 75% chord

2) Flap chord of 27% wing chord

3) Augmentor segments that nest within cruise airfoil profile

4) Design nozzle pressure ratio of 2.5

5) Takeoff flap deflection of 35° and $C_\mu = 1.2$

6) Go-around flap deflection of 50° and $C_\mu = 1.2$

7) $\alpha_{2\text{-}D} = 0°$, $V_\infty = 80$ kn

The design of flap "A" assumed the use of breakup (lobe) nozzles to promote mixing and thus improve both thrust augmentation and noise reduction potential. But the use of a breakup nozzle having the same exit area as a slot nozzle results in a thicker jet, which tends to turn less by coanda action. This becomes a problem at the landing and approach flap deflections.

To assist jet turning, the nozzle axis is rotated 20° down with respect to the wing chord, the lower nozzle lip extension forms a coanda surface, and the lower flap has a generous radius under the jet. At very large flap deflection the sealing of the flap gap should further enhance turning.

To reduce the diffuser length required for a given pressure recovery, the passage formed by the flap and the shroud has a nonlinear area distribution. It is designed to yield, in potential flow, a pressure distribution such that the boundary layer remains attached despite a more adverse pressure gradient than that given by a linear diffuser.

The shapes of the intake and shroud are designed to minimize surface peak velocities. The BLC slot formed by the intake and the shroud is located to take advantage of the suction created by jet entrainment. The design was based on analyses for flap deflection of 35° and 50°. Similar analyses will be made for the landing flap deflection in task II.

7.4 RESULTS OF POTENTIAL FLOW CALCULATIONS

Potential flow solutions for three augmentor flap configurations have been obtained. The lift and pitching moment coefficients are given in table 7-1.

TABLE 7-1.—CALCULATED RESULTS FOR AUGMENTOR FLAP CONFIGURATIONS

Case	Augmentor flap configuration	δ_f	$e_{f/c}$	α	C_μ	C_ℓ	$C_{m/4}$
I	A	35°	0.27	0°	1.2	5.85	-1.23
II	A	50°	0.27	0°	1.2	7.86	-1.56
III	Baseline	50°	0.35	0°	1.2	7.95	-1.65

The surface pressure distributions for the three cases are shown in figures 7-4 through 7-6. The baseline flap represents a typical streamwise section of the Ames phase VI swept wing model (ref. 7-5). Dotted lines are used in the pressure distribution plots to indicate regions where the pressures are questionable because of the mathematical modeling of the ejector. The shapes of the augmentor elements in flap "A" have undergone considerable refinement to achieve the low suction peaks ($C_{P_{min}}$ greater than -9 at $\delta_f = 35°$ and -10 at 50°) shown in figures 7-4 and 7-5. The suction peaks on the intake and the flap are extremely high for the baseline flap. These high peaks could be due partly to the entrainment model. However, the sharp leading edge of the intake is also a likely cause of high local velocities.

The assumed total entrainment and its distribution along the jet path were based on ejector characteristics with multi-element breakup nozzles. The same assumptions were incorporated in all three cases. Since the baseline flap used a slot nozzle, one would expect lower rates of entrainment than those of the multi-element nozzle. To compare the calculated pressure distribution with experimental data, the entrainment model in case III should be adjusted. Reducing the entrainment should lower the flap and intake suction peaks.

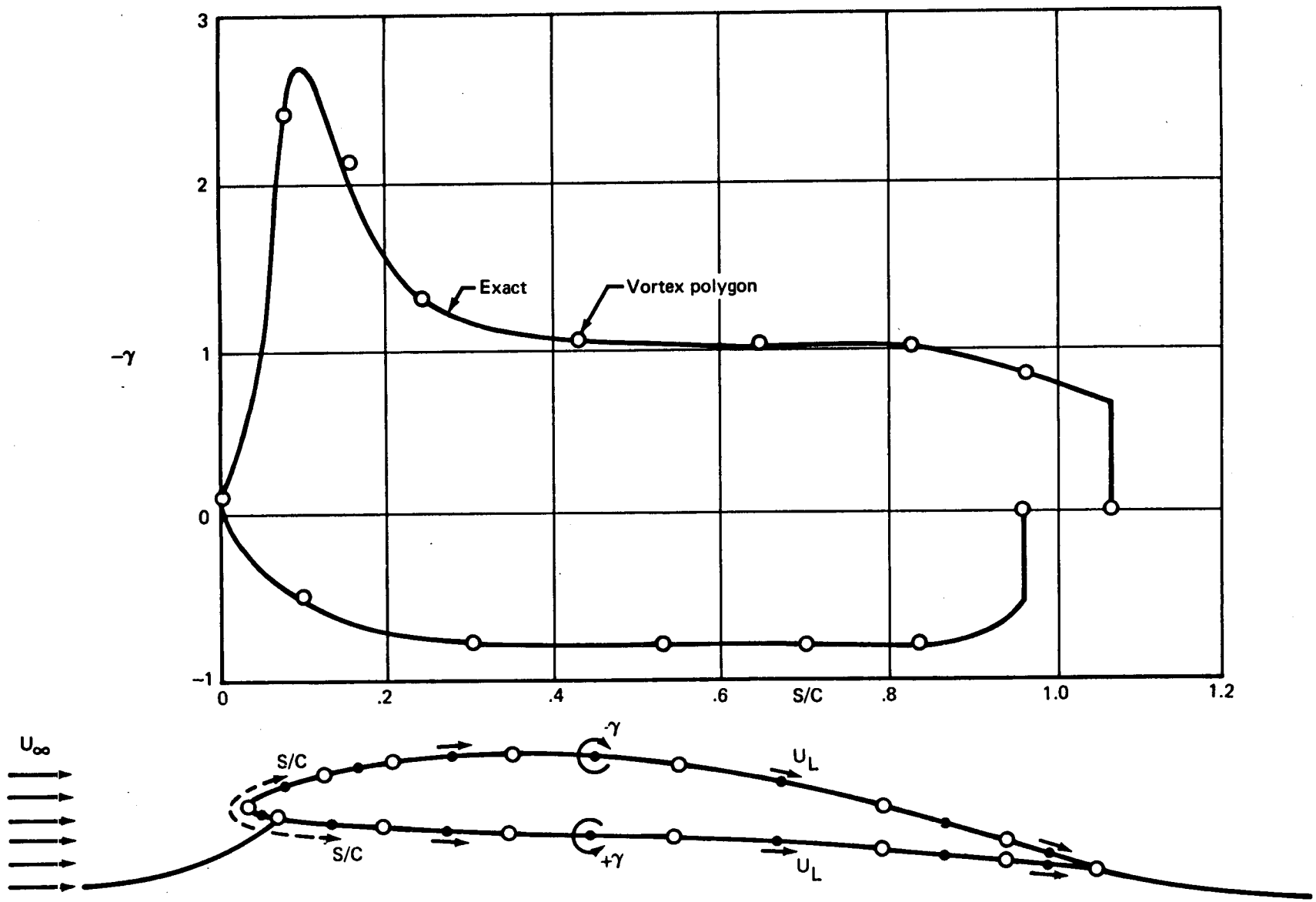

FIGURE 7-1.– EXACT SOLUTION VS VORTEX POLYGON

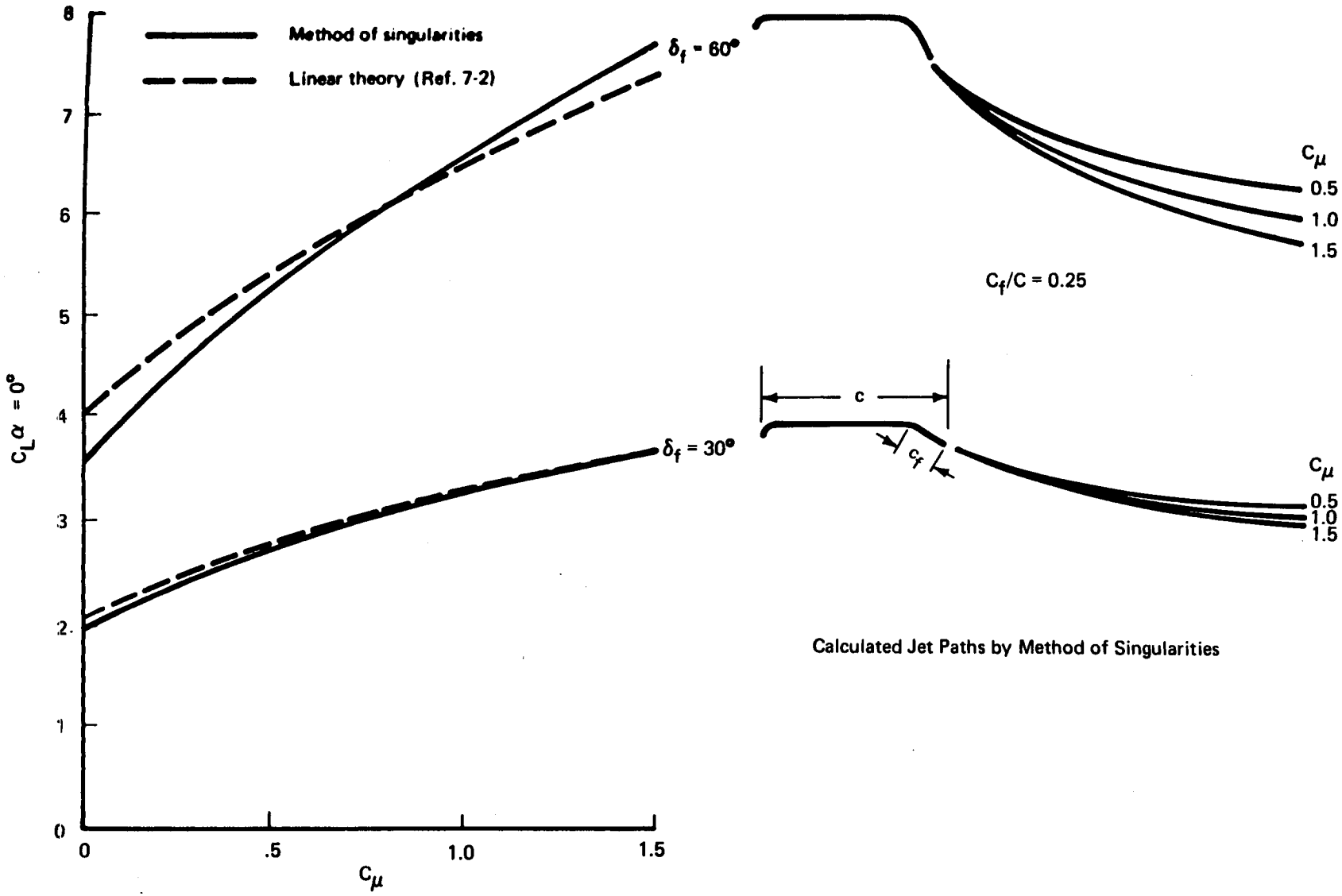

FIGURE 7-2.– CALCULATED LIFT FOR A THIN-JET-FLAPPED AIRFOIL

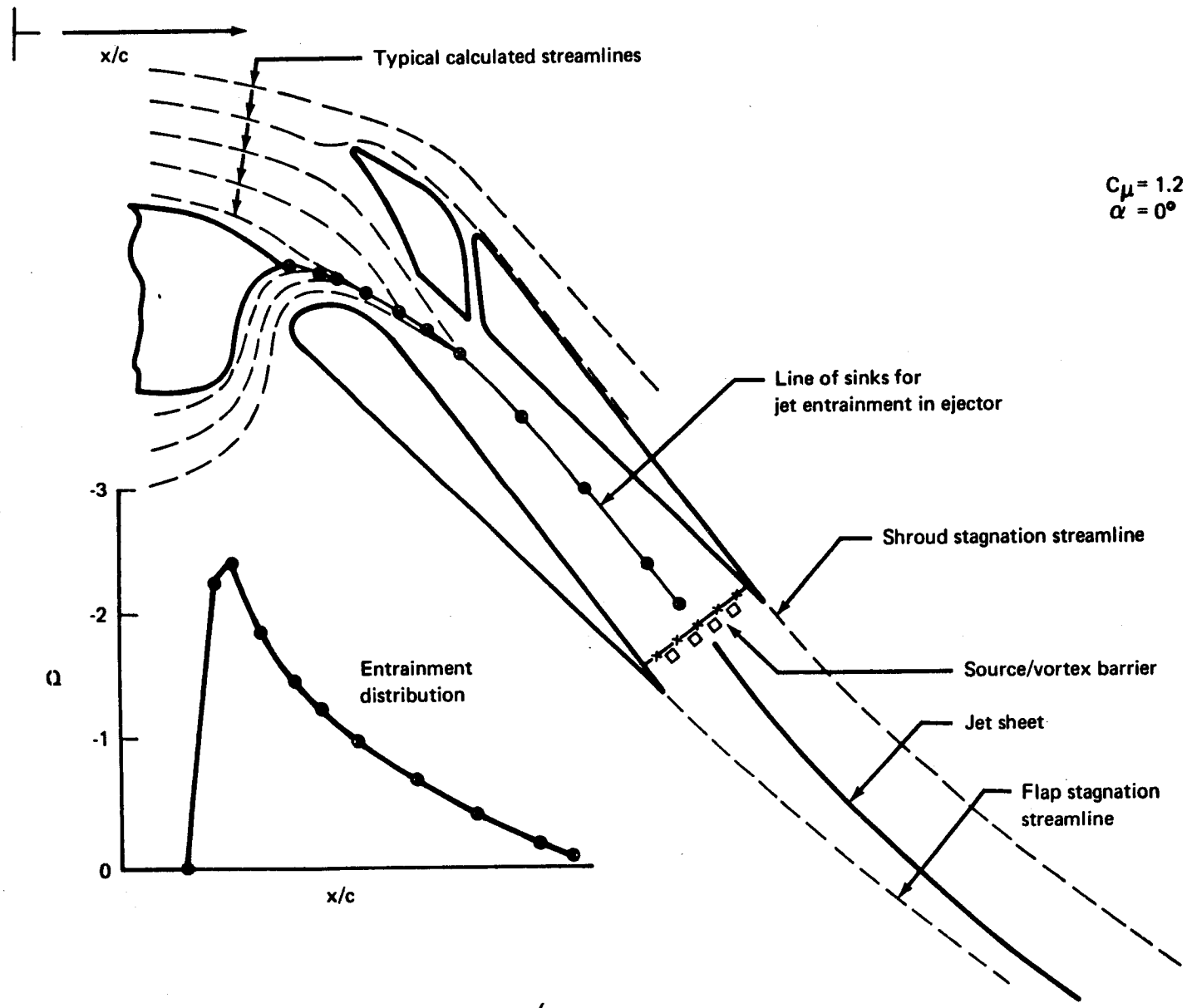

FIGURE 7-3.—AUGMENTOR WING MATHEMATICAL MODEL

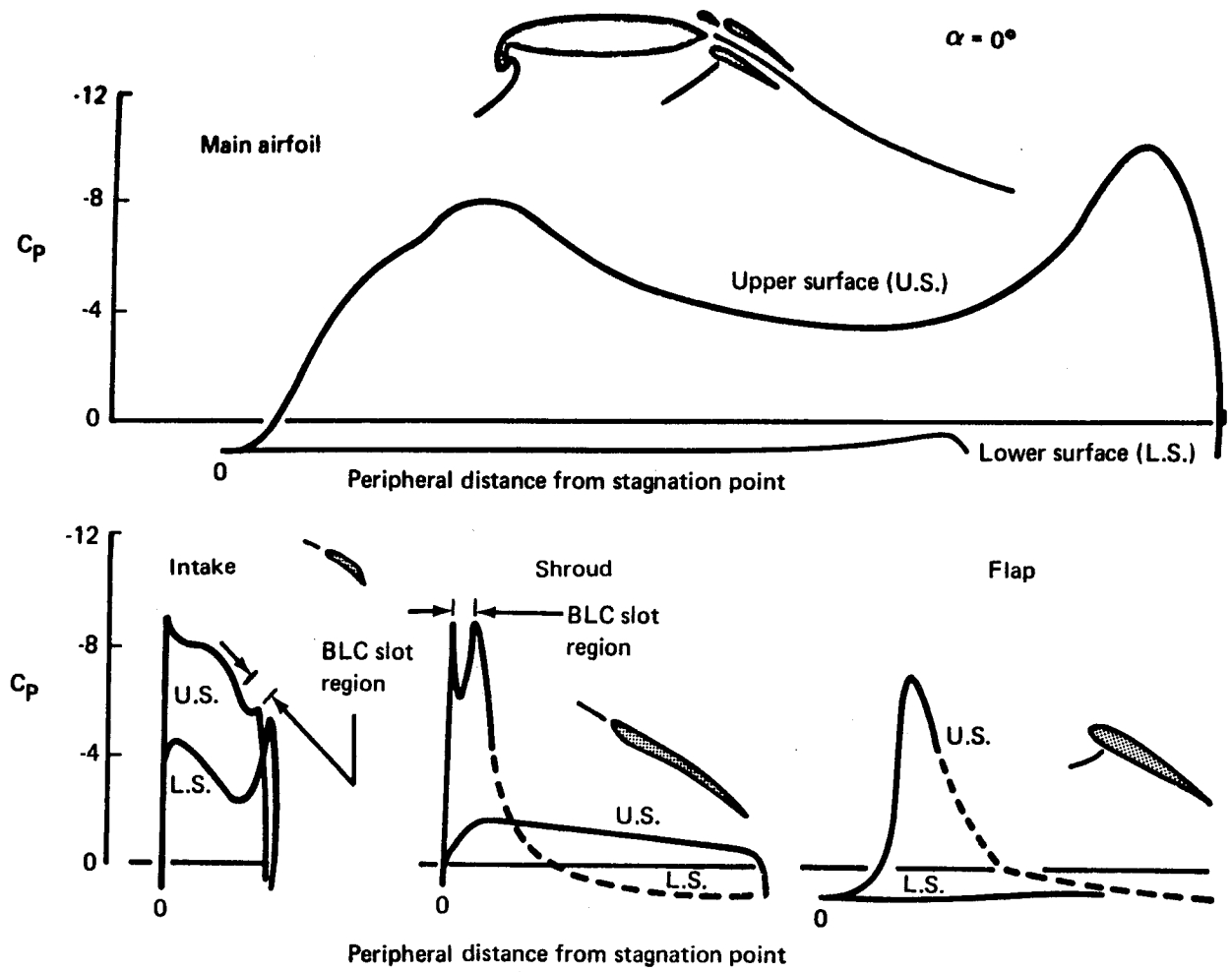

FIGURE 7-4.– CALCULATED PRESSURE DISTRIBUTION FOR FLAP "A", $\delta_f = 35°$

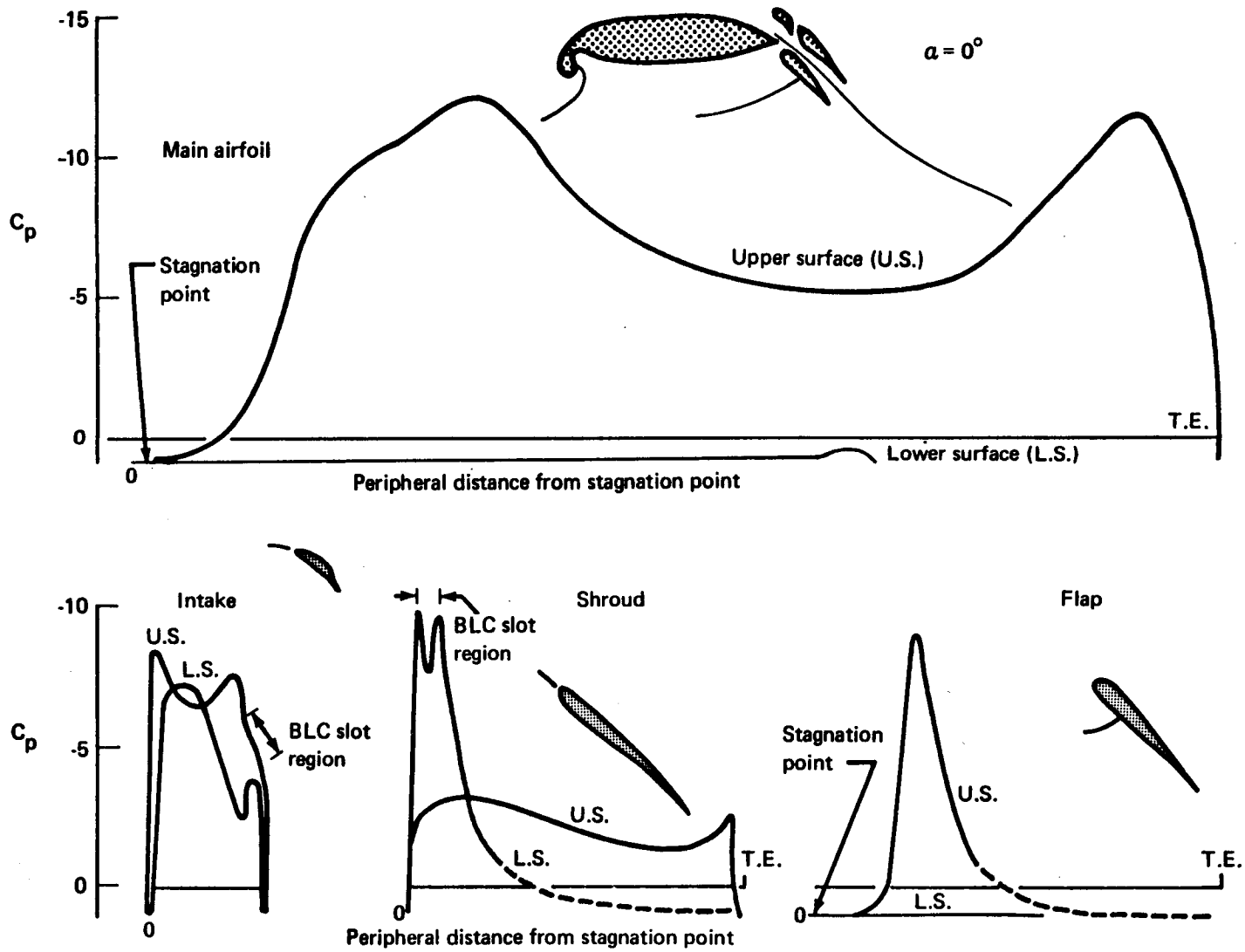

FIGURE 7-5.—CALCULATED PRESSURE DISTRIBUTION FOR FLAP "A", $\delta_f = 50°$

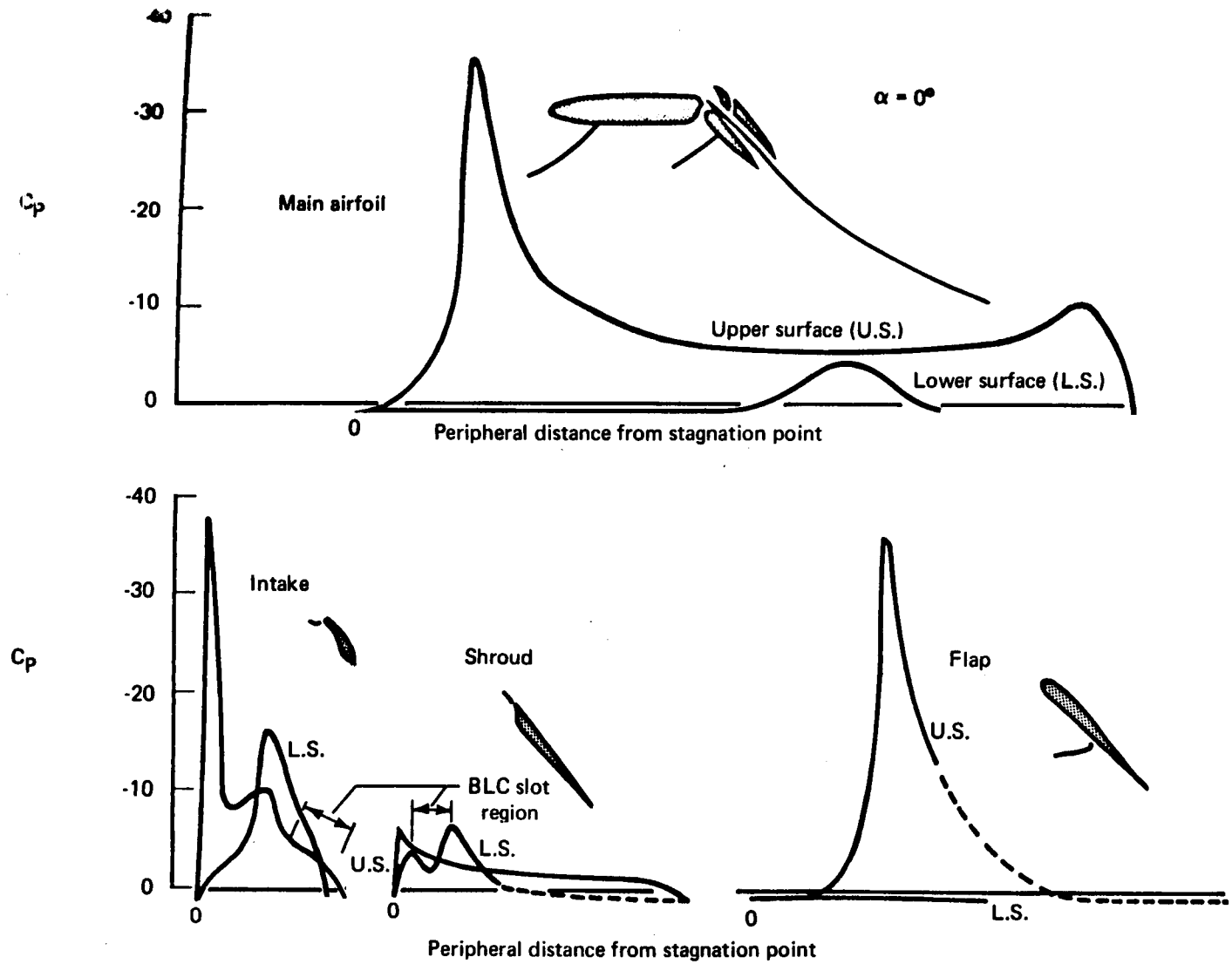

FIGURE 7-6.—CALCULATED PRESSURE DISTRIBUTION FOR BASELINE AUGMENTOR FLAP, $\delta_f = 50°$

8.0 CONCLUSIONS TASK I

(NAS2-6344)

The initial program noise objective of 95 PNdB at 500-ft STOLport sideline distance appears to be achievable for the augmentor wing within the state of the art developed in this program. Precontract noise source estimates and noise level predictions have been confirmed for the basic slot nozzle with large aspect ratios and for the multi-element breakup nozzles. Additional noise reduction methods for these nozzles have been developed which enhance their noise reduction capability. Flap systems are in the process of being tested and hold the excellent technical promise of large amounts of noise suppression, especially with properly designed, frequency tuned, single-layer acoustical lining material installed in the shroud system.

Ninety PNdB at 500-ft STOLport sideline is a realistic extended program target to be obtained for the augmentor wing. Additional noise suppression is achievable with systems design optimization relative to flap mixing length, noise source location and definition, augmentor primary nozzle design, and increased acoustic lining efficiency. Optimization design procedures coupled with multiplayer lining developments collectively produce a system which predicts a 1978 design point, with a 1976 design release date, of 87 to 92 PNdB for the nozzle pressure range of 2.0 to 3.0.

Performance and acoustic data from this test program had a very high degree of accuracy and repeatability. Nozzles tested showed high velocity coefficients.

One of the prime factors in the practicality of the augmentor wing airplane is the capacity of the wing to contain the large amount of ducting required. This question is particularly relevant to the two-stream engine concept, wherein 80% of the thrust is ducted to the wing.

The wing design was compromised in favor of large duct capacity by lowering the aspect ratio and decreasing the width of the wing box. In the initial design it was decided to operate at the lowest possible augmentor nozzle pressure ratio in order to favor low noise. Many ducting and nozzle designs were studied and a system was chosen with four engines operating in parallel feeding a common plenum duct. This design permitted operation at a nozzle pressure ratio of approximately 2.0, which was the objective at the start of the contract.

The plenum ducting system with engines in parallel presents some problems in dynamics and stability of the system, such as the problem of removing a stalled engine from the line without disturbing the remaining engines. This can be accomplished with an independent system, which requires more ducting and a higher pressure to accommodate the required airflow. A nozzle pressure ratio of 2.5 to 2.7 is indicated. With the more favorable noise levels now predicted it appears that the operational advantages of the independent ducting system can be realized within the low noise level objective.

The problem of ducting very large airflows to the wing, as required by the two-stream engine, can be alleviated by using a three-stream engine where a smaller airflow to the wing is used and the remainder of the axial thrust is obtained by exhaust from a

high-bypass-ratio fan. Airplane performance calculations showed that large engine size is required to produce the lift required for wave-off, and the airplane TOGW increases unless as much as 50% of the thrust is ducted to the wing. However, even at this design point the remaining fan thrust results in turbomachinery noise, which is approximately 10 PNdB higher than the level of the two-stream engine version.

The ability of the augmentor wing concept to distribute the thrust along the wing has important advantages during engine-out operation. The most effective design would distribute the thrust of each engine symmetrically with engine out; however, this results in the most difficult ducting design. Analyses of the airplane roll moment characteristics with various amounts of cross-body flow have been related to the roll control necessary for normal operation and cross-wind landing. Allowing for this, the augmentor system can be designed with independent ducting with approximately 25% crossover, permitting a simplification of the duct arrangement and a major reduction in the augmentor nozzle pressure as compared to the original 50% crossover design.

The conclusions derived from the task I study are summarized below:

1) Predict 90 PNdB at 500-ft sideline

2) Ducting possible at NPR = 2.0

3) Inlet noise critical

4) Noise data very close to predicted

5) Higher nozzle pressure acceptable for independent ducting

6) Nozzles show high velocity coefficients

7) Noise and performance data repeatable and accurate

8) System optimization permits significant improvement

9) Two-stream system appears superior

10) Wing airflow crossover of 25% to 30% required

9.0 TASK II AND III RECOMMENDATIONS

Results of parametric tests to determine the noise attenuation and propulsion performance of selected high-aspect-ratio lateral slot nozzles and multi-element nozzles have been presented in this report. The 70-lobe (area ratio 4) and the 100: 1-aspect-ratio slot nozzles have been tested with coanda lips for noise suppression and performance. Preliminary system design studies to integrate the augmentor wing jet flap into a practical STOL airplane have also been completed and reported.

This information has been used to provide program definition for the task II and III parts of the program, where consideration is given to static tests of the noise of the augmentor wing with acoustic lining and two-dimensional wind tunnel tests of the low-noise-level augmentor wing. Continuation of the systems integration effort initiated in task I will involve assessment of the interrelationship of duct designs, wing thickness, engine specific fuel consumption, weight, and their effects on STOL transport aircraft performance and noise.

Task II static rig tests will utilize the various nozzles designed in task I which have indicated the best potential for low noise and optimum performance for initial testing with the augmentor flap systems. Task II investigations shall also include measuring the noise reduction and performance levels attributable to systematic installation of acoustic linings on the flap interior surfaces.

Studies of system design and analysis to integrate the propulsion system and augmentor wing will continue. Included in these studies are ducting component design layouts for minimum pressure loss and weight, diverter valves, variable nozzle area, and other components related to ducting air from the engine fans to the flaps. These studies, as well as the task I systems integration studies, will be continued in task III.

Task III studies are to include analyses and experimental investigations of the effects of various modifications to the augmentor wing jet flap for reduction of noise levels on the sectional aerodynamic characteristics at forward speed conditions. Wind tunnel tests of two-dimensional models will be conducted. The investigations of tasks I and II will determine the static performance of the configurations, and a certain limited number of configurations will be investigated during this task.

Recommendations for work to be conducted by the contractor in tasks II and III are discussed below under three separate headings: static rig tests, wind tunnel tests, and system design studies.

9.1 STATIC RIG TESTS

A schedule which outlines the proposed static rig test program for task II is presented in figure 9-1. Test configurations, estimated design, fabrication, and test flow times are identified. The reasons for testing these designs and the sequence of testing are discussed in the following paragraphs.

To assess the potential of the total augmentor wing concept in a timely manner it is desirable to test the augmentor with and without acoustic lining as soon as a suitable multi-element nozzle configuration has been identified. The 70-lobe, area ratio 4 nozzle tested in task I has demonstrated excellent noise spectrum suppression characteristics compatible with optimum nozzle-augmentor system total suppression goals. This nozzle has been selected for testing with the augmentor flap design in task II.

An augmentor flap system (configuration A) was designed and fabricated in task I. The design was based on aerodynamic, propulsion, and noise suppression considerations. Aerodynamic layout was designed to yield improved static thrust augmentation at flap deflection angles between 30° and 50°. To reduce the amount of jet turning required, the exit plane of the breakup nozzles was tilted by 20° with respect to the wing chord plane. A design nozzle pressure ratio of 2.5 was selected. The contours of the flap system were developed by simulating the flow field of the augmentor-flap airfoil in a two-dimensional potential flow computer program. Flexibility in the augmentor flap components was maintained in the design to ensure optimization capability for propulsion performance. Acoustic design recommendations incorporated into the flap design included a flap length extension segment for further noise attenuation. Since the lower forward air entrainment gap between the nozzle and flaps was considered a possible source of noise radiation, provisions were made to close the lower forward gap to assess the amount of noise which radiated through it. A bulk absorber (fiberglass) acoustic lining of adequate depth was installed on the augmentor flap interior surfaces. Results from tests on this lining material will be used as a baseline for comparison with more flight-worthy acoustic liners to be installed later in task II. Bulk absorber lining will be used to estimate the potential of the lined augmentor. The augmentor was instrumented for static pressure and noise on the interior surfaces. Capability to measure flow profiles at the augmentor throat and exit was also included.

It is recommended that testing of the augmentor include three flap deflections (δ_f = 35°, 50°, and 70°), considered representative of takeoff, go-around, and approach flap settings. Each configuration should be investigated for its noise suppression and performance potential. Special attention should be given to possible coanda turning, augmentation, and flap noise resonance problems. Each configuration should be optimized for performance and then tested for noise.

The flap should be tested with and without the acoustic liner to determine its effect on noise. During this test sequence the influence of additional flap length, lining location, and coanda gap closure on noise attenuation should be studied in a parametric manner. The lining location test will evaluate the individual effectiveness of the lower flap, upper flap, intake, and coanda surface on noise suppression.

It is recommended that each configuration be tested at selected pressure ratios ranging from 1.3 to 3.0. A decision to test with ambient or heated flow will be made early in task II. It is desirable to keep the number of test power settings to a minimum consistent with engine cycle study requirements. The nozzle pressure ratio will be extended lower for relative velocity flight usage.

A majority of the configurations are scheduled for testing at nozzle orientations of 0° and 90°. Task I results have shown orientation to be significant at the sideline condition (β = 90°).

A second test series is recommended for the augmentor flap system (A) with the 100:1-aspect-ratio convergent slot to compare its effectiveness as a suppressor system with the previously tested multi-element system. The three flap deflections, a lined and unlined flap, and selected orientations and nozzle pressure ratios should be included in the test program. Also recommended for comparative test is a configuration which uses the coanda flap section of the augmentor as a jet flap.

Having used the fiberglass acoustic lining to estimate the potential of the lined augmentor for noise reduction, it is recommended that further testing be accomplished with more flightworthy materials incorporated in a tuned lining concept. A two-phase tuned lining test program is suggested. Phase I will determine the effectiveness of basic tuned lining parameters in attenuating jet noise shrouded by an augmentor flap. Basic test hardware will be the 70-lobe area ratio 4 nozzle and an augmentor flap system similar to configuration A. The phase II test objective is to determine optimum lining configurations for the flap ejector.

The basic tuned lining design consists of a honeycomb core sandwiched between a porous facing sheet and a solid backing sheet. Polyimide is to be used for construction. Facing polyimide of several different porosities will be tested with honeycomb cores of different depths. The polyimide facing sheets will have a range of $R/\rho a$ between 2.0 and 0.5; the honeycomb cell size will be 3/16 in. with depths within the range of 1/8 to 1/2 in. Approximately six to eight lining configurations will be tested in phase I. Phase II testing will probably require construction and test of two to four lining configurations.

Two new nozzle designs are scheduled for test with a modified augmentor flap in task II. Before designing these nozzles, it is desirable to have the results of the bulk-absorber-lined augmentor tests anlayzed to determine the frequency range where noise attenuation is most needed. Augmentor test results will provide information as to what frequency range is dominating the perceived noise level and identify any flanking paths or flap resonances which may be limiting the maximum potential of the concept. The technology based on task I results is now available to design nozzles which shape the noise spectrum of the jet in a manner that complements the suppression ability of the lined shroud. The modified flap referred to in the above discussion is considered to be the "A" configuration with improvements derived from the test experience obtained in the initial phase of the test program.

A final test configuration is recommended for task II which combines the best nozzle and augmentor characteristics for optimum noise suppression and augmentation.

9.2 WIND TUNNEL TESTS

The original schedule for task III has been revised such that the two-dimensional wind tunnel test augmentor configurations are now in two phases. A revised schedule is shown in figure 9-2. Phase I consists of evaluating the performance of baseline configurations to determine the effects of leading edge devices and leading edge blowing. A detail test plan appears in figure 9-3. Phase II will include the evaluation of primary nozzle configuration, flap surface condition simulating acoustic lining treatment, flap, shroud, and intake geometry changes based on task II flap static test results.

Although the design and analysis method described in section 7.0 has been used to design the shape of flap "A" elements, the mathematical modeling remains to be verified by experimental data. Static pressure data obtained in phase I wind tunnel testing should be suitable for this purpose. The method should be used to analyse the baseline configuration for a wide range of flap deflections. Where flow separation over shroud and intake upper surface are observed at high flap deflection, this method can be useful in identifying the required geometry changes. It would also greatly accelerate the experimental geometry optimization process if the effect of movement of each element on the pressure distribution is properly understood.

9.3 SYSTEM DESIGN STUDIES

The system design studies of task I provided a baseline augmentor wing airplane configuration which serves:

1) As a guide in establishing scale and configuration of test hardware and range of test variables

2) As a reference size for exploring alternate design approaches in augmentor duct/nozzle/flap/structure/acoustics integration

3) As a reference for parametric studies of wing planform, air distribution system, and engine cycles

The test hardware was designed and several concepts have been identified for the physical integration of the augmentor system components, pending test data confirmation.

Parametric studies were completed covering the range of interest in wing aspect ratio and sweep angle. They showed that a plenum-type duct system with augmentor nozzle pressure ratio of 2.0 is well suited to a wing planform of 5.5 aspect ratio and 30° sweep angle. This planform results in substantially lower airplane gross weight than the reference wing of 6.5 aspect ratio and 25° sweep angle. However, complexity of the the four subduct valves and four back-flow check valves, as well as the potential power management control problems associated with discharging the output of two or more blowing engines into a common plenum, provide incentive to consider the independent duct system.

It was shown that a duct system with independent nozzle and cross-body flow for each engine is best suited to the space available in a wing of 5.5 aspect ratio and 25° sweep angle. A preliminary estimate shows that an augmentor nozzle pressure ratio of 2.6 is required for such a system assuming a nominal duct pressure loss of 15%. The duct system parametric studies suggest that a somewhat higher duct loss would provide more thrust-per-unit-wing-area, permitting either higher wing loading (and attendant reduction in airplane operating empty weight), or a lower nozzle pressure for the required thrust.

This requires further analysis and adjustment of system component flow losses to establish more closely the performance of the independent duct system and take advantage of the space available along the span of a particular wing planform.

Related preliminary design is necessary to integrate the system components with supporting structure and to provide alternate concepts of such items as diverter valves, flexures, and low-loss flow turning schemes. These physical components will be examined as applicable to the wing planform best suited to the independent duct system. While trades were made showing the effect on duct flow area of varying wing rear spar position and flap chord, further analysis and design is necessary to establish the weight effects of those changes.

Flight control and component design concepts are required to accommodate the various steady-state and transition modes of the system.

These variables will be examined in light of existing and new test data to provide appropriate guidance for revising test hardware. The foundation of applicable data thus obtained may then be used to predict STOL airplane performance and noise.

Basic engine cycle analysis was completed providing a consistent family of engines of assumed 1978 technology level to support the continuing system study effort. The ideal engine cycles may now be related to "potential real world" engines and preliminary engine requirements established. Further study of available engine hardware is necessary to identify an engine for the planned task IV static test.

A chart defining these recommended areas of engineering effort is given in figure 9-4.

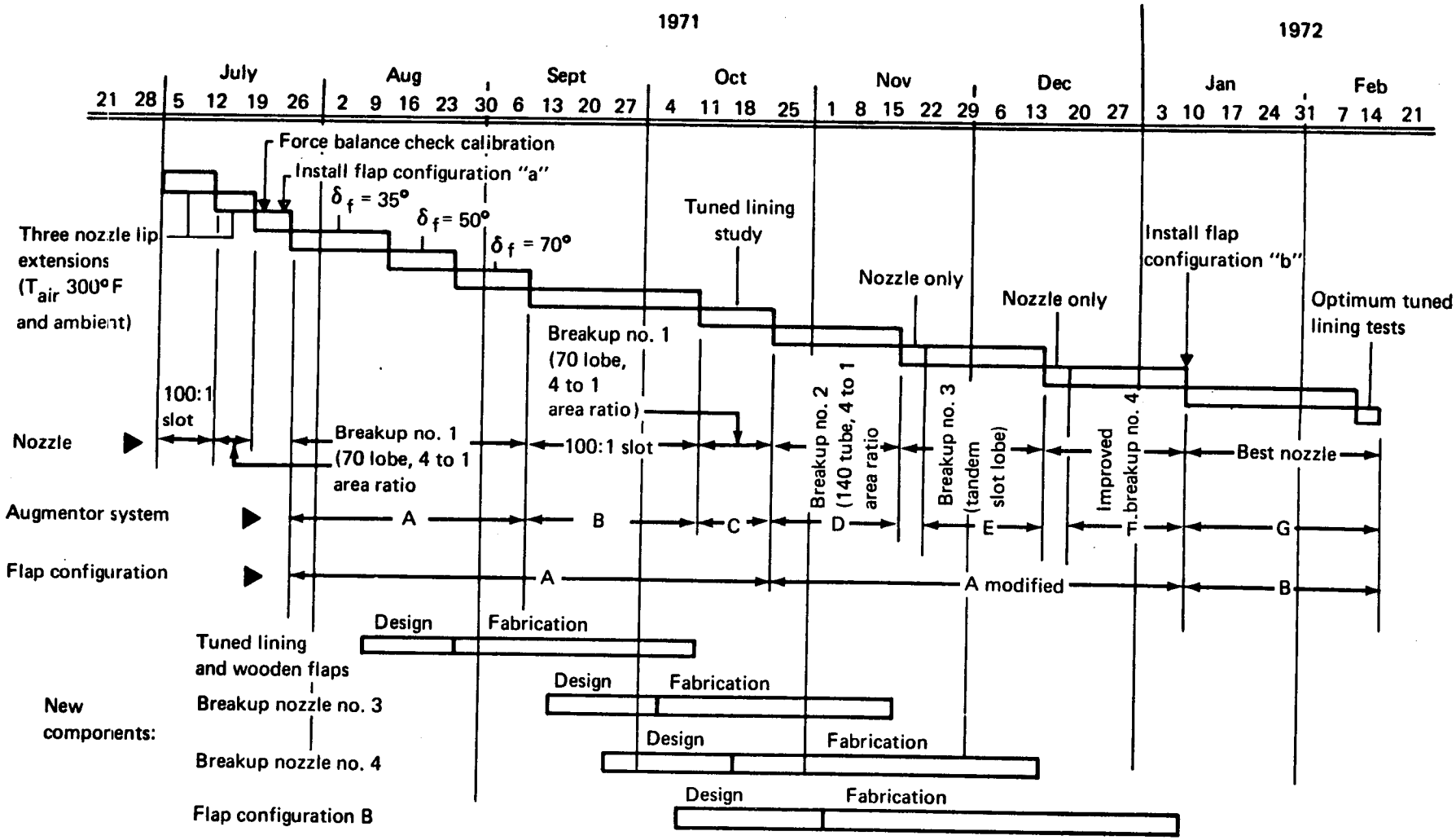

FIGURE 9-1.—TASK II SCHEDULE (STATIC TEST)

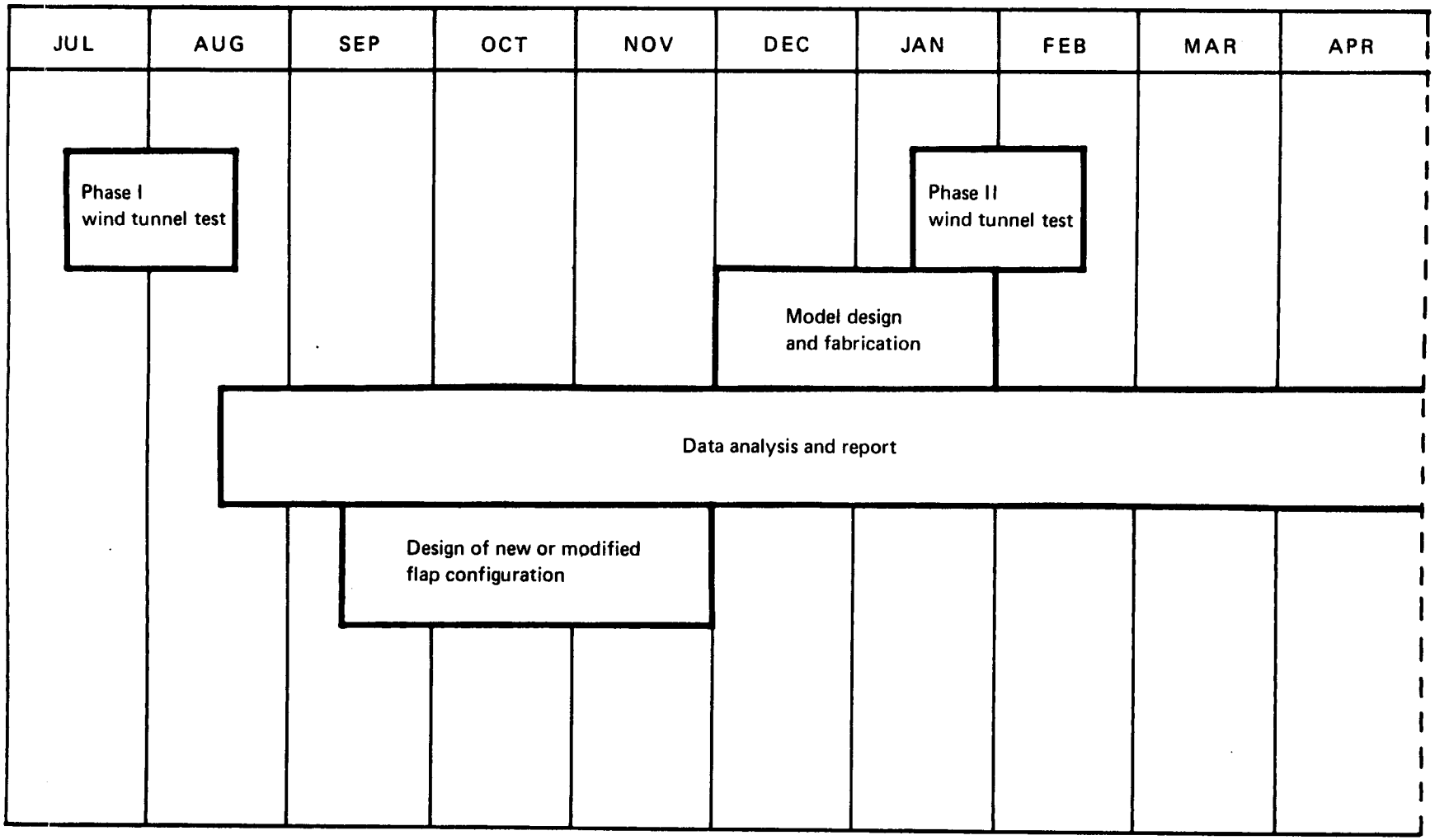

FIGURE 9-2.—AUGMENTOR WING NOISE PROGRAM—TWO DIMENSIONAL WIND TUNNEL TEST SCHEDULE

Configuration	c_f/c	h_s/c	δ_f	Type of test and objective
Scaled down baseline augmentor flap with sealed L.E. flap and blowing BLC 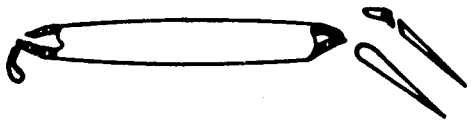	.27	.0054	30° 50° 70°	1. Vary augmentor flap geometry to obtain near optimum performance 2. With this geometry, determine performance with and without L.E. blowing 3. Evaluate effects of forward speed at $\delta_f = 30°$ and 50°
Above augmentor flap with DHC/NASA L.E. slot			30°	Evaluate effects of L.E. geometry. If the effects on quantities other than $C_{L_{max}}$ are significant, test also at $\delta_f = 50°$ and 70°
Baseline augmentor—streamwise section of NASA Ames swept wing model	.35	.0034	30° 40° 50° 60° 70°	Fixed flap geometry, rotate about a single pivot for varying δ_f.

FIGURE 9-3.– PHASE I–2-D WIND TUNNEL TEST PLAN

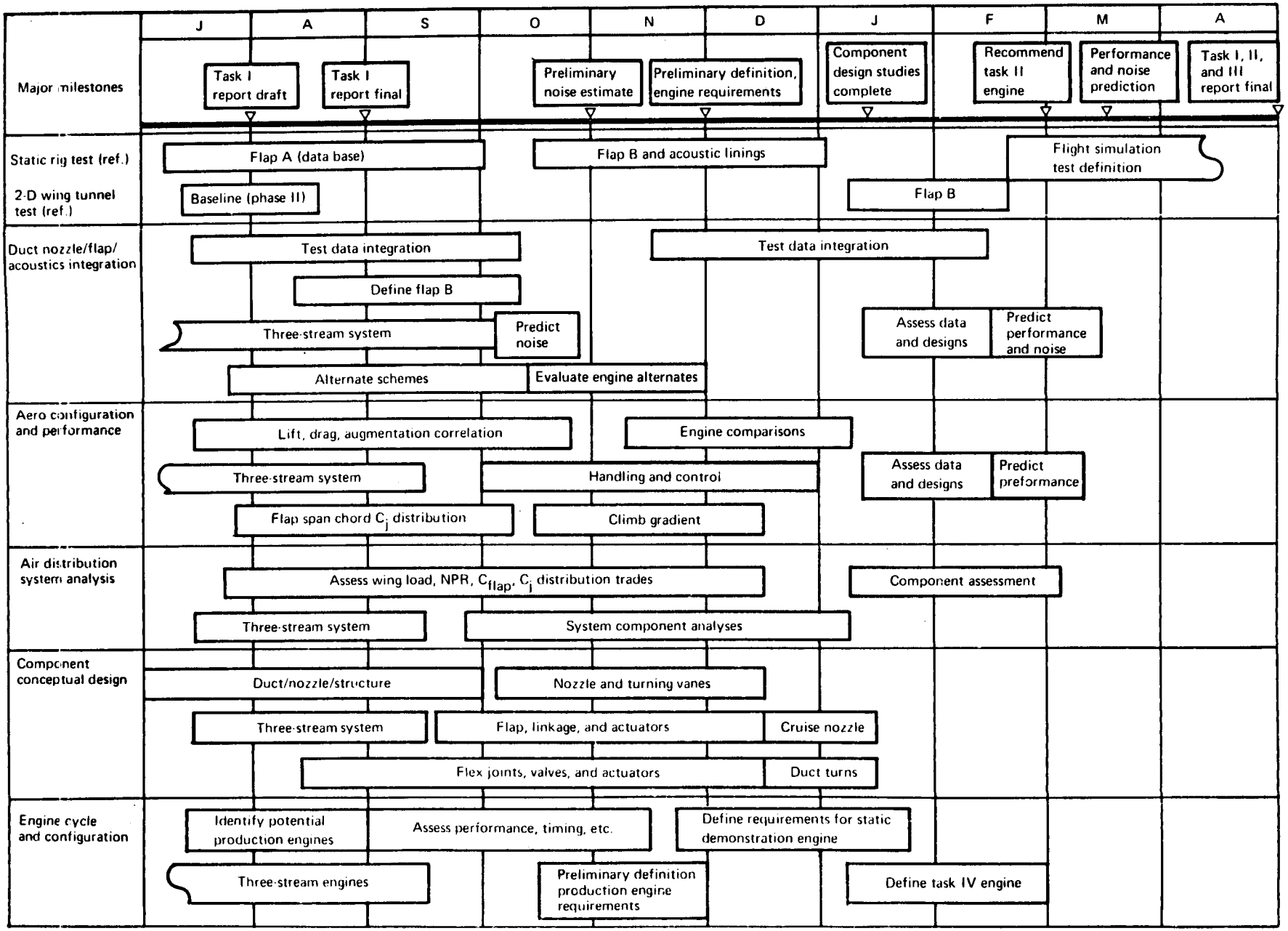

FIGURE 9-4.—SYSTEM DESIGN AND EVALUATION

REFERENCES

5-1 *Operational Requirements and Guidelines for V/STOL Systems,* Eastern Airlines Report, August 12, 1969.

5-2 *A Design Study of a Metropolitan Air Transit System,* Stanford University, NASA Contract NSR 05-020-51, August 1969.

5-3 *Technical Feasibility of Floating Interim Manhattan STOL Port,* American Airlines Report,FAA-RD-70-67, September 1970.

5-4 D. G. Brown and T. K. Sylinkien, *VTOL Transport Aircraft Factors Influencing an Integrating of Airframe, Power Plant and Systems,* Royal Aeronautical Society (Two-Day Convention, Short-Range Transport, May 14 and 15, 1969).

5-5 *Preliminary Performance Estimate for the STF 369 Turbofan Engine,* P&W Brochure TDM2246, August 17, 1970.

5-6 *Preliminary Performance Estimates for the STF 395 Engine,* P&W Brochure, August 8, 1970.

5-7 *Preliminary Proposal, TS1825, RB419-01 Propulsion/Blowing Turbofan Engine,* Rolls-Royce, Ltd., September 1970.

5-8 *Parametric Studies for Multi-Function Propulsion/Blowing Turbofan Engines,* Rolls-Royce Ltd. Brochure PS 261, April 1971.

5-9 *Jet Flap/Augmentor Wing Studies,* P&W Brochure, August 18, 1970.

5-10 S. C. Rayl and A. T. Yamagiwa, *User's Guide for the General Engine Performance Program (TEM 191), Volume 1,* Boeing Document D6-29697, May 8, 1969.

5-11 *Jet Noise Prediction,* SAE AIR 876, July 10, 1965.

5-12 *Standard Values of Atmospheric Absorption as a Function of Temperature and Humidity for Use in Evaluating Aircraft Flyover Noise,* SAE ARP 866, August 31, 1964

5-13 *Definitions and Procedures for Computing the Perceived Noise Level of Aircraft Noise,* SAE ARP 865, November 15, 1964.

5-14 D. G. Dunn, *Calculation of Perceived Noise Levels from Sound Spectra,* Boeing Document D6A10917-1, August 28, 1967.

5-15 D. G. Dunn, *Airport and Community Noise Prediction for Aircraft Using Turbojet or Turbofan Engine(s) with or without Installed Noise Suppressor(s),* Boeing Document D6A11478-1, Revised June 5, 1969.

5-16 D. D. Schrank, *Prediction Procedures for Estimating Noise Levels of High Bypass Ratio Turbofan Engines,* Boeing Document D6-23107TN, 1967.

6-1 W. D. Coles, *Jet-Engine Exhaust Noise From Slot Nozzles,* NASA TN D-60, September 1959.

6-2 J. M. Tyler and T. G. Sofrin, *Rectangular Nozzles for Jet Noise Suppression,* SAE National Aeronautic Meeting, SAE Paper 57T, March 31-April 3, 1959.

6-3 *The Jet Noise of Multi-Nozzle Arrays,* Rolls-Royce Brochure A-P.9, April 1961.

6-4 R. G. Dorsch, E. A. Krejsa, and W. A. Alsen, *Blown Flap Noise Research,* NASA TM X-67850, June 1971.

6-5 C. D. Simcox, *Studies of Shock Related Noise Fields Generated by Hot and Cold Choked Jets,* Boeing Document D6-24486, 1969.

6-6 D. J. Maglieri and H. H. Hubbard, *Preliminary Measurements of the Noise Characteristics of Some Jet Augmented Flap Configurations,* NASA Memo 12-4-58L, January 1957.

6-7 W. D. Coles and E. E. Callaghan, *Full Scale Investigation of Several Jet-Engine Noise-Reduction Nozzles,* NACA R1387, 1958.

6-8 *Augmentor Wing Flap System Model Acoustic Test,* Boeing Document D3-8398, April 1971.

6-9 G. S. Schairer, J. V. O'Keefe, and P. E. Johnson, *Perspective of SST Aircraft Noise Problem,* AIAA Paper 69-1023, October 1968.

6-10 W. V. Morgan, L. C. Sutherland, and K. J. Young, *The Use of Acoustic Scale Models for Investigating Near Field Noise of Jet and Rocket Engines,* WADD TR 61-178, April 1961.

6-11 W. L. Howes, *Ground Reflection of Jet Noise,* NASA TR N-35, 1959.

6-12 J. M. Campbell, *A Method for Determining the Free Field Pressure Spectrum of a Jet Engine From Measurements Taken in the Presence of a Single Reflecting Plane,* Boeing Document D6A-11391-1, September 1968.

6-13 J. M. Campbell and A. W. Elston, *Acoustic Evaluation of Boardman Test Site,* Boeing Document D6A11545-1, August 1969.

6-14 C. C. Higgins, et al., *Exhaust Jet Wake and Thrust Characteristics of Several Nozzles for VTOL Downwash Suppression,* Boeing Document D6-18074, June 1965.

6-15 W. S. Campbell, *Thrust Augmentation for VSTOL,* ARL 67-0065, April 1967.

6-16 A. Powell, "On the Noise Emanating From A Two-Dimensional Jet Above the Critical Pressure," *The Aeronautical Quarterly*, Vol. IV, Part II, February 1953.

6-17 R. E. Franklin, "Noise Measurements on Cold Jets Using Convergent-Divergent Nozzles," *The Aeronautical Quarterly*, Vol. VIII, Part IV, January 1957.

6-18 B. S. Stratford, "The Calculation of the Discharge Coefficient for a Choked Nozzle and the Optimum Profile for Absolute Air Flow Measurements," *Journal of the Royal Aeronautical Society*, Vol. 68, April 1964.

7-1 F. J. Davenport, *Singularity Solutions to Several Potential Flow Airfoil Problems*, Boeing Document D6-7202, 1963.

7-2 D. A. Spence, "The Lift on a Thin Airfoil with a Jet-Augmented Flap," *Aeronautical Quarterly*, Vol. IX, p. 287, 1958.

7-3 I. Wygnanski and B. G. Newman, "The Effect of Jet Entrainment on Lift and Moment for a Thin Aerofoil with Blowing," *Aeronautical Quarterly*, Vol. XV, May 1964.

7-4 D. L. Harkonen, et al., *Static Tests of a 0.7 Scale Augmentor Wing Flap for the Modified C-8A—Test Results and Analysis*, Boeing Document D6-24850, 1971.

7-5 M. D. Falorski and D. G. Koenig, *Aerodynamic Characteristics of a Large Scale Model with a Swept Wing and Augmented Jet Flap*, NASA Ames W.P. No. 271, April 1971.

7-6 G. L. Rabeneck, et al., *Steady Flow Ejector Program*, Lockheed Report ER 4708, AD 251179, December 1960.

DESIGN INTEGRATION AND NOISE STUDY FOR A LARGE STOL AUGMENTOR WING TRANSPORT

TASK I REPORT

APPENDIX

D6-60139

Distribution of this Report is provided in the interest of information exchange. Responsibility for the contents resides in the author or organization that prepared it

Prepared Under Contract NAS2-6344 by
THE BOEING COMPANY
Commercial Airplane Group
P.O. Box 3707
Seattle, Washington 98124

For
Ames Research Center
NATIONAL AERONAUTICS AND SPACE ADMINISTRATION

APPENDIX 5.4.1-I

LO-AWNP-001 A Independent cross-body duct system utilizing L.E. ducts (STF-369B)

-003 B Independent cross-body duct system Mach no. study (concentric ducts - 369B)

-004 C Independent cross-body duct system Mach no. study concentric ducts (STF-395)

-005 D Plenum system, fixed nozzle (STF-395)

-006 E Plenum system, Variable nozzle (369-B)

-007 F Plenum system, Variable nozzle (395)

-008 G Plenum system, fixed nozzle w/sub-duct on inboard flap only (STF-369B)

-009 H Isometric of structure concept

-011 I Variable nozzle plenum system with aileron ~~airframe~~ air foil L.E. ducts (STF-369B)

-012 J Plenum system with full-span sub-ducts, multiple simese ducts integrated with structure. (STF-369B)

-017 K Plenum system with sub-ducts on inboard and out-board flaps, circular ducts, independent structure. (STF-369C) (Baseline)

-019 L Diverter value and check value concept for plenum system (Baseline)

-026 M Independant duct system, circular ducts, independent structure (NPR-2.2)

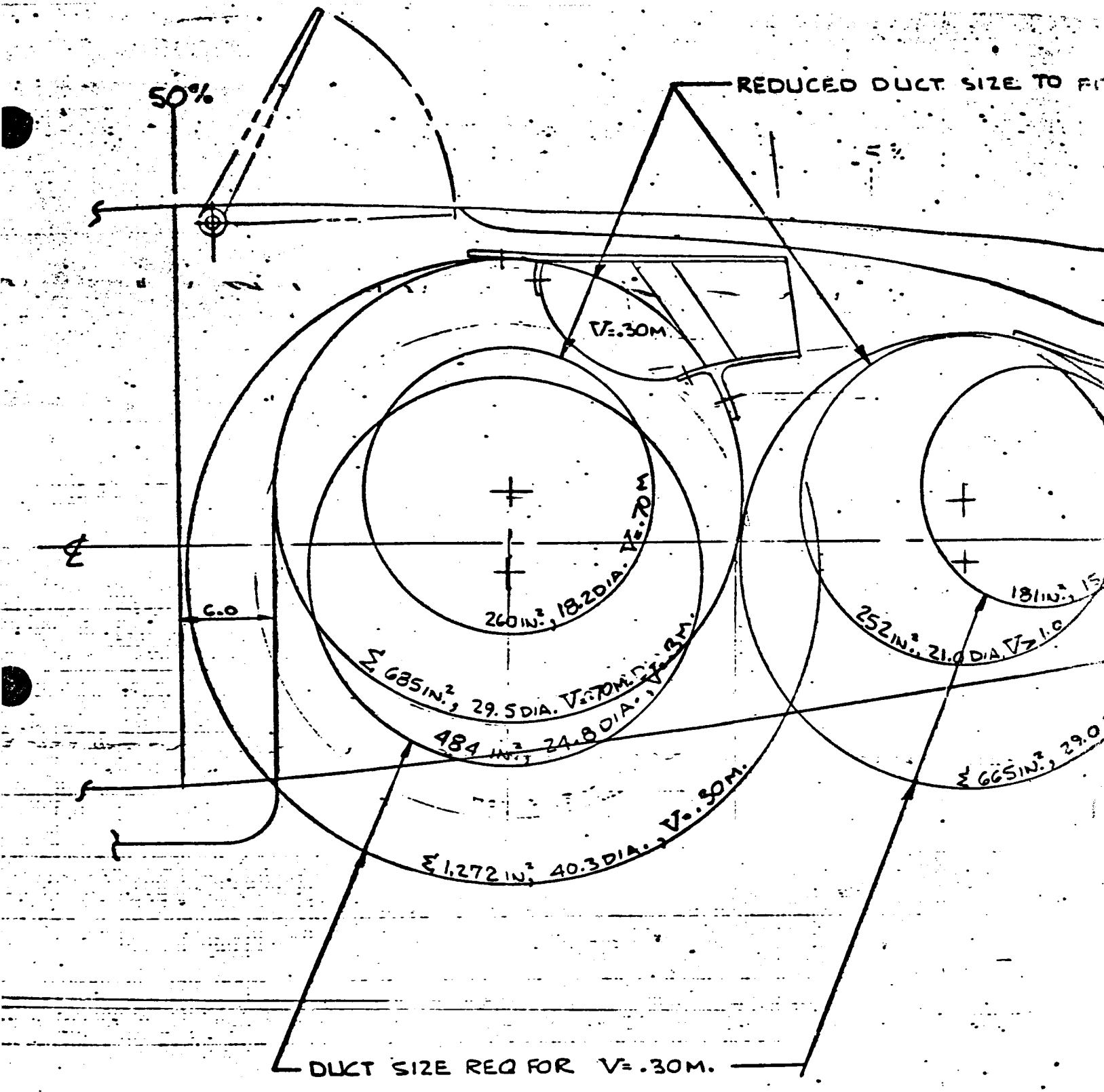

SECTION INBD ENGINE (28%)

SCALE: 1/4.

(1)

T WING

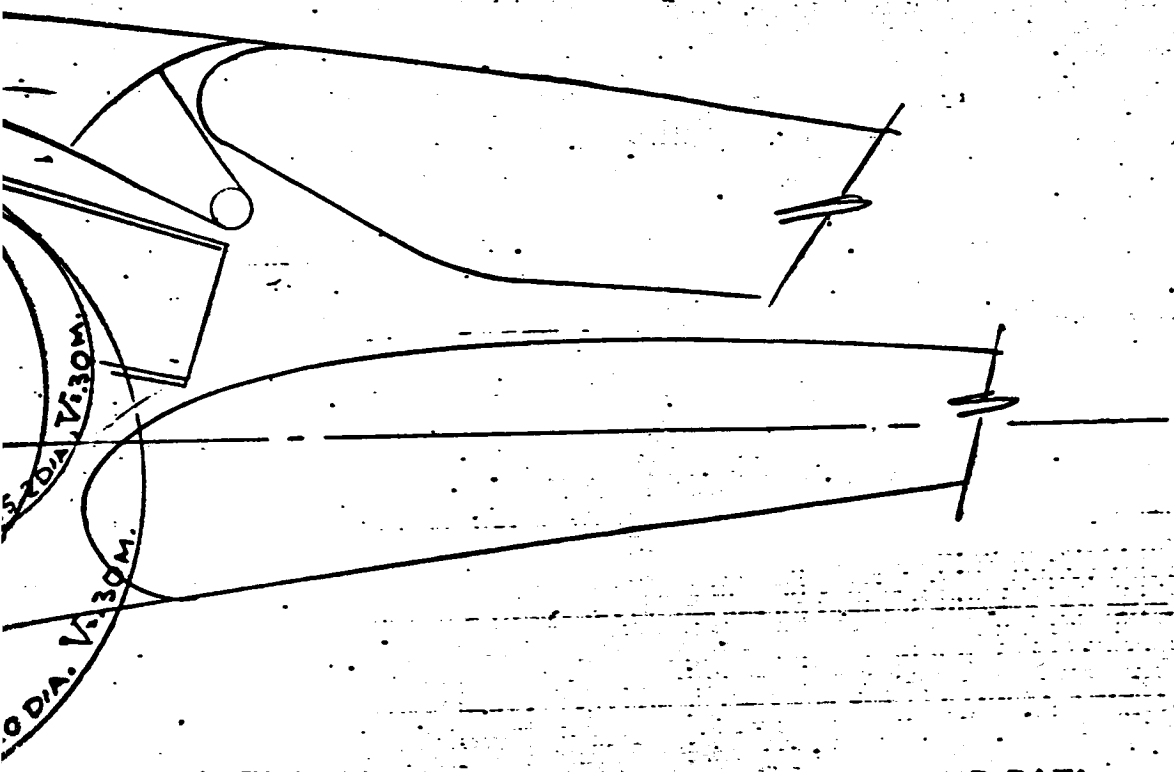

ENGINE DATA.

STF-369B (INSTL)
F_{REF} = 17,800 lbs (UNINSTL.)
W = 258 lbs/sec
P_N = 35.5 PSIA.
P_R = 2.45
T_T = 745.7°R
A^* = 561 in²/ENG.

WING AREA = 2,550 FT²
SEMI-SPAN = 773 IN.

(2)

751-101 C/STOL, STF-369B
INDEPENDENT DUCT SYS.

DON HAPKE 2-2-71

LO-AWNP-003

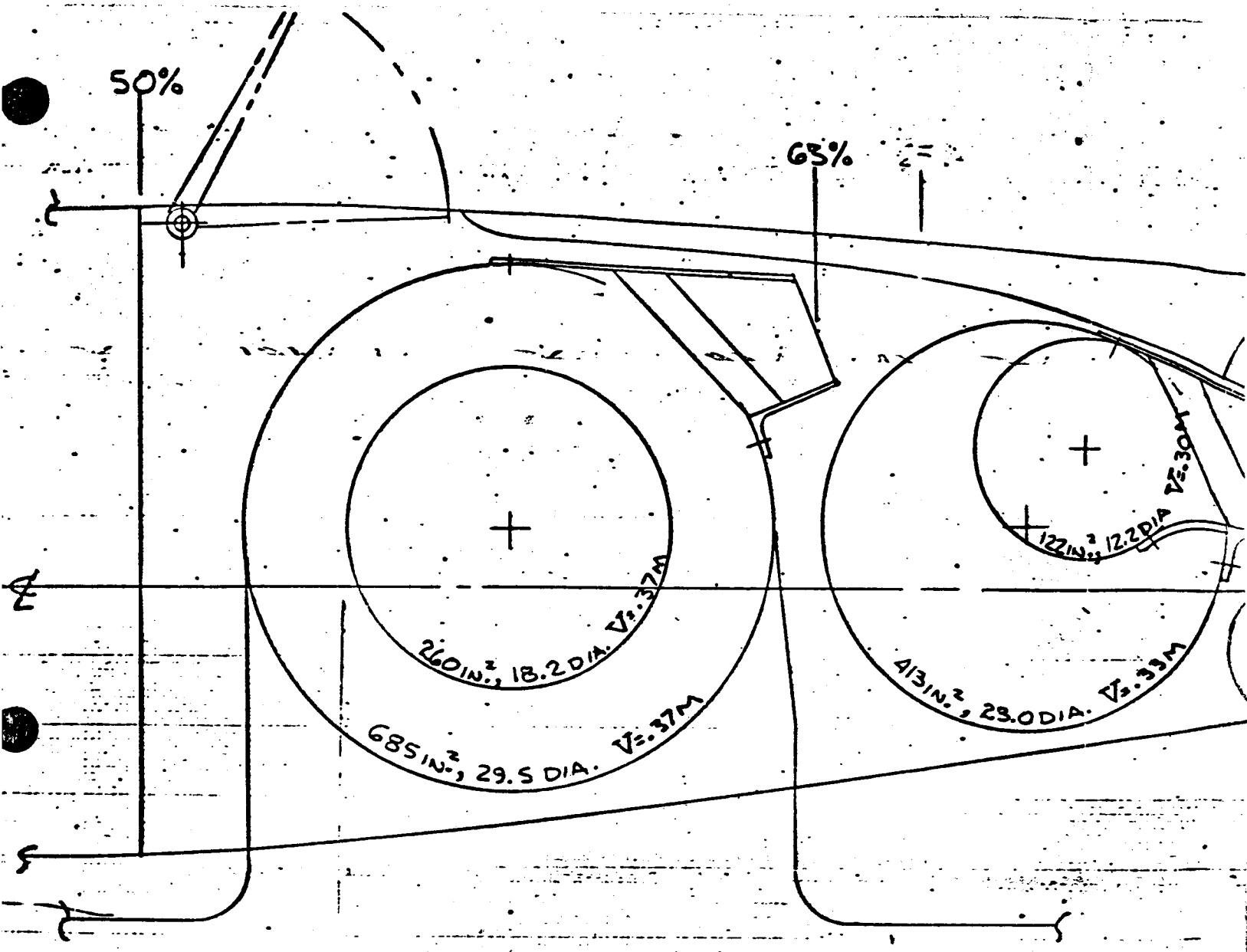

SECTION INBD ENGINE (28%)

SCALE: 1/4

A

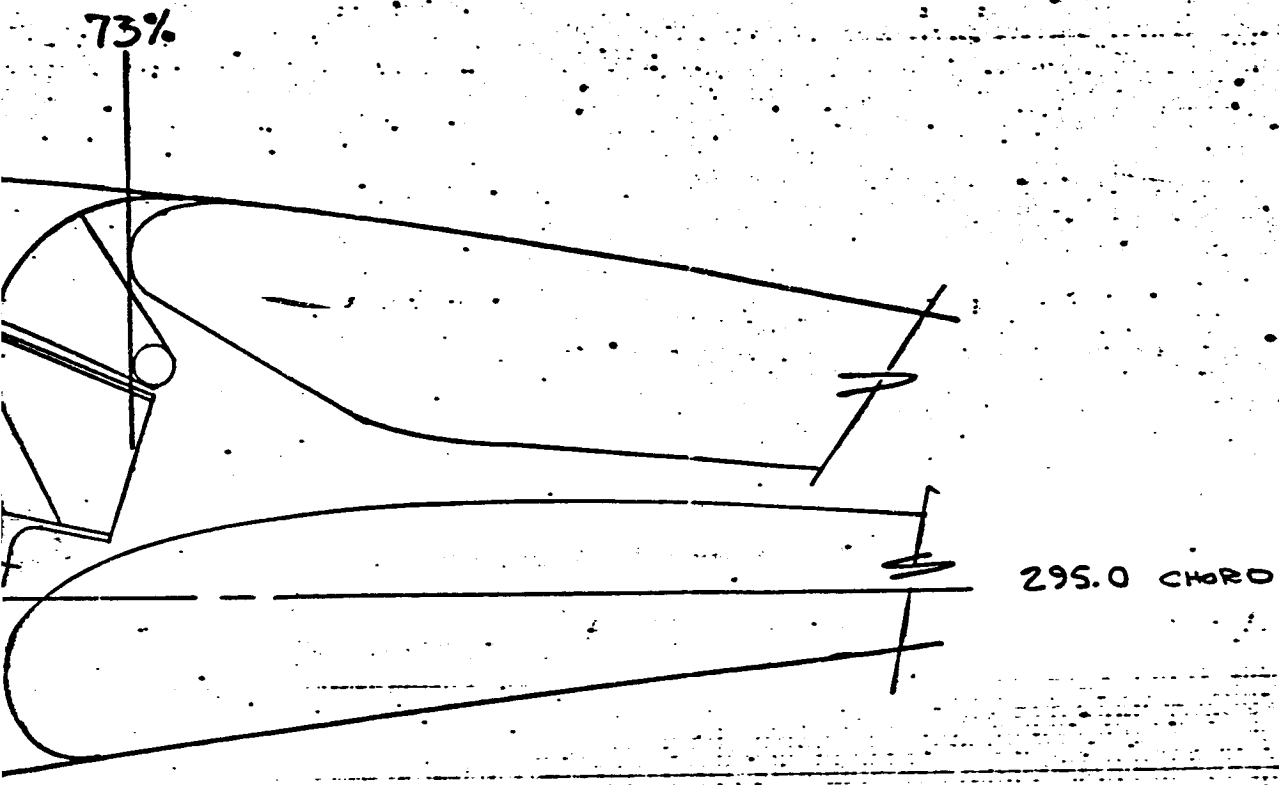

ENGINE DATA

STF-395
$F_{REF.}$ = 17,800 lbs
W = 252 lbs/sec.
P_N = 35.7 PSIA.
PR_P = 2.86
T_T = 748°R
A^* = 373 IN²/ENG.

WING AREA = 2,550 FT.²
SEMI-SPAN = 773 IN.

751-101 C/STOL , STF-395
INDEPENDENT DUCT SYS.

DON HAPKE 2-2-71

LO-AWNP-004

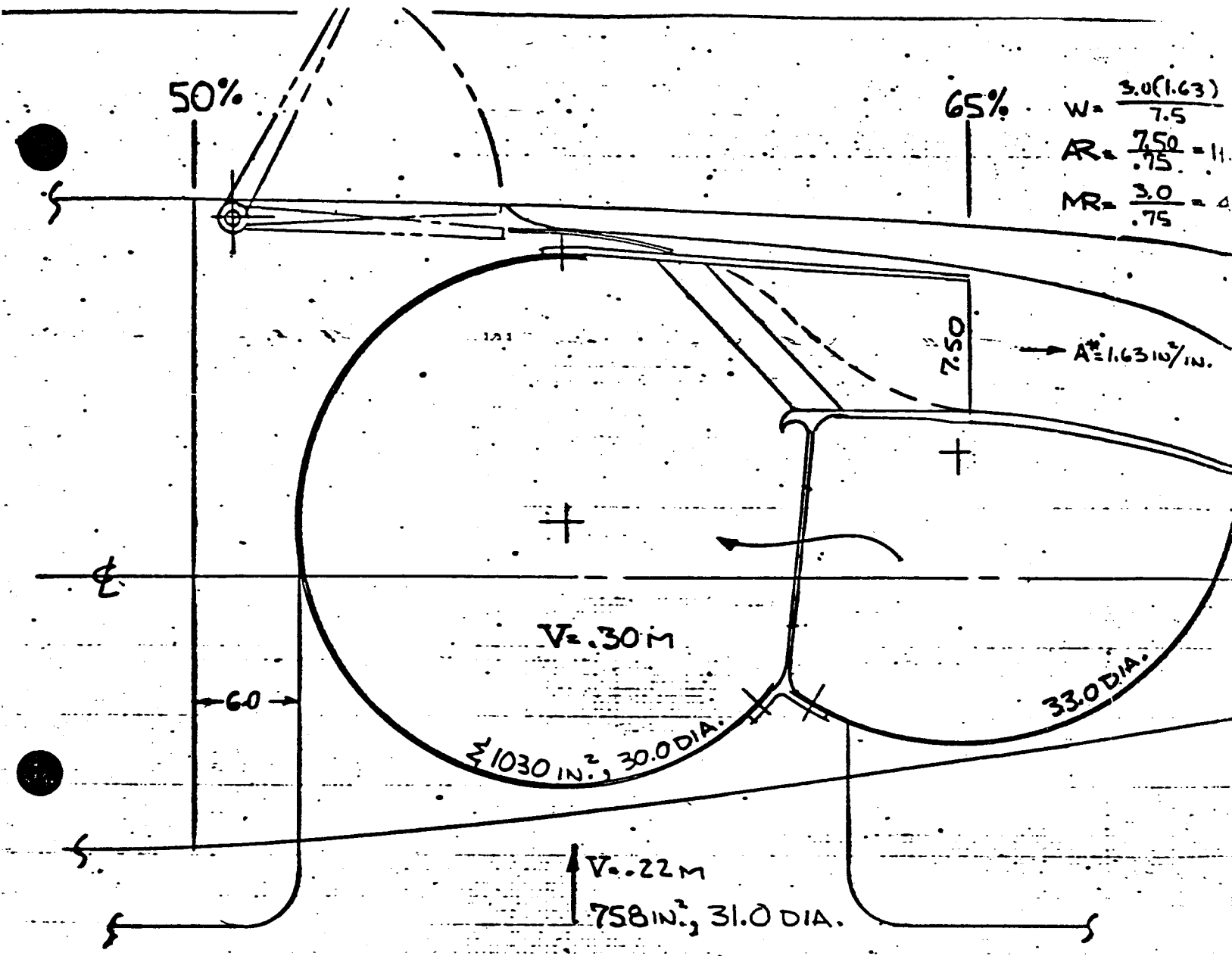

SECTION INBD ENGINE

SCALE : 1/4

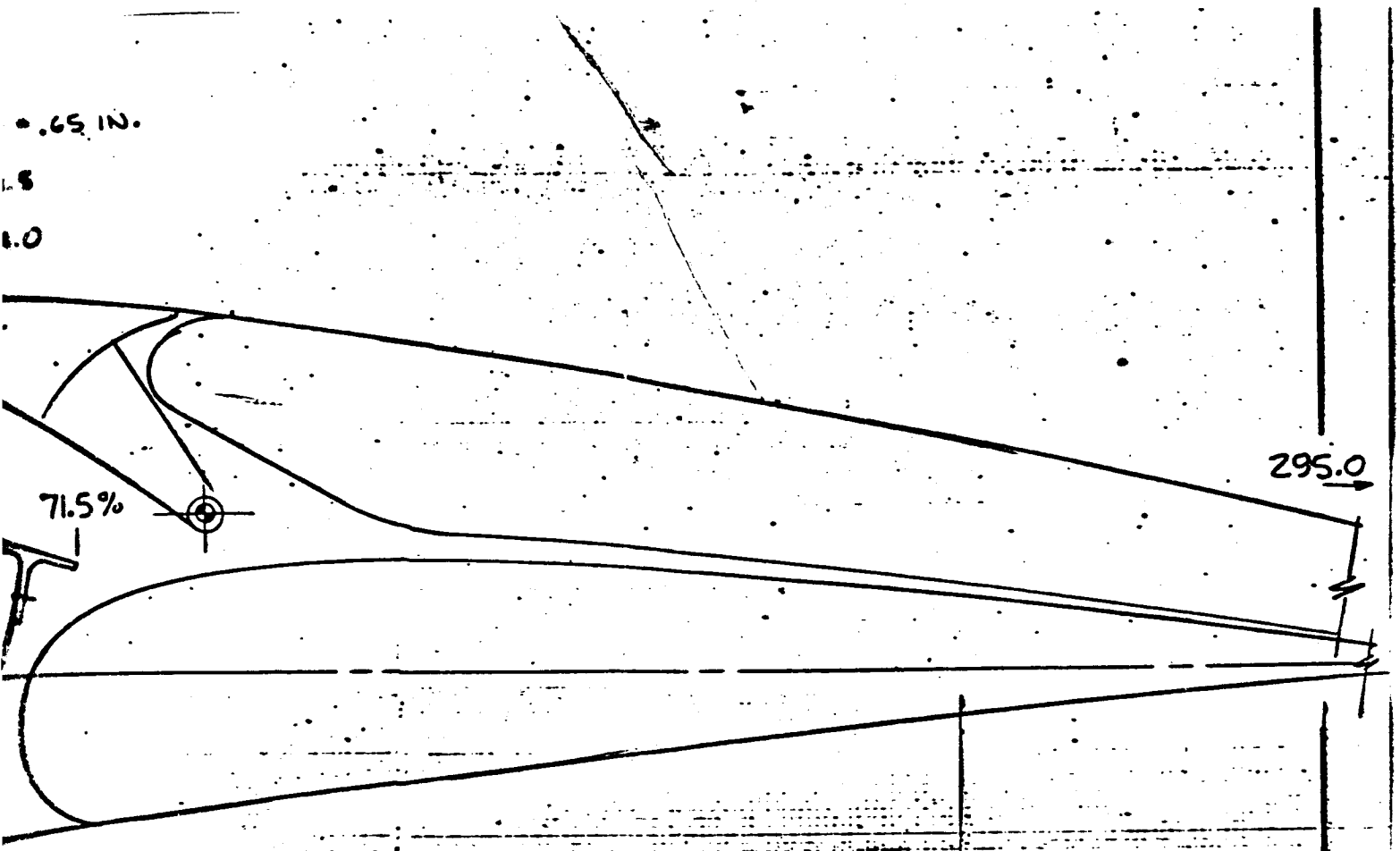

ENGINE DATA:

STF-395 (w/+15% OVER SIZE)
† F_{REF} = 20,400 lbs (UNINSTL)
† W = 378 lbs/SEC
P_N = 35.7 PSIA.
P_R = 2.86
T_T = 748° R
† A^* = 560 IN²/ENG
† = +15% OVER SIZE

WING AREA = 2,550 FT²
SEMI-SPAN = 773 IN.

751-101 C/STOL, STF-395
PLENUM, FIXED NOZZLE
LO-AWNP-005
DON HAPKE 2/4/71

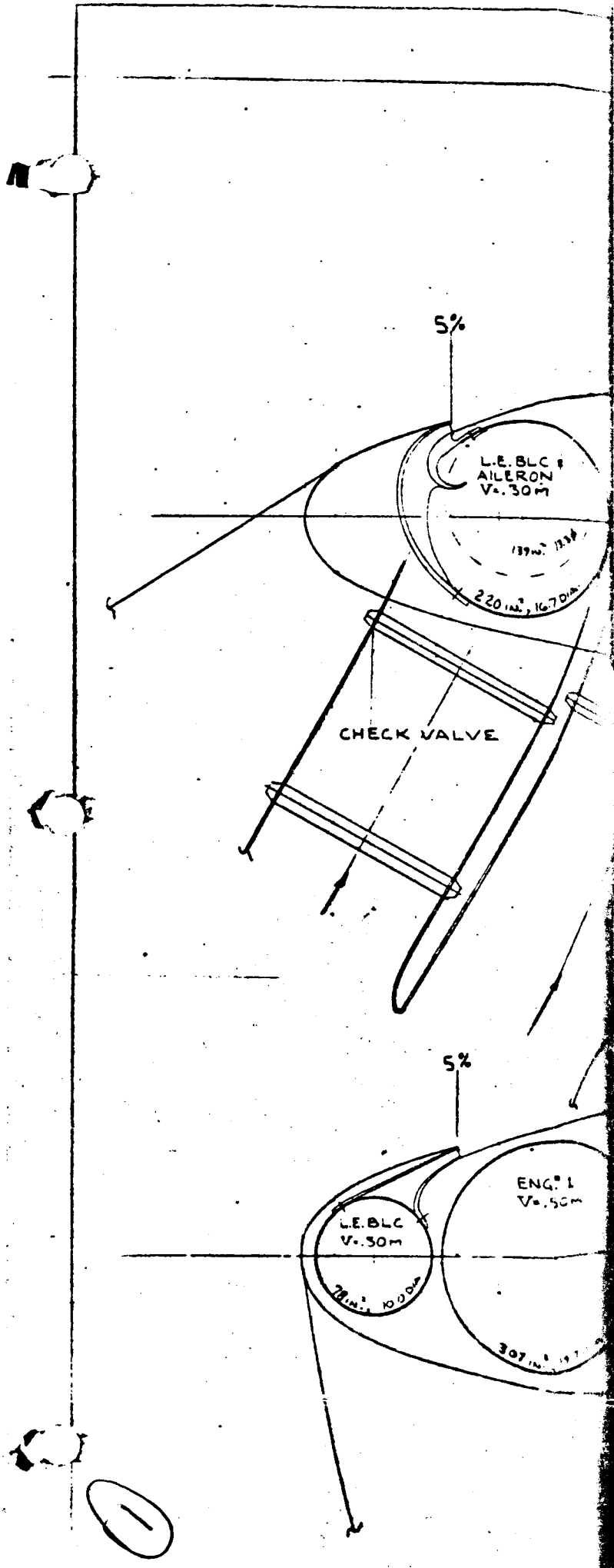
5%
L.E. BLC &
AILERON
V=.30m
139 in.² 13.3 ft
220 in.², 16.7 dia.
CHECK VALVE
5%
ENG.# 1
V=.50m
L.E. BLC
V=.30m
78 in.², 10.0 dia.
307 in.²

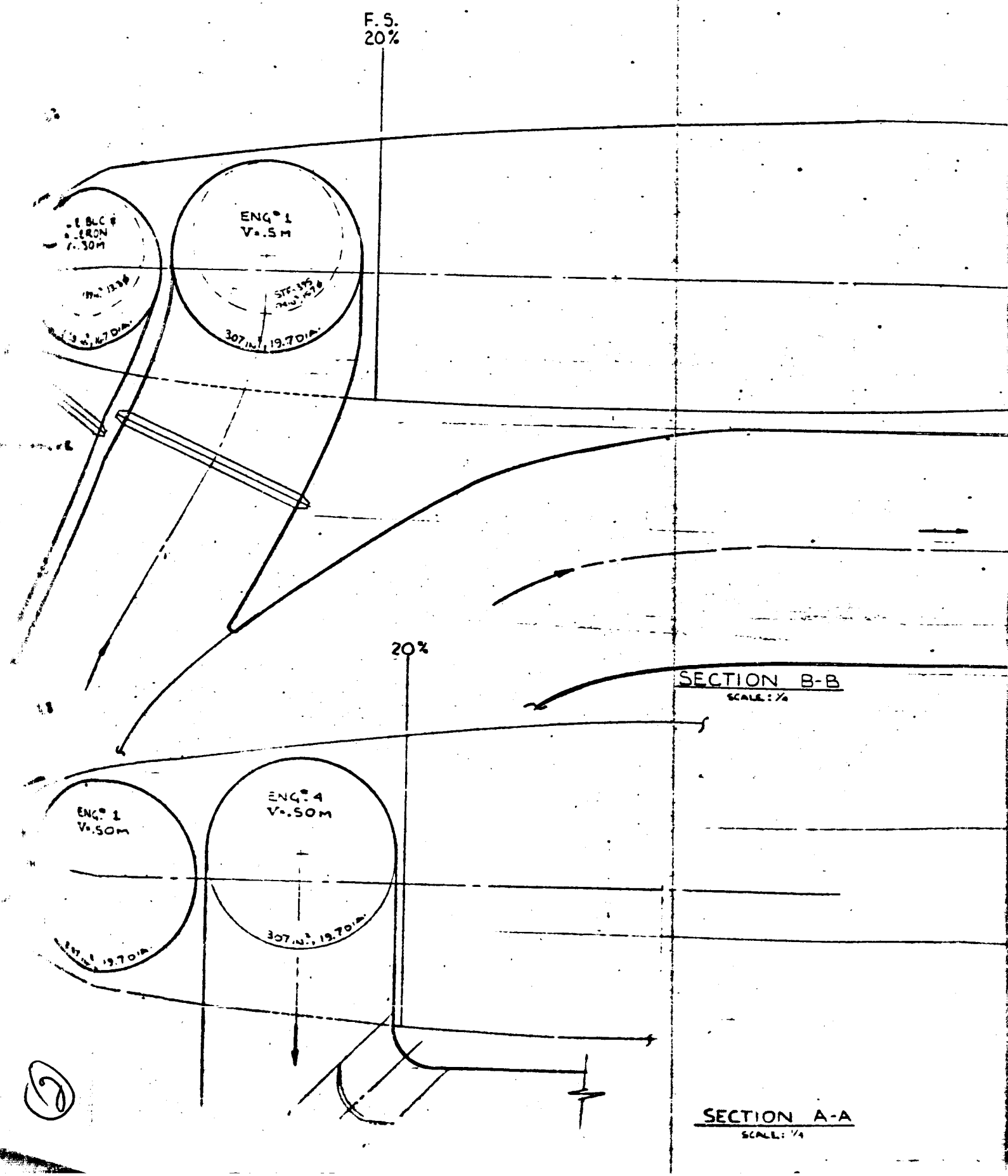
F. S.
20%
ENG# 1
V=.5 M
307 IN², 19.7 DIA.
20%
SECTION B-B
SCALE: 1/4
ENG# 1
V=.50m
ENG# 4
V=.50m
307 IN², 19.7 DIA.
SECTION A-A
SCALE: 1/4

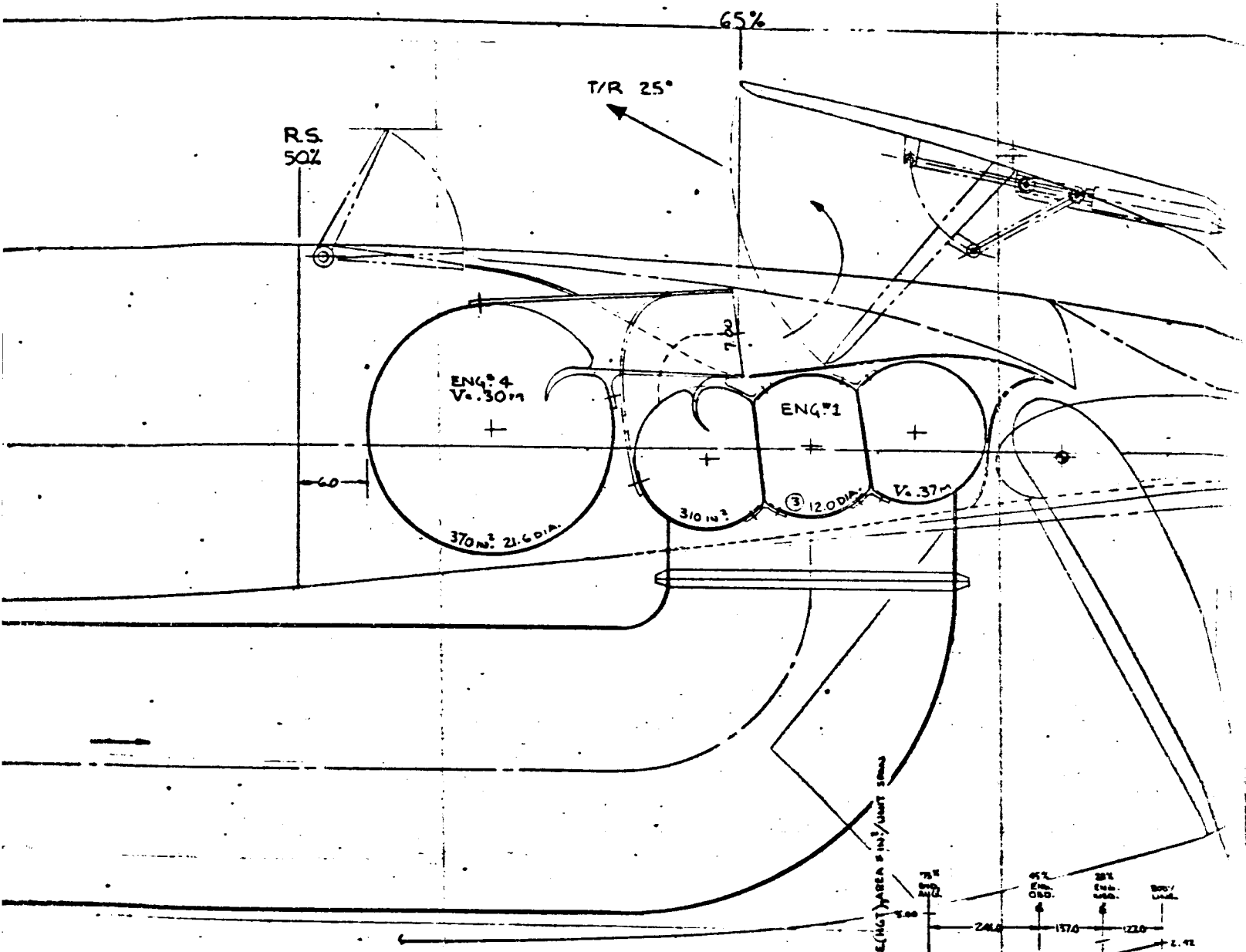

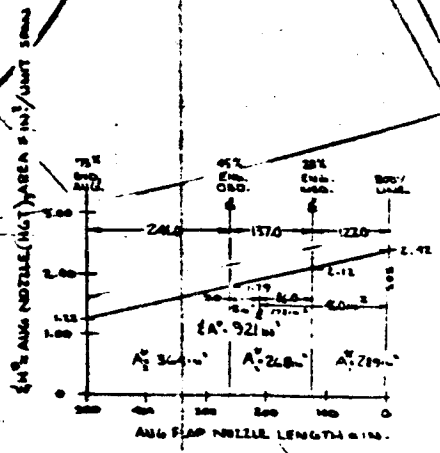

STF-369B
ENGINE DATA

F_{TO} = 17,800 lb (STATIC)
F_{MET} = 15,300 lb
P_{ER} = 2.4
W = 329.5 lb/sec
F_{ENG} = 12,650 lb
F_{ENG} = 4,300 lb
$A^{\#}_{AVG}$ = 921 in² (@ 85% Σ A")
P_{NOZZLE} = 2.04
V_{NOZZLE} = 1,240 ft/sec
$A^{\#}_{SIDE}$ = 108.6 in²/SIDE (@ 10% Σ A")
$A^{\#}_{BOTTOM}$ = 54.3 in²/SIDE (@ 5% Σ A")
ΣA" = 1,083.9 in²/SEAM SPAN

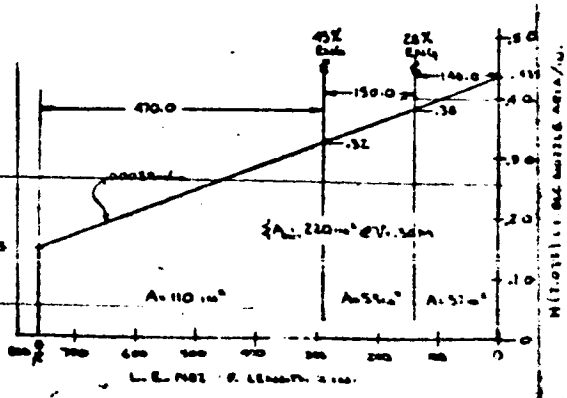

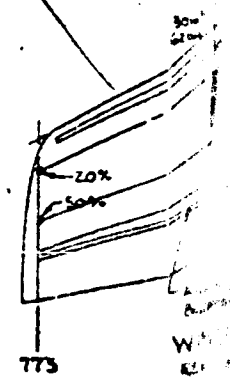

③

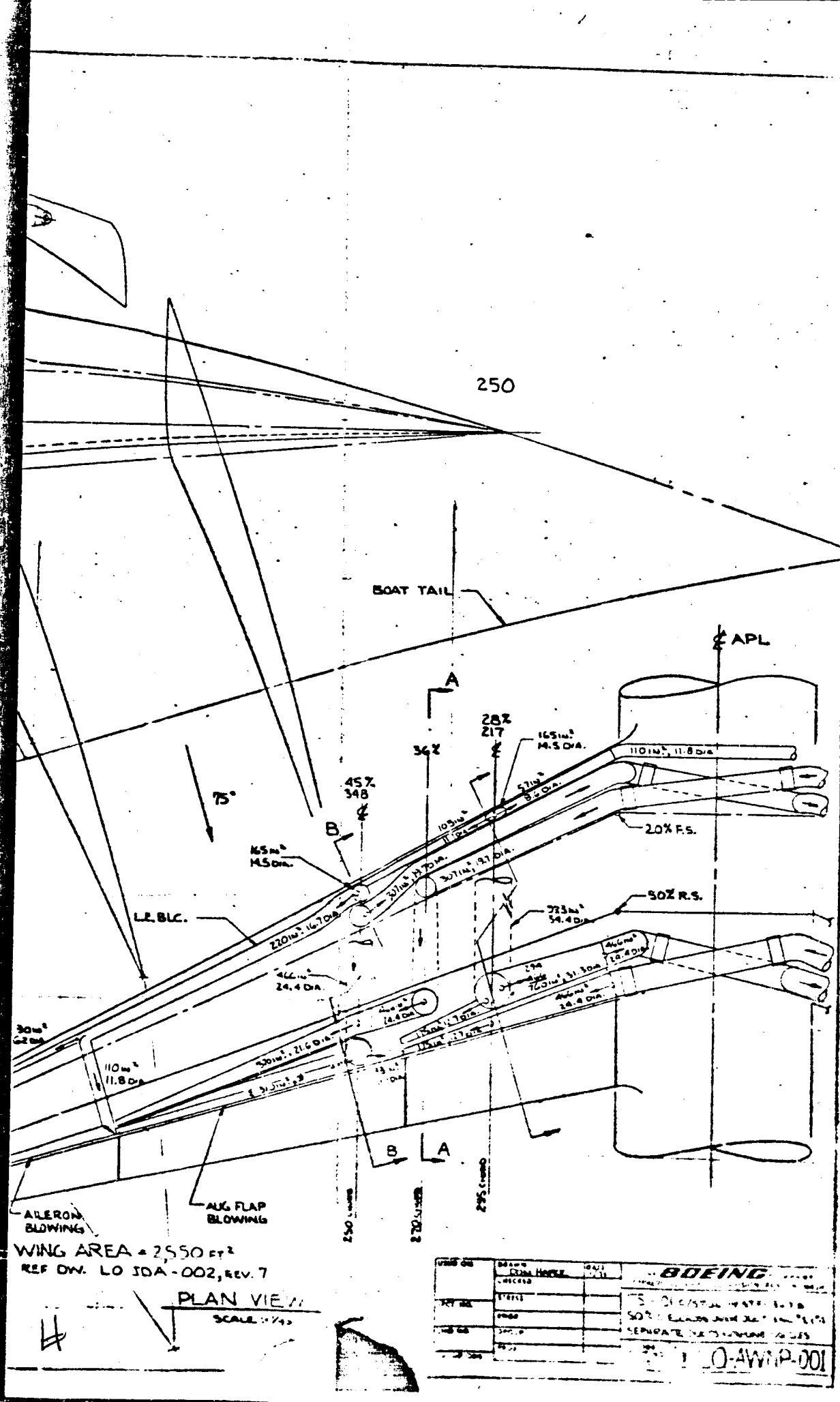
250
BOAT TAIL
℄ APL
A
28%
217
36%
45%
348
75°
B
165 in²
14.5 DIA.
L.E. BLC.
220 in²
16.7 DIA.
110 in²
11.8 DIA.
2.0% F.S.
50% R.S.
373 in²
34.4 DIA.
466 in²
24.4 DIA.
760 in²
31.3 DIA.
30 in²
6.2 DIA.
AILERON BLOWING
AUG FLAP BLOWING
2.50 CHORD
2.70 CHORD
2.95 CHORD
WING AREA = 2,550 FT²
REF DW. LO JDA-002, REV. 7
PLAN VIEW
SCALE: 1/40
BOEING
LO-AWTP-001

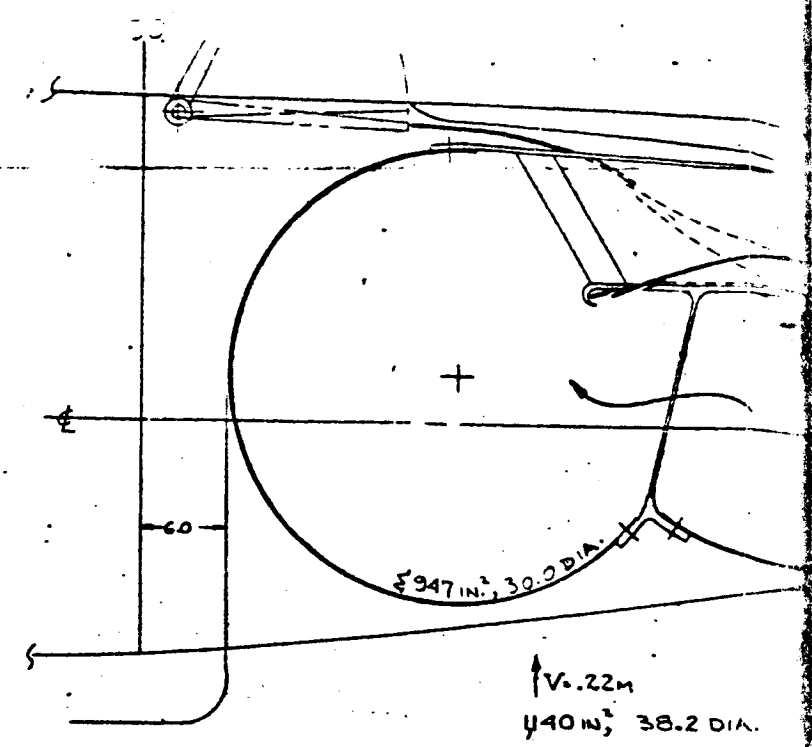

SECTION A-A
SCALE: 1/4

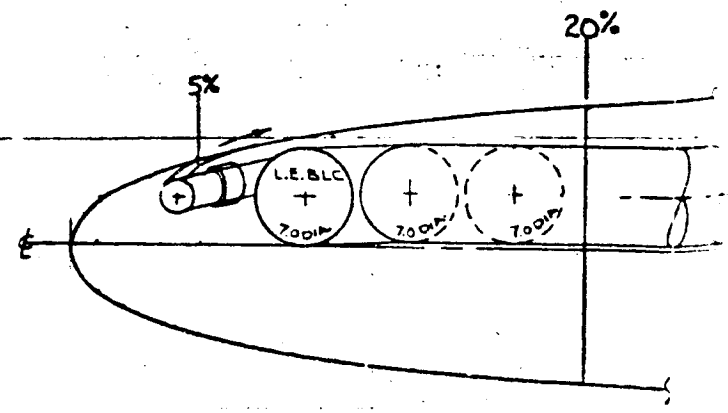

SECT

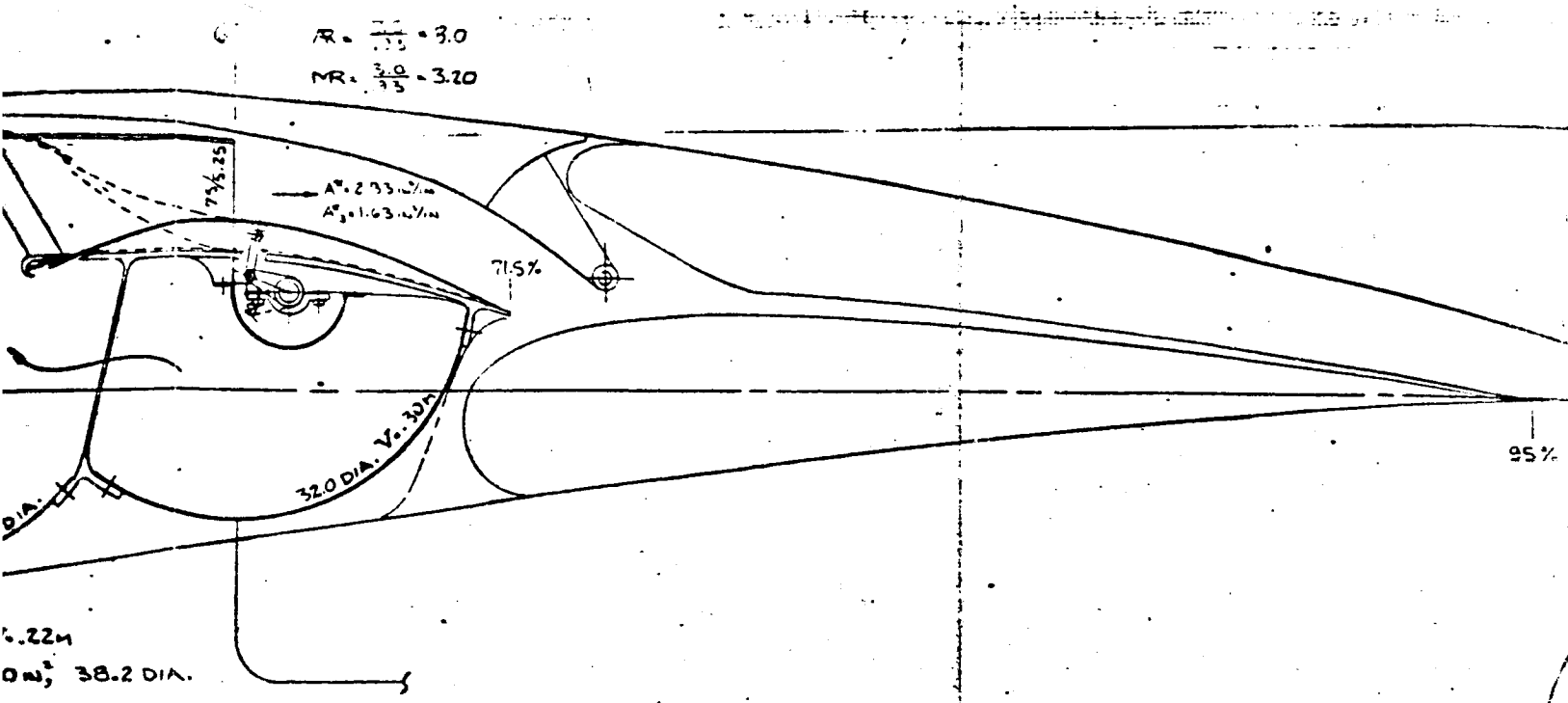

TION A-A
SCALE: 1/4

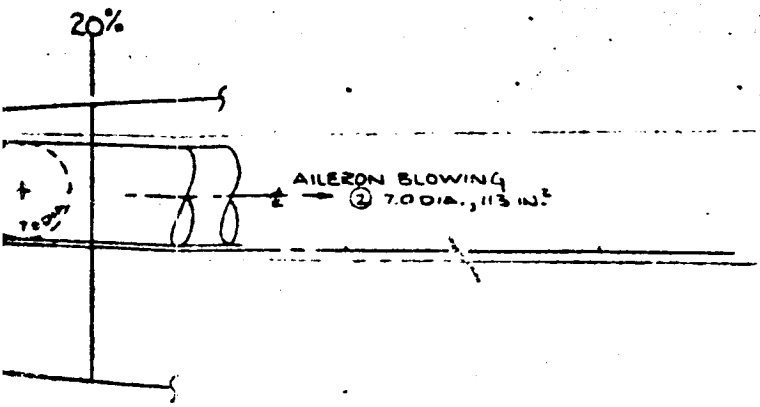

SECTION C-C
SCALE: 1/4

7

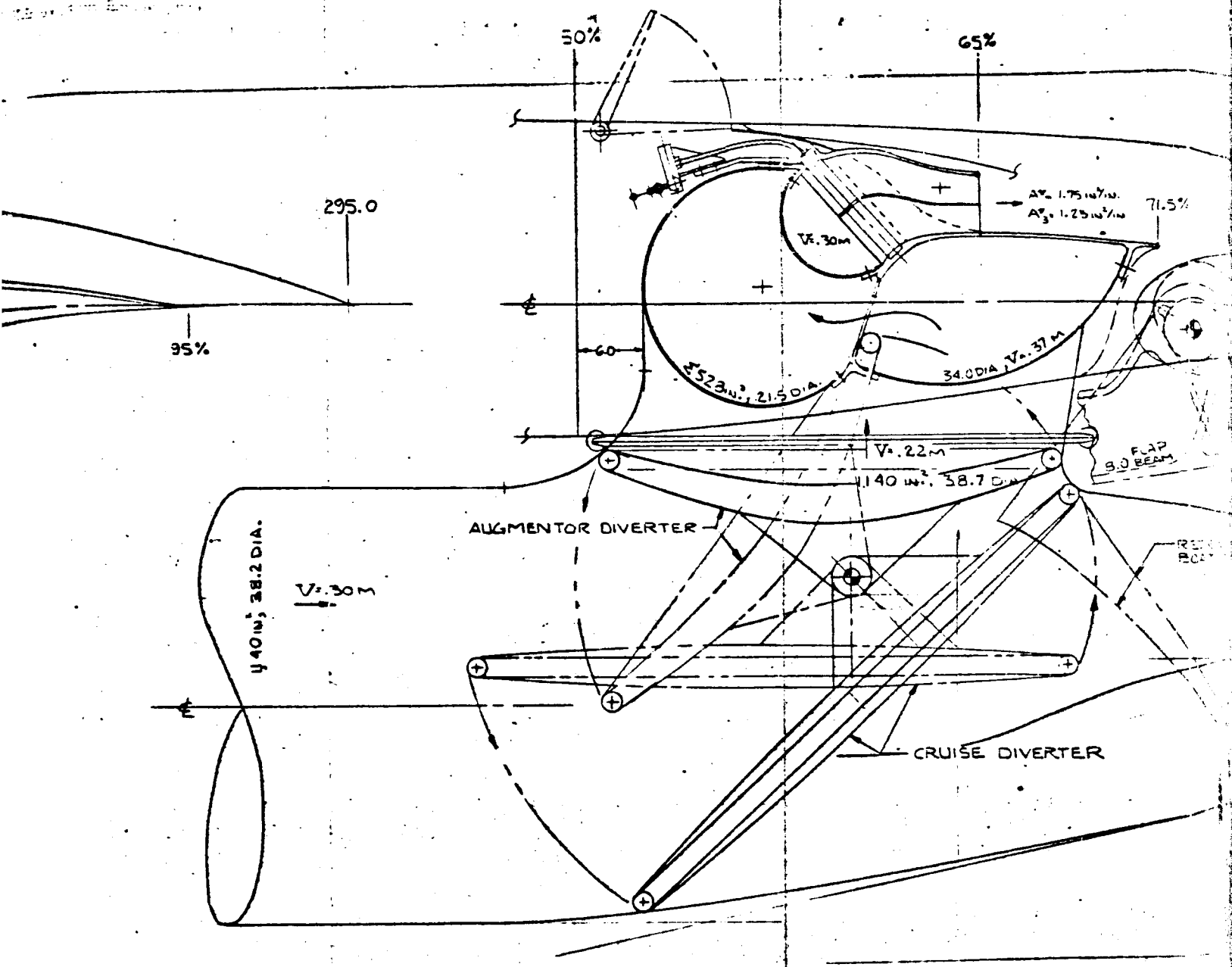

SECTION B-B

SCALE: 1/4

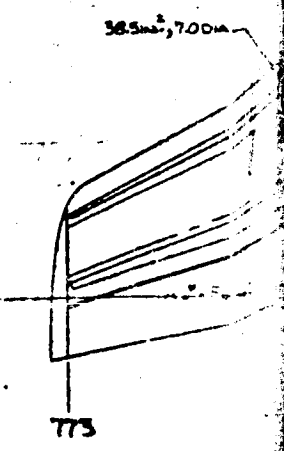

WING AREA = 2,550

SEMI-SPAN = 773 IN.

3

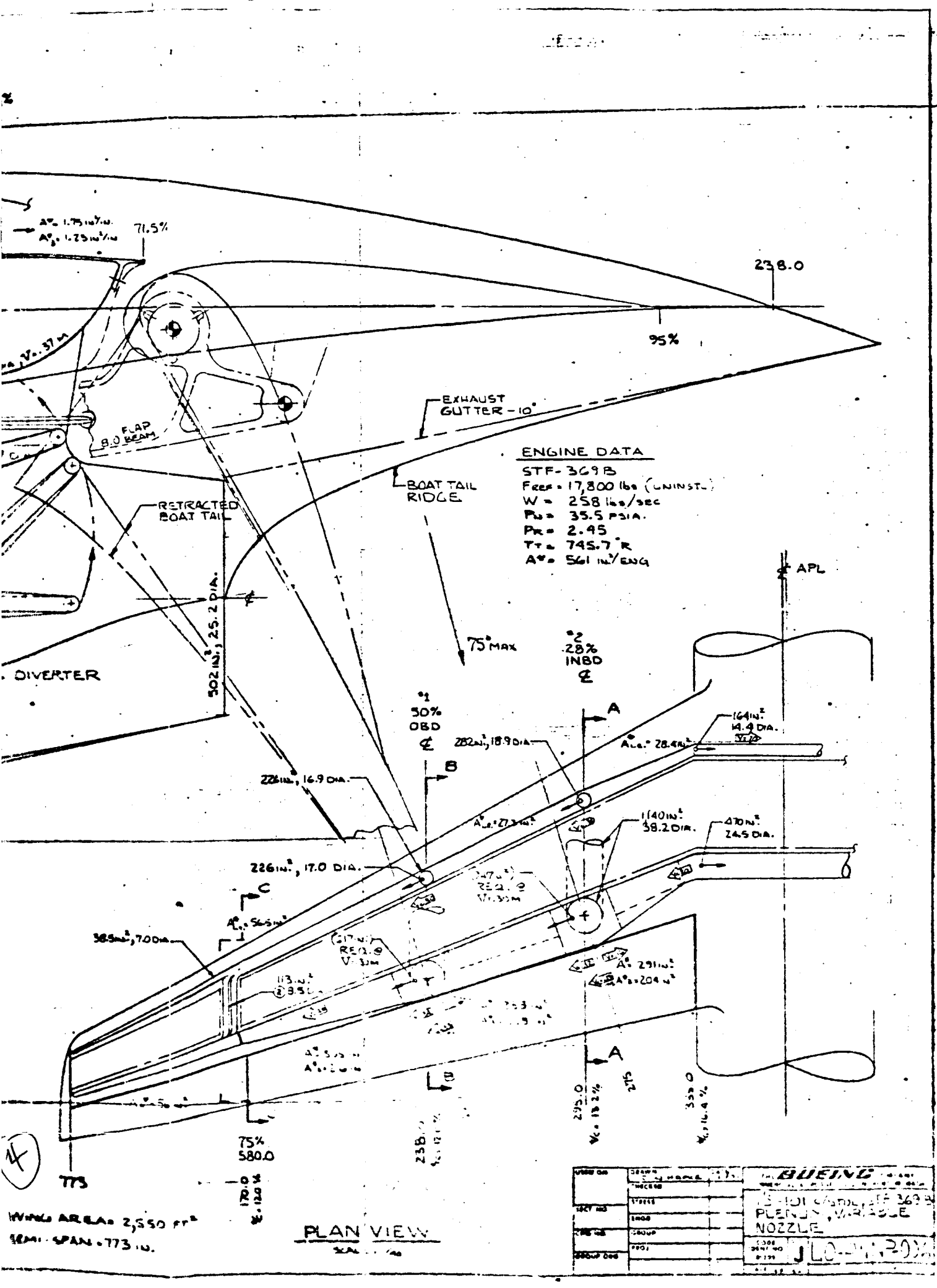
71.5%
238.0
95%
EXHAUST GUTTER - 10°
FLAP BEAM
8.0
BOAT TAIL RIDGE
RETRACTED BOAT TAIL
ENGINE DATA
STF-369B
Fnet = 17,800 lbs (UNINST.)
W = 258 lbs/sec
Pt = 35.5 PSIA.
PR = 2.45
Tt = 745.7 °R
A* = 561 IN²/ENG
℄ APL
75° MAX
28% INBD ℄
50% OBD ℄
DIVERTER
502 IN², 25.2 DIA.
A
B
C
164 IN², 14.4 DIA.
282 IN², 18.9 DIA.
226 IN², 16.9 DIA.
1140 IN², 38.2 DIA.
470 IN², 24.5 DIA.
226 IN², 17.0 DIA.
385 IN², 7.0 DIA.
75% 580.0
TTS
WING AREA = 2,550 FT²
SEMI-SPAN = 773 IN.
PLAN VIEW
BOEING

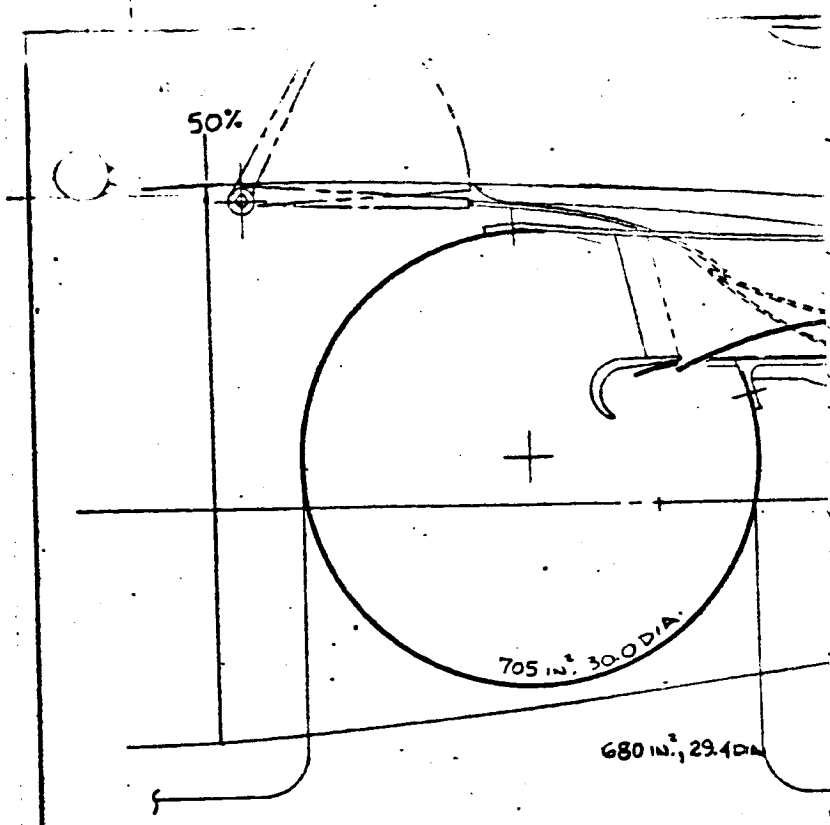

AUG. SECTION A-A
SCALE: 1/4

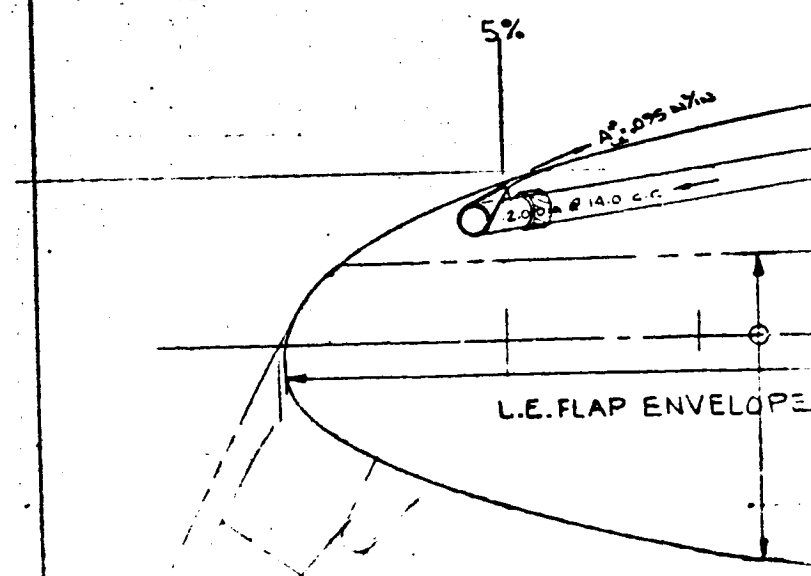

L.E. SECTION
SCALE: 1/4

(1)

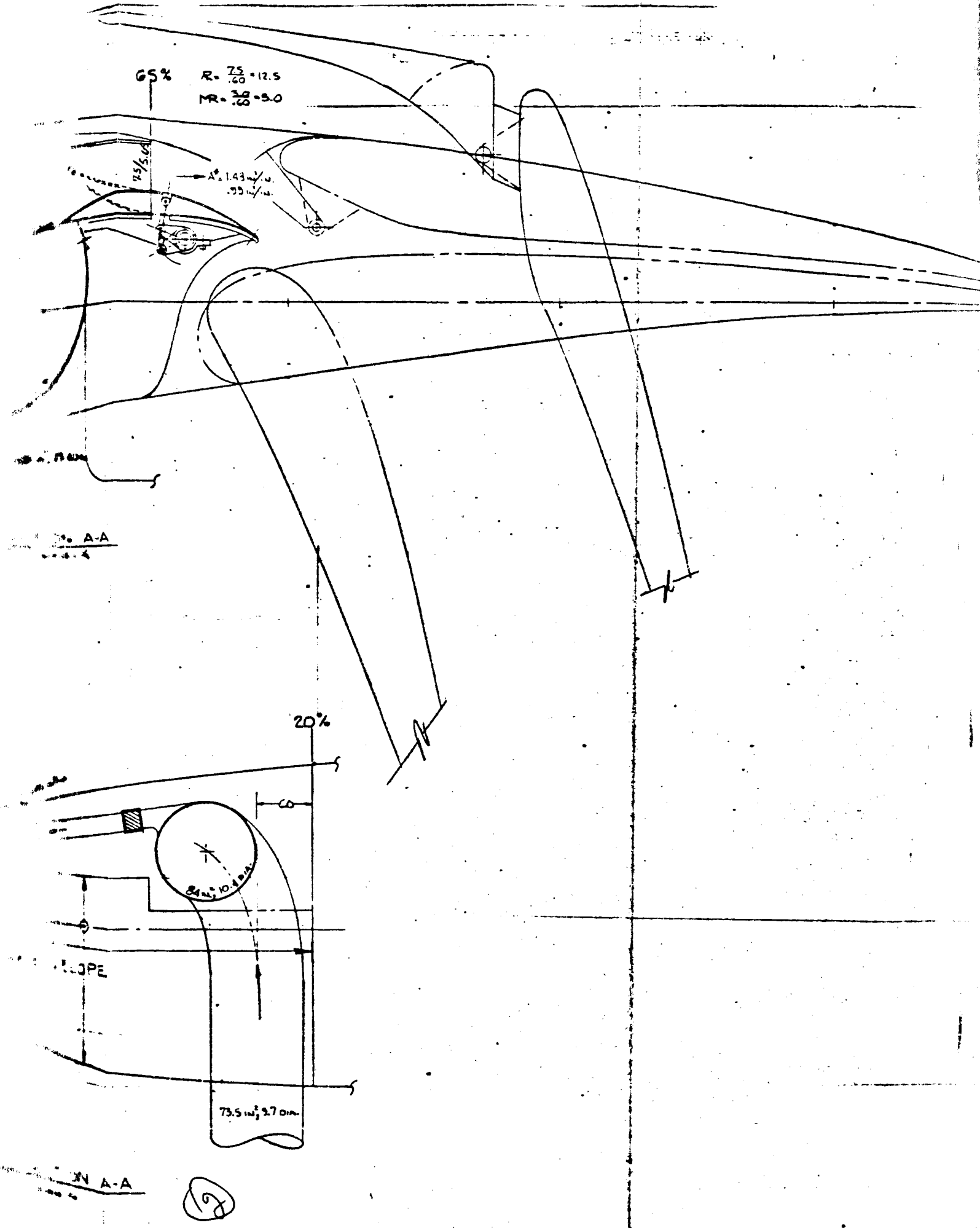
65%
R = 7.5/.60 = 12.5
MR = 3.0/.60 = 5.0
7.5/5.0
A* = 1.43 in²/in.
.99 in²/in.
A-A
20%
CO
84 in² 10.4 DIA.
JPE
73.5 in² 9.7 DIA.
A-A

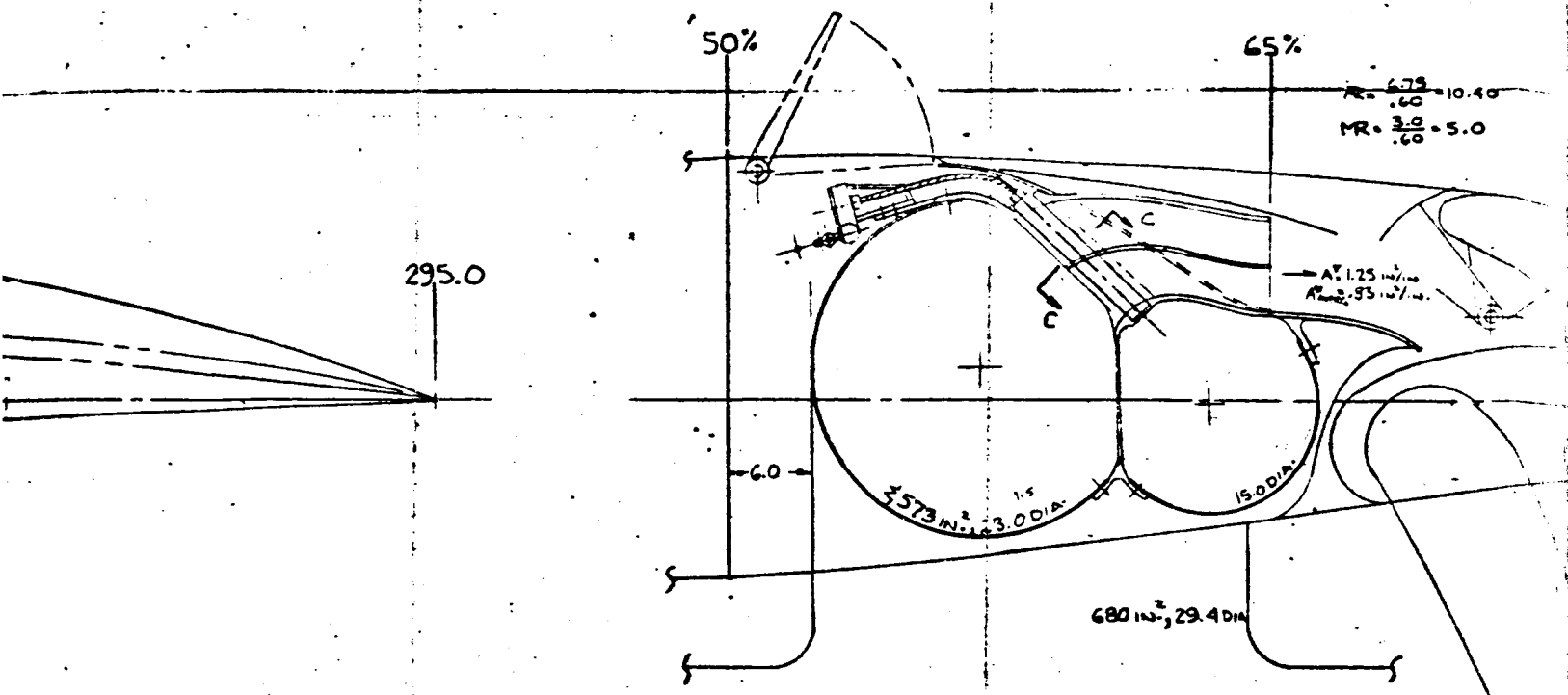

SECTION B-B

SCALE: 1/4

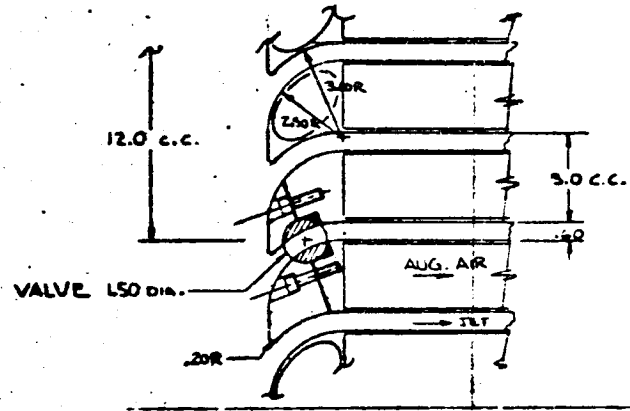

SECTION C-C

SCALE: 1/4

L.E. BLOWING:

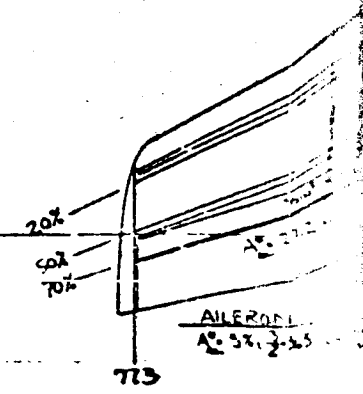

(9)

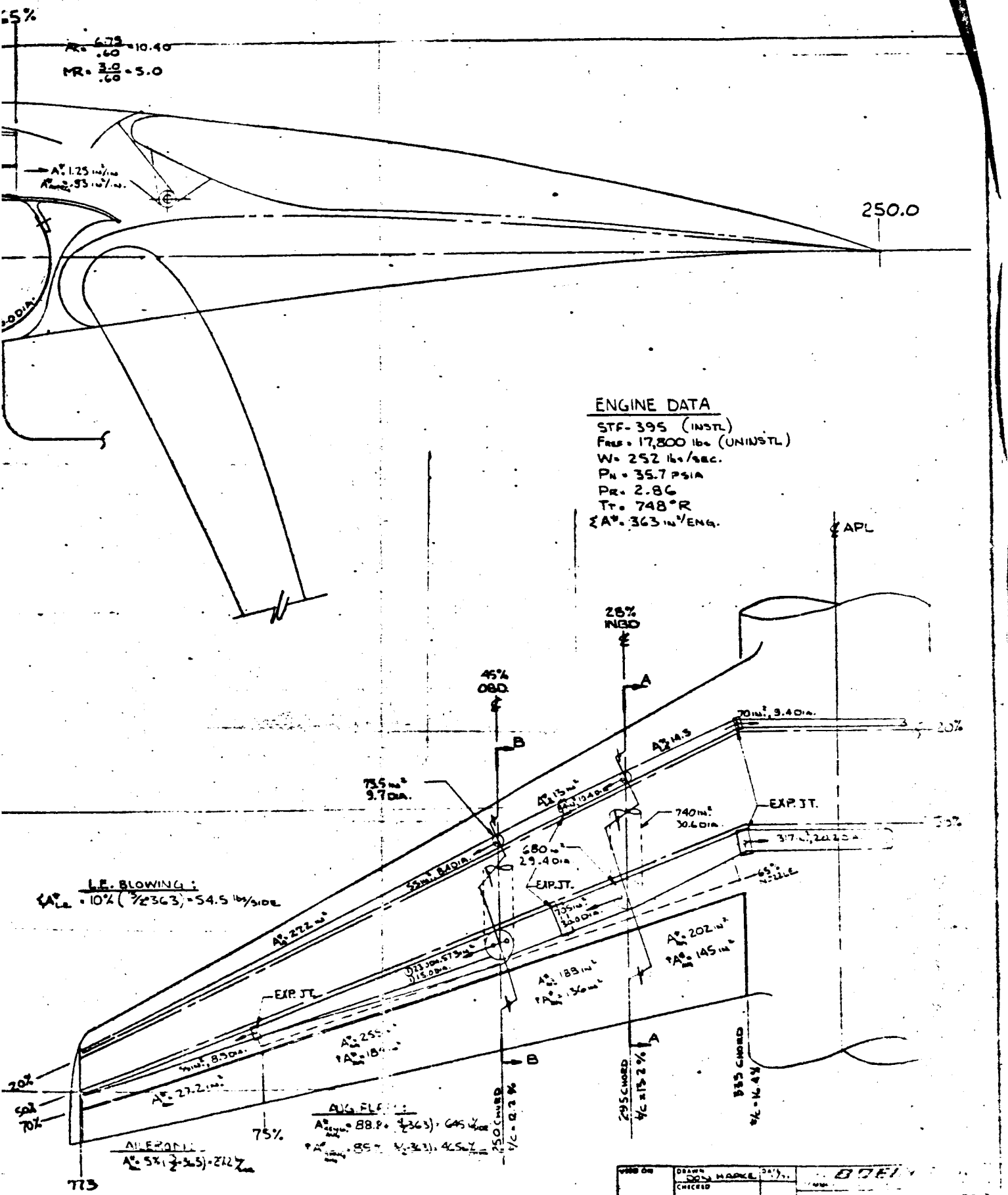
ENGINE DATA
STF-395 (INSTL)
FRES = 17,800 lbs (UNINSTL)
W = 252 lbs/sec.
PN = 35.7 PSIA
PR = 2.86
TT = 748°R
ΣA* = 363 in²/ENG.
250.0
APL
28% INBD
45% OBD
EXP. JT.
740 in²
30.6 DIA.
680 in²
29.4 DIA
73.5 in²
9.7 DIA.
70 in², 9.4 DIA.
L.E. BLOWING:
ΣA*LE = 10% (3/2 363) = 54.5 lbs/SIDE
65° NOZZLE
20%
50%
70%
75%
773
AILERON:
AUG. FLAP:
WING AREA = 2,550 FT²
* ENG. OUT CONDITIONS.
PLAN VIEW
SCALE: NO
BOEING
TS-101 C/STOL STF-395
PLENUM VARIABLE NOZZLE
LO-AWNP-007

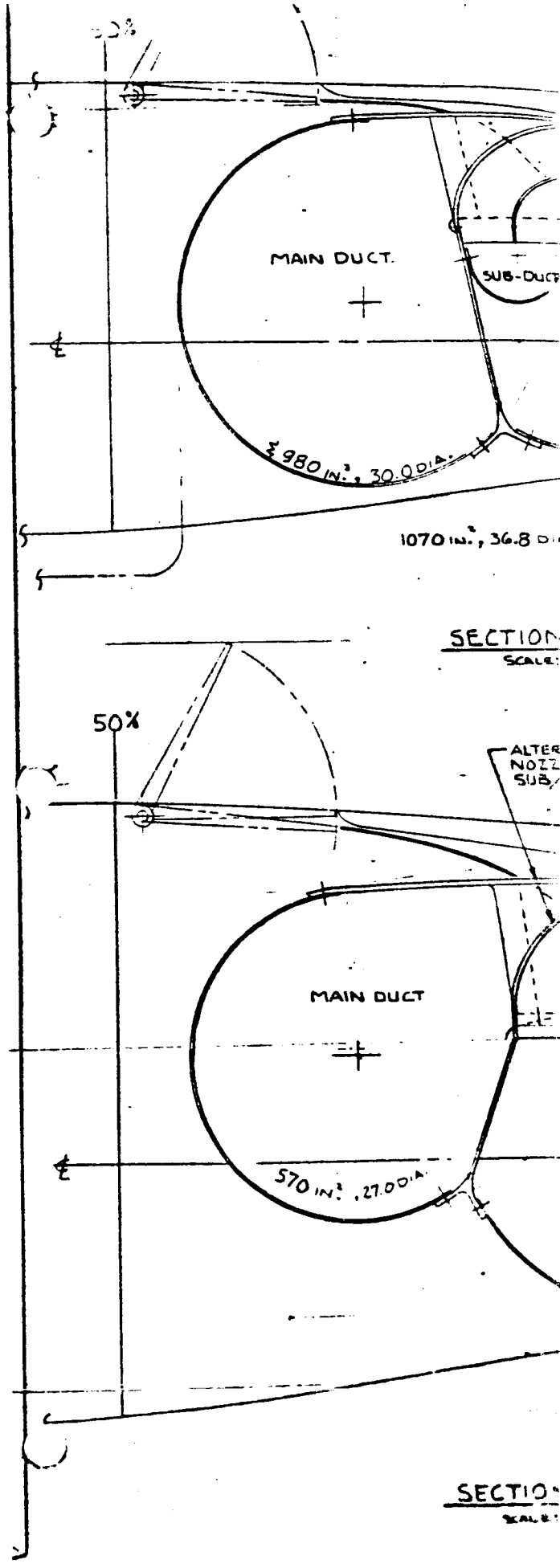
MAIN DUCT.
SUB-DUCT
980 IN.², 30.0 DIA.
1070 IN.², 36.8 DI
SECTION
SCALE:
50%
ALTER
NOZZ
SUB
MAIN DUCT
570 IN.², 27.0 DIA.
SECTIO
SCALE:

1

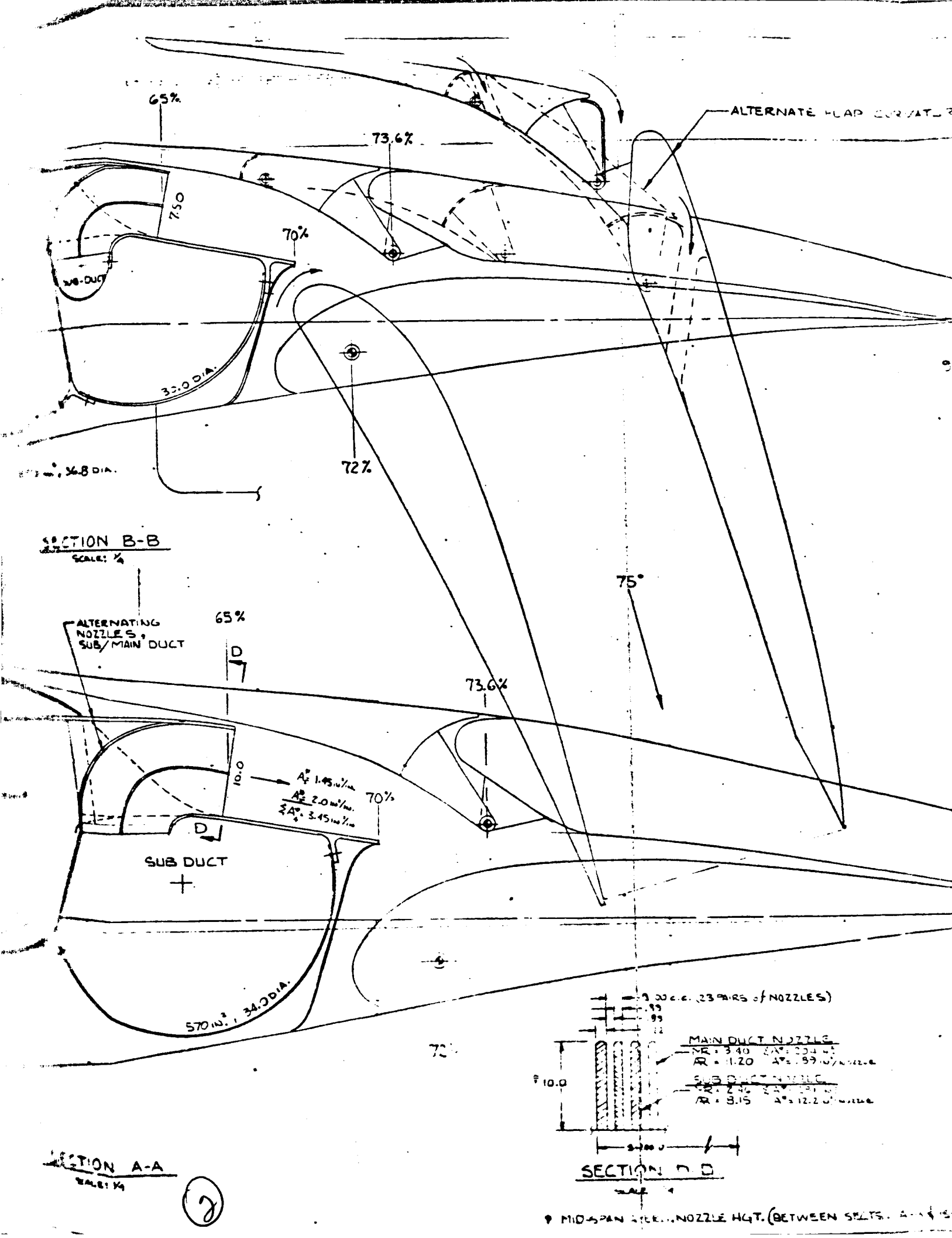
65%
73.6%
ALTERNATE FLAP CURVAT
7.50
70%
SUB-DUCT
30.0 DIA.
72%
36.8 DIA.
SECTION B-B
SCALE: 1/4
75°
ALTERNATING NOZZLES, SUB/MAIN DUCT
65%
D
73.6%
10.0
70%
SUB DUCT
570 IN.², 34.0 DIA.
MAIN DUCT NOZZLE
SUB DUCT NOZZLE
10.0
SECTION D-D
SECTION A-A
SCALE: 1/4
MIDSPAN
NOZZLE HGT. (BETWEEN SPLTS.

RNATE FLAP CURVATURES

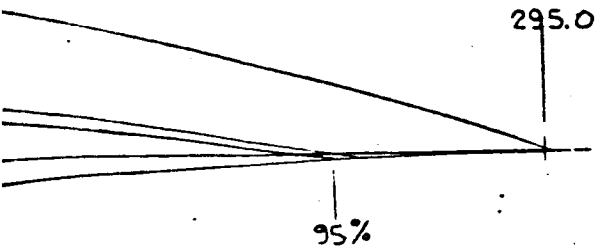

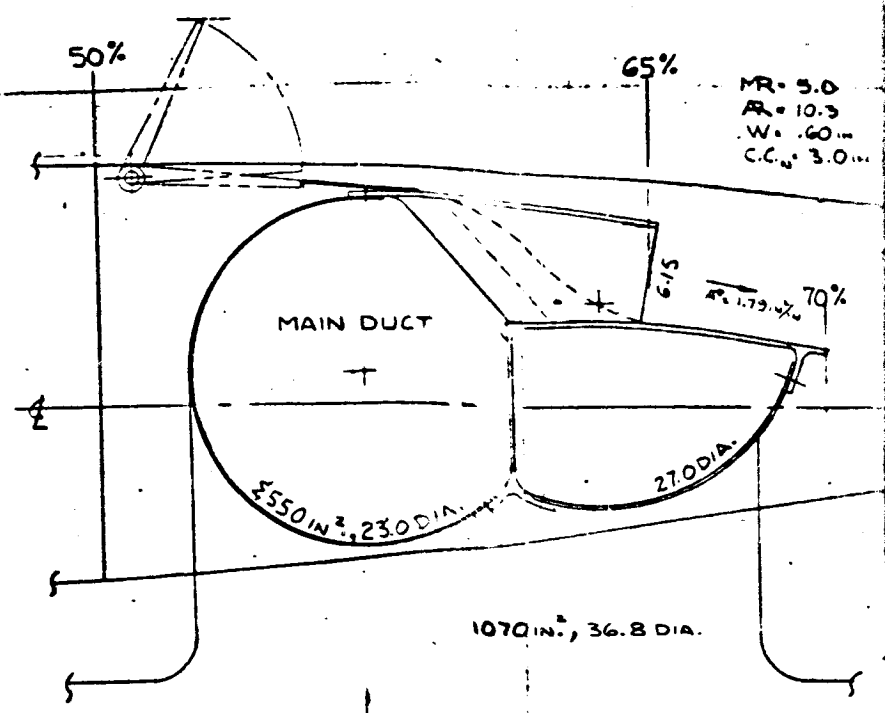

SECTION C-C

SCALE 1 1/4

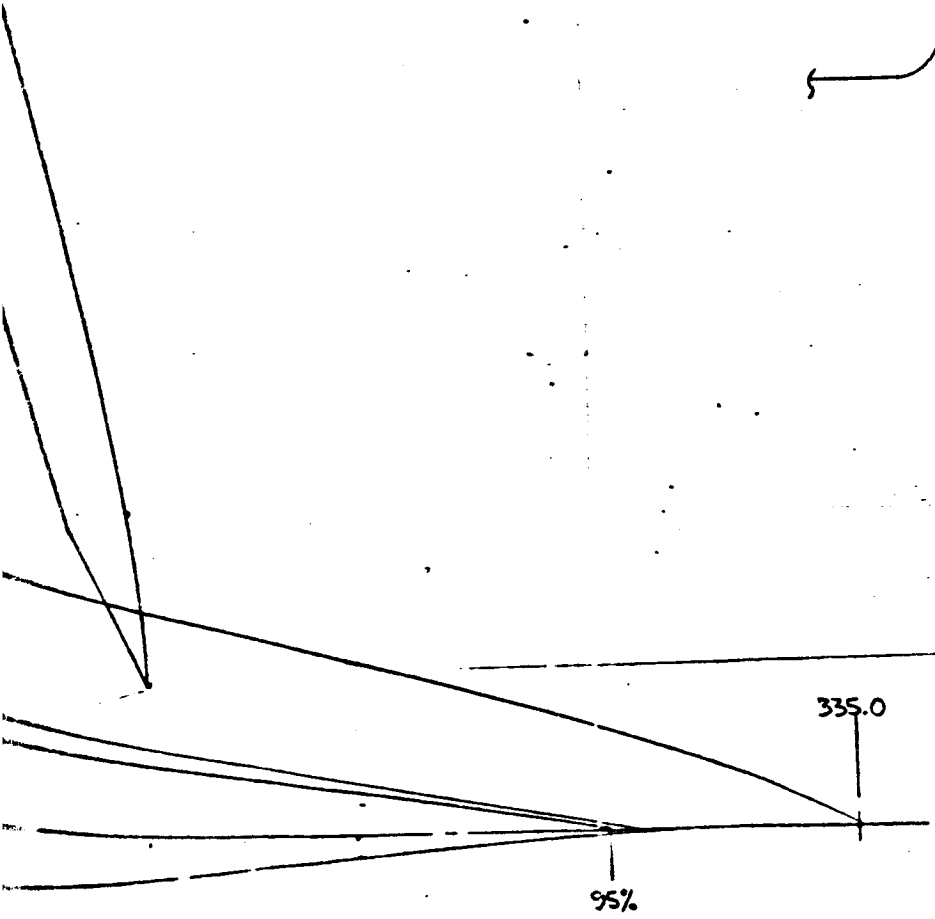

SEE LO-AWNP-007
L.E. BLC
10% of 4 EN

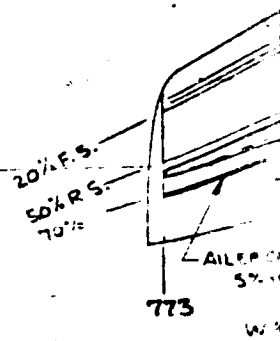

(3)

(BETWEEN SECTS. A-A & B-B)

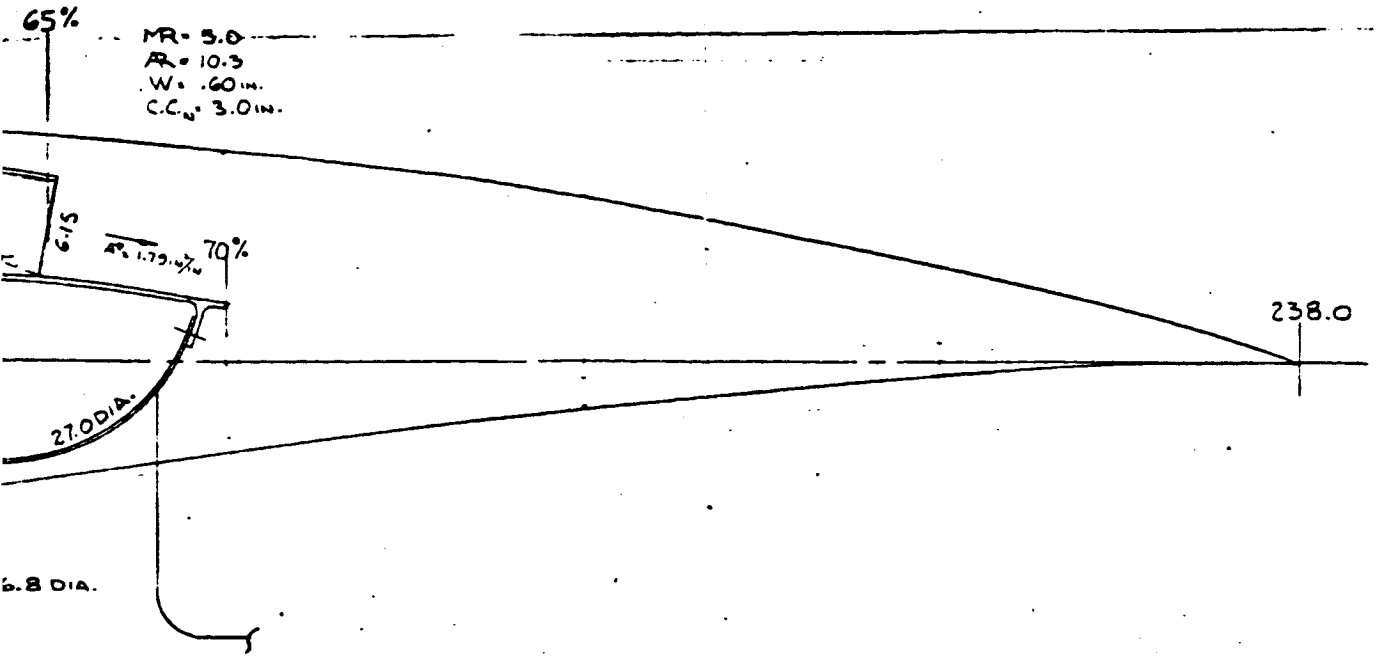
65%
MR = 5.0
AR = 10.3
W = .60 IN.
C.C.N = 3.0 IN.
6.15
70%
238.0
27.0 DIA.
6.8 DIA.

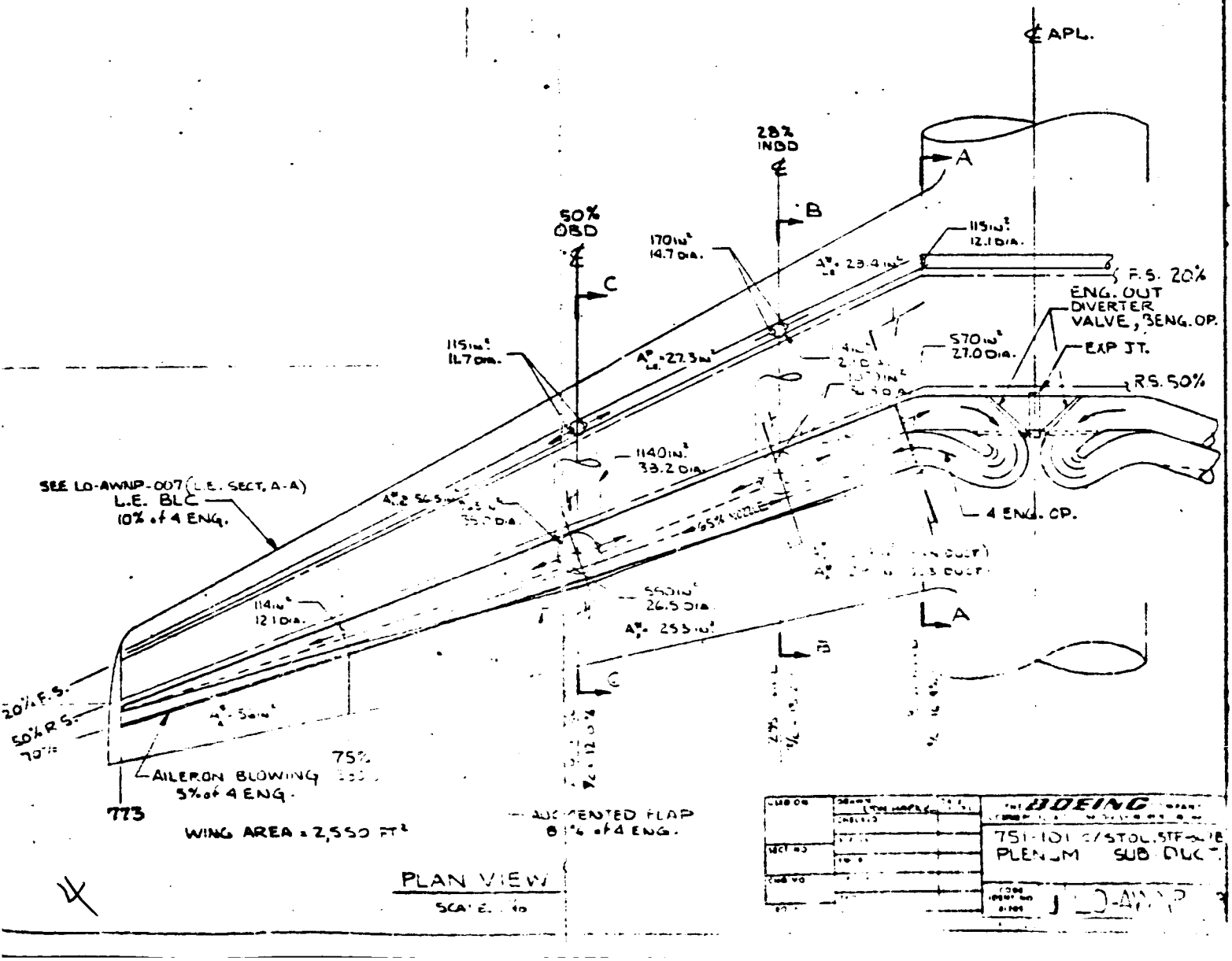
℄ APL.
28% INBD
50% OBD
A
B
C
170 IN²
14.7 DIA.
115 IN²
12.1 DIA.
F.S. 20%
ENG. OUT DIVERTER VALVE, 3 ENG. OP.
570 IN²
27.0 DIA.
EXP JT.
R.S. 50%
115 IN²
11.7 DIA.
1140 IN²
33.2 DIA.
SEE LO-AWNP-007 (L.E. SECT. A-A)
L.E. BLC
10% of 4 ENG.
4 ENG. OP.
65% NOZZLE
550 IN²
26.5 DIA.
114 IN²
12.1 DIA.
20% F.S.
50% R.S.
70%
75%
AILERON BLOWING
5% of 4 ENG.
773
WING AREA = 2,550 FT²
AUGMENTED FLAP
8% of 4 ENG.
PLAN VIEW
SCALE 40
BOEING
751-101 C/STOL STF-18
PLENUM SUB DUCT

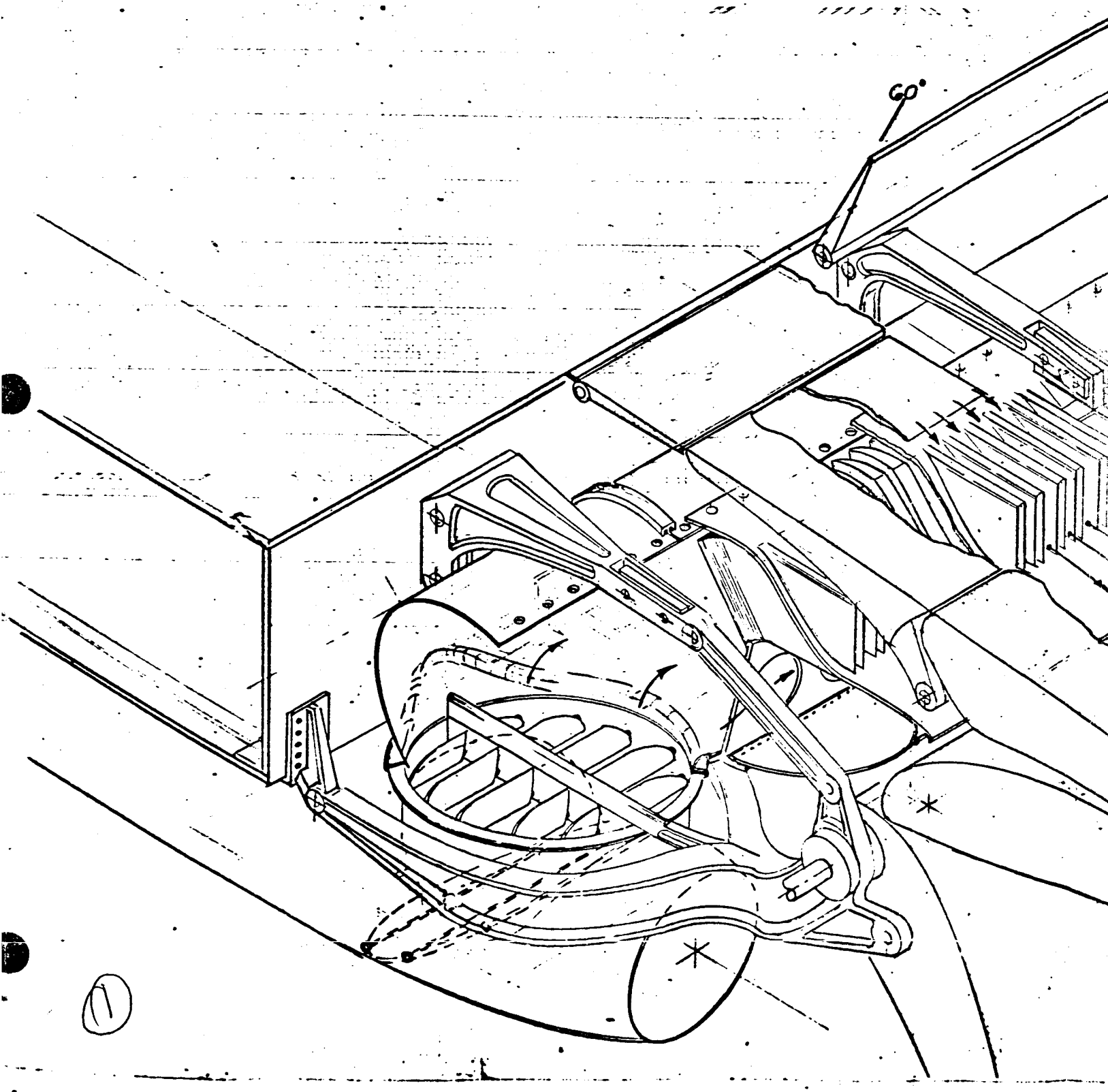
60°
1

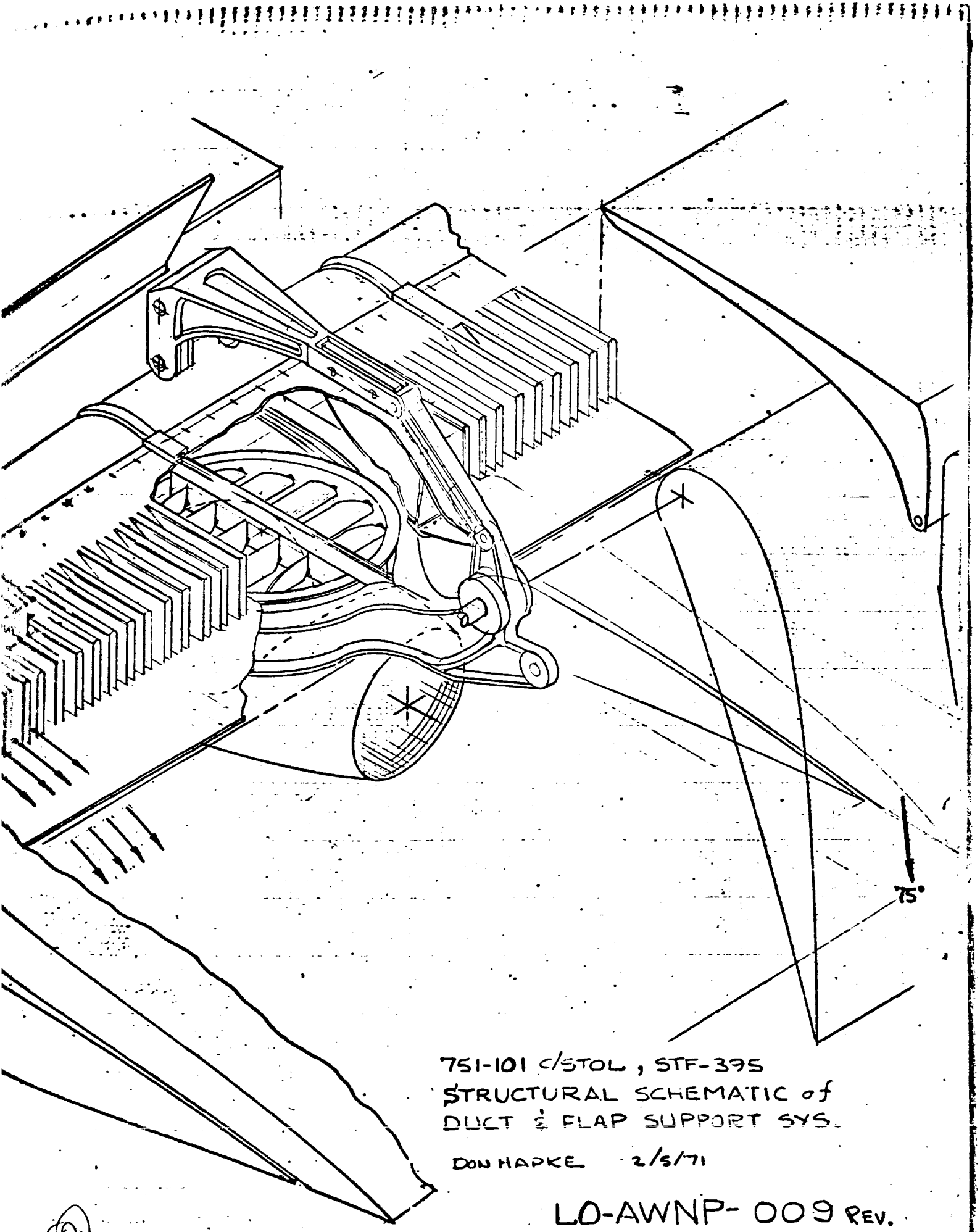

751-101 C/STOL, STF-395
STRUCTURAL SCHEMATIC of
DUCT & FLAP SUPPORT SYS.

DON HAPKE 2/5/71

LO-AWNP-009 REV.

(2)

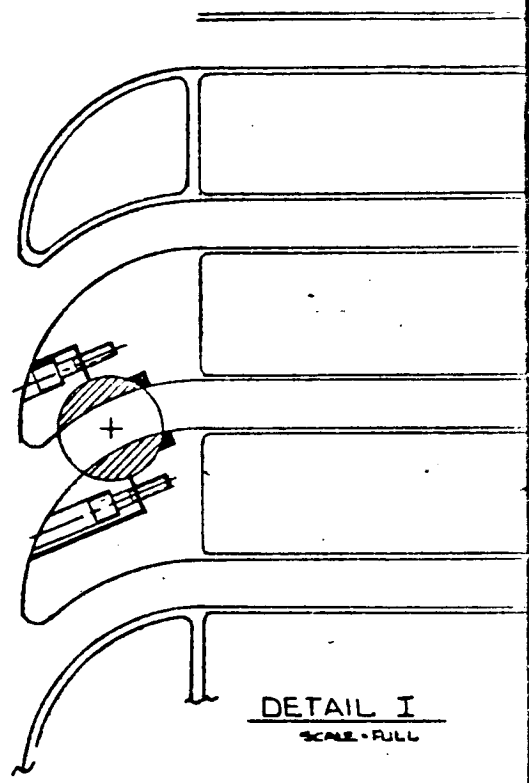

DETAIL I

SCALE - FULL

5%

65%

1

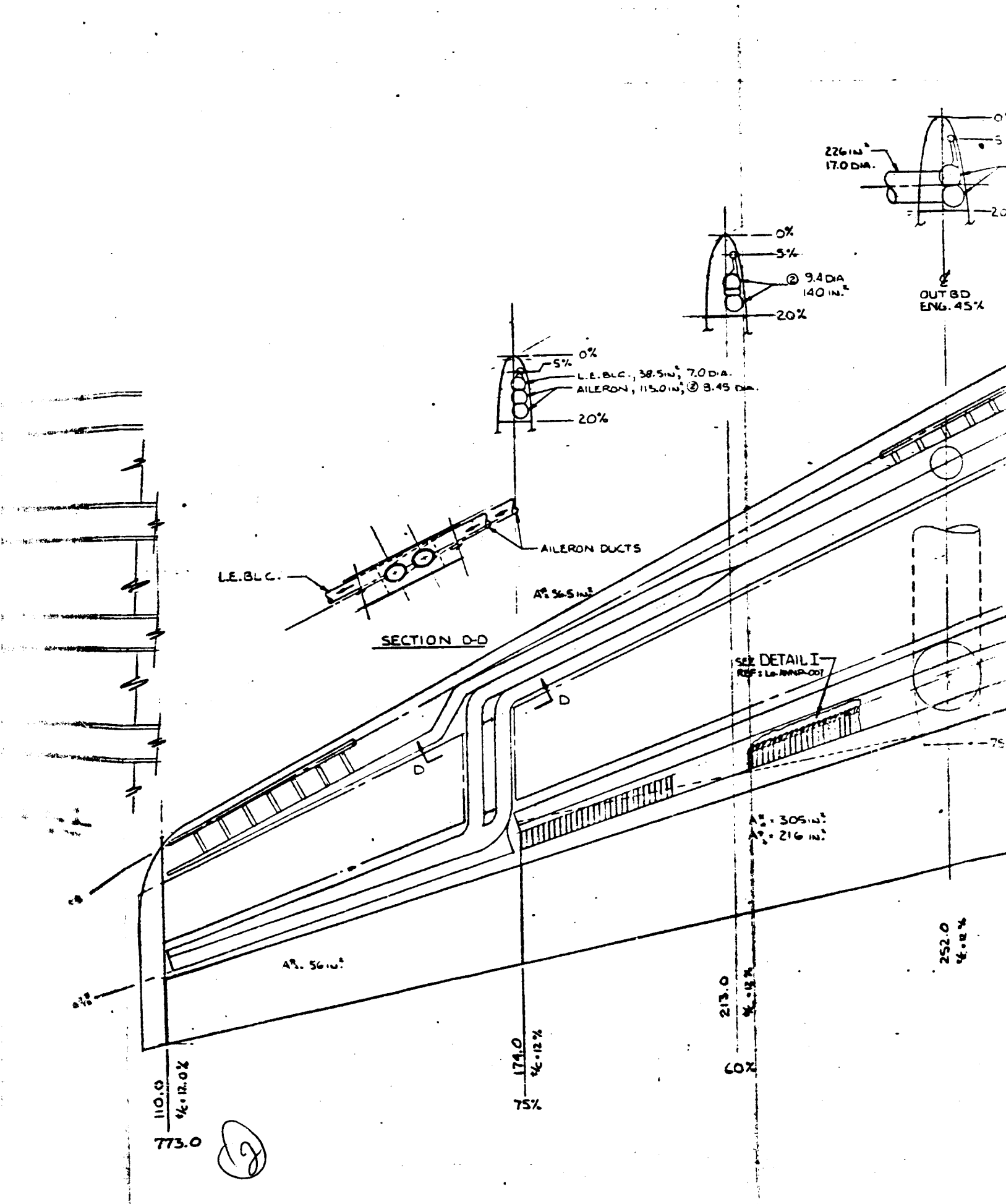
226 IN²
17.0 DIA.
0%
5%
20%
② 9.4 DIA
140 IN.²
OUT BD
ENG. 45%
0%
5%
L.E. BLC., 38.5 IN², 7.0 DIA.
AILERON, 115.0 IN², ② 8.45 DIA.
20%
AILERON DUCTS
L.E. BLC.
A_R = 36.5 IN²
SECTION D-D
SEE DETAIL I
REF: L6-MNP-001
D
D
A_R = 30.5 IN²
A_R = 21.6 IN²
A_R = 56 IN²
110.0
t/c = 12.0%
773.0
174.0
t/c = 12%
75%
213.0
t/c = 12%
60%
252.0
t/c = 12%

17

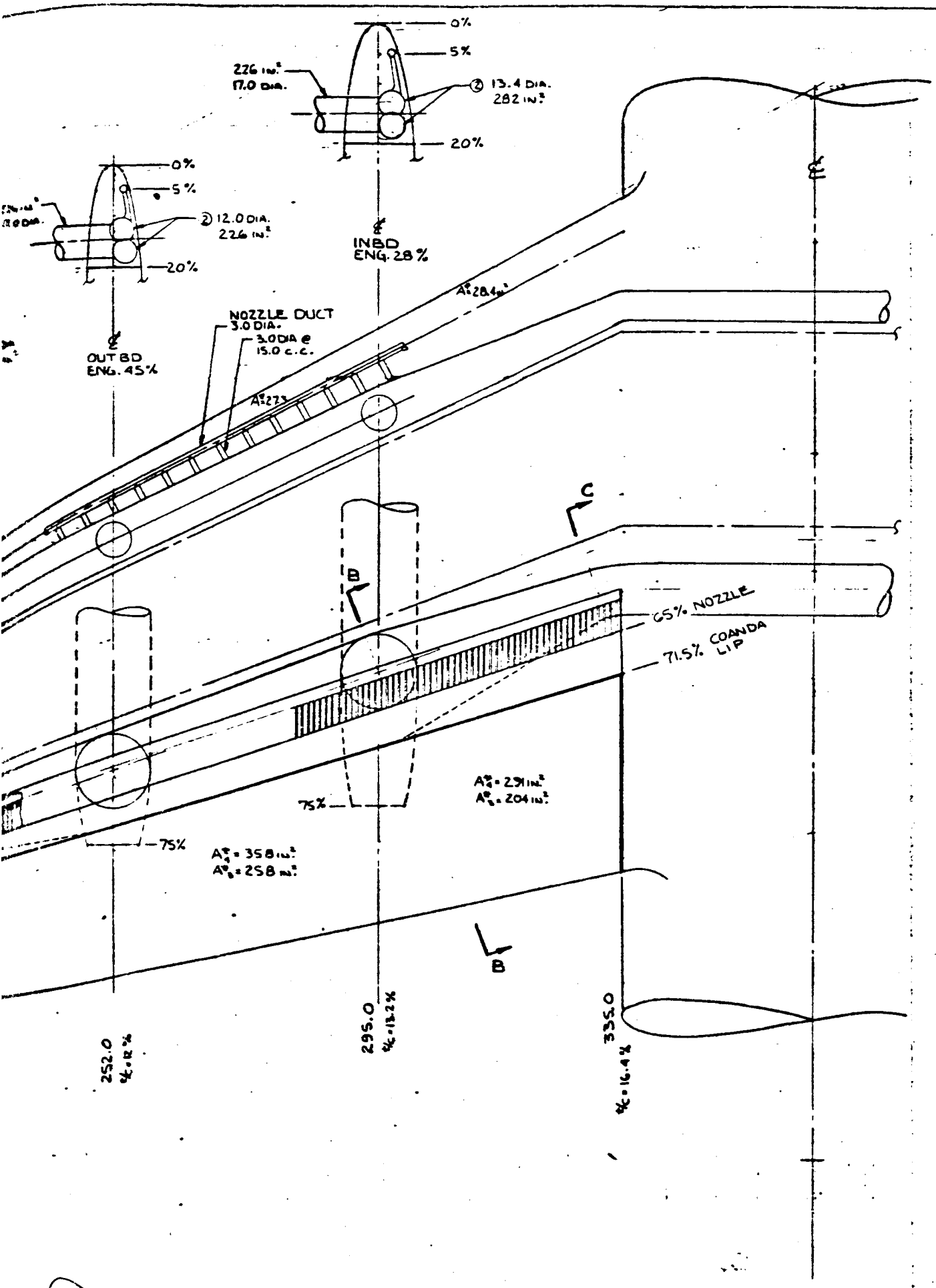
0%
5%
226 in²
17.0 DIA.
② 13.4 DIA.
282 in²
20%
0%
5%
② 12.0 DIA.
226 in²
20%
℄
INBD
ENG. 28%
A* 284 in²
NOZZLE DUCT
3.0 DIA.
3.0 DIA @
15.0 c.c.
A* 273
℄
OUTBD
ENG. 45%
C
B
65% NOZZLE
71.5% COANDA
LIP
A*a = 291 in²
A*b = 204 in²
75%
75%
A*a = 358 in²
A*b = 258 in²
B
252.0
%c = 8%
295.0
%c = 13.2%
335.0
%c = 16.4%
℄

3

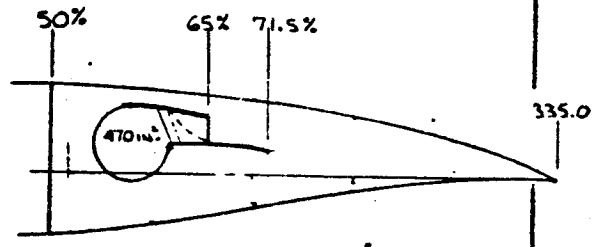

SECTION C-C

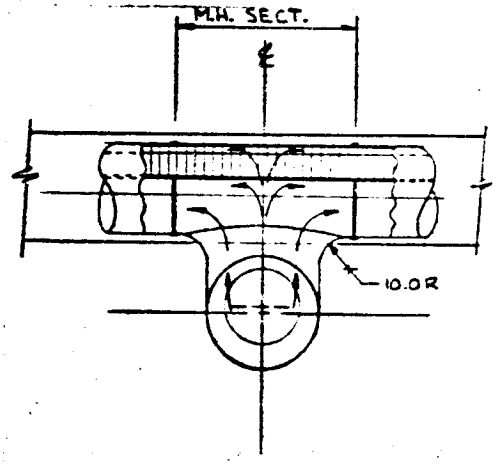

SECTION A-A

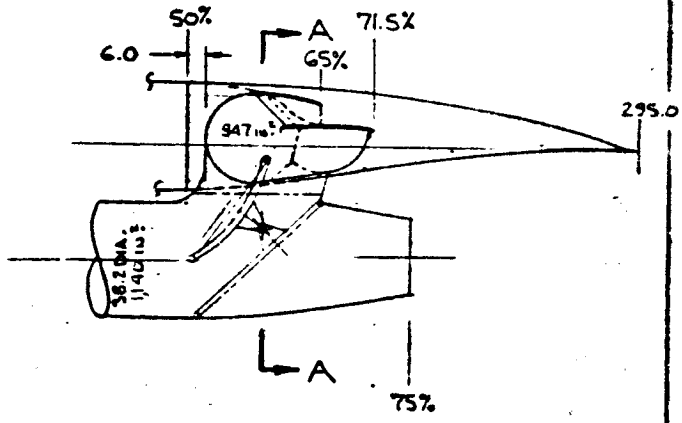

SECTION B-B

MATL	DRAWN	DATE	THE BOEING COMPANY COMMERCIAL AIRPLANE DIVISION RENTON WASH
	CHECKED		
			751-101 C/STOL, CTF-363 B PLENUM VARIABLE NOZZLE REF LO-AWNP-01
			CODE IDENT NO. 81205 — 1 — LO-AWNP-01

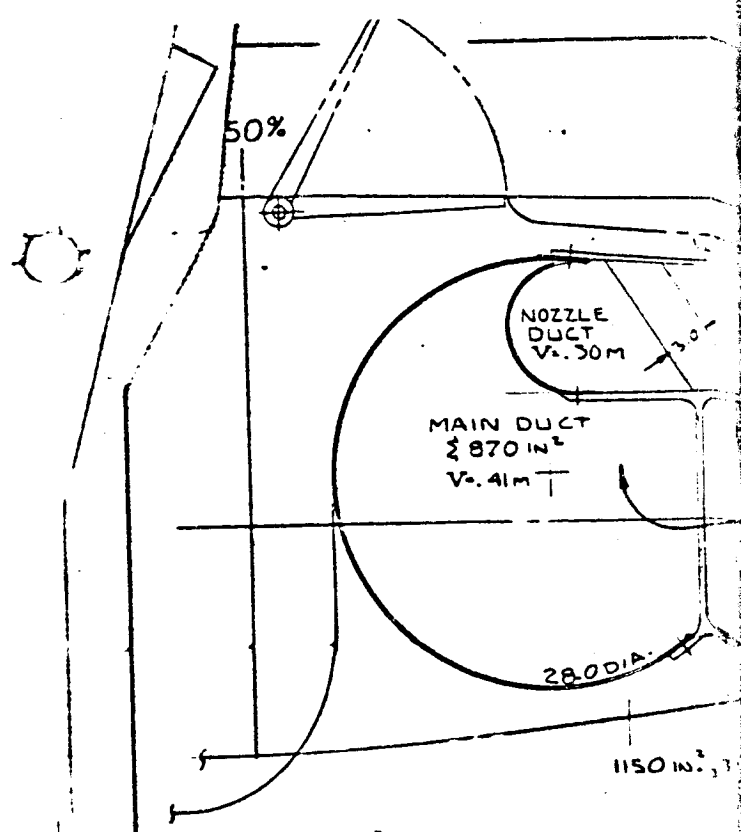

SECTION B
AT 28% WING
SCALE: ¼

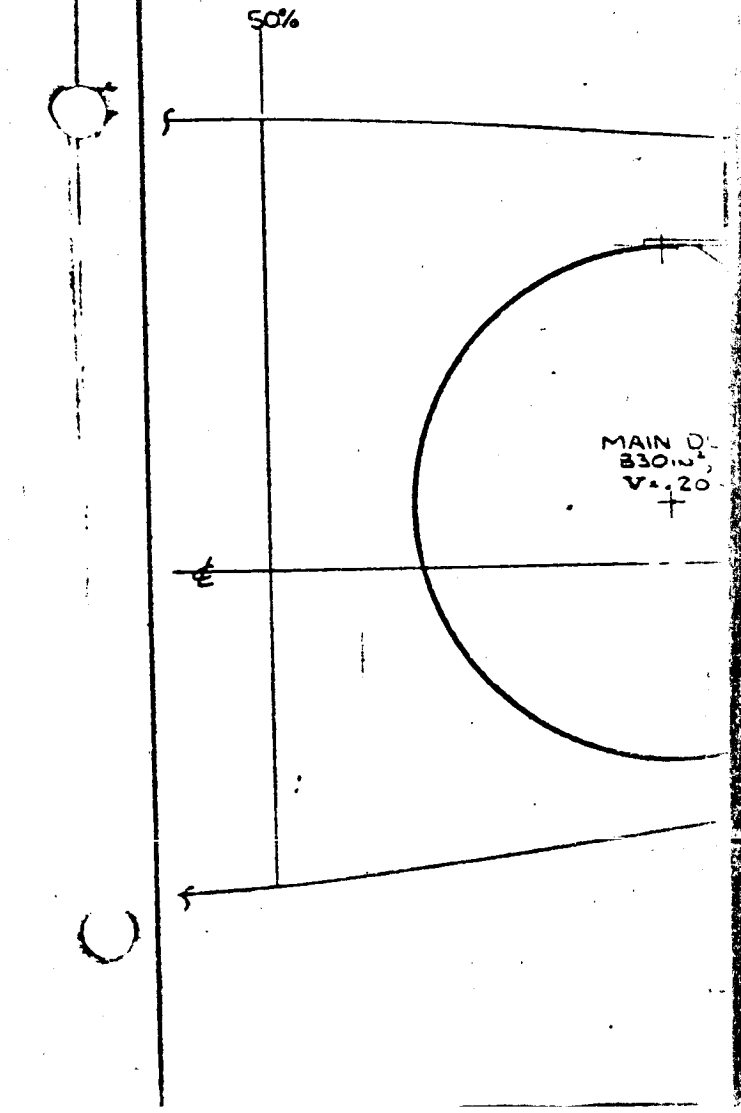

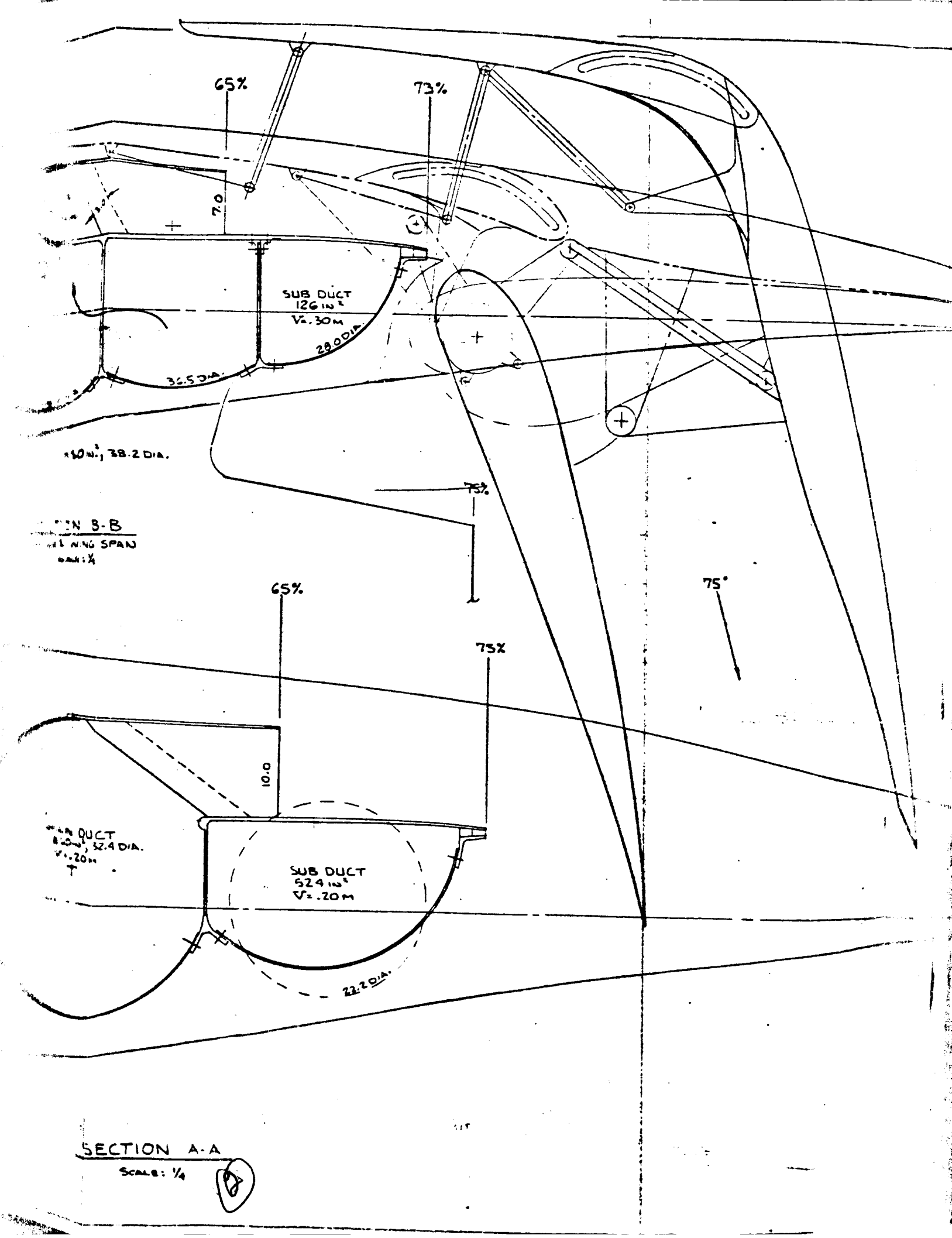
65%
73%
7.0
SUB DUCT
126 IN²
V=.30M
28.0 DIA.
36.5 DIA.
38.2 DIA.
75%
WING SPAN
65%
75%
75°
10.0
SUB DUCT
524 IN²
V=.20M
22.2 DIA.
SECTION A-A
SCALE: 1/4

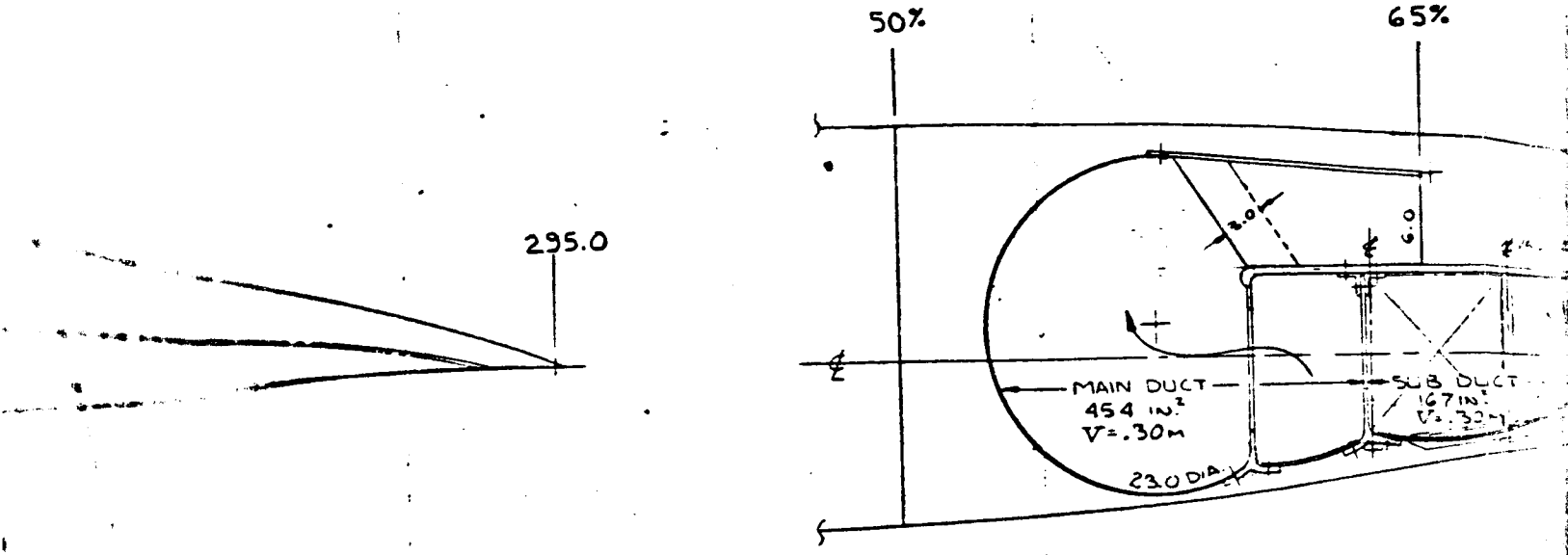

SECTION C-C
AT 50% WING SPAN
SCALE: 1/4

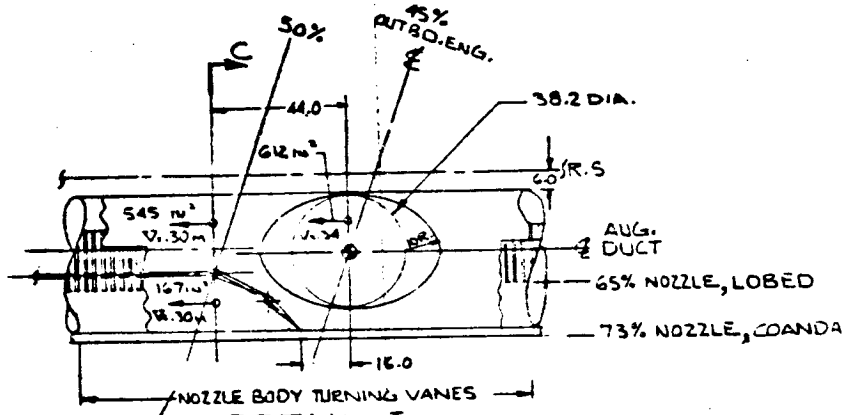

DETAIL-I
SCALE: 1/20

SEE DETAIL-II

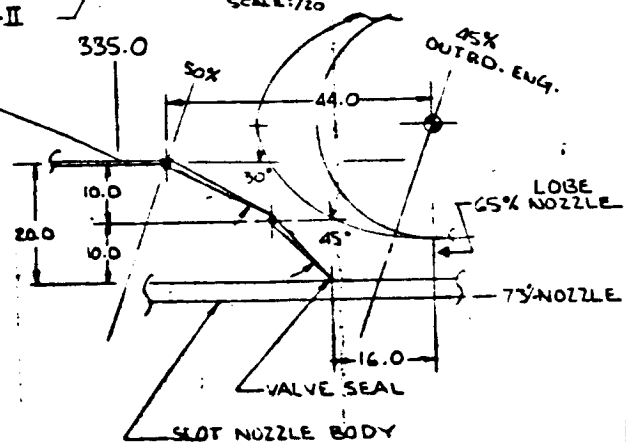

DETAIL-II
SCALE: 1/6

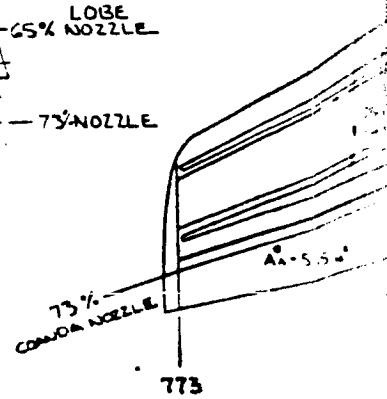

WING AREA - 25,500

(3)

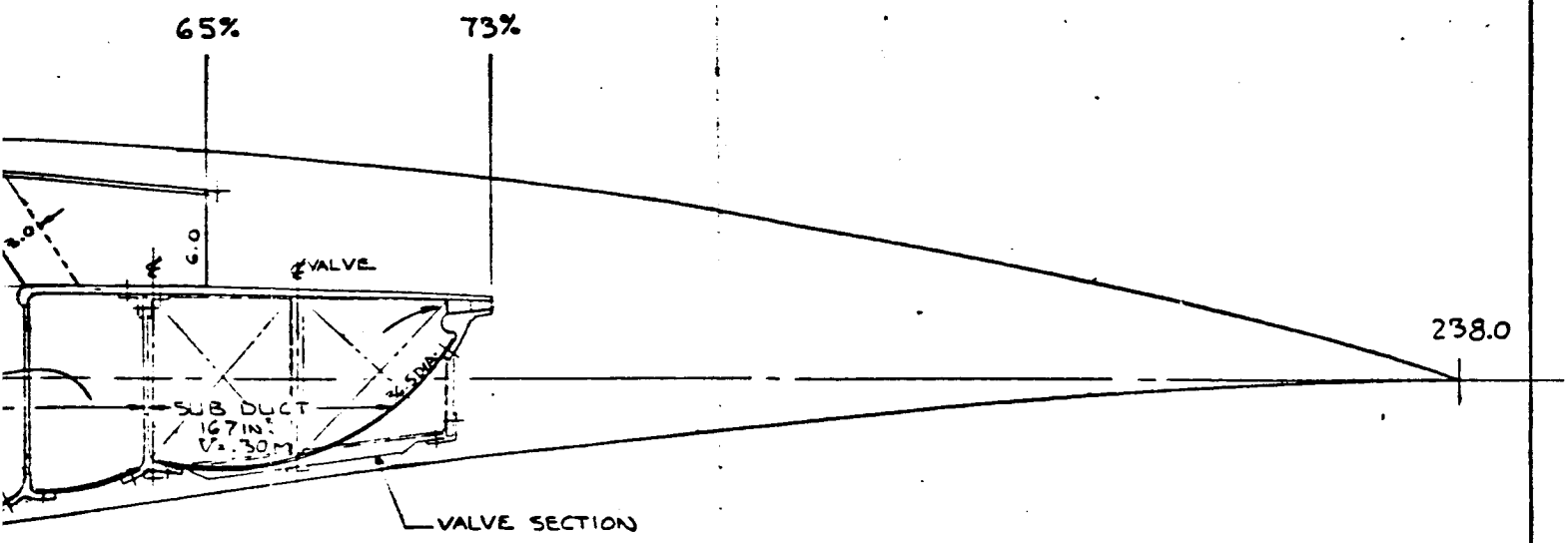

CTION C-C
50% WING SPAN
SCALE: 1/4

ENGINE DATA

STF-369 B
F_{REQ} = 17.800 lb (UNINSTL.)
W = 328.5 lbs/SEC.
P_N = 29.2 PSIA
P_R =
T_N = 703°R
A^* = 565 IN²/ENG.

.2 DIA.

R.S

℄ AUG. DUCT
— 65% NOZZLE, LOBED
— 73% NOZZLE, COANDA

ENG.

LOBE NOZZLE

NOZZLE

13% DA NOZZLE

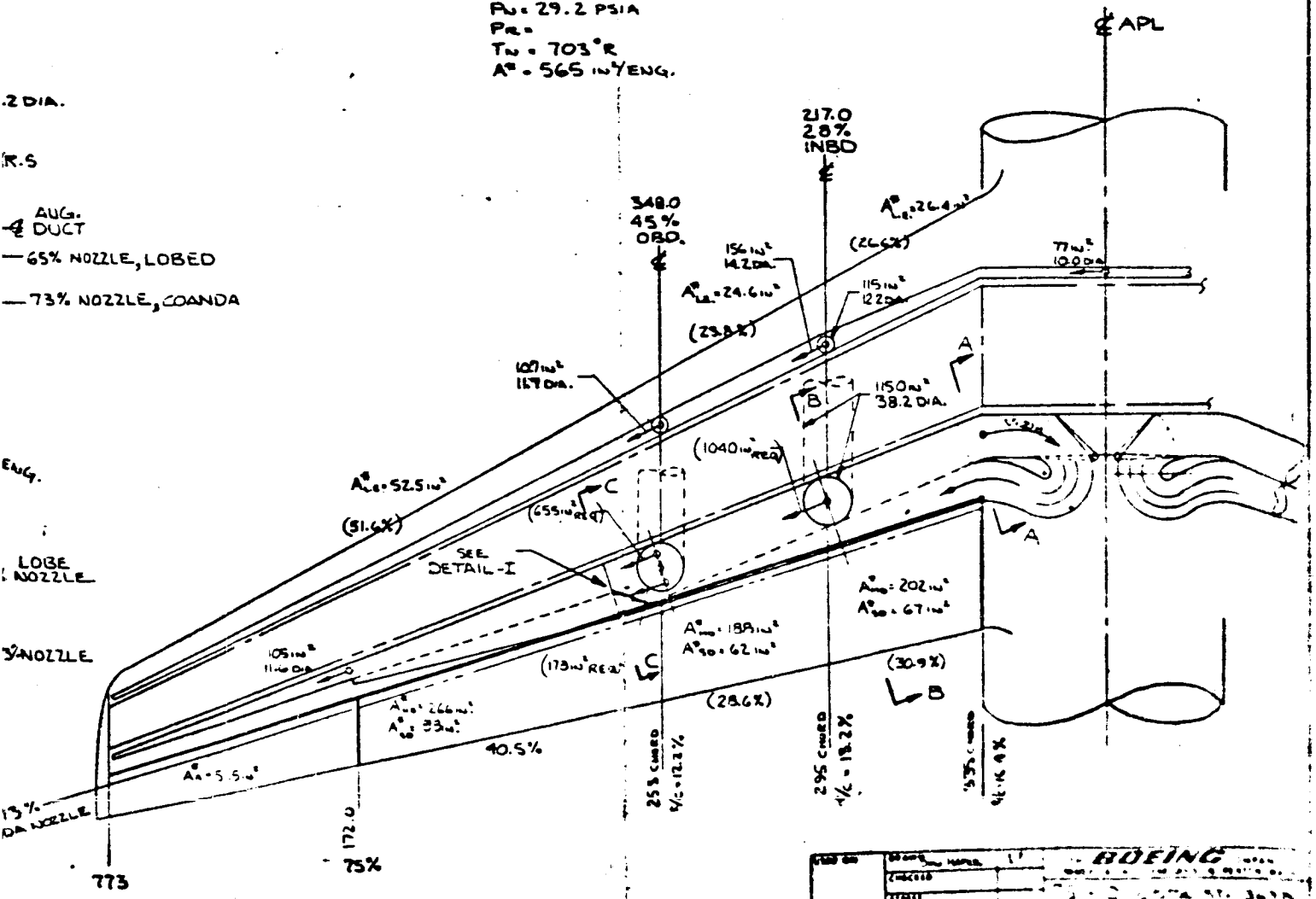

WING AREA = 25,500 FT.²

PLAN VIEW
SCALE: 1/40

BOEING

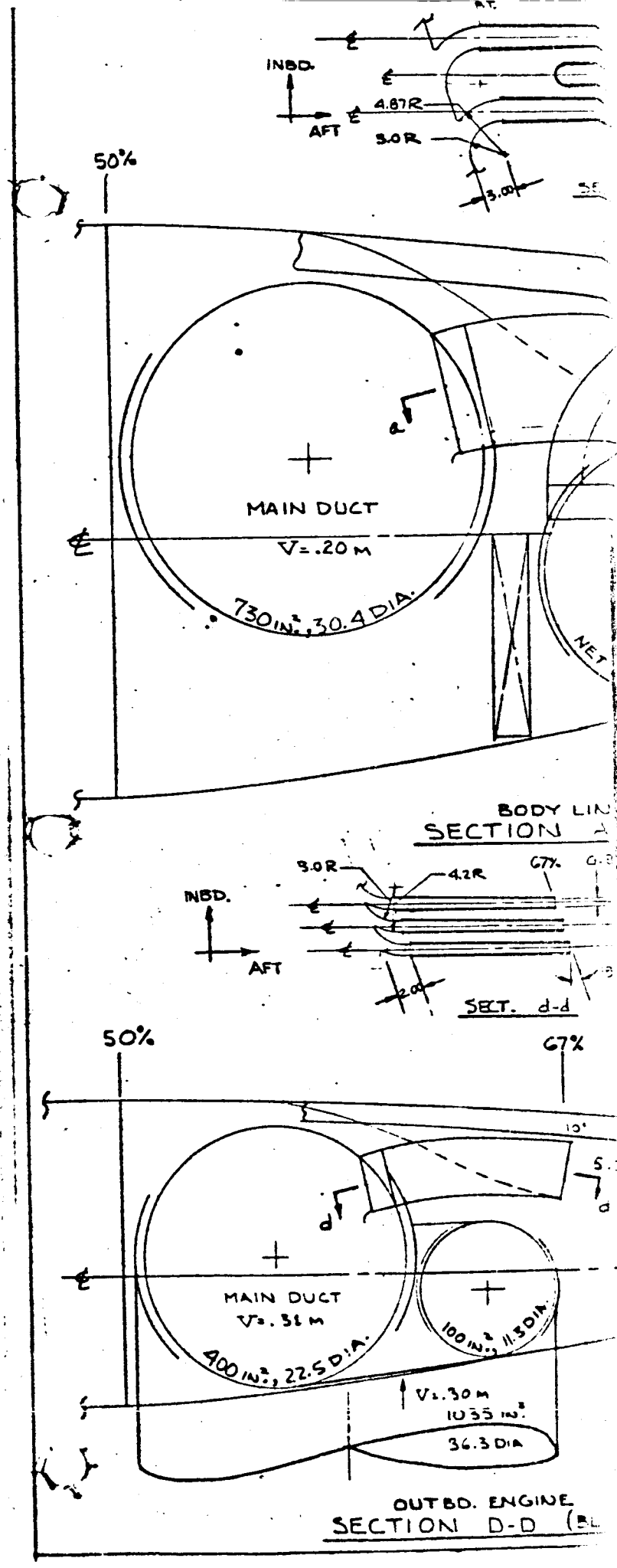
INBD.
AFT
4.87R
3.0R
3.00
50%
MAIN DUCT
V=.20 M
730 IN², 30.4 DIA.
BODY LIN
SECTION A
3.0R
4.2R
67%
INBD.
AFT
2.00
SECT. d-d
50%
67%
MAIN DUCT
V=.31 M
400 IN², 22.5 DIA.
100 IN², 11.5 DIA.
V=.30 M
1035 IN²
36.3 DIA
OUTBD. ENGINE
SECTION D-D

1

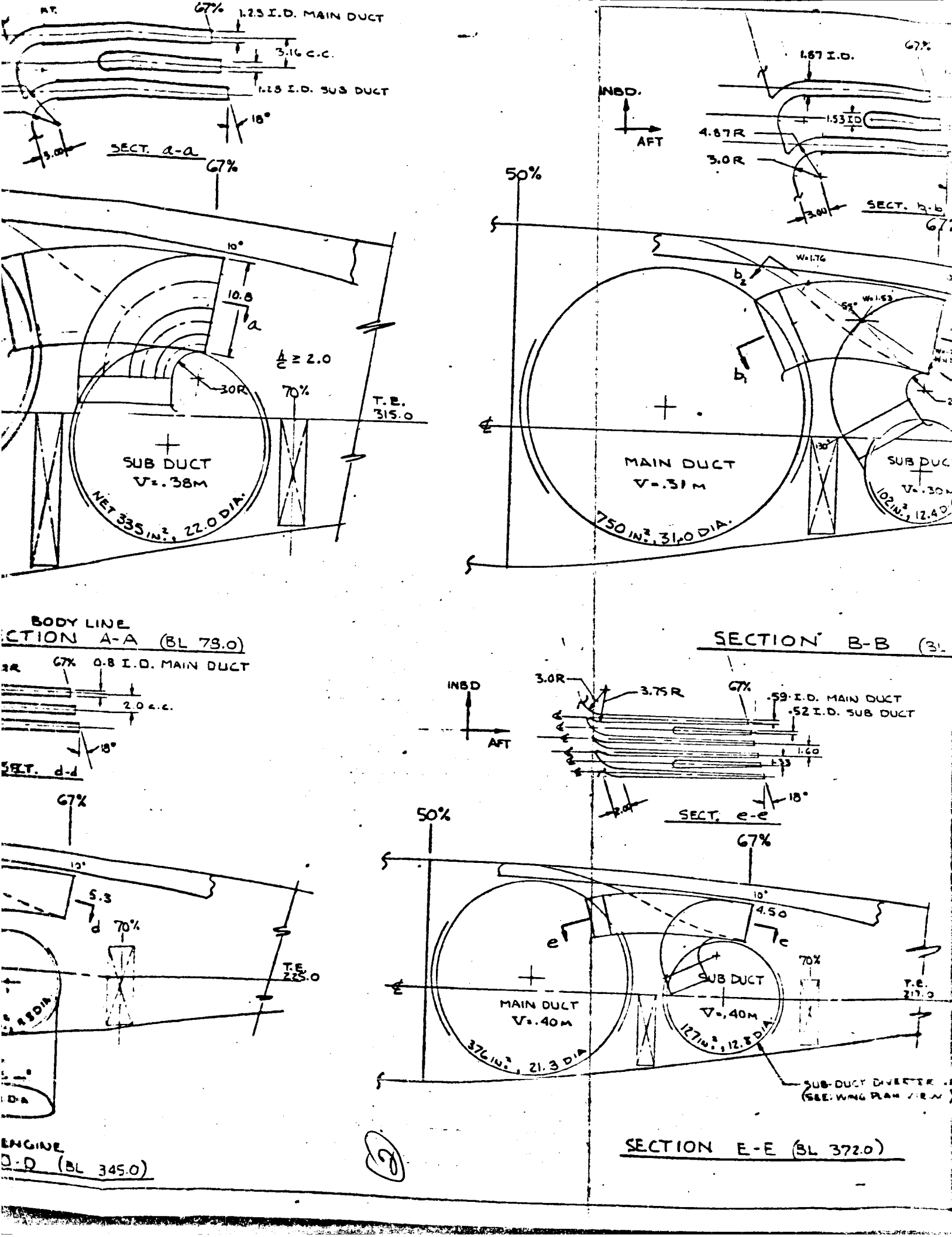
AFT
67%
1.25 I.D. MAIN DUCT
3.16 c.c.
1.25 I.D. SUB DUCT
18°
SECT. a-a
67%
10°
10.8
a
a/c ≥ 2.0
30R
70%
T.E. 315.0
SUB DUCT
V=.38M
NET 335 IN.², 22.0 DIA.
1.87 I.D.
67%
INBD.
AFT
1.53 ID
4.87R
3.0R
SECT. b-b
50%
W=1.76
b
W=1.53
53°
b
MAIN DUCT
V=.31M
750 IN.², 31.0 DIA.
SUB DUC
BODY LINE
CTION A-A (BL 73.0)
67%
0.8 I.D. MAIN DUCT
2.0 c.c.
18°
SECT. d-d
67%
10°
5.3
d
70%
T.E. 225.0
SECTION B-B
INBD
AFT
3.0R
3.75R
67%
.59 I.D. MAIN DUCT
.52 I.D. SUB DUCT
1.60
18°
SECT. e-e
50%
67%
10°
4.50
e
e
70%
SUB DUCT
MAIN DUCT
V=.40M
V=.40M
376 IN.², 21.3 DIA.
127 IN.², 12.8 DIA.
T.E. 217.0
SUB-DUCT DIVERTER
(SEE WING PLAN VIEW)
ENGINE
D-D (BL 345.0)
SECTION E-E (BL 372.0)

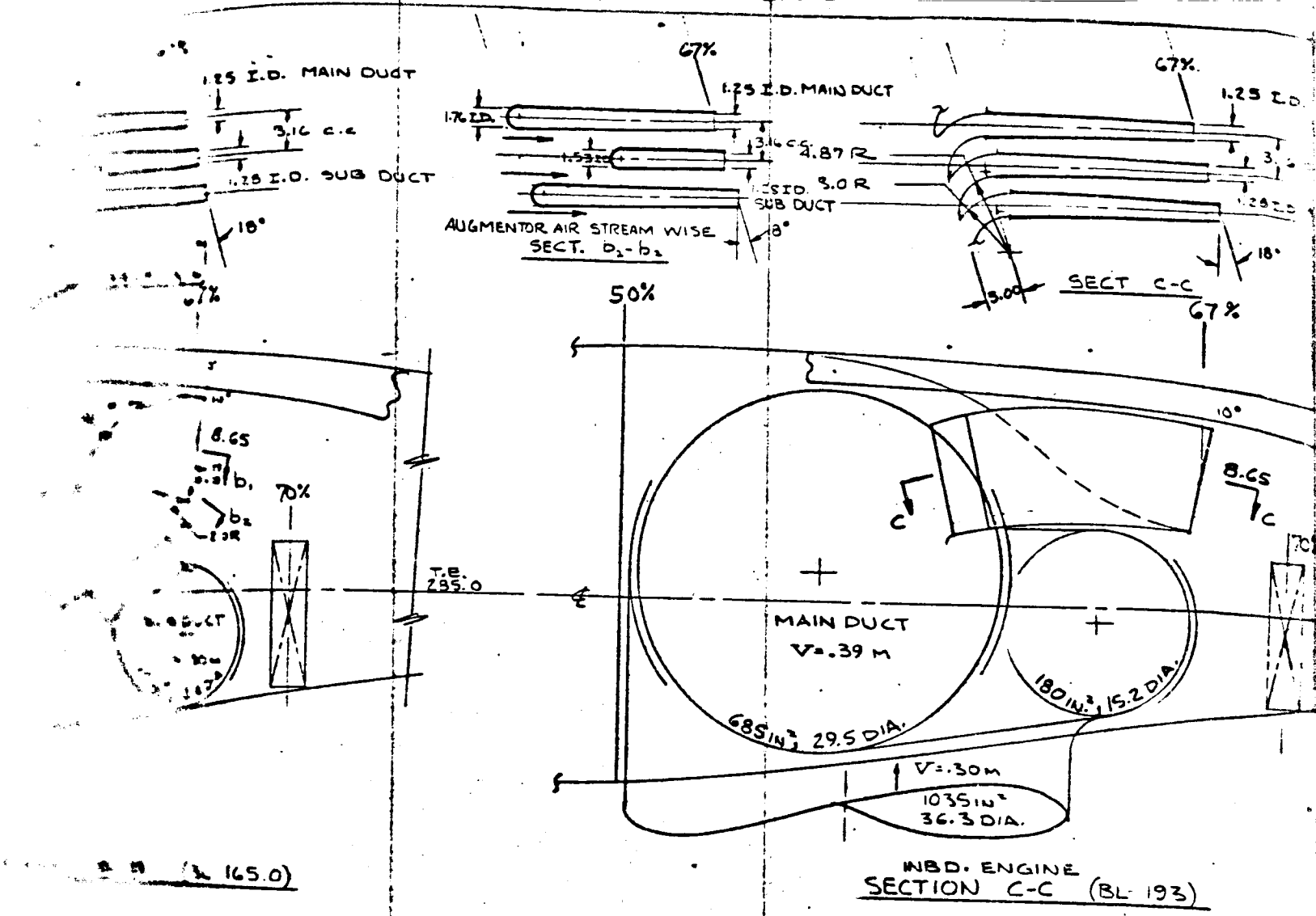

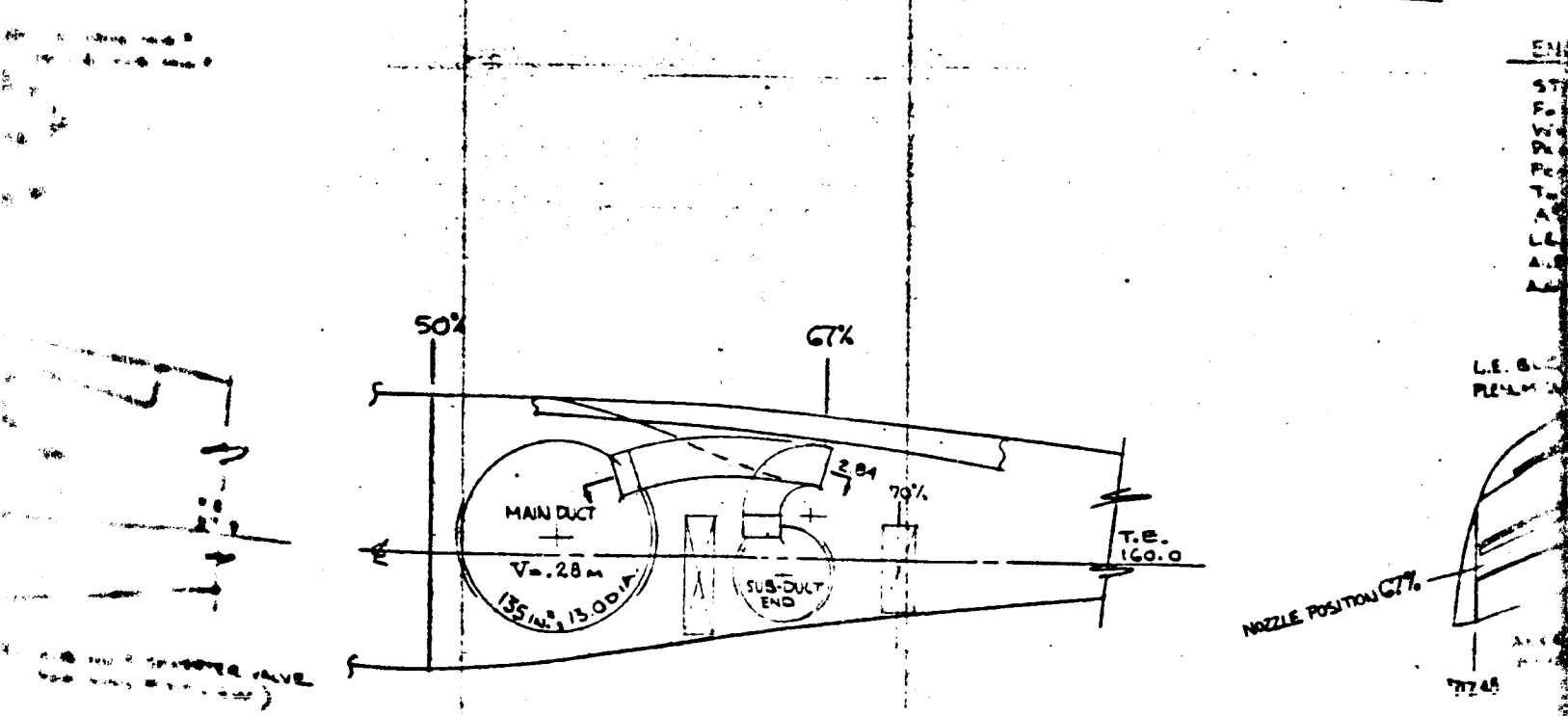

SECTION F-F (BL 536.0)

3

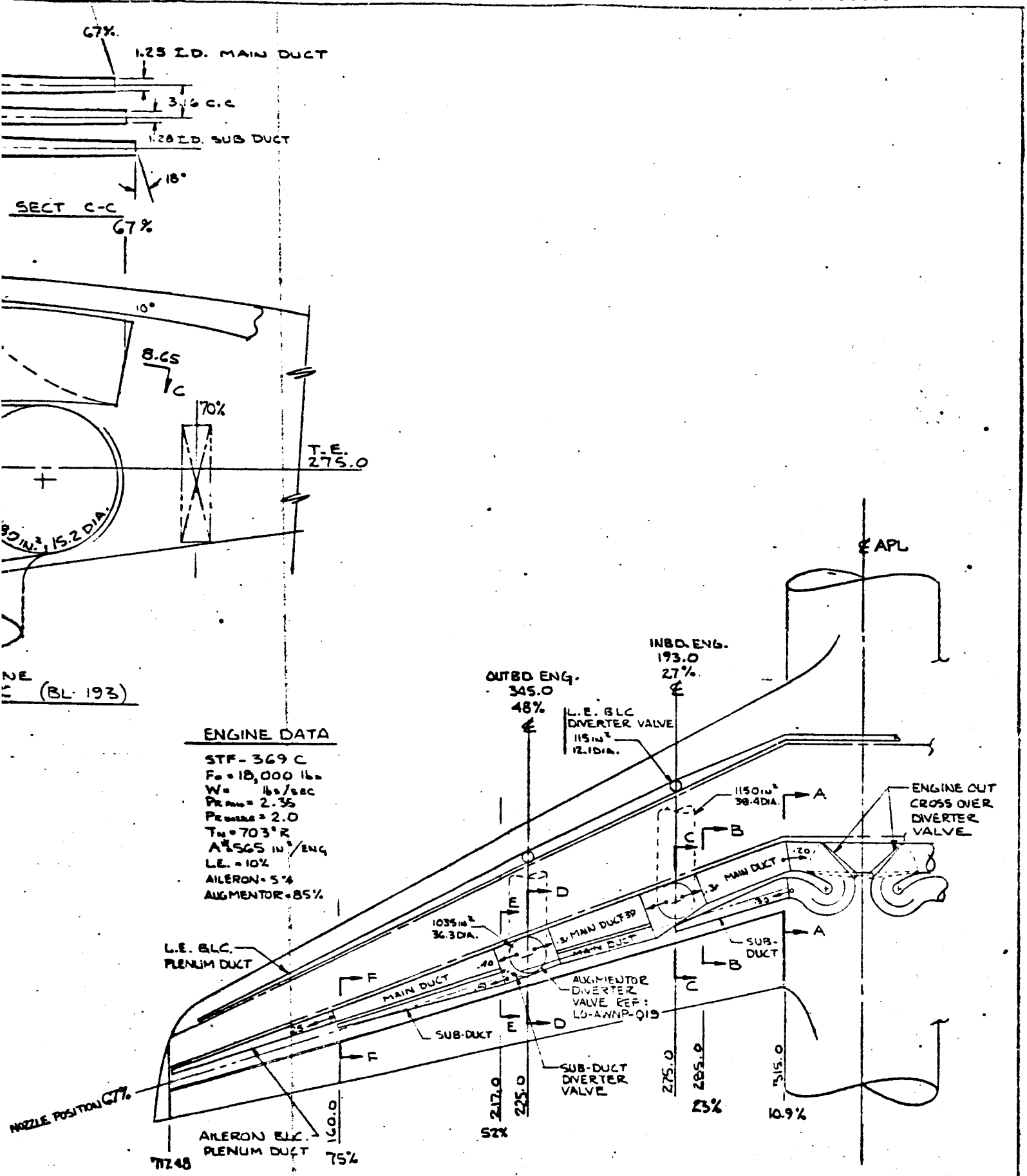

(14)

WING PLAN VIEW

SCALE: 1/60

REF: NOZZLE SIZE DATA: AWNP-CS-047 & -053

DRAWN	DAN HARKER	3/71	THE BOEING COMPANY
CHECKED			751-103 C/STOL, STF 369C
STRESS			PLENUM SUB-DUCT SYS.
ENGR			BASELINE NOZZLE
GROUP			
PROJ			J LO-AWNP-017

AIR VELOCITY, MAX FOR OUTBD ENG. OUT.

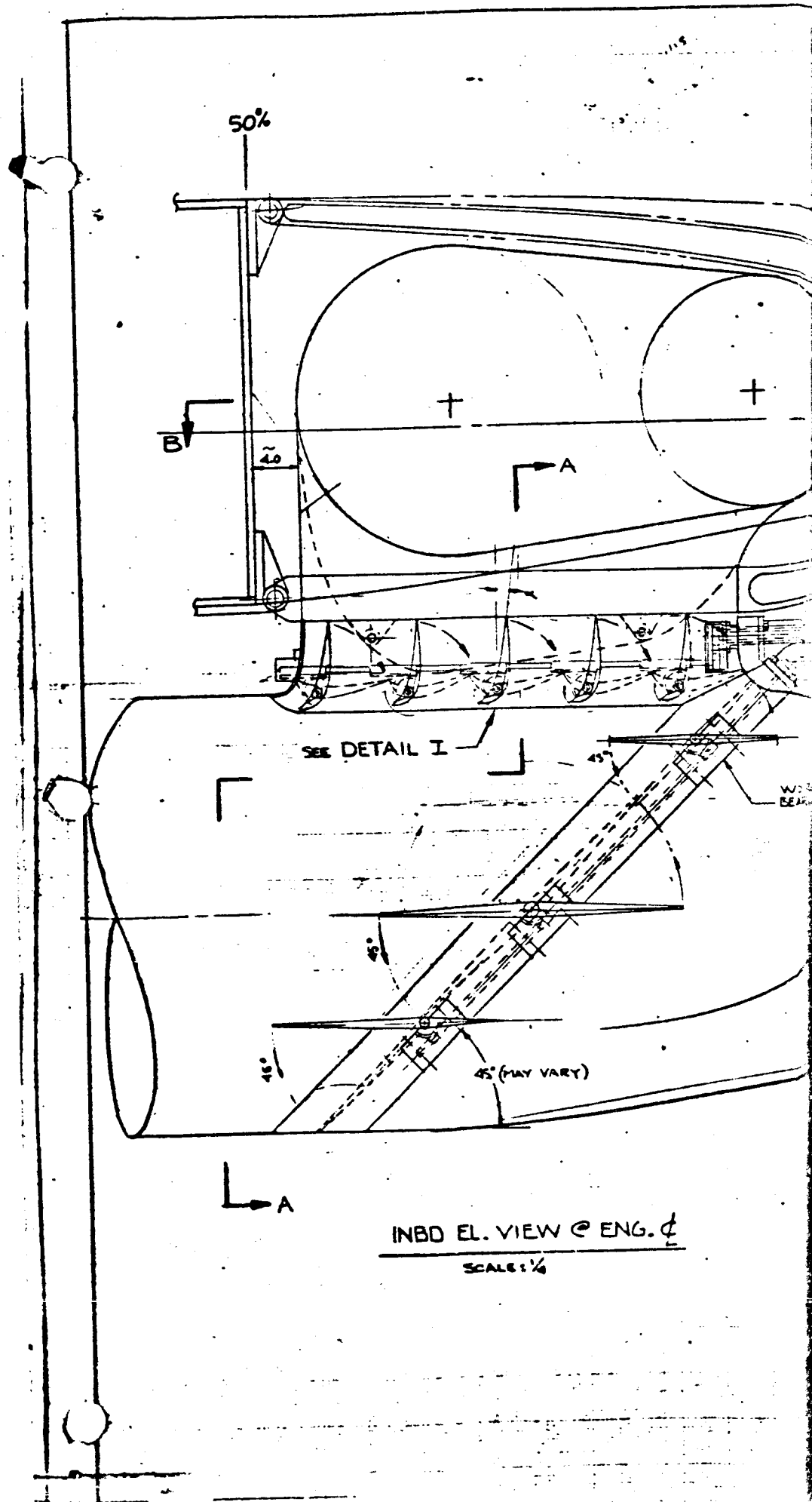

INBD EL. VIEW @ ENG. ℄

SCALE: 1/4

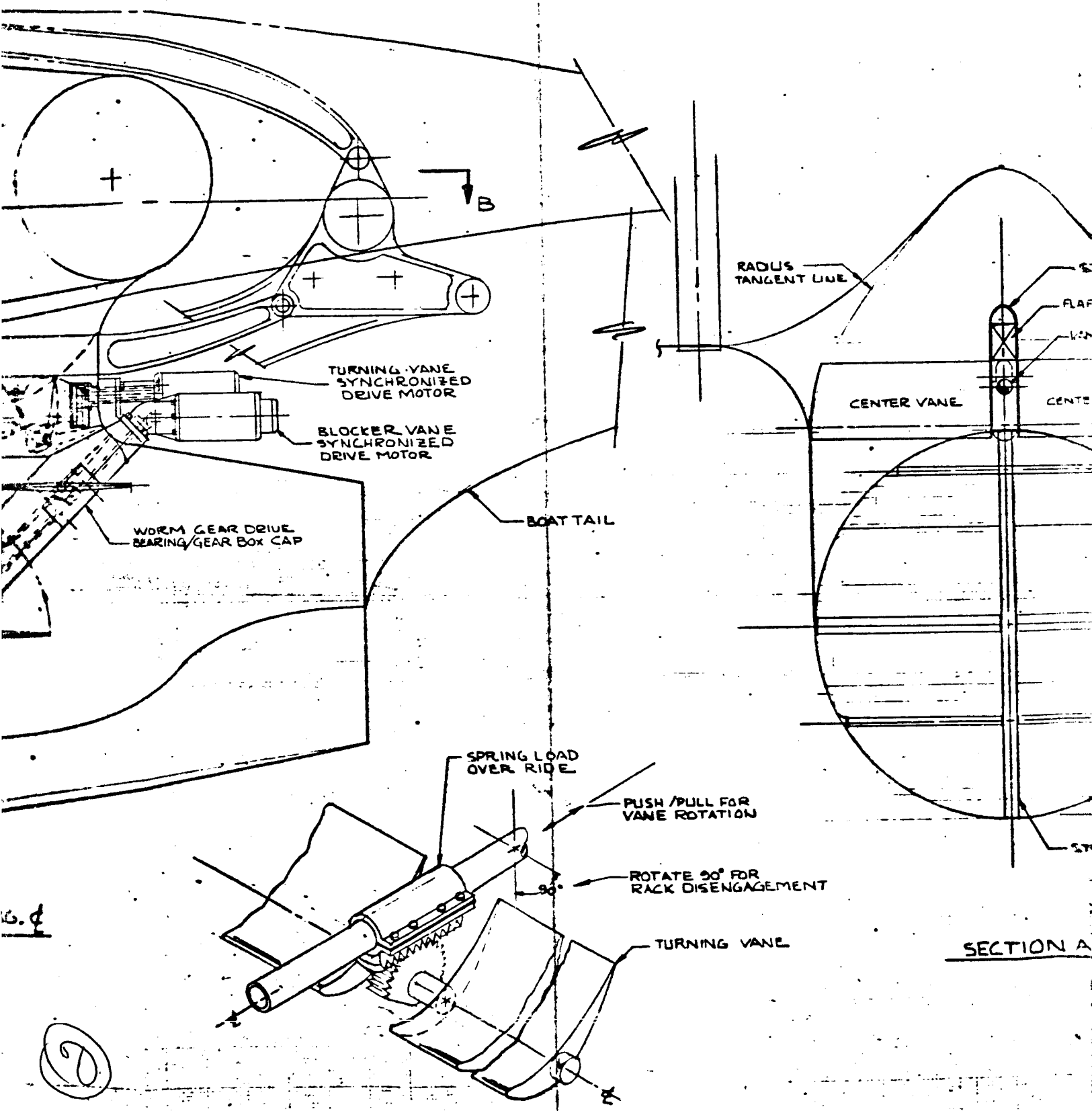
B
TURNING VANE SYNCHRONIZED DRIVE MOTOR
BLOCKER VANE SYNCHRONIZED DRIVE MOTOR
WORM GEAR DRIVE BEARING/GEAR BOX CAP
BOAT TAIL
RADIUS TANGENT LINE
CENTER VANE
SPRING LOAD OVER RIDE
PUSH /PULL FOR VANE ROTATION
90°
ROTATE 90° FOR RACK DISENGAGEMENT
TURNING VANE
SECTION A
DETIAL I
SCALE: NONE

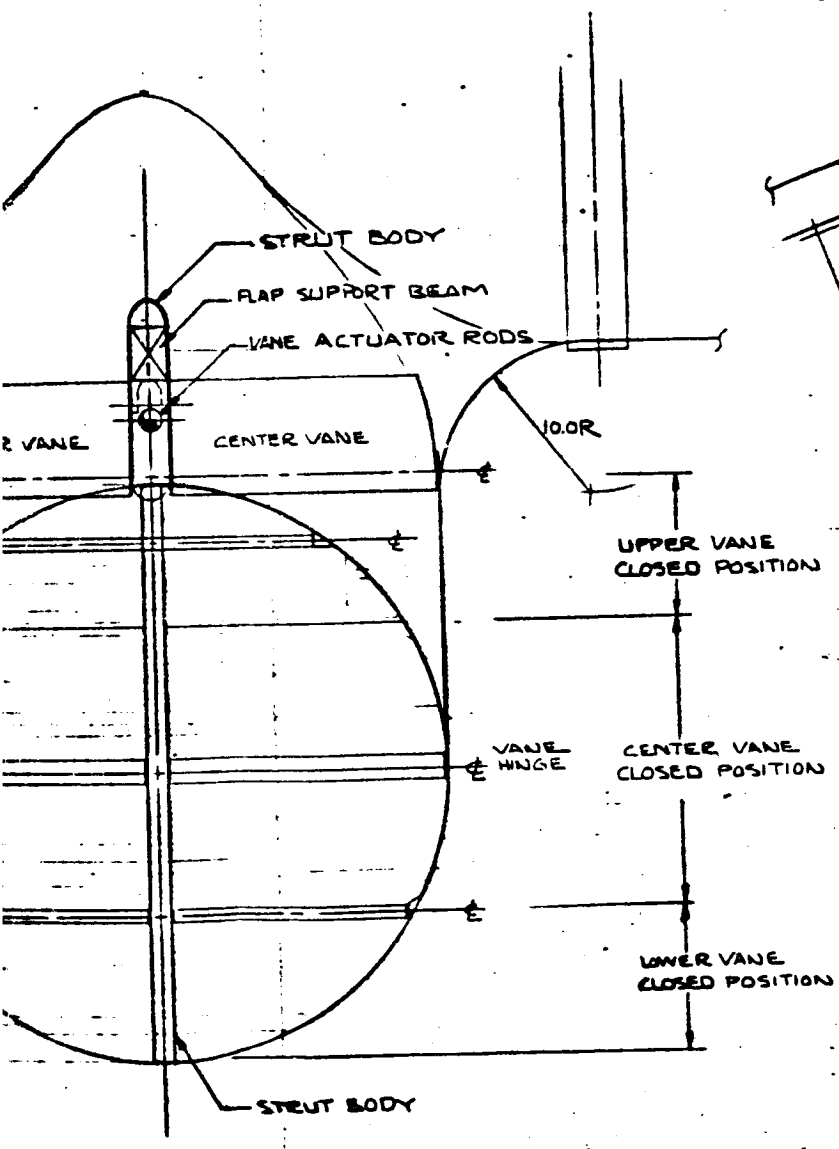

SECTION A-A

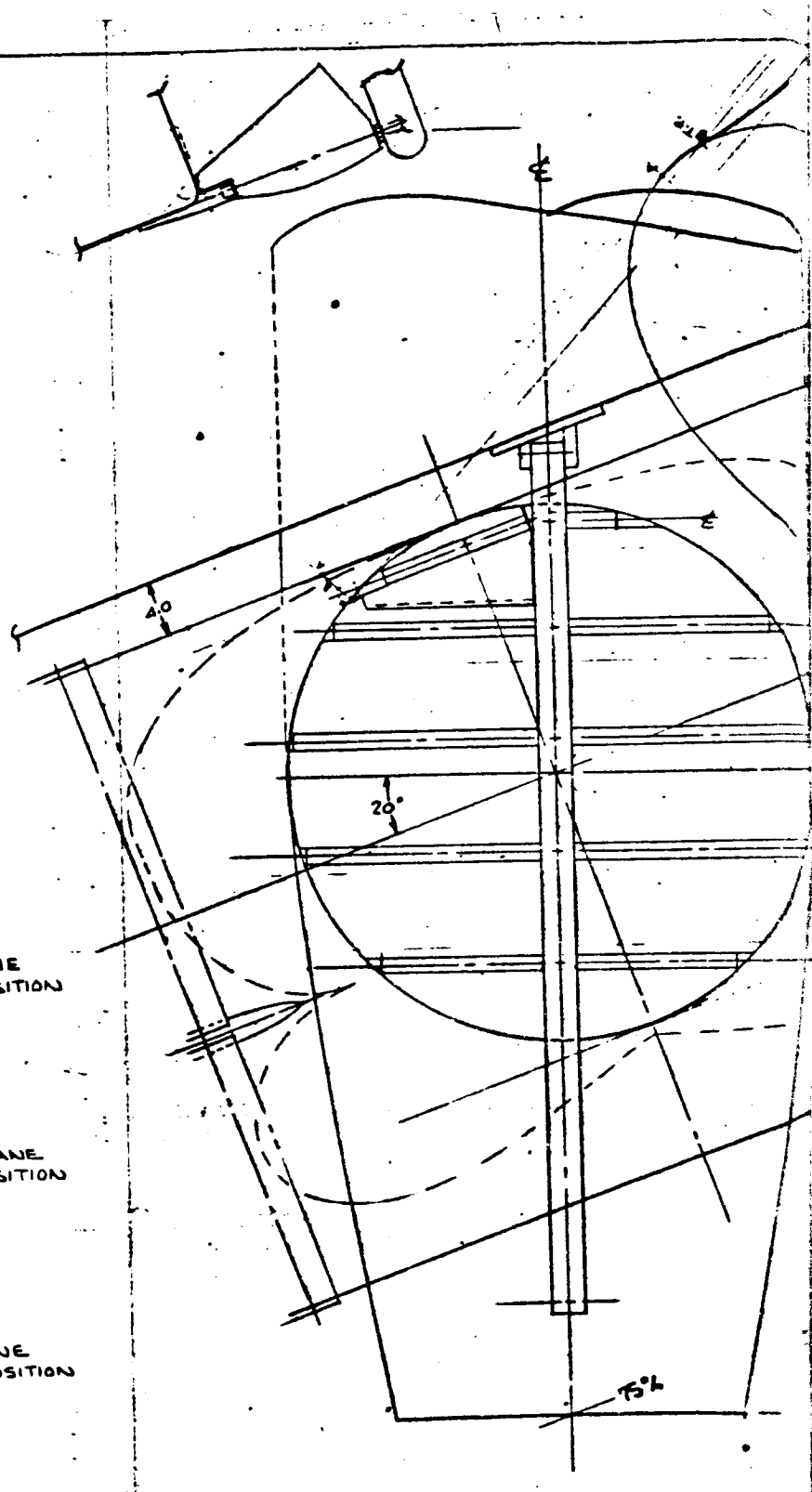

SECTION B-B

3

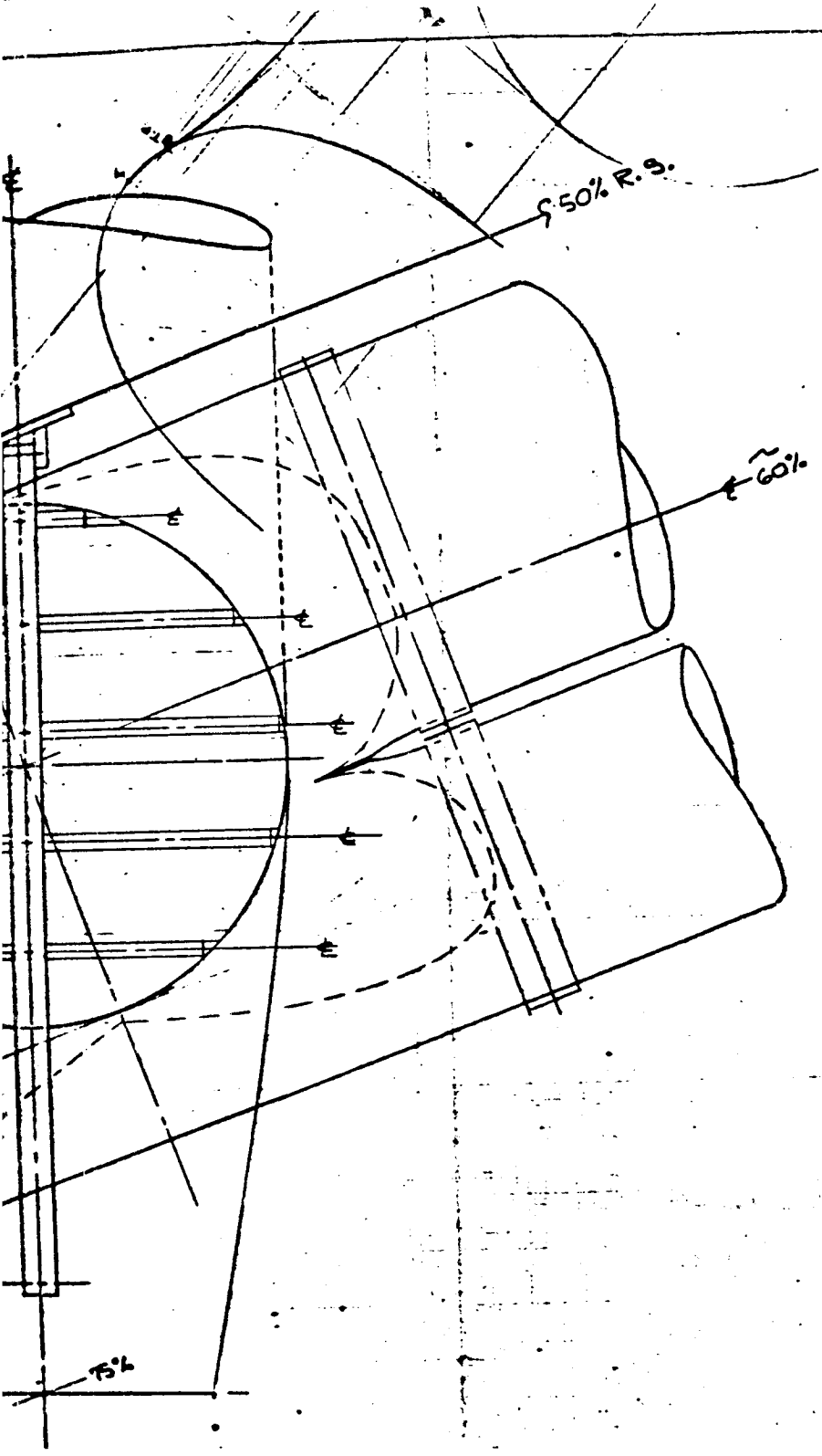

ON B-B

(4)

DRAWN			THE BOEING COMPANY
CHECKED			751-103 C/STOL, STF-369 B PLENUM SYS.-DIVERTER VALVE, VANE TYPE
			LO-AWNR(

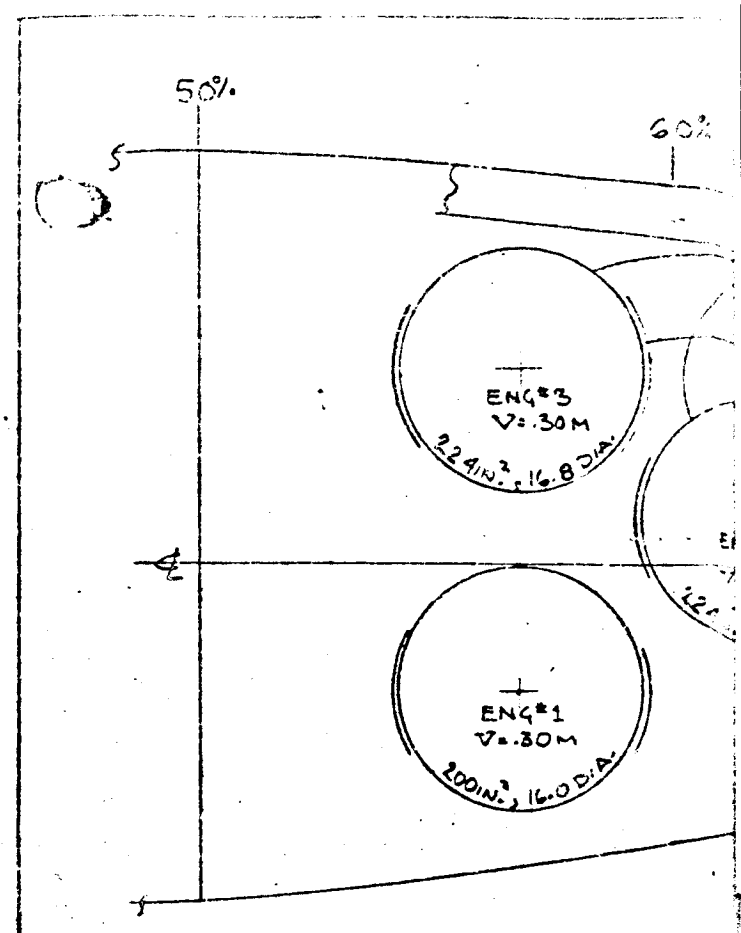
50%
60%
ENG#3
V=.30M
224 IN², 16.8 DIA.
ENG#1
V=.30M
200 IN², 16.0 DIA.
SECTION

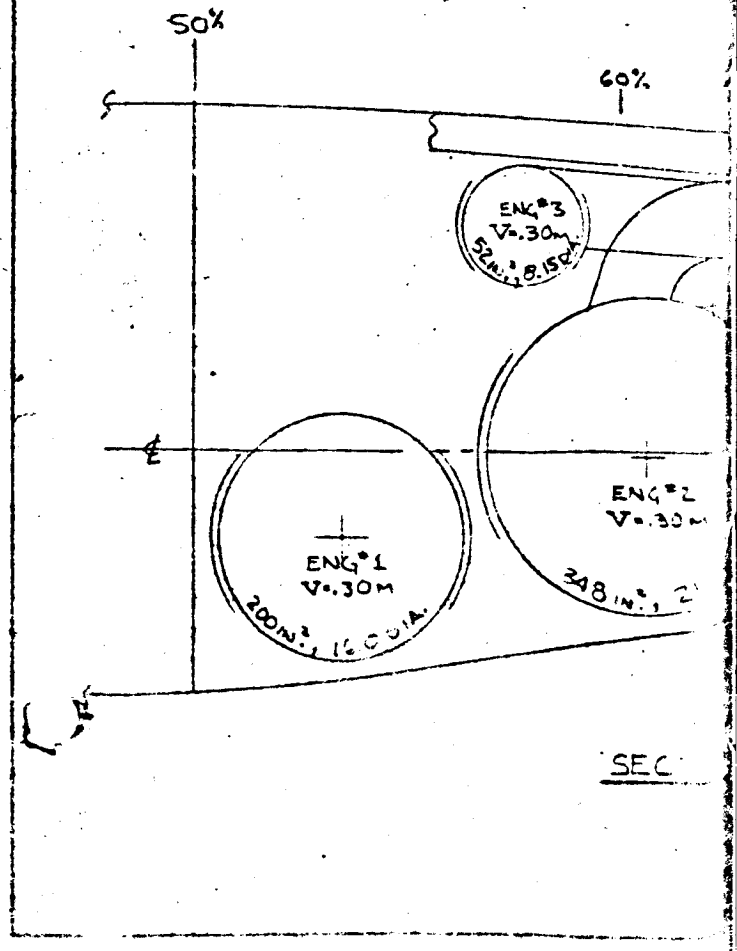
50%
60%
ENG#3
V=.30M
52 IN², 8.15 DIA.
ENG#1
V=.30M
200 IN², 16.0 DIA.
ENG#2
V=.30M
348 IN²,
SEC

1

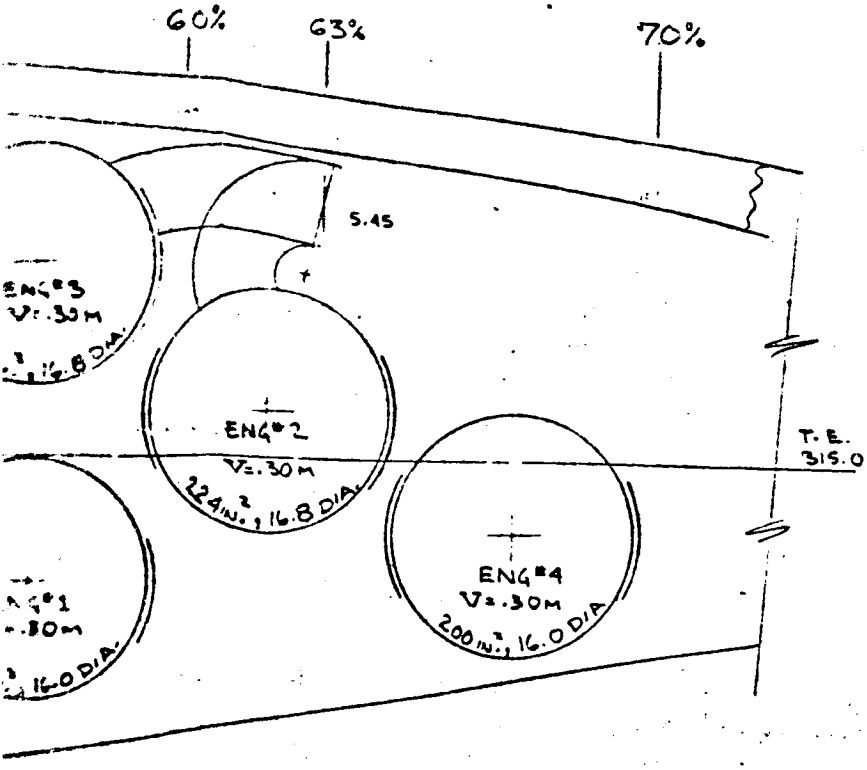

SECTION: A-A

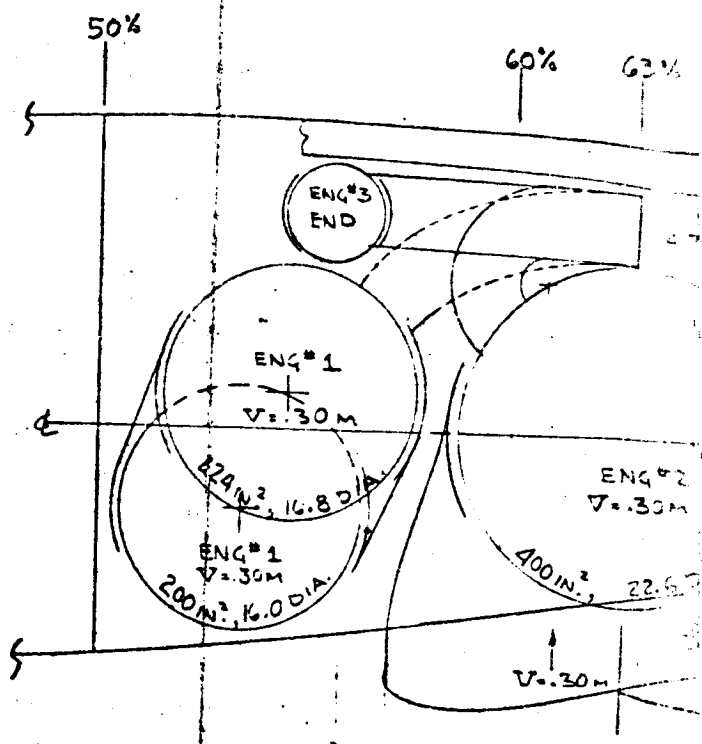

SECTION C-C

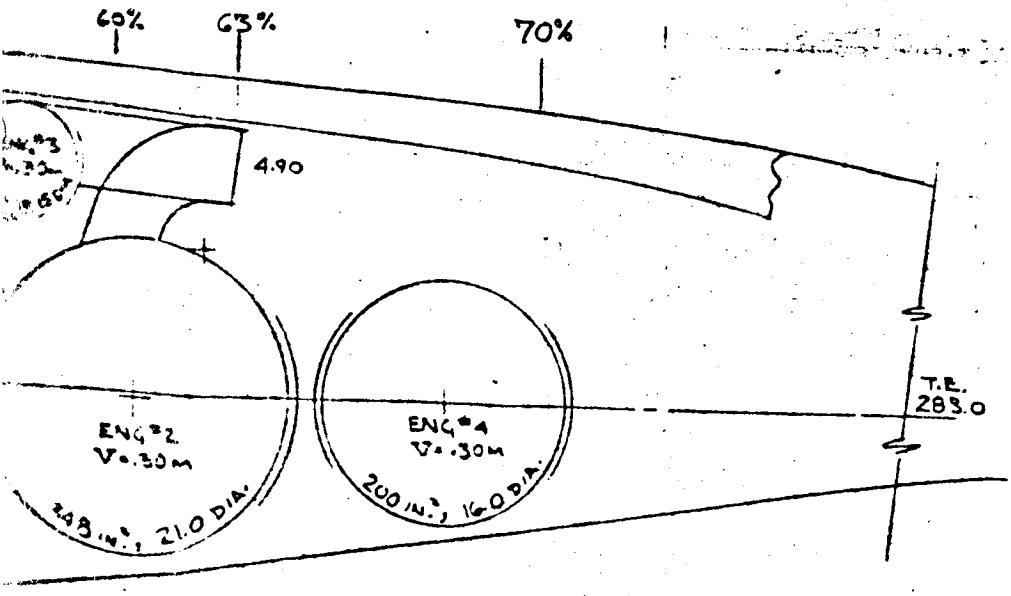

SECTION B-B

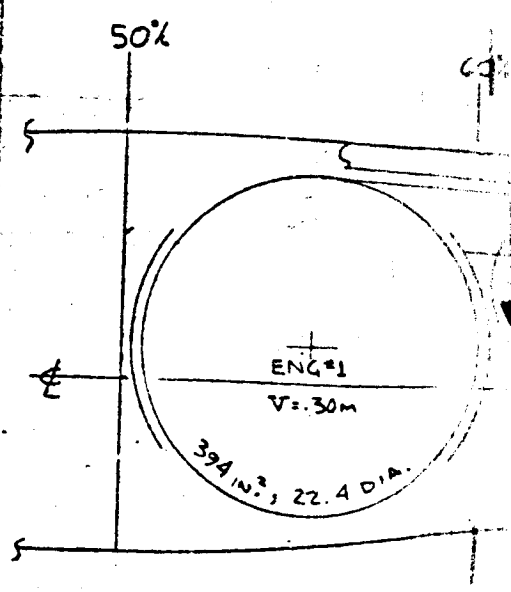

SEC

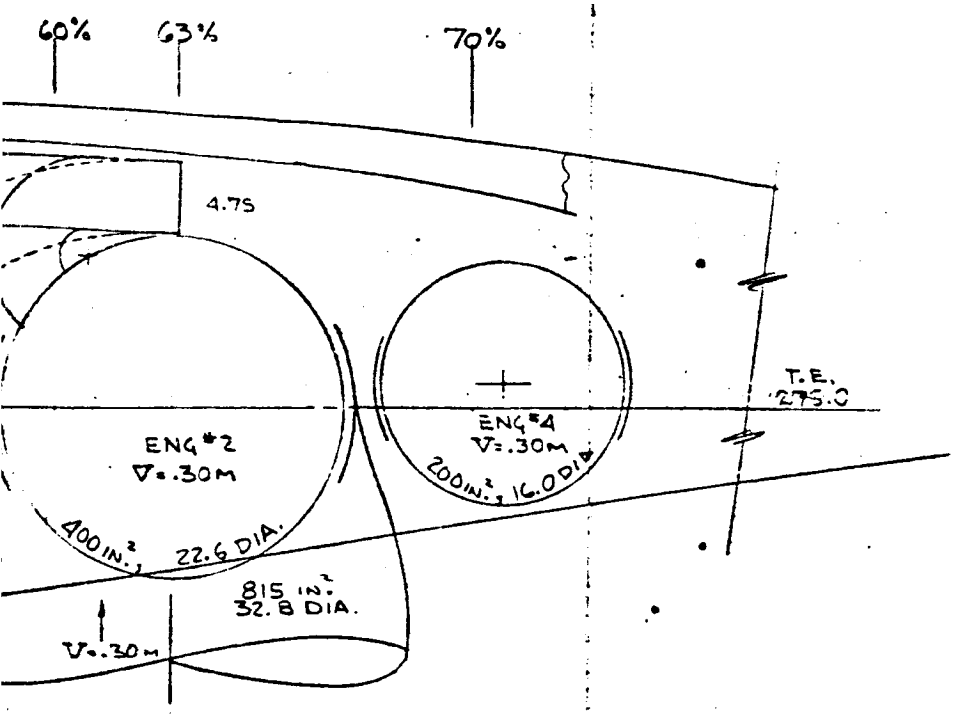

TION C-C

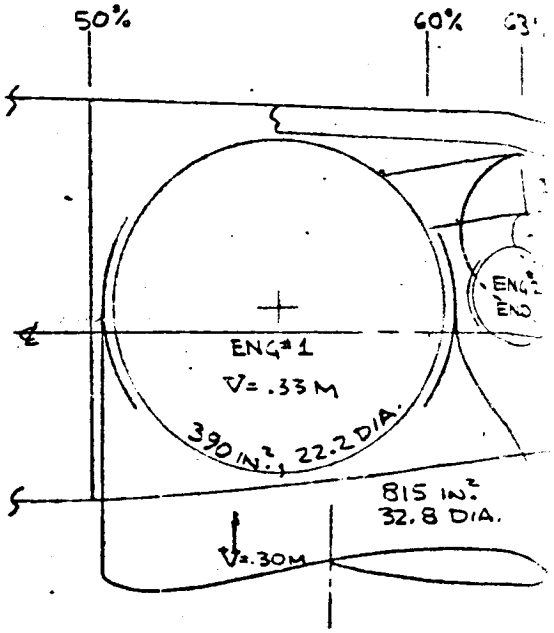

SECTION

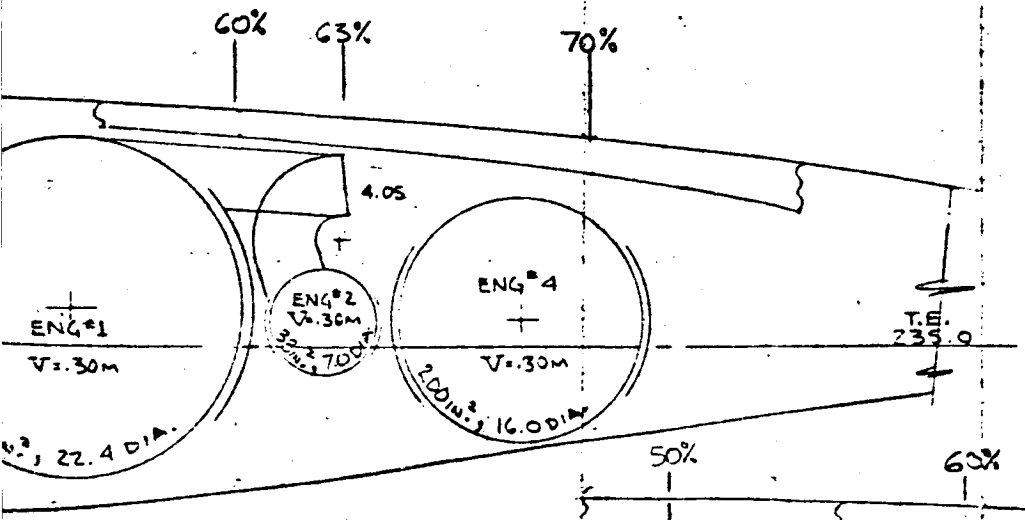

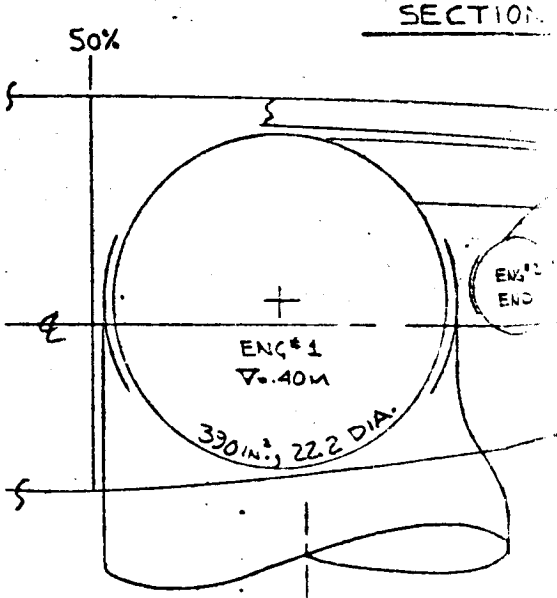

ALTERNATE SECTION E-E

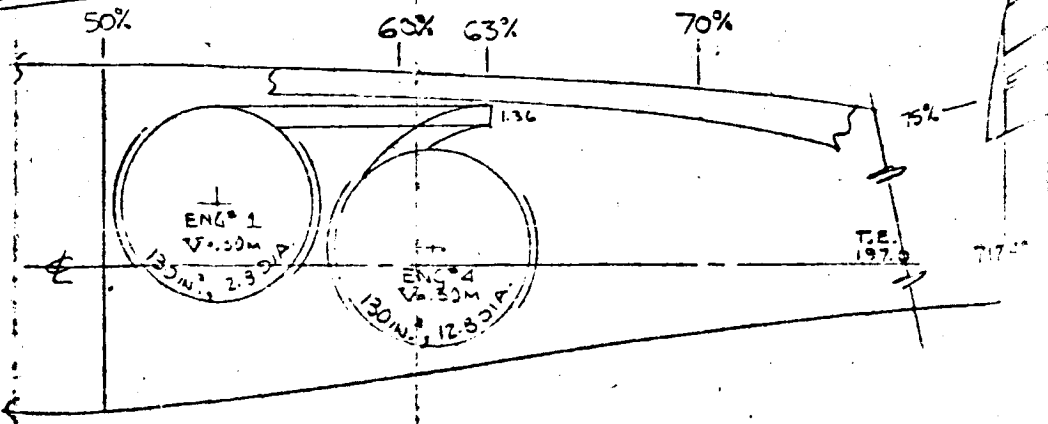

SECTION D-D

SECTION F-F

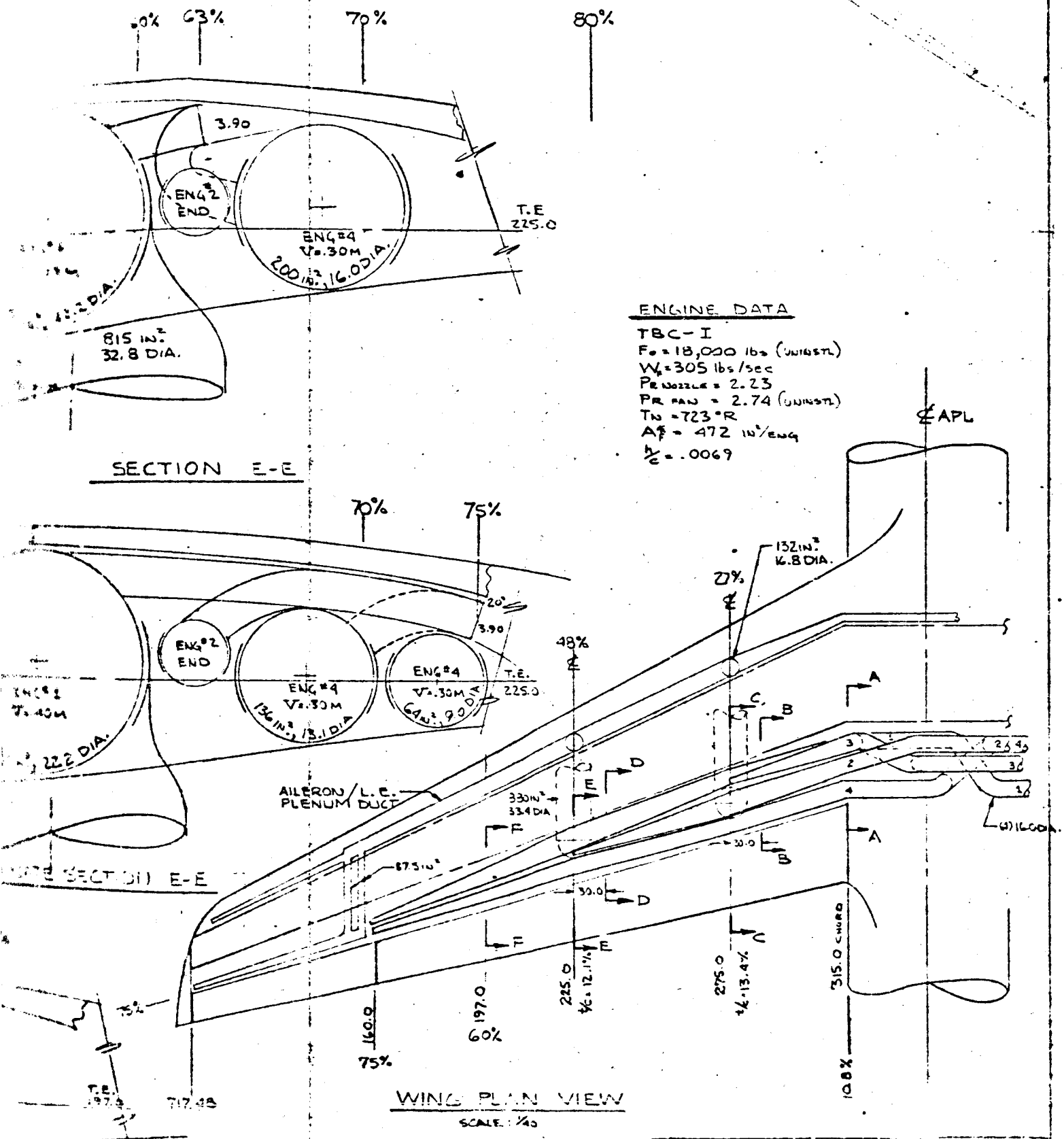
63%
70%
80%
3.90
ENG #2 END
ENG #4 V=.30M
200 IN², 16.0 DIA.
T.E 225.0
815 IN² 32.8 DIA.
SECTION E-E
ENGINE DATA
TBC-I
F₀ = 18,000 lbs (UNINSTL)
W = 305 lbs/sec
PR NOZZLE = 2.23
PR FAN = 2.74 (UNINSTL)
TN = 723°R
A = 472 IN²/ENG
h/c = .0069
℄ APL
70%
75%
20°
3.90
ENG #2 END
ENG #4 V=.30M
136 IN², 13.1 DIA
ENG #4 V=.30M
64 IN², 9.0 DIA
T.E. 225.0
22.2 DIA.
132 IN² 16.8 DIA.
27%
48%
AILERON/L.E. PLENUM DUCT
330 IN² 33.4 DIA
87.5 IN²
30.0
30.0
(4) 16.0 DIA.
315.0 CHORD
160.0
197.0
60%
75%
225.0
h/c = 12.1%
275.0
h/c = 13.4%
108%
T.E. 197.4
717.48
WING PLAN VIEW
SCALE: 1/40
TBC-I
INDEPENDENT DUCT
LO-AWNP-026